JAERI-Conf
97-005

PROCEEDINGS OF THE 1996 SYMPOSIUM ON NUCLEAR DATA
November 21-22, 1996, JAERI, Tokai, Ibaraki, Japan

March 1997

(Eds.) Tetsuo IGUCHI* and Tokio FUKAHORI

日 本 原 子 力 研 究 所
Japan Atomic Energy Research Institute

Proceedings of the 1996 Symposium on Nuclear Data
November 21-22, 1996, JAERI, Tokai, Ibaraki, Japan

(Eds.) Tetsuo IGUCHI* and Tokio FUKAHORI

Japanese Nuclear Data Committee
Tokai Research Establishment
Japan Atomic Energy Research Institute
Tokai-mura, Naka-gun, Ibaraki-ken

The 1996 Symposium on Nuclear Data was held at Tokai Research Establishment, Japan Atomic Energy Research Institute (JAERI) , on 21st and 22nd of November, 1996. This symposium was organized by Japanese Nuclear Data Committee and Nuclear Data Center, JAERI. In the oral sessions, presented were 18 papers on integral testing of JENDL-3.2, international collaboration, delayed neutron, new experiments, JENDL special purpose file and high energy nuclear data. In the poster session, presented were 32 papers concerning experiments, evaluations, benchmark tests and on-line database on nuclear data. Those presented papers are compiled in this proceedings.

---

* Nagoya University

1996年核データ研究会報文集
1996年11月21日～22日，日本原子力研究所，東海村

日本原子力研究所東海研究所
シグマ研究委員会
（編）井口 哲夫*・深堀 智生

　1996年核データ研究会が，1996年11月21日と22日の両日，日本原子力研究所東海研究所において開催された。この研究会は，日本原子力研究所のシグマ研究委員会と核データセンターが主催して開いたものである。口頭発表では，JENDL-3.2の積分テスト，国際協力，遅発中性子，特殊目的ファイル，高エネルギー核データ，新しい実験・測定の18件の報告があった。ポスター発表では，32件の発表があり，それらは，核データの測定，評価や評価済核データのベンチマークテスト，オンラインデータベース等に関するものであった。本報文集は，それらの論文をまとめたものである。

東海研究所：〒319-11　茨城県那珂郡東海村白方白根2－4
* 名古屋大学

Program Committee

Tetsuo IGUCHI (Chairman)	Nagoya University
Satoshi CHIBA	Japan Atomic Energy Research Institute
Tokio FUKAHORI	Japan Atomic Energy Research Institute
Kazuki HIDA	Toshiba, Co.
Hideo HIRAYAMA	High Energy Physics Institute
Makoto ISHIKAWA	Power Reactor and Nuclear Fuel Development, Co.
Jun-ichi KATAKURA	Japan Atomic Energy Research Institute
Ken NAKAJIMA	Japan Atomic Energy Research Institute
Yutaka NAKAJIMA	Research Organization for Information Science and Technology
Naoteru ODANO	Ship Research Institute, Ministry of Transport
Etsuro SAJI	Toden Software Inc.
Hiroshi TAKADA	Japan Atomic Energy Research Institute
Yasushi TAMURA	Japan Atomic Energy Research Institute
Yoshitomo UWAMINO	The Institute of Physical and Chemical Research
Takashi WATANABE	Kawasaki Heavy Industries, Co. Ltd.
Tadashi YOSHIDA	Musashi Institute of Technology

プログラム委員会

井口	哲夫 （委員長）	名古屋大学
千葉	敏	日本原子力研究所
深堀	智生	日本原子力研究所
肥田	和毅	（株）東芝
平山	英夫	高エネルギー物理学研究所
石川	真	動力炉・核燃料開発事業団
片倉	純一	日本原子力研究所
中島	健	日本原子力研究所
中島	豊	（財）高度情報科学技術研究機構
小田野	直光	運輸省船舶技術研究所
佐治	悦郎	東電ソフトウェア（株）
高田	弘	日本原子力研究所
田村	康志	日本原子力研究所
上蓑	義明	理化学研究所
渡部	隆	川崎重工業（株）
吉田	正	武蔵工業大学

Contents

目 次

1. Introduction

The 1996 symposium on nuclear data was held at Tokai Research Establishment, Japan Atomic Energy Research Institute (JAERI), on 21st and 22nd of November, 1996. The symposium was organized by Japanese Nuclear Data Committee and Nuclear Data Center, JAERI.

The program of the symposium is listed below. In the second oral sessions, three invited talks were addressed on integral testing of JENDL-3.2. As an international session, nuclear data research activities in China, Korea and Karlsruhe were presented. In the other sessions, total 12 papers were presented on delayed neutron, new experiments, JENDL special purpose file and high energy nuclear data. In the poster session, presented were 32 papers concerning nuclear data experiments, evaluations, benchmark tests and on-line database on nuclear data. Those papers are compiled in this proceedings.

Program

Oral Presentation [Talk + Discussion (min.)]
Nov. 21 (Thu.)
10:00 - 10:10

1. Opening Address   Y. Murao (JAERI)

10:10 - 12:00

2. Integral Test of JENDL 3.2   Chairman: M. Kawai (Toshiba)
2.1 Isotopic Analyses and Calculations by Use of JENDL-3.2
  for High Burn-up UO2 and MOX Spent Fuels [35+5]   A. Sasahara(CRIEPI)
   comment: Collection of Assay Data on Isotopic Composition
     in LWR Spent Fuels [10+5]   Y. Naito(JAERI)
2.2 Integral Test of JENDL Fusion File [25+5]   F. Maekawa(JAERI)
2.3 Toward JENDL-3.3: Comments on the Problems of JENDL-3.2
  for the Next Version Developments [10+5]   A. Hasegawa(JAERI)

12:00 - 13:00   LUNCH

13:00 - 14:50

3. Topics 1: International Collaboration   Chairman: T. Fukahori(JAERI)

3.1 Status and Future Plan of Nuclear Data Activities

in China [30+10]   Zhuang Youxiang(CIAE)

3.2 Status and Future Plan of Nuclear Data Activities in Korea [25+5]

Oh Soo-Youl and Chang Jonghwa(KAERI)

3.3 Status of Nuclear Data Activities at Karlsruhe [25+5]   T. Kawano(Kyushu U.)

14:50 - 15:10   COFFEE BREAK

15:10 - 16:50

4. Topics 2: Delayed Neutron   Chairman: T. Yoshida (Musashi Inst. Technol.)

4.1 Status of International Benchmark Experiment for

Effective Delayed Neutron Fraction (β eff) [25+5]   S. Okajima(JAERI)

4.2 Review of Experimental Methods for Evaluating Effective

Delayed Neutron Fraction [25+5]   Y. Yamane(Nagoya U.)

4.3 Delayed Neutron Spectra and their Uncertainties

in Fission Product Summation Calculations [25+5]   T. Miyazono(Nagoya U.)

16:50 - 17:40

5. Poster Session 1 (Introduction)

18:00 - 20:00   Reception at Akogi-ga-ura Club

Nov. 22 (Fri.)

9:00 - 10:10

5'. Poster Session 2 (Discussion)

10:10 - 12:00

6. Topics 3: New Experiments   Chairman: Y. Uwamino(RIKEN)

6.1 Status and Future Plan of Measurements by RIKEN Accelerator Facility[30+10]

I. Tanihata(RIKEN)

6.2 Simultaneous Measurement of Fission Fragments and Prompt Neutrons

for Thermal Neutron Induced Fission of U-235 [25+5]   K. Nishio(Kyoto U.)

6.3 Development of a Helium Accumulation Fluence Monitor

for Fast Reactor Dosimetry [25+5]

C. Ito(PNC), Y. Kanda(Oita Professional Eng. School), Y. Takao(Kyushu U.)

12:00 - 13:00   LUNCH

13:00 - 14:10
7. JENDL Special Purpose File   Chairman: Y. Nakajima(RIST)
7.1 Activities on Covariance Evaluation in Japanese Nuclear Data Committee [25+5]

K. Shiabata(JAERI)

7.2 PKA Spectrum [25+5]   M. Kawai(Toshiba)

14:10 - 16:20
8. High Energy Nuclear Data   Chairman: H. Hirayama(KEK)
8.1 Spallation Integral Experiment Analysis by High Energy
    Nucleon-Meson Transport Code [25+5]   H. Takada(JAERI)
8.2 The South African National Accelerator Centre and
    its Research Programme [25+5]   Y. Watanabe(Kyushu U.)
8.3 Measurement of Double Differential Charged Particle Emission Cross Sections and
    Development of a Wide Range Charged Particles Spectrometer for Ten's MeV
    Neutrons[25+5]   Y. Nauchi(Tohoku U.)
8.4 Status of Spallation Neutron Source [25+5] Y. Oyama(JAERI)

16:20 - 16:35
9. Summary Talk   M. Baba(Tohoku U.)

Poster Session
Thu. 11/21 17:00 - 17:40 and Fri. 11/22: 9:00 - 10:10

P01. Measurements of keV-Neutron Capture g Rays of Fission Products(3)

M. Igashira(TIT)

P02. Integral Test on Activation Cross Section of Tag Gas Nuclides Using

a Fast Neutron Spectrum Field   T. Aoyama(PNC)

P03. Comparison of Yield and Decay Data among JNDC2, ENDF/B-VI

and JEF2.2   K. Oyamatsu(Nagoya U.)

P04. Measurement of Helium Production Cross Sections of Iron for d-T

Neutrons by Helium Accumulation Method   Y. Takao(Kyushu U.)

P05. Measurements of Double-Differential Neutron Emission Cross Sections

of Li-6 and Li-7 for 18 MeV Neutrons   M. Ibaraki(Tohoku U.)

P06. Measurement of (n,2n) Cross-sections for Sc, Mn, Cr and In between

12 and 19 MeV with Activation Technique   S. Iwasaki(Tohoku U.)

P07. (n,a) Cross Section Measurement for Gaseous Samples Using Gridded

Ionization Chamber   -Determination of Cross Section-

T. Sanami(Tohoku U.)

P08. Development of Whole Energy Absorption Spectrometer for Decay Heat

Measurement on Fusion Reactor Materials   F. Maekawa(JAERI)

P09. Evaluation of Induced Activity, Decay Heat and Dose Rate

Distribution after Shutdown in ITER   K. Maki(Hitachi)

P10. Measurements of Neutron Spallation Cross Sections (2) E. Kim(Tohoku U.)

P11. Measurements of Secondary Neutrons Producted from Thick Targets

Bombarded by Heavy Ions   T. Kurosawa(Tohoku U.)

P12. Measurements of Neutron Spectrum from Stopping-length Target

Irradiated by Several Tenth-MeV/u Particles   S. Meigo(JAERI)

P13. Calculation of the Intermediate Energy Activation Cross Section

S. Furihata(MRI)

P14. Measurement of Reaction Cross Sections of I-129 Induced by DT Neutrons

D. Nakano(Osaka U.)

P15. Measurement of Thermal Neutron Cross Section and Resonance Integral

of the Reaction Cs-135(n.g)Cs-136

T. Kato(PNC, Gifu College Med. Technol.)

P16. Calculation of Prompt Neutron Spectra for Curium Isotopes

T. Osawa(Kinki U.)

P17. One-Group Constants Libraries for Nuclear Equilibrium State

A. Mizutani(TIT)

P18. Development of a System of Measuring Double-differential
Cross Sections for Proton-induced Reactions   M. Harada(Kyushu U.)

P19. Measurement of Fission Cross Section with Pure Am-243 Sample Using
Lead Slowing-Down Spectrometer   K. Kobayashi(Kyoto U.)

P20. Quasi-Elastic Cross Sections from He-4, C-12 Induced by 1 GeV Protons

M. Nishimura(Kyushu U.)

P21. Cross Section Measurement for (n,n α) Reactions by 14 MeV Neutrons

Y. Kasugai(JAERI)

P22. Measurement of Cross Sections Producing Short-lived Nuclei by 14 MeV
Neutron -Br, Te, Dy, Ho, Yb-   H. Sakane(Nagoya U.)

P23. Systematic Measurement of Beta-decay Half-lives of Short-lived Nuclei

T. Hirose(Nagoya U.)

P24. Double Differential Charged Particle Emission Cross Sections
of Vanadium for 14.1 MeV Incident Neutron   Ko-Ko-Oo(Osaka U.)

P25. Direct Neutron Capture in a Dispersive Potential of Light Nuclei

H. Kitazawa(TIT)

P26. The Influence of Impurities for Cross Section Measurement of
Am-241,243(n,f) Reactions   T. Kai(Kyoto U.)

P27. Modification of EXIFON Code and Analysis of O-16 + n Reactions
in En=20-50 MeV   T. Murata(NFD)

P28. HETC-3step Included Fragmentation Process   N. Shigyo(Kyushu U.)

P29. Phenomenological Dirac Optical Potential for Neutron Cross Sections

S. Maruyama(Kyushu U.)

P30. A Consistent Analysis of (p,p') and (n,n') Reactions Using
the Feshbach-Kerman-Koonin Model   S. Yoshioka(Kyushu U.)

P31. Construction of a Nuclear Data Server Using TCP/IP   T. Kawano(Kyushu U.)

P32. Decay Data File Based on the ENSDF File   J. Katakura(JAERI)

2. Papers Presented at Oral Session

2.1 Integral Test of JENDL 3.2

2.1.1 Isotopic Analyses and Calculation by Use of JENDL-3.2 for High Burn-up U O2 and MOX Spent Fuels

Akihiro SASAHARA and Tetsuo MATSUMURA

Central Research Institute of Electric Power Industry(CRIEPI)
2-11-1, Iwado Kita, Komae-shi, Tokyo 201 Japan
e-mail : sasa@criepi.denken.or.jp

G.NICOLAOU, M.BETTI and C.T.WALKER
European Commission, Joint Research Centre,
Institute for Transuranium Elements(ITU)
Postfach 2340, D-76125 Karlsruhe, Germany

The post irradiation examinations (PIE) were carried out for high burn-up UO2 spent fuel (3.8%U235, average burn-up:60GWd/t) and mixed oxide (MOX) spent fuel (5.07%Pu, average burn-up:45GWd/t). The PIE includes, a) isotopic analysis, b) electron probe microanalysis(EPMA) in pellet cross section and so on. The results of isotopic analyses and EPMA were compared with ORIGEN2/82 and VIM-BURN calculation results. In VIM-BURN calculation, the nuclear data of actinides were proceeded from new data file, JENDL-3.2. The sensitivities of power history and moderator density to nuclides composition were investigated by VIM-BURN calculation and consequently power history mainly effected on Am241 and Am242m and moderator density effected on fissile nuclides. From EPMA results of U and Pu distribution in pellet, VIM-BURN calculation showed reasonable distribution in pellet cross section.

1. Introduction

Development of advanced spent fuel storage technology is necessary for high burn-up UO2 and MOX spent fuel in the near future. These high burn-up UO2 and MOX spent fuel have much higher neutron emission and heat generation than that of conventional burn-up UO2 fuel (table 1). It is therefore necessary to obtain basic data in order to verify computations prior to their use in the design and safety analyses for spent fuel storage. Such data include the neutron and gamma-radiation source, actinide and fission product isotopic composition, elements distribution in a pellet and so on[1,2].

In this study, post irradiation examinations (PIE) were carried out and subsequently the predictions of the ORIGEN2/82 and VIM-BURN code were compared with PIE results on isotopic analyses and EPMA. In VIM-BURN calculation, the nuclear data of actinides were prepared from JENDL-3.2 and the sensitivities of linear power and moderator density to nuclides composition were investigated. The U and Pu distribution profile along pellet radius obtained by EPMA were also compared with VIM-BURN calculation.

2. Fuel Specification

The spent fuels used in this study were irradiated in commercial PWRs : a high burn-up UO2 fuel pin (3.8%U-235, 60.2GWd/t declared average burn-up) ; two segments (MOX1 and MOX2) from middle parts of two MOX fuel pins (5.07%Pu, 44.5GWd/t and 45.7GWd/t declared burn-up). There are Pu agglomerates(Pu enrichment : 30%) in MOX fuel pellets which were manufactured by the mechanically blending. Both

segments have similar irradiation histories. The PIE of these fuels were carried out at the Institute for Transuranium Elements(ITU), Karlsruhe in Germany.

3. Isotopic Analyses
3.1 Preparation of Sample and Measurement Process

Isotopic analyses were performed on dissolved solution contained samples which were chose from MOX1 segment (i.e. one sample) and differential axial four positions (i.e. four samples) for a high burn-up UO2 fuel. The analyses techniques include α-/γ- spectrometry, thermal ionization mass spectrometry (TIMS) and ICP-MS coupled to an ion chromatography column. For high burn-up UO2 fuel, the local burn-up of four samples obtained from different axial positions were 54GWd/t, 61GWd/t, 65GWd/t (at axial lower position) and 65GWd/t (at axial upper position). These burn-up values were estimated from Nd148 obtained by isotopic analyses. For MOX sample, the burn-up was 46GWd/t.

3.2 Calculation Process of ORIGEN2 and VIM-BURN Code

In ORIGEN2/82 calculation, the libraries prepared in ORIGEN2/82 were used for high burn-up UO2 and MOX fuel calculation.

The VIM-BURN code is composed of VIM2 and BURN. The VIM2 is a continuous neutron energy Monte-Carlo code developed in Argonne National Laboratory. The burn-up module, BURN was added to VIM2 in CRIEPI. The VIM-BURN code can treat resonance cross section of nuclides such as U238 in detail and calculate nuclides distribution profile in pellet during irradiation[3]. In VIM-BURN calculation, the cross section library was proceeded from JENDL-3.2 for nuclides such as actinides, Xe135, Sm149 and Ag107(as lumped FP) and JENDL-2 was used as 67 multigroup constant library (MGCL) for other FPs. Fig.1 shows calculation flow of the VIM-BURN code. The actinides, U234 up to Cm245, were considered in the burn-up chain. Fig.2 shows the calculation geometry applied to high burn-up UO2 and MOX fuel in VIM-BURN calculation. In high burn-up UO2 fuel, the pellet was divided into 9 sub-regions and in MOX fuel, that was divided into 7 sub-regions. A 80,000-history and 200,000-history were produced in calculations for high burn-up UO2 fuel and MOX fuel respectively. Table 2 shows calculation parameters. The sensitivities of linear power density and moderator density to nuclides composition were investigated by VIM-BURN calculation.

3.3 Results of Isotopic Analyses and Calculation

Fig.3 shows the C/E (Calculation/Experiment) values obtained by ORIGEN2/82 calculation at upper and lower position of high burn-up UO2 fuel, which have similar burn-up of 65GWd/t. The reason why the discrepancy of the C/E values from U234 till Pu242 between both positions is difference of neutron spectrum distribution. The neutron spectrum at lower axial position is softer than that at upper axial position due to higher moderator density. Thus the burning of fissile nuclides in sample were advanced at lower axial position. For Cm242 at axial lower position, it is necessary to review the measurement data. Fig.4 shows the C/Es of MOX fuel. In ORIGEN2/82 calculation, the C/Es in U and Pu agree within 20% for high burn-up and MOX fuel.

Fig.5 and Fig.6 show the sensitivities of linear power density and moderator density for high burn-up UO2 fuel (at axial upper position, burn-up:65GWd/t) obtained from VIM-BURN calculation. In Fig.5, the linear power density effects on Am241 produced by β-decay from Pu241 and consequently change of Am242m is enhanced. The moderator density mainly effects on burning of fissile nuclides. Fig.7 and Fig.8 show the C/Es of VIM-BURN and ORIGEN2/82 calculation at 61GWd/t and 54GWd/t for high burn-up UO2.

In VIM-BURN calculation, the C/Es of minor actinides are improved except with Np237 and Cm242. For Cm242, it is necessary to review the measurement data at 61GWd/t and 54GWd/t.

Fig.9 and Fig.10 show the sensitivities of linear power density and moderator density for MOX fuel. The C/Es show the similar behavior in high burn-up UO2 fuel by change of the linear power density and moderator density. In VIM-BURN calculation, the C/Es of Cm are improved more than that in ORIGEN2/82 calculation.

4. EPMA Measurements
4.1 Measurement Process

For high burn-up UO2 fuel, the concentration distribution of U, Pu, Nd, Xe and Cs along a pellet radius were measured by EPMA. For MOX fuel, the average distribution of U, Pu, Nd, Xe and Cs along a pellet radius were measured along a pellet radius. The burn-ups were estimated from Nd concentration.

4.2 Results of EPMA and Calculation

The average burn-up estimated by EPMA was 74.5GWd/t and at pellet surface was 157GWd/t for high burn-up UO2 fuel. For MOX fuel, the average burn-up was 47.3GWd/t and at pellet surface was 61.8GWd/t.

Fig.11 and Fig.12 show concentration distribution of U and Pu obtained by EPMA and VIM-BURN calculation. There is an accumulation of Pu transformed from U238 by neutron surface resonance effect at pellet surface in high burn-up UO2 fuel. VIM-BURN calculations show reproduction of U and Pu distribution profile at pellet surface. In MOX fuel, Pu distribution is scattered due to Pu agglomerates in EPMA.

5. Summaries

The results of isotopic analyses and EPMA measurements for high burn-up UO2 and MOX spent fuel were compared with ORIGEN2/82 and VIM-BURN calculation. The nuclear cross section library, JENDL-3.2 was used for actinides in VIM-BURN calculation. The sensitivities of power history and moderator density to nuclides composition were investigated by VIM-BURN calculation. There is the discrepancy of the C/Es obtained by ORIGEN2/82 calculation between upper and lower position of high burn-up UO2 fuel at 65GWd/t. The reason why the discrepancy of the C/Es from U234 till Pu242 are difference of neutron spectrum distribution. In ORIGEN2/82 calculation, the C/Es in U and Pu agree within 20% for high burn-up and MOX fuel.

In VIM-BURN calculation, the linear power density effects on Am241 produced by β-decay from Pu241 and consequently change of Am242m is enhanced. The moderator density mainly effects on burning of fissile nuclides.

From EPMA results of U and Pu distribution in pellet radius, there is an accumulation of Pu at pellet surface in high burn-up UO2 fuel. VIM-BURN calculations show reproduction of U and Pu distribution profile at pellet surface. The U and Pu distribution of VIM-BURN calculation agree with EPMA results.

References

[1] Sasahara A., Matsumura T. and Nicolaou G. : "Post Irradiation Examinations and the Validity of Computational Analysis for High burn-up UO2 and MOX Spent Fuels", CRIEPI report, T95012(in Japanese).

[2] Sasahara A., Matsumura T., Nicolaou G., Glatz J.P., Toscano E. and Walker C.T.: "Post Irradiation Examinations and Computational Analysis of High Burn-up UOX

and MOX Spent Fuels for Interim Dry Storage", Proc. 10th Pacific Basin Nuclear Conference, Oct.20-25, 1996, Kobe, Japan, p.1073.
[3] Kameyama T. and Matsumura T. : "Development and Verification of Rim Effect Analysis Code for High Burnup LWR Fuel", CRIEPI report, T88301(in Japanese).

Table1 An Example of Neutron Emission and Heat Generation
in High Burn-up UO2 and MOX fuel

	Conventinal UO2	High Burn-up UO2	MOX
Neutron Emission	1.0	1.5	18.4
Heat Generation	1.0	1.3	2.4

ratio to conventional UO2 fuel

Table2 Parameters in VIM-BURN Calculation

	Reference	Paramerter
linear power	206W/cm(High Burn-up UO2 fuel) 185W/cm(MOX fuel)	+5%, -5% +5%, -5%
moderator density	typical PWR(High Burn-up UO2 fuel) typical PWR(MOX fuel)	+5%, -5% +5%, -5%
burn-up	65GWd/t(High Burn-up UO2 fuel) 45GWd/t(MOX fuel)	—— ——
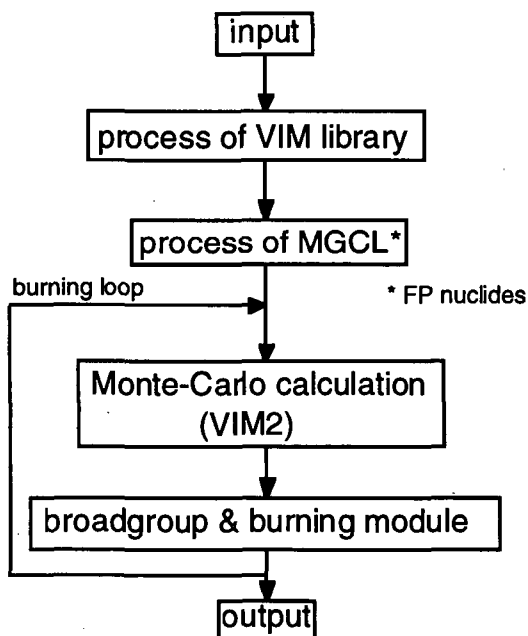
Fig.1 Calculation Flow of VIM-BURN code
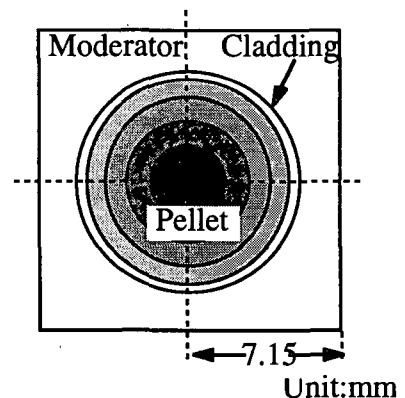
Fig.2 Calculation Geometry of High Burn-up UO2 and MOX fuel
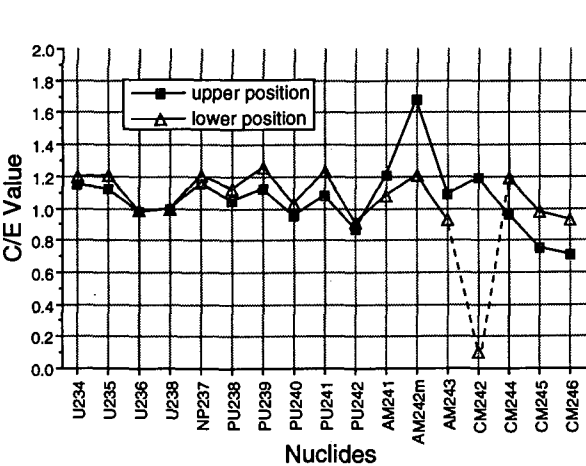
Fig.3 ORIGEN2 Results of High Burn-up UO2
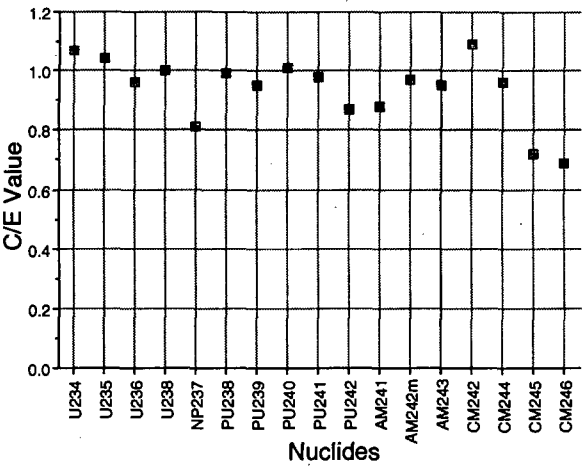
Fig.4 ORIGEN2 Results of MOX
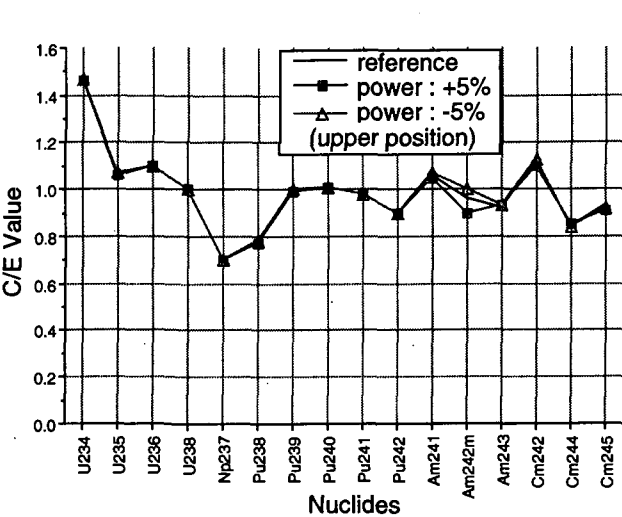
Fig.5 Effect of Linear Power Density
(VIM-BURN Calculation of High Burn-up UO2)
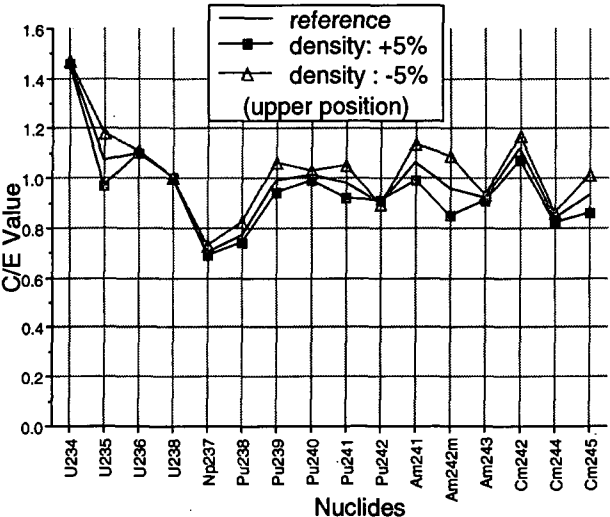
Fig.6 Effect of Moderator Density
(VIM-BURN Calculation of High Burn-up UO2)
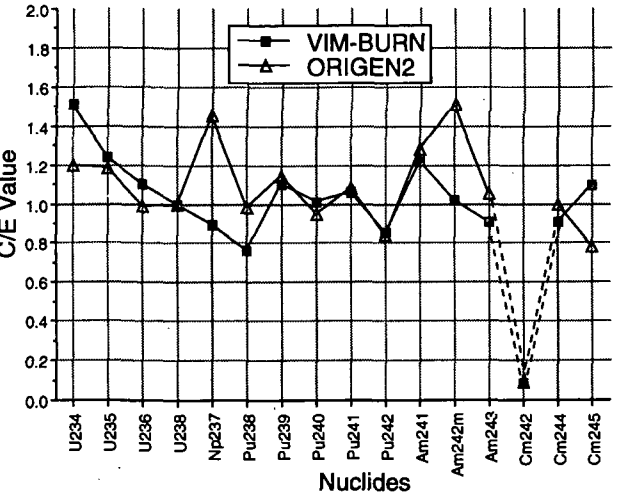
Fig.7 VIM-BURN and ORIGEN2
(High Burn-up UO2:61GWd/t)
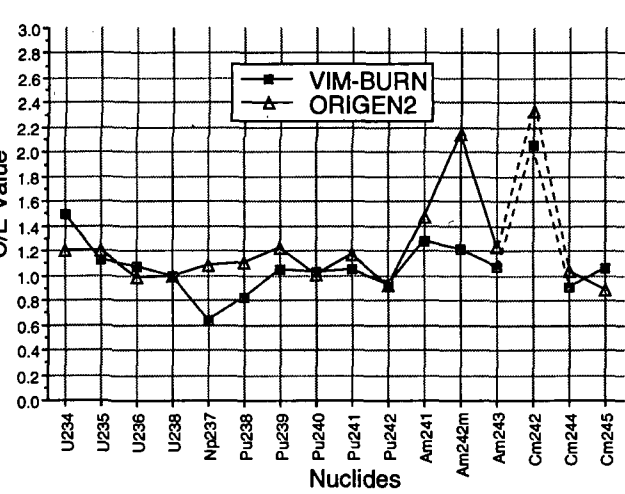
Fig.8 VIM-BURN and ORIGEN2
(High Burn-up UO2:54GWd/t)
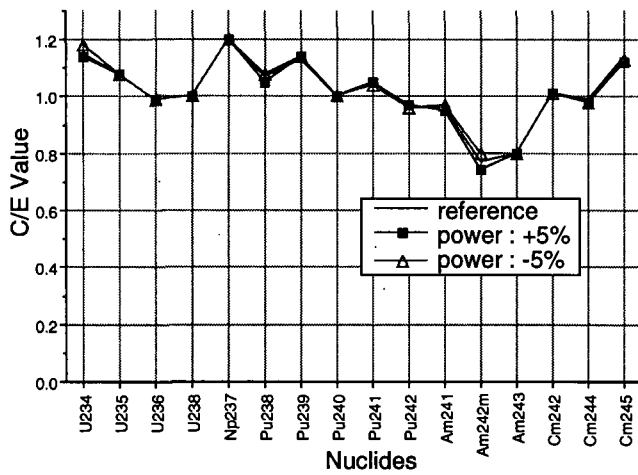
Fig.9 Effect of Linear Power Density
(VIM-BURN Calculation of MOX)
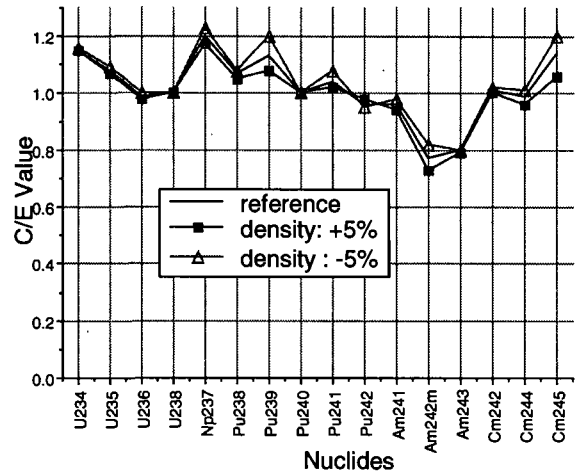
Fig.10 Effect of Moderator Density
(VIM-BURN Calculation of MOX)
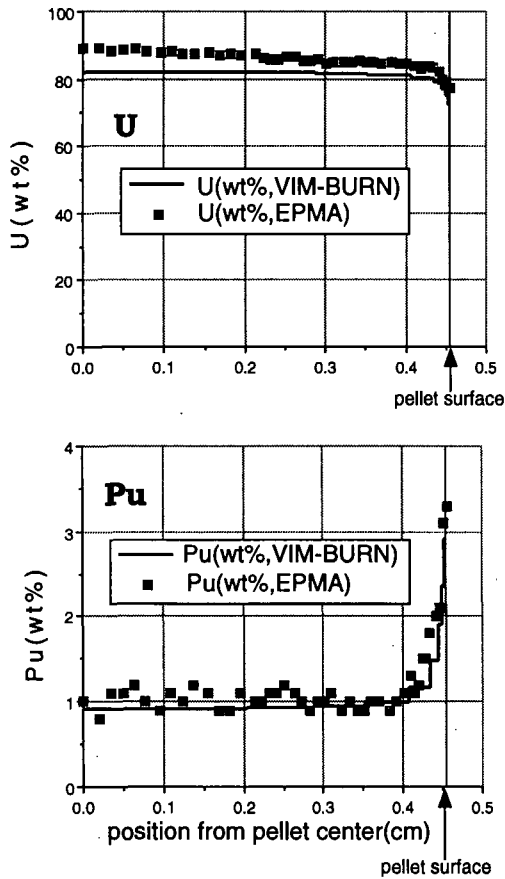
Fig.11 U and Pu distribution
(High Burn-up UO₂)
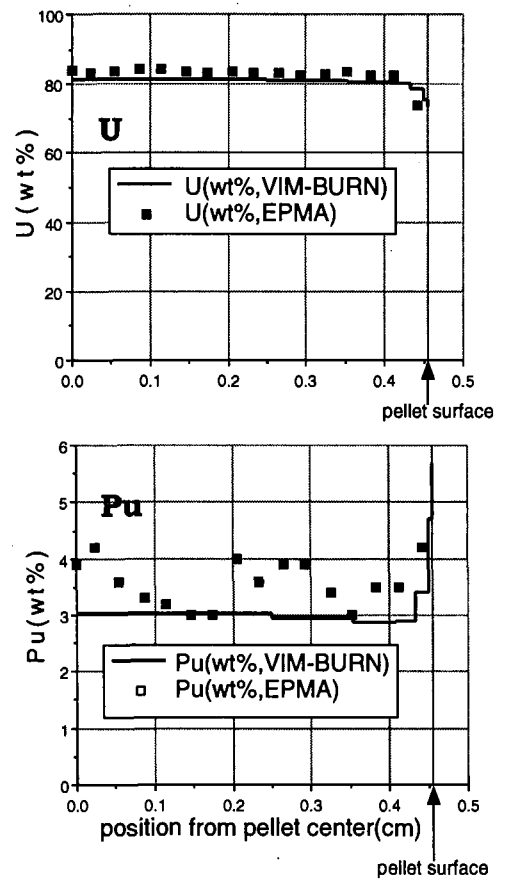
Fig.12 U and Pu distribution
(MOX1)

Comment: Collection of Assay Data on Isotopic Composition in LWR Spent Fuel

Yoshitaka NAITO, Masayoshi KUROSAWA and Kenya SUYAMA

Fuel Cycle Safety Research, Japan Atomic Energy Research Institute
Tokai-mura, Naka-gun, Ibaraki-ken, 319-11
e-mail: naito@popsvr.tokai.jaeri.go.jp

Many assay data of LWR spent fuels have been collected from reactors in the world and some of them are already stored in the database SFCOMPO which was constructed on a personal computer IBM PC/AT. On the other hand, Group constant libraries for burnup calculation code ORIGEN-II were generated from the nuclear data file JENDL3.2. These libraries were evaluated by using the assay data in SFCOMPO.

1. Introduction

In the Nuclide Production Evaluation WG in the Sigma Committee, we have been collecting the assay data on isotopic composition in LWR spent fuels. Some of these collected data are stored in SFCOMPO database. On the other hand, we have been generating one group constant libraries for burnup calculation codes;ORIGEN-II and COMRAD using the JENDL 3.2 nuclear data library. The ORIGEN-II libraries for the representative PWR and BWR in Japan were generated already. Furthermore, we are going to verify these burnup codes by comparing the calculated isotopic composition with the measured one in SFCOMPO. The flow chart of these works is shown in Fig. 1.

2. Isotopic composition database SFCOMPO

The spent fuel assay data from 13 LWRs(7 PWRs and 6 BWRs) had been already reviewed and published[1]. Such data collection woks have been continued. To supply worldwide users with these assay data, isotopic composition database system:SFCOMPO[2] was developed and constructed on an IBM PC/AT. As a result of data selection with a consideration of data quality, the isotopic composition data from 10 LWRs and the axial gamma activity profile data from a PWR and a BWR in Japan are stored in SFCOMPO at present. These lists are shown in Table 1 and Table 2.

SFCOMPO has functions of data storage, data revision, data search and table output, has not a function of graphical output. But, it can prepare the input for external graphic soft. The figures 2 and 3

show total-Pu/total-U of collected data and axial gamma (Cs-137) activity profile data, they were obtained using a Kaleida Graph Soft and the prepared input for it by SFCOMPO.

3. Group constant libraries for ORIGEN-II from JENDL3.2

One group constant libraries for ORIGEN-II were generated using SWAT[3] code from the latest Japan Nuclear Data File : JENDL3.2. A flow chart of generation of one group constant library is shown in Fig. 4. The libraries for typical PWR fuel and BWR fuels(with 0%, 40%,70% coolant void) were prepared using these procedures. At that time, one pin model with keeping the fuel pitch and H/U of the objective fuel assembly was used for generations of these group constant libraries. The OIGEN-II burnup calculations of 17 x 17 BWR Step II fuel were performed using these new libraries and the original one. The calculated results on the burnup dependent Pu-239 density of the fuel are shown in Fig. 5. The result with the new library for BWR 40% void is almost same as one with the original library: BWRUS.

4. Conclusions

The calculated results:total-Pu/total-U using the original library and new ones were compared with the collected assay data. Those are shown in Fig. 6. Most measured data are located in the area between the calculated line of BWR 40% void and the 70% void. It shows that these new libraries give reasonable results. On the other side, we are going to collect assay data on isotopic composition in MOX spent fuels, high burnup UO2 spent fuels. These future works are described in Table 3. By using these collected assay data, the verifications of burnup calculation codes will be performed successfully.

References
[1] Naito Y., Kurosawa M., Kaneko T.: " Data Book of Isotopic Composition of Spent Fuel in Light Water Reactors", JAERI-M 94-034(1994).
[2] Kurosawa M., Naito Y., Sakamoto H., Kaneko T.: " The Isotopic Composition Database System on Spent Fuels in Light Water Reactors(SFCOMPO)", JAERI Data/Code 96-036(1997).
[3] Suyama K., Iwasaki T., Hirakawa N.: "Improvement of Burnup Code System SWAT for Use in Burnup Credit Problem", Proc. Int. Conf. on the Physics of Reactors, September 16-20, 1996, Mito, Japan, p. L-53(1996).

Table 1 Isotopic Composion Data Contents in SFCOMPO

No	Reactor Name	Reac Type	Power	Rod Array	Enrichment(w/o)
1	Trino Vercellese	PWR	825 MWth	15 x 15	2.7/3.1/3.9
2	Obligheim	PWR	908	14 x 14	2.5/2.8/3.1
3	Mihama-3	PWR	2440	15 x 15	3.24 w/o
4	Genkai-1	PWR	1650	14 x 14	3.42
5	Robinson-2	PWR	2200	15 x 15	1.9/2.6/3.1
6	Gundremmingen	BWR	(250MWe)	6 x 6	1.87/2.53
7	Monticello	BWR	(536MWe)	8 x 8	1.5/1.9/2.1/2.9
8	Calvert Cliffs-1	PWR	(825MWe)	14 x 14	3.04
9	Cooper	BWR	(825MWe)	7 x 7	1.3/1.7/1.9/2.9
10	Fukushima-No1-3	BWR	(784MWe)	8 x 8	1.5/1.9/2.2/3.0

Table 2 Axial Burnup Profile Data Contents in SFCOMPO

No.	Reactor Name	Assembly Name	Rod Pos.	Gamma-ray Data
1	Genkai-1 (PWR)	C33	E11	Cs-134,137,Eu-154,Total
			N1	Cs-137, Total
			N10	Cs-137, Total
2	Tsuruga-1 (BWR)	JAB-73	A1	Cs-134,137,Eu-154
			C3	C3-134137,EU-154

Table 3 Future Works on Collection of Assay Data

1. ARIAN Program:

MOX,high burnup UO_2 spent fuels assay

1) Peak burnup:50 GWd/t(MOX and UO_2)
2) Assay data: Nd, Pu, U, Am, Cm, Np,Cs,I
3) Report publication:1998
   (This program will be completed in 1996)

2. PIE program on MOX,UO_2 fuels

conducted by CRIEPI

1) Rod average burnup:45 GWd/t(MOX)
   60 GWd/t(UO_2) and lower B.U.
2) Assay data: Nd, Pu, U, Am, Cm, Np, FPs
3) Report publication: Jan.,1996 and 1997 or 1998.

3. PIE program on high burnup UO_2 fuels by JAERI

1) Assembly average burnup: 40-50 GWd/t(UO_2)
2) Assay data: Nd, Pu, U, Am, Cm, Np, FPs
3) Report publication: at the end of every fiscal year.
   (It is supported by STA at present that this program will
   be continued from 1994 until 1998)

4. Other data in Japan(NUPEC, etc,)

1) PIE of Phase III fuel.

Neutron Cross Section Libraries
JENDL3.2, ENDF/B

Nuclear Stucture Data
ENSDF

Mult-Group Constant
MGCL

Decay Data Liblary
JDDL

ORIGEN-II
Library

Cell Burnup Calculation

Burnup Dependent One Group Constant Libraries

Point Burnup Code
COMRAD , ORIGEN-II

Isotopic Composition in Spent Fuels ; Calc.

Exposure of Test Fuels

Comporison of Isotopic Compositions obtained by Calc. and Measurement

Isotopic Composition Database System
SFCOMPO

Isotopic Composition in Spent Fuels ; Meas.

Nuclear Fuel Management Data

Post Irradiation Test

Fig.1 Flow Diagram for Verification of Burnup Codes

total-Pu / total-U

burnup (GWd/t)

Legend:
- ○ Obrigheim 3.0wt% (PWR)
- □ Obrigheim 2.83wt% (PWR)
- ● Gundremmingen 2.53wt% BOT(BWR)
- ■ Gundremmingen 2.53wt% TOP(BWR)
- ◇ Mihama-3 3.24wt% (PWR)
- × Genkai-1 3.42wt% (PWR)
- + H.B.Robinson-2 2.55wt% (PWR)
- ▲ Cooper 2.939wt% (BWR)
- ⊞ Calvert Cliffs-1 3.04wt% (PWR)
- ⊙ Calvert Cliffs-1 2.72wt% (PWR)
- ⊠ Calvert Cliffs-1 2.45wt% (PWR)
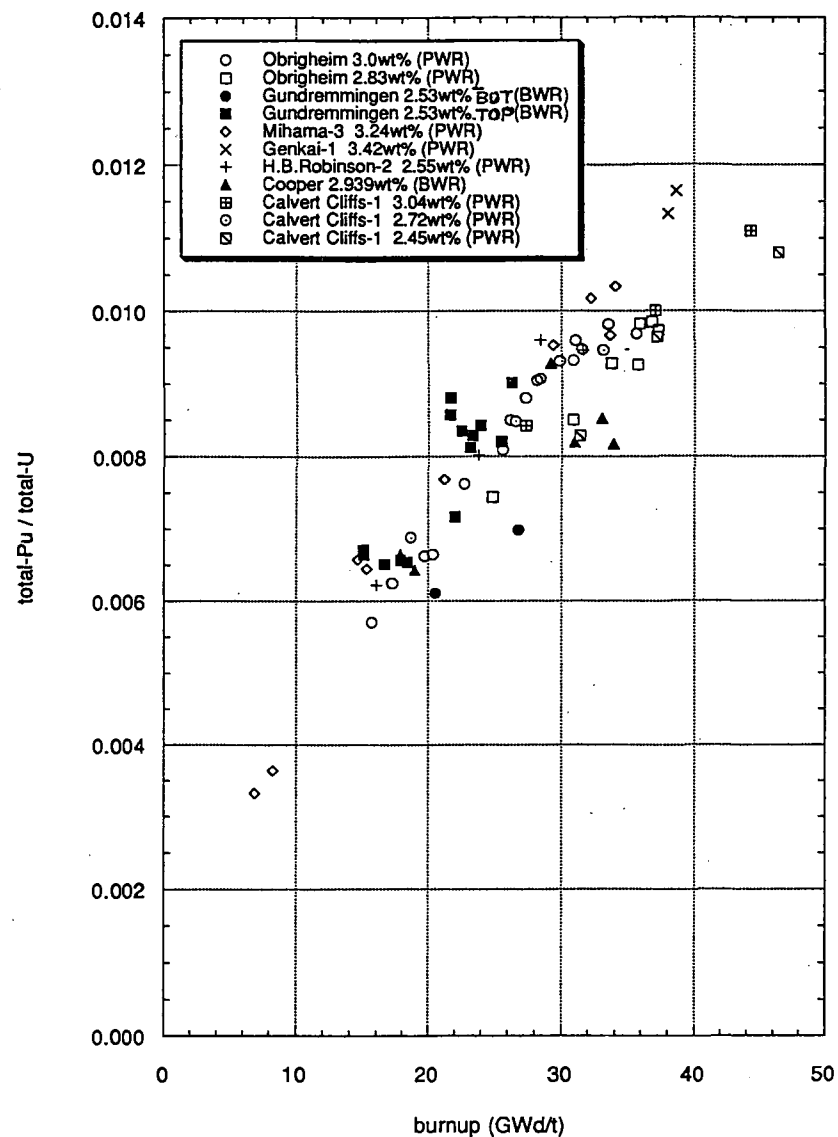
Fig. 2 Isotopic composition data in SFCOMPO
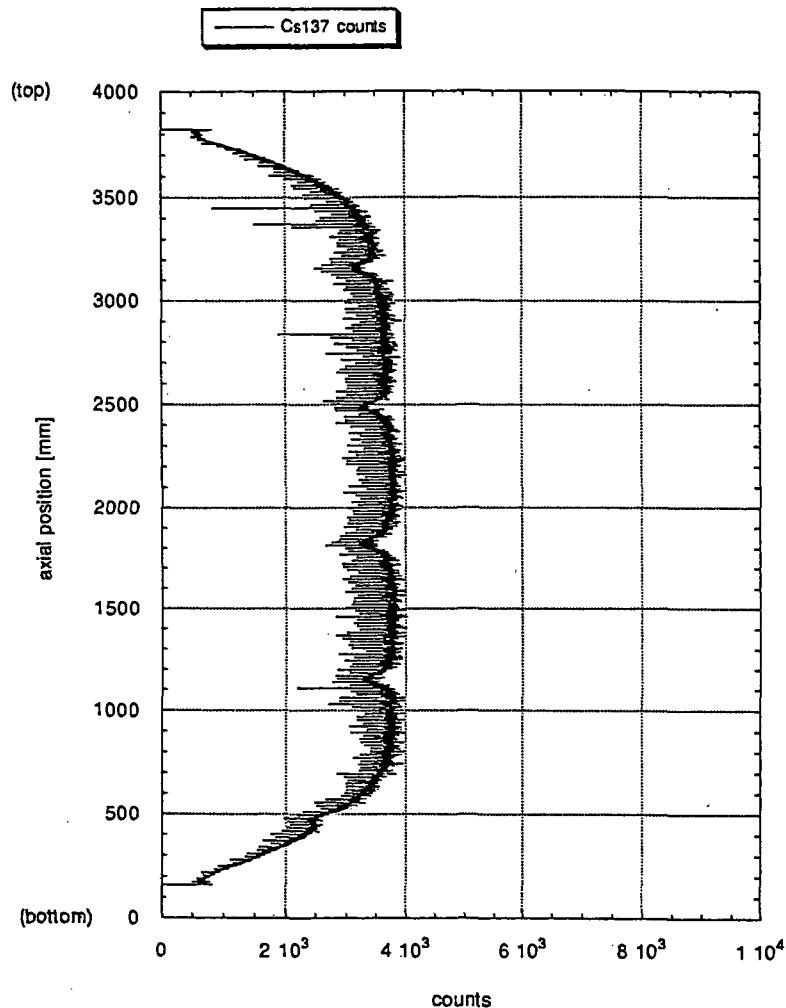
Fig. 3 Axial gamma activity profile data in SFCOMPO
(Cs-137 in the spent fuel rod of Genkai-1)
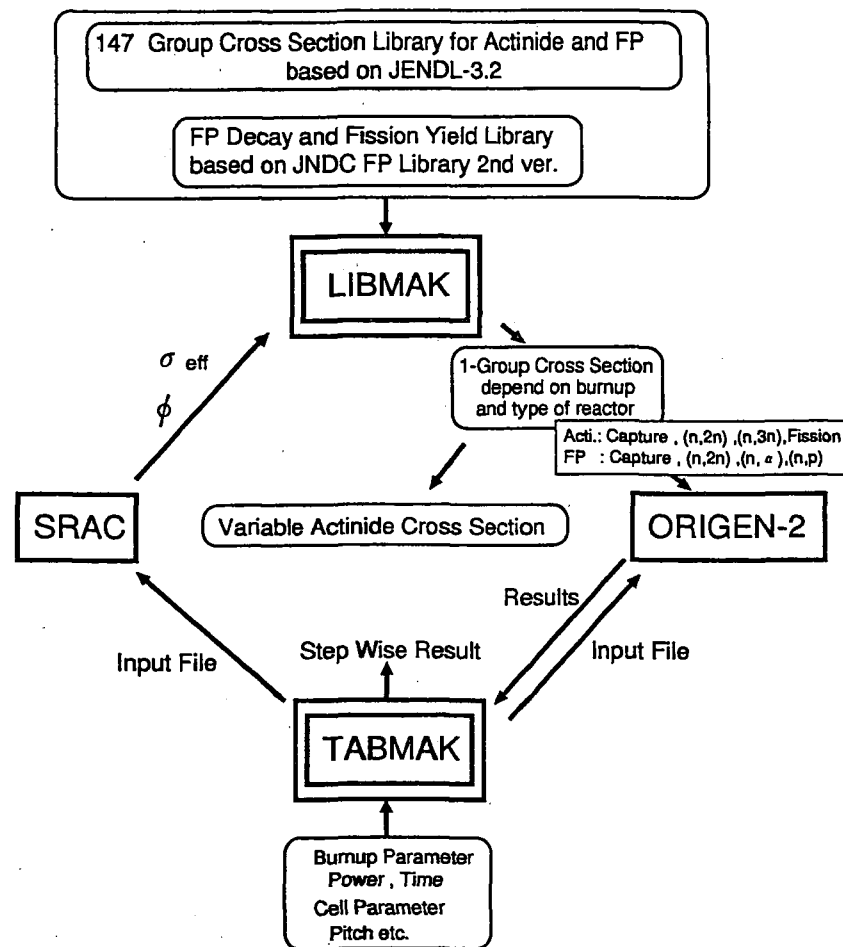
Fig.4 Generation of 1 group constant libraries
for ORIGEN-II from JENDL 3.2
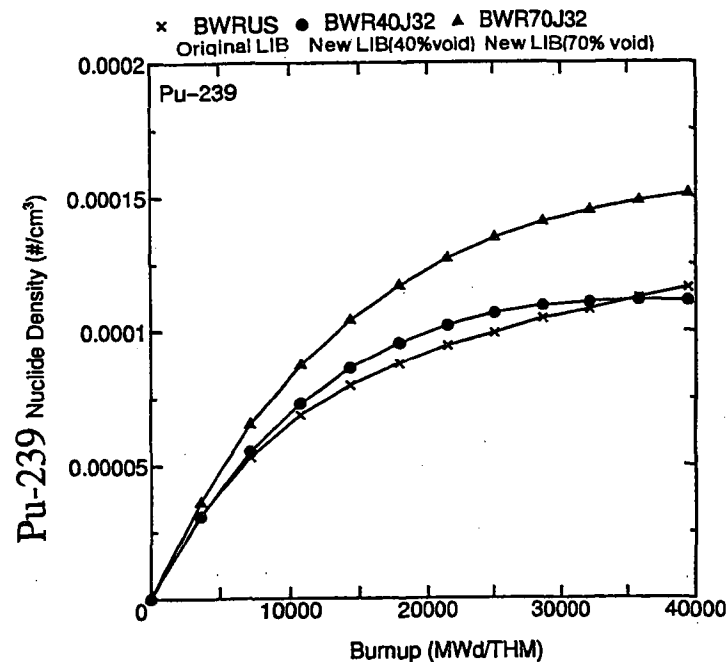
Fig. 5 Burnup dependent Pu-239 by
ORIGEN-II(17 x 17 BWR fuel : step II)
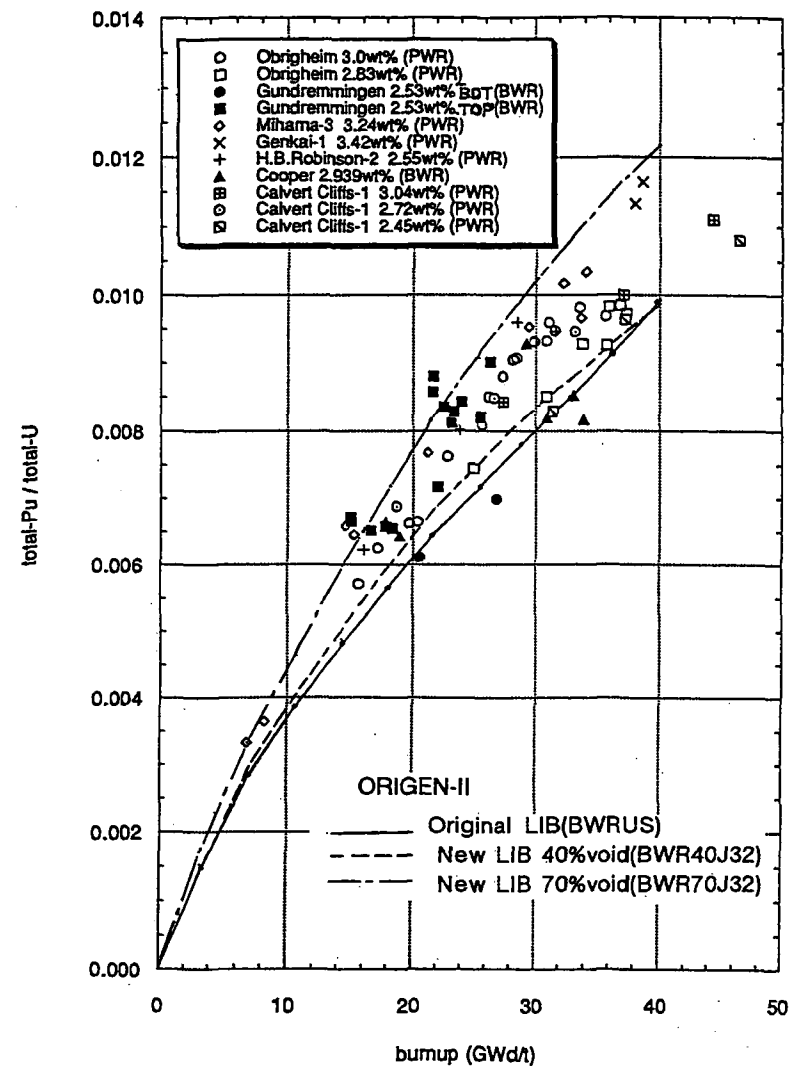
Fig. 6 Comparison of measured and calculated

2.1.2 Integral Test of JENDL Fusion File

Fujio MAEKAWA

Fusion Neutronics Laboratory, Japan Atomic Energy Research Institute

Tokai-mura, Naka-gun, Ibaraki-ken 319-11

e-mail: fujio@fnshp.tokai.jaeri.go.jp

Integral test of JENDL Fusion File (J-FF) is performed through analyses of available benchmark experiments. As a result, good agreement between the calculated results with J-FF and the measured data is observed as a whole. Thus, J-FF is qualified to be used for nuclear design of fusion reactors. Owing to the high quality evaluation of J-FF, cross section data in J-FF for many nuclides are recommended to be assigned as data in FENDL/E-2.0 in the IAEA Consultants' Meeting held at Karlsruhe, Germany, 24-28 June, 1996.

1. Introduction

JENDL Fusion File [1] (J-FF) is one of the JENDL special purpose files, to be used for fusion applications. The most remarkable feature of J-FF is the representation of secondary neutrons in the double-differential cross section (DDX) form in the ENDF-6 format needed to treat precisely the correlated energy-angle distributions of secondary neutrons produced by 14-MeV neutrons, in stead of the energy- and angle-differential cross sections (EDX and ADX, respectively). Cross section data in J-FF for most of nuclides are identical to those in JENDL-3.2 [2] (J-3.2) except for the representation of secondary neutrons. Newly evaluated data for beryllium and modified data for several nuclides are included in addition. To validate cross section data in J-FF, integral tests were performed with available benchmark experiments.

J-FF along with ENDF/B-VI, BROND-2, EFF-3 and CENDL-2 is one of the candidate evaluations for FENDL/E-2.0, the Fusion Evaluated Nuclear Data Library version 2 [3], to be released from IAEA/NDS in 1997. The integral tests also contributed to give a guide for the selection of cross section data for FENDL/E-2.0.

2. Benchmark Experiment and Transport Calculation

Benchmark experiments [4-8] served for the integral test, listed in Table 1, include both basic and engineering benchmark experiments carried out at the two D-T neutron source facilities, FNS/JAERI and OKTAVIAN/Osaka University. Material compositions and geometrical configurations for the

three basic benchmark experiments were simple to make sure of testing of the cross section data. Integral tests for these basic benchmark experiments were performed by the Fusion Neutronics Integral Test Working Group of the Japanese Nuclear Data Committee. On the other hand, integral tests for the engineering benchmark experiment were performed under the Engineering Design Activities of International Thermonuclear Experimental Reactor (ITER). The practical shielding configuration of ITER was simulated with the experimental assemblies, i.e., layered shield made of type 316 stainless steel (SS316) and water, and simulated superconducting magnet (SCM) behind the shield. The experiment was in a sense a mock-up experiment of ITER.

The continuous energy Monte Carlo transport calculation code MCNP-4A [9] was used for through the integral tests. The cross section library for MCNP, FSXLIB-JFF [10], was prepared from J-FF. Results for the calculations were compared to the experimental data for neutron spectrum, dosimetry reaction rate, gamma-ray spectrum and gamma-ray heating rate.

3. Results of Basic Benchmark Experiment

Figure 1 shows neutron spectra leaking from the beryllium slab for the FNS/TOF experiment. The spectrum calculated with J-3.2 is larger than measured one around 0.5~2 MeV, while very good agreement with the experiment is found for the spectrum calculated with J-FF due to the reevaluation of the energy-angle distribution of secondary neutrons.

Measured and calculated neutron spectra leaking from the spherical titanium pile are shown in Fig. 2. Although neutron cross section data for titanium in J-FF and J-3.2 are completely the same, the expression of secondary neutrons is different: DDX and EDX+ADX forms, respectively. No remarkable difference is, however, observed between the calculated spectra with J-FF and J-3.2, as shown in Fig. 2. This is a general trend in most of comparisons between J-FF and J-3.2, and indicates that the DDX format does not give large impact on the results for integral experiments, although J-FF reproduces the measured DDX better than J-3.2.

Calculated to experimental (C/E) ratios corresponding to neutron fluxes in the energy ranges of 10-100 keV and 0.1-1 keV for the FNS iron benchmark experiment are shown in Fig. 3. In this case, from the comparisons between J-FF and J-3.2, improvements of C/E ratios are found in both the low energy neutron fluxes. This improvement is simply due to the expression of secondary neutrons in the different formats.

It was reported that most of secondary gamma-ray data in J-3.2 are valid through the analysis of the OKTAVIAN experiment [11]. Too large gamma-ray production cross section, however, was pointed out from the FNS iron benchmark experiment, as shown in Fig. 4. On the other hand, results by J-FF agree within 20 % with the experiment because the gamma-ray production cross sections in J-3.2 for threshold reactions are modified in J-FF to be consistent in terms of the energy balance.

As a result for the basic benchmark experiments, it is found that most of problems which were pointed out for JENDL-3.1 and -3.2 are solved in J-FF, and results of J-FF are in good agreement

with the experimental data, as a whole.

4. Results of Engineering Benchmark Experiment

Figure 5 shows neutron spectra in the SS316/water shield assembly. The calculated neutron spectrum with J-FF is in good agreement with the measured one from 14-MeV to the thermal energy. Reaction rate distributions for threshold reactions (^{93}Nb(n,2n)^{92m}Nb and ^{115}In(n,n')^{115m}In), ^{235}U fission and gamma-ray heating in the SS316/water/SCM assembly in comparisons with calculated ones by JENDL-FF are shown in Fig. 6. This figure indicates that the adequacy of J-FF for the various quantities is considerably excellent because the calculation with J-FF predicts the experimental results with uncertainties of 20 % although neutron and gamma-ray fluxes attenuate 4~6 orders of magnitude behind the thick shield of ~ 1 m. Consequently, J-FF is qualified to be used for such shielding designs of fusion reactors.

5. FENDL/E-2.0 Selection

The IAEA Consultants' Meeting on Selection of Basic Evaluations for the FENDL-2 Library was held at Karlsruhe, Germany, 24-28 June, 1996. The consultants recommended best evaluations to be assigned for FENDL/E-2.0, as listed in Table 2. Many cross section data in FENDL/E-1.0 are replaced by J-FF, resulting in major contribution of J-FF for FENDL/E-2.0. This fact suggests that the superiority of J-FF is approved in the world.

Acknowledgments

Reference
[1]   Chiba S., Fukahori T., Yu B. and Kosako K.: JAERI-Conf 96-005, pp. 45-54 (1996).

[2]   Nakagawa T., et al.: J. Nucl. Sci. Technol., 32, pp. 1259-1271 (1995).

[3]   Ganesan S. and McLaughin P. K.: IAEA-NDS-128, (1995).

[4]   Oyama Y. and Maekawa H.: JAERI-M 94-014, pp. 126-216 (1994).

[5]   Maekawa H., et al.: JAERI-M 94-014, pp. 217-301 (1994).

[6]   Ichihara C., et al.: JAERI-M 94-014, pp. 63-125 (1994).

[7]   Yamamoto J., et al.: JAERI-M 94-014, pp. 32-62 (1994).

[8]   Konno C., Maekawa F., et al.: JAERI-Research 94-043, 94-044 (1994), 95-017, 95-018 (1995).

[9]   Briesmeister J. F. (Ed.): LA-12625 (1993).

[10]   Kosako K.: JAERI-Conf 96-005, pp. 55-62 (1996).

[11]   Maekawa F.: Nucl. Sci. Eng., 123, 272 (1996).

Table 1. Benchmark experiments used for the integral test.

Basic Benchmark Experiment	Material	Measured Quantities
FNS time-of-flight experiment [4]	Li2O, Be, C, N, O, Fe, Pb	n-spec (> 50keV)
FNS clean benchmark experiment [5]	Li2O, Be, C, Fe, Cu, W	n-spec (1eV~14MeV) RR, γ-spec, γ-heat
OKTAVIAN pulsed sphere experiment [6,7]	Be, LiF, CF2, Al, Si, Ti, Cr, Mn, Fe, Co, Ni, Cu, As, Se, Zr, Nb, Mo, W, Pb	n-spec (> 0.1 MeV)
Engineering Benchmark Experiment	Material	Measured Quantities
FNS bulk shielding experiment [8]	SS316, SS316/water, SS316/water/SCM	n-spec (1eV~14MeV) RR, γ-spec, γ-heat

Table 2. Selected evaluated nuclear data libraries for FENDL/E-1.0 and -2.0.

Nuclide	FENDL/E-1.0	FENDL/E-2.0	Nuclide	FENDL/E-1.0	FENDL/E-2.0
1-H -1	ENDF-VI	ENDF-VI	25-Mn-55	ENDF-VI	ENDF-VI
1-H -2	ENDF-VI	JENDL-FF+BROND-2	26-Fe-54	ENDF-VI.1	ENDF-VI.1
1-H -3	ENDF-VI	ENDF-VI	26-Fe-56	ENDF-VI.1	EFF-3/ENDF-VI.1
2-He-3	ENDF-VI.1	ENDF-VI.1	26-Fe-57	ENDF-VI.1	ENDF-VI.1
2-He-4	ENDF-VI	ENDF-VI	26-Fe-58	ENDF-VI.1	ENDF-VI.1
3-Li-6	ENDF-VI.1	ENDF-VI.1	27-Co-59	ENDF-VI.2	ENDF-VI.2
3-Li-7	ENDF-VI	ENDF-VI	28-Ni-58	ENDF-VI.1	ENDF-VI.1
4-Be-9	ENDF-VI	JENDL-FF	28-Ni-60	ENDF-VI.1	ENDF-VI.1
5-B -10	ENDF-VI.1	ENDF-VI.1	28-Ni-61	ENDF-VI.1	ENDF-VI.1
5-B -11	ENDF-VI.1	ENDF-VI.1	28-Ni-62	ENDF-VI.1	ENDF-VI.1
6-C -12	ENDF-VI.1	JENDL-FF+ENDF-VI.1	28-Ni-64	ENDF-VI.1	ENDF-VI.1
7-N -14	BROND-2	JENDL-FF+BROND-2	29-Cu-63	ENDF-VI.2	ENDF-VI.2
7-N -15	BROND-2	BROND-2	29-Cu-65	ENDF-VI.2	ENDF-VI.2
8-O -16	ENDF-VI	JENDL-FF	31-Ga-nat	-----	JENDL-3.2
9-F -19	ENDF-VI	ENDF-VI	40-Zr-nat	BROND-2	JENDL-FF
11-Na-23	JENDL-3.1	JENDL-3.1	41-Nb-93	BROND-2	JENDL-FF
12-Mg-nat	JENDL-3.1	JENDL-3.1	42-Mo-nat	JENDL-3.1	JENDL-FF
13-Al-27	JENDL-3.1	EFF-3/JENDL-FF	50-Sn-nat	BROND-2	BROND-2
14-Si-nat	BROND-2	ENDF-VI/JENDL-FF	56-Ba-138	ENDF-VI	ENDF-VI
15-P -31	ENDF-VI	ENDF-VI	73-Ta-181	JENDL-3.1	JENDL-3.1
16-S -nat	ENDF-VI	ENDF-VI	74-W -182	ENDF-VI	JENDL-FF
17-Cl-nat	ENDF-VI	ENDF-VI	74-W -183	ENDF-VI	JENDL-FF
19-K -nat	ENDF-VI	ENDF-VI	74-W -184	ENDF-VI	JENDL-FF
20-Ca-nat	JENDL-3.1	JENDL-3.1	74-W -186	ENDF-VI	JENDL-FF
22-Ti-nat	JENDL-3.1	JENDL-3.1	82-Pb-204	ENDF-VI.1	ENDF-VI.1
23-V -51	ENDF-VI	JENDL-FF	82-Pb-206	ENDF-VI	ENDF-VI
24-Cr-50	ENDF-VI	ENDF-VI	82-Pb-207	ENDF-VI.1	ENDF-VI.1
24-Cr-52	ENDF-VI	ENDF-VI	82-Pb-208	ENDF-VI	ENDF-VI
24-Cr-53	ENDF-VI	ENDF-VI	83-Bi-209	JENDL-3.1	JENDL-3.1
24-Cr-54	ENDF-VI	ENDF-VI			

+: Data in both evaluations are merged.

/: One of them is selected after benchmark testing.
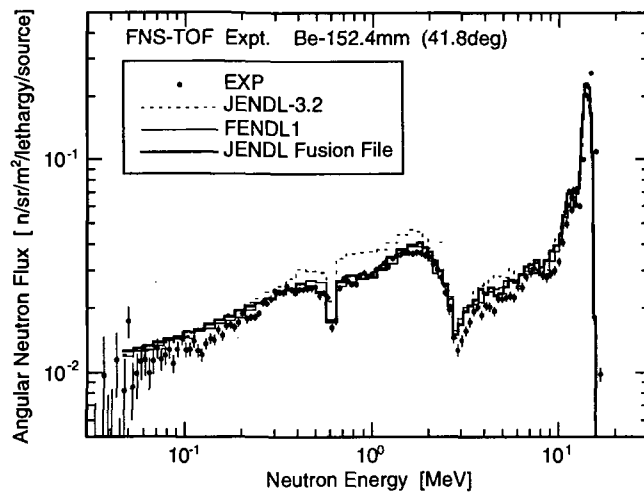
Fig. 1   Neutron energy spectra leaking from the beryllium slab assembly measured at FNS in comparisons
with calculated ones by JENDL-FF, -3.2 and FENDL-1.
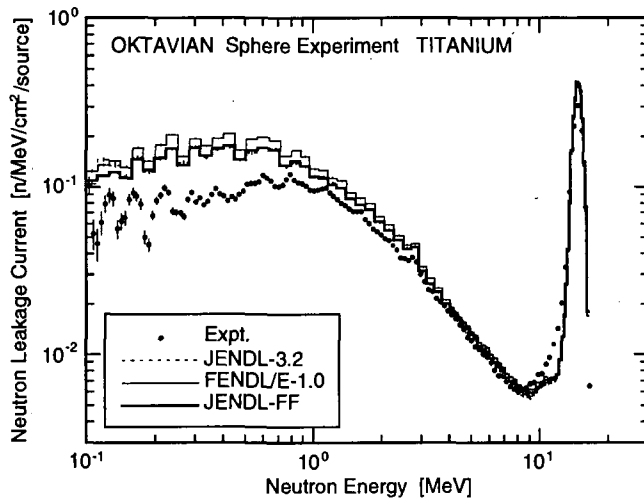
Fig. 2   Neutron energy spectra leaking from the titanium spherical pile measured at OKTAVIAN in
comparisons with calculated ones by JENDL-FF, -3.2 and FENDL-1.
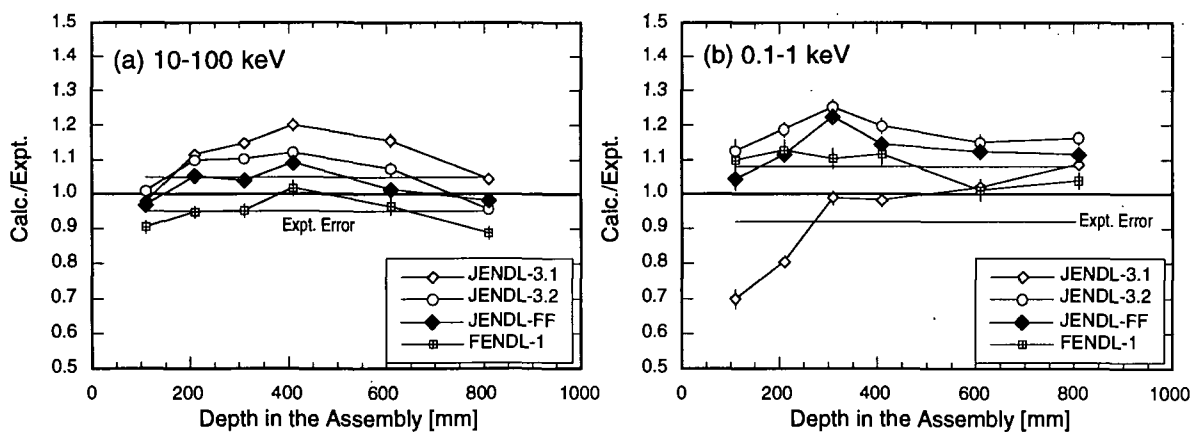
Fig. 3   Calculated to experimental ratios of integral fluxes for energy regions of (a) 10-100 keV and (b)
0.1-1 keV for the FNS iron benchmark experiment.
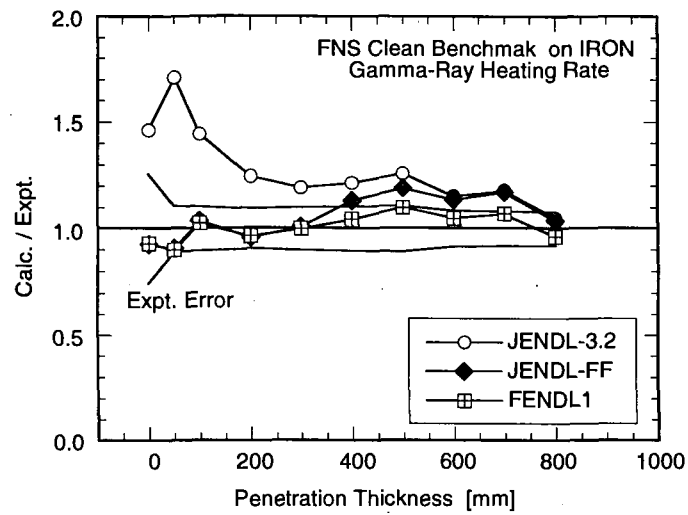
Fig. 4　Calculated to experimental ratios of gamma-ray heating rates for the FNS iron benchmark experiment.
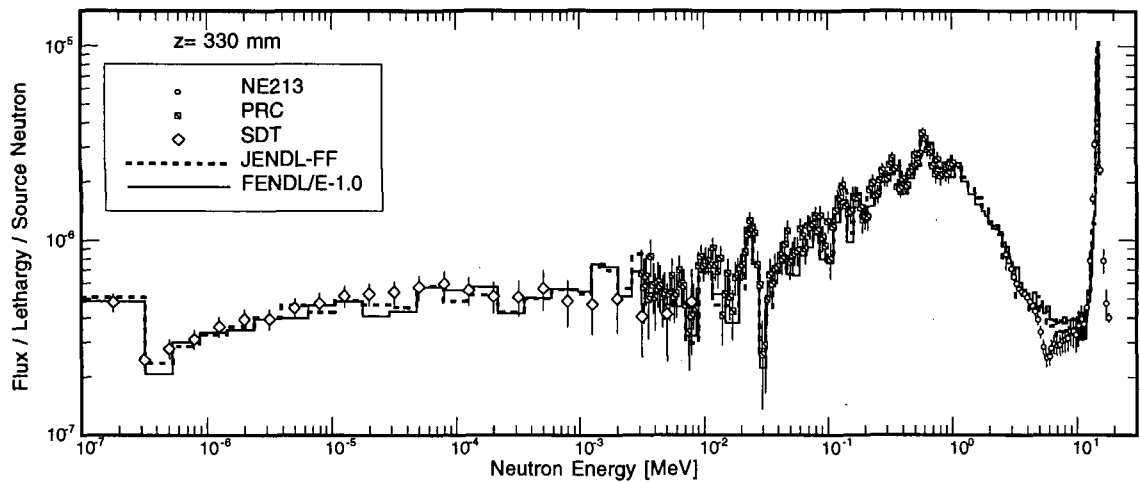
Fig. 5　Neutron energy spectra in the SS316/water shield assembly measured at FNS in comparisons with calculated ones by JENDL-FF and FENDL-1.
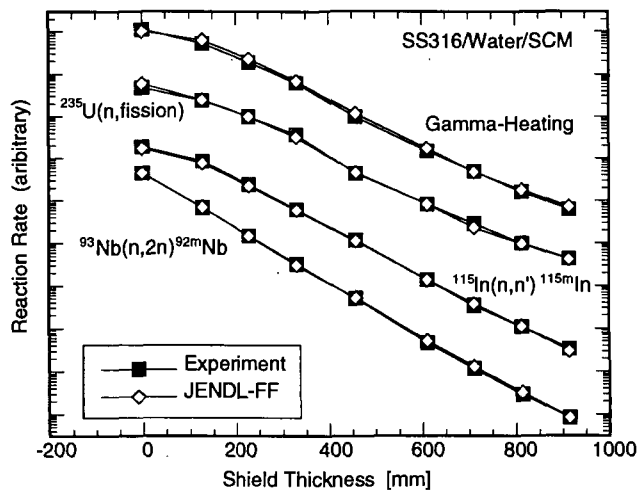
Fig. 6　Reaction rate distributions in the SS316/water/SCM assembly measured at FNS in comparisons with calculated ones by JENDL-FF.

2.1.3 *Toward JENDL-3.3: Comments on the Problems of JENDL-3.2 for the next version developments*

A. Hasegawa

Nuclear Data Center

Japan Atomic Energy Research Institute

Tokai-mura Ibaraki-ken, 319-11, Japan

Abstract

Revision work for JENDL-3.2 is foreseen and the discussions about the problems of JENDL-3.2 is under going in a small advisory group of JNDC (Japanese Nuclear Data Committee) since this April. In this article main discussion points in that group are presented. Problems from evaluators' point of view, problem from users' point of view and request from anticipated users are summarized. Some discussions on U-235 cross sections in the thermal and epi-thermal energy range are made in relation of the new evaluation of resolved resonance parameters performed by Leal/Derrien.

1. Introduction

Already more than two years have past since the latest version of JENDL-3.2[1] was released. This file aims general use in the applications of the atomic power fields such as fission reactors, fusion reactors, shielding, fuel processing plants and so on. We think that much feed back information to this file has been piled up as various users' experiences. Now JAERI NDC(Nuclear Data Center) has a plan to revise the current version to update to JENDL-3.3, a consolidated new version, including covariance data for important nuclides in the fast reactor applications. Covariance data preparation is one of the main items in the new version of JENDL-3.3. This is a reflection of a requests from urgent and strong needs by the fast reactor development groups in Japan. At the same time, a thorough re-evaluation work is also foreseen for the problems raised from users.

A small advisory group for discussing the problems of JENDL-3.2 evaluations [+] was set up last April. Up to now several meetings have been held and a number of problems were raised and discussed. In Chapter2, we summarize main discussion

---

[+] Members are following: M.Ishikawa(PNC), H.Matsunobu(DEI), M.Kawai(Toshiba), N.Yamano(SAEI), Y.Nakajima(RIST), H.Takano, F.Maekawa, K.Shibata and A.Hasegawa(JAERI)

points raised from evaluators and/or application users as well as requests by big potential users for the next version of JENDL.

In this article, a special emphasis is placed on the U-235 data for the fission reactor applications, especially for Light Water Reactors. There are two main reasons. One is that the change from JENDL-3.1[2] to 3.2 causes overestimation about 1% on the Keff values for light water reactor. This tendency is also found in the analyses of the experimental reactors JRR-3 and JRR-4 in JAERI and also in the analysis of STACY experiments in the criticality safety. The other is that a newest evaluation by Leal/Derrien[3] for the resolved resonance parameters in the energy range from 0 to 2250eV was released recently and much attentions are drawn to this data due to their data freshness and detailed error analyses. This data should be one of the candidates to the next version of JENDL. But the new data has fairly drastic differences in the capture cross sections, which is one of the key reactions influencing to the criticality of reactors. Some discussions are made in chapter 3.

2. Problems of JENDL-3.2

Main discussion points are summarized here in the following 3 items, evaluators' points of view, users' point of view, requests from big potential users.

2.1 Evaluators' points of view

2.1.1 Notified problems to Nuclear Data Center as of Nov. 1996.

- N-14(n,p) : too small cross-section values.

- O-16(n,2n) : 10 times larger values are given due to some compilation errors.

- Fe-natural(total/elastic/inelastic) cross-sections in the energy range 800keV to several MeV from the benchmark tests for ASPIS, FNS transmission experiments.

- W: energy balance of gamma-ray production cross sections is inconsistent.

- Ta-181(n, alpha): relatively large values (several hundreds mb) are given in the low energy range (several tens of keV).

- U-235(n, gamma): possibility of smaller values in the resonance energy range.

- Pu-236(n,f): too small value for less than 1MeV cross-sections compared with the measurements.

- Energy spectrum in the continuum energy range for heavy nuclides: Especially energy spectrum for U-233, U-236 is largely different from the evaluation by Maslov et.al. Other nuclides should be checked also.

2.1.2 JENDL-3.2 FP data

(1) Thermal cross-section and Resonance Integral

Reflection of latest measurements by PNC group are partly made but not yet included for Tc-99, I-129, Cs-135. These data will be included soon.

(2) Resonance parameters

We think that JENDL-3.2 FP data is the latest evaluations for this item in the world. But for some nuclides like Ru-99, potential compilation errors due to so many data manipulation paths in the compilation step has resulted in the wrong assignment of spin and parity values. For such nuclides, revision work will be made in the next version.

(3) capture cross-sections

For sample worth of FP, some nuclides show inconsistencies against the integral values measured by ECN Petten. But we cannot put full responsibility on the cross-sections itself, because inadequacy of the integral measurements are also conceivable. For these nuclides, we must gather other back up data to judge the validity of cross-sections to make final decisions whether to re-evaluate or not. Some limited number of nuclides such as Eu-152 and 154, cross-sections are determined only by the data adjustments at JENDL-2 evaluations because no differential data are available. These nuclides have potential problems in the model parameters because the parameters of these nuclides might be inconsistent with the value used in the evaluations mostly adopted in JENDL-3.2.

(4) Inelastic scattering cross-sections

Secondary energy distributions assigned at the threshold energy in JENDL-3.2 for the continuum reactions (i.e., continuum inelastic, (n,alpha), (n,p), etc.) shows unphysical shape. This is a long history. Some computer code like MCNP stop whenever it detect these data because up-scattering process is just generated but physically it is completely forbidden. The users of such code are always burdened with this problems because whenever up-scattering process is detected the code would not go further. At the first stage in the JENDL-3 evaluations, delta function is always assigned at the threshold energy. But these presentation gives strange (unphysical) shape of flux if the data are used in the transport calculations of neutrons due to the interpolation of energy distributions between threshold energy point and the next energy point. So the energy distribution of the next energy points to the threshold is re-assigned at the threshold,i.e., the same energy distributions, regardless it's unphysical assignments.

To fix the problem, following three actions are anticipated,

a. Logics in MCNP should be changed.

For the moments, it is affordable. But it is very difficult to take effect for all users of MCNP.

b. Library of MCNP should be changed.

This take effects only for updated library supplied from us and not to the other libraries processed by themselves.

c. JENDL-3 original data should be change.

This is the right way but we think it takes huge time and man powers.

Nuclides having very small number of levels (especially less than 12 levels) among which total of 100 nuclides succeeding the original evaluation of JENDL-2 have some potential problems, because these data are taken from rather old level schemes and capture cross-sections might be rather large.

(5) Benchmark test for the post irradiated analysis

Through the burn-up calculation made for PWR, prediction for the production of Eu-154 is well reproduced by JENDL-3.2 compared with ENDF/B-IV data. But experimental data for post irradiated analysis are very scarce up to now, therefore we must make much efforts to obtain measured data under the good irradiation conditions. Even if we get post irradiated data from power reactors, usually irradiation history is not known completely to perform the detailed calculation for the depletion. Therefore we cannot state meaningful conclusions for the nuclear data by these power reactor's irradiated data. Recently we have some possibility to get these data through JRR-3 clean irradiation.

2.2 Users' point of view

2.2.1   Fission Reactors

For LWR (Light Water Reactor), comments are given by following three main users,

> (i)   Reactor Integral Test Working Group of JNDC,
>
> (ii)   Research Reactor Design Group of JAERI,
>
> (iii)   NUCEF group of JAERI.

For FBR (Fast Breeder Reactor), comments are given by following three groups,

> (i)   Reactor Integral Test Working Group of JNDC,
>
>   :International benchmark cores, small core benchmarks.
>
> (ii)   PNC FBR design group,
>
>   :from JUPITER analysis using JENDL-3.2   and ENDF/B-VI library for criticality, reaction rate ratio, space dependence of rod-worth , Na-void worth.
>
> (iii)   FCA experimental group,

from the experimental analysis for enriched U cores, metallic Pu fueled cores and Doppler worth.

(1) For major actinides, following items are pointed out:
● Secondary neutron distributions of heavy nuclides

Unphysical data are given for some heavy nuclides mainly calculated by PEGASUS code such as U-233, U-235 as shown in Fig.1[4]. Fixing this problem a consistent evaluation among all reaction channels should be requested.

● Capture cross-section in MeV range

Direct capture process is not included in JENDL-3.2 evaluation, therefore rather steep decreasing shapes are given as shown in Fig.2 . As the values of these cross section is very small, thus not significant effects are foreseen for reactor applications. But for other applications such as astrophysics, these values are very sensitive to the estimation of nuclear synthesis even if it is the order of milli-barn. We must give right values and true shape for the capture cross-sections in these energy range.

● U-238 inelastic cross-sections

Significant differences are found in Keff values between the results using JENDL-3.2 and ENDF/B-VI inelastic cross-section by the substitution method for FBR benchmarks. The differences come from the secondary energy distributions as well as the cross-section shape of total inelastic scattering.

● U-233 fission cross sections

There are about 2% differences found in Keff between JENDL-3.2 and ENDF/B-VI[5] evaluations for the analysis of small spherical cores of U-233 system of FBR. This differences are suspected to be in the differences of fission cross-sections.

● U-235 capture cross-sections

Latest evaluation by Leal/Derrien of U-235 data for resolved resonance region shows quite huge differences, i.e., 20 to 80% larger values are assigned in the energy range 200 eV to 2.2 keV compared with that of JENDL-3.2. Details are described in section 3. This data gives rather small contribution to the Keff of thermal reactor benchmarks but rather larger effects for FCA IX series assemblies.

The data differences between JENDL-3.2 and 3.1 gives 0.3 to 1.1% change in reactivity(the former shows more reactive) for thermal benchmarks. This differences in Keff comes from capture cross-sections in the thermal energy range. From these two reasons, we must re-evaluate this reaction data carefully for the

next revision of JENDL.

● U-235 ν structure

The data of JENDL-3.2 shows some clear structure in ν, none of the evaluations other than JENDL has such tendency. NEA NSC WG-18 (epi-thermal U-235 cross-sections) shows some interests for this matter.

● Other important reactions

Following reactions are listed up through the discussions mainly from FBR benchmarks and FBR sensitivity analyses,

Pu-239 fission, capture, fission-spectrum,

Pu-240 fission capture,

Pu-241 fission.

(2) structural materials or coolant materials

Following cross-sections are listed-up;

Fe inelastic,

Na elastic, inelastic cross-section, elastic

O elastic cross-section, elastic μ :

For FBR applications, the differences in the evaluations between JENDL-3.2 and ENDF/B-VI gives non-negligible contribution to the reactor parameters from the sensitivity analyses studies made by M.Ishikawa (PNC).

(3) Comments from FCA:

· From the analyses of FCA-IX series assemblies (7 cores: composed from C moderated and SUS moderated cores) for enriched U cores, criticality calculation by JENDL-3.2 shows over-estimation in Keff. If we replace U-235 JENDL-3.2 data with that of 3.1, Keff approaches to 1.0, this tendency is amplified with increase of C density.

· For metallic fuel (Pu) mock-up assemblies (FCA-XVI-1, XVI-2), criticality calculation by JENDL-3.2 shows under-estimation in Keff. Spectral indices by foil measurements are very well predicted by JENDL-3.2 i.e., all values are within the measurements accuracy(ex, C/E of F28/F49 using foil measurement is nearly 1.0. This value is improved considerably compared with C/E value for the measurements by fission counters, the latter is in the value of 1.05).

· For the Doppler reactivity worth, JENDL-3.2 predicts it very well for the cores ranging from experimental reactors to large FBRs including demonstration plants within the measurements errors.

(4) Comments from NUCEF

・Benchmark results from STACY shows that Keff by JENDL-3.2 over-estimates the experiments by 0.8% . This value seems rather large compared with the experimental accuracy, which is thought to be about 0.1% .Some questions about U-235 thermal data are raised.

・Calculation by JENDL-3.2 shows about 0.5-0.7% reactive results compared with JENDL-3.1. In the sensitive energy range for this calculation, differences in fission and capture cross-section are attributable. Considering the differences in the magnitude of these cross-sections, main contributor to this difference is fission reaction cross-section.

2.2.1 Shielding

For Iron data, problems still remained. Items to be re-evaluated for this nuclide are:

・Total and elastic cross-section shape adjustment for valley and peak values from 1 to 3 MeV

・Inelastic / elastic scattering cross-section sharing from 600keV to 1MeV.

To fix these values, high resolution experimental data are inevitable, Geel's new data will play a very important role.

From the analyses for the transmission spectrum experiments (Benchmarks from Broomstick, ASPIS, FNS) following remarks has been pointed out:

At the revision work from JENDL-3.1 to 3.2, significant improvements were obtained for the transmitted spectrum taking account the re-grouping of levels of inelastic scattering cross-sections of Fe. Number of levels used in the latest version is less than 40, i.e., we have still chance to include more levels to improve the data.

As to the evaluation policy, whether to take isotope evaluation or natural isotope evaluation is still unresolved problems. For the user's points of view, natural evaluation is more favorable. In the experiments, a number of natural-element data are obtained rather than the isotope data for structural materials or shielding materials. Further consistency should be maintained between these evaluations i.e., isotope evaluation and natural element evaluations. Keeping consistency is a big burden in the evaluation process.

2.2.3   Fusion Reactors

For this application, requests from users are fundamentally satisfied by the JENDL-Fusion File completed last year.   The main points of the evaluations are

placed for the good prediction for DDX data and gamma-ray spectra. For the General purpose file these results will be feedbacked. Still further problems are pointed out from experimental analyses for the applications in ITER.

● Common problems in the evaluation:

Increasing of data accuracy using individual isotope evaluations, not using natural element evaluations is requested. Because it aviods the ambiguity of threshold energy or insufficient number of levels to represent all of the inelastic levels. In some nuclides, energy balance of gamma-ray emission and particle emission are not represented properly.

● Individual problems:

Fe:

The prediction of heat production rate by gamma-ray is over-estimate for FNS experiments. This problem is solved in JENDL Fusion File. Reflection of iron data in the fusion file to the General Purpose File is requested.

Elastic scattering cross-sections around 14MeV seems rather small by the comparison of transmission experiments performed by FNS. Also reevaluation for total cross section around 5 keV is requested.

Ni:

Energy balance of capture gamma-ray has problems. (n,alpha) cross section has low energy components below threshold.

W:

Energy balance of gamma-ray is inconsistent.

Cu:

Resonance parameters either of Cu-63 or Cu-65 in the energy range of several hundreds keV has some problems from the analyses for neutron spectrum observed in the Cu block..

Neutron spectrum:

Leakage spectrum for F, Ti and Co, are not well predicted by the analyses of OKTAIAN experiments.

Secondary gamma-ray spectrum:

For Ti, Cr, Nb and W, secondary gamma-ray spectrum is not well predicted for the analyses of OKTAIAN experiments.

2.3 Requests from potential users

(1) Requests from ITER group.

Nearly all nuclides are already available in the JENDL-3.2 for the design purpose of

ITER. So no additional nuclides are requested to evaluate any more. But gamma-ray production data should be prepared for all of the nuclides necessary. In this sense, a number of nuclides are still necessary to be evaluated in the JENDL-3.2. This is because the heat production in the super conducting magnet is one of the key parameters in the design.

For the estimation of damage by the irradiation of 14MeV high energy neutron, KERMA/DPA data plays a very important role. To do the damage calculation, energy spectra of exit charged particle data are inevitable. These data has been evaluated in the JENDL Fusion file. Requesting data accuracy from the user side is about 5% for all of the data items to be considered, but this value seems very severe for the experimenters. For the designers, in some cases only 1cm differences in the shielding thickness might result in the cost up of 1 billion yen. Designers want reducing the cost ambiguity due to the cross section ambiguities.

3. U-235 data in thermal and epi-thermal energy region

U-235 epi-thermal cross-section is a hot topics in the OECD/NEA NSC(Nuclear Science Committee) WPEC SG-18 (Working Party of International Evaluation Cooperation Sub-Group-18). Recently Leal/Derrien's new evaluation data has been released. This data is believed as the last evaluation in this century for the resonance parameters of this nuclide. The data is given in ENDF6 FORMAT. The current data of ENDF/B-VI.2 is the evaluation made by Leal and de Saussure, but some problems has been pointed out. One of these problems is Resonance Integrals, the values for fission reaction seems good but that for capture too small(10-13%) (see Table 3.3).

The new data show η energy dependence ($\eta = \nu \sigma_f / \sigma_a$) for the energy range 0.02- 0.4 eV. This energy dependence was introduced from the evidence of experiments made by Geel and ILL. This energy dependence is suggested by reactor physics group for the inconsistency of temperature coefficient in thermal reactors.

The newly evaluated resolved resonance parameters are following:

energy range :	0 - 2250 eV
number of resonances:	3170 resonances
number of resonances in the boundstate:	14 resonances
number of resonances above 2.25keV:	14 pseudo resonances

A complete single set of resonance parameters are obtained by high resolution transmission data fitting for fission and capture reactions using SAMMY code. The code SUMMY is multilevel multi-channel R-matrix resonance analysis program based on the Bayes approach for Reich-Moore formalism with multiple scattering correction

for capture reactions.

Table 3.1   Fitting Data Sources

---

thermal(0.0253)	Wageman(Geel/1988)		0.001-0.4eV
< 1eV	total: transmission by Spencer(ORNL/1984)		0.01-1eV
<20eV	fission: Gwin(ORNL/1984) Schrack(RPI/1988)		0.01-20eV
	total: 3 transmissions by Harvey		0.4-2250eV
		high resolution data	
	fission:	Weston(ORNL/1984)	14-2250eV
		Weston(ORNL/1992)	100-2000eV
	capture: de Saussure(RPI/1967)		0.01-2250eV
		Perez(ORNL/1967)	0.01-200eV
	η :Wartena(Geel/1987)		0.0018-1.0eV
		Weigmann(ILL/1990)	0.0015-0.15

For this new evaluation several problems have been pointed out by Moxon and others. Used code is one of the problems. REFIT code fitting is recommended by him because Doppler broadening is calculated by more rigorous Einstein model. SUMMY code uses Gas model, i.e., less accurate model. In the course of fitting effective temperature of the sample should be carefully checked and assigned. From the fitted data observation several peaks in one resonance are seen, i.e., not completely separated for very narrow resonances in this fitting. The most important point among the problems is radiation widths, because it fluctuate too much compared with expected.

Table 3.2   Fluctuation of $< \Gamma_\gamma >$

Evaluation	$< \Gamma_\gamma >$	1 σ
ENDF/B-VI.2	34.9 meV	3.0meV
JENDL-3.2	34.9	3.0
Leal/Derrien	41.9	11.4

n.b.   1 σ : standard deviation

Here the value of Leal/Derrien's 11.4meV is nearly theoretical upper bound i.e., too high. Theoretically it is about 1meV. From Table 3.2,the value of fluctuation seems normal for the current evaluations of JENDL-3.2 and ENDF/B-VI .

If this new evaluation is true then we must check α value(ratio of capture to fission cross-sections) above 2250eV,because the same tendency might be appeared in this energy range.

The data validation by Benchmark test has been made by the members of NSC WPEC SG-18 in early 1996 using pre-released data for reviewing. Benchmark calculation was made mainly by two groups, US CSEWG group and JEF group of FRANCE. Former group calculates ORNL benchmarks(ORNL-1,2,3,4and10) which are unreflected sphere of U-235 uranyl nitrate and H_2O mixture. FRANCE CEA (JEF group) calculated LWR Lattices. And no significant impact to Thermal Lattices are found and 0.2-0.3% decreasing Keff tendency found. This tendency is nearly the same as our calculation performed by TAKANO et.al. (JAERI).

Table 3.3 Present Data Status for U-235

data source	I_γ	I_f	α	$<\Gamma_\gamma>$	
unit	b	b		meV	
Mughabghab	144±6	275±5	0.523±0.24		
ENDF/B-6.2	133.5	279.1	0.478	35.0	
JENDL-3.2	134	279	0.478	35.0	38.5
MOXON				~38.2	
Leal/Derrien	140	275	0.509	41.9	

n.b
· I_γ : capture Resonance Integral
· I_f : fission Resonance Integral
α : ratio of capture to fission
$<\Gamma_\gamma>$: average radiation widths

2 values are given foe JENDL-3.2 the first number is for lower energy the other is for higher energy.

Data status of JENDL-3.2 compared with Leal/Derrien's evaluation, is shown in

Table 3.1-3.3, Fig. 3.1 to 3.3. Significant differences are found for capture cross-sections, some for fission cross-sections compared with current evaluations.

In the course of re-evaluation step, we must take into consideration this new data as one of the candidate for JENDL-3.3. Much works still remains to take this data.

4. Conclusions

Brief descriptions of the problems recognized in the current version of JENDL-3.2 was described. A revision work toward JENDL-3.3 will start in 1997 by JNDC. A new version of JENDL-3.3 will be scheduled .within next 3 years. This does not means new data will be available after 3 years from now. Any new revised data (nuclide wise) will be open to the publics at any times when the evaluation work is completed and review is made.

5. References

1) Nakagawa,T., et al.:J. Nucl.Sci. Technol.,32[12], 1259 (1995)

2) Shibata, K., et al.: JAERI-1319, (1990)

3) Leal,L C., Derien,H., et al. : "Final report on evaluation of U-235 cross sections", distributed NEA NSC WPEC 8th meeting,(1996).

4) Porodzinskij,Y.V., Sukhovitskij,e.s.,: Private communication,(1995).

5) Rose, P.F., (ed.) : "ENDF/B-VI Summary Documentation", BNL-NCS-17541 (ENDF-201), (1991), Data Library ENDF/B-VI. Update, 1995, by the U.S. National Nuclear Data Center.

^{235}U E$_n$=8 MeV
COMPARISON WITH JENDL-3
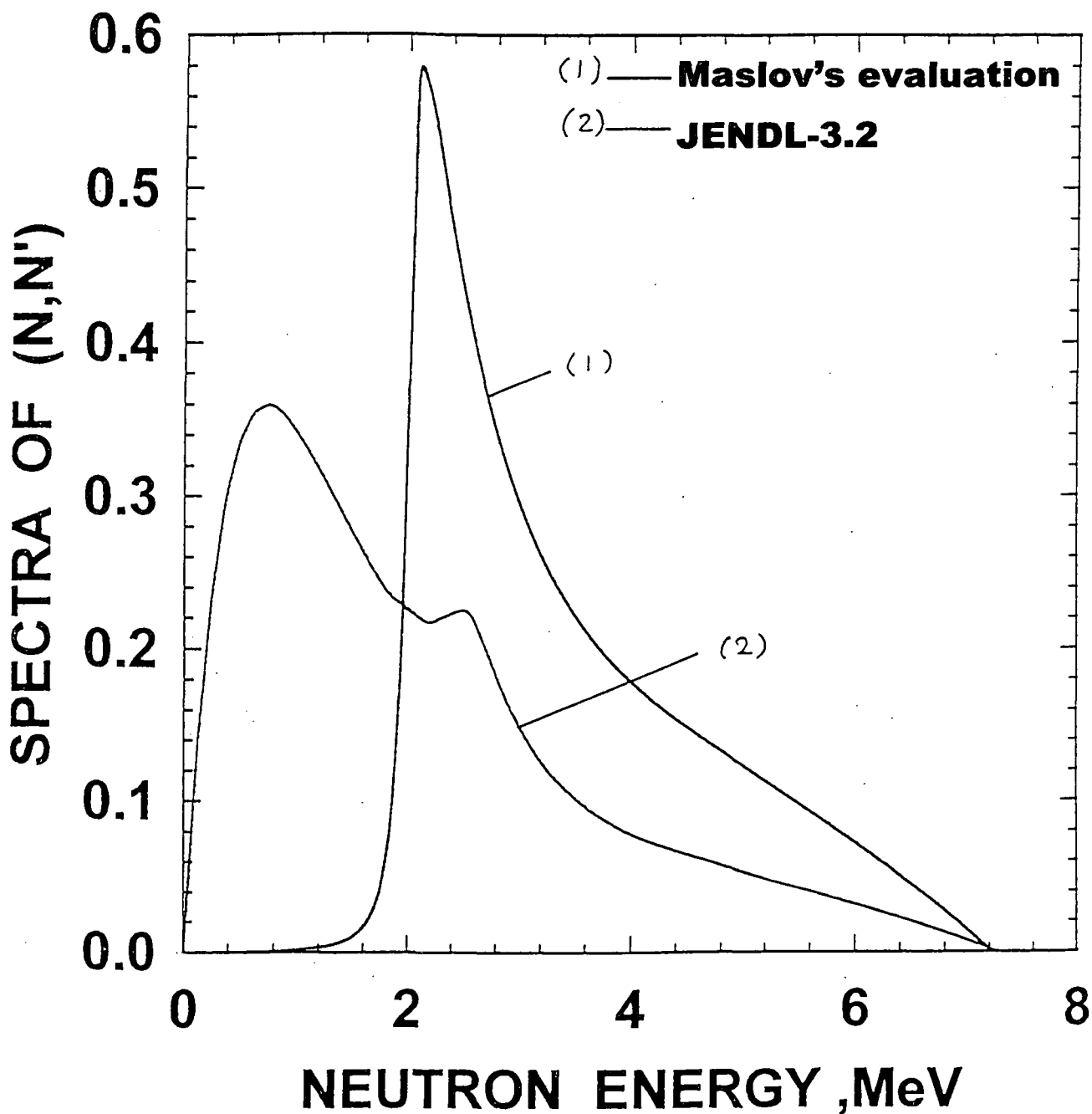
Fig. 1   Secondary energy distributiond for U-235
(JENDL-3.2 and Maslov's evaluation)

U-235 Capture

ENDF-VI (n,gamma) xsec
JENDL-3.2 (n,gamma) xsec
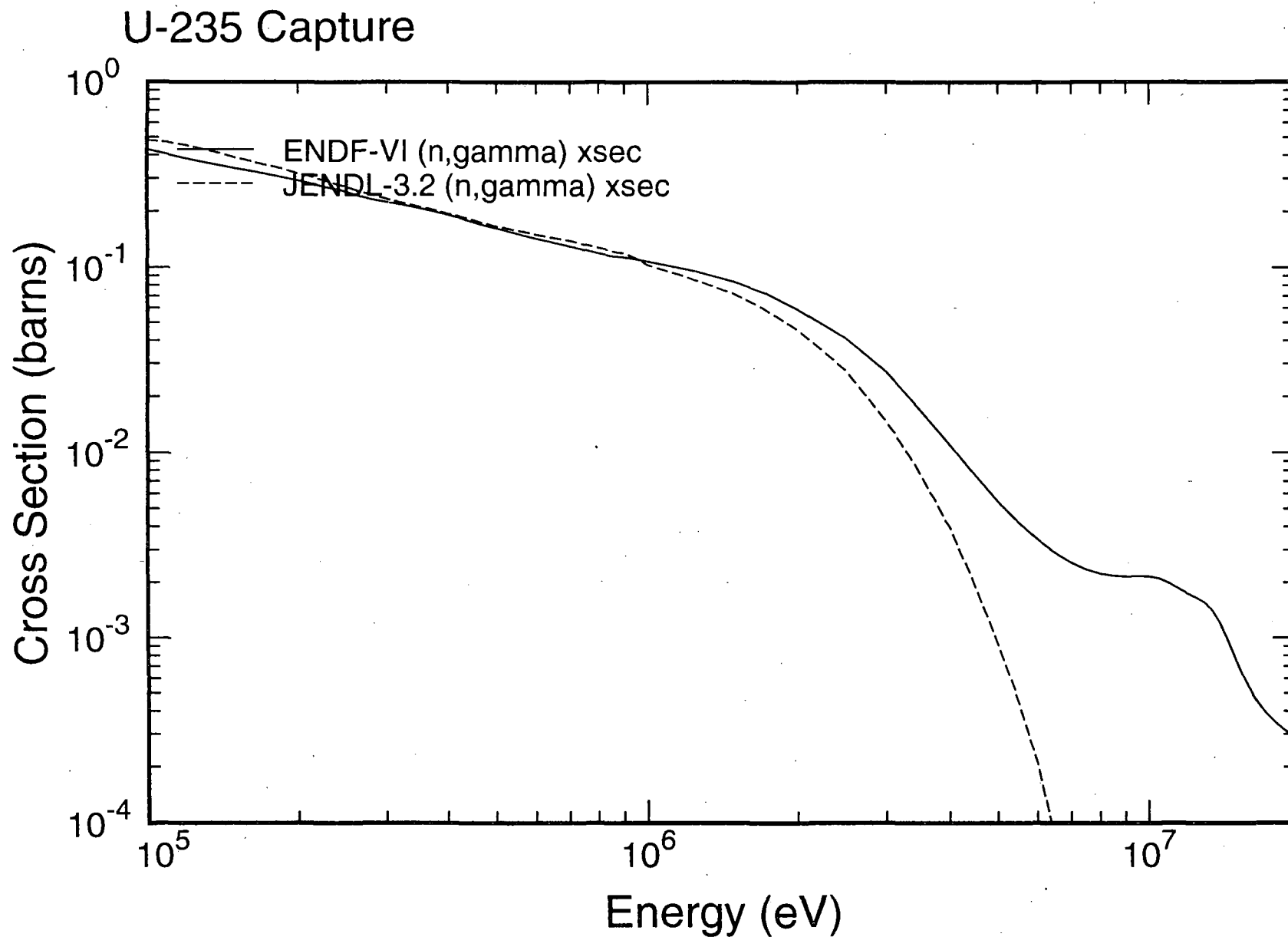
Fig. 2   U-235 capture cross-sections (MeV range)

Fig. 3-1 U-235 capture percent differences

(LEAL/DERRIEN - JENDL-3.2) / JENDL-3.2
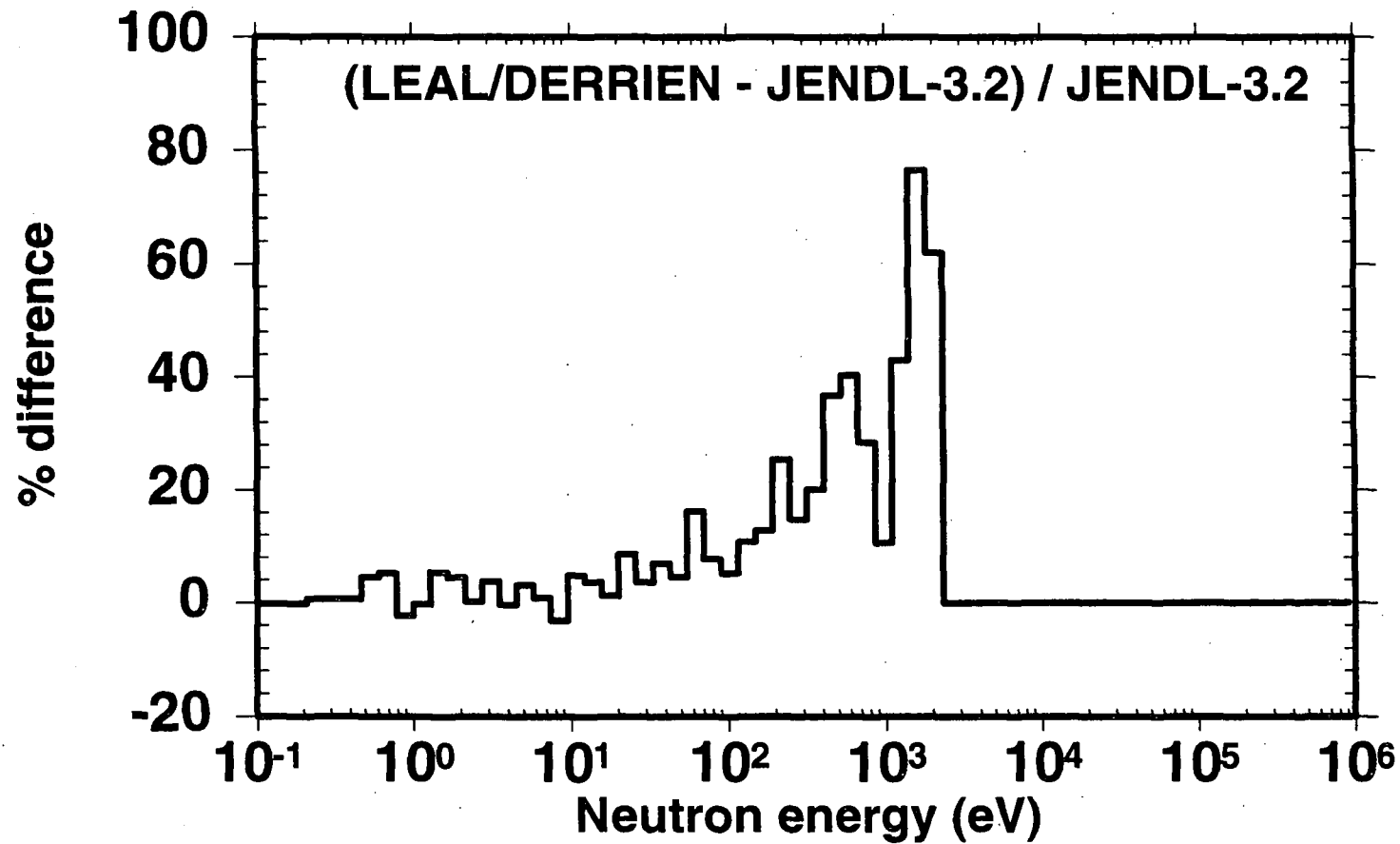
Fig. 3-2 U-235 Fission percent differences
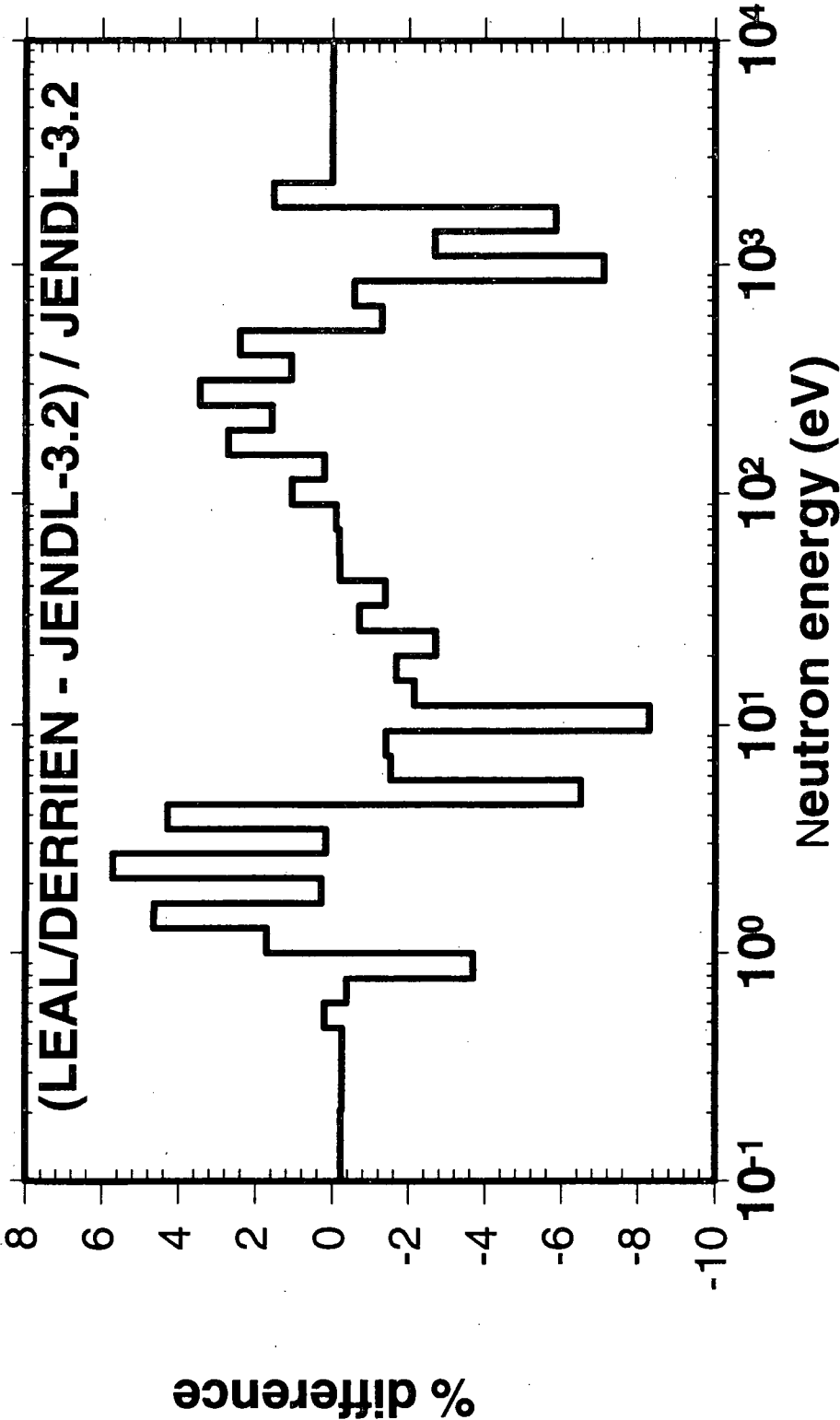
Fig. 3-3 Comparison of 100 Group Average for capture^{235}U
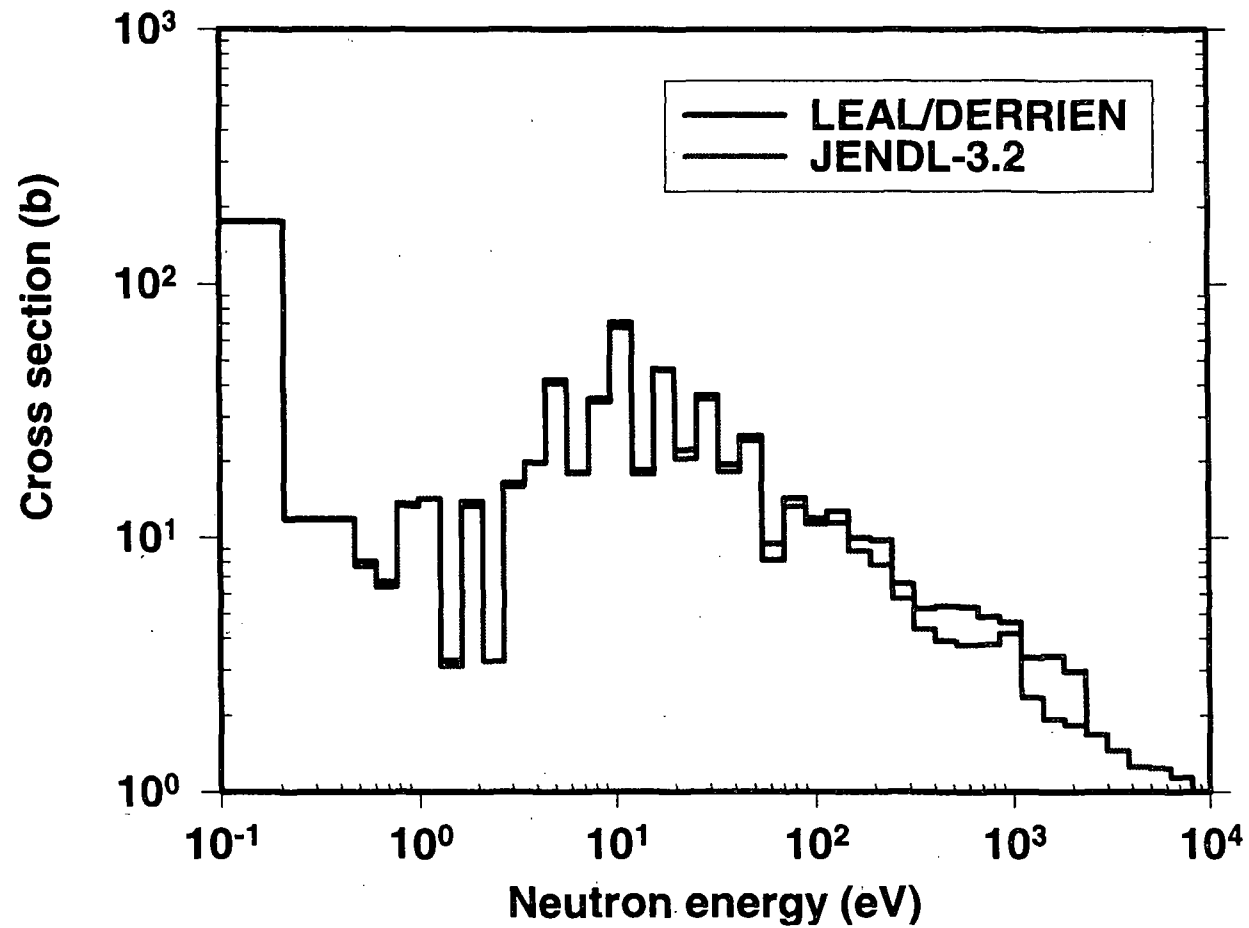
2.2.1 STATUS AND FUTURE PLAN OF NUCLEAR DATA ACTIVITIES IN CHINA

Zhuang Youxiang and Tang Hongqing

China Institute of Atomic Energy
P. O. Box 275, Beijing 102413
P. R. China

Abstract

The present status and future plan of nuclear data measuremant and evaluation in China are presented, including the supplement, improvement on CENDL-2.1 and benchmark test of CENDL-2.1, the progress on nuclear data measurement and CENDL-3.

I. Introduction

Nuclear data requirements in the nineties are shifting from conventional to advanced fission and to fusion reactor technology, nuclear waste incineration and fission reactor decommissioning, as well as to intermediate energy applications such as biomedical applications, spallation sources, accelerator shielding, space and cosmic research.

Nuclear data has played a significant role in the growing economy and energy demands, nuclear science and technology of the developing P. R. China.

The China Nuclear Data Center (CNDC) and China Nuclear Data Coordination Network (CNDCN) have made a lot of progress on nuclear data measurement, evaluation and nuclear reaction theory as well as its application since 1993.

II. Nuclear Data Measurement

Since last symposium in 1990, some progress has been made of nuclear data measurement and related experimental facilities.

The measurement program is focused on the nuclear data for fusion

and fission reactor technology. It includes measurements of differential and double differential cross sections of secondary neutrons, activation cross sections, neutron-induced charged particle outgoing reactions, fission yields, prompt fission neutron spectrum, radiative capture γ-rays and neutron emission spectrum on (α,n) reactions .

2.1 DDXs of secondary neutrons

At the incident neutron energy of 10MeV, the DDXs of secondary neutrons have been measured on ^{9}Be, Fe, ^{238}U and ^{209}Bi using CIAE method. Namely, the higher energy part (greater than ~3.5 MeV of the secondary neutron spectrum) was measured by the normal TOF spectrometer and the lower energy part was measured by the abnormal spectrometer. Some results are shown in figs.1-4.

At 14MeV, the DDXs of C and ^{9}Be were measured at the pulsed Van de Graaff accelerator of Peking University. The data of ^{7}Li which were obtained by an associated α-particle TOF method are shown in figs.5 and 6.

At 37MeV, measurement of differential cross sections of C and ^{209}Bi was carried out at the HI-13 tandem accelerator using a tritium gas target . Some preliminary results (neutron attenuation, multiple scattering and finite geometry have not been corrected yet) are shown in figs.7and 8. Measurement for light elements is planned in the future.

2.2 Activation cross sections

2.2.1 Neutron-induced reactions

The following reaction cross sections have been measured:
(n, p): ^{46}Ti, ^{54}Fe, ^{59}Co, ^{58,60,61}Ni, ^{64}Zn and ^{182}W in the energy range from 6 to 11 Mev, ^{92}Mo, ^{58}Ni, ^{64}Zn and ^{54}Fe around 14MeV.

(n,np+pn+d): ^{58}Ni in the 6-11MeV region.

(n, α): ^{54}Fe, ^{62}Ni and ^{63}Cu in the neutron energy range from 6 to 11MeV.

(n, 2n): ^{93}Nb and ^{176,179}Hf in the 7-12MeV region.

(n, γ): ^{159}Tb, ^{169}Tm and ^{180}Hf in the energy range 0.1-1.5MeV. Some results are shown in figs.9 and 10. In the near future the effort will be

concentrated on the energy range from 6 to 12 MeV and reaction residuals with short half lives at 14MeV.

2.2.2 Charged particle induced reactions

Cross sections of d+Ti and d+Mo reactions have been studied in the incident energy below 24MeV.

2.3 DDXs of (n, x) reactions

DDXs of outgoing charged particles of neutron-induced reactions have been studied for structural materials. The data of ^{58}Ni(n, α) and ^{40}Ca (n, α) reactions at incident neutron energies of 5,6 and 7MeV and (n, p) reactions on Fe, ^{93}Nb and Ni at 14MeV were obtained. Measurements of (n, p) reactions on ^{58}Ni, ^{54}Fe, ^{64}Zn and ^{45}Sc in the incident energy range 4-5MeV and (n, α) reactions on Fe, Ni and Cu at 14MeV are planned.

2.4 Fission yields

The yields of fission products of ^{235}U at about 5,8 and 14MeV have been measured using the thermal neutron-induced fission yield as a reference standard. The dependence of the yield on the incident neutron energy for some products is obtained. The uncertainty of the data is about 3%. The yield measurements of ^{235}U at 3MeV and other fissile nuclides are scheduled in the coming years.

2.5 Prompt fission neutron spectrum

After the measurement of the prompt fission spectra of ^{238}U at 10 and 12MeV, a measurement at 5.4MeV was finished recently. The result is shown in fig.11.

2.6 Radiative Capture γ-rays

After the measurement of the excitation function and angular distribution of the ^{12}C(n, γ) reaction, the excitation functions of ^{6}Li(n, γ)

^{7}Li, ^{16}O(n, γ)^{17}O, ^{56}Fe(n, γ)^{57}Fe and ^{238}U(n, γ)^{239}U reactions in 9-18MeV and ^{11}B(p, γ)^{12}C in the 5-15MeV region have been measured recently. Some results are shown in fig.12.

The fusion γ-rays of hydrogen isotopes at low energies will be studied and γ-ray production cross sections at 14MeV will be measured in the near future.

2.7   Neutron emission spectra of (p, n) and (α, n) reactions

To obtain nuclear level density parameters of reaction residual nuclei in the excitation energy range 2-7MeV, besides the measurement of neutron emission spectra of (p, n) reactions on ^{45}Sc, ^{107,109}Ag, ^{147,152}Sm and Mo isotopes, the spectra of ^{54}Fe(α, n), ^{93}Nb(α, n) and ^{115}In(α, n) reactions have been measured at 12.3, 16.3 and 18.3MeV recently. Part of results are shown in fig.13 and Table 1. A further study will be focused on (α, n) and heavy ion reactions.

In the recent years, some new experimental facilities have been built. A new Cockcroft-walton accelerator with a maximum voltage of 600keV and direct beam current of 3 to 5 mA is under construction. It is designed to provide pulsed beam with a pulse width of ~1.5ns, an average beam current of 30-50μA and repetition rate of 1.5MHZ. Besides measurements of microscopic nuclear data, such as DDX of secondary neutrons, γ-ray production cross sections, activation cross sections, fission product yields etc. around 14MeV, an integral experiment will be arranged at the accelerator. So far the accelerator has already provided several hundreds of hours direct beam for neutron experiment. It will give pulsed beam soon.

An ultraviolet vacuum spectrometer has been built at the HI-13 tandem accelerator for atomic and molecular physics study. Beam foil spectroscopy of highly ionized atoms will be studied with this facility.

A tritium gas target has been built at the tandem accelerator. It has been used for ~900 hours for neutron scattering experiment at 37MeV and other measurements. A schematic diagram and some neutron spectra of the T(d, n) reaction are shown in figs.14 and 15.

III   Nuclear Data Evaluation

3.1   The Supplement and Improvement on CENDL-2.1

A modified version of CENDL-2, i.e. CENDL-2.1 was completed and released in 1995.

The library contains evaluations of neutron reaction data for 68 elements or isotopes from ^{1}H to ^{249}Cf in the neutron energy range from 10^{-5} eV to 20 MeV.

Compared to CENDL-2, the size of the library has been increased significantly, the modifications have been made to most materials, so the accuracy of the data have been improved. For example:

(1)   14 new evaluations completed by Chinese or Chinese/Japanese cooperation have been added. They are: Cl, ^{50,52,53,54}Cr, ^{54,56,57,58}Fe, ^{63,65}Cu, Lu, Hg, and Ti.

(2)   9 evaluations have been updated or re-evaluated, which were done by Chinese or Chinese/Japanese cooperation. They are: ^{27}Al, ^{nat}Ca, ^{nat}Cr, ^{55}Mn, ^{nat}Fe, ^{nat}Cu, ^{93}Nb, ^{nat}Ag and ^{238}U.

(3)   The secondary neutron energy spectra have been modified for 20 nuclides. They are: ^{16}O, ^{23}Na, Mg, Si, P, S, K, Ti, ^{51}V, Ni, Zr, Cd, In, Sb, Hf, W, ^{197}Au, Pb, ^{237}Np and ^{239}Pu.

(4)   The total cross section and elastic scattering cross section have been updated for 8 elements. They are: S, K, Ti, Ni, Zr, Sb, Hf, and Pb.

(5)   The double differential cross section, gamma production data and covariance data have been added for many nuclides.

The comparison of the CENDL-2.1 with CENDL-2 is as follows:

	Nuclides	MF6	MF12-15	MF31-33
CENDL-2	54	4	10	7
CENDL-2.1	68	25	38	10
Increment	14	21	28	3

All the n-D interaction data for CENDL-2.1 have been calculated from the three-body model based on the Faddeev equation. The double-differential cross sections of nertron and spallation proton in ^{2}H(n, 2n)^{1}H reaction are shown in Figs.16~20, as seen, the coincidence of theoretical results with experimental data is generally good .

3.2 The Benchmark Test of CENDL-2.1

CENDL-2.1 has been tested for ten homogeneous, eight heterogeneous thermal and nine homogeneous fast assemblies, which were recommended by CSEWG of USA. 123 - group (for thermal) and 175- group (for fast) cross sections were generated with code system NJOY91.91/NSLINK, MILER, the effective multiplication factors and reaction rate ratios were calculated with code system PASC - 1.

The calculated K_{eff} are shown in Figs.21~22 for homogeneous and heterogeneous thermal assemblies. It can be seen that the K_{eff} are much close to 1.0 for first five homogeneous (Fig.21) and eight heterogeneous (Fig.22) uranium assemblies, ranging from 0.9944 to 0.9995 and from 0.9965 to 1.0027, respectively; but they are considerably overestimated (maximum 2.44%) for last five homogeneous plutonium assemblies (Fig.21). The K_{eff} for homogeneous fast assemblies are shown in Fig.23. It can be seen that they are very close to 1.0 (ranging from 0.9994 to 1.0014) for first three ^{235}U assemblies with different spectra. They are overestimated by about 0.4% for two plutonium metal bare sphere assemblies (JEZEBEL and JEZEBEL - Pu), but it becomes better for plutonium assembly with natural uranium reflector (FLATTOP - Pu). They are changed from 0.9946 to 1.0093 for three different ^{233}U assemblies without, with natutal U and ^{232}Th reflector.

In conclusion, the agreements of the calculated K_{eff} with expermental ones are quite well for U fast, thermal (homogenous and heterogeneous) assemblies, but the K_{eff} are overestimated for Pu thermal, fast assemblies. This means that the data of ^{235}U, $^{238}U(O, H)$ in CENDL - 2.1 are reliable, but the data of Pu need to be improved. The similar conclusion also obtained from analysis of the calculated reaction rate ratio data for above assemblies.

To compare, the calculations have also been done with ENDF/B-6 data for above assemblies and the K_{eff} are shown in Figs.21~23.

3.3 Nuclear Parameter Library, Charged Particle and Photonuclear Data

(1) China Evaluated Nuclear Parameter Library (CENPL)

The six sublibraries, atomic masses and characteristic constants, discrete level schemes and gamma radiation branching ratios, giant

dipole resonance, level density, fission barrier and optical model parameters, have been set up. The studies of the relevant model parameters are being carried out. A plan on developing the CENPL-2 has been worked out.

(2) Charged - Particle Nuclear Data (CPND)

The evalnation and calculation of ^{11}B(p,n)^{11}C, ^{13}C(p,n)^{13}N, ^{16}O(p, α)^{13}C, ^{77}Se(p,n)^{77}Br and ^{186}W(p,n) ^{186}Re reaction cross sections have been accomplished for medical radioisotope production under IAEA research contract No. 8600/RB. There is a result of ^{77}Se(p, n)^{77}Br reaction cross section, see Fig.24.

The renewal contract No.8600/R1/RB has started, the scope of the research project is as follows:

a. Evaluate experimental data for 13 proton reactions, including 7 monitor exitation functions and 6 exitation functions of gamma-emitters;

b. Perform theoretical calculations of proton induced reactions on ^{27}Al, ^{Nat}Cu, ^{111}Cd, ^{127}I and ^{203}Tl up to 80 MeV, and recommend excitation function on ^{22}Na, ^{56}Co, ^{111}In, ^{123}Xe→^{123}I and ^{201}Pb→^{201}Tl, respectively.

The activation cross sections of CPND were also evaluated and calculated by code CUNF, for example, ^{57}Fe(p, 2n)^{56}Co reaction cross section is given in Fig.25.

(3) Photonuclear Data

The collections and evaluations of experimental photonuclear data and complete theoretical calculations on ^{54,56,57,58,nat}Fe and $^{63,65, nat}$Cu for photons up to 30 MeV have been completed under IAEA research contract No.8833/RB using code GUNF, a result is shown in Fig.26.

3.4 Nuclear Theory and Computational Code

The recent progress on nuclear reaction theory and its application are presented in the following.

3.4.1 Double Differential Cross Section Formulations of Light Composite Particle Projectile

The semi-classical multi-step compound and direct interaction double differential cross section formulations of light composite particle projectile considering (1, m) and (2, m) pick-up type reactions simultaneously are presented. The calculated results of cross section, spectra, and double differential cross sections indicate that the contributions of the (2, m) pick-up type reactions are about 15~25% when incident energy is less than 50 MeV and become dominant when incident energy is larger than 50 MeV in some region of the outgoing energy and angles. Whereas the forward tendency of the calculated angular distributions by (2, m) configuration are weaker than that by (1, m) configuration. It also concludes that for the reactions of outgoing composite particle with higher incident energy the semi-classical multi-step direct process must be considered.

3.4.2 Consistent Dynamic and Statistical Description of Fission

The research survey of consistent dynamical and statistical description of fission is briefly introduced. The channel theory of fission with diffusive dynamics based on Bohr channel theory of fission and Fokker-Planck equation and Kramers-modified Bohr-Wheeler expression according to Strutinsky method given by P.Frobrich et al. are compared and analyzed.

3.4.3 The Quantum-Mechanical Preequilibrium Theory

(1) Unified theory of nuclear compound reaction and multistep compound theory

A unified theory formula describing the multistep compound emission of preequilibrium and compound nucleus emission of full equilibrium is presented by using the optical model in the FKK theory.

(2) The FKK theory of Spin 1/2 particle

A multistep compound formula with the spin-half particle, a non-zero spin target and the angular momentum coupling treated in j-j representation has been deduced.

(3) Two-component multistep compound theory

The neutrons and protons are distinguished rigorously by isospin in wave function. The formulas of double differential cross-sections, damping and escape width are deduced in this two component theory.

(4) Quasi-quantum model for calculating multistep direct reaction of continuum and discrete levels.

3.4.4 Intermediate and High Energy Reactions

(1) Averaged analytical forces in intermediate and high energy reactions

By use of the effective Skyrme-type potentials, we derived the averaged analytical forces which include the two-body Skyrme force, three-body Skyrme force, Yukawa force and the Coulomb force. Comparing with the difference method, the application of the analytical forces can raise the calculation speed to 6 times and raise the accuracy significantly.

(2) Light particle emissions in fission diffusion process and the nuclear friction coefficient

In order to include the emissions of other light particles (such as p, α, ...) into the fission diffusion process, we give out the extensive Smoluchowski equation with the inclusion of these light particle emissions. We also showed the formulas for the multiplicities of these particles, with them the comparisons to experimental data can be made and the nuclear friction coefficient can be extracted.

3.4.5 Effective Nucleon-Nucleon Cross Sections Based on Skyrme Interactions

A major goal in the study of intermediate-energy heavy-ion collisions is to measure the time evolution process of nuclear matter under violet collisions as well as nuclear properties under extreme conditions of high density and temperature. However, the interesting information on these problems can only be obtained indirectly through certain theoretical model. Thus one has to choose a good theoretical tool, which should be as general and basic as possible on the one hand and as practicable as possible on the other hand. At present, there exist various approaches to

this subject; the most ambitious one is to obtain the transport equation starting from the time-dependent G-matrix theory. In this approach the time evolution of the heavy-ion collision process is described by a kinetic equation, the G matrix serves as a dynamical input of two-body interaction. It would be more practical to take the effective interaction rather than the G matrix as the transport model for heavy-ion collision. In this work we obtain a self-consistent Boltzmann-Uehling-Uhlenbeck approach which is used to study heavy-ion collisions based on the effective Skyrme interactions, and reproduced empirical optical potentials. The temperature and density dependence of the effective elastic cross section in nuclear matter have been studied. Bacause of the fundamental assumption of the temperature independence of the effective Skyrme interaction and the limitation due to the zero-range force used, our results might be considered to be reasonable for $T \leqslant 10$ MeV and for kinetic energies $E_p \leqslant 120$MeV.

3.4.6 Computational Code

A series of codes UNF has been developed and perfected for nuclear data calculation with the unified treatment of the pre-equilibrium and equilibrium reaction processes with angular momentum and parity conservations. The pick-up mechanism of composite particle emission and the discrete level effects are taken into account for improving the calculations of reaction cross section concerned. This series is capable of calculating DDX of particles, recoil nuclei and γ-ray produced in the reactions.

NUNF is for structural material calculation, FUNF for fission nuclides, SUNF for fission product ones, LUNF for light nuclides, all the mentioned-above codes for neutron incident; CUNF for charged particle incident on structural material, and GUNF for photonuclear reactions.

3.5 China Evaluated Nuclear Data Library, the third version (CENDL-3)

A five year plan(1996-2000) for nuclear data have been made and endorsed by the First Plenary Session of the Second China Committee of Nuclear Data held in Beijing in June, 1995. To make the plan in detail

and workable, follow after, the joint meeting of Nuclear Data Evaluation and Nuclear Theory Working Groups, the meetings of Nuclear Data Measurement and Macroscopic Data Working Groups were held in Oct., Dec. 1995 and May 1996, respectively.

According to the plan , CENDL — 3 will be completed by 2000, and will contain 200 nuclides. Among them, the data of following nuclides will be newly or reevaluated: fissile nuclides 15, structure materials 18, light nuclides 5, fission products 91. It will contain consistent data between natural element and its isotopes for structure material, newly evaluated data for fission products, and more γ -production data (files 12-15), double differential cross section(file 6), covariance matrix (files 31-35).

According to the plan, also the special files for fission yield, activation cross section, nuclear decay data and intermediate data will be developed. An expert system for nuclear data evaluation will be established. CENPL will be improved and revised.

To complete the plan, many subgroups on different subjects have been organized at CNDC and China Nuclear Data Coordination Network, and the various works are underway smoothly.

Table 1 Comparison of "a" parameter (MeV-1)

	$^{59}Ni_{28}$	$^{95}Tc_{43}$	$^{96}Tc_{43}$	$^{97}Tc_{43}$	$^{98}Tc_{43}$	$^{100}Tc_{43}$
G-C	6.00	8.34	9.04	9.80	10.56	11.77
Su	6.50	11.94	13.04	13.52	14.25	15.52
Fit	6.30	10.70	11.00	ᵕ11.20	11.20	11.80

	$^{147}Eu_{63}$	$^{152}Eu_{63}$	$^{107}Cd_{48}$	$^{109}Cd_{48}$	$^{45}Ti_{22}$
G-c	21.02	21.75	14.70	16.12	6.84
Su	20.69	22.77	16.30	16.31	7.06
Fit	15.92	18.00	13.25	14.03	6.01
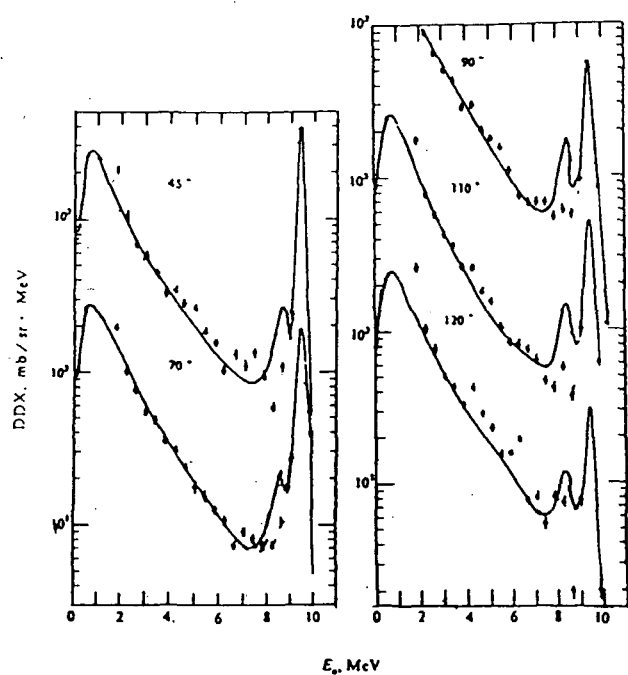
Fig. 1 Double differential cross sections of ^{238}U at 9.6MeV
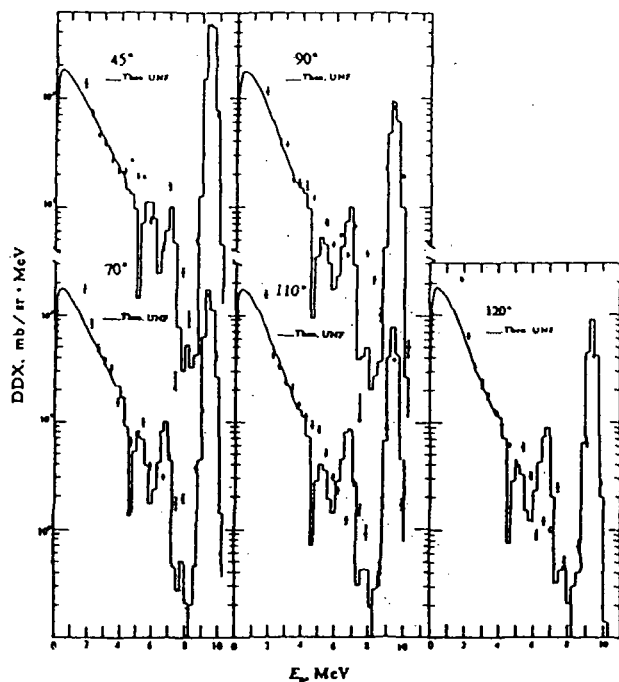
Fig. 2 Double differential cross sections of ^{209}Bi at 9.6MeV
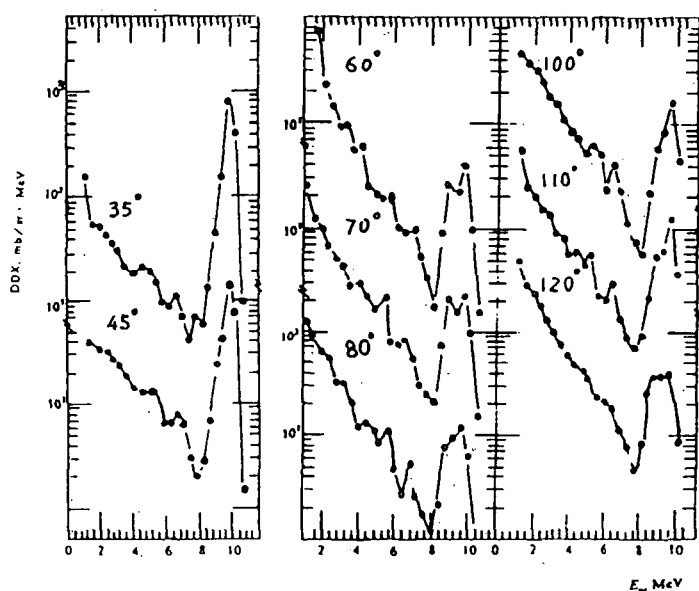
Fig. 3 DDCSs of secondary neutrons
of Fe at 10. 1 MeV
• present work
——eye guide
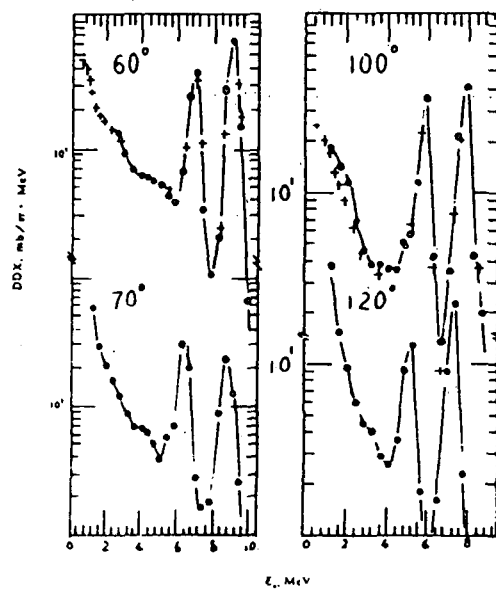
Fig. 4 DDCSs of secondary neutrons
of ^{9}Be at 10. 1 MeV
• present work
┼ M. Drake et al.
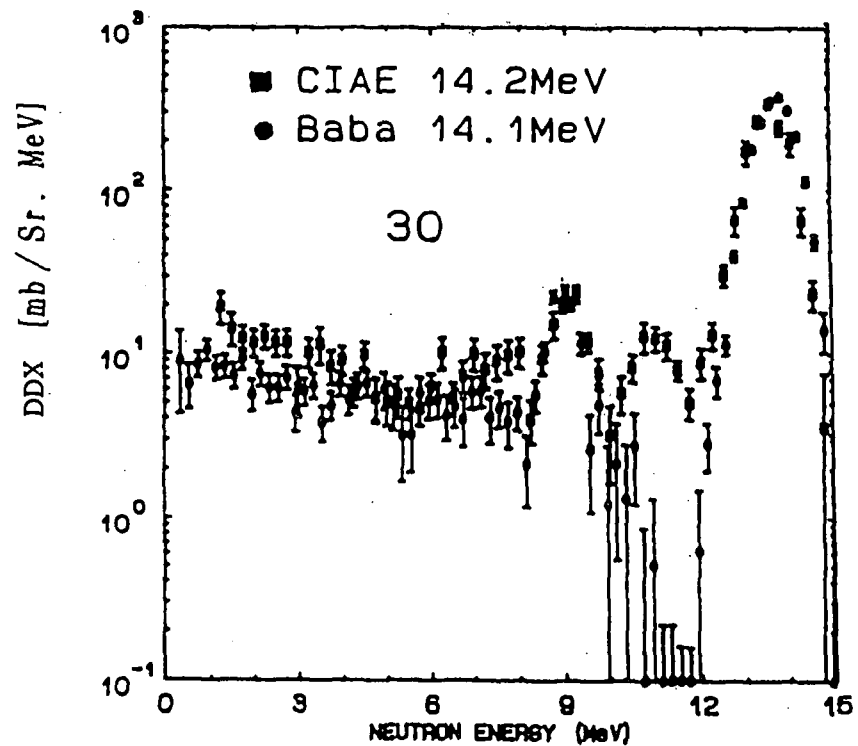
Fig.5 Dou.Diff.x-Sec. of Li-7
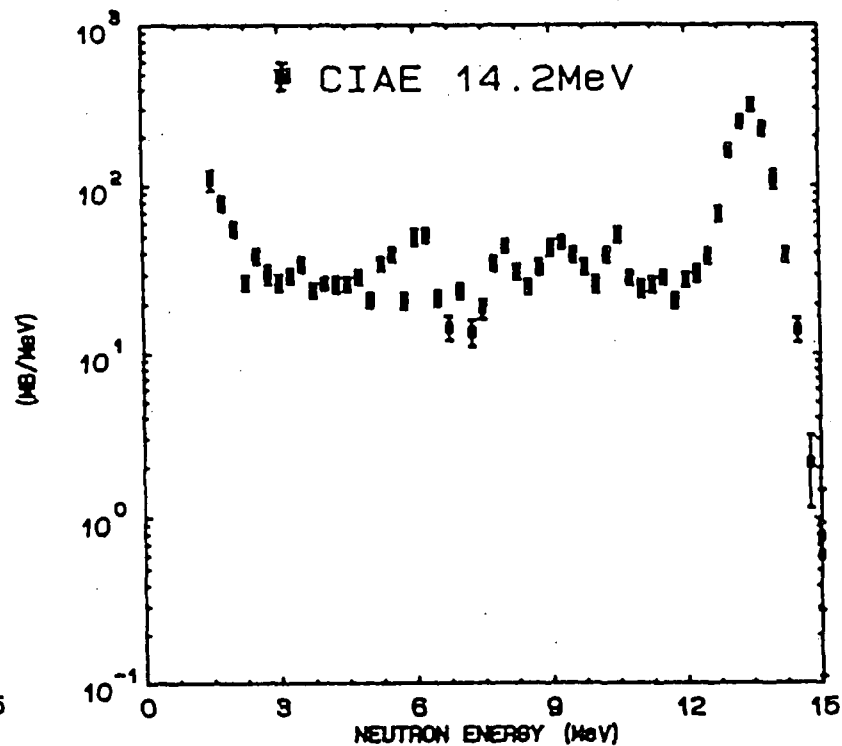
Fig.6 Space Integ. x-Sec. of Li-7
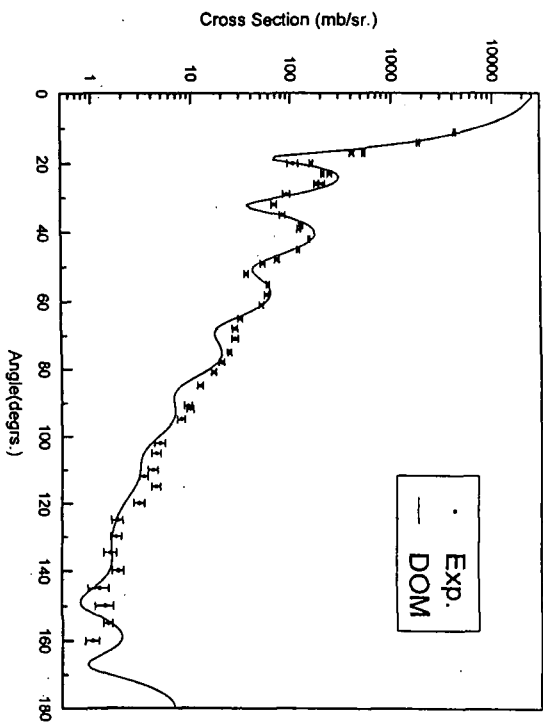
Fig.7 Angular Distribution of 37 MeV Neutrons Scattered from Bi
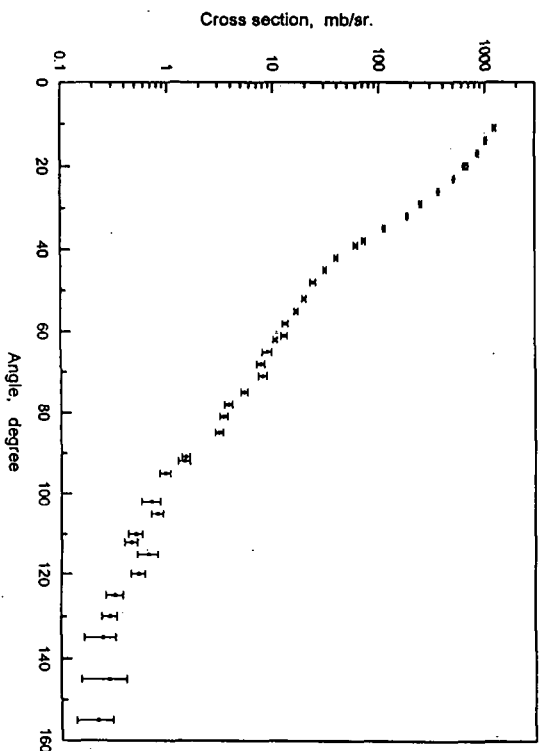
Fig. 8 Angular distribution of 37 MeV neutrons scattered from C
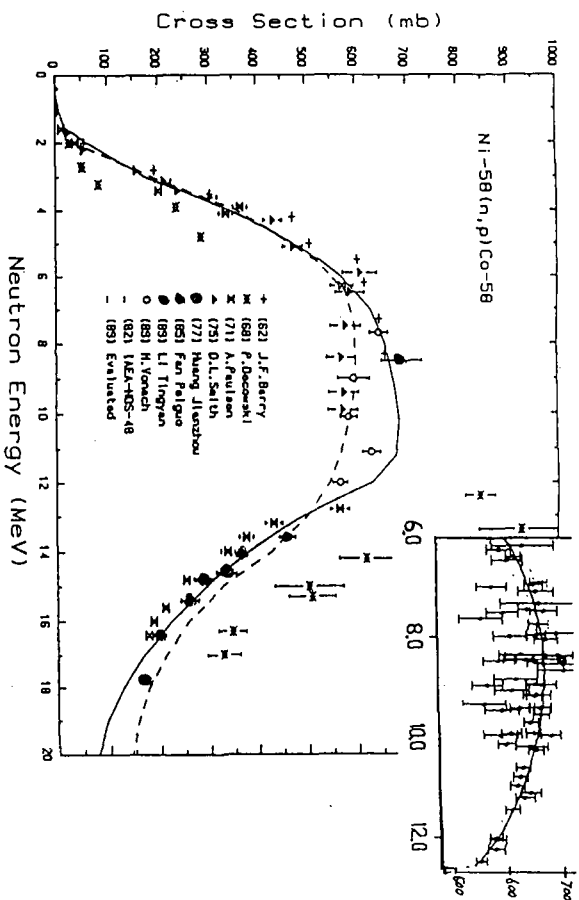
Fig.9 Cross sections of $^{58}Ni(n,p)^{58}Co$ reaction
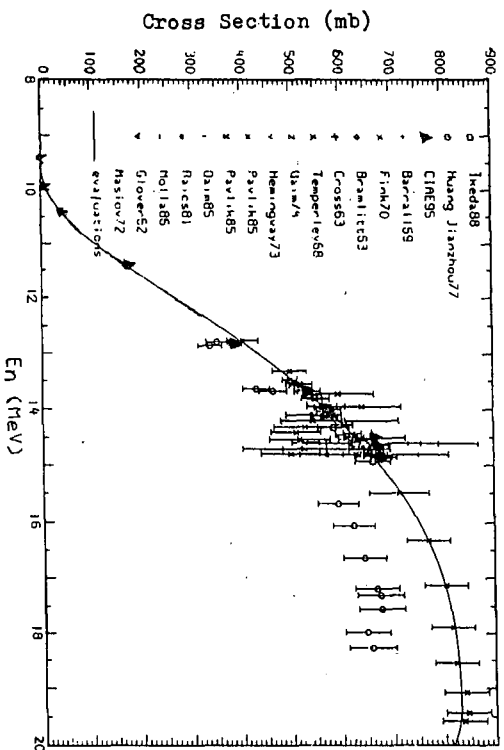
Fig.10 Cross sections of $^{58}Ni(n,np+pn+d)^{57}Co$ reaction

Ein=12 MeV Maxwellian T=1.47MeV

ratio

Ein=10 MeV Maxwellian T=1.40MeV

--- ENDF/B5

ratio

En(MeV)
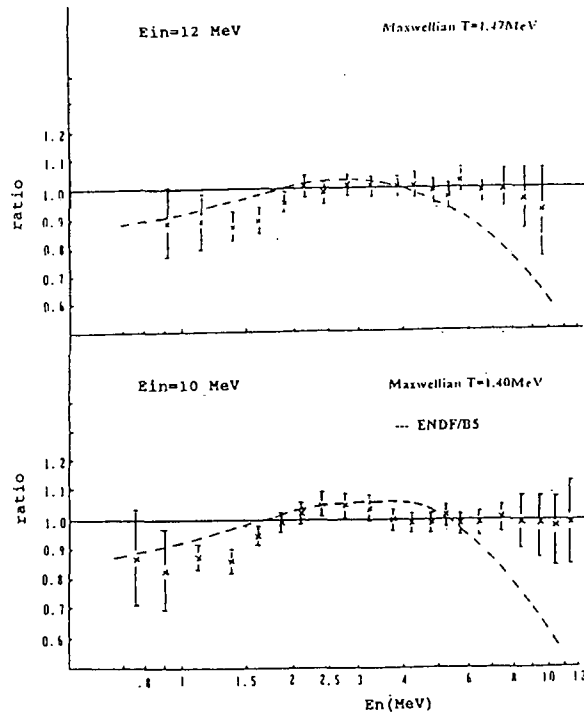
Fig.11 Ratio of prompt fission neutron spectrum to
the Maxwellian distribution

^{56}Fe(n,γ)^{57}Fe

$(4\pi d\sigma/d\Omega)/\mu b$

E_n/MeV
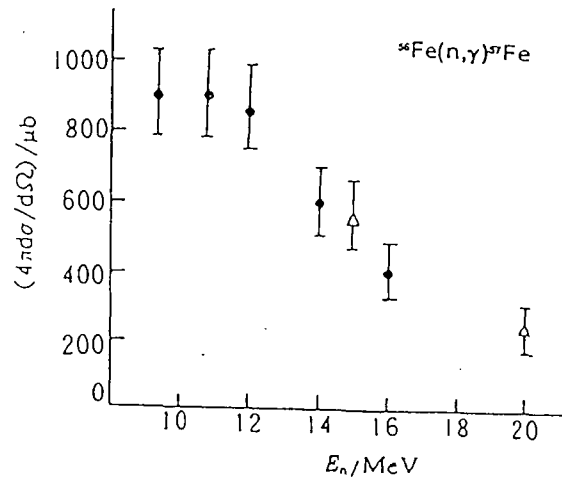
Fig.12 Cross sections of ^{56}Fe(n,γ)^{57}Fe reaction

Level density, MeV^{-1}

B_n, MeV
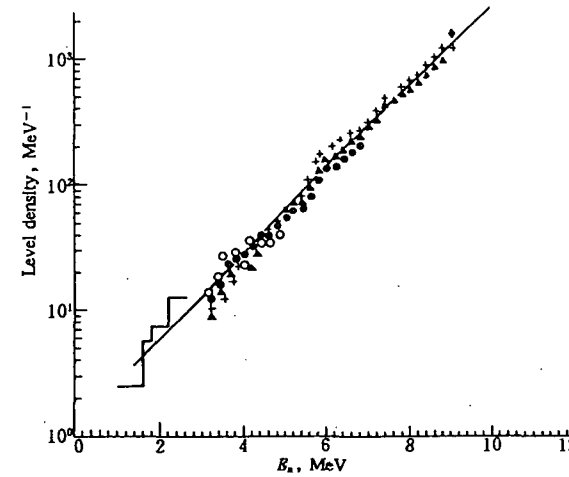
Fig.13 Level densities of ^{59}Ni. $\bigcirc$ $E_p=9$ MeV; $\bullet$ $E_p=11$ MeV; $\blacktriangle$ $E_p=13$ MeV; + $E_p=15$ MeV; Histogram from Ref. [8]; $\blacklozenge$ from s-wave neutron resonance spacing; Solid line: calculated, $a=6.3$, $\delta=1.0$, $\sigma=3.17$.

2cm
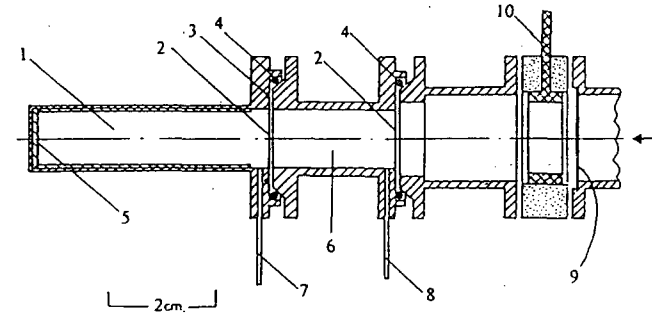
Fig.14 Cross sectional view of the tritium gas target

1. Tritium gas cell 2. Mo foil 3. Indium O—ring 4. O—ring 5. Au beam stop 6. Helium gas cell
7. Tritium gas filling tube 8. Helium gas filling tube 9. Ta collimator 10. Electron suppressor ring
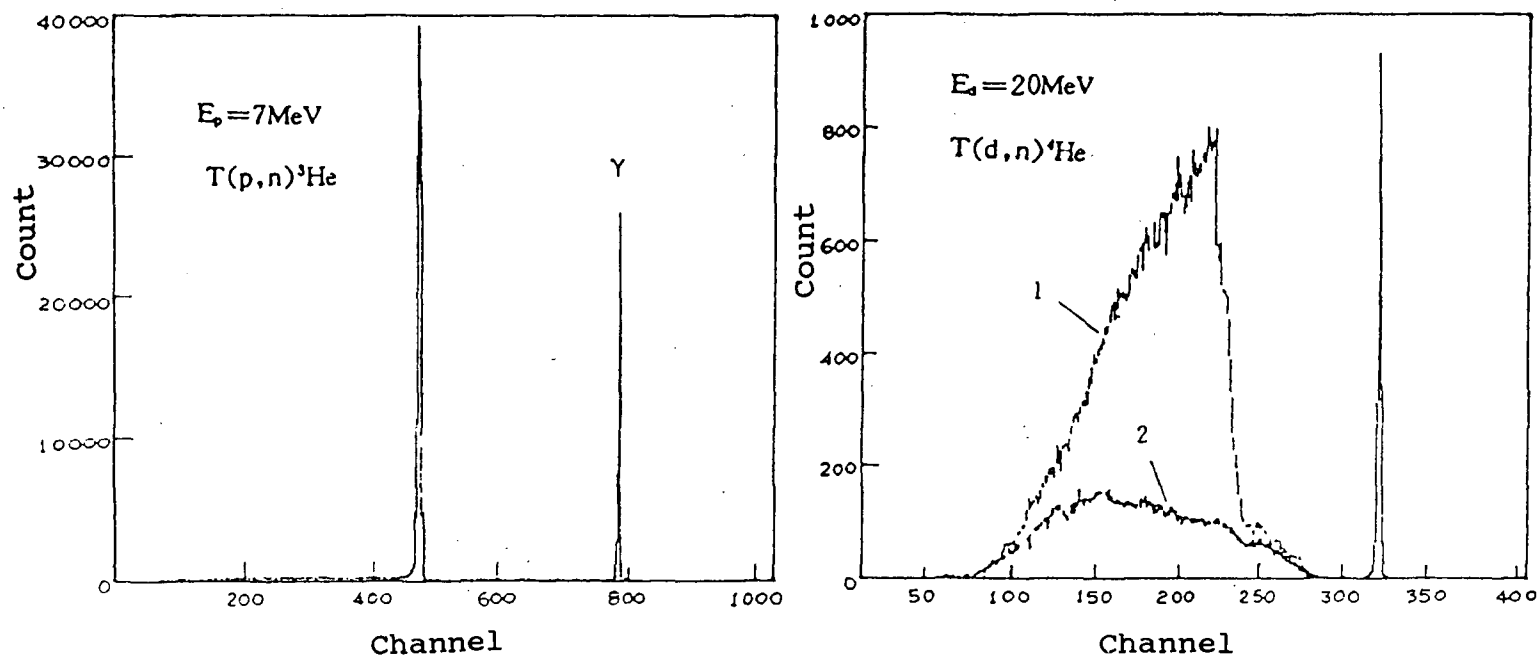
Fig.15 Neutron TOF spectra of T(p,n)³He and T(d,n)⁴He reactions

$E_p = 7\text{MeV}$ and $E_d = 20\text{MeV}$.

(1——tritium gas in, 2——tritium gas out)
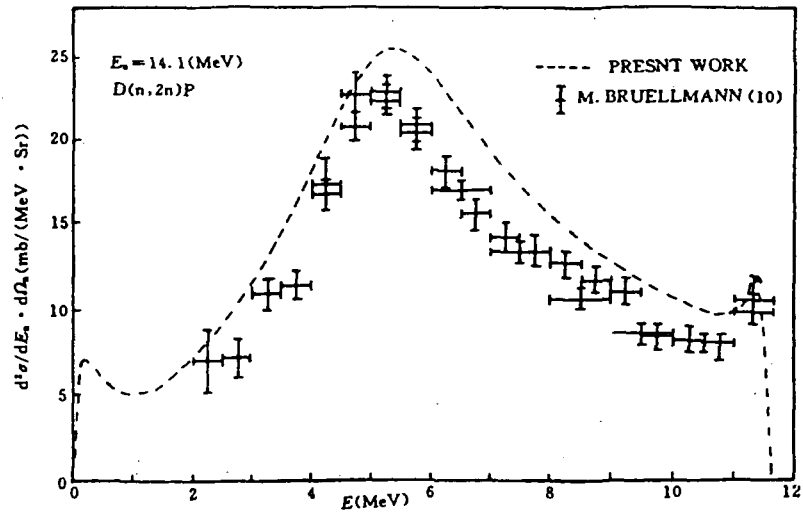
Fig. 16 Measured and evaluated double-differential E (MeV) cross sections for the (n,2n) reaction at 1.0°
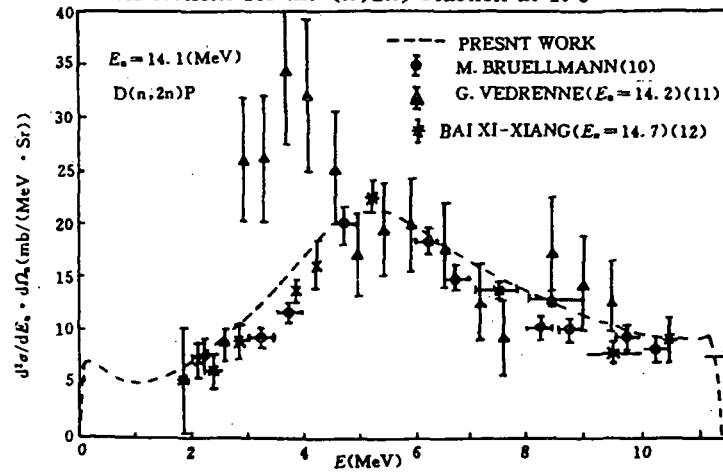
Fig. 17 Measured and evaluated double-differential cross sections for the (n,2n) reaction at 15°
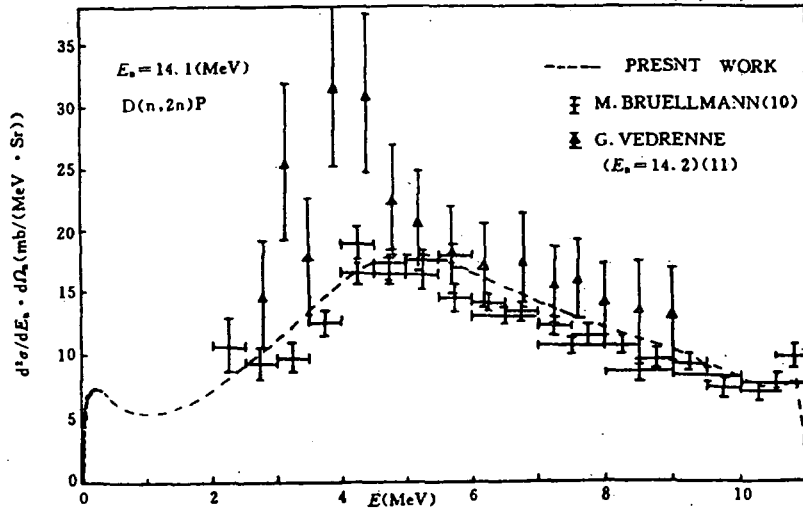
Fig. 18 Measured and evaluated double-differential cross sections for the (n,2n) reaction at 20°
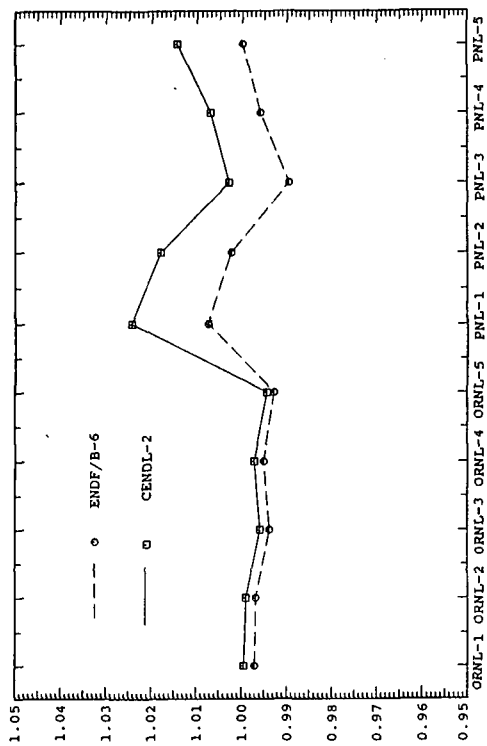
Fig.21 Keff for thermal homogeneous assemblies
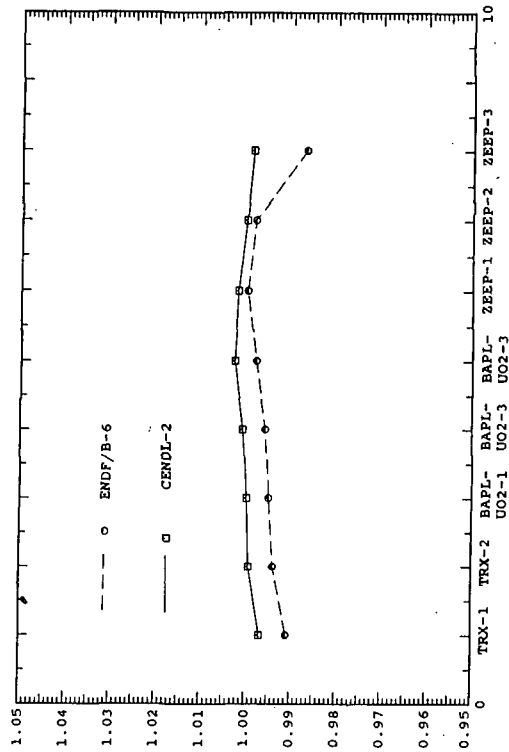
Fig.22 Keff for thermal heterogeneous assemblies
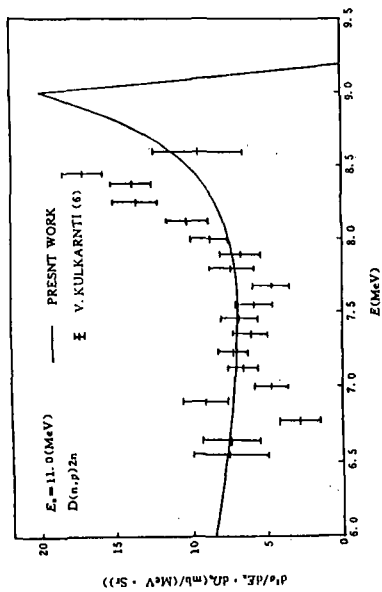
Fig.19 Measured and evaluated protons double-differential cross sections for the D(n,p)2n reaction at 2.50°
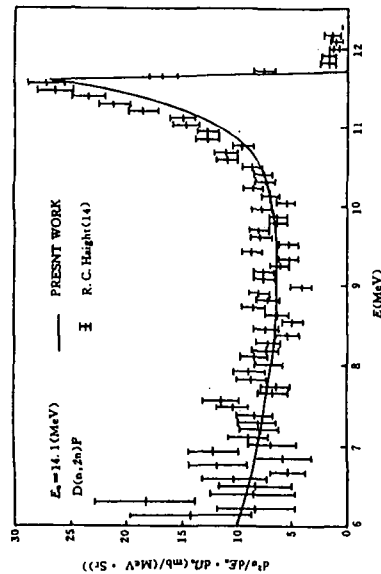
Fig.20 Measured and evaluated double-differential cross sections for the D(n,p)2N reaction at 1.6°

Fig.25 Cross sections of $^{57}Fe(p,2n)^{56}Co$ reaction

Fig.26 Cross sections of $^{63}Cu(g,n)^{62}Cu$ reaction
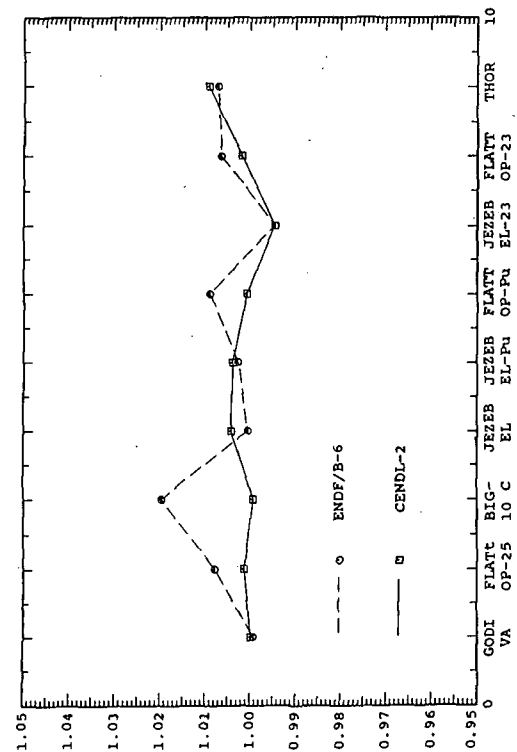
Fig.23 Keff for homogeneous fast assemblies
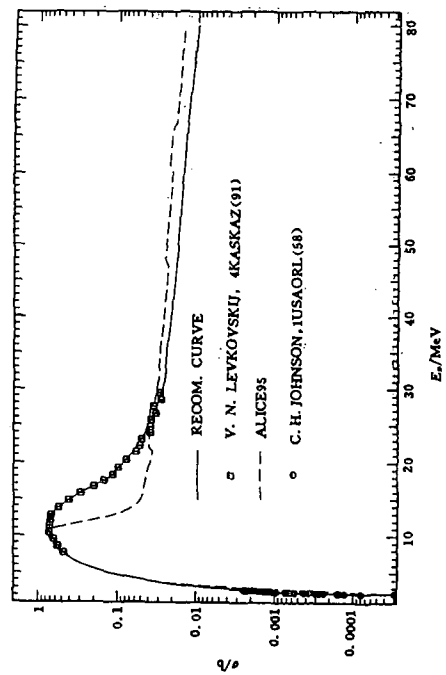
Fig.24 Comparison of calculated $^{77}Se(p,n)$ cross section with exp. data

2.2.2 Status and Future Plan of Nuclear Data Activities in Korea

OH, Soo Youl and CHANG, Jonghwa

Nuclear Data Team

Korea Atomic Energy Research Institute

P.O.Box 105, Yusung, Taejeon, 305-600, Korea

Phone: +82-42-868-2961 e-mail: syoh@kaeri.re.kr

Abstract

It was reviewed the nuclear data related activities in Korea, and was explained a 15-year term nation-wide R&D project that had been launched at 1996. The experiences up to now show, as a whole, that the nuclear data field in Korea is in the early stage. Through the long term project, however, it is expected that a firm foundation be established. Then it would be possible to contribute actively to the international nuclear data community as well as to meet domestic requests for nuclear data. Also it was pointed out the necessity of the international collaboration such as consultings and co-works.

I. Introduction

The nuclear power in Korea has taken an important role in electricity generation during last two decades. There are now 10 PWRs and 1 CANDU plant in operation and 4 PWRs and 3 CANDUs under construction. The nuclear share in the total electricity generation at 1995 was about 36%, and the share of 40% in capacity has been the basis of the long-term national electricity supply plan. These numbers show directly the importance of nuclear power in Korea. Accordingly the nuclear related R&D activities have been focused on the design and construction of nuclear power plant and, as a result, the key technology for conventional nuclear plants had been settled down. This trend, however, also results in basic research fields fallen behind in a relative sense. It is worthy here to quote the science and technology policy in Korea. The basis of the policy is *to enter at midway*, not from the most fundamental stage. It looks an avoidable choice due to the limited man power and research fund; for instance, the number of researchers in nuclear related research institutes in Korea is less than 1,000 persons.

The nuclear data field has been regarded as one of the basic fields, and it is hard to say that the current level in Korea is satisfactory. In section II, it was introduced the experiences in Korea in three categories; nuclear data measurement, evaluation, and processing. Section III summarized the demand for nuclear data in the increasing phase, and Section IV was devoted to explain a 15-year nuclear data R&D project, which is one of the nation-wide long-term nuclear projects[1]. It is expected that a firm foundation be established through this project, however, as it was pointed out in the final section, the international collaboration is indispensable for the project.

II. Status of Nuclear Data Activities

The authors expect that there would be no special objection to categorize the nuclear data activities into three groups from top to down stream; the data measurement, evaluation, and processing. Korea Atomic Energy Research Institute (KAERI) has been the center of nuclear data related activities as well as of other nuclear related researches. So the most of experiences introduced here is of KAERI.

Regarding the processing of evaluated data library, there are relatively fair experiences through conventional PWR projects and a project on the research reactor HANARO[2]. NJOY system has been used to process ENDF/B, JENDL, or JEF. WIMS/D library for HANARO and CANDU reactor is one of the major libraries produced. MCNP4A library was produced for HANARO simulation, CASMO3 library for Mixed Oxide (MOX) fuel research, and SPINX, TRANSX/MATX libraries for the fast reactor nuclear design. Also a benchmark test of evaluated Fe data for OECD/NEA is one of the examples in the processing category.

In the category of evaluation, a database construction has been the major work scope. Evaluated nuclear data have been collected since 1979 and processed for domestic applications. It has been developed since 1994 a machine system in the form of World Wide Web to redistribute these data[2]. The collection list also includes nuclear structure data. For the evaluation itself, many well known methodologies are under studying and testing. Meanwhile building man-power is the other subject.

In the category of measurement, there are only a few experiences. Nuclear structure data at universities, proton reaction data by using cyclotron, etc. fill the list for this category. However, two major facilities had started the operation at 1995, HANARO reactor and a light source from accelerated electrons at Pohang Accelerator Laboratory(PAL)[3]. HANARO is a multi-purpose research reactor constructed at KAERI. It is a pool type 30MW reactor of which neutron flux level is 5E+14. On the other hand, PAL has a 150m-long LINAC to provide electrons to the storage ring. Three electron beam exits, from 100 MeV to 2 GeV, were prepared. It is expected that these facilities provide good environment for measurements. Experiment facilities for nuclear data measurement will be added in those two sites, and a high energy proton accelerator is under planning related to the spallation research. The plan will be explained at Section IV.

III. Demand for Nuclear Data

The demand for the nuclear data in Korea is in the increasing phase. This trend is closely related to the endeavor to expand the horizon from the conventional technology to the advanced ones and from the power generation to other ones such as nuclear therapy.

There are internationally available evaluated cross sections nowadays such as JENDL-3.2, ENDF/ B-6, JEF-2, etc. During the period of introducing fully developed nuclear technology, there was nearly no need to elaborate in nuclear data producing activity. However, as Korea becomes one of the most nuclear power dependent country, she needs for more economic nuclear power generation, she is confronting a problem of nuclear waste, and so she needs for new technology such as fusion, accelerator driven fissile reactor. In the new regime of nuclear technology, Korea has no patience to wait for a well developed product. So Korean government supports the budget for long- or mid-term developments of such as liquid metal reactor, tokamak reactor, nuclear waste management technology, research reactor application,

radioisotope application, nuclear medical diagnosis/treatment as well as light water and heavy water reactor fuel and safety.

The need for nuclear data at current stage may be satisfied by introducing well proven nuclear software tool from the other countries. However, as the design of new application becomes detailed and diverted from original one, we eventually recognize the need for own customized and proven tool. Such lesson was learned during the feasibility studies on extended burnup fuel, erbia and halfnium poison for the light water reactor fuel, and the spent fuel management. In addition, many other fields of nuclear development are lacking of reliable nuclear data and experimental facilities for verification. So the needs for nuclear data applicable to new technologies are in the increasing phase.

On the other view point, the current plan in Korea is to build an infra structure to collaborate with more developed countries and to fulfill domestic need for some specific data. This infra structure may include the trained man-power as well as data measurement facility.

IV. Future Plan

A R&D project titled "Development of Nuclear Data System" had been launched this year, even this year's activity is a kind of pre-project for the real project. The full scale project will start at next year. This is a nation-wide long-term, more than 10 years, project. It might be possible to prospect the future, at least till the end of the first decade of next century, of Korean nuclear data related activities through this project.

Before to introduce each activity of the project, an overview is presented. While Korea Atomic Energy Research Institute (KAERI) plays the initiative role, other related organizations will participate in the project in part. The Pohang Accelerator Laboratory is the major participant outside KAERI, and laboratories affiliated to universities will join the project. It was estimated that 170 man-year for the first 10 years from 1997 is necessary inside KAERI. In the other organizations, they have their own plan on the man-power assignment, so much more researchers shall join the project. For the same period, about 50 billion Korean Won, equivalent to about 7 billion Japanese Yen, was requested for the whole project.

It was summarized in the Table what activities have been planned. The goals of each stage are the establishment of foundation, preparation for self-reliance, and self-reliance, respectively. Among many activities in the table, construction of experiment facilities is the foundation itself for both the self-reliance and contribution to the international nuclear data community. A target room will be constructed at the end of one of the electron beam exits of LINAC at Pohang Accelerator Lab. In this facility, measurements for differential quantities such as energy dependent cross section will be conducted. For integral measurements, another facility will be constructed at HANARO. At stage 2, Isotope Separation On Line facility for nuclear data of fission products has been scheduled at HANARO. A heavy particle accelerator for medium energy data and DDX measurements has been planned also at stage 2. Meanwhile, there is a different project on a high energy proton accelerator. If that project goes on schedule, we would like to add a facility for the data measurement which is necessary for spallation research. The target of measurement category at stage 1 is the man-power buildup. So researchers will join to foreign experiments, and we are now searching for counter parts. After that, own experiments will be conducted from the relatively easy ones. In addition to the new man-power buildup, it is pointed out that concentrating or organizing the existing measurement activities in Korea is equally important. Concerning the evaluation,

the database related activities will be continued throughout all of the stages as an indispensable part of evaluation. It has been scheduled from the evaluation system setup to the evaluation of data necessary for advanced researches such as transmutation. Processing technique will be enhanced throughout the project. Activities in this category will cover the processing for from Mixed OXide fuel and fast reactor applications at stages 1 and 2 to fusion and transmutation applications at stage 3. In addition to the activities above, many other activities have been planned. These are related to the other projects on such as Boron Neutron Capture Therapy, crystal structure research with cold neutron, and production of isotopes for Positron Emission Tomography. Nuclear design and analyses for these are included in the work scope.

All of the detail activities are subjected to change to reflect the results of periodical review of national nuclear R&D projects. However, the skeleton will be maintained throughout the period.

V. Concluding Remark

Even the nuclear data field in Korea is in the early stage now, this field will grow up soon because the Korean nuclear industry asks for that. A big project had been launched as it was presented in Section IV. This project will provide a firm foundation to Korean nuclear data researches. Furthermore it is important to recognize that the nuclear data activities in Korea will be vigorously continued even after this project. The nuclear-drive policy in Korea supports this prospect.

However, there are many fields that need international collaboration. Consulting needs for the design of experiment facilities and for practices in the data measurement and evaluation are the examples. It seems co-works in the measurement and evaluation are also indispensable. Such collaborations shall be valuable for both Korea and her counter parts.

References

[1] For instance, Nam Zin Cho, "Nuclear Energy Policy and R&D Prospects : The Korean Case," *Proc. Int'l Conf. on the Physics of Reactors* (PHYSOR 96), Vol. 1, O-21, Sept. 16-20, 1996, Mito, Japan.
[2] http://hpngp01.kaeri.re.kr and http://hpngp01.kaeri.re.kr/hanaro
[3] http://pal.postech.ac.kr

Table. Activities and Milestone of Development of Nuclear Data System Project

Activity	Stage 1 (1997-2000)	Stage 2 (2001-2004)	Stage 3 (2005-2009)
Experiment Facility Construction	• differential measurement facility[1] • integral measurement facility[4]	• isotope separation on line facility[2] • facility for reaction with heavy particle	• facility for spallation data[3]
Measurement	• participation in foreign experiments	• CS of stable isotopes	• CS of fission products • data for fusion, transmutation research, etc.
Evaluation	• database setup, data collection, and maintenance • evaluation system setup	• continuing database activities • evaluation for stable isotopes	• continuing database activities • evaluation for short-lived isotopes, transmutation related isotopes
Processing	• technique development / enhancement for MOX fuel, fast reactor, etc.	• continuing technique development	• continuing technique development for fusion, transmutation research, etc.
Others	• design system setup for BNCT, etc. • man-power development	• nuclear design and analyses for other project	

1) utilizing LINAC at Pohang Accelerator Lab.
2) at HANARO
3) A high energy proton accelerator has been scheduled in another project.
4) utilizing filter-beam at HANARO

2.2.3 Status of Nuclear Data Activities at Karlsruhe

Toshihiko KAWANO

Energy Conversion Engineering, Kyushu University
6-1 Kasuga-kouen, Kasuga 816, Japan
e-mail: kawano@ence.kyushu-u.ac.jp

This is a brief introduction to nuclear data activity at Karlsruhe Research Center. Some URLs concered are given. Topics mentioned here are, the FENDL and JEF/EFF project at INR, and measurements of neutron capture cross sections at IK III.

1. Introduction

The Karlsruhe Research Center (*Forschungszentrum Karlsruhe*, FZK) was called Karlsruhe Nuclear Research Center (*Kernforschungszentrum Karlsruhe*, KfK) formerly, and it is one of the largest non-commercial science and engineering research institutions in Germany nowadays. The research program is concentrated on,

1. Environment

2. Energy

3. Microsystems engineering, and

4. Fundamental research.

Detailed information about FZK is found at their WWW server:

```
http://www.fzk.de/
```

2. Institutes

Despite their research is diverted to environment and technology INR (*institut für Neutronenphysik und Reactortechnik*) is still active in the field of the nuclear data since they produced KEDAK (*Kerndaten-Datei Karlsruhe*). The nuclear data activity in INR is stimulated by fusion reactor research projects and the JEF, EFF, and FENDL projects.

Nuclear data concerning to fusion reactor neutronics have been studied by Dr.Kiefhaber's group (*Theoretische Abteilung 3*), and recent studies[1] are focused on the fusion blanket engineering. The fusion data library FENDL which gathered the existing nuclear data libraries — ENDF/B-VI, JENDL, EFF, and BROND — is a reference library for the ITER project, and FZK coordinates international data test program of the library.

Dr.Fischer and Dr.Wiegner studied the FENDL data testing[2]. Measurements of neutron leakage spectra from beryllium shells were performed at IPPE, Obninsk. These spectra were analyzed with the one-dimensional S_N code and the Monte Carlo code, and it was reported at Gatlinburg conference[3].

Dr.Fröhner has responsibility for a data evaluation and a covariance file of JEF/EFF. He has been developed sophisticated covariance evaluation methodology which is based on "the Principle of Maximum Entropy[4, 5, 6, 7]". Uncertainty analysis in the resolved/unresolved

resonance region appeared at the Gatlinburg conference[8]. High-resolution iron transmission measurements were made at Geel[9]. It was shown that the fluctuations of the total cross section can be derived from the Hauser-Feshbach theory, and self-shielding effects are important up to 4 or 5 MeV[10].

The INR's Web page is :

    http://hbksun17.fzk.de:8080/INR/

and a few private home pages are shown at :

    http://inrrisc6.fzk.de:8080/inrprivate.html

The other activity concerning to the nuclear data is found at IK (*Institut für Kernphysik*). A 3.75 MV Van de Graaf accelerator is used to study stellar nucleosynthesis by Dr.Käppeler's group in IK III – Nuclear Astrophysics, and measurements of neutron capture cross sections were carried out there[11]. Their Web page is :

    http://ik3indigo.fzk.de/

and the abstracts of their recent paper can be obtained from :

    http://ik3indigo.fzk.de/papers.html

References

[1] "*Ergebnisbericht über Forschung und Entwicklung*, 1995, Institut für Neutronenphysik und Reaktortechnik," Wissenschaftlische Berichte FZKA 5535 (1996).

[2] Fischer, U. and Wiegner, E. : *Fusion Engineering and Design*, **28**, 437 and 624 (1995).

[3] Fischer, U. and Wiegner, E. : *Proc. Int. Conf. Nuclear Data for Science and Technology*, Gatlinburg, 916 (1994).

[4] Jaynes, E.T. : "*Papers on Probability, Statistics and Statistical Physics*," R.D.Rosenkrantz(ed.), Reidel, Dordrecht (1983).

[5] Fröhner, F.H. : "*Principles and Techniques of Data Evaluation*," Karlsruhe report KfK 4099 (1986).

[6] Fröhner, F.H. : *Proc. Nuclear Data Evaluation Methodology*, 209 (1993).

[7] Fröhner, F.H. : *Proc. Reactor Physics and Reactor Computations*, 287 (1994).

[8] Fröhner, F.H. : *Proc. Int. Conf. Nuclear Data for Science and Technology*, Gatlinburg, 597 (1994).

[9] Berthold, K., Nazareth, C., Gohr, and G., Weigmann, H. : *Proc. Int. Conf. Nuclear Data for Science and Technology*, Gatlinburg, 218 (1994).

[10] Fröhner, F.H. : Final Status Report of NSC Subgroup 15 – Self-Shielding in the Unresolved Region, (1996).

[11] Käppeler, F., *et al.*, : For Example, *Phys. Rev.*, **C 53**, 459 (1996), *Phys. Rev.*, **C 53**, 977 (1996), *Phys. Rev.*, **C 53**, 1397 (1996).

2.3 Topics 2: Delayed Neutron

2.3.1 Status of International Benchmark Experiment
for Effective Delayed Neutron Fraction (βeff)

S. Okajima, T. Sakurai, T. Mukaiyama

Japan Atomic Energy Research Institute

Tokai-mura, Naka-gun, Ibaraki-ken 319-11

E-mail:okajima@fca001.tokai.jaeri.go.jp

To improve the prediction accuracy of the βeff, the program of the international benchmark experiment (Beta Effect Reactor Experiment for a New International Collaborative Evaluation: BERNICE) was planned. This program composed of two parts; BERNICE-MASURCA and BERNICE-FCA. The former one was carried out in the fast critical facility MASURCA of CEA, FRANCE between 1993 and 1994. The latter one started in the FCA, JAERI in 1995 and still is going. In these benchmark experiments, various experimental techniques have been applied for in-pile measurements of the βeff. The accuracy of the measurements was better than 3%.

1. Introduction

The effective delayed neutron fraction, βeff, which allows the conversion between calculated and measured reactivity values, plays an important role in the theoretical interpretation of reactivity measurement. In recent systematic analysis for the βeff experiments which were previously performed in ten different core configurations, the ratio between calculation and experiment, C/E values, ranged from 0.93 to 1.04[1]. From this result the current prediction accuracy of βeff was estimated to be about ±5% (1σ). This prediction accuracy strongly affects the uncertainty for the reactivity measurement either in a power reactor or in a critical facility.

To improve the prediction accuracy of the βeff, the international benchmark experiments of the various techniques under the international collaboration have been carried out: the experiment at MASURCA facility of CEA-Cadarche and that at FCA facility of JAERI-Tokai. In these experiments six different core configurations were selected taking into consideration of the systematic change of the nuclide contribution from U-235, U-238 and Pu-239 to the βeff. The several countries participated in this experimental program. The βeff measurement was carried out by each participant with their own measurement technique, and the measured

results were compared with each other. These experiments have been conducted under the NEA/NSC Working Party on International Evaluation Cooperation (WPEC), Subgroup 1.6 on Delayed Neutron Data Validation.

2. International βeff Benchmark Experiment at MASURCA (BERNICE-MASURCA) [2]

There were three different core configurations: R2 (U-core), Zona2 (MOX-core) and Compact (MOX-core). Table 1 shows the main characteristics of these cores. The purpose of the R2 core was to calibrate and to optimize experimental techniques. Those of others was to obtain the different contribution to βeff for U-238 and Pu-239. The core was surrounded by a 50-50 UO_2-Na mixture blanket. The thickness of the blanket was 30 cm in radial direction and 20 cm in axial direction. The detail of core configuration was described in the reference (2).

The experiments in the first two cores, namely R2 and Zona2, were carried out between April, 1993 and March, 1994. The experiment in the third core, Compact, was postponed. Five countries participated in these experiments: France (CEA), Italy (ENEA), Russia (IPPE/Obninsk), USA (LANL) and Japan (JAERI) [3].

Prior to the βeff measurement, the CEA, IPPE and JAERI teams measured fission rates of U-235, U-238 and Pu-239, and corresponding rate ratios in the core center with using their own absolute fission chambers. The results were compared with each other to reduce the uncertainty of the fission integral for βeff evaluation, and were found to be in good agreement within the experimental error of 2% or less. Consequently, the uncertainty of the fission integral was estimated to be about 2%.

The βeff was measured within the experimental error of ~3%. The experimental results of βeff by each participant were shown in Fig. 1.

3. International βeff Benchmark Experiment at FCA (BERNICE-FCA)

As the complementary program to that at MASURCA, JAERI proposed the βeff benchmark experiments at FCA.

Three different core configurations were selected so that these cores could be complementary to those of MASURCA: XIX-1 (U-core), XIX-2 (Pu/NU core) and XIX-3 (Pu core). Figure 2 shows the nuclide contribution to βeff for each core. The systematic change of nuclide contribution was found. The nuclide contribution to βeff in the XIX-2 core is similar to that in the MASURCA Zona2 core. The purpose of the XIX-1 core is to compare the experimental techniques among participating parties through the βeff measurement for standard material, U-235, since the contribution of U-235 in this core is about 95%. The purpose of the XIX-3 core is to evaluate the βeff for Pu-239.

The main characteristics of these cores were shown in Table 2. The core is surrounded by

an inner blanket of 30 cm thickness containing a significant amount of depleted uranium-oxide and sodium, and an outer blanket of 15 cm thickness containing only depleted uranium metal. The contribution of these blanket regions to βeff was less than 10%.

The following are participating groups; CEA/Cadarche (France), IPPE/Obninsk (Russia), KAERI (Korea), LANL (USA), Nagoya Univ. (Japan) and JAERI (Japan).

The experimental schedule was also shown in Table 2. The first core, XIX-1 core, construction started in October, 1995. The βeff measurement in this core was carried out between January, and April, 1996. The measurement in the third core will finish in 1997.

The preliminary results in the XIX-1 core was shown in Fig. 3. The tentative measured results of βeff was determined with the accuracy of 3 - 5 %. Further works, such as the evaluation of experimental error etc. are needed.

4. Summary

To improve the prediction accuracy of the βeff, the international benchmark experiments have been carried out. The primary intent of these benchmark experiments was to obtain an in-pile measurement of the βeff with an accuracy better than 3% using a wide variety of experimental techniques. On the basis of these results, the reliability of delayed neutron data can be verified using current computational methods.

References

(1) A. D'Angelo and A. Filip: *Nucl. Sci. and Eng.*, **114**, 332-341 (1993).

(2) P. Bertrand et al.: *Proc. of Int. Conf. on the Physics of Reactors PHYSOR 96*, Mito, Japan, E-190 - E-199, (1996).

(3) T. Sakurai and T. Nemoto: *Proc. of The 1995 Symposium on Nuclear Data*, *JAERI-Conf 96-008*, 98-103, (1996).

Table 1 Major characteristics of the BERNICE-MASURCA

Core name	Enrichment	Geometry R*H (cm)	βeff (pcm)	Experimental period
R2	30% U	49.5*60	734 (75%:25%:0%)†	Apr. '93 - Sep. '93
Zona2	25% Pu	52.5*60	343 (2%:48%:42%)	Dec. '93 - Mar. '94
Compact	11% Pu	79.6*60	402 (5%:59%:32%)	postponed

† Nuclide contribution to βeff: (U-235 : U-238 : Pu-239)

Table 2 Major characteristics of the BERNICE-FCA

Core name	Enrichment	Geometry R*H (cm)	βeff (pcm)	Experimental period
XIX-1	93% U	33*51	756 (95%:5%:0%)	Jan. '96 - Apr. '96
XIX-2	22% Pu	36*61	364 (11%:45%:42%)	Jul. '96 - Oct. '96
XIX-3	92% Pu fiss.	33*61	246 (8%:9%:80%)	Jul. '97 - Oct. '97

† Nuclide contribution to βeff: (U-235 : U-238 : Pu-239)
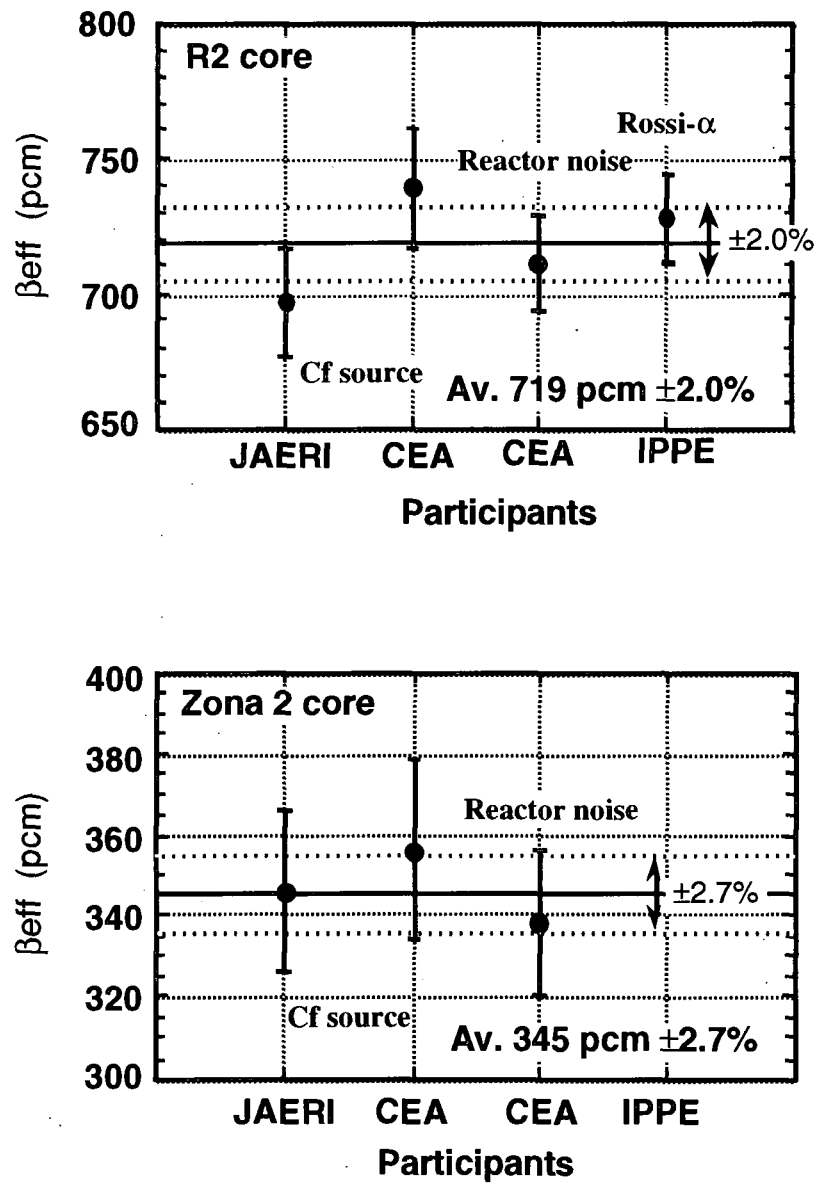
Fig. 1 Experimental results of βeff in the BERNICE-MASURCA
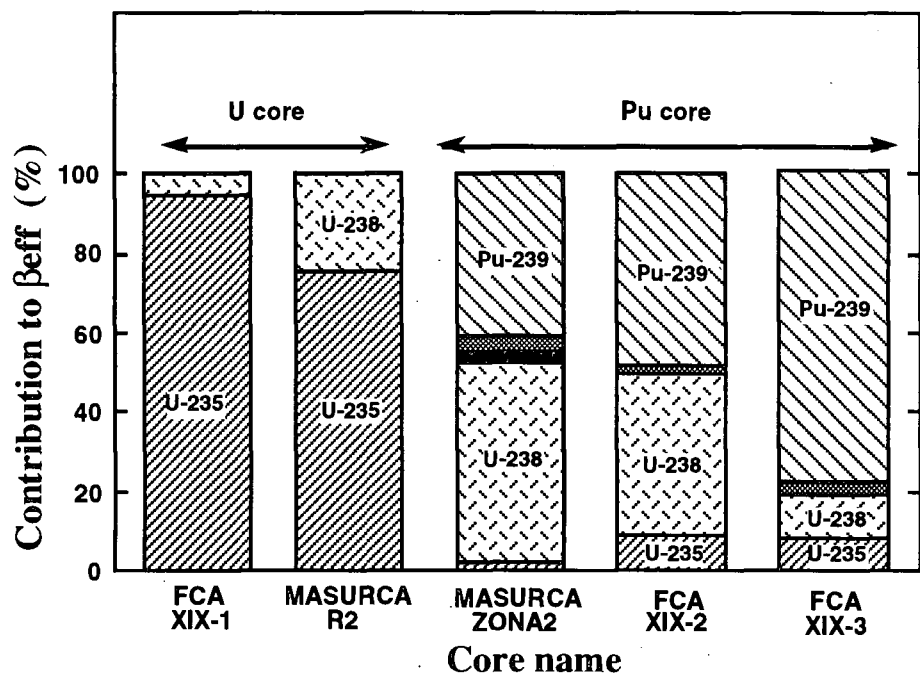
Fig. 2 Nuclide contribution to βeff for BERNICE program
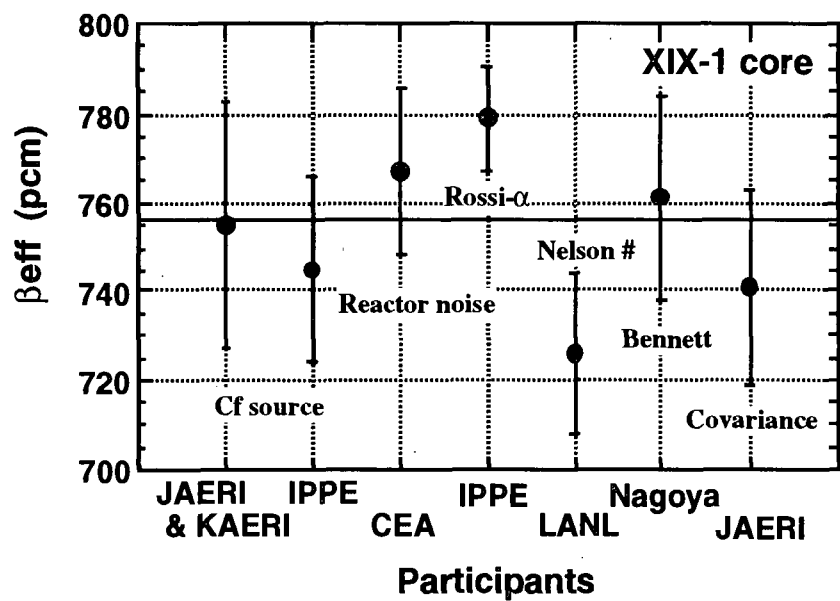
Fig. 3 Preliminary results of βeff in the BERNICE-FCA

2.3.2

Review of Experimental Methods for Evaluating Effective Delayed Neutron Fraction

Yoshihiro Yamane

Nuclear Engineering, School of Engineering, Nagoya University

Furoh-cho, Chikusa-ku, Nagoya 464-01

e-mail:yamane@mail.nucl.nagoya-u.ac.jp

The International Effective Delayed Neutron Fraction β eff Benchmark Experiments have been carried out at the Fast Critical Assembly of Japan Atomic Energy Research Institute since 1995. Researchers from six countries, namely France, Italy, Russia, U.S.A., Korea, and Japan, participate in this FCA project. Each team makes use of each experimental method, such as Frequency Method, Rossi-α Method, Nelson Number Method, Cf Neutron Source Method, and Covariance Method. In this report these experimental methods are reviewed.

1. Introduction

Since 1995, the International Effective Delayed Neutron Fraction β eff Benchmark Experiments have been carried out at the Fast Critical Assembly of Japan Atomic Energy Research Institute. This project took over the similar international project by using MASURCA facility at Cadarache. Researchers from France, Italy, Russia, U.S.A., Korea, and Japan participate in this FCA project. Each team makes use of each experimental method measuring the β eff as follows: (1)France-Italy team(Frequency Method), (2)Russia team(Rossi-α Method), (3)U.S.A. team(Nelson Number Method), (4)FCA-Korea team(Cf Neutron Source Method), and (5)Nagoya Univ. team(Covariance Method).

2. Experimental Methods

(1) Frequency Method

France-Italy team makes use of Frequency Method, which is based on measuring cross-power-spectral-density(CPSD) between two neutron counters. This CPSD is described on the basis of the prompt neutron approximation as follows:

$$\Phi_{12}(\omega) = \varepsilon_1 \varepsilon_2 F^2 \delta(\omega) + \varepsilon_1 \varepsilon_2 F \frac{\overline{\nu_p(\nu_p - 1)}}{2\tau_f^2} \frac{1}{\alpha^2 + \omega^2} , \qquad (1)$$

where $\alpha = \frac{\beta_{eff} - \rho}{\Lambda}$ is the prompt neutron decay constant, $\tau_f = (\nu\Sigma_f)^{-1}$ is the mean fission time,

$\Lambda = (\nu\nu_p\Sigma_f)^{-1}$ is the neutron generation time, and F is fission rate.

As the frequency, ω, is less than the prompt neutron decay constant, α, the plateau value of the CPSD is represented as

$$(CPSD)_{pl} = \varepsilon_1 \varepsilon_2 F \frac{\overline{\nu_p(\nu_p - 1)}}{2\tau_f^2} \frac{1}{\alpha^2} . \qquad (2)$$

Rearranging the above equation about β_{eff}, we can obtain the following expression,

$$\beta_{eff} = \frac{D}{2 F \left(1 - \rho_s\right)^2} \frac{V_{01} V_{02}}{\left(C P S D\right)_{pl}^2} \quad , \quad (3)$$

where $V_{0i} = \varepsilon_i F$ for $i = 1,2$ is average voltage. The Diven factor, D, and subcriticality in dollar unit, ρ_s, are defined by

$$D = \overline{v_p(v_p - 1)} / \left(\overline{v_p}\right)^2 \quad , \quad (4)$$

$$\rho_s = \rho / \beta_{eff} \quad . \quad (5)$$

At critical state, namely $\rho_s = 0$, the following expression is obtained,

$$\beta_{eff} = \frac{D}{2 F} \frac{V_{01} V_{02}}{\left(C P S D\right)_{pl}^2} \quad , \quad (6)$$

Then we measure the CPSD and the average voltage of each detector output. Moreover the absolute integral of fission rate, F, is measured by using the fission foil irradiation technique, and the Diven factor is calculated. The β_{eff} is evaluated by Eq.(6).

(2) Rossi-α Method

The Russian team makes use of Rossi-α Method[1]. This method is based on the Rossi-α measurement with two neutron detectors by using time analyzer. Scan of the time analyzer starts by the pulse from the first detector, then the pulses from the second detector with a time delay τ are registered. Then a profile of neutron counts consists of a peak and a decaying part following this peak. The background counts appearing in the left side of the peak ,namely $\tau < t$, are randomly coincidence pulses. Hence this background counts, $C_b(t)$, is represented as

$$C_b(t) = \varepsilon_{ct} v Q \left\{ 1 - \frac{D v \left(1 - \beta_{eff}\right)^2}{2} \varepsilon_{st} \alpha \int_{-\infty}^{\tau} e^{-C(\tau - t')} e^{-\alpha |t - t'|} dt' \right\} \quad , \quad (7)$$

where efficiencies of the first and second detector are ε_{st} and ε_{ct}, respectively. Fission-source intensity is Q, and the counts C is equal to $\varepsilon_{st} v Q$.

Integrating the above equation over $t > \tau$, we obtain the following result for the background counts,

$$C_b(t) = \varepsilon_{ct} v Q \left\{ 1 - \frac{D v \left(1 - \beta_{eff}\right)^2}{2} \varepsilon_{st} \frac{\alpha}{\alpha + C} e^{-\alpha(t - \tau)} \right\} \quad . \quad (8)$$

This background counts consists of a constant part and a time-dependent part corresponding to a correlated part. As total amount of counts in this correlated part is defined by S, we can obtain it by means of integrating Eq.(8),

$$S\alpha = \frac{DC}{2F} \frac{\alpha}{\alpha + C} \frac{\left(1 - \beta_{eff}\right)^2}{\left(1 - \rho_s\right)^2} \frac{\alpha}{\beta_{eff}^2} \quad . \quad (9)$$

The final expression can be derived by rearranging Eq.(9) about β_{eff},

$$\beta_{eff} = \left\{ 1 + \left(1 + \rho_s\right) \sqrt{\frac{2 F S \Delta t}{ND} \frac{\alpha + C}{\alpha}} \right\}^{-1} \quad , \quad (10)$$

where F denotes total integral of fission rate, and average counts per a channel is N. When a channel

width is Δt, the count rate of trigger pulse, C, is equal to $N/\Delta t$.

Various quantities S,N,C,α can be determined by the Rossi-α experiment, and the subcriticality $\rho_{\$}$ is measured. Then we measure the total integral of fission rate, F, and calculate the Diven factor, based on the same procedure as Frequency Method. Then we can estimate the β_{eff} by Eq.(10).

(3) Nelson Number Method

Nelson Number Method was proposed by G.D. Spriggs at 1993[2]. This is based on measuring the Nelson Number which is defined by the α-value and the amplitudes of the correlation and non-correlation part of the Rossi-α decay curve. As U.S.A. team, Spriggs joins in the FCA project by himself.

The probability P(t), which means that a count occurs at the time t after a count occurred at t=0, is represented as

$$P(t) = Ae^{\alpha t} + C \ . \qquad (11)$$

Here a correlation amplitude, A, is represented as

$$A = \varepsilon_c \overline{v_p} \left(\frac{D_s D}{2l}\right) \frac{K}{1-K} \quad , \qquad (12)$$

where K is prompt neutron maltiplication factor, which is equal to $\left(1-\beta_{eff}\right)k_{eff}$, and detector efficiency is ε_c , neutron life time is l, and spatial correction factor is D_s.

The first term is the correlation term and the second is non-correlation term. This non-correlation term can be given by the neutron multiplication method as follows:

$$C = \frac{D_s^* \varepsilon_c S}{1-\dfrac{K}{1-\beta_{eff}}} \qquad , \qquad (13)$$

where S is the strength of fixed neutron source, D_s* is spatial correction factor for this source.

Here Nelson Number is defined by

$$N = -\frac{2D_s^* S}{D_s D \overline{v_p}} \frac{A}{\alpha C} \quad . \qquad (14)$$

Substituting the expressions of A,C and α, and using the reactivity in dollar unit, we can easily get the following equation,

$$N = -\frac{\left\{\left(1-\beta_{eff}\right)-K\right\}K}{\left(1-\beta_{eff}\right)\left(1-K\right)^2} = \frac{1-\beta_{eff}}{\beta_{eff}} \frac{\rho_{\$}}{\left(1-\rho_{\$}\right)^2} \quad . \qquad (15)$$

The final expression is obtained by rearranging about β_{eff} ,

$$\beta_{eff} = \frac{-\rho_{\$}}{N\left(1-\rho_{\$}\right)^2 - \rho_{\$}} = \frac{\alpha_0/\alpha - \left(\alpha_0/\alpha\right)^2}{N + \alpha_0/\alpha - \left(\alpha_0/\alpha\right)^2} \quad . \qquad (16)$$

The second expression is derived by the following relationship between subcriticality and prompt neutron decay constant,

$$\rho_{\$} = 1 - \alpha/\alpha_0 \quad , \qquad (17)$$

where the decay constant at critical is denoted by α_0.

The quantities A,C and α are determined by the Rossi-α experiments at various subcritical states. Subcrirticalities are estimated by the decay constant α and α_0. Strength of the fixed neutron source is measured. The Diven factor and spatial correction factor are calculated by using neutron flux and adjoint flux.

(4) Cf Neutron Source Method

This method was proposed by Fischer at 1977[3]. The FCA of JAERI and Korea team use this method. This is based on measuring an apparent reactivity change by introducing a Cf neutron source into the system investigated.

A steady state hold by an inherent neutron source is represented by the following equation, when one-group diffusion theory is assumed for simplicity.

$$D\nabla^2 \phi(r) + \nu\Sigma_f \phi(r) - \Sigma_a \phi(r) + S_i(r) = 0 . \qquad (18)$$

Here the effective multiplication factor is defined by

$$k_{eff} = \frac{\mathrm{Pr}\,oduction}{Disappearance} = \frac{<\nu\Sigma_f \phi>}{-<D\nabla^2\phi> + <\Sigma_a\phi>} , \qquad (19)$$

and reactivity is defined as

$$\rho = \frac{k_{eff} - 1}{k_{eff}} = -\frac{<S_i>}{<\nu\Sigma_f \phi>} . \qquad (20)$$

Reactivity ρ' due to an insertion of a point ^{252}Cf neutron source, S_{cf}, on the other hand, is represented as

$$\rho' = -\frac{<S_i> + S_{cf}}{<\nu\Sigma_f \phi>} . \qquad (21)$$

Moreover we defined an apparent reactivity change, $\delta\rho$, due to the ^{252}Cf source insertion,

$$\delta\rho = \rho - \rho' = \frac{S_{cf}}{<\nu\Sigma_f \phi>} . \qquad (22)$$

Then the apparent reactivity change in dollar unit is

$$\beta_{eff}\delta\rho_{\$} = \frac{S_{cf}}{\nu R_f F} . \qquad (23)$$

We use the following notations. The fission rate of core material at the core center is $R_f = \Sigma_f \phi(0)$, and the total fission integral is $F = <\Sigma_f \phi(r)> / R_f$.

The following multigroup version can be derived by taking account of the difference between fission spectrum of ^{252}Cf spontaneous fission and core material fission by using importance ratio, Φ^+_{Cf} / Φ^+_f,

$$\beta_{eff} = \frac{S_{cf}}{\delta\rho_{\$} R_f F \overline{\nu}} \frac{\Phi^+_{Cf}}{\Phi^+_f} . \qquad (24)$$

Apparent reactivity change can be evaluated as the control rod worth to adjust the reactor power with ^{252}Cf to one without ^{252}Cf neutron source. Absolute fission rate averaged in the cell is measured by fission foil. Other quantities, ν,F and the importance ratio are calculated. The characteristics of this method is that the absolute strength of ^{252}Cf source is needed in addition to the absolute fission integral.

(5) Covariance Method

This method was proposed by E.F.Bennett at 1981[4]. Nagoya University team makes use of this

method. This is based on measuring the covariance of neutron counts between two neutron detectors. Then this method is regarded as the time-region version of the Frequency Method.

The m-th sample of neutron counts accumulated during the time interval τ with detector #1 is represented by

$$C^{(i)}{}_m(\tau) = \int\limits_{(m-1)\tau}^{m\tau} v^{(i)}(t)dt \quad . \qquad (25)$$

A local fluctuation $\delta u^{(i)}{}_m(\tau)$ is defined by using three sequential samples, namely m-1,m and m+1 as follows:

$$\delta u^{(i)}{}_m(t) = \frac{C^{(i)}{}_m(\tau) - (1/2)\left\{C^{(i)}{}_{m-1}(\tau) + C^{(i)}{}_{m+1}(\tau)\right\}}{< C^{(i)}(\tau) >} \quad , \qquad (26)$$

where $<C^{(i)}(\tau)>$ is average counts.
A covariance between two detectors is defined as follows:

$$\sigma^2{}_{12} = \frac{1}{M-2}\sum_{m=2}^{M-1}\left\{\delta u^{(1)}{}_m(\tau)\cdot\delta u^{(2)}{}_m(\tau)\right\} \quad . \qquad (27)$$

Assuming the symmetry of detector, the covariance defined by Eq.(27) can be represented by three kinds of covariance[5], such as covariance within the same gate, $< C^{(1)}{}_0 C^{(2)}{}_0 >$, covariance between two adjacent gates, $< C^{(1)}{}_{-1} C^{(2)}{}_0 >$, and covariance between two gates apart by one gate, $< C^{(1)}{}_{-1} C^{(2)}{}_{+1} >$. Then the following expression is derived

$$\sigma^2{}_{12} = \frac{1}{4 < C^{(1)} >< C^{(2)} >}\left\{6 < C^{(1)}{}_0 C^{(2)}{}_0 > -8 < C^{(1)}{}_{-1} C^{(2)}{}_0 > +2 < C^{(1)}{}_{-1} C^{(2)}{}_{+1} >\right\} \quad . \qquad (28)$$

To derive three kinds of covariance, we use the compound detection probability, which means that a neutron count occurs at t_2 by detector #j after a neutron count occurring at t_1 by detector #i,

$$P_{ij}(t_1,t_2)dt_1 dt_2 = \varepsilon_i \varepsilon_j \left\{F^2 + F\frac{\overline{v_p(v_p-1)}}{2\tau_f{}^2\alpha}e^{-\alpha(t_2-t_1)}\right\}dt_1 dt_2 \quad , \qquad (29)$$

where the detection efficiency per total fission is ε_i, and the average fission time is $\tau_f = (v \Sigma_f)^{-1}$. By using this compound detection probability, the final expression is obtained as follows:

$$\sigma^2{}_{12}(\tau) = \frac{DD_s}{F\left(\dfrac{\beta_{\mathit{eff}}}{1-\beta_{\mathit{eff}}}\right)^2(1+\rho_s)^2\tau}\left\{\frac{3}{2} - \frac{5-15/2e^{-\alpha\tau}+3e^{-2\alpha\tau}-1/2e^{-3\alpha\tau}}{2\alpha\tau}\right\} \quad , \qquad (30)$$

where total fission rate is F, and spatial correction factor is D_s.

Counts during the time interval τ are registered with two detectors. Covariance for various time intervals are measured. These data are fitted to the Eq.(30) to evaluate the correlation amplitude. An absolute fission rate at the specific position in the core is measured. Total fission rate integrated over the whole core is calculated. This value is normalized by the above absolute value. Subcriticality in the dollar unit is determined by using the calibrated control rod worth. The Diven factor and spatial correction factor are calculated. Then we can estimate β_{eff} by the correlation amplitude of Eq.(30).

3. Summary

The characteristics of these methods are summarized in Table. Characteristics of the experimental method for evaluating the effective beta is to need both experimental and calculated

values. Absolute values of fission integral and strength of ^{252}Cf neutron source are needed. The accuracy shown in this Table is cited from Ref.[6,7]. At this time, the accuracy of these methods except for Covariance Method attained to less than 3%. But, the way of evaluating the Diven factor and its value are important, especially in the multiple fissile system, because this calculation depends directly on nuclear data to calculate neutron flux and adjoint flux.

Table Summary of Experimental Methods

Method	Measurement	Calculation	Accuracy
(1) Frequency	(CPSD)$_{pl}$, Average voltage (V$_{01}$,V$_{02}$), ρ_s=0, Fission rate F (Absolute)	Diven factor	2.6% (*)
(2) Rossi-α	Total counts S, Average count N, α, ρ_s, Trigger rate C, Fission rate F(Absolute)	Diven factor	2.2% (*)
(3) Nelson number	Correlation amplitude A, Background C, α, α_0, Source strength S (Absolute)	Diven factor, Spatial correction	2.5% (**)
(4) Cf source	Apparent reactivity $\delta\rho_s$, Fission rate R$_f$, Source strength S$_{cf}$(Absolute)	Fission integral F, Importance ratio $\Phi_{cf}^{+}/\Phi_{f}^{+}$	2.6%(*)
(5) Covariance	Covariance $\sigma^2_{12}(\tau)$, ρ_s Fission rate F (Absolute)	Diven factor, Fission integral F, Spatial correction	4.0%

(*) P.Bertrand, et al., PHYSOR'96, E-190 (1996).   (**) G.D.Spriggs, et al., LA-UR-96-2032 (1996).

References

[1] V.A.Dulin and G.M.Mikhailov: Atomic Energy,78,147(1995).

[2] G.D.Spriggs: Nucl.Sci.Eng.,113,161(1993).

[3] E.F.Fischer: Nucl.Sci.Eng., 62,105(1977).

[4] E.F.Bennett: "An Experimental Method for Reactor-Noise Measurements of Effective Beta,"ANL-81-72, Argonne National Laboratory (1981).

[5] Yamane Y. and Takemoto Y.: J. of the Atomic Energy Society of Japan,38,1001(1996)(in Japanese).

[6] P.Bertrand, et al., "BERENICE-Inter Laboratory Comparison of β eff Measurement Techniques at MASURCA," Proc. Int. Conf. on Physics of Reactors, PHYSOR96, Sept.16-20, Mito, Japan, p.E-190(1996).

[7] G.D.Spriggs, Sakurai T. and Okajima S.: "Rossi-α and β eff Measurements in the Japanese Atomic Energy Research Institute's FCA XIX-1 Assembly," LA-UR-96-2032, Los Alamos National Laboratory (1996).

2.3.3 Delayed Neutron Spectra and their Uncertainties in Fission Product Summation Calculations

T. Miyazono, M. Sagisaka, H. Ohta, K. Oyamatsu and M. Tamaki

Department of Energy Engineering and Science, Nagoya University

Furo-cho, Chikusa-ku, Nagoya 464-01

e-mail: toshi@luna.nucl.nagoya-u.ac.jp

Uncertainties in delayed neutron summation calculations are evaluated with ENDF/B-VI for 50 fissioning systems. As the first step, uncertainty calculations are performed for the aggregate delayed neutron activity with the same approximate method as proposed previously for the decay heat uncertainty analyses. Typical uncertainty values are about 6~14% for ^{238}U(F) and about 13~23% for ^{243}Am(F) at cooling times 0.1~100 (s). These values are typically 2~3 times larger than those in decay heat at the same cooling times. For aggregate delayed neutron spectra, the uncertainties would be larger than those for the delayed neutron activity because much more information about the nuclear structure is still necessary.

1. INTRODUCTION

It is well known that the kinetic behavior of any fission reactors is determined largely by the delayed neutron properties although these neutrons comprise only ~1% of total neutrons released after fission. The summation method has several advantages for the delayed neutron calculations. The primary advantage is that a single set of precursor decay data (emission probabilities, decay constants and spectra) can be used to predict delayed neutron yields at arbitrary cooling times for any fissioning system provided that fission yields are available. As for integral measurements of the delayed neutrons, there are evaluations of experimental delayed neutron yields by Tuttle [1][2], measurements for spectra at the University of Lowell [3], etc. However, these properties has been measured only for limited fissioning systems such as U and Pu at limited cooling times.

In the future, delayed neutron properties for minor actinide fissioning systems such as Am and Cm isotopes will be of greater importance in connection with transmutations. However measurements are still not adequate for these fissioning systems because of difficulties in obtaining isotopically pure samples as is also the case with decay heat measurements for these systems. For more precise prediction of the fission product properties, it is important to evaluate and reduce uncertainties in summation calculations.

2. DELAYED NEUTRON SUMMATION CALCULATION

The summation method simulates an actual mechanism of decay heat generations and delayed neutron emissions. The fission product properties are given by summing up the individual fission

product contributions. The decay heat power $P(t)$ and the delayed neutron activity $n_d(t)$ at cooling time t after a burst fission is given as

$$P(t) = \sum_{i=1}^{\text{all FP's}} E_i \lambda_i N_i(t),$$

(1)

and

$$n_d(t) = \sum_{i=1}^{\text{all FP's}} b_{i \to d.n.} \lambda_i N_i(t)$$

(2)

where E_i, λ_i, $b_{i \to d.n.}$ and $N_i(t)$ are the average decay energy, the decay constant, the delayed neutron emission probability and the number of atoms of nuclide i. Noted that E_i in Eq. (1) is simply replaced by $b_{i \to d.n.}$ in Eq. (2). The value of $N_i(t)$ are obtained by solving about 900 simultaneous liner differential equations for production and decay of fission product nuclides:

$$\frac{dN_i(t)}{dt} = -\lambda_i N_i(t) + \sum_j b_{j \to i} \lambda_j N_j(t),$$

(3 a)

with

$$N_i(0) = y_i,$$

(3 b)

where $b_{j \to i}$ and y_i are the production rate of nuclide i from a decay of nuclide j and the independent fission yield of nuclide i. Practically, we compute $N_i(t)$ using FPGS90N-code [4] in Bateman's method. The calculation with this code is referred to as the '*exact calculation*' in the following.

3. APPROXIMATION

In delayed neutron summation calculations, it has often been assumed

$$N_i(t) \approx Y_i \exp(-\lambda_i t)$$

(4)

where Y_i is the cumulative yield of nuclide i. However, as shown in Fig. 1, this approximation, referred to as the '*one nuclide approximation*', has errors of about 5% compared with the exact method (FPGS90N-code). Since the uncertainty evaluation based on the exact method requires very complicated calculations, we adopt the '*three nuclide approximation*' which was used previously for our decay heat uncertainty analyses [5]. In this approximation, $N_i(t)$ is assumed to be determined only by the decay of itself i, its parent $i-1$(*mother of i*) and her parent $i-2$(*grandmother of i*) as shown in Fig. 2. From Fig. 1, we see that the 3 nuclide approximation is excellent at the whole cooling time (10^{-1} ~ 10^3 s).

4. UNCERTAINTY CALCULATION

We examine uncertainties in summation calculations for delayed neutron properties based on the law of error propagation. As the first step, uncertainty calculations are performed for aggregate delayed neutron activity (as a function of the cooling time), which can be done in the same way as those for the decay heat [5].

$$\left(\delta n_d(t)\right)^2 = \sum_{i=1}^{\text{all FP}} \left\{ \left(\frac{\partial n_d}{\partial b_{i \to d.n.}}\right)^2 \left(\delta b_{i \to d.n.}\right)^2 + \left(\frac{\partial n_d}{\partial \lambda_i}\right)^2 \left(\delta \lambda_i\right)^2 + \left(\frac{\partial n_d}{\partial y_i}\right)^2 \left(\delta y_i\right)^2 + \left(\frac{\partial n_d}{\partial Y_i}\right)^2 \left(\delta Y_i\right)^2 \right\}$$

(5)

Here, the symbol δX denotes the uncertainty of each parameter X. In this calculation, we use values of

nuclear data ($b_{i \to d.n.}$, λ_i, y_i and Y_i) and their uncertainty data ($\delta b_{i \to d.n.}$, $\delta\lambda_i$, δy_i and δY_i) in ENDF/B-VI. As for the uncertainty values which are not available in ENDF/B-VI equal to themselves, we assume

$$\delta b_{i \to d.n.} = b_{i \to d.n.}, \qquad \delta\lambda_i = \lambda_i \qquad\qquad (6)$$

because the estimated values of decay constant may be too large or too small by an order of magnitude in any theories or systematics. As for independent fission yields, the correlation effects among their values are also taken into account in the same way as in Ref. [5].

5. RESULTS and DISCUSSIONS

Uncertainties in the aggregate delayed neutron activity are calculated for 50 fissioning systems in ENDF/B-VI. The results are shown in Figs. 3 and 4 for typical fissioning systems. In Table 1, we also list uncertainties both in delayed neutron activity and in decay heat at the same cooling times 0.1~100 (s). From these figures and the table,

    (a)   The uncertainties for Np, Am and Cm isotopes are typically 2~3 times larger than those for ^{235}U, ^{238}U and ^{239}Pu because of large uncertainties in fission yields for the minor actinides.

    (b)   The uncertainties in the delayed neutron activity are typically 2~3 times larger than those in decay heat at the cooling times 0.1~100 (s) because of large uncertainties in fission yields and decay data of precursors which are the most unstable of all fission products.

From our uncertainty evaluation, we are able to show the calculated activity with error bars as shown in Fig. 5. As for ^{235}U(T) and ^{239}Pu(T), there are, at some cooling times, significant disagreements between the calculated results and Tuttle's recommendation values beyond error bars while the result for ^{238}U(F) is in fair agreement with Tuttle's.

Here, we note that the uncertainties for ^{235}U(T) in Fig. 3 are remarkably large at cooling times shorter than 1 (s). In the following, we discuss this peculiar behavior in some detail. Figure 6 depicts uncertainties in delayed neutron activity without taking correlation effects among independent yields for simplicity. Table 2 shows the identified nuclides and their nuclear data which are responsible for the uncertainties. From this table, the decay constant and emission probability for ^{86}Ge should be responsible for the large uncertainties at these cooling times. However, the uncertainties for ^{238}U(F) and ^{239}Pu(T) calculated with the same decay data are not so large as that for ^{235}U(T). Then, how about the independent yield of ^{86}Ge for these fissioning systems? Figure 7 shows independent yields of nuclides with mass number 86 for ^{235}U(T), ^{235}U(F) and ^{235}U(H). From this figure, we see that the yield of ^{86}Ge for ^{235}U(T) is distinctly doubtful. Therefore we conclude that the large uncertainties for only ^{235}U(T) are mainly due to the too large value of independent yield of ^{86}Ge. The wrong prediction in Table 2 stems from the fact that our analysis is based on the first order perturbation theory (Eq. (5)). We also remark that as in this example for delayed neutron calculations there may still exist some other data which are too erroneous to use Eq. (5) in uncertainty analyses.

6. CONCLUSION

We examine uncertainties in summation calculations for delayed neutron properties. As the first step, uncertainty calculations are performed for aggregate delayed neutron activity. Typical

uncertainty values are about 6~14% for ^{238}U(F) and about 13~23% for ^{243}Am(F) at cooling times 0.1~100 (s). These values are 2~3 times larger than those for decay heat calculations. The uncertainties in aggregate delayed neutron spectrum calculations would be larger than those in delayed neutron activity because much more information about the nuclear structure is still necessary. Therefore more precise values for both decay and yield data are still necessary for summation calculations to achieve the precision in integral measurements. We hope that our results can feed back much information to experimentalists of nuclear data.

REFERENCES

[1] Tuttle R. J.: Nucl. Sci. and Eng., **56**, 37-71(1975)

[2] Tuttle R. J.: *Proc. Consultants' Mtg. Delayed Neutron Properties*, INDC-NDS-107/G+Special, 29(1979).

[3] Tanczyn R. S., et al.: Nucl. Sci. and Eng., **94**, 353-364(1986)

[4] Ihara H., Katakura J. and Nakagawa T.: "A Computer Code for calculation of Radioactive Nuclide Generation and Depletion, Decay Heat and γ Ray Spectrum -FPGS90-", JAERI-Data/Code 95-014 (1995).

[5] Ohta H., Oyamatsu K. and Tasaka K.: JAERI-Conf 96-008 , 290-295(1996).
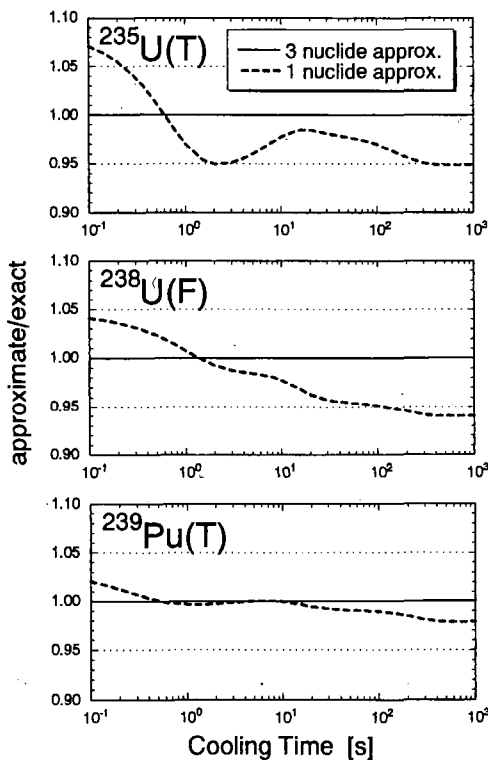
Fig. 1 The ratio of delayed neutron activity calculated with the approximate method to that with the exact one.
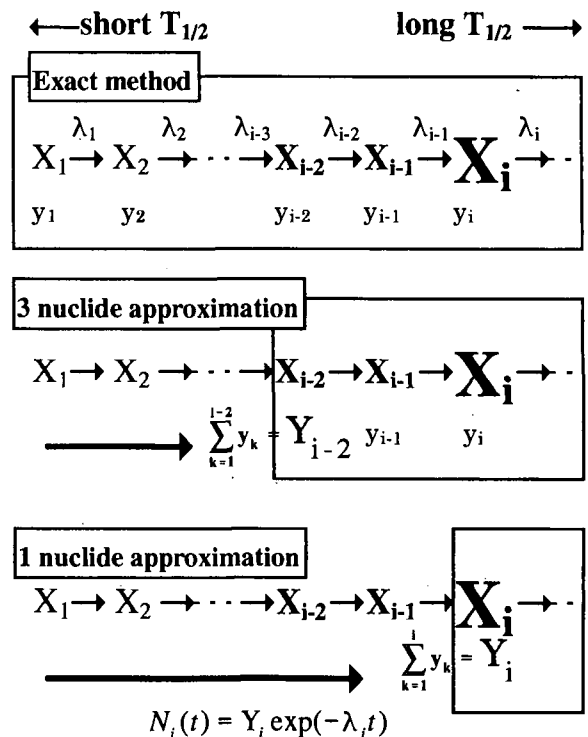
Fig. 2   Approximate summation method.
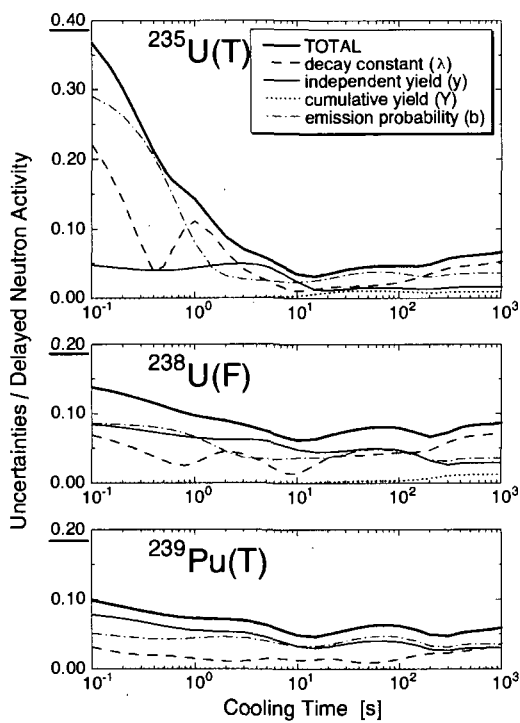
Fig. 3 Uncertainties in delayed neutron activity for ^{235}U(T), ^{238}U(F) and ^{239}Pu(T).
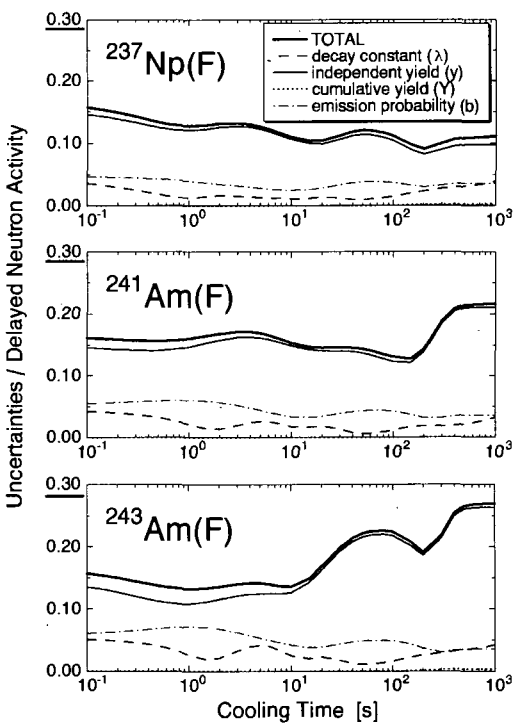
Fig. 4 Uncertainties in delayed neutron activity for ^{237}Np(F), ^{241}Am(F) and ^{243}Am(F).

Table 1 Uncertainties in summation calculations for several fissioning systems at cooling times 0.1~100[s]

Fissioning Systems	delayed neutron activity [%]	(β+γ) decay heat [%]
^{235}U(T)	3~37	2~7
^{238}U(F)	6~14	3~6
^{239}Pu(T)	5~10	3~7
^{239}Pu(F)	10~16	3~8
^{237}Np(F)	10~16	3~7
^{241}Am(F)	13~17	4~8
^{243}Am(F)	13~23	4~8
^{244}Cm(F)	15~24	4~8
^{246}Cm(F)	13~20	4~8
^{248}Cm(F)	11~17	4~8
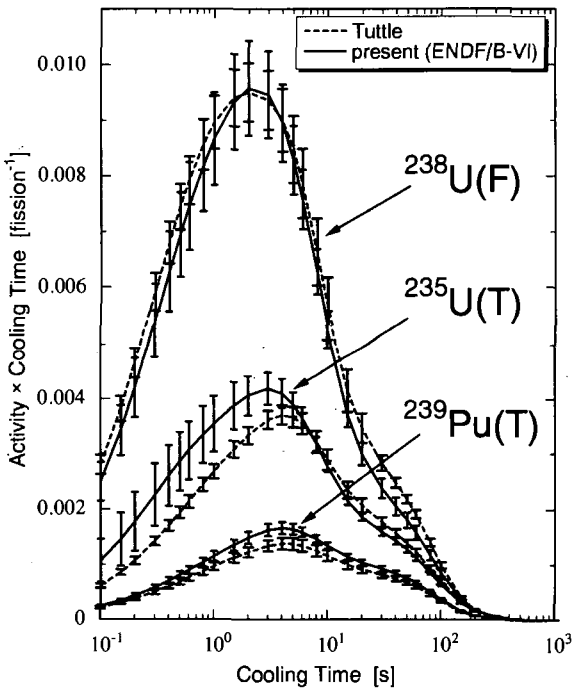
Fig. 5 Delayed neutron activity after a burst fission.
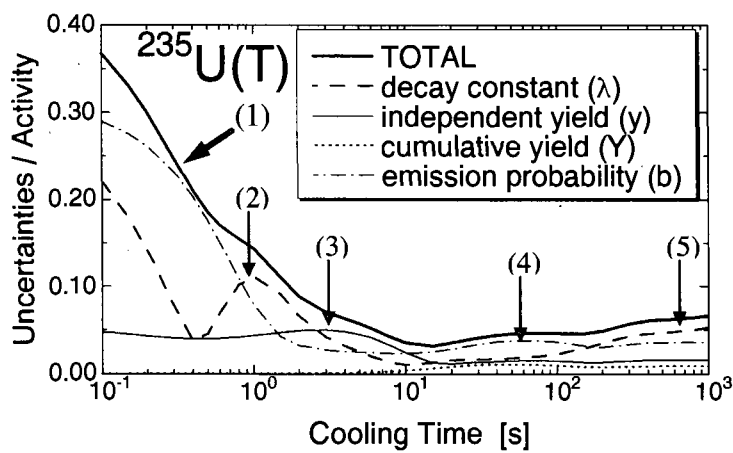
Fig. 6   Uncertainties in delayed neutron activity without
taking correlation effects into account.

Table 2 The main causal nuclides for large uncertainties
in delayed neutron activity for ^{235}U(T).

No.	t [s]	Parameter	Nuclide	Ratio [%]	δX/X [%]
(1)	**0~1**	Independent Yield	^{86}Ge	30	16
			^{88}As	52	64
		Decay Constant	**^{86}Ge**	**87**	100*
		Emission Probability	**^{86}Ge**	**87**	100*
(2)	1	Decay Constant	^{86}Ge	94	100*
(3)	1~10	Independent Yield	^{85}As	68	64
			^{86}Ge	22	16
(4)	~10^2	Emission Probability	^{137}I	85	5.97
(5)	10^3	Decay Constant	^{87}Se	74	100*
			^{87}Br	26	0.23
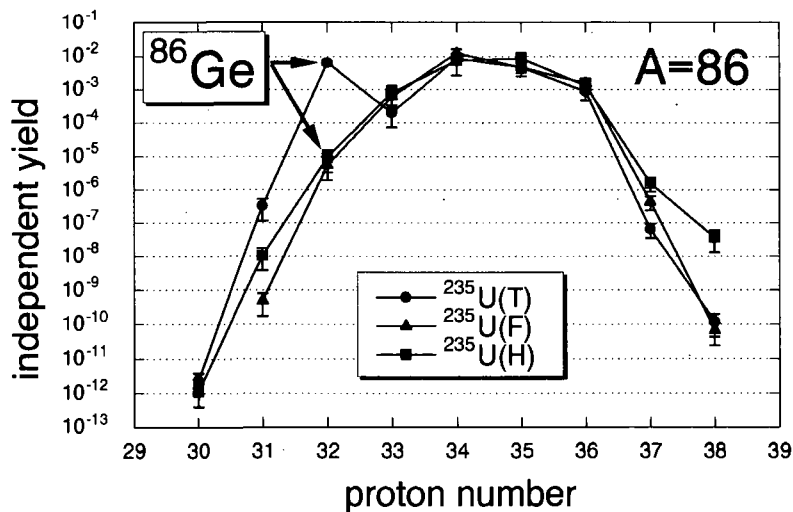
Fig. 7   Independent yields for ^{235}U(T, F, H).

2.4 Topics 3: New Experiments

2.4.1 Status and Future Plan of Measurements by RIKEN Accelerator Facility

I. Tanihata

Accelerator Facility

The Institute of Physical and Chemical Research, RIKEN,

2-1 Hirosawa, Wako, Saitama 351-01 Japan

Abstract

The RI beam creator has been developed and many kinds of research by using this facility are under going in RIKEN. In this presentation, some of topics from above research will be explained, especially for recent creation of new isotopes, and for mechanism of neutron skin and halo of neutron rich nuclei.

2.4.2 Simultaneous Measurement of Fission Fragments and Prompt Neutrons for Thermal Neutron-induced Fission of U-235

Katsuhisa NISHIO [1], Hideki YAMAMOTO [1], Itsuro KIMURA [1] and Yoshihiro NAKAGOME [2]

1. *Department of Nuclear Engineering, Kyoto University*
   Yoshida, Sakyo-ku, Kyoto 606-01, Japan
2. *Research Reactor Institute, Kyoto University*
   Kumatori-cho, Sennan-gun, Osaka 590-04, Japan

Simultaneous measurement of fission fragments and prompt neutrons following the thermal neutron induced fission of U-235 has been performed in order to obtain the neutron multiplicity (ν) and its emission energy (η) against the specified mass (m^*) and the total kinetic energy (TKE). The obtained value of $-d\nu/dTKE(m^*)$ showed a saw-tooth distribution. The average neutron energy $<\eta>(m^*)$ had a distribution with a reflection symmetry around the half mass division. The measurement also gave the level density parameters of the specified fragment, $a(m^*)$, and this parameters showed a saw-tooth trend too. The analysis by a phenomenological description of this parameters including the shell and collective effects suggested the existence of a collective motion of the fission fragments.

1. Introduction

The energy which is equivalent to the Q-value of a nuclear fission reaction is converted into the TKE and the excitation energies (E_{ex}) of two fission fragments. The former value is assumed to be equal to the Coulomb potential at the scission point, and the latter reflects the deformation energy of the fragment at this point. Therefore, the simultaneous measurement of TKE and E_{ex} gives an important information to understand the fission process. Since most of E_{ex} is dissipated by the prompt neutrons, we can estimate it by measuring the ν and η. These values for ^{252}Cf(sf) [1][2] can be available now with good statistical accuracy. On the other hand, those for thermal neutron induced fissions are still not satisfactory for detailed discussion of the fission mechanism. So we tried to determine $\nu(m^*,TKE)$ and $<\eta>(m^*)$ for ^{235}U(n_{th},f).

Nuclear level density parameter is a fundamental quantity to relate the nuclear temperature (T) and E_{ex} of a nucleus. The a of fission fragments following ^{235}U(n_{th},f) were determined with the similar measurement to Jørgensen *et al.* [2]. The advantages of this method is that : (1) giving the absolute value, (2) obtaining the a for the neutron-rich nuclei, and (3) covering the data of wide-mass range by one measurement. We also remarked the shell and collective effects of the fragment from the analysis by using the phenomenological expression by Iljinov *et al.* [3].

2. Experimental method

The experiment was carried out by using the neutrons from the Kyoto University Reactor. The experimental layout with electronic circuits is shown in Fig. 1. At the exit of the super-mirror neutron guide tube, a vacuum fission chamber made of aluminum, in which a ^{235}U target and two fission fragment detectors were mounted, was positioned.

An uranium target with 99.9 % enriched ^{235}U was made by the electrodeposition of $UO_2(NO_3)_2$ on a nickel foil of 90 μg/cm^2. The target thickness was 140 μg^{235}U/cm^2.

The kinetic energy of the fragment 1 (FF1) was obtained with a silicon surface barrier detector (SSBD). Another fragment (FF2) was detected by a parallel plate avalanche counter (PPAC) with an active diameter of 22.0 cm, and the energy was determined by the time difference between the signals of the SSBD and the PPAC. The PPAC was designed so as to determine the incident position of FF2, by which the fragment flight direction (θ) was determined. The maximum acceptable angle of the fragment was determined by the diameter of the PPAC, and it became 19°. The details about the structure and the characteristics of the PPAC are described elsewhere [4].

The neutron emitted from the FF1 was detected with a liquid organic scintillator (NE213) of 12.8 cm in diameter and 5.1 cm in thickness. The neutron energy was determined by the TOF method with the flight path length of 75.8 cm, for which the start signal was triggered by the pulse from the SSBD. In the present detector arrangement, the neutron emission angle from FF1 was equal to the fragment direction θ, which was used to transform the neutron energy to the value of the fragment center-of-mass system. To discriminate the neutron signals from the gamma ray signals, a pulse shape discrimination technique was applied.

Two types of coincidence events were stored in the data acquisition computer with a list mode for the off-line analysis. One is the coincidence event of two fragment, and the other is that of both fragments and the neutron. The details of the data processing are described elsewhere [4][5].

3. Experimental Results

3.1 Center-of-mass neutron energy

The obtained neutron energy spectra in the c.m. system are shown in Fig. 2. The numeral on each subfigure represents the mass number of the neutron emitter. The data points are fitted to the following Maxwell distribution and the result is shown by the solid line.

$$\phi(\eta) = const\ \eta^{1/2} \exp(-\eta / T_{eff}) \ . \tag{1}$$

Where, T_{eff} is the effective nuclear temperature. It is seen that this expression can represent the data well.

The mean value of the neutron energy $<\eta>(m^*)$ is shown in the upper part of Fig. 3. From this figure, it is found that : (1) $<\eta>(m^*)$ distributes of bell-type and is nearly symmetrical about the half mass division of the compound nucleus, and (2) the minimal energy appear around the mass of 90 u and 145 u. The shape of $<\eta>(m^*)$ for $^{235}U(n_{th},f)$ is similar to that for $^{252}Cf(sf)$ [2] as shown in the lower part of Fig. 3, especially the minimum at 145 u is clearly seen for both reactions. Although the data points for $^{233}U(n_{th},f)$

[6] scatter greatly, their shape seem to agree with the present data on the whole.

3.2 Neutron multiplicity

The average neutron multiplicity as a function of the fragment mass is shown in Fig. 4. The neutron multiplicity averaged in the light and heavy fragment groups became 1.42 and 1.01, respectively. For comparison, the data by Apalin et al. [7], Maslin et al. [8] and Boldeman et al. [9] are depicted in the same figure. The data by Apalin et al. underestimate the $<v>$ in the ranges of $80 < m^* < 90$ u and $126 < m^* < 133$ u, and overestimate it in $m^* > 145$ u. The present result shows a dent or a shoulder about 100 u and a hump about 140 u. The former structure is commonly seen for all previous works in Fig. 4. But both data of Apalin et al. and Boldeman et al. have no hump, whereas that by Maslin et al. clearly show it as well as the present.

In Fig. 5., The total neutron emission from both fragments, $<v^{tot}>$, is plotted against the TKE as well as the previous two works [8][9]. The data points are fitted to a linear function for TKE > 150 MeV, and its slope is obtained as $- dv^{tot} / dTKE = 17.1 \pm 0.3$ neutron/MeV. Below 150 MeV, the present $<v^{tot}>$ value deviate from this line drastically as well as the data by Maslin et al.

The neutron multiplicity versus TKE is plotted in Fig. 6 for the selected mass gates. The most attracting trend in this figure is the change of the slope, $-dv/dTKE$, against the mass. By fitting the data points to the linear function, the $-dv/dTKE(m^*)$ is obtained and the result is shown in Fig. 7. The curve of $-dv/dTKE(m^*)$ shows the saw-tooth structure as well as the $<v>(m^*)$. We can find the dip around 142 u which is close to the to the hump position of $<v>(m^*)$ in Fig. 4. The physical meaning of the $-dv/dTKE$ is explained by the scission point model by Terrell [10]. If we assume that two spheroidally deformed fragments are nearly touching at the scission point, the TKE value can be calculated from the charge-center distance between both fragments. The deformation energy of the fragment at this point is nearly proportional to the neutron multiplicity. Consequently, we can consider that the slope $-dv/dTKE$ is an index of the fragment deformability at the scission point. From Fig. 7., it is seen that the fragment about the mass of 105 u is very deformable or soft, whereas the complementary fragment is hard or stiff. However for the system with very asymmetric mass division, the deformability of both fragments are similar with each other.

4. Level density parameter
4.1 Derivation of level density parameter

The level density parameter, a, relates the excitation energy and the temperature of the fragment by

$$E_{ex} = a T^2 . \qquad (2)$$

As described above, the neutron spectrum in the c.m. system can be represented by the Maxwellian shape as eq. (1). Therefore, the nuclear temperature of the fragment is estimated by $T = (3/4) <\eta>$. And the excitation energy of the fragment is determined by

$$E_{ex} = <v> (<\eta> + <B_n>) + <B_n>/2 , \qquad (3)$$

where the first and the second term in the right hand side are the energy dissipated by the neutrons and the gamma rays, respectively. The neutron binding energy $<B_n>$ is determined from the mass table from Ref. [11].

The obtained $a(m^*)$ for $^{235}U(n_{th},f)$ from eqs.(2)-(3) is shown in Fig. 8 and is compared with that for $^{252}Cf(sf)$ [2]. From this figure, it is found that the $a(m^*)$ for $^{235}U(n_{th},f)$ as well as for $^{252}Cf(sf)$ shows a saw-tooth trend with the minimum value around 130 u, which reflects the strong shell effect. The values of a in the light fragment group for $^{235}U(n_{th},f)$ are slightly larger than those for $^{252}Cf(sf)$, but in the heavy group the present data lie below those for $^{252}Cf(sf)$.

4.2 Analysis and discussion

The level density of a nucleus, $\rho(E_{ex})$, is described by [3]

$$\rho(E_{ex}) = K_{rot}K_{vib} \, \rho_{int}(E_{ex}) \, , \qquad (4)$$

where K_{rot} and K_{vib} are the coefficients for rotational and vibrational enhancements of the non-collective internal nuclear level density $\rho_{int}(E_{ex})$, respectively. The $\rho_{int}(E_{ex})$ is a function of the following level density parameter [3], a.

$$a(E_{ex}, Z, N) = \tilde{a}(A) \, [\, 1 + \delta W(Z, N) f(E_{ex})/E_{ex} \,] \, , \qquad (5)$$

$$f(E_{ex}) = 1 - \exp(- \gamma E_{ex}) \, , \qquad (6)$$

$$\tilde{a}(A) = \alpha A + \beta \, . \qquad (7)$$

The $\delta W(Z, N)$ in eq. (5) is the shell-correction energy of nucleus consisting of N-neutrons and Z-protons, and is taken from Myers and Swiatecki [12]. The δW of fission fragments for $^{235}U(n_{th},f)$ are shown in Fig. 9(a). Iljinov et al. [3] determined the (α, β, γ) so as to mostly represent the $\rho(E_{ex})$ values determined from the neutron resonance measurements and others. They obtained the two sets of parameters as (0.090, - 0.040, 0.070) and (0.114, 0.098, 0.051), when the collective enhancement of the $\rho(E_{ex})$ is included ($K_{rot} \neq 1$, $K_{vib} \neq 1$) or not ($K_{rot} = K_{vib} = 1$) , respectively.

In Fig. 9(b), the $a(m^*)$ calculated by eqs.(5)-(7) is shown for the two cases. The corresponding lines in the same figure mean the asymptotes of the level density parameters, $\tilde{a}(A)$, when the excitation energies increase to infinity. It is said that (1) the saw-tooth distribution of $a(m^*)$ by experiment can be well represented by using the $\delta W(m^*)$, and (2) the fission fragments have collective motions.

5. Conclusions

We obtained the $\nu(m^*, TKE)$ for the system of $^{235}U(n_{th},f)$ with superior statistical accuracy to previous works. The obtained $-d\nu/dTKE(m^*)$, which is a good index to represent the $\nu(m^*, TKE)$, showed the saw-tooth trend. The present $<\eta>(m^*)$ showed the reflection symmetry around the half mass division, and was similar to that for $^{252}Cf(sf)$. The $a(m^*)$ for $^{235}U(n_{th},f)$ showed the saw-tooth trends with minimum value about 130 u, which is seen to be the result of the shell-effect on the fragment. The analysis of $a(m^*)$ with the model by Iljinov et al. suggested the existence of the collective motions of the fragments.

References

[1] H.R. Bowman *et al.*, Phys. Rev. C **129** (1963) 2133.

[2] C. Budtz-Jørgensen and H.-H. Knitter, Nucl. Phys. **A490** (1988) 307.

[3] A.S. Iljinov *et al.*, Nucl. Phys. **A543** (1992) 517.

[4] K. Nishio *et al.*, Nucl. Instrum. Meth. A, in press.

[5] K. Nishio *et al.*, submitted to Nucl. Phys. A.

[6] J.C.D. Milton and J.S. Fraser, in Symposium on the Physics and Chemistry of Fission, 1965 (IAEA, Vienna, 1965), Vol. 2, p. 39.

[7] V.F. Apalin *et al.*, Nucl. Phys. **71** (1965) 553.

[8] E.E. Maslin *et al.*, Phys. Rev. **164** (1967) 1520.

[9] J.W. Boldeman *et al.*, Aust. J. Phys. **24** (1971) 821.

[10] J. Terrell, Proc. IAEA Symposium on Physics and Chemistry of Fission, Salzburg 1965. Vol. 1 p. 3. Vienna 1965.

[11] P. Möller and J.R. Nix, At. Data and Nucl. Data Tables, **26** (1981) 165.

[12] W.D. Myers and W.J. Swiatecki, Ark. Phys. **36** (1967) 343.

PA   : Preamplifier

CFD : Constant-Fraction Discriminator

TAC : Time-to-Amplitude Converter

TA   : Timing Amplifier

AMP : Amplifier

PSA : Pulse Shape Analyzer

ADC : Analog-to-Digital Converter
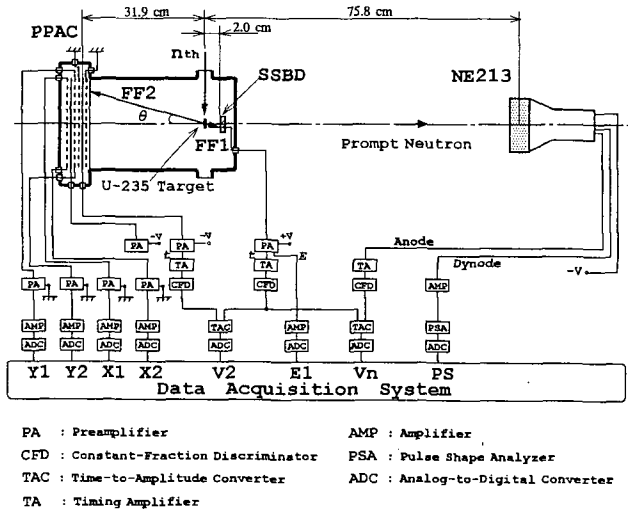
Fig.1   Experimental setup
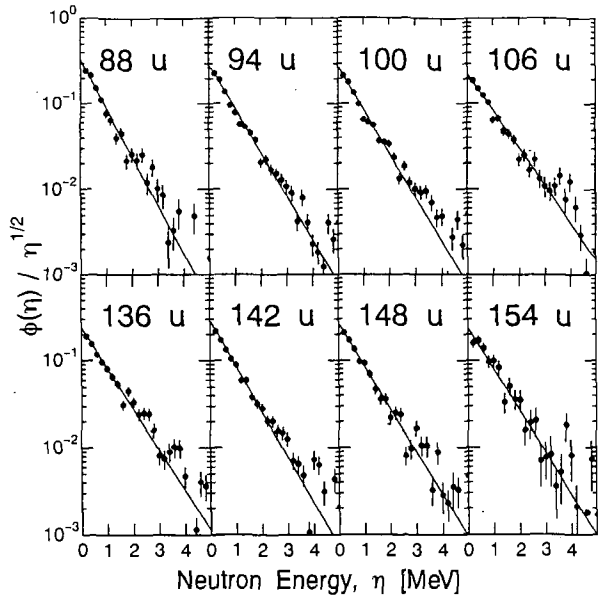
Fig.2   Neutron spectrim in the c.m. system
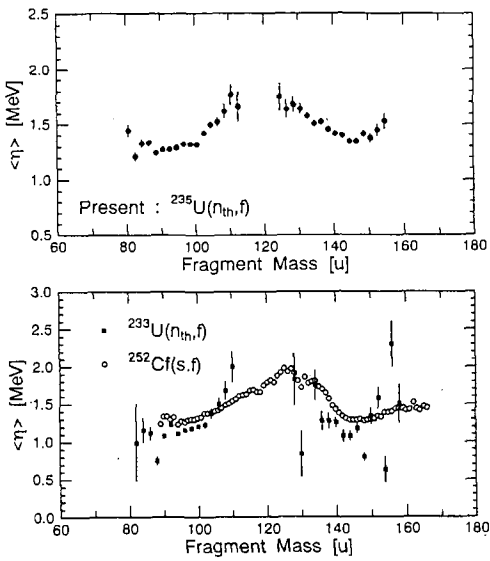
Fig.3   Average neutron energy $<\eta>(m^*)$
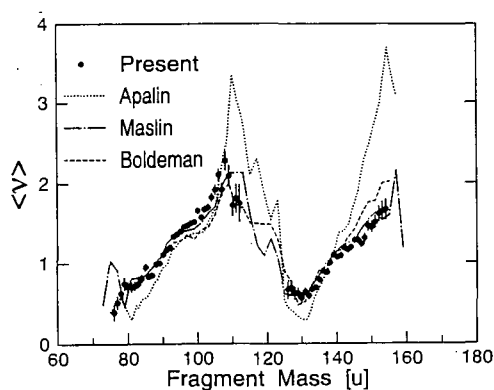
Fig.4 Average neutron multiplicity $<\nu>(m^*)$
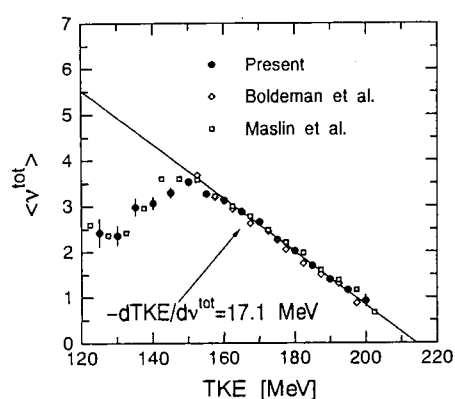
Fig.5 Total neutron multiplicity versus *TKE*
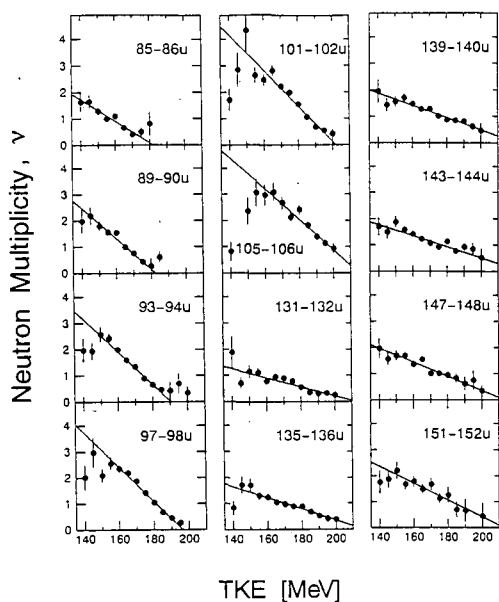
Fig.6 Neutron multiplicity versus *TKE*
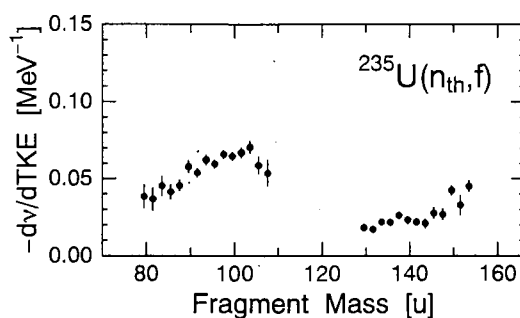
Fig.7 - dν / d*TKE*
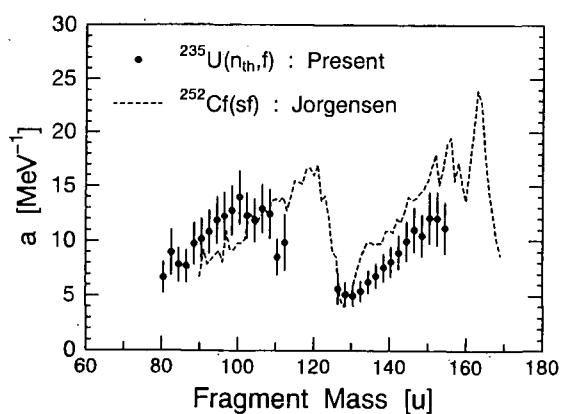
Fig.8 Level density parameter $a(m^*)$
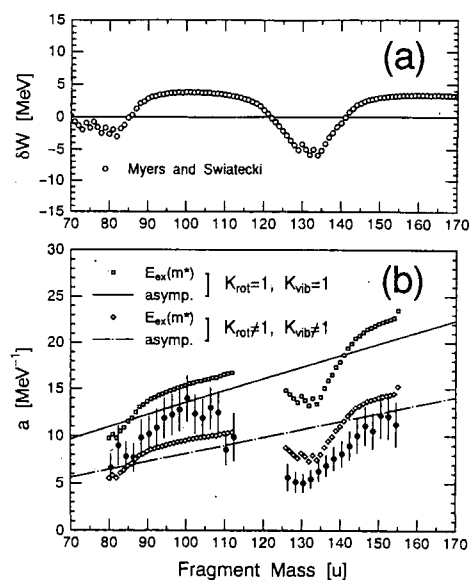
Fig.9 (a) Shell-correction energy $\delta W(m^*)$

(b) Calculation with the expression by Iljinov *et al.*

2.4.3 Calibration of a He Accumulation Fluence Monitor for Fast Reactor Dosimetry

Chikara ITO

Reactor Technology Section, Experimental Reactor Division, Oarai Engineering Center
Power Reactor and Nuclear Fuel Development Corporation
4002 Narita-cho, Oarai-machi, Ibaraki-ken 311-13 Japan
E-mail: ito@oec.pnc.go.jp

The helium accumulation fluence monitor (HAFM) has been developed for a fast reactor dosimetry. The HAFM measurement system was calibrated using He gas and He implanted samples and the measurement accuracy was confirmed to be less than 5%. Based on the preliminary irradiation test in JOYO, the measured He in the ^{10}B type HAFM agreed well with the calculated values using the JENDL-3.2 library.

1. Introduction

The He accumulation method [1] is a technique for determining the He production rate in materials by measuring their He content, which was produced mainly by (n, α) reaction. This method is suitable for measuring the neutron fluence in long-term irradiation tests and for reactor surveillance. This is due to stability of the produced He during the irradiation. The He accumulation method has also the advantage of directly measuring the He production in fast reactor stainless steels, whereas the standard foil activation method relies on the calculation of the He production rate using its cross section and the neutron spectrum.

In the He accumulation method, the accuracy of He measurements determines the overall accuracy. The HAFM measurement system was calibrated using both He gas and He implanted samples and the measurement accuracy of the system was also determined.

2. The HAFM and HAFM Measurement System

Fig. 1 illustrates the HAFM and its monitor material enclosed in a vanadium capsule to assure containment of the accumulated He. For fast reactor dosimetry B, Be, Li and Al will be used as the monitor materials.

The He accumulated inside the HAFM materials is released by melting the material and the amount is measured by means of a gas mass spectrometry. The HAFM measurement system consists of an electric furnace and a magnetic type mass spectrometer as shown in Fig. 2. This system has the capability of measuring $10^{13} \sim 10^{19}$ He atoms per sample, which covers the amount of He production with the neutron fluences in a typical fast reactor irradiation field.

3. Calibration Tests
3.1 Calibration by He Gas

In the calibration with He gas, known amounts of He were determined by the HAFM measurement system, the quantity of He is proportional to the mass spectrometer output voltage. The measurements only calibrated the mass spectrometer. As a result, the calibration curve for $10^{13} \sim 10^{15}$ atoms of He is shown as the broken line in Fig. 3, note the good linearity.

3.2 Calibration by He Implanted Samples

The calibration of the HAFM measurement system was performed by melting the He implanted samples in this system [2]. The He containing samples (Cu, Al and V chips) had been implanted with $1 \times 10^{13} \sim 3 \times 10^{15}$ He ions by using the ion source and accelerator in Kyushu University. The extent of melting in a sample was determined by the measurements of He released at various temperatures. Complete He release was assured by heating the sample above the melting point ($T_m \times 1.3$).

The relation between the quantity of He and the mass spectrometer output was shown by the solid line in Fig. 3. This calibration curve also showed good linearity. The mean deviation of the measured values indicated that the error was $\sim 5\%$. This result also agreed with the calibration for He gas within 5%.

Stainless steel is one of the major fast reactor component materials. The He production in type 316 stainless steel (316 SS) samples were independently measured by the HAFM measurement system and an analogous He atoms measurement system (HAMS) [3] at Kyushu University. Fig. 4 shows these results. Even though the 316 SS samples did not melt completely, due to the sample reaction with the tungsten boat in the furnace, the measurement agreed with the He implanted content. This indicates that most of the He inside the 316 SS samples can be released around its melting temperature.

In consideration of the effect of long term storage some 4 years old He

containing samples were measured with the HAFM measurement system and the HAMS. The results are shown in Fig. 5. The He was retained during long term storage. Thus enabling a periodical calibration of the system using the He implanted samples at specifical time intervals.

4. Irradiation Test

The He production of the HAFM materials irradiated in JOYO have been measured by the HAFM measurement system. The monitor material, ^{10}B sample, was irradiated to a total fluence of 1.3×10^{22} n/cm^2 in the JOYO Mark-II core. The measured He amount was compared with the calculated value with the JENDL-3.2 [4] as shown in Table 1. The neutron spectrum in JOYO was determined by the foil activation method using the J1-Unfolding code NEUPAC [5] with the JENDL-3 dosimetry file [6]. As a result, the C/E value was 0.92, which confirms that the HAFM measurement system is applicable to fast reactor dosimetry. For a typical irradiation condition in JOYO, the calculated value of He production is shown in Table 2.

Prior to using HAFMs in JOYO, the measurement accuracy of the HAFM system will be determined by calibration tests using samples which have been irradiated in the standard neutron field of the fast neutron source reactor YAYOI at University of Tokyo.

5. Conclusion

A HAFM method has been developed for fast reactor dosimetry and for direct measurement of He production in fast reactor component materials. The HAFM measurement system was calibrated using He implantation samples and the accuracy was found to be $\sim$ 5 %. As a result of measuring the He production of the HAFM materials irradiated in JOYO, the C/E value was 0.92. HAFMs are presently under irradiated in YAYOI to further validate the measurement accuracy of the HAFM and HAFM measurement system.

The He accumulation method will be qualified and applied to the fast reactor dosimetry and the measurement of He production in fast reactor component materials. This method will improve reliability of the measured neutron fluence and provide an accurate measurement of the He production in fast reactor component materials.

Acknowledgements

References

[1] ASTM: 1994 Annual Books of ASTM Standards Vol. 12.02, American Society for Testing and Materials (1994) E910-89, p. 507

[2] C. ITO and T. AOYAMA: "Accuracy of Neutron Fluence Measurement by a Helium Accumulation Fluence Monitor," PNC report (in Japanese) PNC TN9410 96-115 (1996)

[3] Y. TAKAO and Y. KANDA: "A system for measurement of sub-parts-per-trillion helium in solids," Review of Scientific Instruments Vol. 67, No. 1, American Institute of Physics (1996) p. 198

[4] K. SHIBATA et al.: "Japanese Evaluated Nuclear Data Library, Version-3," JAERI 1319, Japan Atomic Energy Research Institute (1990)

[5] M. NAKAZAWA and A. SEKIGUCHI: "The Basic Reports of J1-Unfolding Code "NEUPAC"," UTNL-R0096 (1981)

[6] M. NAKAZAWA et al.: "JENDL Dosimetry File," JAERI 1325, Japan Atomic Energy Research Institute (1992)
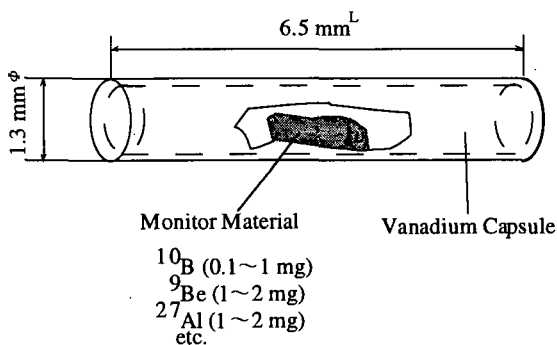
Fig. 1 HAFM
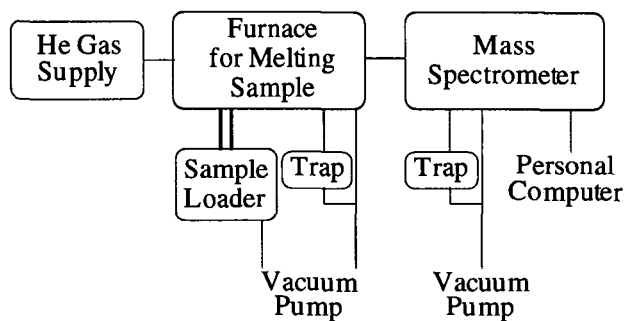
Fig. 2 HAFM Measurememt System
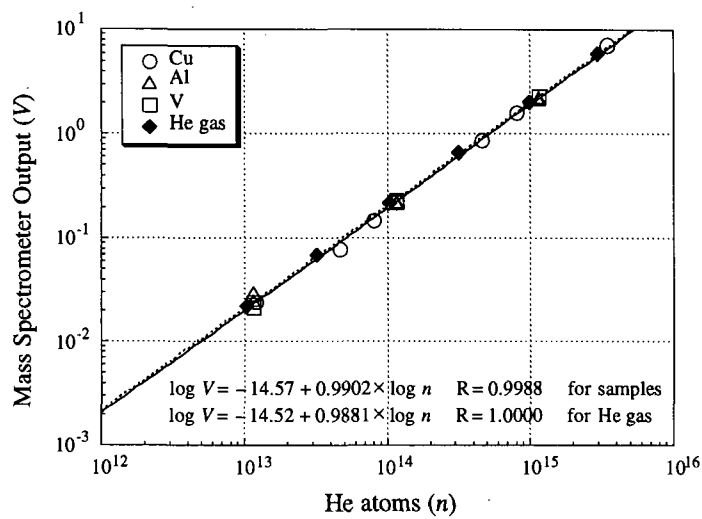
Fig. 3   Relation between He Atoms and Mass Spectrometer Output

$$\log V = -14.57 + 0.9902 \times \log n \quad R = 0.9988 \quad \text{for samples}$$
$$\log V = -14.52 + 0.9881 \times \log n \quad R = 1.0000 \quad \text{for He gas}$$
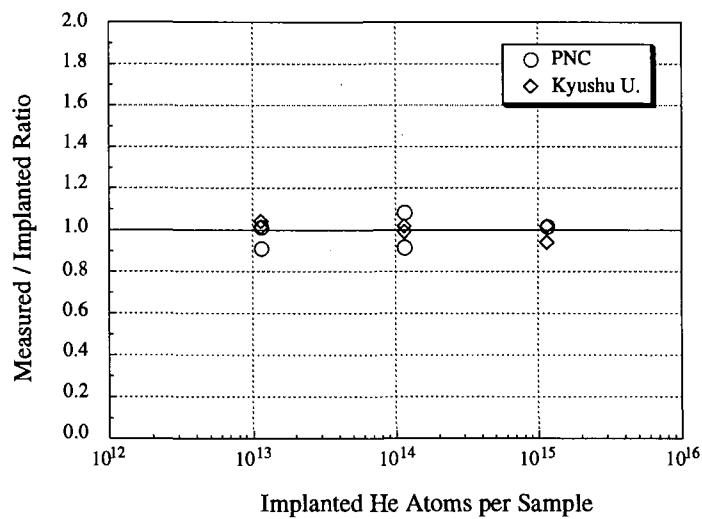
Fig. 4 Measurement of 316 SS Samples with Implanted He Atoms
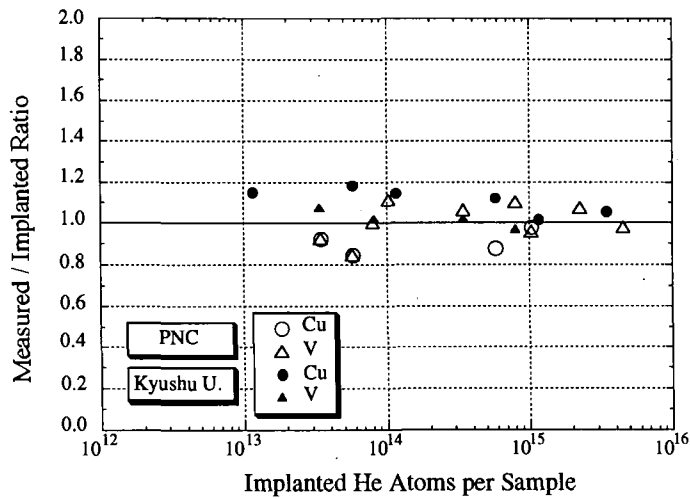
Fig. 5   Effect of Storage on He Content of Samples
(Measurement of Samples after 4 Years)

Table 1 Result of the HAFM Irradiation Test in JOYO

Monitor Material	He Production [atoms/sample]		Calculated vs Measured
	Measured	Calculated	
Natural B 2.15 mg	1.03×10^{18}	0.95×10^{18}	0.92

Irradiated Location: The 5th Row [5F5]
Total Neutron Fluence: 1.3×10^{22} n/cm²

Table 2 Calculation of He Production on the HAFM Irradiation Test in JOYO

Fuel Region

Total Flux [n/cm² s]	DPA Rate [dpa/s]	Irradiation Time [EFPD]	He Production [atoms/sample]		
			^{9}Be 2 mg	^{10}B 0.1 mg	^{27}Al 2 mg
3.6×10^{15}	1.3×10^{-6}	70	2.4×10^{16}	2.3×10^{17}	1.1×10^{14}
		350	1.2×10^{17}	1.1×10^{18}	5.4×10^{14}

Reflector Region

Total Flux [n/cm² s]	DPA Rate [dpa/s]	Irradiation Time [EFPD]	He Production [atoms/sample]		
			^{9}Be 2 mg	^{10}B 0.1 mg	316 SS 10 mg
8.3×10^{14}	1.3×10^{-7}	70	5.5×10^{14}	5.1×10^{17}	7.3×10^{13}
		350	2.8×10^{15}	2.5×10^{18}	3.7×10^{14}

2.5 JENDL Special Purpose File

2.5.1 Activities on Covariance Estimation in Japanese Nuclear Data Committee

Keiichi SHIBATA

Nuclear Data Center
Japan Atomic Energy Research Institute
Tokai-mura, Naka-gun, Ibaraki-ken 319-11
e-mail: shibata@cracker.tokai.jaeri.go.jp

Described are activities on covariance estimation in the Japanese Nuclear Data Committee. Covariances are obtained from measurements by using the least-squares methods. A simultaneous evaluation was performed to deduce covariances of fission cross sections of U and Pu isotopes. A code system, KALMAN, is used to estimate covariances of nuclear model calculations from uncertainties in model parameters.

1. Introduction

Nuclear data should be accompanied with uncertainties since they are regarded as universal constants. Covariances are required to estimate design and safety margins of nuclear facilities. Sensitivity analyses of various reactor calculations also need uncertainties in nuclear data. Moreover, for those who try to adjust group cross-section libraries, covariances of microscopic evaluated data are requisite to know the range of data variation which is physically allowed.

As mentioned above, there are a lot of needs on covariance data from library users. However, we did not respond to the needs satisfactorily. As a matter of fact, the revision 2 of the Japanese Evaluated Nuclear Data Library-3 (JENDL-3.2)[1] did not contain covariance files. Moreover, the first version of JENDL Dosimetry File[2] took covariance data from IRDF-85[3]. Therefore, it is an urgent task to make our own covariance files for JENDL.

To make covariance files is time-consuming and tedious. Thus, the progress was very slow as compared with the conventional cross-section evaluation. However, we should overcome the difficulty since JENDL is now used in a world-wide range, and regarded as one of the 3 major libraries in the world. In 1993, Prof. Kanda founded a working group (WG) on covariance estimation in the Japanese Nuclear Data Committee (JNDC). The objective of the WG was to establish the methodologies of covariance estimation. In addition, the WG members are actually making covariance files relevant to fast reactors. The quantities needed are covariances of cross sections, average number of neutrons emitted by a fission, resonance parameters, angular and energy distributions of secondary neutrons.

Re-evaluation of JENDL Dosimetry File is in progress at a WG on dosimetry integral test. Not only cross sections but covariances are evaluated in the work. This WG uses the same methodologies developed by the WG on covariance estimation.

This paper presents the methodologies in covariance estimations together with the results obtained by the two WGs.

2. Methods

2.1 Simultaneous evaluation

In JENDL-3.2, important cross sections of fissile and fertile nuclides were simultaneously evaluated[4] by taking account of ratio measurements as well as absolute ones in the energy region above 50 keV. The cross sections obtained in the simultaneous evaluation are the fission cross sections of ^{235}U, ^{238}U, ^{239}Pu, ^{240}Pu and ^{241}Pu and the capture cross sections of ^{197}Au and ^{238}U. These cross sections were determined by a least-squares method, and covariance data were also obtained although the covariances were not given in JENDL-3.2.

Figures 1-4 show standard deviations of the fission cross sections of ^{235}U, ^{238}U, ^{239}Pu and ^{240}Pu, respectively.

2.2 Least-squares fit with GMA

A least-squares code GMA[5] was installed on a workstation and on a mainframe at JAERI, and has been used to derive covariances for JENDL-3.2. With this code, the percentage of the systematic and statistical errors to the cross-section value is required as input. The correlation matrix for data points in each experiment is calculated from this percentage. The procedure is very simple and appropriate for producing covariance files without knowing detailed error information for each experiment. The WGs on both covariance estimation and dosimetry integral test have used this code.

Figure 5 shows a fitted curve of the ^{6}Li total cross section obtained by a GMA analysis. In general, the accuracy of measured total cross sections is good, and the estimated error of ^{6}Li is about 1.5% in the entire energy region. Figure 6 shows the ^{46}Ti(n,p) reaction cross sections and standard deviations obtained by an activity of the WG on dosimetry integral test. It is found from Fig. 6 that the uncertainties around 14 MeV are smaller than those in other energy region.

2.3 Uncertainties in nuclear model calculations

The evaluated data in JENDL consist of the one estimated from nuclear model calculations and the one inferred from measurements. In the former case, nuclear models are regarded as fitting functions and the evaluation is equivalent to the search for suitable model parameters.

The parameters required for model calculations are adjustable within a certain acceptable limit which is given by a priori knowledge and theoretical consideration. When the nuclear model calculation is fitted to experimental data, uncertainties in the model parameters are determined according to a prior covariance of the parameters and a covariance of the experimental data used. Uncertainties in the parameters lead to uncertainties in calculated cross sections by the law of error propagation.

We have used a computer code system KALMAN[6], which was developed at the Kyushu University, to deduce uncertainties in model calculations. At present, this system enables one to estimate covariances of cross sections calculated from the optical, statistical models and coupled-channel method

One can see the advantage of this method when a multistep statistical model code such as GNAH[7] is employed in the evaluation. With the same parameters and their covariances, one can obtain uncertainties in the reaction cross sections for which measurements are not available.

Table 1 gives initial and final optical-model parameters and correlation of the final parameters when KALMAN was used to analyze the total cross section of ^{239}Pu. A strong negative correlation is seen between a real depth V and a real radius r_V, which is known as the

discrete ambiguity in the optical model. The calculated cross section is shown in Fig. 7.

3. Conclusions

The activities on covariance estimation in JNDC was discussed together with several results. Covariances for JENDL are being estimated at two WG in JNDC. The WG on covariance estimation performs a work on the preparation for JENDL-3.2 covariance files relevant to fast reactor applications, while the WG on dosimetry integral test is engaged in revising the JENDL Dosimetry File. Covariances of important cross sections of fissile and fertile nuclides were obtained by the simultaneous evaluation. A lest-squares code GMA was used to estimate covariances of the cross sections which were determined on the basis of measurements in the JENDL-3.2 evaluation. Covariances of nuclear model calculations were derived from uncertainties in model parameters by using the KALMAN code system.

References

[1] Nakagawa T.: *J. Nucl. Sci. Technol.*, **32**, 1259 (1995).

[2] Nakazawa M. et al.: "JENDL Dosimetry File", *JAERI* 1325 (1992).

[3] Cullen D.E. et al.: "The International Reactor Dosimetry File (IRDF-82)", *IAEA-NDS*-41/R, rev. 0 (1982). IRDF-85 is a modified version with additional cross section data.

[4] Kanda Y. et al.: "Simultaneous Evaluation of Fission and Capture Cross Sections and their Covariances for Heavy Nuclei", Proc. Int. Conf. Nuclear Data for Basic and Applied Science, Santa Fe, 1985, p.1567 (1986), Gordon and Breach.

[5] Poenitz W.P.: "Data Interpretation, Objective Evaluation Procedures and Mathematical Techniques for the Evaluation of Energy-Dependent Ratio, Shape and Cross Section Data", Proc. Conf. Nuclear Data Evaluation Methods and Procedures, *BNL-NCS*-51363, p.249(1981).

[6] Kawano T. and Uenohara Y.: Private communication (1995).

[7] Young P.G. and Arthur E.D.: "GNASH: A Preequilibrium, Statistical Nuclear-Model Code for Calculation of Cross Sections and Emission Spectra", *LA*-6947 (1977).

Table 1　Optical Model Parameters for ^{239}Pu

Parameter	Initial	Final	Error(%)	Correlation (×1000)					
V (MeV)	40.7	41.3	0.95	1000					
r_V (fm)	1.32	1.31	0.99	-966	1000				
a_V (fm)	0.47	0.46	4.87	651	-611	1000			
W_S (MeV)	6.78	6.22	4.23	-558	492	-20	1000		
r_S (fm)	1.36	1.39	1.24	497	-627	4	-252	1000	
a_S (fm)	0.47	0.42	4.92	-153	292	-47	-294	-818	1000
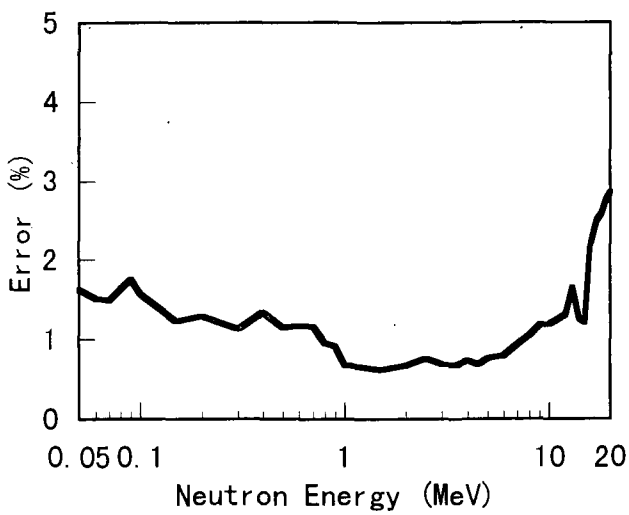
Fig. 1　Error of U-235(n, f) cross sections.
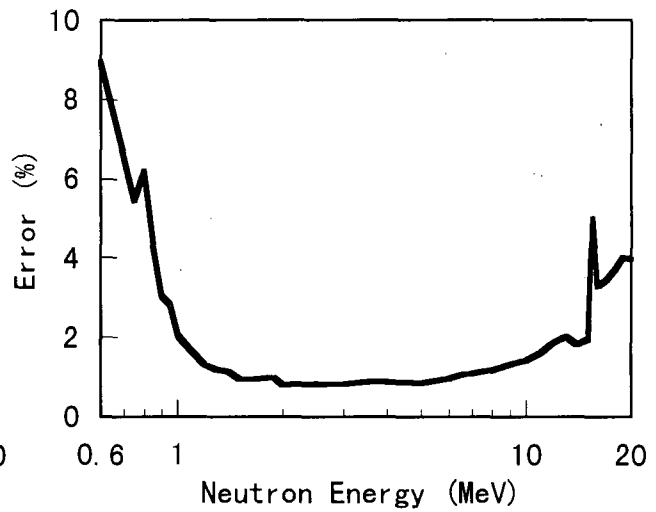
Fig. 2　Error of U-238(n, f) cross sections.
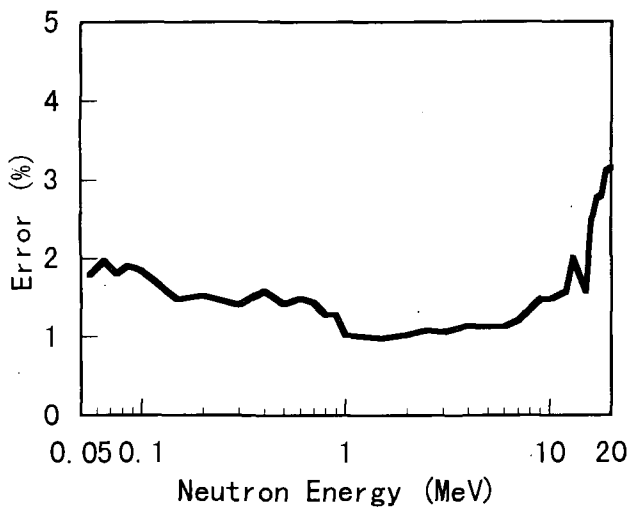
Fig. 3　Error of Pu-239(n, f) cross sections.
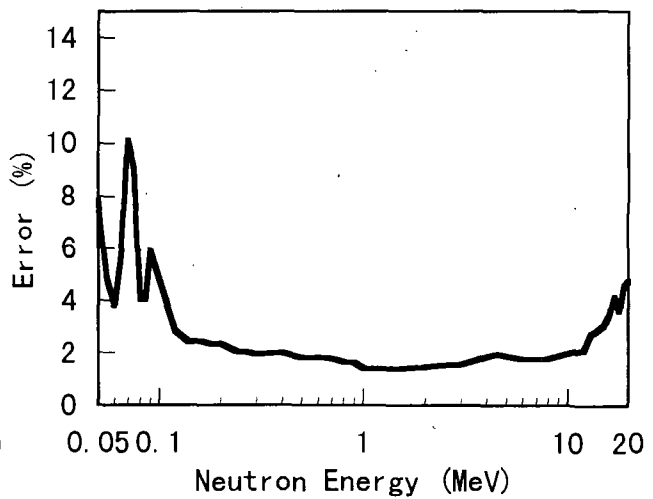
Fig. 4　Error of Pu-240(n, f) cross sections.
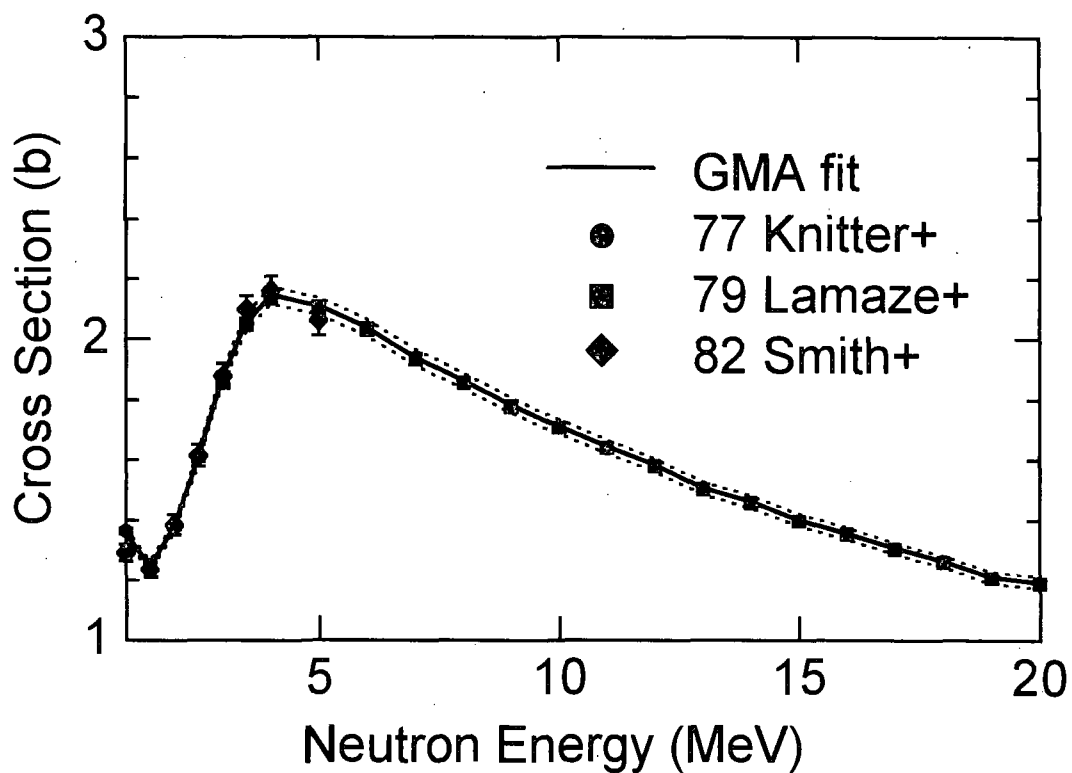
Fig. 5 Total cross section of Li-6.
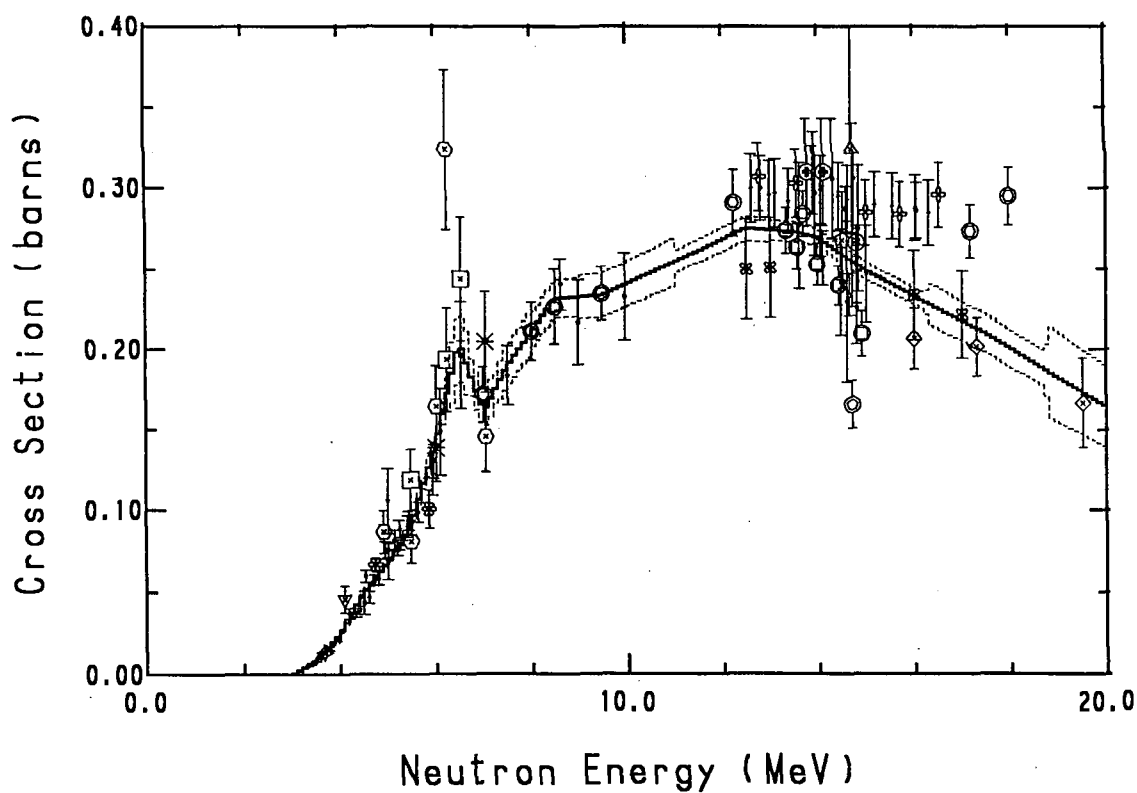
Fig. 6 Ti-46(n,p) reaction cross section.
The lines were obtained by a GMA fit.
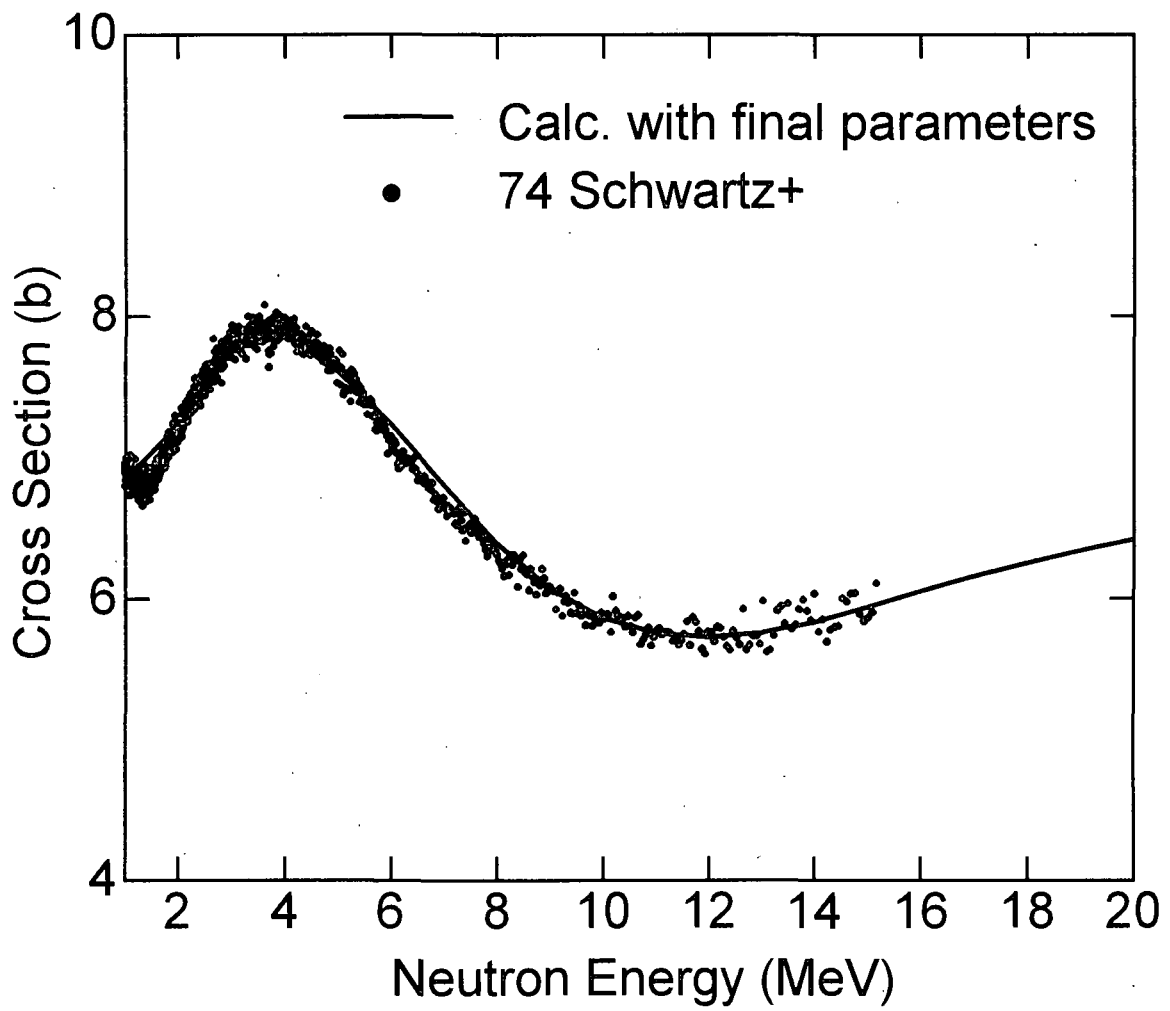
Fig. 7   Total cross section of Pu-239.

2.5.2 PKA Spectrum File

M. Kawai

Nuclear Engineering Laboratory, Toshiba Corp., 4-1 Ukishima-cho, Kawasaki-ku, Kawasaki, 210 Japan

ABSTRACT

In the Japanese Nuclear Data Committee, the PKA/KERMA file containing PKA spectra, KERMA factors and DPA cross sections in the energy range between 10^{-5} eV and 50 MeV is being prepared from the evaluated nuclear data. The processing code ESPERANT was developed to calculate quantities of PKA, KERMA and DPA from evaluated nuclear data for medium and heavy elements by using the effective single particle emission approximation (ESPEA). For light elements, the PKA spectra are evaluated by the SCINFUL/DDX and EXIFON codes, simultaneously with other neutron cross sections. The DPA cross sections due to charged particle emitted from light elements are evaluated for high neutron energy above 20 MeV.

1. Introduction

In the PKA Spectrum Working Group of Japanese Nuclear Data Committee, the PKA/KERMA file containing primary knock-on atom (PKA) spectra, KERMA factors and displacement per atom (DPA) cross sections in the energy range between 10^{-5} eV and 50 MeV is prepared[1] from the evaluated nuclear data file, for radiation damage calculations used to such as the International Fusion Material Irradiation Facility (IFMIF)[2] which is an FMIT-type accelerator facility using Li(d,n) neutron source for irradiation tests of fusion reactor materials. The processing code system, ESPERANT, was developed to calculate quantities of PKA, KERMA and DPA from evaluated nuclear data for medium and heavy elements by using an effective single particle emission approximation (ESPEA). The PKA spectra of light elements are evaluated by the SCINFUL/DDX code[3] for Li, Be, B, C and by modified version of the EXIFON code[4] for N and O, simultaneously with other neutron cross sections. The DPA cross sections for light elements are calculated taking into account of contribution of charged particle emitted from high energy neutron reactions above 20 MeV. Finally, the PKA/KERMA file will contain the data for 78 isotopes of 29 elements in the energy region up to 50 MeV.

As a trial task of ESPERANT, a file of PKA spectra for 69 nuclides from ^{19}F to ^{209}Bi in the energy region up to 20 MeV has been generated for fusion application from the JENDL Fusion File[5], in order to supply the PKA data to the FENDL-2 project[6]. The considered reactions to process were elastic (MT=2) and discrete inelastic (MT=51-90) scattering, continuum neutron emission reaction (MT=201) and charged particle emission reactions (MT=203-207). Damage energy spectra were also generated. The calculated PKA spectra were compared with the results of Monte Carlo calculation using MCEXCITON[7] and of Doran's processing[8] ENDF/B-IV[9], the DPA cross sections in the KERMA Files were compared with calculations by RADHEAT-V4[10] and Doran, and the KERMA factors processed by ESPERANT were compared with Howerton's calculation[11] as data and method check of ESPERANT. It was concluded that processed result of present work had an good accuracy for above physical quantities. In this report, the processing method, ESPEA, is explained and the results of comparison are discussed as well as an example of lighter mass nuclei calculation by SCINFUL/DDX.

2. Effective Single Particle Emission Approximation (ESPEA)

It is often impossible to calculate PKA spectra exactly for reactions emitting two or more particles from evaluated nuclear data file which usually has no separated spectrum of each reaction step and channel. For these cases, the effective single particle emission approximation (ESPEA) has been developed[1] to calculate

spectra. In ESPEA, it is assumed that the particles are emitted from sequential reactions, which can not emit the particles simultaneously, and only the first emitted particle contributes to determination of energy and angular distributions of PKA.

Double-differential cross section (DDX) of emitted particle in CMS, DDX_1^C (E_p^L, E_1^C, μ_1^C), is assumed to be given in evaluated nuclear data files, where superscripts of C and L mean center-of-mass system (CMS) and laboratory system (LAB), subscripts of p, t, 1 and 2 show incident particle, target nucleus, outgoing particle and residual nucleus, and symbols of E, m and θ are energy, mass and emitted angle (μ = cos θ). PKA spectrum in CMS, DDX_2^C(E_p^L, E_2^C, μ_2^C), is directly calculated by using energy and momentum conservation lows. That for particle emission reaction is written

$$DDX_2^C (E_p^L, E_2^C, \mu_2^C) = \frac{m_2}{m_1} DDX_1^C (E_p^L, E_1^C, \mu_1^C) \tag{1}$$

$$E_2^C = \frac{m_1}{m_2} E_1^C \tag{2}$$

$$\mu_2^C = -\mu_1^C \tag{3}$$

and that for γ-ray emission reaction is

$$DDX_2^C (E_p^L, E_2^C, \mu_2^C) = \frac{m_2 c^2}{E_\gamma} DDX_\gamma (E_p^L, E_\gamma, \mu_\gamma) \tag{4}$$

$$E_2^C = \frac{E_\gamma^2}{2 m_2 c^2} \tag{5}$$

$$\mu_2^C = -\mu_\gamma \tag{6}$$

where c is light speed. Since particle production cross sections (MT=201, 203-207 in ENDF-6 format, similar as following) are compiled by summing up individual production cross sections, which are given as a product of reaction cross section and particle multiplicities, exceeds the total reaction cross section, some re-normalization is necessary to maintain a number of recoil nuclei by means of single particle emission procedure. A normalization factor, R, for ESPEA is given as following.

$$R = \frac{\sigma_R}{\sum_x \int_{\varepsilon_x^{(min)}} d\varepsilon_x \int d\mu_x \sigma_x (E_p^L, \varepsilon_x, \mu_x)} \tag{7}$$

where σ_R and σ_x indicate cross sections of total reaction and each particle emission channel, and $\varepsilon_x^{(min)}$ is lower limit of energy for spectrum considered, which means the first emitted particles are distributed in higher energy region in the emitted spectra. It is assumed that no PKA is created by light particles emitted below this energy. The lower energy limit, $\varepsilon_x^{(min)}$, is determined to be satisfied the following equation of average energy for light particle emitted from the reaction x.

$$\int_{\varepsilon_x^{(min)}} \varepsilon_x f_x (\varepsilon_x) d\varepsilon_x = \left[\frac{m_t}{m_p + m_t} E_p^L + Q_x \right] \Big/ \left[1 + (\frac{m_{1x}}{m_{2x}})^2 \right] \tag{8}$$

$$\int_0^\infty f_x (\varepsilon_x) d\varepsilon_x = 1 \tag{9}$$

where Q_x is Q-value of reaction x, and f_x the normalized DDX_1^C of reaction x.

DDX of PKA in LAB, $DDX_D^L(E_D^L, E_2^L, \mu_2^L)$, is obtained after conversion from CMS to LAB, then the damage energy spectra, σ_D, can be given by

$$\sigma_D(E_p^L, E_2^L, \mu_2^L) = E_D(E_2^L) \cdot DDX_2^L(E_p^L, E_2^L, \mu_2^L) \tag{10}$$

where E_D is given by Lindhard-Robinson model[11] with unit of E_2^L in eV as following.

$$E_D(E_2^L) = \frac{E_2^L}{1 + k \cdot g(\varepsilon)} \tag{11}$$

$$k = 0.13372 \cdot Z^{2/3} / A^{1/2} \tag{12}$$

$$g(\varepsilon) = 3.48008\varepsilon^{1/6} + 0.40244\varepsilon^{3/4} + \varepsilon \tag{13}$$

$$\varepsilon = E_2^L / 86.931 Z^{7/3} \tag{14}$$

The DPA Cross Section, σ_{DPA}, can be obtained by using the above damage energy spectra,

$$\sigma_{DPA}(E_p^L) = \iint v(E_2^L)\sigma_D(E_p^L, E_2^L, \mu_2^L) dE_2^L d\mu_2^L \tag{15}$$

$$v(E_2^L) = \frac{\kappa}{2\varepsilon_d} E_D(E_2^L) \tag{16}$$

$$\kappa = 0.8 \tag{17}$$

where ε_d is the threshold energy for knock-on atom displaced from lattice point, and its amount strongly depends on materials. The KERMA factor for x-reaction, $KERMA_x(E_p^L)$, is also calculated by using double differential PKA spectrum as following.

$$KERMA_x(E_p^L) = \iint (E_{1x}^L + E_{2x}^L) DDX_{2x}^L(E_p^L, E_{2x}^L, \mu_{2x}^L) dE_{2x}^L d\mu_{2x}^L \tag{18}$$

For neutron and photon emission reactions, the term of E_{1x} is eliminated.

3. PKA/KERMA File as a Test of ESPERANT

The PKA File has been generated to supply the PKA data as a trial task of ESPERANT, processing from the JENDL Fusion File below 20 MeV. Nuclides processed for the PKA File are 69 and listed in Table 1. Considered reactions are elastic (MT=2) and discrete inelastic scattering (MT=51-90), continuum neutron emission reaction (MT=201), and charged particle emission reactions (MT=203-207). Damage energy spectra has been also processed. The processing accuracy was 1.0 %, including uncertainties of CMS-LAB

Table 1   Nuclides Included in PKA File for FENDL-2 Project (En=10^{-5} eV - 20 MeV)

69 isotopes included in JENDL Fusion File is processed.
^{19}F, ^{27}Al, $^{28, 29, 30}$Si, $^{40, 42, 43, 44, 46, 48}$Ca, $^{46, 47, 48, 49, 50}$Ti, ^{51}V, $^{50, 52, 53, 54}$Cr, ^{55}Mn, $^{54, 56, 57, 58}$Fe, ^{59}Co, ^{64}Ni, $^{63, 65}$Cu, ^{75}As, $^{90, 91, 92, 94, 96}$Zr, ^{93}Nb, $^{94, 95, 96, 97, 98, 100}$Mo, $^{121, 123}$Sb, $^{182, 183, 184, 186}$W, $^{114, 115, 116, 117, 118, 119, 120, 122, 124}$Sn, $^{204, 206, 207, 208}$Pb, ^{209}Bi

conversion, averaging, PKA energy calculation, and so on.

The results of PKA spectra processed by ESPERANT from JENDL Fusion File were compared[1] with those calculated with MCEXCITON[7] and given by Doran[8]. Since the PKA spectrum strongly depends on emitted light particle spectrum, the particle spectra in PKA file and calculated by MCEXCITON were also compared. For example, the PKA spectra for ^{27}Al at incident neutron energies of 10 and 20 MeV are shown in Fig. 1. The PKA spectra processed by ESPERANT are in good agreement with those calculated by MCEXCITON with considering the large secondary particle energy meshes of the ESPERANT calculation. In Fig. 1(a), the PKA spectra given by Doran at incident energies of 9 and 11 MeV is also indicated. Doran processed the PKA spectra from ENDF/B-IV with assuming evaluation spectra for charged particles, since ENDF/B-IV does not have charged particle spectrum. However, his processing gives similar result to present result.
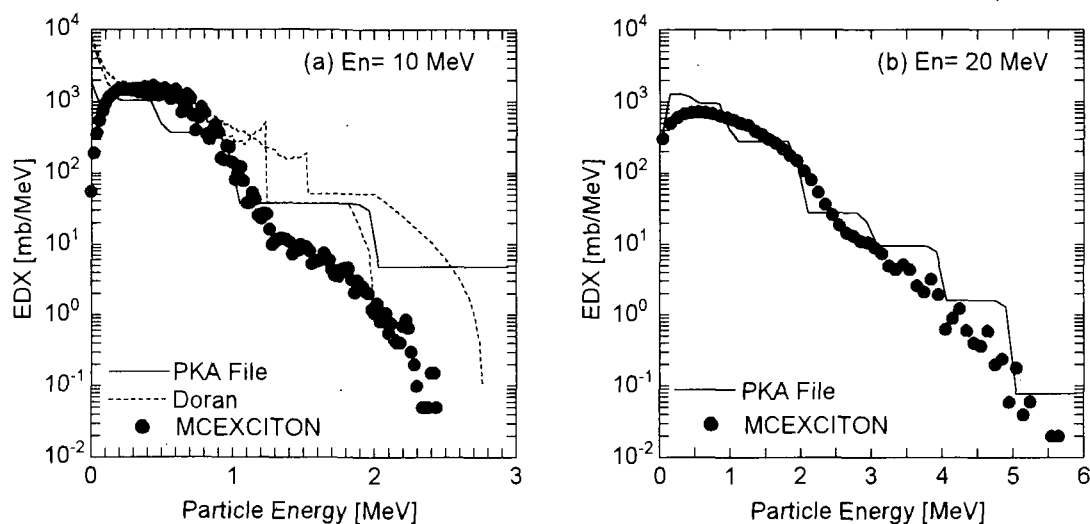
Fig.1 ^{27}Al PKA Spectra of PKA File Compared with Calculations by
MCEXCITON and Doran at (a) En=10 MeV and (b) En=20 MeV

The DPA cross sections for ^{27}Al and ^{56}Fe in the KERMA Files are also compared with calculations by RADHEAT-V4[10] and Doran[8] as function of incident neutron energy in Fig. 2. Processed results by ESPERANT are in good agreement with other two calculations.

The KERMA factors for ^{27}Al and ^{56}Fe in the KERMA Files are illustrated with Howerton's calculation[11] in Fig. 3. KERMA factors processed by ESPERANT agree with the calculations. As an example of KERMA factor calculations for light mass nuclei such as ^{12}C, the results by SCINFUL/DDX is shown in Fig. 4, comparing with the experimental data and the calculated one calculated by using JENDL-3.2. Present work can reproduce almost all experimental data while the JENDL-3.2 results, which include no "break-up" spectrum, give larger value above 14 MeV. Because of this importance including break-up reactions, the SCINFUL/DDX code is good to use instead of ESPERANT for lighter mass nuclei. By using the SCIFUL/DDX results, the DPA cross section for carbon are calculated[13] with the E-DEP-1-ext code[14] taking into an account of the contribution from emitted charged particles slowing down in one-element material irradiated with highly energetic neutrons. The contributions of charged particles to total DPA cross section are 28% at the neutron energy of 20 MeV and 36% at 50 MeV.
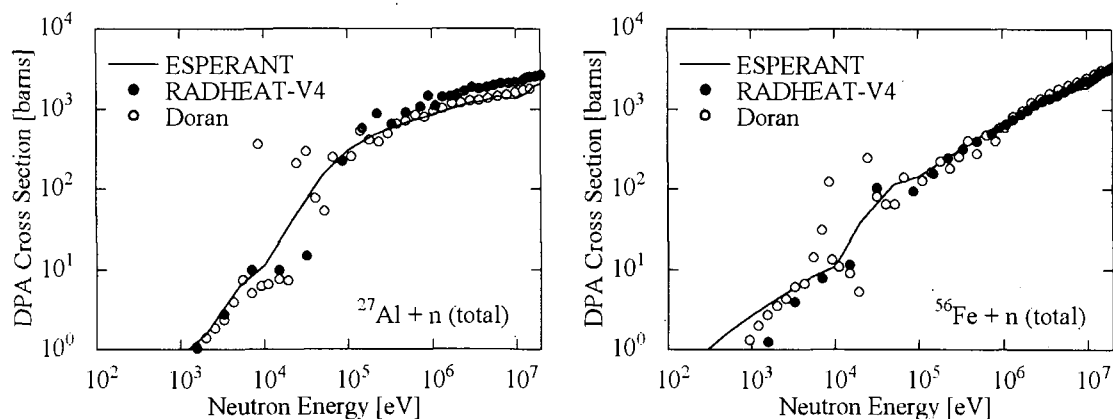
Fig.2 ^{27}Al and ^{56}Fe DPA Cross Sections of KERMA File Compared
with Calculations by RADHEAT-V4 and Doran
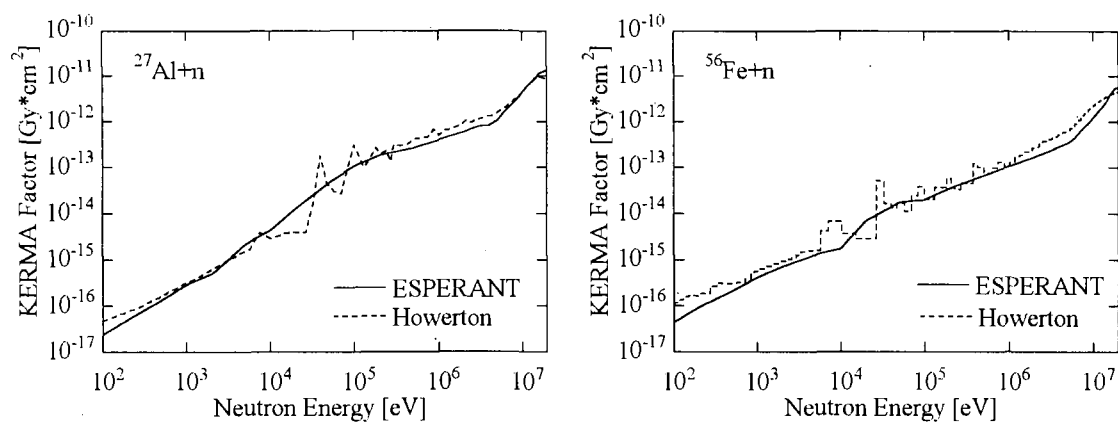
Fig.3 ^{27}Al and ^{56}Fe KERMA Factors of KERMA File Compared
with Calculations by Howerton
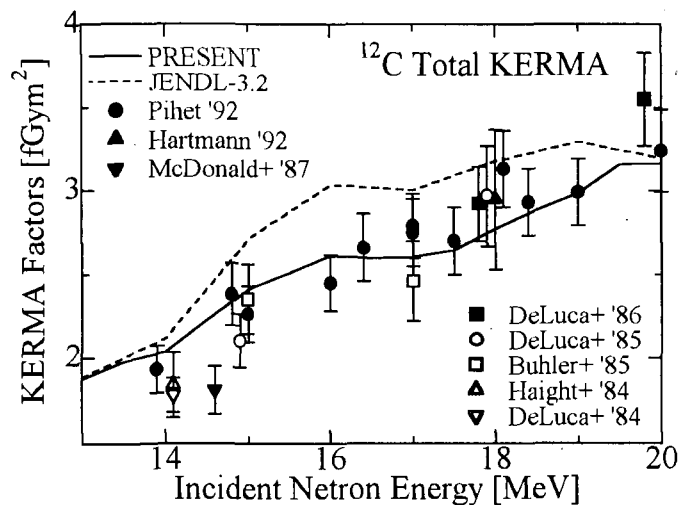
Fig.4 KERMA Factors of ^{12}C Calculated by SCINFUL/DDX

4. Summary

The present status of the JENDL PKA/KERMA File was reviewed, especially for FENDL usage (En < 20 MeV). The processing method, ESPEA, was explained and the results of comparison were discussed. It was confirmed by comparing with the results of Monte-Carlo code, MCEXCITON, calculation and of Doran's processing by using ENDF/B-IV, as data and method test that ESPEA was well worked for calculating PKA spectra from the evaluated file. The SCINFUL/DDX code was clarified to calculate KERMA factors as well as neutron cross sections for light elements suxh as Li, Be, B and C with good accuracy. It was also found that the charged particles emitted from high energy neutron reactions highly contributed to DPA cross sections for light elements.

The evaluation of nuclear data for JENDL High Energy File is now in progress. Finally, the PKA/KERMA file will contain the data for 78 isotope of 29 elements in the incident neutron energy range up to 50 MeV. The benchmark test of the KERMA data for C, Ti, Cu, Mo, etc. will be made by using the FNS experiments of nuclear heating. After the test, the PKA/KERMA file will be released in 1998.

Acknowledgments

References

1. T. Fukahori, S. Chiba and M. Kawai, *JAERI-Conf* **96-005** (1996) p.130.
2. K. Noda, *JAERI-Conf* **95-008** (1995) p.112.
3. H. Kashimoto, Y. Watanabe, Y. Koyama, H. Shinohara and S. Chiba, *JAERI-M* **93-046** (1993) p.287.
4. H. Kalka, *Proc. Int. Conf. on Nuclear Data for Science and Technology, Julich, May 13-17, 1991* (Springer-Verlag, Berlin, Heidelberg, 1992) p.897.
5. Y. Baosheng, S. Chiba and T. Fukahori, *J. Nucl. Sci. Technol.*, **29** (1992) 677.
6. e.g. for FENDL-1: S. Ganesan and P.K. McLaughlin, *IAEA-NDS-128 Rev.1* (1995).
7. N. Kishida and H. Kadotani, *Proc. Int. Conf. on Nuclear Data for Science and Technology, Mito, May 30 - June 3, 1988* (Saikon Publishing, Tokyo, 1988) p.1209.
8. D.G. Doran and N.J. Graves, *HEDL-TME* **7670** (1976).
9. (Ed.) D. Garber, *BNL-17541*, 2nd Edition (1975).
10. N. Yamano et al., *JAERI*-**1316** (1989).
11. R.J. Howerton, *UCRL-50400* **Vol. 27** (1986).
12. J. Lindhard, et al., *Kgl. Danke Vidensk Selsk. mat-fis. Medd.*, **33** (1963) p.10 and N.T. Robinson, *Proc. BNES Conf. on Nuclear Fission Reactors, Culham 1969* (BNES, London, 1969) p.346.
13. T. Aruga, S. Chiba, M. Harada, H. Kashimoto, Y. Watanabe and M. Kawai, *JAERI-Conf* **95-008** (1996) p.211.
14. T. Aruga, K. Nakata and S. Takamura, *Nucl. Instr. and Meth.* **B33** (1988) 748.

2.6 High Energy Nuclear Data

2.6.1 Spallation Integral Experiment Analysis by High Energy Nucleon-Meson Transport Code

Hiroshi Takada[1], Shin-ichiro Meigo[1], Toshinobu Sasa[1], Tokio Fukahori[1], Nobuaki Yoshizawa[2], Shiori Furihata[2], Vladimir I. Belyakov-Bodin[3], Gennady I. Krupny[3] and Yuriy E. Titarenko[4]

1) Japan Atomic Energy Research Institute, Tokai-mura, Naka-gun, Ibaraki-ken, 319-11, JAPAN
2) Mitsubishi Research Institute Inc., Ote-machi, Chiyoda-ku, Tokyo, 100, JAPAN
3) Institute of Theoretical and Experimental Physics, B.Cheremushkinskaya, 25, Moscow, RUSSIA
4) Institute of High Energy Physics, Protvino, Moscow Region, RUSSIA
    E-mail: takada@omega.tokai.jaeri.go.jp

Abstract: Reaction rate distributions were measured with various activation detectors on the cylindrical surface of the thick tungsten target of 20 cm in diameter and 60 cm in length bombarded with the 0.895 and 1.21 GeV protons. The experimental results were analyzed with the Monte Carlo simulation code systems of NMTC/ JAERI-MCNP-4A, LAHET and HERMES. It is confirmed that those code systems can represent the reaction rate distributions with the C/E ratio of 0.6 to 1.4 at the positions up to 30 cm from beam incident surface.

1. Introduction

Monte Carlo simulation code system which consists of the nucleon-meson transport code such as LAHET[1], HETC-KFA2[2] and NMTC/JAERI[3] and the neutron transport code of MORSE[4] and MCNP-4A[5] has been employed in neutronics design studies of accelerator-based transmutation system for long-lived transuranic nuclides and intense spallation neutron sources. It is important to understand the accuracy of the code system for estimating the neutron yield, neutron energy spectra and reaction rates in the accelerator-based transmutation systems. For this purpose, code intercomparisons were conducted by OECD/NEA.[6-8] As for the thick target benchmark in the code intercomparison, only the calculated results were compared.

In order to validate the code system for thick target calculations, a reaction rate distributions on a thick tungsten target were measured with various activation detectors for the proton incidence of 0.895, 1.09 and 1.21 GeV as a cooperative work between JAERI and Institute of Theoretical and Experimental Physics under the contract of International Science and Technology Center project #157. Analytical study has just started using the code systems of NMTC/JAERI-MCNP-4A, LAHET and HERMES (HETC-KFA2-MORSE)[2].

2. Experimentals

The experiment was carried out at the booster beam line of Institute of High Energy Physics in Russia. In the experiment, protons were injected into a cylindrical tungsten target of 20 cm in diameter and 60 cm in length. The purity and density of the tungsten target was 19.1 g/cc and 99.95%, respectively. Reaction rate distributions on the cylindrical surface of the target were measured using various kinds of activation detectors of ^{27}Al, ^{12}C, ^{31}P, ^{32}S, ^{103}Rh, ^{115}In, ^{197}Au and ^{209}Bi at the distances of 2, 8, 12, 17, 30 and 55 cm from the beam incident surface. In this study, the reaction rates of the ^{27}Al, ^{31}P, ^{32}S and ^{209}Bi detectors for the 0.895 and 1.21 GeV proton incidence were analyzed. The physical and nuclear characteristics of the activation detectors are summarized in Tables 1 and 2, respectively.

During the irradiation period, proton beam intensity was monitored using an induction current sensor with an accuracy of about 3 %. The profile of the beam was the Gaussian distribution with a FWHM of 2.4 cm. The number of protons injected in the target was 1.3×10^{14} to 4.3×10^{15}. The γ and ß rays from the activation detectors were measured using Ge-detectors and polystyrene scintillation counters, respectively. The error in determining the activities of the activation samples were less than 3% at 0.95 confidential interval for the γ-ray measurement, while less than 22% at 0.95 confidential interval for the ß-ray measurement.

3. Calculation

The calculations were carried out using the code systems of NMTC/JAERI-MCNP-4A, LAHET,

HERMES. In NMTC/JAERI and LAHET, preequilibrium process was taken into account in the nuclear reaction calculation. A closed from exciton model[9] was employed in the preequilibrium calculation in the former, while a multistage multistep preequilibrium exciton model[10] was incorporated in the latter. The level density parameter derived by Ignatyuk[11] with the parameters proposed by Mengoni et al.[12] was selected in the evaporation calculation in NMTC/JAERI and LAHET. The level density parameter proposed by Baba [13] was employed in HERMES.

In the particle transport calculation, the cutoff energy was set to be 1 MeV for charged particles and 20 MeV for neutron. The treatment of nucleon-nucleus collision cross sections were different among the three code systems. NMTC/JAERI employs the systematics derived by Pearlstein[14] in the energy region below 1 GeV and the geometric cross sections in the energy region above 1 GeV. For elastic scattering, HERMES employs the cross sections compiled in HILO library in the energy region below 150 MeV and those from NASA library above 150 MeV.[2] LAHET uses the cross sections of elastic scattering obtained by a global phenomenological optical model in the energy region below 400 MeV and those from NASA library above 400 MeV. [1]

In the neutron transport calculation in the energy region below 20 MeV, a continuous cross section library processed from the nuclear data file JENDL-fusion file[15] was employed in all the code systems.

As for the nuclide production cross section, the data of JENDL Dosimetry file[16] were used in the energy region below 20 MeV. In the energy region above 20 MeV, on the other hand, the nuclide production cross sections calculated with the ALICE-F code[17] were employed. Fig. 1 shows the experimental[18] and calculated cross section of the $Bi(n,4n)^{206}Bi$ reaction.

4. Results and Discussion

Figure 2 shows the calculated neutron energy spectra on the cylindrical surface between 7 and 9 cm from the beam incident surface for the 1.21 GeV proton bombardment. It is observed that LAHET gives much higher neutron yield in the energy region below 60 MeV than HERMES because LAHET takes account of the preequilibrium process. NMTC/JAERI-MCNP-4A does not give such high neutron yield between 20 and 60 MeV in spite it also includes the preequilibrium process. The code system, however, produces neutrons higher than LAHET between 1 and 3 MeV. This is because the difference of prequilibrium calculation model and the transport cross sections between NMTC/JAERI and LAHET.

Figures 3 and 4 show the reaction rate distributions for the 0.895 GeV proton incidence. The C/E ratios of each reaction are also shown in Fig. 7. It is observed that the calculated reaction rates of NMTC/JAERI, LAHET and HERMES reproduce the experimental ones with the C/E ratio of 0.6 to 1.4. The HERMES code system tends to estimate the reaction rate lower than the other code systems because of lack of preequilibrium process. The LAHET code are in preferable agreement with the experimental results than NMTC/JAERI and HERMES. The LAHET code system can predict the experimental reaction rates with an accuracy of 0.8 to 1.2 in C/E ratio. As seen in Fig. 1, the ambiguity of the calculated nuclide production cross sections seem to be small for Bi(n,xn) reactions whose threshold energies are higher than 20 MeV. Therefore, it is indirectly proved that LAHET can estimate neutron spectra on cylindrical surface of the tungsten target quite well. At the position of 55 cm, however, the agreement between the calculated and experimental results becomes worse than at the other positions. This may indicate the neutron transport is not estimated accurately in all the code systems.

The similar tendency is obtained in the comparison between the calculated and experimental reaction rates for the 1.21 GeV proton incidence as shown in Figs 5 and 6.

5. Concluding Remarks

The reaction rate distributions of various activation detectors on the cylindrical surface of a tungsten target of 20 cm in diameter and 60 cm in length bombarded with 0.895 and 1.21 GeV protons were analyzed with the code systems of NMTC/JAERI-MCNP-4A, LAHET and HERMES. It was confirmed that those code systems agreed with the experimental results in the range of 0.6 to 1.4 in C/E ratio up to 30 cm from the beam incident surface. Among the code systems, LAHET had preferable accuracy of 0.8 to 1.2 in C/E ratio. This comes from the fact that the code system gives higher the neutron yield in the energy region below 60 MeV than the other codes because of the inclusion of the preequilibrium process. It is, therefore, concluded that the inclusion of the preequilibrium process improves the accuracy of nucleon-meson transport code. At the position

of 55 cm, however, the agreement between the calculated and experimental results became worse. More detailed study is required in the nucleon transport calculation part of the nucleon-meson transport code. Since NMTC/JAERI could not give as many neutron yield as LAHET in spite it took account of the preequilibrium, it is necessary to investigate the accuracy of preequilibrium calculation model in NMTC/JAERI. For more strict comparison between the calculated reaction rate with the experimental one especially in the energy region above 20 MeV, it is necessary to take into consideration of the ambiguity of nuclide production cross sections calculated by ALICE-F.

References

[1]   Nakahara Y., Tsutsui T.: "NMTC/JAERI A Code System for High Energy Nuclear Reactions and Nucleon-Meson Transport Code", JAERI-M 82-198, (1982), [in Japanese].

[2]   Prael R. E., Lichtenstein H.: LA-UR-89-3014, "Users Guide to LCS: The LAHET Code System", (1989).

[3]   Cloth P., et al.: "HERMES A Monte Carlo Program System for Beam Materials Interaction Studies", Jül-2203, (1988).

[4]   Emmett M. B.: "The MORSE Monte Carlo Radiation Transport Code System", ORNL-4972, (1975).

[5]   Briesmeister J.F. (Ed.) : MCNP A General Monte Carlo N-Particle Transport Code, Version 4A, LA-12625, (1993).

[6]   OECD/NEA: "Proc. of Specialists' Mtg. on Intermediate Energy Nucl. Data: Models and Codes", May 31 - June 1, Issy-les-Moulineaux, OECD Publications, Paris, (1994).

[7]   Filges D., Nagel P., Neef R. D. (Eds.): "International Code Comparison for Intermediate Energy Nucl. Data: The Thick Target Benchmark", NEA/NSC/DOC(95)-2, (1995).; Sobolevsky N. : "Conclusions of International Code Comparison for Intermediate Energy Nucl. Data, Thick Target Benchmark for Lead and Tungsten", NEA/NSC/DOC(96)-15, (1996).

[8]   Michel R., Nagel P.:"Specifications for An International Codes and Model Intercomparison for Intermediate Energy Activation Yields", NEA/NSC/DOC(95)-8, (1995).

[9]   Yoshizawa N., Ishibashi K, Takada H.: J. Nucl. Sci. Technol. 32, 601, (1995).

[10]   Prael R.E., Bozoian M.:"Adaptation of the Multistage Preequilibrium Model for Monte Carlo Method", LA-UR-88-3238, (1988).

[11]   Ignatyuk A. V., Smirenkin G. N., Tishin A. S.: Sov. J. Nucl. Phys., 21, 256 (1975).

[12]   Mengoni A., Nakajima Y.: J. Nucl. Sci. Technol., 31, 151 (1994).

[13]   Baba H. : Nucl. Pys. A 159, 625 (1970).

[14]   Pearlstein, S.: Astrophys. J., 346, 1049 (1989).

[15]   Chiba S., Yu B., T., Fukahori T. : "Evaluation of JENDL Fusion File", Proc. of the 1991 Symp. on Nucl. Data, Nov. 28-29, 1991, JAERI, Tokai, Japan, JAERI-M 92-027, pp. 35-44 (1992).

[16]   Nakazawa M., et al..: "JENDL Dosimetry File", JAERI-1325, (1992).

[17]   Fukahori T.:"ALICE-F Calculation of Nuclear Data up to 1 GeV", Proc. of the Specialists' Mtg. on High Energy Nucl. Data, Oct. 3-4, 1991, JAERI, Tokai, JAERI-M 92-039, pp. 114-122 (1992).

[18]   Kim E., et al.: "Measurement of Neutron Spallation Cross Sections", Proc. of the 1995 Symp. on Nucl. Data, Nov. 16-17, 1995, JAERI, Tokai, Japan, JAERI-Conf 96-008, pp.236-241 (1996).

Table 1. Physical characteristics of activation detectors.

Sample	Size (mm)	Density (g/cc)	Purity (%)
P	20ϕ x 3	2.20	100
S	20ϕ x 3	2.07	95.02
Al	25 x25x1.6	2.699	100
Bi	20ϕ x 1	9.747	99.99

Table. 2. Nuclear characteristics of activation detectors.

Reaction	Half-Life	γ-/β-ray Energy	Emission Rate	Threshold Energy
$^{32}S(n,p)^{32}P$	14.3 days	694.7 keV (β)	1.0	0.96 MeV
$^{31}P(n,p)^{31}Si$	157.3 min	595.7 keV (β)	0.999	0.73 MeV
$^{27}Al(n,p)^{27}Mg$	9.45 min	843 keV (γ)	0.7	1.9 MeV
$^{27}Al(n,\alpha)^{24}Na$	15.0 hours	1369 keV (γ)	1.0	3.27 MeV
$^{209}Bi(n,4n)^{206}Bi$	6.243 days	803.1 keV (γ)	0.989	22.56 MeV
$^{209}Bi(n,5n)^{205}Bi$	15.31 days	703.4 keV (γ)	0.311	29.63 MeV
$^{209}Bi(n,6n)^{204}Bi$	11.22 hours	374.7 keV (γ)	0.737	37.99 MeV
$^{209}Bi(n,7n)^{203}Bi$	11.76 hours	820.2 keV (γ)	0.296	45.31 MeV
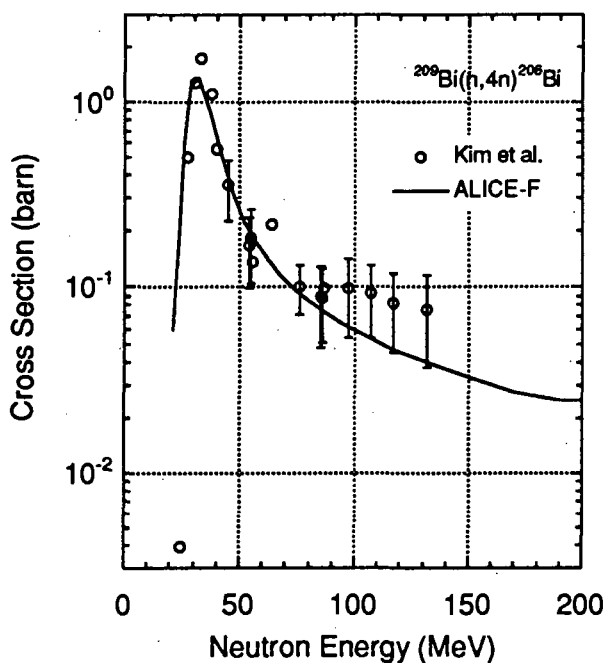
Fig. 1 Cross section of $^{209}Bi(n, 4n)^{206}Bi$. The open circle indicates the experimental data[18]. The solid line stands for the calculated results of ALICE-F[17].
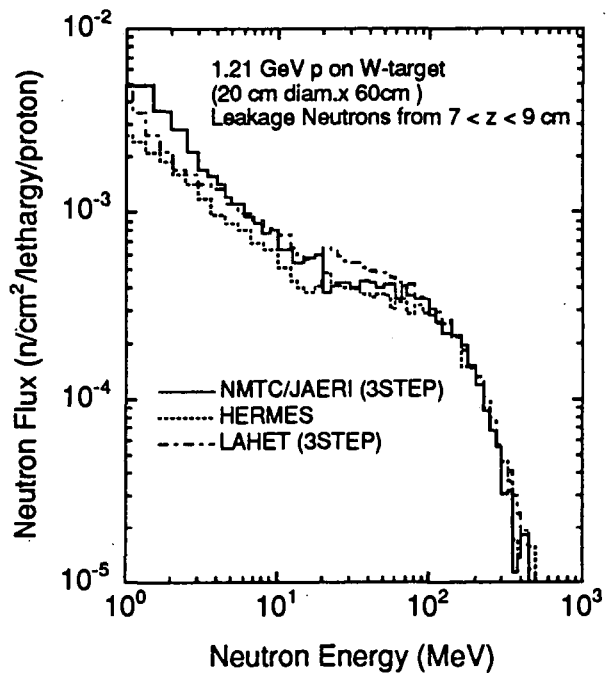
Fig. 2 Calculated neutron leakage spectra on the cylindrical surface at the position between 7 and 9 cm from the front surface of thick tungsten target bombarded with 1.21 GeV protons. The solid, dotted and dot-dashed lines indicate the calculated results of NMTC/JAERI-MCNP-4A, HERMES and LAHET, respectively.
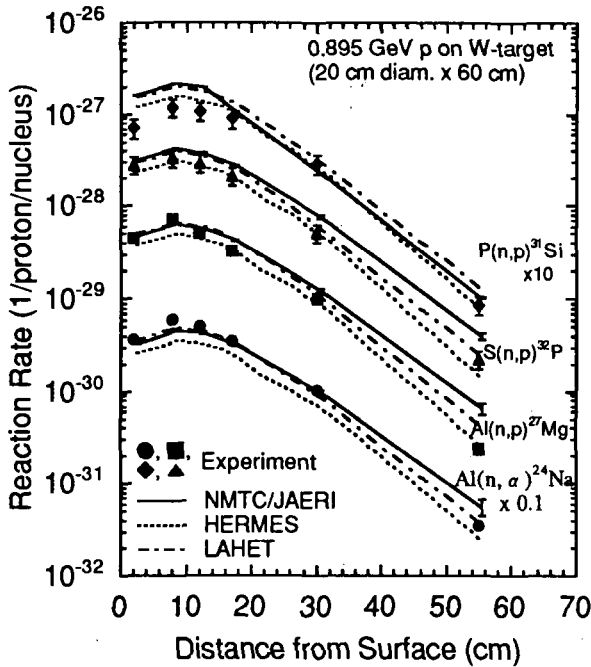
Fig. 3 Reaction rates of $S(n,p)^{32}P$, $P(n,p)^{31}Si$, $Al(n,p)^{27}Mg$ and $Al(n,\alpha)^{24}Na$ for the 0.895 GeV proton incidence on thick tungsten target. The solid marks indicate the experimental results. The solid, dotted and dot-dashed lines stand for the calculated results of NMTC/JAERI-MCNP-4A, HERMES and LAHET, respectively.
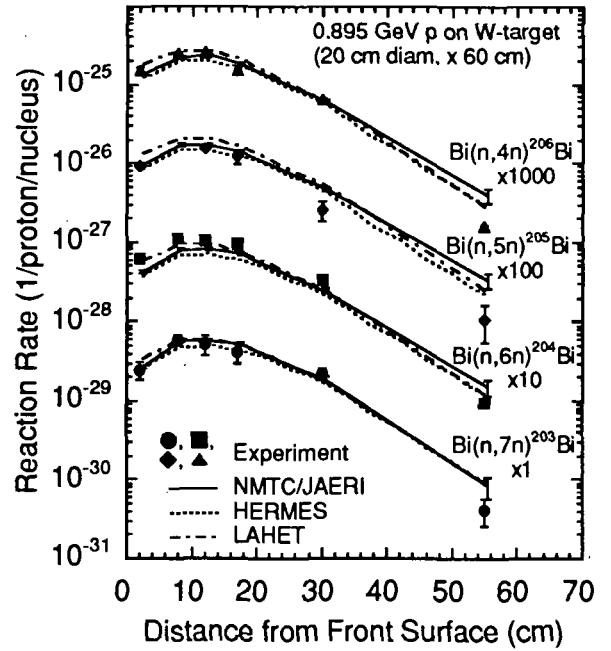
Fig. 4 Reaction rates of $Bi(n,4n)^{206}Bi$, $Bi(n,5n)^{205}Bi$, $Bi(n,6n)^{204}Bi$ and $Bi(n,7n)^{203}Bi$ for the 0.895 GeV proton incidence on thick tungsten target. The notes to the marks and lines are the same as for Fig. 3.
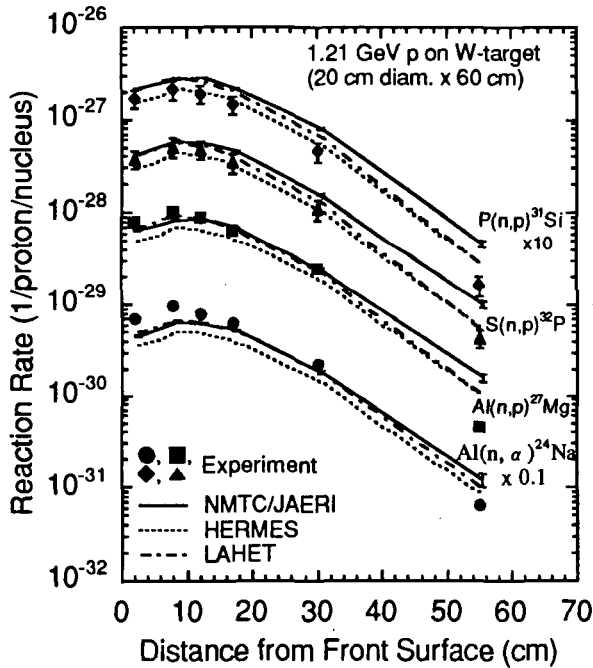
Fig. 5 Reaction rates of $S(n,p)^{32}P$, $P(n,p)^{31}Si$, $Al(n,p)^{27}Mg$ and $Al(n,\alpha)^{24}Na$ for the 1.21 GeV proton incidence on thick tungsten target. The notes to the marks and lines are the same as for Fig. 3.
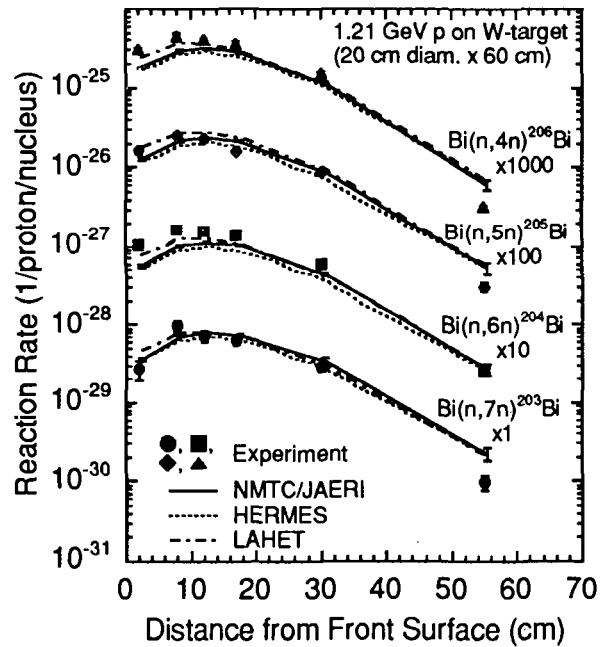
Fig. 6 Reaction rates of $Bi(n,4n)^{206}Bi$, $Bi(n,5n)^{205}Bi$, $Bi(n,6n)^{204}Bi$ and $Bi(n,7n)^{203}Bi$ for the 1.21 GeV proton incidence on thick tungsten target. The notes to the marks and lines are the same as for Fig. 3.
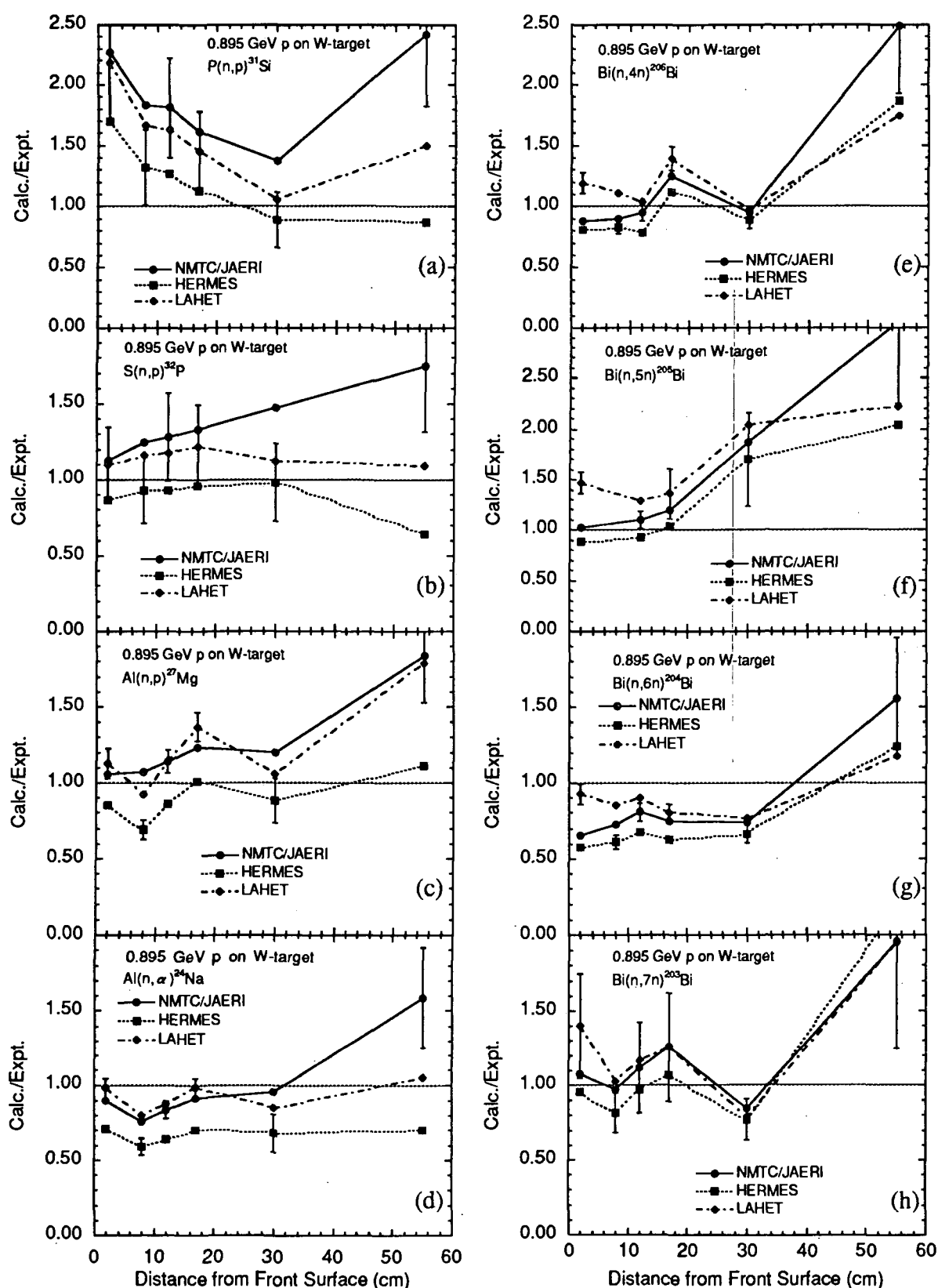
Fig. 7 C/E ratios of reaction rates for the 0.895 GeV proton incidence on thick tungsten target. The solid, dotted and dot-dashed lines indicate the results of NMTC/JAERI-MCNP-4A, HERMES and LAHET, respectively.

(a) $P(n, p)^{31}Si$ reaction, (b) $S(n, p)^{32}P$ reaction, (c) $Al(n, p)^{27}Mg$ reaction, (d) $Al(n, \alpha)^{24}Na$ reaction,

(e) $Bi(n, 4n)^{206}Bi$ reaction, (f) $Bi(n, 5n)^{205}Bi$ reaction, (g) $Bi(n, 6n)^{204}Bi$ reaction, (h) $Bi(n, 7n)^{203}Bi$ reaction.

2.6.2   The South African National Accelerator Centre and its Research Programme

Y. Watanabe
Department of Energy Conversion Engineering,
Kyushu University, Kasuga, Fukuoka 816, Japan
e-mail : watanabe@ence.kyushu-u.ac.jp

An overview of the South African National Accelerator Centre and its research activities is given with emphasis on medium energy nuclear physics and nuclear data measurements for medical use. Also presented is a preliminary result of $^{40}Ca(p,p'x)$ spectrum measurement for 392 MeV which has been carried out at RCNP, Osaka University, under the South Africa-Japan collaborative programme.

1. Introduction

For the past few years, the author has been keeping collaboration with several researchers who are studying nuclear physics at National Accelerator Centre (NAC) in Faure, South Africa. The collaborative work is related to the study of preequilibrium nuclear reactions which become a dominant reaction process in the intermediate energy region more than 20 MeV. He had an opportunity to visit University of Stellenbosch and NAC in October 1996. Based on the experiences, he introduces an overview of NAC and its research programme in connection with intermediate energy nuclear data evaluation in this report.

The NAC group has started a new measurement of $(\vec{p},p' p")$ and (p,p'x) at 392 MeV at RCNP, Osaka University with Japanese collaborators (RCNP, Kyoto University and Kyushu University) in April 1996. The preliminary result is also presented.

2. NAC and its research programme

2.1. Overview

NAC is a multidisplinary research centre established in 1977, operated by the Foundation for Research Development (FRD), South Africa. It provides facilities for (i) basic and applied research using particle beams, (ii) particle radiotherapy for the treatment of cancer, and (iii) the supply of accelerator-produced radioactive isotopes for nuclear medicine and research. The accelerators now operated by NAC are a 6 MeV Van de Graaff accelerator, an 8 MeV injector cyclotron which provides light ions for a 200 MeV cyclotron, a second injector cyclotron which provides heavy ions and polarized light ions for the 200 MeV machine, and the 200 MeV separated-sector cyclotron (SSC). A layout of the SSC facility is illustrated in Fig.1.

The protons and other heavy ions accelerated by the SSC are transported into three facilities located inside the building: radiotherapy facilities, radioisotope production facilities, and nuclear physics facilities. The machine operating schedule in a week is presented in Fig.2. The experiments related to nuclear physics are limited only in the weekend, because the treatment of cancer and the radioisotope production have a high priority as the daily business.

2.2. Neutron and proton radiotherapy and related nuclear data measurements

The NAC has the only particle therapy facility in the world where both high-energy neutrons and high-energy (>150 MeV) protons are used for patient treatment. Three treatment vaults are included in the facility. One of them contains the isocentric neutron therapy unit (gantry) in which neutrons are produced by the reaction of 66 MeV protons on a thick beryllium target. It is located in vault "N" in Fig.1. The 200 MeV horizontal beam proton therapy facility occupies a second vault marked "M" (left) in Fig.1. Additional proton therapy

beam lines are foreseen for the third vault marked "M" (right) in Fig.1. Details of the facility and the treatment are described in Ref.[1].

Nuclear data related to neutron and proton therapy are being measured at NAC. Fig.3 shows typical double-differential cross sections of $^{16}O(p,p'x)$ which have been measured in the comprehensive investigation of continuum spectra of light ejectiles induced by protons of 100-200 MeV on ^{12}C, ^{14}N, and $^{16}O[2]$. In addition, the cross sections for $^{12}C(n,\alpha)^9Be$ and $^{12}C(n,n')3\alpha$ for $E_n=5$ to 53 MeV have been measured using the neutron beam of the NAC neutron therapy facility. The preliminary result[3] is presented in Fig.4.

2.3. Nuclear physics with the SSC

A variety of research programme on medium energy nuclear physics are in progress at NAC. In this report, particular attention is paid to a topics on preequilibrium particle emission which has extentively been studied by Cowley (Univ. of Stellenbosch) and his co-workers.

So far, their group has been carrying out (p,p'x) experiments in the incident energy range from 80 to 200 MeV as summarized in Table I. Those experiments have been done using a ΔE-E counter telescope placed in a multi-purpose scattering chamber which is installed in the experimental arena marked "E" in Fig.1. The counter telescope consists of an active collimator made of a plastic scintillator, a silicon ΔE-detector and an NaI(Tl) E-detector. The detail has been described in the references in Table I. The experimental data have been analyzed in terms of the Feshbach-Kerman-Koonin theory, and the dependence of strength V_0 of effective N-N interaction on energy and mass number was investigated with their particular interest. A typical example of their results is presented in Fig.5. In the future, their experimental data are expected to contribute to intermediate energy nuclear evaluation because there are few available data in the energy range of 100 to 200 MeV.

More recently, they have extended the experiment so as to measure inclusive (p,α) spectra for ^{27}Al, ^{59}Co, and ^{197}Au at incident energies of 120, 160 and 200 MeV[6]. The typical result is shown in Fig. 6. As the next experimental project, they have undertaken measuerements of the analyzing powers of inclusive (p,p') spectra using a polarized proton beam in order to investigate the mechanism of preequilibrium proton emission in more details.

Table I. (p,p') experiments carried out at National Accelerator Centre, Faure. This table is taken from Ref. [4].

• Nov. 1989	^{90}Zr	$E_p = 80, 120$ MeV
		PRC 43 (1991) 678
• Feb.– Aug. 1991	^{90}Zr ^{89}Y ^{92}Mo ^{94}Mo ^{96}Mo ^{98}Mo	$E_p = 120, 160, 200$ MeV
		PRC 49 (1994) 1001
• May– Oct. 1992	^{115}In ^{141}Pr ^{167}Er ^{173}Yb ^{181}Ta	$E_p = 120, 150, 175, 200$ MeV
		PRC 54 (1996) 1756
• Also older data for MSD calcs:	^{58}Ni ^{100}Mo ^{197}Au	$E_p = 120, 150, 175, 200$ MeV
		PRC 46 (1992) 1030

3. South Africa and Japan Collaboration for Experiment at RCNP

Under the South Africa-Japan collaborative programme*, the experiment was carried out for the measurement of coincident proton emission from the continuum in the $^{40}Ca(\vec{p},p'p'')$ reaction at an incident energy of 392 MeV at RCNP. The purpose of the experiment is to investigate the rescattering effects in nucleon knockout reactions. The dual magnetic spectrometer system illustrated in Fig. 7 was used. "Grand Raiden" was set up at a fixed forward angle and a fixed momentum. The large acceptance spectrometer "LAS" was operated in coincidence to measure the angle-energy distributions of ejectile protons. The data analysis is now in progress.

Additional measurement of inclusive (p,p') spectra for the same target and incident energy was carried out at six angles of 25.5°, 40°, 60°, 80°, 100° and 120° using the LAS in order to study the mechanism of preequilibrium proton emission. The preliminary result is shown in Fig. 8. The data with the two highest field setting shows unacceptable matching in the overlap region (around 255 MeV). However, the other data look reasonable. Further detailed data analysis will be necessary to obtain the final result. From the viewpoints of the intermediate energy nuclear data evaluation as well as the study of the multistep direct processes, the present experimental data is expected to be valuable because there is no available data in this energy region.

4. Summary

The South African National Accelerator Centre and its research activities was described briefly, with respect to neutron and proton radiotherapy, its related nuclear data measurements and the study of preequilibrium nuclear reactions. The new experiment which has been started at RCNP by the South Africa and Japan collaboration was also introduced. In the experiment, the inclusive (p,p') spectra were measured from the basic and applied points of view. We hope that our collaboration will continue and bring great results in both the fields of nuclear physics and nuclear data evaluation in the future.

Acknowledgments

The author is deeply grateful to Prof. A.A. Cowley and his colleagues for inviting him to University of Stellenbosch and NAC and their warmest hospitality during his stay. The $(\vec{p},p'p'')$ experiment was performed at RCNP under the experimental-program-number E82.

References
[1] D.T.L. Jones, Hospital Supplies, June (1996) pp.8.
[2] G.J. Arendse et al., NAC Annual Report, NAC/AR/95-01 (1995), p. 9.
[3] M.R. Nchodu et al., NAC Annual Report, NAC/AR/95-01 (1995), p. 16.
[4] W.A. Richter, acta physica slovaca **45**, 733 (1995).
[5] W.A. Richter et al., Phys. Rev. C **46**, 1030 (1992).
[6] A.A. Cowley et al., Phys. Rev. C **54**, 778 (1996).
[7] T. Noro, *Proc. of the 14th RCNP OSAKA Int. Symp. on Nuclear Reaction Dynamics of Nucleon-Hadron Many Body System*, Eds. H. Ejiri, T. Noro, K. Takahisa, and H. Toki, (World Scientific, 1996), p.86.

*Participants: A.A. Cowly, G.J. Arendse, R. Visser, J.J. Lawrie, J.V. Pilcher, F.D. Smit, G.F. Steyn, S.V. Förtsch, T. Noro, M. Kawabata, K. Tamura, Y. Mizuno, Y. Yuasa, S. Nakanishi, K. Takahisa, H. Hatanaka, N. Matsuoka, M. Nomachi, H. Sakaguchi, M. Itoh, and Y. Watanabe

A: Separated-sector cyclotron (SSC)
   Oopsektorsiklotron (OSS)
B: Solid-pole injector cyclotron SPC1
   Soliedepool-injektorsiklotron SPS1
C: Solid-pole injector cyclotron SPC2
   Soliedepool-injektorsiklotron SPS2
D: Low-energy experimental area
   Lae-energie eksperimentele gebied
E: Charged-particle experimental area
   Gelaaide-deeltjie-eksperimentele gebied
F: Neutron-beam experimental area
   Neutronbundeleksperimentele gebied
G: Gamma-ray measurement area
   Gammastraalmeetgebied
H: Magnetic spectrometer
   Magneetspektrometer
J: Radioisotope production vault
   Radioisotoopproduksiekluis
K: Electronics areas
   Elektronikagebiede
L: Beam-swinger magnet vault
   Bundelswaaiermagneetkluis
M: Proton therapy vaults
   Protonterapiekluise
N: Isocentric neutron therapy vault
   Isosentriese neutronterapiekluis
P: Polarized-ion source (basement)
   Gepolariseerde-ioonbron (kelder)
Q: ECR ion source (basement)
   ESR-ioonbron (kelder)
▣ Shielding walls
   Afskermmure

Fig.1   Layout of the cyclotron facility of NAC.

PH   Nuclear Physics
E   Energy Change
N   Neutron Therapy
P   Proton Therapy
I   Production of Radioisotopes
C   Calibration

Fig.2   Operationing schedule for the separated-sector cyclotron
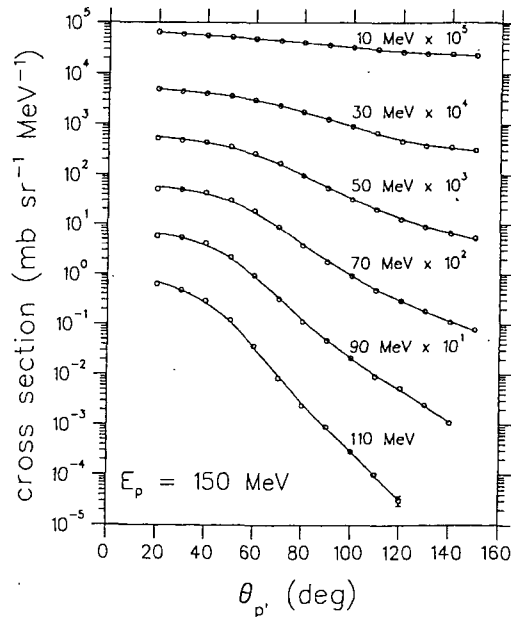
Fig.3   Angular distribution for the reaction $^{16}O(p,p')$ at selected ejectile energies. This figure is taken from Ref.[2].
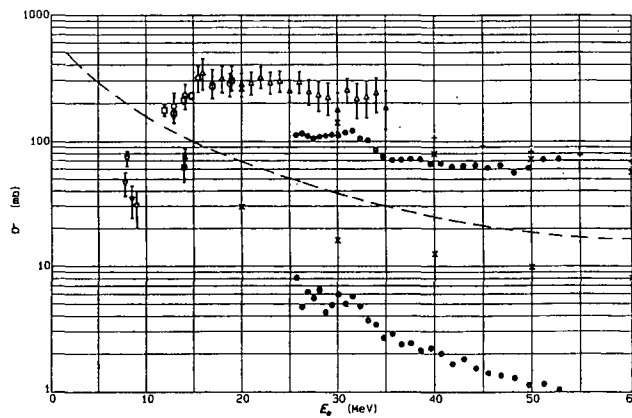
Fig.4   Cross sections for the ^{12}C(n,α)^{9}Be reaction (below dashed line) and ^{12}C(n,n')3α reaction (above dashed line). This figure is taken from Ref.[3].
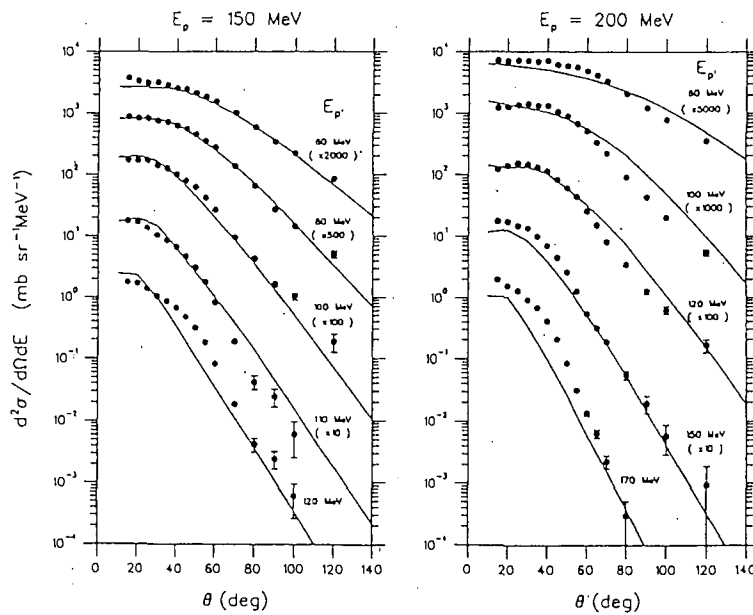
Fig.5   Comparisons of experimental angular distributions for ^{58}Ni(p,p') at two incident energies E_p and emission energies $E_{p'}$ and results of MSD calculations (solid lines). The figures are taken from Ref. [5].
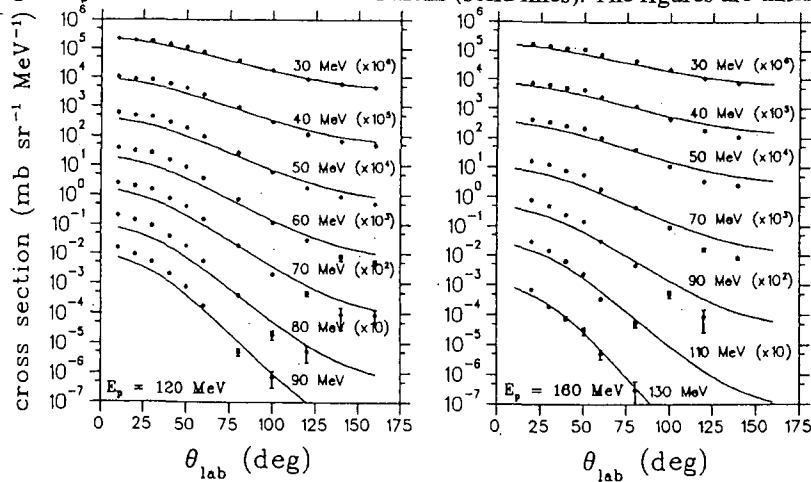
Fig.6   Laboratory angular distributions for the inclusive reaction ^{27}Al(p,α) at incident energies E_p of 120 and 160 MeV and various emission energies. The curves are distributions, predicted by the Kalbach systematcs, normalized to the experimental data. This figure is taken from Ref. [6].
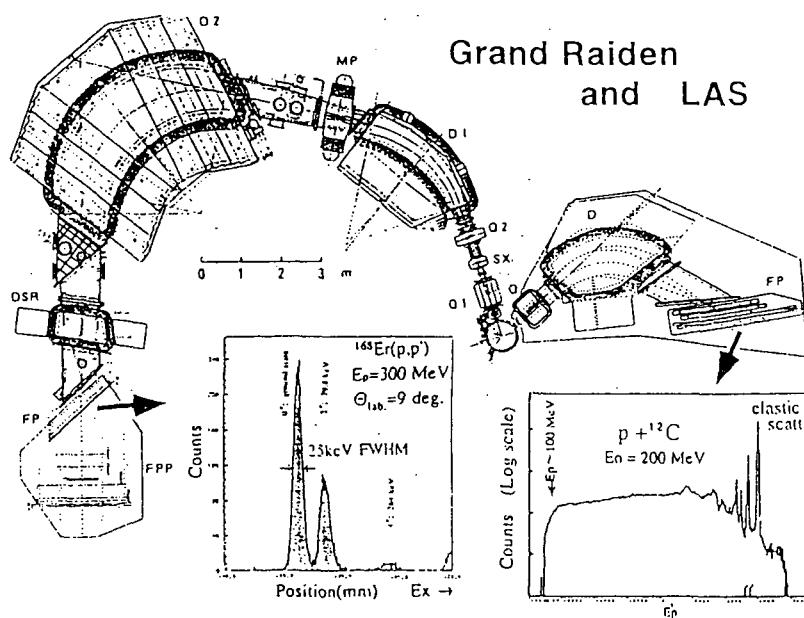
Fig.7 Layout of Grand Raiden and Large Acceptance Spectrometer (LAS). This figure is taken from Ref. [7].
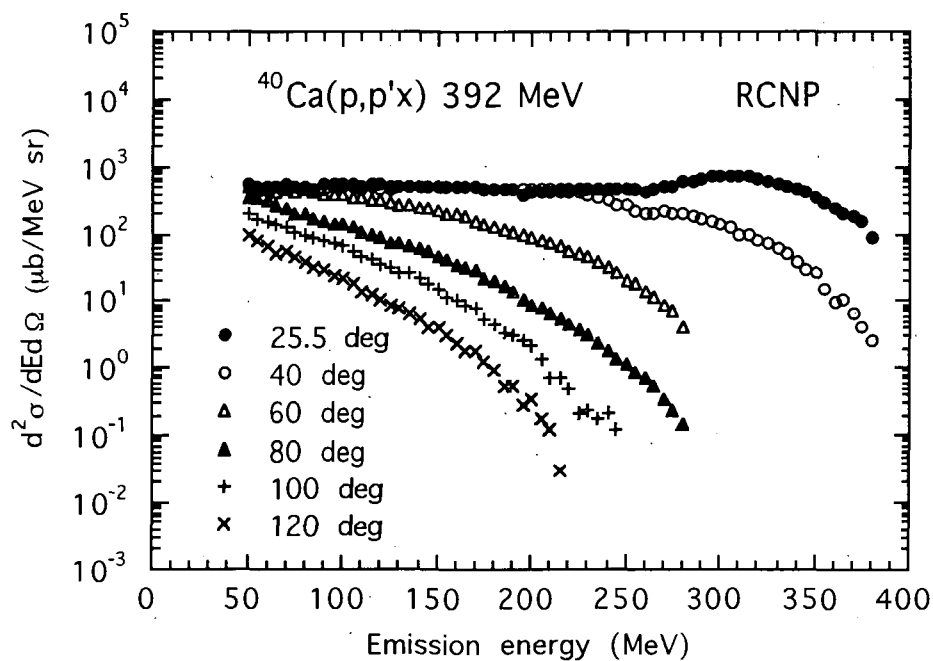
Fig.8 Experimental double-differential cross sections of the $^{40}Ca(p,p'x)$ reaction at an incident energy of 392 MeV.

2.6.3 Measurements of Double Differential Charged Particle Emission Cross Sections and Development of a Wide Range Charged Particles Spectrometer for Ten's MeV Neutrons

Yasushi NAUCHI, Mamoru BABA, Takehide KIYOSUMI, Tomohiko IWASAKI,
Toshiya SANAMI, Shigeo MATSUYAMA, Naohiro HIRAKAWA
Department of Quantum Science and Energy Engineering, Tohoku University, Sendai 980-77
Susumu TANAKA
Takasaki Establishment, Japan Atomic Energy Research Institute, Takasaki 370-12
Shin-ichiro MEIGO, Hiroshi NAKASHIMA
Tokai Establishment, Japan Atomic Energy Research Institute, Tokai-mura 319-11
Takashi NAKAMURA
Cyclotron Radioisotope Center, Tohoku University, Aoba-ku, Sendai 980-77
Yukinobu WATANABE, Masahide HARADA
Department of Energy Conversion Engineering, Kyushu University, Kasuga-ku, Fukuoka 816

Abstract

We measured (n,xp), (n,xd) cross sections of C and Al for En=64.3MeV neutrons at the ^{7}Li(p,n) neutron sources facility at TIARA (Takasaki Establishment, JAERI) by using a conventional SSD-NaI telescope placed in the air. They show characteristic energy and angular dependence in high energy regions.

In order to extend the measurements to low energy protons and α particles, a new spectrometer consisting of low pressure gas counters and BaF$_2$ scintillators is now under development. A low threshold for low energy α particles will be achieved by using the gas counters. The particle identification over a wide energy range will be achieved by combining the ΔE-E method for low energy particles with the pulse shape discrimination (PSD) method of BaF$_2$ for high energy particles.

1. Introduction

Double differential cross section (DDX) data of charged particle emission reactions for intermediate energy neutrons are important for the study of radiation damage, fast neutron therapy, and accelerator-based reactors. However, DDXs data beyond 20 MeV are scarce.

We are conducting the measurements of (n,xz) DDXs using the ^{7}Li(p,n) source at TIARA (Takasaki Ion Accelerator for Advanced Radiation Application) LC course [Fig. 1] using a conventional SSD-NaI ΔE-E telescope [1]. Recently, we measured (n,xp), (n,xd) DDXs of C and Al for 64.3MeV neutrons those are important in various applied fields. The results of this measurement were compared with cascade model calculations.

The detection threshold of the telescope, however, was still too high (Ep~9MeV), thus a new wide range charged particle spectrometer was designed for simultaneous measurements of low energy protons and α particles together with high energy protons. The improvements in signal to noise ratio and the counting efficiency are also intended.

2. (n,xp), (n,xd) Measurements

2.1 Experiment

Figure [1] shows a schematic view of the ^{7}Li(p,n) neutron source facility at TIARA. Accelerated

protons are injected into a ^{7}Li target of 5.07mm thickness, then quasi monoenergetic of 64.3MeV neutrons were generated. The neutron spectrum was measured with a proton recoil telescope[1] and the TOF method. It consists of 64.3MeV peak part and low energy continuum part as shown in Fig. [2]. The peak flux was 1.4×10^4 n · cm^{-2} · μC^{-1}. During the experiment, the neutron intensity was monitored by a ^{238}U fission chamber set near the Li target.

The C and Al samples were placed at 5.6m from the target in the air, and irradiated by the neutron beam. Emitted protons and deuterons were measured by a counter telescope consisted of a SSD ΔE detector (150μm thick, 900mm^2 wide) and a NaI(Tl) scintillator (5.08cm in diameter, 3cm thick). To obtain the spectra for very forward angles < 25°, we use an "annular geometry"; the counter telescope is located on the neutron beam line behind a 50cm brass shadowbar as shown in Fig. [3a]. The data for angles > 25° were taken by a normal "inclined geometry" as shown in Fig. [3b].

The pulse heights and TOF signals of detectors were taken event by event. Particle identification was done by the ΔE-E method, then the events induced by the peak neutrons were selected using TOF information.

The energy scale was determined by the recoil proton peak corresponding to 64.3MeV peak neutrons and the linear response of NaI(Tl) [2]. Then the spectra were corrected for the energy loss assuming the avarage values of energy loss in the sample, air, Al window (0.115mm in thickness) and SSD. At last, DDXs are obtained by considering the neutron flux, the number of sample atoms and the solid angle.

2.2 Carbon (n,xp), (n,xd) spectra

Figure [4a] shows (n,xp) DDXs of carbon. In high energy region, peaks are seen with very strong angular dependencies. These peaks will correspond to the ground state and the first excited state of residual nucleus ^{12}B. The low energy continuum spectra show much milder angular dependencies.

In Fig. [5], our (n,xp) data are compared with the experimental data reported by Subramanian[3] et. al. and Slypen et al. [4]. Our data are consistent with the others both in shape and magnitude. In the energy region lower than our detection threshold (Ep=9MeV), however, the other two data show marked differences in magnitude.

In Fig. [6a], we compeared our data with calculations of cascade model code, ISOBAR. ISOBAR trace the shape of experimental spectra but underestimates generally, probably because the ISOBAR ignors inelastic scattering processes.

Figure [4b] show (n,xd) DDXs. A prominent peak is seen at the high energy end of the spectrum. This peak intensity depend strongly on angles and will due to the pick-up reactions.

2.3 Aluminum (n,xp), (n,xd)

Figure [7a] shows (n,xp) DDXs of Al. In contrast to C case, the spectra are continuum-like and the spectra are softer because of equilibrium and/or multi-boy reactions, while the angular dependencies are strong in high energy region (> 40MeV). Figure [6b] shows the comparison of our data with ISOBAR. ISOBAR traces the experimental data fairly well, while it still underestimates at forward angles.

Figure [7b] shows Al(n,xd) DDXs. Similarl with carbon data, isolated peaks attributable to pick up reactions exist in high energy region at forward angles (< 20°).

3. Developments of New Spectrometer

It is desirable to measure low energy protons and α particles with high energy protons simultaneously. Furthermore, backgrounds should be reduced greatly. Background protons and deuterons were stemmed from the air and other materials exposed by the source neutrons.

To be low the detection threshold, it is necessary to use a vacuum reaction chamber and a low pressure gas counter with a thin window as the ΔE detector. On the other hand, particle identification (PI) by the ΔE-E method becomes difficult for high energy particles because of the small energy deposition in the gas counter. Therefore, the pulse shape discrimination (PSD) method utilizing light outputs of BaF$_2$ will be employed to PI for high energy particles[5]. By combining two methods, all emitted particles will be separated each other for the whole energy range.

Figure [8] shows a test telescope. The gas counter is of cylinder shape (54mm long, 45mm in diameter), with a gold plated tungusten wire (0.05mm in diameter) on the central axis. Entrance and exit window of the counter are 3.4μm thick mylar films, supported by tungusten wires. The BaF$_2$ scintillator is 4cm in diameter and 2.2cm thick to stop 85MeV protons. Each of detectors is now investigated.

Figure [9] shows the spectrometer now under fabrication. The vacuum chamber is 35cm in diameter and holds a sample (5cm in diameter) at the center. The sample is viewed by 3 gas-BaF2 telescopes simultaneously (11mstr×3). The neutron entrance window to the chamber is 7cm in diameter, and the neutron beam is collimated to avoid exposure of wall materials of the chamber. With this spectrometer, DDXs at from 25° to 155° can be obtained. Data for very forward angles (< 25°) are obtained utilizing the annular geometry.

Acknowledgement

References

(1) M. Baba et. al., : *Proc. Int. Conf. on Nucl. Data for Sci. Technol.* (1994 Gatlinburg) pp. 90

(2) J. L. Romero et al., : *Nucl. Instr. and Meth. in Phys. Res.* **A301** 241 (1991)

(3) T. S. Subramanian et. al., : *Phys. Rev.* **C 28** 521 (1983)

(4) I. Slypen et. al., *Phys. Rev.* **C 51** 1303 (1995)

(5) G. Lanzano et. al., : *Nucl. Instr. and Meth.* **A312** 515 (1992)

Fig. 1: TIARA neutron source

Fig. 2: Li(p,n) neutron spectrum
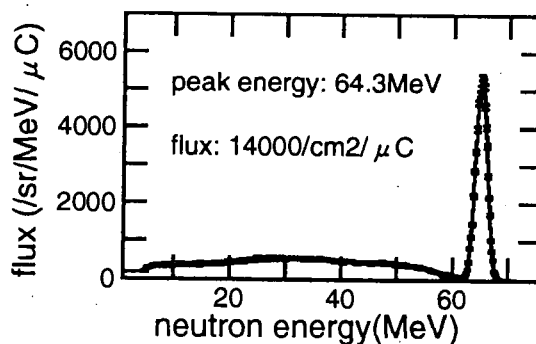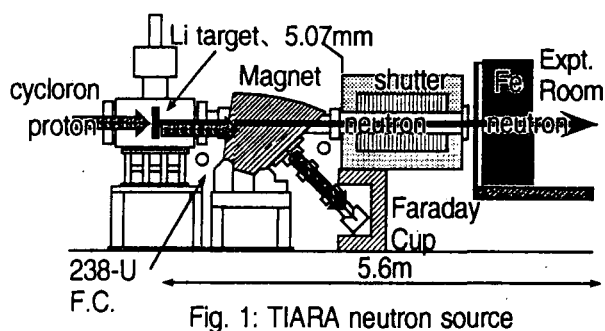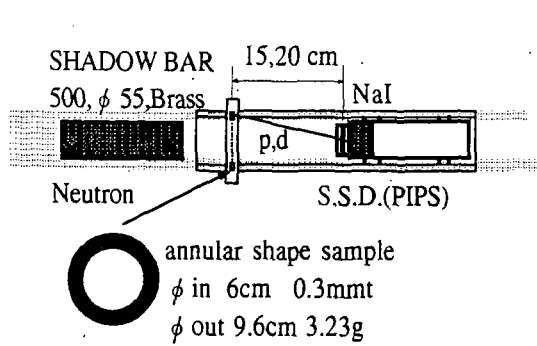
Fig.3a: annular geometry
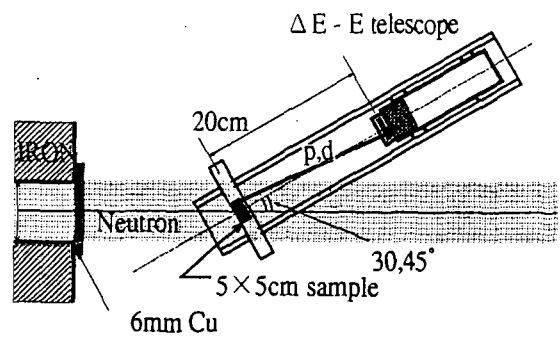
Fig. 3b: inclined geometry
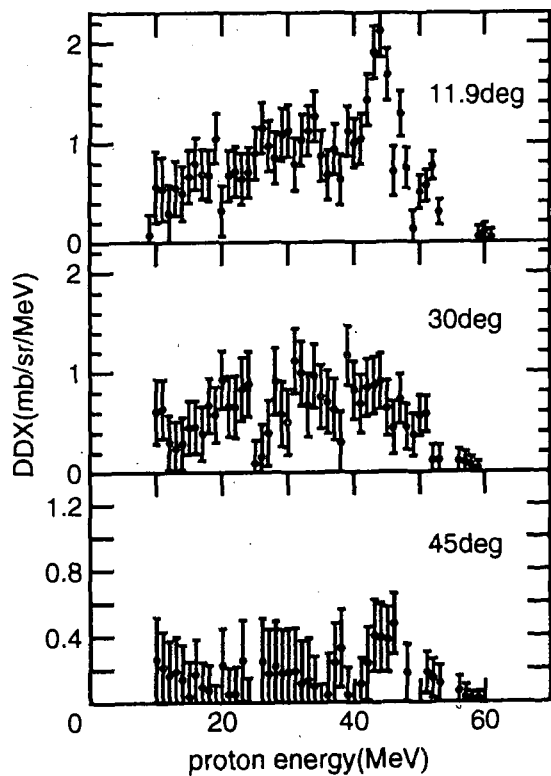
Fig. 4a: C(n,xp) DDX
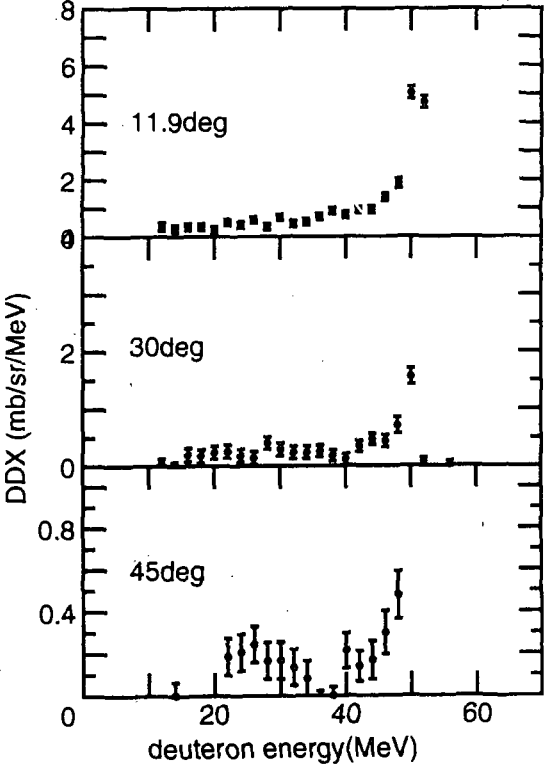
Fig. 4b: C(n,xd) DDX
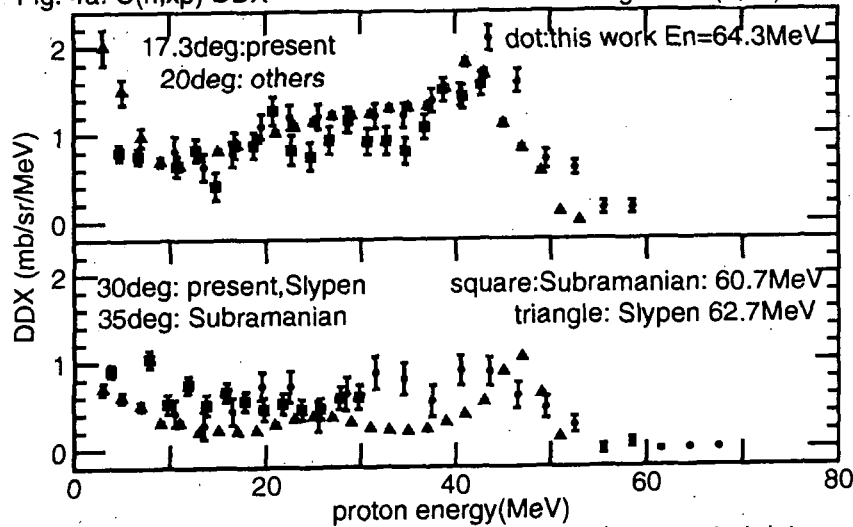
Fig. 5: Comparison present work with other reported data
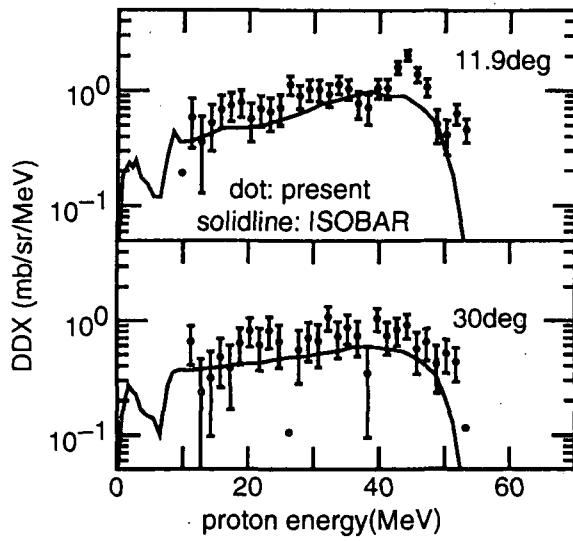
Fig. 6a: Comparison C data with ISOBAR
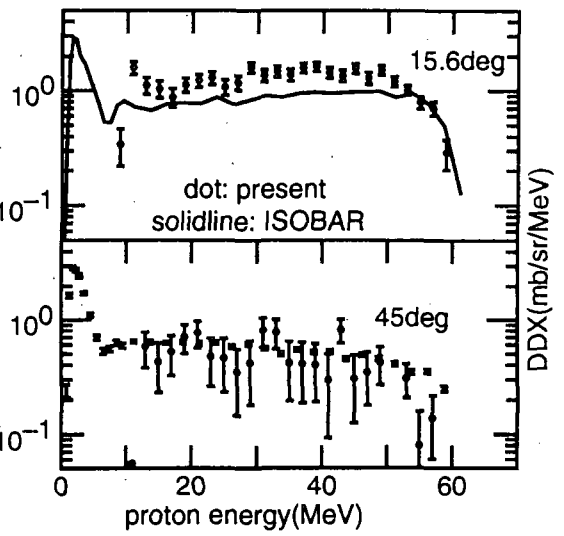
Fig. 6b: Comparison Al data with ISOBAR
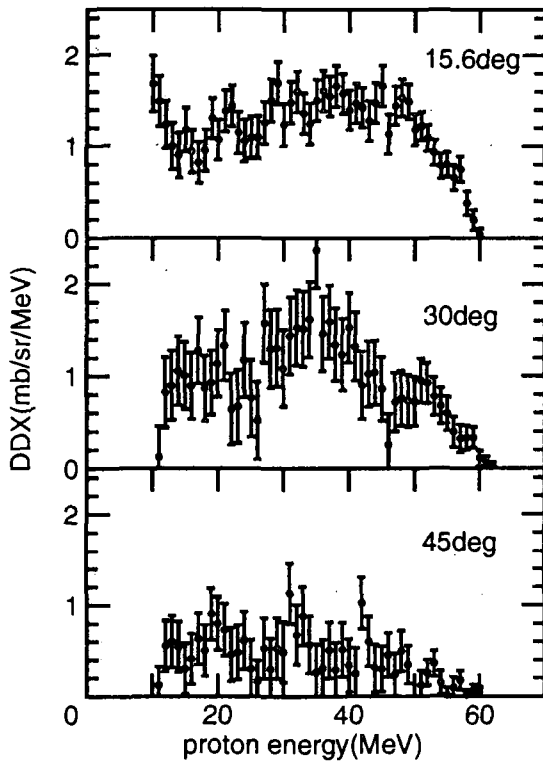
Fig. 7a: Al(n,xp) DDX
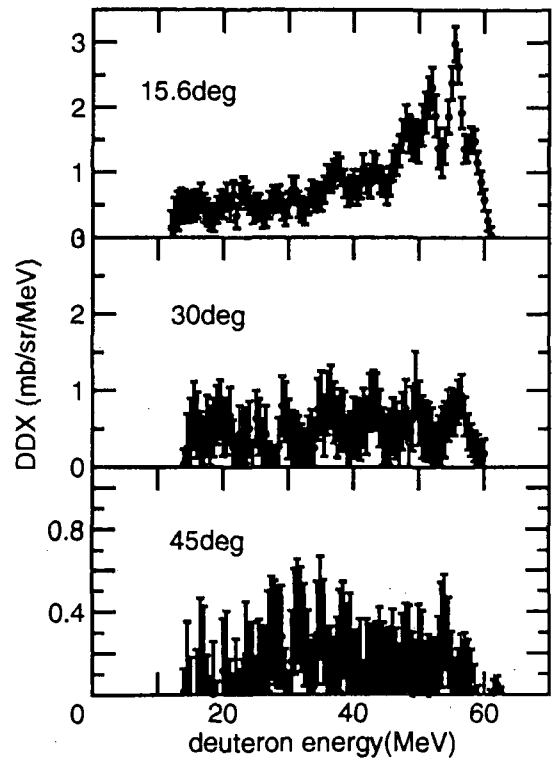
Fig. 7b Al(n,xd) DDX
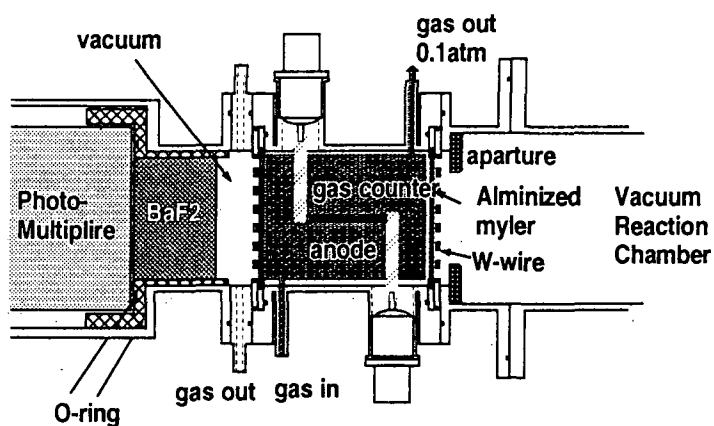
Fig. 8: Gas-BaF2 telescope
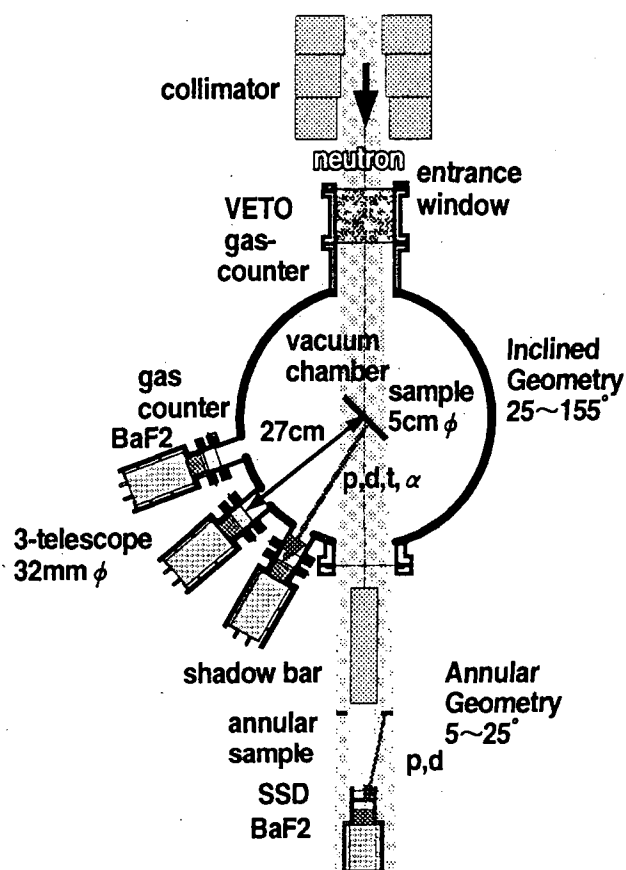
Fig. 9: Shematic view of the new spectrometer

2.6.4 Status of Spallation Neutron Source

Yukio OYAMA

Japan Atomic Energy Research Institute
Tokai-mura, Naka-gun, Ibaraki-ken 319-11
e-mail: oyama@fnshp.tokai.jaeri.go.jp

Existing and planned facilities using proton accelerator driven spallation neutron source are reviewed. These include new project of neutron science proposed from Japan Atomic Energy Research Institute. The present status of facility requirement and accelerator technology leads us to new era of neutron science such as neutron scattering research and nuclear transmutation study using very intense neutron source.

1. Introduction

Recently spallation neutron sources as a next generation neutron source have been extensively investigated and are planned in the world. Many programs are proposed now such as the ESS (European Spallation Source) [1] at Europe, the NSNS (National Spallation Neutron Source) [2] at ORNL, and in Japan there is two programs of the N-arena in JHP (Japan Hadron Project)[3] at National Laboratory for High Energy Physics (KEK) and the Neutron Science Program at JAERI. Also most intense spallation source SINQ will be operated at Paul Sherrer Institute in Switzerland [4] this year. These neutron source programs are motivated by a lack of neutron source in future[5] because of termination of many research reactors in the world.

In Japan, the KENS at KEK has supplied pulsed spallation neutrons for neutron scattering research. However, its intensity is two order lower than the ISIS at Rutherford Appleton Laboratory. Thus the research community in neutron scattering field called for Japanese intense neutron source. On the other hand, new research areas utilizing high energy proton beam are raised; one is for K-on and neutrino physics and another is for nuclear transmutation study of long-lived nuclear wastes. Specially, nuclear transmutation study requires enormous number of neutrons as well as neutron scattering science that can be realized only by a high energy proton driven spallation neutron source. Thus JAERI proposes multi-purpose spallation source with a proton accelerator of 1.5 GeV and beam current up to 6 mA.

The present paper describes status of recent spallation source projects, mainly the Neutron Science Program proposed by JAERI in comparison with the other projects.

2. Feature of Spallation Source and Its Utilization

Spallation reaction is not defined clearly but usually means the high energetic proton induced neutron production reaction, i.e., (p,xn) for proton energy above 100 MeV. Above this energy, various types of nuclear reactions are included, i.e., intranuclear cascade, evapolation, fission and so on. Specially around GeV region, intranuclear cascade is dominant, and then the neutron production yield is presented as multiplication of the mass number of target nuclei and the incident proton energy. The yield can be well expressed by the following formula:

$$Y_n \ [\text{n/proton}] = a \ (A+20) \ (E-b) \ ,$$

where a=0.1[GeV^{-1}] for A=9-210 and =0.2[GeV^{-1}] for U-238, and b=0.12[GeV]. Figure 1 plots neutron production yields for thick targets of various materials from experimental data. From the figure, though the data are scattered, below 200 MeV the data do not show clear mass dependence and fall rather in a band of a factor.

On the other hand, from the viewpoint of production efficiency, i.e., neutron yield for deposited energy that expresses difficulty to realize a heat removal system, a spallation source is comparable to a plasma D-T fusion system [6]. When we consider an intense neutron source, we should remember that the heat removal is always a problem. Thus the smaller the deposited heat for unit neutron production is, the better it is to construct the maximum neutron source. However if you consider the attainable maximum flux, we also should take a care for the neutron yield for unit particle incident.

From the above comparison, the spallation source could have a compact source space, so that it can give high flux and is suitable to produce cold neutrons using close coupled moderators, specially for neutron scattering research. This is a reason that spallation sources were built in the world. In addition, the spallation source can provide pulsed neutrons of micro second by a usage of accelerator.

2. Existing and Planned Facilities

There are several facilities of proton accelerator based spallation neutron source. Those were built mainly for neutron scattering research. In this research area a fission reactor is also used. However recently many reactors were shut down and will be shut down soon. By a public acceptance problem or technical difficulty to construct new intense research reactors, the total number of available neutron sources decrease and the situation is making a lack of neutrons. i.e., Neutron Gap. By this reason many proposals for accelerator based spallation source are raised in Europe and the United State as summarized in Table 1. The existing facilities are consists of synchrotron and linac accelerators below 1 GeV. The maximum power is given by SINQ at PSI, and it has got the first beam in December 1996. The SINQ is also operated in continuos beam and got higher efficiency for cold neutrons than the reactors. In Japan, the neutron scattering facility is proposed as a part of the JHP program at National Laboratory for High Energy Physics. As a next generation of spallation neutron source, very intense sources of 5 MW class are proposed from Europe (ESS), the United State (NSNS) and JAERI (Neutron Science Project). Those facilities utilizes linac accelerator with the energy above 1 GeV.

Figures 2 show the neutron target used in the ISIS facility. This facility was the maximum power

in the world and operated many years. This target system of Tantalum can be used three year (1752 mA-hr) till break down by irradiation damage. The most significant problem is a damage of the beam window of the target and a cooling of the target material. The beam window of the target is easily break down by proton-neutron irradiation, and a cooling structure for solid material is very difficult. In addition a break-down of cooling system leads to a release of radio-activities. Therefore For 5 MW class high power target in the ESS program, mercury is proposed because of liquid property at room temperature and high heat removal efficiency. Figure 3 shows the proposed target system for the ESS project.

3. Neutron Science Project at JAERI

Since late 1970' s a study of partitioning and transmutation (P-T) have been started at JAERI. In early 1980's an accelerator application to nuclear engineering was discussed, and at 1988 the OMEGA program was started to study a R&D program on P-T of minor actinides and long-lived fission products. This study included an accelerator -driven transmutation system. Under this program some basic R&D, i.e., ion source, RFQ, DTL, for high energy and intense proton accelerator has been carried out. In 1995 these activities and ideas of accelerator utilization were integrated to a project to construct a multi-purpose research facility using intense proton accelerator, we called, Neutron Science Project.

The research areas in the project are divided to three main categories: 1) Basic science utilizing very intense neutron source, 2) Accelerator transmutation study and 3) Extended development of accelerator engineering for a future application to a nuclear energy system. The most expected area in the basic science is to study structural biology using neutron scattering, because this study is effective only by a source overcoming the existing neutron source. The transmutation study will be possible only by this facility because there is no other plan in the world.

The basic parameters of the planned facility are summarized in Table 2. The maximum power of accelerated beam is about 8 MW in total. A 5 MW of the power is provided to the neutron scattering facility. The continuos beam is also required for the stage of experimental verification of nuclear transmutation system. The proposed accelerator complex is made of RFQ, DTL linacs and a linac with super conducting cavities. The total length of accelerator will be 800 meter. The spallation neutron target system for the maximum power, i.e., for neutron scattering, will use a liquid target system of mercury, for example. The proton beam is distributed by three main pulse structures, short (<1 µs) for neutron scattering , long(~mA) for transmutation study and very short (~ns) pulses for neutron nuclear physics as illustrated in Fig. 4.

The schedule of R&D and construction is set preliminary as to start a construction in 2002, to start commissioning in 2005, and to complete an accelerator facility in 2008. To keep this schedule, many R&D studies should be on time, so we are strongly requesting an approval for the proposed plan.

4. Concluding Remarks

The spallation neutron source is almost only one way to get most intense and highest flux of neutrons, because of limitation of fission reactors. Neutron utilization could be a frontier of science in the next century, because neutrons should be more attractive as both a probe for looking a micro-structure and a particle for catalyzing and controlling nuclear energy.

Acknowledgment

The author would like to express his thanks to an extensive effort of a conceptual study by the members of neutron science project group in JAERI.

References

[1] G.S. Bauer, " The European Spallation Source Study, ESS" , Proc. 2nd Int. Conf. on Accelerator -Drive Tranmutation Technologies and Applications, 3-7,June, Kalmar, Sweden (1996)

[2] B. Appleton, " NSNS Collaborative Project" , NSNS Workshop on Instrumentation Needs and Performance Metrics, 31 Oct. -1 Nov., ORNL, USA (1996)

[3] Y. Mori," The 50 GeV high-intensity proton synchrotron complex of Japanese Hadron Project," JAER-Conf 96-014 (1996) 17

[4] W.E. Fischer, " SINQ-A Continuous Spallation Neutron Source," Proc. 13th Mtg. of Int. Collaboration on Advanced Neutron Sources, 11-14 Oct., PSI, Switzerland (1995) 75

[5] " The Looming Neutron Gap" , Science, 267 (1995) 952

[6] Ed. S. Cierjacks ," Neutron Sources for Basic Physics and Applications," Pergamon Press (1983) 220

Table 1   Comparison of Neutron Scattering Facilities

	Proton Energy	Average Current	Target Power	Repettion Rate	Operation
KENS-I	500 MeV	5 μA	2.5 kW (DeU)	15 Hz	1985
LANSCE	800 MeV	100 μA	70 kW (W)	12 Hz	1985
ISIS	800 MeV	200 μA	160 kW (DeU,Ta)	50 Hz	1985
SINQ	590 MeV	1.2 mA	720 kW (Pb/Zyrcaloy)	CW	1997
JHP	3 GeV	200 μA	600 kW (Ta, W)	25 Hz	2002
ESS	1.35 GeV	3.7 mA	5 MW (Hg)	50 Hz	2006
NSNS	1 GeV	1 mA(4.4 mA)	1 MW(Hg) (4.4 MW)	60 Hz	2003 upgrade
JAERI	1.5 GeV	3.3 mA and 1.3 mA	5 MW (Hg) 2 MW (W)	50 Hz CW	2007
APT	1.3 GeV	100 mA	130 MW(W/Pb)	CW	?

Table 2 Refernce Parameters for Accelerator and Proton Beam

Accelerator	
Proton energy	1.5 GeV
Maximum current	- 6 mA
Linac frequency	200MHz DTL/600MHz SCC-Linac
Max. peak current	- 30 mA
Neutron Scattering Facility	
Macro pulse width	- 3 ms
Chopping factor	0.6
Pulse width	400 ns
Repetition	50 Hz
Target power	5 MW
Nuclear Tranmutation	
Mode	CW
Target power	2 MW
Irradiation Effect	
Mode	Pulse/CW
Target power	- 1.5 MW
Neutron Nuclear Physics	
Pulse width	< 1 ns
Average current	10 µA
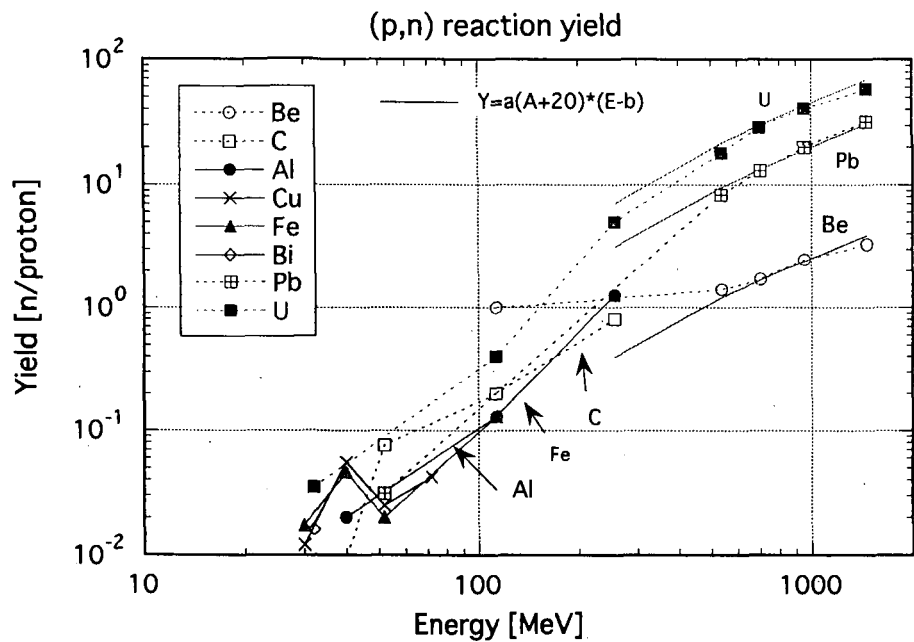
Fig. 1   Neutron production yield by (p, xn) reaction vs. proton energy
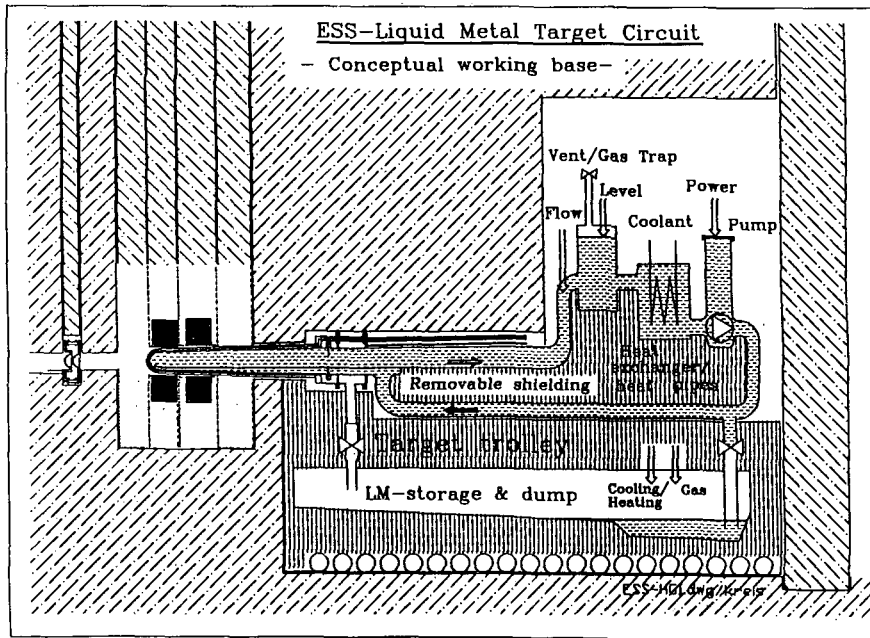
Fig. 2   The conceptual design of mercury liquid target system in the ESS program
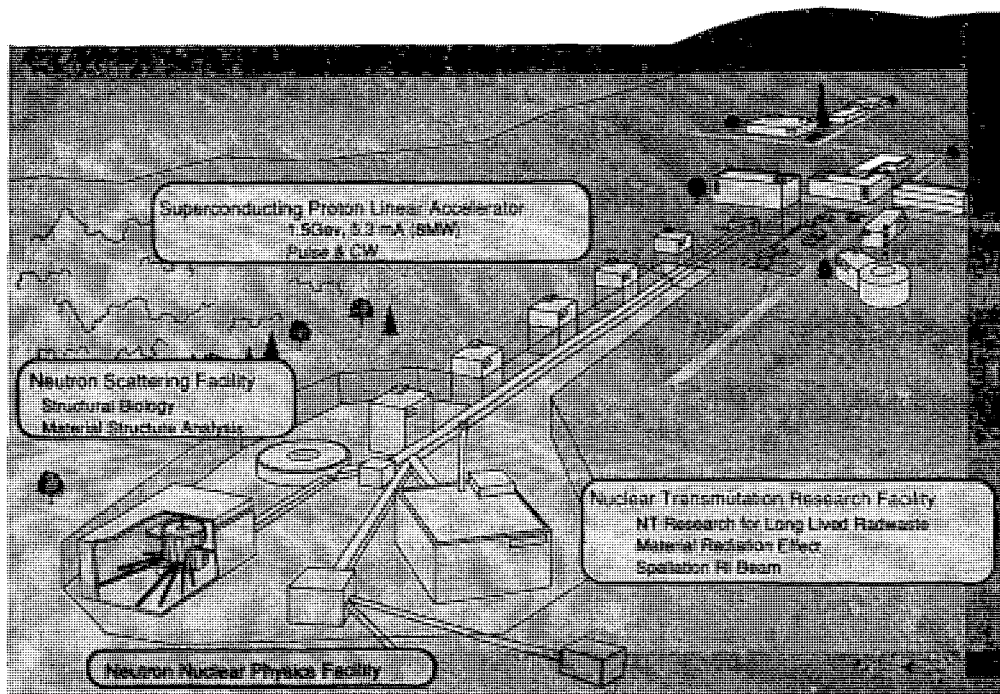
Fig. 3   Conceptual drawing of facility layout of the JAERI Neutron Science Project

3. Papers Presented at Poster Session

3.1 Measurements of keV-Neutron Capture γ Rays of Fission Products(III)

Masayuki IGASHIRA
Research Laboratory for Nuclear Reactors, Tokyo Institute of Technology
2-12-1 O-okayama, Meguro-ku, Tokyo 152, Japan
e-mail:iga@nr.titech.ac.jp

γ rays from the keV-neutron capture reactions by ^{143,145}Nd and ^{153}Eu have been measured in a neutron energy region of 10 to 80 keV, using a large anti-Compton NaI(Tl) γ-ray spectrometer and the ^{7}Li(p,n)^{7}Be pulsed neutron source with a 3-MV Pelletron accelerator. The preliminary results for the capture cross sections and γ-ray spectra of those nuclei are presented and discussed.

1. Introduction

The keV-neutron capture cross sections of fission products(FPs) are indispensable for studies on innovative nuclear energy systems, and those of some FPs also for studies on the s-process nucleosynthesis in stars. Moreover, keV-neutron capture γ-ray spectra are necessary for studies on neutron capture reaction mechanism, and those of largely deformed nuclei would provide important information on nuclear excitation modes such as the M1 scissors mode[1]. However, those data, especially spectrum data, are quite inadequate both in quality and in quantity. Therefore, we are measuring keV-neutron capture γ rays of important FPs to obtain those nuclear data. For the past one year, we finished the measurements for ^{143,145}Nd and ^{153}Eu in a neutron energy region of 10 to 80 keV. Preliminary results are presented and compared with previous results in literature.

2. Experimental Procedure

The measurements were performed, using the 3-MV Pelletron accelerator of the Research Laboratory for Nuclear Reactors at the Tokyo Institute of Technology. A typical experimental arrangement is shown in Fig. 1.

Pulsed keV neutrons were produced from the ^{7}Li(p,n)^{7}Be reaction by bombarding a Li-evaporated copper disk with the 1.5-ns bunched proton beam from the Pelletron accelerator. The average proton beam current was 5 to 7 μA at a 2-MHz pulse repetition rate. The incident neutron spectrum on a capture sample was measured by means of a time-of-flight(TOF) method without the sample, employing a 0.5-cm diameter by 0.5-cm ^{6}Li-glass scintillation detector. The detector was located 30 cm away from the neutron source, and the angle between the detector axis and the proton beam direction was adjusted so as to observe the average incident neutron spectrum.

Highly enriched oxide powder contained in a case made of graphite was used for each capture sample. The samples were disks with a diameter of 2 cm and a thickness of 0.3 to 0.5 cm. The sample was located 11.8 cm away from the neutron source at an angle of 0° with respect to the proton beam direction. A standard Au sample with a diameter of 2 cm and a thickness of 0.2 cm was used to determine the absolute number of neutrons incident on each capture sample.

Capture γ rays were detected with a large anti-Compton NaI(Tl) spectrometer[2], employing a TOF method. The main detector of spectrometer is a 15.2-cm diameter by 20.3-cm NaI(Tl) detector, and is centered in a 33.0-cm outer diameter by 35.6-cm NaI(Tl) hollow anti-Compton detector. The spectrometer was set in a heavy shield consisting of borated paraffin, borated polyethylene, cadmium, and potassium free lead. A ^{6}LiH shield that absorbed effectively the neutrons scattered by the sample was added in the collimetor of the spectrometer shield. The distance between the sample and the spectrometer was 86 cm. Capture γ rays were observed at an angle of 125° with respect to the proton-beam direction. Because the second Legendre polynomial is zero at this angle, the differential measurement at this angle gave approximately the integrated γ-ray spectrum for the dipole transition. Capture events detected by the spectrometer were stored in a workstation as two-dimensional data on TOF and pulse height(PH).

The measurement with each sample and the measurements with and without the standard Au sample were made cyclically to average out changes in experimental conditions such as the incident neutron spectrum. The three measurements were connected by the neutron counts of the ^{6}Li-glass scintillation detector. Measurement time for each capture sample was 20 to 30 h.

3. Data Processing

The data processing method has been described in detail elsewhere[3,4] and so is summarized briefly in the present paper.

A typical incident neutron spectrum is shown in Fig. 2. The spectrum was extracted from the TOF spectrum observed with the ^{6}Li-glass scintillation detector and its relative neutron detection efficiencies.

Figure 3 shows a typical TOF spectrum observed with the γ-ray spectrometer. The sharp peak around 900 channel is due to γ rays from the ^{7}Li(p,γ)^{8}Be reaction. The broad peak around 750 channel is due to keV-neutron capture γ rays from the ^{143}Nd sample. Digital windows (DWs) were set on the TOF spectrum in Fig. 3 to obtain foreground and background PH spectra. The net capture γ-ray PH spectra were extracted by subtracting the background PH spectrum from the foreground PH spectra.

A PH weighting technique[5] was applied to the net PH spectra to obtain the capture yields. The capture yields of Au and the standard capture cross section of Au[6] were used to determine the absolute number of neutrons incident on each sample. Furthermore, the net PH spectra were unfolded by using a computer program FERDOR[7] to obtain the corresponding capture γ-ray spectra.

Corrections were made for the self-shielding and multiple-scattering of neutrons in the sample, for the absorption of capture γ rays in the sample, and for the dependence of γ-ray detection efficiency on the position in the sample. The oxide powder samples are hygroscopic, and the exact characterization of the samples is a severe problem for accurate cross section measurements. However, we have not yet performed the characterization. Therefore, the correction for the water in the sample is not made, but the effect of the correction is investigated with a Monte-Calro program, TIME-MULTI[8].

4. Results and Discussion

Preliminary cross section results of ^{143,145}Nd and ^{153}Eu are shown in Figs. 4-6, respectively, and are compared with previous values in literature[9-16]. The present values of ^{143}Nd are in good agreement with those of Musgrove et al.[9] and Bokhovko et al.[10] in the low energy region and with those of Nakajima et al.[11] in the high energy region.

The present results of ^{145}Nd are about 10 % larger than those of Bokhovko et al.[10] and Hockenbury et al.[12]. The results of Nakajima et al.[11] are much larger than our results in the high energy region contrary to the case of ^{143}Nd. The energy dependency of the results of Musgrove et al.[9] is stronger than that of our results in both cases of ^{143}Nd and ^{145}Nd. The present results of ^{153}Eu are 10 to 20 % larger than those of Macklin and Young[13], but about 20 % smaller than those of Kononov et al.[15]. The results of Mizumoto et al.[16] are in good agreement with the present ones in the low energy region, but become larger than the present ones in the high energy region.

The capture γ-ray PH spectra of ^{143,145}Nd and ^{153}Eu are shown in Figs. 7-9, respectively. A shoulder is clearly observed around 2.5 MeV in the ^{153}Eu spectrum and barely observed around 2 MeV in the ^{143,145}Nd spectra. The energy position of the shoulder is consistent with the systematics obtained from our early work[3] as shown in Fig. 10. The shoulder, referred to as the bump in our early work, was attributed only to a resonance structure of the E1 γ-ray strength function at that time, but its origin should be investigated also from different aspects such as the excitation of nuclear M1 scissors mode.

References

[1] N. Lo Iudice and F. Palumbo, Phys. Rev. Lett. **41** (1978) 1532.

[2] M. Igashira, K. Tanaka and K. Masuda, Proc. the 8th Int. Symp. on Capture Gamma-Ray Spectroscopy and Related Topics, Fribourg, Switzerland, 1993, edited by J. Kern (World Scientific, Singapore, 1994) p.992.

[3] M. Igashira, H. Kitazawa, M. Shimizu, H. Komano and N. Yamamuro, Nucl. Phys. **A457** (1986) 301.

[4] S. Raman, M. Igashira, Y. Dozono, H. Kitazawa, M. Mizumoto and J. E. Lynn, Phys. Rev. **C41** (1990) 458.

[5] R. L. Macklin and J.H. Gibons, Phys. Rev. **159** (1967) 1007.

[6] ENDF/B-VI data file for ^{197}Au (MAT=7925), evaluated by P. G. Young (1984).

[7] H. Kendrick and S. M. Sperling, **GA-9882** (1970).

[8] K. Senoo, Y. Nagai, T. Shima, T. Ohsaki and M. Igashira, Nucl. Instrum. Methods, **A339** (1994) 556.

[9] A. R. de L. Musgrove, B. J. Allen and J. W. Boldeman, Proc. Int. Conf. on Neutron Physics and Nuclear Data for Reactors and Other Applied Purposes, AERE Harwell, 1978, p.449.

[10] M. V. Bokhovko, L. E. Kazakov, V. N. Kononov, E. D. Poletaev, V. M. Timokhov, and A. A. Voevodskiy, Yaderye Konstanty, **3** (1985) 12.

[11] Y. Nakajima, A. Asami, Y. Kawarasaki and Y. Furuta, Proc. Int. Conf. on Neutron Physics and Nuclear Data for Reactors and Other Applied Purposes, AERE Harwell, 1978, p.438.

[12] R. W. Hockenbury, W. R. Koste and R. A. Shaw, Bull. Am. Phys. Soc. **20** (1975) 560.

[13] R. L. Macklin and P. G. Young, Nucl. Sci. Eng. **95** (1987) 189.

[14] V. A. Konks, Yu. P. Popov and Yu. I. Fenin, Sov. J. Nucl. Phys. **7** (1968) 310.

[15] V. N. Kononov, B. D. Yurlov, E. D. Poletaev and V. M. Timokhov, Sov. J. Nucl. Phys. **26** (1977) 500.

[16] M. Mizumoto, A. Asami, Y. Nakajima, Y. Kawarasaki, T. Fuketa and H. Takekoshi, J. Nucl. Sci. Technol. **16** (1979) 711.
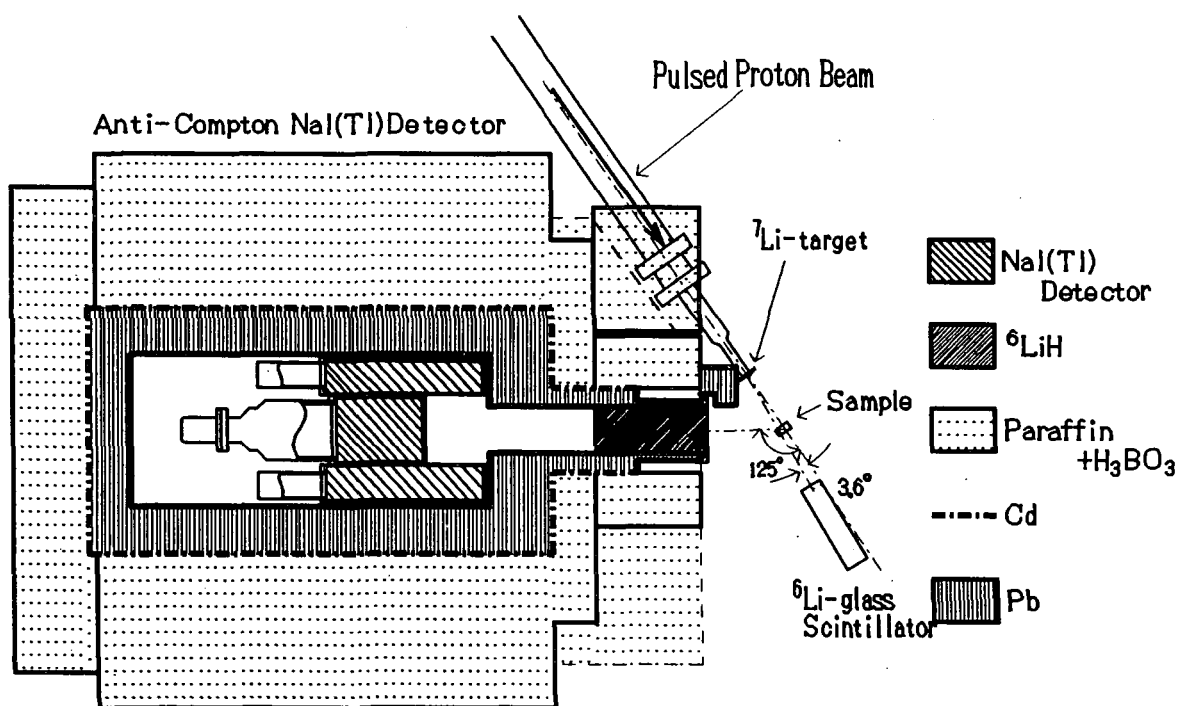
Fig. 1. Typical experimental arrangement.
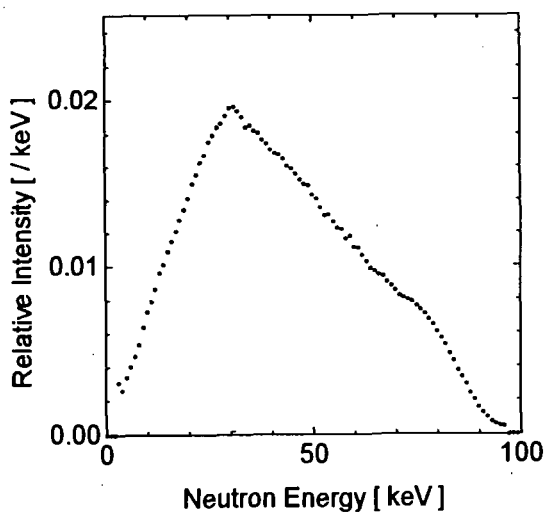
Fig. 2. Typical incident neutron spectrum.
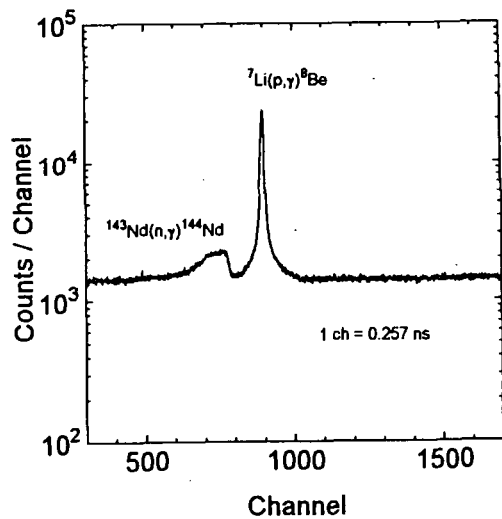
Fig. 3. Typical TOF spectrum observed by the γ-ray spectrometer.
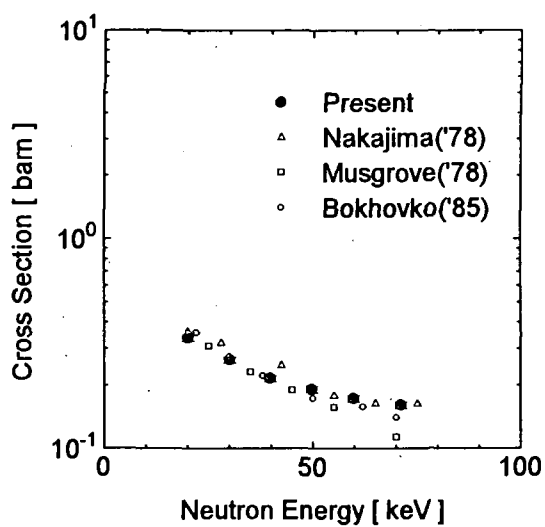
Fig. 4. Capture cross sections of ^{143}Nd.
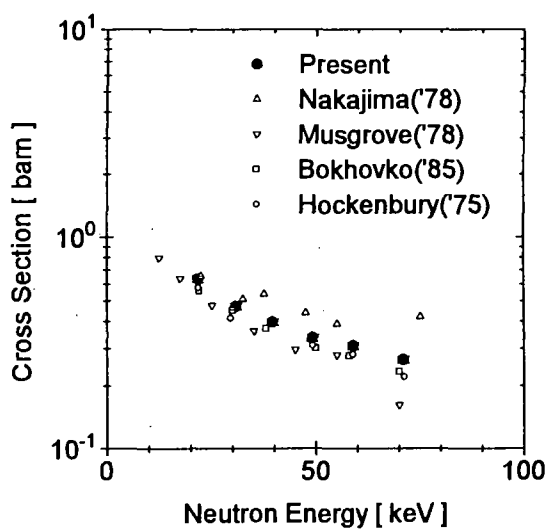
Fig. 5. Capture cross sections of ^{145}Nd.
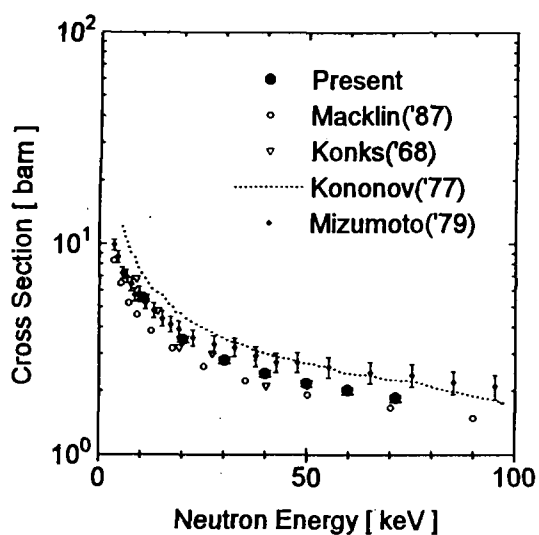
Fig. 6. Capture cross sections of ^{153}Eu.
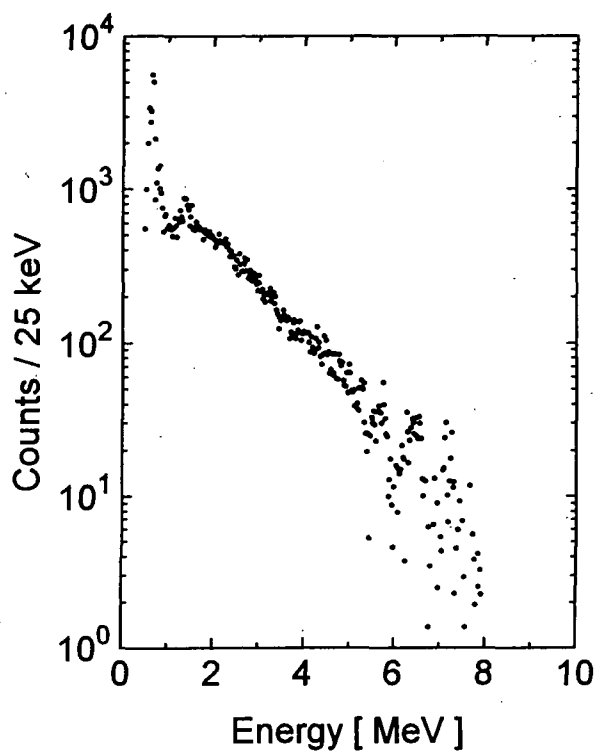
Fig. 7. Capture γ-ray PH spectrum of ^{143}Nd.
The average incident neutron energy is 30 keV.
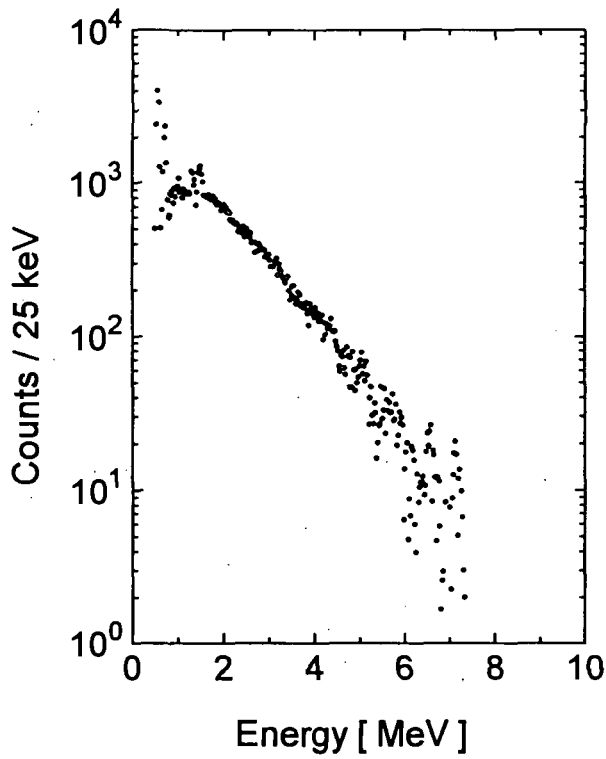
Fig. 8. Capture γ-ray PH spectrum of ^{145}Nd.
The average incident neutron energy is 30 keV.
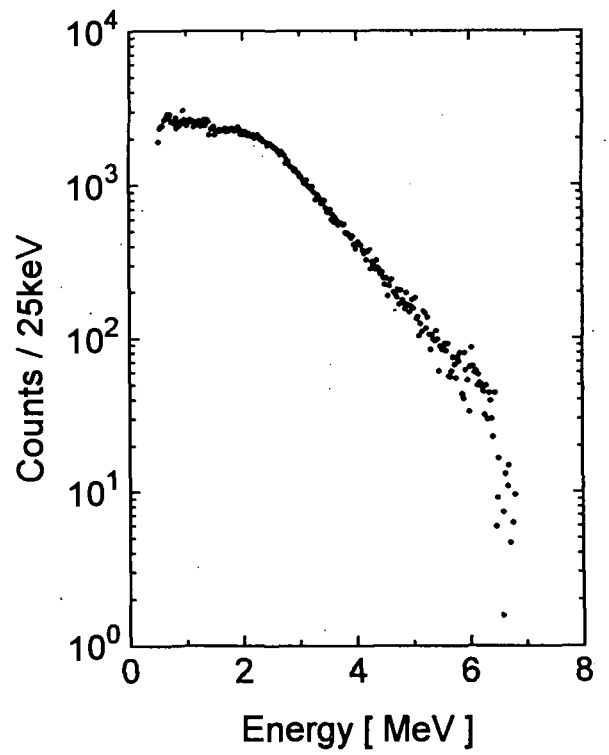
Fig. 9. Capture γ-ray PH spectrum of ^{153}Eu.
The average incident neutron energy is 30 keV.
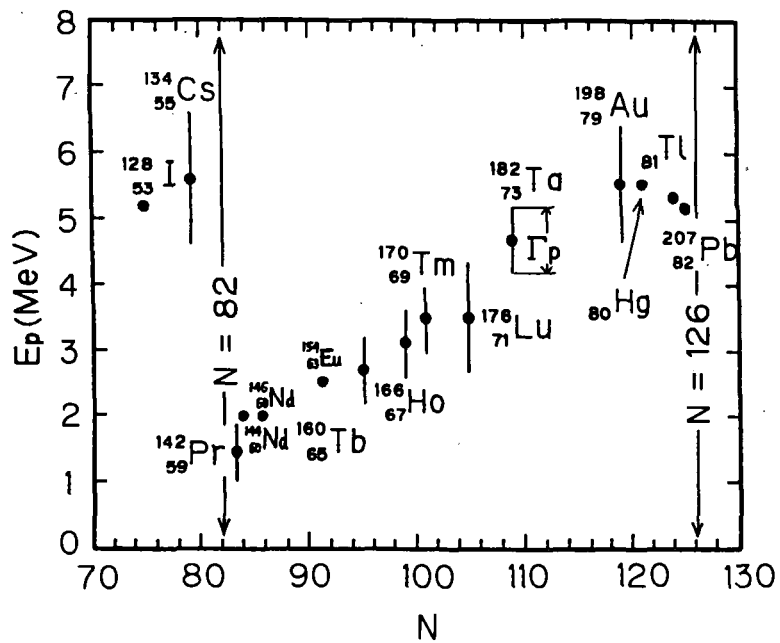
Fig. 10. Energy position of shoulder or bump
vs. the neutron number of residual nucleus.

3.2 Integral Test on Activation Cross Section of Tag Gas Nuclides Using Fast Neutron Spectrum Fields

Takafumi AOYAMA and Soju SUZUKI

Reactor Technology Section, Experimental Reactor Division, Oarai Engineering Center
Power Reactor and Nuclear Fuel Development Corporation
4002 Narita-cho, Oarai-machi, Ibaraki-ken 311-13 JAPAN
E-mail : aoyama@oec.pnc.go.jp

Activation cross sections of tag gas nuclides, which will be used for the failed fuel detection and location in FBR plants, were evaluated by the irradiation tests in the fast neutron spectrum fields in JOYO and YAYOI. The comparison of their measured radioactivities and the calculated values using the JENDL-3.2 cross section set showed that the C/E values ranged from 0.8 to 2.8 for the calibration tests in YAYOI and that the present accuracies of these cross sections were confirmed.

1. Introduction

Unique ratios of stable xenon and krypton gases (tag gas) are used in fast reactor fuel pins. In the event of fuel pin failure, the gases are released into the reactor cover gas where they are collected and analyzed for their isotopic ratios by means of mass spectrometry to identify the failed pins. The tag gas nuclides are also activated through (n, γ) reaction during the irradiation and these activation products can be identified by measuring the gamma-ray spectrum of the cover gas.

The gamma-ray spectrometry has a higher sensitivity than the mass spectrometry for tag gases diluted in the cover gas space, possibly less than ppm. Therefore, measuring of the activated tag gas nuclides by this method is expected to be an alternative in the failed fuel detection and location (FFDL). This method will enhance the reliability of the FFDL in sodium cooled FBRs.

2. Irradiation Tests in JOYO and YAYOI
2.1 In-Core Tag Gas Release Test in JOYO

To demonstrate this method, the in-core tag gas release tests were carried out in JOYO. In the tests as shown in Fig. 1, highly pressurized

(more than 30MPa) tag gas capsules were placed in the core region of the JOYO Mark-II core. These capsules eventually breached via creep rupture and the krypton and xenon gases were released into the cover gas space. The activated tag gas nuclides were measured with a high purity germanium gamma-ray detector of the On-line Gamma-ray Monitor [1] (OLGM), which uses a charcoal bed to selectively adsorb xenon and krypton.

The measured gamma-ray spectrum and the trend of cover gas activities for each activation nuclide are shown in Figs. 2 and 3. It can be seen that the distinct photo-electron peaks of the activated nuclides ^{125}Xe, ^{127}Xe, ^{129m}Xe, ^{131m}Xe, ^{133}Xe and ^{135}Xe were determined with high resolution. These nuclides among the background fission products were clearly detected by the OLGM and this method was found to be applicable to the FFDL.

2.2 Cross Section Calibration Test in YAYOI

In order to apply this technique it is important to assure the accuracy of the tag gas activation (n, γ) cross section. Several tag gas calibration samples, which were contained in capsules, were irradiated in the standard neutron field of the fast neutron source reactor YAYOI. The tag gas sample specifications are shown in Table 1. After irradiation the radioactivities of the tag gas activation nuclides were measured with a high purity germanium gamma-ray detector.

3. Comparison with the Calculation

The measured radioactivities were compared with the calculated values using the ORIGEN2 code [2] based on the 70 group cross sections processed from JENDL-3.2 [3]. The 70 group cross sections were collapsed into one group, using the neutron spectra of YAYOI and JOYO as shown in Fig. 4. The neutron spectrum in YAYOI, which is the preliminary result, was determined by the foil activation method using the J1-Unfolding code NEUPAC [4] with the JENDL-3 dosimetry file [5]. The JOYO spectrum was calculated by the two-dimensional discrete ordinate transport code DOT3.5 [6] with JENDL-2 [7].

By comparing the measured radioactivities and calculated values based on the JENDL-3.2 cross section library, the C/E values for ^{79}Kr, ^{125}Xe, ^{127}Xe, ^{133}Xe and ^{135}Xe ranged from 0.8 to 2.8 for the YAYOI calibration tests, shown in Fig. 5. As the total neutron fluences of irradiation tests in YAYOI are small (0.63 $\sim$ 1.27 $\times$ 10^{16} n/cm^2), the discrepancy appears due

to the uncertainty of these cross sections. The C/E values for the JOYO tests are similar to those from YAYOI results except for ^{125}Xe and ^{127}Xe, which appears to be mainly due to the sensitivity difference to the neutron energy of these nuclides. These results imply that further investigation of these cross section accuracies must be performed.

4. Conclusion

Activation cross sections of krypton and xenon were evaluated by the irradiation tests in the fast neutron spectrum fields in JOYO and YAYOI. It was found that the tag gas activation method is applicable for the FFDL in sodium cooled FBR plants and the present accuracies of the tag gas activation cross sections were confirmed.

Acknowledgements

References

[1] T. AOYAMA and S. SUZUKI, "Nuclear Instrumentation and Radiation Measurement Technology in the Experimental Fast Reactor "JOYO"," PNC report (in Japanese) TN9420 96-058 (1996)

[2] A. G. CROFF, "A User's Manual for the ORIGEN2 Computer Code," ORNL-TM-7175, Oak Ridge National Laboratory (1980)

[3] K. SHIBATA et al., "Japanese Evaluated Nuclear Data Library, Version-3," JAERI 1319, Japan Atomic Energy Research Institute (1990)

[4] M. NAKAZAWA and A. SEKIGUCHI, "The Basic Reports of J1-Unfolding Code "NEUPAC"," UTNL-R0096 (1981)

[5] M. NAKAZAWA et al., "JENDL Dosimetry File," JAERI 1325, Japan Atomic Energy Institute (1992)

[6] W. A. RHOADES et al., "DOT3.5 Two Dimensional Discrete Ordinates Radiation Transport Code," CCC-276 (1977)

[7] H. TAKANO and K. KANEKO, "Revision of Fast Reactor Group Constant Set JFS-3-J2," JAERI-M 89-141, Japan Atomic Energy Institute (1989)

Table 1 Tag Gas Specifications Used in YAYOI

Tag ID	No. 1		No. 2		No. 3	
Tag Gas Volume (cc)	Xe	Kr	Xe	Kr	Xe	Kr
	1.25	1.25	1.62	1.06	1.56	1.11
Xe Isotope Ratio						
124 / 129	0.079		0.059		0.074	
126 / 129	0.048		0.083		0.104	
128 / 129	0.185		0.249		0.296	
130 / 129	0.057		0.132		0.125	
131 / 129	0.060		0.682		0.646	
132 / 129	0.025		0.862		0.816	
134 / 129	0.006		0.329		0.312	
136 / 129	0.001		0.266		0.253	
Kr Isotope Ratio						
78 / 80	0.261		0.494		0.495	
82 / 80	1.35		7.56		7.55	
83 / 80	0.217		3.54		3.60	
84 / 80	0.066		16.2		16.0	
86 / 80	0.003		4.90		4.84	

Irradiated at Glory Hole. Total Neutron Fluence = $0.63 \sim 1.27 \times 10^{16}$ n/cm^2

Test Rig

Rotating Plug
Sodium Level
Upper Core Structure
Core

Loading Diagram

Fig. 1 In-Core Tag Gas Release Test in JOYO

Cable
Gas Pipe
Tag Gas Specimen
Capsule
Thermocouple
Support Structure
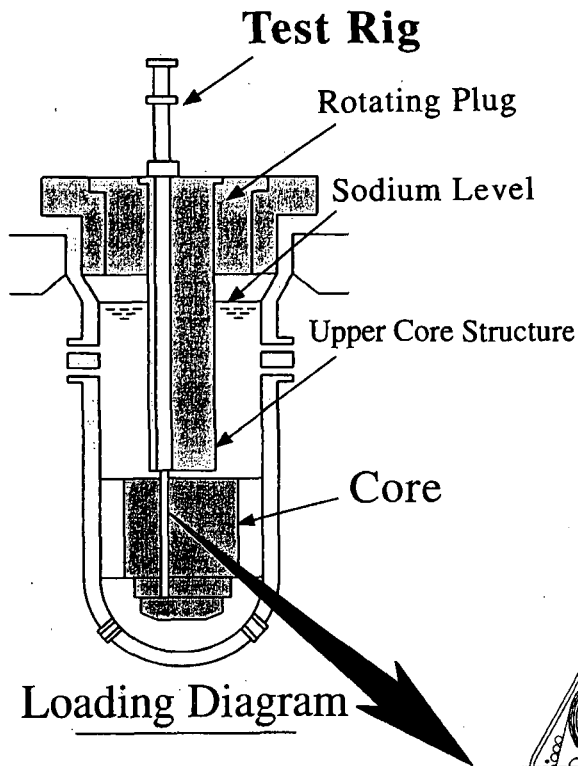
Tag Gas Specifications Used in JOYO

Tag Gas Volume (cc)		
Xe	Kr	He
0.77	3.1	$52 \sim 62$

Xe Isotope Ratio	Kr Isotope Ratio
124/129 =0.038	78/84 =0.022
126/129 =0.053	80/84 =0.110
128/129 =0.183	82/84 =0.260
130/129 =0.139	83/84 =0.213
131/129 =0.720	86/84 =0.298
132/129 =0.911	
134/129 =0.353	

Total Neutron Fluence = $0.77 \sim 3.3 \times 10^{21}$ n/cm^2

Tag gas was released to the reactor cover gas volume of 6.5m^3 (6.5×10^6 cc)
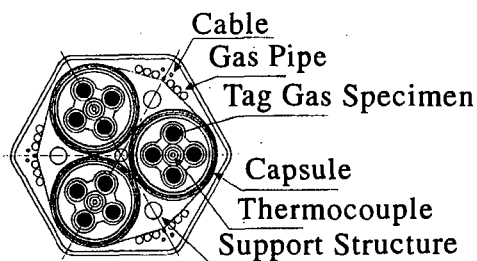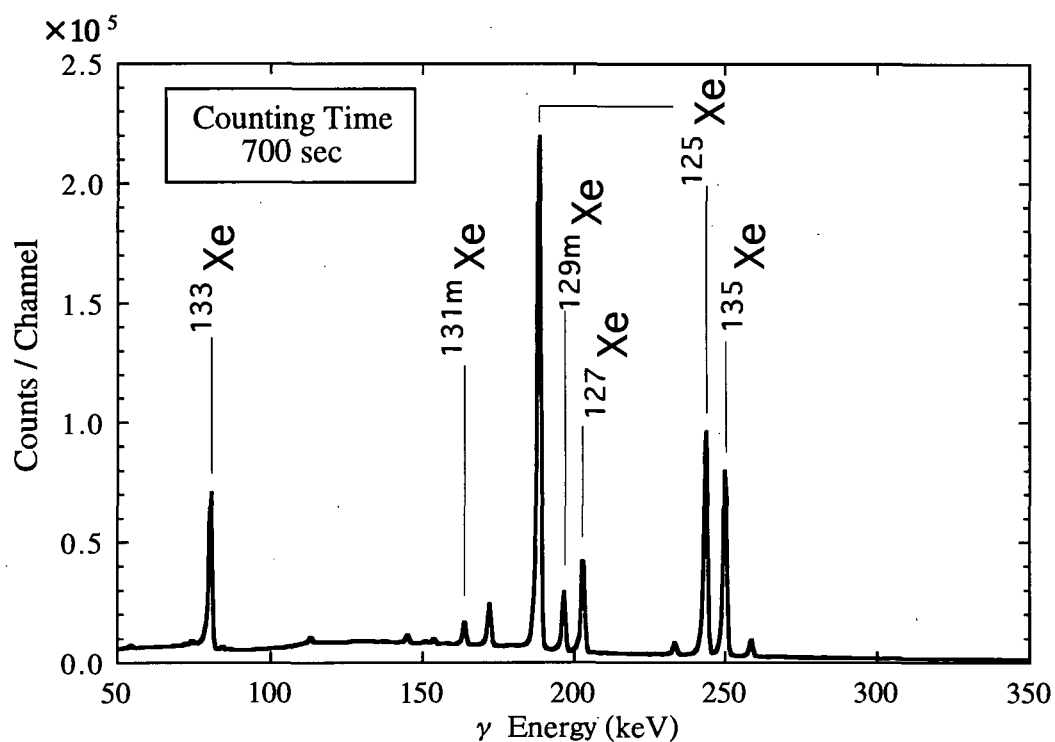
Fig. 2 Gamma-Ray Spectrum of the JOYO Cover Gas
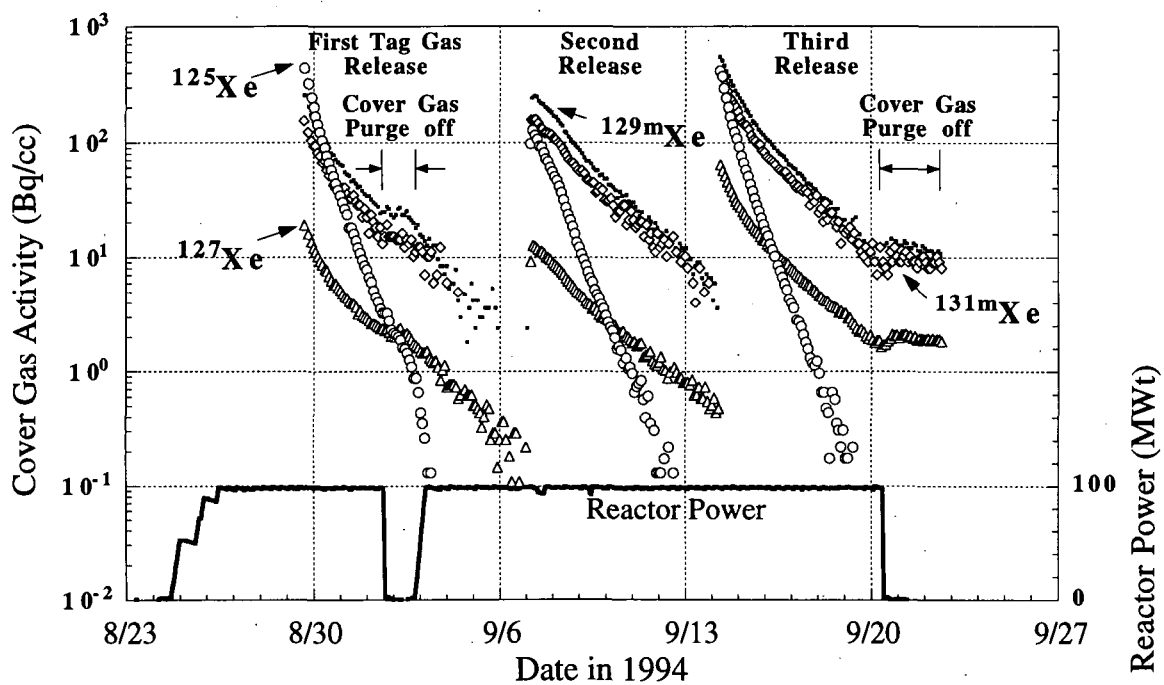
Fig. 3 Measured Tag Gas Activation Products in JOYO
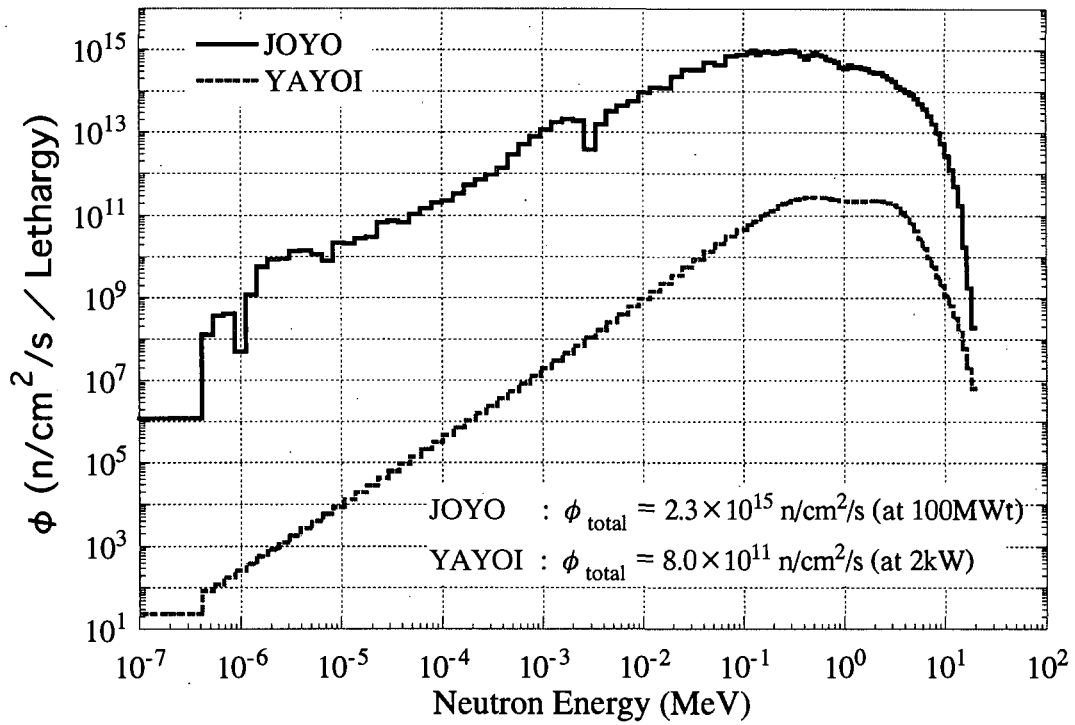
Fig. 4   Neutron Spectrum of JOYO and YAYOI
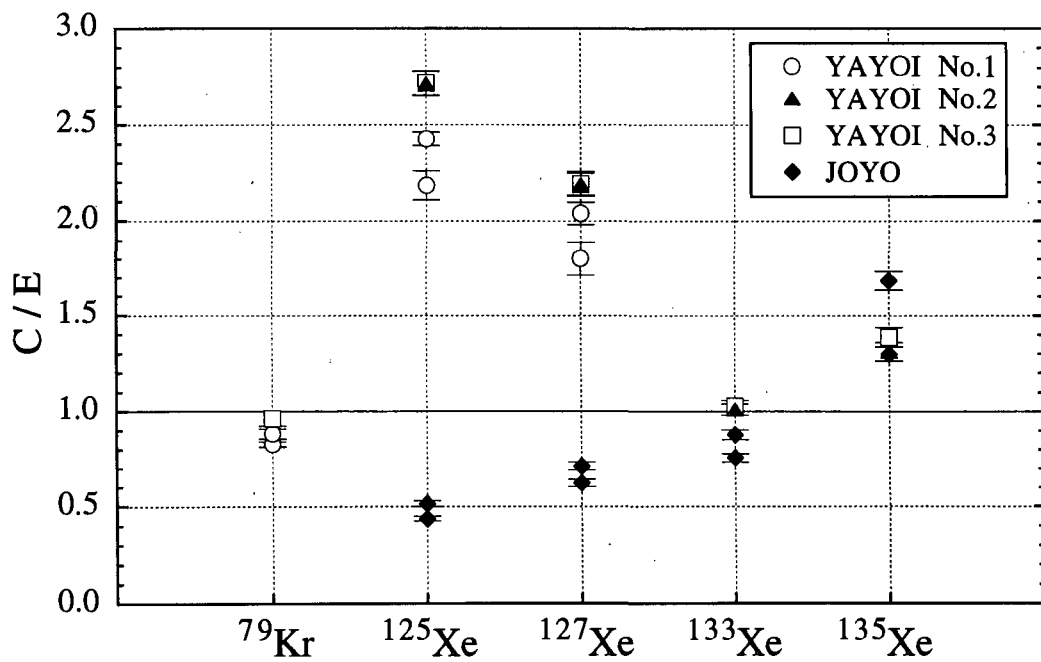
Fig. 5   Calculated (C) to Measured (E) Values
of Tag Gas Radioactivities

3.3 Comparison of Yield and Decay Data among JNDC2, ENDF/B-VI and JEF2.2

Kazuhiro OYAMATSU, Mitsuyuki SAGISAKA and Toshimitsu MIYAZONO

Department of Energy Engineering and Science, Nagoya University

Furo-cho, Chikusa-ku, Nagoya 464-01, Japan

e-mail : oyak@luna.nucl.nagoya-u.ac.jp

Fission yields and decay data for fission product summation calculations are compared among JNDC2 and ENDF/B-VI and JEF2.2. Special attention is paid to the summation calculation of the total delayed neutrons per fission because it requires the data of the most unstable nuclides among all fission products. The cumulative fission yields of delayed neutron precursors are found to be appreciably different among the libraries even though values of the independent fission yields and the total number of delayed neutrons are chosen to be in fair agreement with each other. This suggests that there still exist large uncertainties in delayed neutron emission probabilities (or decay chains) for the precursors far from the stability line.

1. Introduction

Fission product properties can be calculated from fission yields for a given neutron energy spectrum, and decay data which are basic properties of unstable nuclei. The three major nuclear data libraries, JNDC2, ENDF/B-VI and JEF2.2, have come to give more or less similar results for summation calculations of aggregate decay heat power for thermal and/or fast fissions of ^{235}U, ^{238}U and ^{239}Pu. This suggests that most of the yield and decay data in these libraries are essentially equal. Therefore we believe that it is time to examine and eliminate still existing differences which cause substantial differences in calculated fission product properties among the libraries.

The purpose of this paper is to assess differences of the yield and decay data among the three libraries. We mainly discuss the total number of delayed neutrons per fission because the delayed neutron precursors are most unstable and rarely known nuclei among all fission products.

2. Expressions for delayed neutron summation calculations

The fission product properties are calculated from fission yields and decay data (decay constants, branching ratios, average decay energies and delayed neutron emission

probabilities). Let us first see how the total number of delayed neutrons is given in the matrix representation. Consider a vector of the independent fission yields of M fission product nuclides;

$$y = \begin{pmatrix} y_1 \\ y_2 \\ \vdots \\ y_M \end{pmatrix}. \tag{1}$$

Here, the value of the i-th component, y_i, is equal to the independent yield of nuclide i. A decay from nuclide i to nuclide j is characterized by the branching ratio $b_{i \rightarrow j}$. A matrix of the branching ratios,

$$B = \begin{pmatrix} 0 & b_{2 \rightarrow 1} & \cdots & b_{M \rightarrow 1} \\ b_{1 \rightarrow 2} & 0 & \cdots & b_{M \rightarrow 2} \\ \vdots & \vdots & \ddots & \vdots \\ b_{1 \rightarrow M} & b_{2 \rightarrow M} & \cdots & 0 \end{pmatrix}, \tag{2}$$

describes the decay chains. It is also useful to define a vector of the cumulative fission yields, Y, defined in the same way as y. Between the independent and cumulative yields, we have a relation

$$y = (I - B) Y \tag{3}$$

with I being the unit matrix. Alternatively, the cumulative yield vector is given by

$$Y = (I - B)^{-1} y. \tag{4}$$

Then, the total number of delayed neutrons, v_d, is written as

$$v_d = \begin{pmatrix} b_{1 \rightarrow n} & b_{2 \rightarrow n} & \cdots & b_{M \rightarrow n} \end{pmatrix} Y = \begin{pmatrix} b_{1 \rightarrow n} & b_{2 \rightarrow n} & \cdots & b_{M \rightarrow n} \end{pmatrix} (I - B)^{-1} y. \tag{5}$$

Here, the value of the delayed neutron emission probability of nuclide i, $b_{i \rightarrow n}$, is equal to one of the components in the matrix B. We can also write a vector, v_d, whose i-th component gives the number of delayed neutrons emitted from nuclide i;

$$v_d = \begin{pmatrix} b_{1 \rightarrow n} & 0 & \cdots & 0 \\ 0 & b_{2 \rightarrow n} & \cdots & 0 \\ \vdots & \vdots & \ddots & 0 \\ 0 & 0 & \cdots & b_{M \rightarrow n} \end{pmatrix} Y = \begin{pmatrix} b_{1 \rightarrow n} & 0 & \cdots & 0 \\ 0 & b_{2 \rightarrow n} & \cdots & 0 \\ \vdots & \vdots & \ddots & 0 \\ 0 & 0 & \cdots & b_{M \rightarrow n} \end{pmatrix} (I - B)^{-1} y. \tag{6}$$

In principle, the quantities

$$\begin{pmatrix} b_{1 \rightarrow n} & b_{2 \rightarrow n} & \cdots & b_{M \rightarrow n} \end{pmatrix} \text{ and } \begin{pmatrix} b_{1 \rightarrow n} & 0 & \cdots & 0 \\ 0 & b_{2 \rightarrow n} & \cdots & 0 \\ \vdots & \vdots & \ddots & 0 \\ 0 & 0 & \cdots & b_{M \rightarrow n} \end{pmatrix}$$

can be constructed from the branching matrix B. However, we do not discuss it in detail to avoid further complications.

In a similar way, time dependent fission product properties can also be represented in the matrix representation. We give a few examples here. Let us define a vector of the number of atoms of nuclide i $N_i(t)$ at a cooling time t after instantaneous irradiation;

$$N(t) = \begin{pmatrix} N_1(t) \\ N_2(t) \\ \vdots \\ N_M(t) \end{pmatrix}.$$

(7)

The differential equation for $N(t)$ is

$$\frac{d}{dt}N(t) = (B - I) \Lambda_0 N(t)$$

(8)

with the initial condition

$$N(0) = y.$$

(9)

The time evolution is determined principally by a matrix of decay constants,

$$\Lambda_0 = \begin{pmatrix} \lambda_1 & 0 & \cdots & 0 \\ 0 & \lambda_2 & \cdots & 0 \\ \vdots & \vdots & \ddots & \vdots \\ 0 & 0 & \cdots & \lambda_M \end{pmatrix}.$$

(10)

The solution of this equation is given by

$$N(t) = \exp\left((B - I) \Lambda_0 t\right) y.$$

(11)

Here, the exponential function of a matrix A is defined as

$$\exp(A) = I + A + \frac{1}{2!}A^2 + \frac{1}{3!}A^3 + \frac{1}{4!}A^4 + \cdots.$$

(12)

With the solution (11), the decay heat power and delayed neutron activity can be written as

$$P(t) = \left(E_1 \; E_2 \; \cdots \; E_M \right) \Lambda_0 \exp\left((B - I) \Lambda_0 t\right) y$$

(13)

and

$$n(t) = \left(b_{1 \to n} \; b_{2 \to n} \; \cdots \; b_{M \to n} \right) \Lambda_0 \exp\left((B - I) \Lambda_0 t\right) y,$$

(14)

respectively.

3. Overlap of two vectors

Apart from the branching ratio matrix B, the expressions for the decay heat power and delayed neutron properties are composed of vectors of fission yields y, average decay energies E and delayed neutron emission probabilities P_n together with the diagonal matrix of decay constants Λ_0. Therefore it is a good idea to compare these vectors among JNDC2, ENDF/B-VI and JEF2.2. For this comparison, we make use of the value of the directional cosine of two vectors v and v',

$$\mu = \frac{v \cdot v'}{|v||v'|}.$$

(15)

We call this quantity "overlap" of the two vectors [1,2]. The value of μ is equal to unity when the two vectors are identical, and smaller than unity when the directions of the two are different. Therefore, the value of $1 - \mu$ provides us with a good measure of difference between the two vectors.

We can specify the components of the two vectors which differ largely between the two vectors by evaluating the value of

$$\varepsilon_i = \frac{1}{2} \frac{|v_i|^2 + |v'_i|^2 - 2 v_i v'_i}{|v||v'|} = \frac{1}{2} \frac{|v_i - v'_i|^2}{|v||v'|} . \tag{16}$$

The value of ε_i is zero when $v_i = v'_i$ and large when the value of the i-th component differs significantly.

4. Decay constants, decay energies and delayed neutron emission probabilities

We examine the difference of decay data between two of the three nuclear data libraries JNDC2, ENDF/B-VI and JEF2.2. Specifically, the μ values are evaluated for decay energy vectors E and delayed neutron emission probability vectors P_n as well as decay constant vectors

$$\lambda = \begin{pmatrix} \lambda_1 \\ \lambda_2 \\ \vdots \\ \lambda_M \end{pmatrix} \tag{17}$$

in place of the diagonal matrices Λ_0 .

The results for decay data are shown in Table 1. As for energies, β decay Q values are almost equivalent among the three libraries. However, the γ decay energies in JEF2.2 are significantly different from the other two. This may stem from the fact that both JNDC2 and ENDF/B-VI adopt the gross theory of β decay while JEF2.2 does not. More remarkable differences are seen in decay constants and especially in Pn values. These differences may imply that the decay constants of delayed neutron precursors which are most unstable among all fission products do not have sufficient accuracy. If we notice that the Pn values are branching ratios to delayed neutron emission, decay chains may also be uncertain for the delayed neutron precursors.

5. Fission yields and total number of delayed neutrons per fission

We only discuss total number of delayed neutrons per fission, ν_d , as an application of our method to results of summation calculations. Figure 1 depicts μ values for independent fission yields y (upper bar), cumulative fission yields Y (middle bar) and delayed neutron yields ν_d (lower bar) for each fissioning system between two libraries. The μ values in this figure are calculated with only delayed neutron precursors. We see that the values of the lowest

Table 1. Comparison of decay data among JNDC2, ENDF/B-VI and JEF2.2. The symbol M stands for the number of fission products nuclides and isomers available in the two libraries. The other symbols Q, E_β, E_γ. λ and Pn mean β decay Q values, average β and γ decay energies, decay constants and delayed neutron emission probabilities, respectively.

	M	Q	E_β	E_γ	λ	P_n
JNDC2 - ENDF/B-VI	750	0.995	0.997	0.994	0.838	0.637
JNDC2 - JEF2.2	762	0.996	0.934	0.841	0.853	0.573
ENDF/B-VI - JEF2.2	634	0.997	0.940	0.887	0.877	0.455

bars for most fissioning systems are closest to unity. This means that the delayed neutron yields from individual precursors are not very different among the three libraries.

It is strange that the differences of the cumulative yields Y are larger than the independent fission yields y and the delayed neutron yields ν_d. The cumulative fission yields are made of the independent fission yields y and branching ratios (Eq. (4)) while ν_d is also made of these two if we notice that the Pn values are the branching ratios to delayed neutron emission. Taking into account the large differences of Pn values in Table 1, the large differences of the cumulative yields seem to suggest that the branching ratios or decay chains for the delayed neutron precursors are not well known at present even though the number of delayed neutrons from individual precursors ν_d is not very different among the three libraries.

6. Conclusion

The present study shows that values of the decay constants and branching ratios for short-lived nuclides differ substantially among libraries while the decay energies are in reasonable agreement among the three except for E_γ in JEF2.2. We note the large differences in the Pn values and cumulative fission yields of delayed neutron precursors. These differences make us doubt if some artificial adjustments are made to be consistent with ν_d values obtained from integral measurements. We conclude that delayed neutron summation calculations are far less reliable than decay heat calculations. Further spectroscopic studies for delayed neutron precursors are still necessary for the evaluation of delayed neutron properties based on the summation method.

References

[1] Oyamatsu K. and Sagisaka M.: A simple method to evaluate differences of fission yields from various fissioning systems, Proc. 1995 Symposium on Nuclear Data, Tokai, Japan, JAERI-Conf 96-008, pp. 344-349 (1996).

[2] Oyamatsu K., Sagisaka M. and Miyazono T.: Comparison of decay and yield data between JNDC2 and ENDF/B-VI, Proc. Internet Sympo. on Nucl. Data 1996, in press.

232Th(F) 232Th(H) 233U(T) 233U(F) 233U(H) 235U(T) 235U(F) 235U(H) 236U(F) 238U(F) 238U(H) 237Np(F) 239Pu(T) 239Pu(F) 240Pu(F) 241Pu(T) 242Pu(F) 252Cf(S)

0.70   0.80   0.90   1.00
overlap μ between JNDC2 and JEF2.2

0.70   0.80   0.90   1.00
overlap μ between JNDC2 and ENDF/B-VI

0.70   0.80   0.90   1.00
overlap μ between ENDF/B-VI and JEF2.2
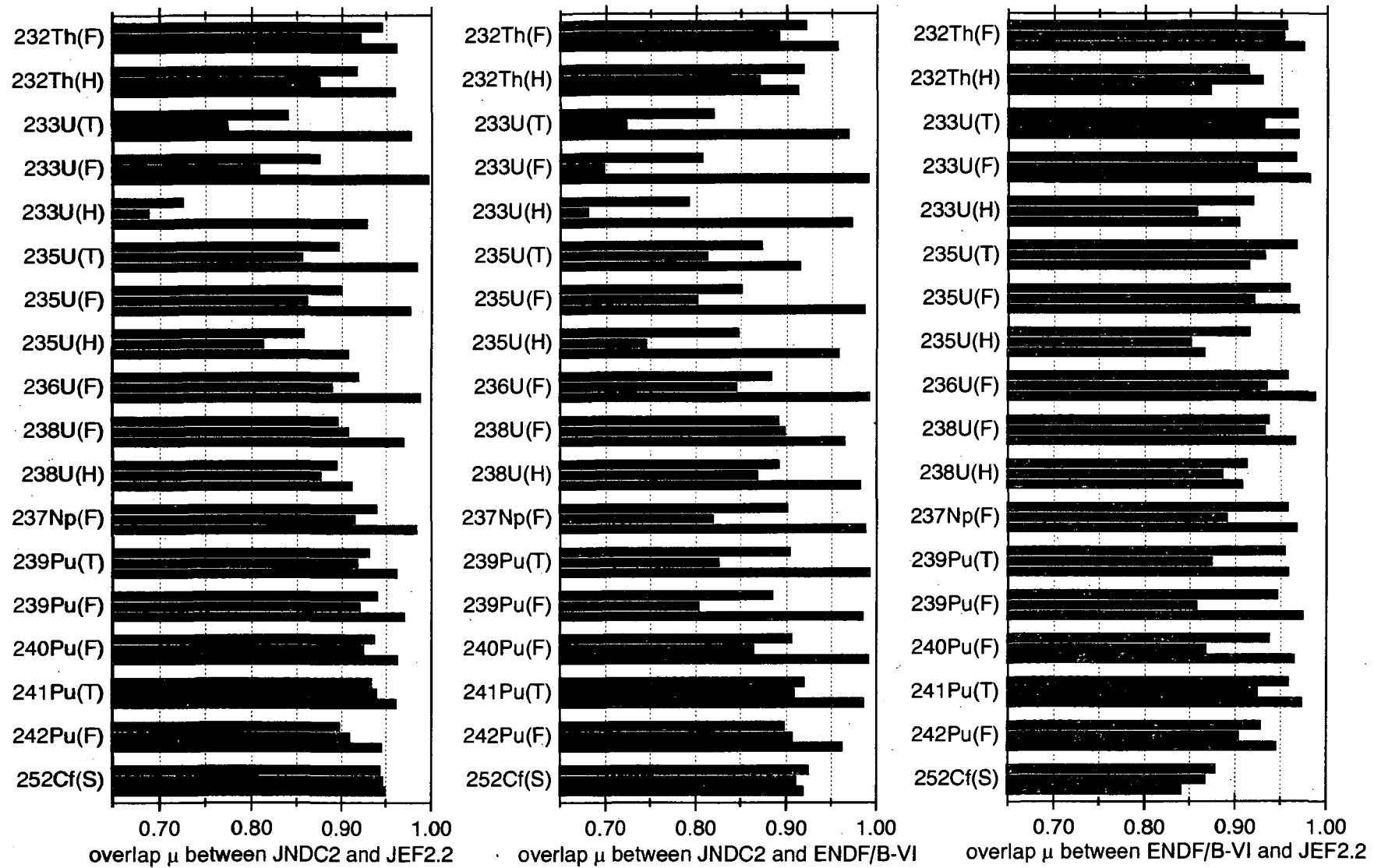
Fig. 1. Comparison of the independent fisson yields (upper), cumulative fission yields (middle) and the total number of delayed neutrons (lower) among JNDC2, ENDF/B-VI and JEF2.2.

3.4 Measurement of Helium Production Cross Sections of Iron for d-T neutrons by Helium Accumulation Method

Yoshiyuki TAKAO, Yukinori KANDA, Koji NAGAE, and Toshihiro FUJIMOTO
Department of Energy Conversion Engineering,
Kyushu University, Kasuga, Fukuoka 816, Japan

Yujiro IKEDA
Department of Reactor Engineering, Japan Atomic Energy Research Institute,
Tokai-mura, Naka-gun, Ibaraki-ken, 319-11, Japan

Helium production cross sections of Iron were measured by helium accumulation method for neutron energies from 13.5 to 14.9 MeV. Iron samples were irradiated with FNS, an intense d-T neutron source of JAERI. As the neutron energy varies according to the emission angle at the neutron source, the samples were set around the neutron source and were irradiated by neutrons of different energy depending on each sample position. The amount of helium produced in a sample was measured by Helium Atoms Measurement System at Kyushu University. The results of this work are in good agreement with other experimental data in the literature and also compared with the evaluated values in JENDL-3.

1. INTRODUCTION

Helium production cross sections are required in design for structural materials of fusion reactors. The structural materials such as a first wall are exposed to heavy irradiation of high energy neutrons. They are severely damaged by gas production reactions induced by neutrons. Helium production reaction is especially important, because helium produced in the materials changes the mechanical property of the structural materials and causes embrittlement of them. Therefore, helium production cross sections are needed for predicting the property changes and knowing the life of the fusion materials. However, the experimentally measured cross sections are few and are measured at one or two points of neutron energy near 14MeV. Most of available experimental data about helium-emitted-reactions are not always equivalent to the helium production data because they are measured with the activation method which does not detect the helium produced reactions but count identical residual nuclei of a type of helium-emitted-reactions. As the helium production reaction is not always a single type of reaction, the helium production cross section must be obtained with detecting helium produced in all available reactions. Helium accumulation method is one of the useful techniques to detect all helium produced in samples and to determine helium production cross sections. We have been measured helium production cross sections by this method and by using the Helium Atoms Measurement System (HAMS)[1] developed at Kyushu University.

In the present study, several natural iron samples were irradiated with neutrons ranging from 13.5 to 14.9 MeV and helium production cross sections of iron, $Fe(n,x\alpha)$ cross sections, were decided by measuring helium atoms produced in the samples with the HAMS. Helium production cross section of iron is important, because iron is the major constituent of stainless steels which are the most likely materials for the fusion reactor materials at present.

2. EXPERIMENTAL

2.1. Sample Preparation

Fe samples had a size $12 \times 9 \times 0.8 mm^3$ and a nominal chemical purity of 99.99%. The Fe samples were cut out of an as-given Fe plate. Fe foils as sample covers had a thickness of 0.1mm and a nominal chemical purity of 99.998%. These Fe samples and Fe foils were cleaned ultrasonically in an acetone bath for 20 minutes and were then heated at a pressure of less than $7 \times 10^{-4}Pa$ for an hour of outgassing at 1273K. Ten Fe samples sets were prepared. An Fe sample set was consisted of two Fe samples covered with the Fe foil. This structure of the Fe sample set was for getting rid of the outgoing phenomenon of energetic a-particles produced by neutron irradiation from the sample surface. The incoming a-particles from the adjacent Fe sample and foil canceled out the outgoing ones. We measured the produced He atoms in the Fe sample after removing the Fe foil from the Fe sample set.

2.2. Neutron Irradiation

The sample sets were irradiated by d-T neutrons at Fusion Neutronics Source (FNS) of an intense d-T neutron source at Japan Atomic Energy Research Institute. Ten Fe sample sets together with Nb foils for fluence monitor were set around the neutron source. Neutron energies at the sample sets varied from 13.5 to 14.9MeV according to the neutron emission angles. The arrangement of the sample sets around the neutron source and neutron energy at each sample position are shown in Fig.1. Neutron energies were determined by using MORSE-DD of a Monte Carlo code. The neutron fluence decided by referring to the $^{93}Nb(n,2n)^{92m}Nb$ cross section of 455mb$\pm$2%[2] and was ranged from 4x10^14 to 4x10^14 n/cm^2.

2.3. Helium Atoms Measurement

The amount of He atoms accumulated in the samples after neutron irradiation was measured with the HAMS. Figure 2 shows the block diagram of the HAMS. The HAMS consisted of three blocks: a gas releaser, a mass spectrometer, and a standard He supply. Each block was evacuated with a turbo-molecular pump to keep it at an ultra-high vacuum. An Fe sample was put on an evaporating boat made of tantalum in a furnace contained on the gas releaser. The boat was heated electrically up to more than a melting point of the sample. The gas released from the sample was purified by traps of Ti-getter pumps. The gas was then admitted into a quadrupole mass spectrometer (QMS) controlled by a personal computer (PC) and was analyzed to determine the mass distribution, which was converted into the numerical data, and was stored in the PC. The measured mass spectrum was displayed on a CRT of the PC and the number of He atoms was calculated from the integration of the mass-4 spectrum.

The helium measuring efficiency of the HAMS was calibrated by a series of measurements of standard He gases: a known amount of He gas which is prepared by using the standard He supply (Fig.3). The standard He supply consisted of four vessels (V1~V4), three absolute pressure gages, and a thermometer. The V5 was the furnace. The absolute volumes of the five vessels (V1~V5) were previously measured. A certain He gas was admitted into the V2 and a pressure and a temperature were measured and the amount of He in the V2 is estimated from these measured values. The He gas was then admitted into the V3 and was diluted between the V3 and the V4 which were alternately evacuated. A volume of the V4 was about 10 times larger than that of the V3. A known amount of He was then produced in the V3 and was admitted into the V5. The He gas was analyzed and the He measuring efficiency of the HAMS was known.

2.4. Experimental Errors

The overall errors for the measurement of individual samples were estimated to be 4.2%(sample No.1~5) and 4.3%(sample No.6~10). Major errors were 2% for the $^{93}Nb(n,2n)$ cross section[2], ~1.5% for the γ-ray counting efficiency, 2% for the γ-ray counting statistical uncertainty, 1.5% for the fluctuation of He measuring efficiency of the QMS, 2.3% for the calibration of the HAMS,

and 0.2%(sample No.1~5), 0.8%(sample No.6~10) for the fluctuation of the mass-4 background. The measurement uncertainties are summarized in Table 1.

3. RESULTS AND DISCUSSION

The results of this experiment are shown in Fig.4 together with cross sections measured in available experiments and the most recent evaluations of the Fe(n,xα) excitation function from 13 to 15MeV.

Fe(n,xα) cross sections have been measured by Baba et al.[3], Kneff et al.[4], Grimes et al.[5], and Wattecamps et al.[6]. The Baba et al., Kneff et al., and Wattecamps et al. Fe(n,xα) cross section are in good agreement with the present measurements. The Grimes et al. Fe(n,xα) cross section is lower than, but consistent with, the present measurements.

The comparison with the evaluated values of JENDL-3 indicates that the JENDL-3 values are fairly close to the present measurements.

REFERENCES

[1] TAKAO,Y., KANDA,Y.: A System for Measurement of Sub-Parts-Per-Trillion Helium in Solids, *Rev. Sci. Instrum.*, **67**[1], 198(1996).

[2] IKEDA,Y., KONNO,C., OYAMA,Y., KOSAKO,K., OISHI,K., MAEKAWA,H.: Absolute Measurements of Activation Cross Sections of ^{27}Al(n,p)^{27}Mg, ^{27}Al(n,α)^{24}Na, ^{56}Fe(n,p)^{56}Mn, ^{90}Zr(n,2n)$^{89m+g}$Zr and ^{93}Nb(n,2n)^{92m}Nb at Energy Range of 13.3~14.9 MeV, *J. Nucl. Sci. Technol.*, **30**[9], 870(1993).

[3] BABA,M., ITO,N., MATSUYAMA,I., MATSUYAMA,S., HIRAKAWA,N., CHIBA,S., FUKAHORI,T., MIZUMOTO,M., HASEGAWA,K., MEIGO,S.: Measurement of Double-Differential (n,α) Cross Sections of Fe, Ni, Cu and ^{50}Cr for 4.5-14.1 MeV Neutrons, *Porc. Int. Conf. on Nucl. Data for Sci. and Technol., May 9-13, 1994, Gatlinburg, Tennessee*, Vol.2, 941(1994).

[4] KNEFF,D.W., OLIVER,B.M., FARRAR IV,H., GREENWOOD,L.R.: Helium Production in Pure Elements, Isotopes, and Alloy Steels by 14.8-MeV Neutrons, *Nucl. Sci. Eng.*, **92**, 491(1986).

[5] GRIMES,S.M., HAIGHT,R.C., ALVAR,K.R., BARSCHALL,H.H., BORCHERS,R.R.: Charged-Particle Emission in Reactions of 15-MeV Neutrons with Isotopes of Chromium, Iron, Nickel, and Copper, *Phys. Rev. C*, **19**, 2127(1979).

[6] WATTECAMPS,E., LISKIEN,H., ARNOTTE,F.: Measurement of (n,α) Cross-Sections for Cr, Fe and Ni at 14 MeV Neutron Energy, *Porc. Int. Conf. on Nucl. Data for Sci. and Technol., September 6-10, 1982, Antwerp*, D.Reidel Publishing, Dordrecht, 156(1983).

Table 1. Sources and magnitude of uncertainties in the measured Fe(n,xα) cross sections.

	Sources of uncertainty	uncertainty (%)
Determination of neutron fluence	γ-ray counting statistical uncertainty	±2.0
	Reference cross section of ^{93}Nb(n,2n)^{92m}Nb	±2.0
	Efficiency of γ-ray counting	±1.0~1.5
Helium atoms measurement	Fluctuation of mass-4 background	±0.2 (Sample No.1~5) ±0.8 (Sample No.6~10)
	Uncertainty of Standard He Gas	±2.3
	Fluctuation of He measuring efficiency of the QMS	<±1.5
Combined uncertainty		±4.2 (Sample No.1~5) ±4.3 (Sample No.6~10)

Sample No.	Angle (degree)	Energy (MeV)	Sample No.	Angle (degree)	Energy (MeV)
1	0	14. 92	6	90	14. 06
2	20	14. 85	7	100	13. 98
3	40	14. 66	8	110	13. 84
4	60	14. 49	9	120	13. 69
5	80	14. 22	10	135	13. 52
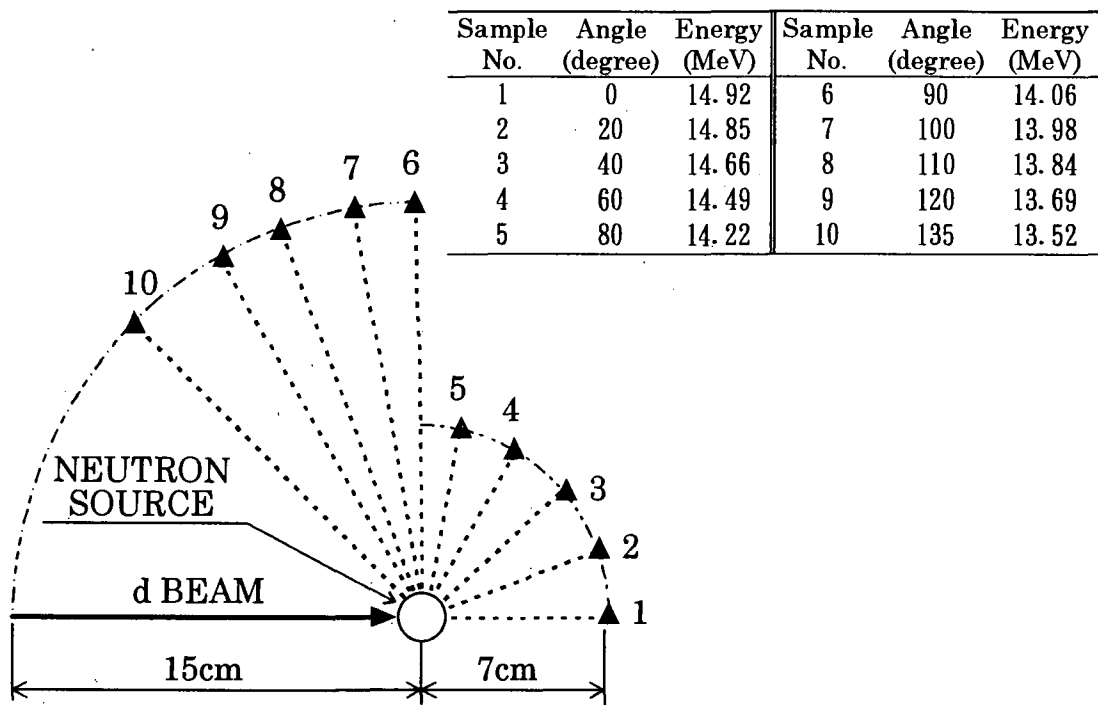
Fig.1. Sample positions and neutron energy at each position.
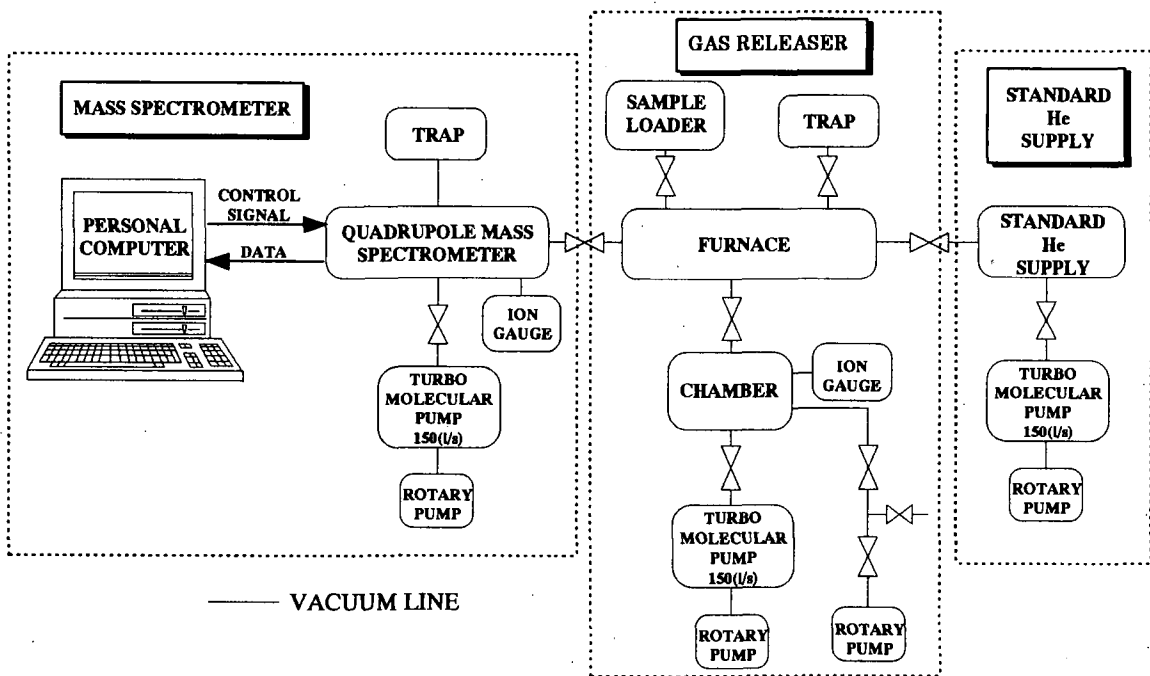
Fig.2. A block diagram of the Helium Atoms Measurement System (HAMS).
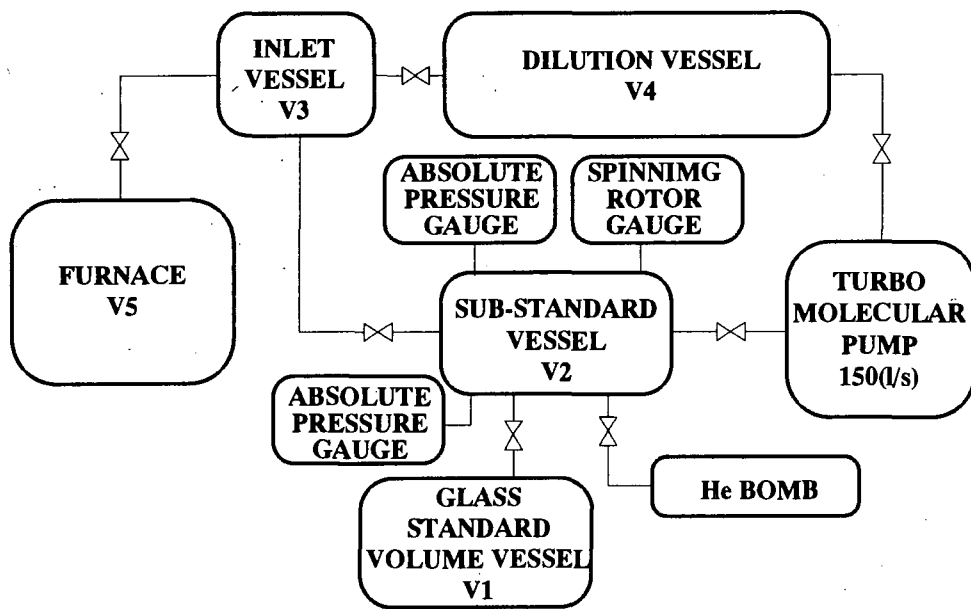
Fig.3. A block diagram of the standard helium supply.
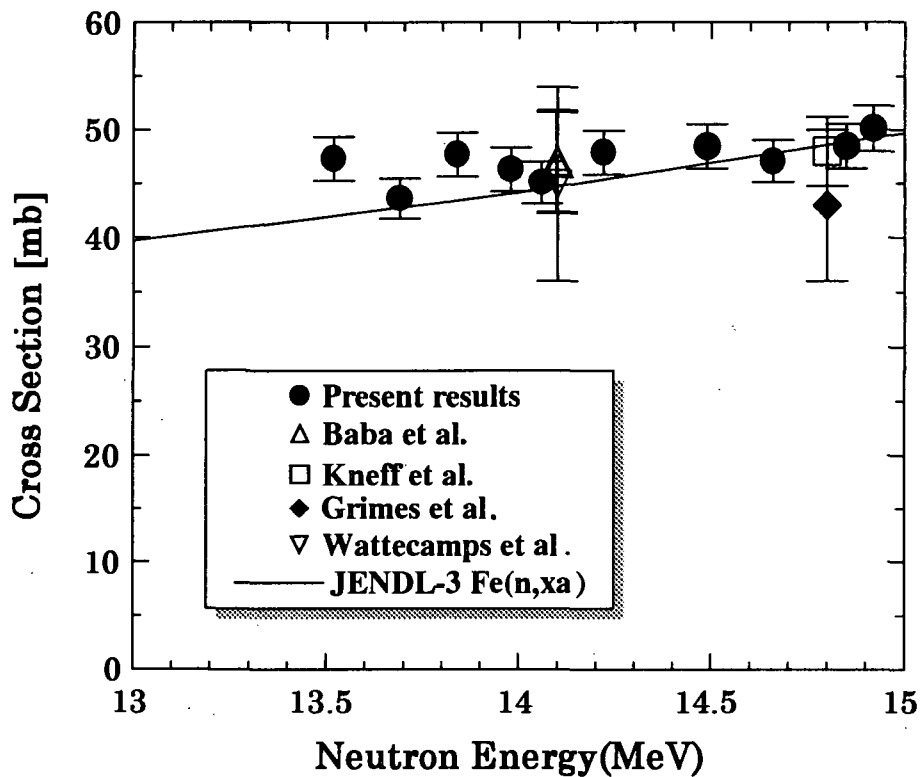
Fig.4. The Fe(n,xα) cross sections.

3.5 Measurements of Double-differential Neutron Emission Cross Sections of ^{6}Li and ^{7}Li for 18 MeV Neutrons

Masanobu Ibaraki, Mamoru Baba, Shigeo Matsuyama, Toshiya Sanami,
Than Win, Takako Miura and Naohiro Hirakawa
Department of Quantum Science and Energy Engineering, Tohoku University
Aramaki-Aza-Aoba, Aobaku, Sendai, 980-77, Japan
Email : iba@rpl.nucle.tohoku.ac.jp

Double-differential neutron emission cross sections of ^6Li and ^7Li were measured for $18MeV$ neutrons at Tohoku University 4.5MV Dynamitron facility. Neutron emission spectra were obtained down to $1MeV$ at 13 angles with energy resolution good enough to separate discrete levels. A care was taken to eliminate the sample-dependent background due to parasitic neutrons. Experimental results were in fair agreement with the JENDL-3.2 data and a simple model considering a three-body breakup process and discrete level excitations.

1 Introduction

Double-differential neutron emission cross sections (DDXs) of ^6Li and ^7Li are very important for the neutronics design of fusion reactors and high energy accelerator facilities and are required for various incident energies. In the energy region above $15MeV$, however, there have been only a single DDX measurement by our group /1/. We measured DDXs of ^6Li and ^7Li at $18MeV$ using the $T(d,n)$ source at Tohoku University 4.5MV Dynamitron facility. In this study, the energy resolution was improved markedly than in our previous study /1/ by employing a longer flight path and a thinner target. A long liquid scintillation detector (LLSD) /2/ was used for secondary neutron detection to compensate the lower counting rate. The DDXs deduced were corrected with a care for the sample-dependent background and the effects of finite sample-size by a Monte-Carlo code SYNTHIA /3/. Experimental results were compared with the evaluated data and the simple model calculations considering a three-body breakup process and discrete level excitations.

2 Experiment and Data Reduction

2.1 Experiment

Experiments were carried out using the Tohoku University Dynamitron time-of-flight spectrometer /4/. Figure.1 shows the experimental geometry. The neutrons were produced by bombarding a $Ti - T$ target with a pulsed deuteron beam with $\sim 2ns$ duration and 2 MHz repetition rate. Scattering samples were cylinders of enriched metallic lithium (95% in ^6Li and 99% in ^7Li) encased in thin SUS cases, $3.2cm\phi \times 4cm$.
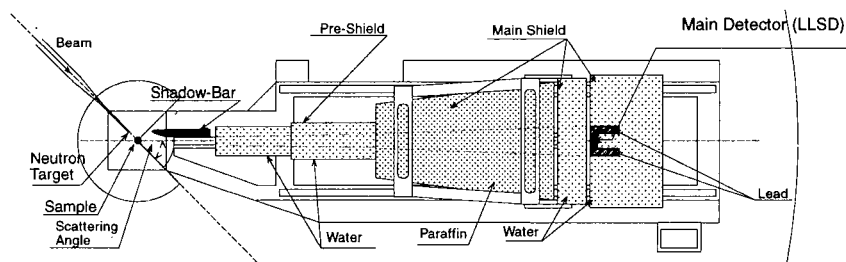
Figure 1: Experimental geometry of the S-TOF method

In this study, the energy resolution was improved markedly than in our previous study for ^6Li and ^7Li /1/ by employing a longer flight path and a thinner $Ti - T$ target. To compensate the lower counting rate, we employed a long liquid scintillation detector (LLSD, 80cm long, 10cm wide and 6.5cm thick) /3/ as a secondary neutron detector. LLSD was placed vertically in a massive shield on a turning table. The flight path was around 6m. The data were obtained at 13 scattering angles between 20° ~ 150°. Figure.2 shows the energy spectrum of the source neutrons. In addition to 18MeV primary neutrons, the parasitic neutrons by $D(d, n), C(d, n)$ and $etc.$ appear in low energy region. These parasitic neutrons give rise to serious sample-dependent backgrounds and their yields vary in the experiment. Therefore, we monitored the yields of parasitic neutrons during the experiment using the monitor neutron detector (NE-213, 2-$inch\phi$ × 2-$inch$) for normalization between foreground and background runs.
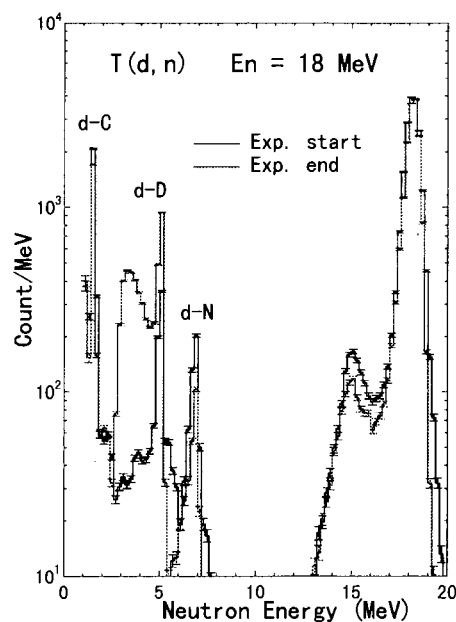
Figure 2: Energy spectrum of the source neutrons

2.2 Data Reduction

The TOF spectra were converted into the energy spectra considering the effects of sample-independent background and the detection efficiency. Absolute cross sections were determined by referring the $H(n, n)$ cross section by measuring scattering yield from a polyethylene sample, 1.5$cm\phi$ × 5cm. The energy spectra were corrected for the sample-dependent background due to parasitic neutrons and the effects of finite sample-size by a Monte-Carlo code SYNTHIA /3/. The correction is very important in this study because of large amount of parasitic components in the source neutrons. In the Monte-Carlo calculation, we used the JENDL-3.2 data as the input data for neutron interaction

with the sample nuclide. Figure.3 shows the results of the Monte-Carlo calculation in comparison with the uncorrected experimental data. The calculation results reproduce the experimental data generally well over the energy and angle and will provide reliable correction. We deduced the corrected DDXs by multiplying the uncorrected experimental data by the correction factor obtained from Monte-Carlo calculation.
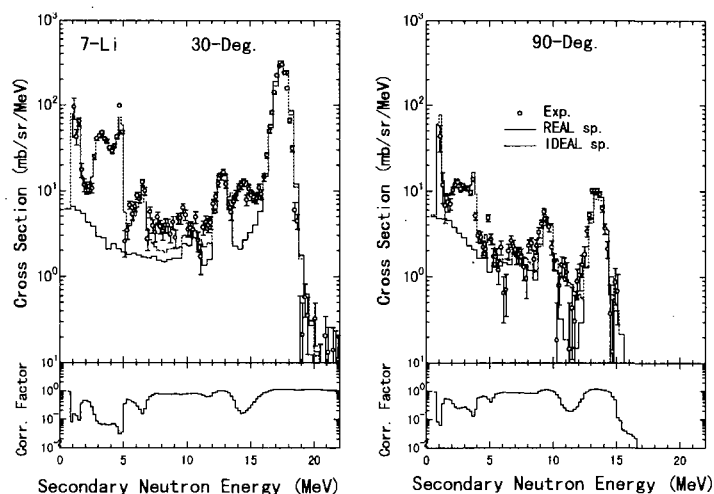
Figure 3: the results of the Monte-Carlo calculation

3 Results and Discussion

Figure.4 shows DDX of ^6Li and ^7Li at 30° in comparison with our previous data /1/. General trends are reproduced. The energy resolution is much improved in the present experiment. Larger values in previous results in $3 - 5MeV$ region might be attributed to underestimation of the sample-dependent background.
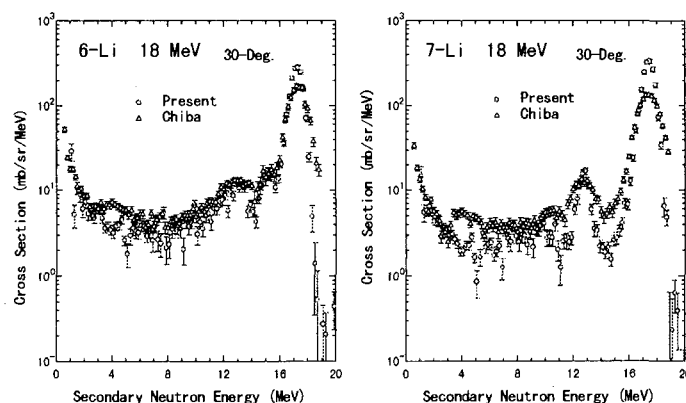
Figure 4: DDXs in comparison with our previous data

JAERI—Conf 97—005

3.1 Comparison with evaluated data

Figure.5 shows DDXs of ^6Li and ^7Li in comparison with the evaluated nuclear data. The experimental data show some discrete structures on the continuum spectra. The JENDL-3.2 data reproduce the experimental data generally well for both ^6Li and ^7Li, but the ENDF/B-VI data differ markedly, in particular in low energy region ($< 4MeV$) corresponding to $(n, 2n)$ neutrons. This comparison indicates that the inadequacy of the assumption of the ENDF/B-VI that $^{6,7}Li(n, 2n)$ spectra to be the multi-body phase space distributions. For ^7Li, the inelastic peaks($E_X = 6.68MeV, 7.47MeV$) observed in experimental data are not considered in the ENDF/B-VI.
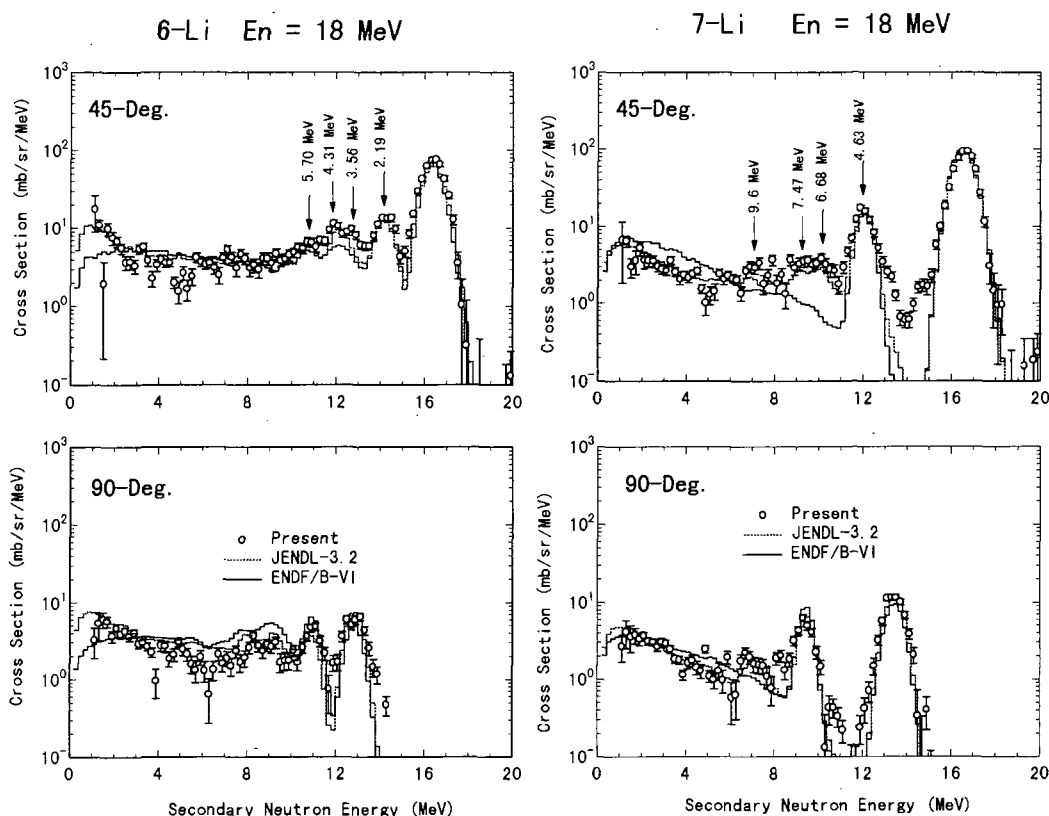
Figure 5: DDXs in comparison with evaluated data

3.2 Comparison with model calculation

The calculation assumes the contributions of 1) elastic and discrete inelastic scattering, 2) simultaneous three-body breakup reaction of $^6Li(n, n'd)\alpha$, $^7Li(n, n't)\alpha$ and 3) $^{6,7}Li(n, 2n)$ reaction. The spectra of these components were expressed in terms of 1) Gaussian distribution considering the energy resolution in the experiment, 2) three-body phase space distribution (isotropic in center of mass system) and 3) evaporation spectrum (isotropic in laboratory system), respectively. The evaporation temperatures

- 167 -

are extrapolated from $14MeV$ data by $T = C \cdot \sqrt{E_{in}/14.2}$ MeV (C =0.665 for ^6Li and 0.862 for ^7Li)/5/. Figure.6 shows calculated DDXs in comparison with the experimental data. The calculations reproduced the shape and angular dependence of experimental results in spite of physically unreasonable assumption of evaporation spectrum for light nuclei. This calculation is similar to that employed in JENDL-3.2 and reproduce the experimental data generally well at $E_n = 14MeV$.
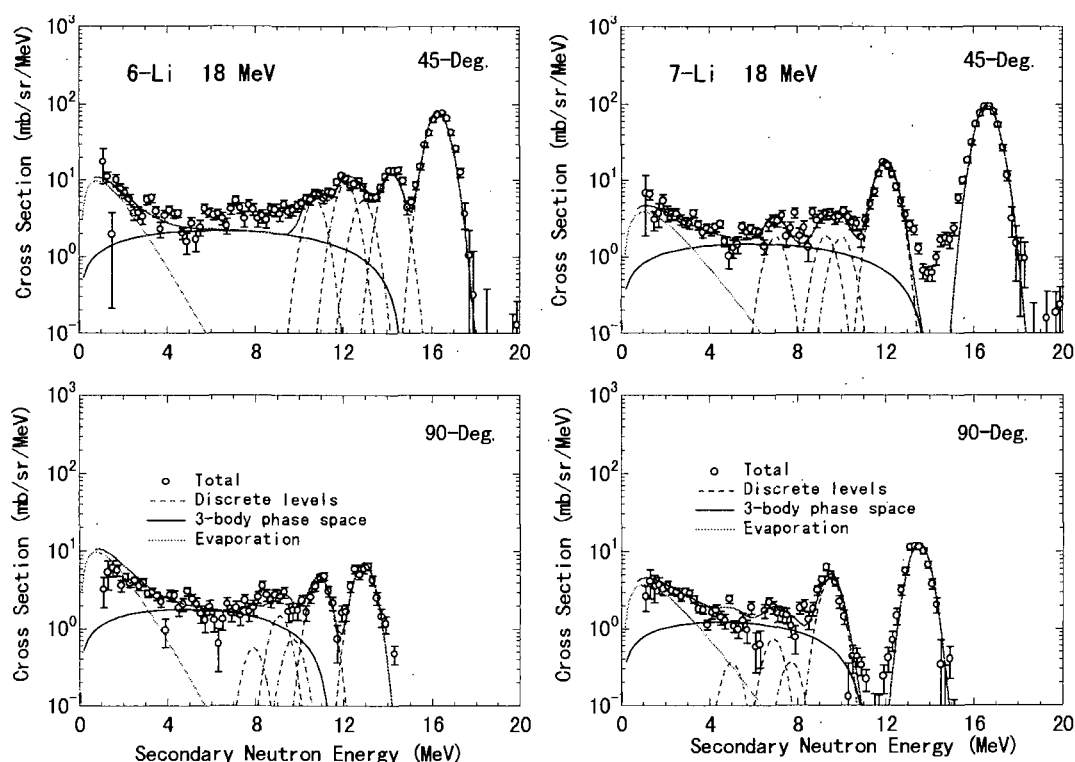
Figure 6: DDXs in comparison with model calculation

References

[1] S.Chiba et al ., Proc. Int. Conf. Nuclear Data for Science and Technology (1988 Mito) p.253

[2] S.Matsuyama et al., Nucl. Instrum. Methods A 372 (1996) p.246

[3] M.Baba et al., *ibid.*, 366 (1995) p.354

[4] S.Matsuyama et al., *ibid.*, 348 (1994) p.34

[5] S.Chiba et al., J. Nucl. Sci. Technol., 22(10) (1985) p.771

3.6 Measurement of (n,2n) Cross-sections for Sc, Mn, Cr and In between 12 and 19 MeV with activation technique

S. Iwasaki, Than Win, S. Matsuyama, and N. Odano*

Department of Quantum Science and Energy Engineering, Tohoku University

Aramaki-Aza-Aoba, Aobaku, Sendai 980-77, Japan

*Tokai-branch, Ship Research Institute, 319-11 Tokai, Ibaragi, Japan

ABSTRACT

Activation cross-sections for scandium, manganese, chromium and indium have been measured in the neutron energies from 12 to 19 MeV. Source neutrons were produced via the $T(d,n)^4He$ reaction by bombarding a 3.2-MeV deuteron beam from the Dynamitron accelerator of Fast Neutron Laboratory at Tohoku University. Ten packages of high or ultra-high purity metal foils for chromium and indium, alloy foils for manganese, and oxide powder for scandium were set around the neutron source at 5 cm from the target in the angular range from 0 to 140 deg covering the incident neutron energies from 19 to 12 MeV at the center position of each package. Activation rates of the samples were obtained by the gamma-ray measurements using a high purity germanium detector. Neutron flux at each sample was determined using the activation rates of two niobium foils locating both sides of that sample; the reference reaction was $^{93}Nb(n,2n)^{92m}Nb$ of which cross-section data was taken from the 1991 NEANDC/INDC standard files. The source neutrons distributions have been measured in detail by the time-of-flight technique. The measured cross-sections are the following important dosimetry or activation reactions: $^{45}Sc(n,2n)^{44m}Sc$, $^{55}Mn(n,2n)^{54}Mn$, $^{52}Cr(n,2n)^{51}Cr$, and $^{115}In(n,2n)^{114m}In$. These cross-sections are compared with available activation file, dosimetry files and previous experimental data.

1. INTRODUCTION

Precise cross sections above 12 MeV are still sparse except for the special energy point around 14 MeV. These are important for the high energy dosimetry, and estimation of damage rates and/or activation level of structural materials tested or used in the proposed high energy accelerator-based neutron fields. Such cross sections also provide indispensable information to establish the nuclear

model parameters for high energy cross sections evaluation.[1] In this study, (n,2n) activation cross sections for scandium, chromium, manganese and indium have been measured between 12 and 19 MeV, as the series of the neutron activation experiment at Fast Neutron Laboratory of Tohoku University.

2. EXPERIMENTAL

The source neutrons were produced via the $T(d,n)^4He$ reaction by bombarding a 2.9-MeV deuteron beam from the Dynamitron accelerator at Tohoku University. Ten packages of high purity metal foils for chromium and indium, Manganine-alloy foils for manganese, and oxide powder for scandium enclosed by plastic bag were set around the neutron source at 5 cm from the tritium metal target in the angular range from 0 to 140 deg. which covered the incident neutron energies from 19 down to 12 MeV. Sizes of the samples were all the same as $0.5^tx10x20mm^3$ except for the chromium of $2^tx3x20mm^3$, and that of the niobium foils was $0.2^tx10x20mm^3$. The neutron irradiation, neutron source characterization, and gamma ray measurement were carried out as before.[2,3,4,5] Neutron flux at each foil was determined from the activation rates of two niobium foils which sandwiched each sample foil in between; the reference cross section for the $^{93}Nb(n,2n)^{92m}Nb$ reaction was taken

Table 1 Related nuclear data for the expected activities of the samples.[7]

reaction*	half-life	decay mode	main γ - rays (keV)	emission probability (%)	abundance (%)
$^{45}Sc(n,2n)^{44m}Sc$	58.6(2)h	IT+β+	1157.03	98.6(0.2)	100
$^{52}Cr(n,2n)^{51}Cr$	27.702(4)d	EC	320.1	9.85(9)	87.789(12)
$^{55}Mn(n,2n)^{54}Mn$	312.14(5)d	EC	834.8	99.9750(10)	100
$^{93}Nb(n,2n)^{92m}Nb$	10.15(2)d	EC,weak β+	934.5	99.0(2)	100
$^{115}In(n,2n)^{114m}In$	4.486(4)d	IT, weak β-	336.2	45.9(2)	95.7(2)

from the 1991 NEANDC/INDC standard file.[6] Table 1 shows the related nuclear data[7] for the expected activities of the samples after the (n,2n) reactions. In the gamma ray measurement, the effect of the gamma ray self attenuation effects in the samples were corrected using the simple slab geometry approximation. The correction was important especially for the two cases: chromium because the sample thickness was 2 mm, which was enough to attenuate gamma rays of 300 keV, and indium because the high Z metal foil of the thickness of 0.5 mm could absorb 190 keV gamma appreciably. The sum coincidence effect for the measured main gamma lines were negligible in the decay of all residual nuclei of the four (n, 2n) reactions.

3. RESULTS

The derived sections cross data for the four (n,2n) reactions: ^{45}Sc(n,2n)^{44m}Sc, ^{52}Cr(n,2n)^{51}Cr,^{55}Mn(n,2n)^{54}Mn, and ^{115}In(n,2n)^{114m}In. are compared with the previous experimental data and cross section files: JENDL Activation File[8] and JENDL Dosimetry File[9] in Fig. 1. through 4. Filled circles show the tentative present results with the errors within the circles.

3.1. ^{45}Sc(n,2n)^{44m}Sc cross section

There have been many sets of the experimental data from '60 to'90 as shown in Fig.1, whereas there are some odd experimental data which show discrepant trends with major data sets. The old data by Rayburn, et al. ('61), Prestwood, et al.('61) and Tiwari, et al.('66) are discrepant with each other and with other major data beyond the experimental errors. The present data lie in the main trend of the major data, and are consistent with the Bayhurst, et al's ('75) data, which gave many reliable data set above 16 MeV to 25 MeV for the other reactions.

The present result shows similar trend of the cross section curve of the JENDL ACT(IVATION) file which shows flat trend above 16 MeV, but the present cross section values are larger by about 5 %. It is recommended that the evaluators should take into account the present data as well as the Bayhurst, et al's data if they want to extend the cross section curve to higher energy region.

3.2. ^{52}Cr(n,2n)^{51}Cr cross section

There are two cross section trends above 16 MeV among the experimental data sets: one is

Fig. 1 Comparison of the present data with the previous experimental data as well as the curve of the files of JENDL ACT for ^{45}Sc(n,2n)^{44m}Sc reaction.

Fig. 2 Comparison of the present data with the previous experimental data as well as the curve of the files of JENDL ACT, -DOS, ENDF/B-VI and IRDF-90 for ^{52}Cr(n,2n)^{51}Cr reaction.

higher group (e.g., Wagner, et al.('89), and Liskien, et al.('89)) which had been adopted in the IRDF file, while another one is lower group (e.g., Ikeda, et al.('88), Bormann, et al.('68) and Ghorai, et al.('87)) which is followed by the JENDL ACT and JENDL DOS(IMETRY) files.

The present measurement data are consistent with other experimental data, more precisely the higher group below 15 MeV, whereas above this energy, the cross section values are between two groups, and are consistent with the Bormann, et al's data, except for the present odd data around 18 MeV.

The data by JENDL DOS show a consistent cross section curve with the present data, while the JENDL ACT file shows a little smaller values. The ENDF/B-VI and IRDF-90 are seriously discrepant with the present data in the higher energy range, and should be re-evaluated.

3.3. ^{55}Mn(n,2n)^{54}Mn cross section

First of all, the present cross section data with larger estimated errors are now preliminary because there is uncertainty in the number of atom ratio for the used alloy sample, and were normalized with the average value of the main trend of the previous cross section at 14 MeV. The trend of the present data are quite consistent with those by Bormann, et al. ('68) and our previous data, Sakuma, et al. ('93) in the entire energy range except for the odd data at 18.9MeV. These are a little lower compared with other data above 16 MeV.

The present data clearly supports the JENDL DOS cross section. Thus, the cross section of this reaction is almost established from threshold to around 20MeV.

3.4. ^{115}In(n,2n)^{114m}In cross section

There are several cross section data sets in the entire energy range, but are inconsistent with each other, as shown in Fig. 3.4. But, there exist very few previously measured experimental data covering the energy range above 16 MeV. The present data are similar to Peggoug, et al. ('82), and IRDF-90, but do not support the JENDL ACT File in the higher energy region, which might be based on the experimental data by Pestwood, et al. ('61) and Li Jianwei, et al. ('88).
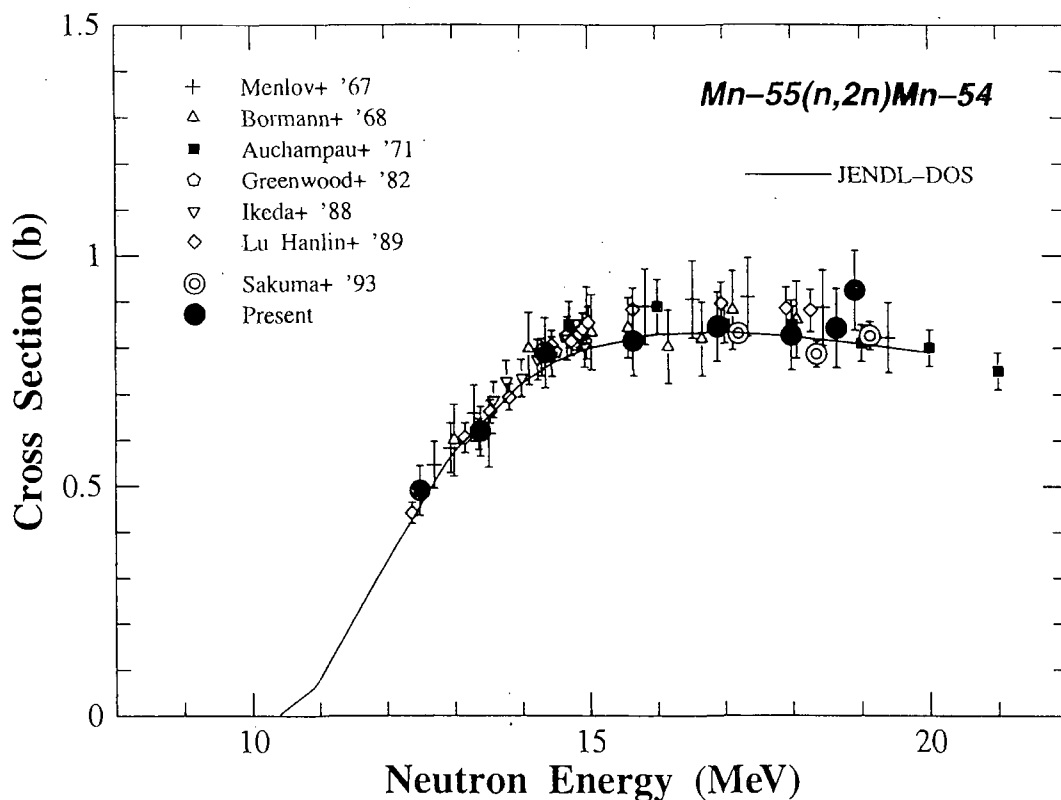
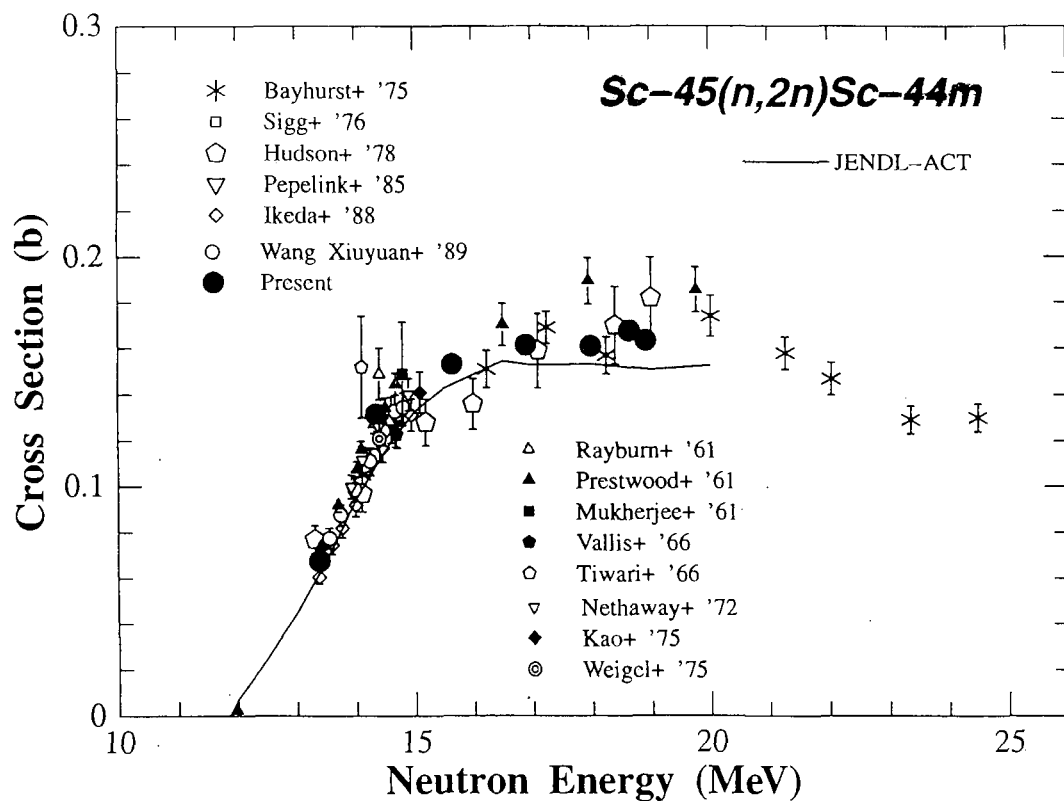Fig. 3 Comparison of the present data with the previous experimental data as well as the curve of the files of JENDL DOS for ^{55}Mn(n,2n)^{54}Mn reaction.
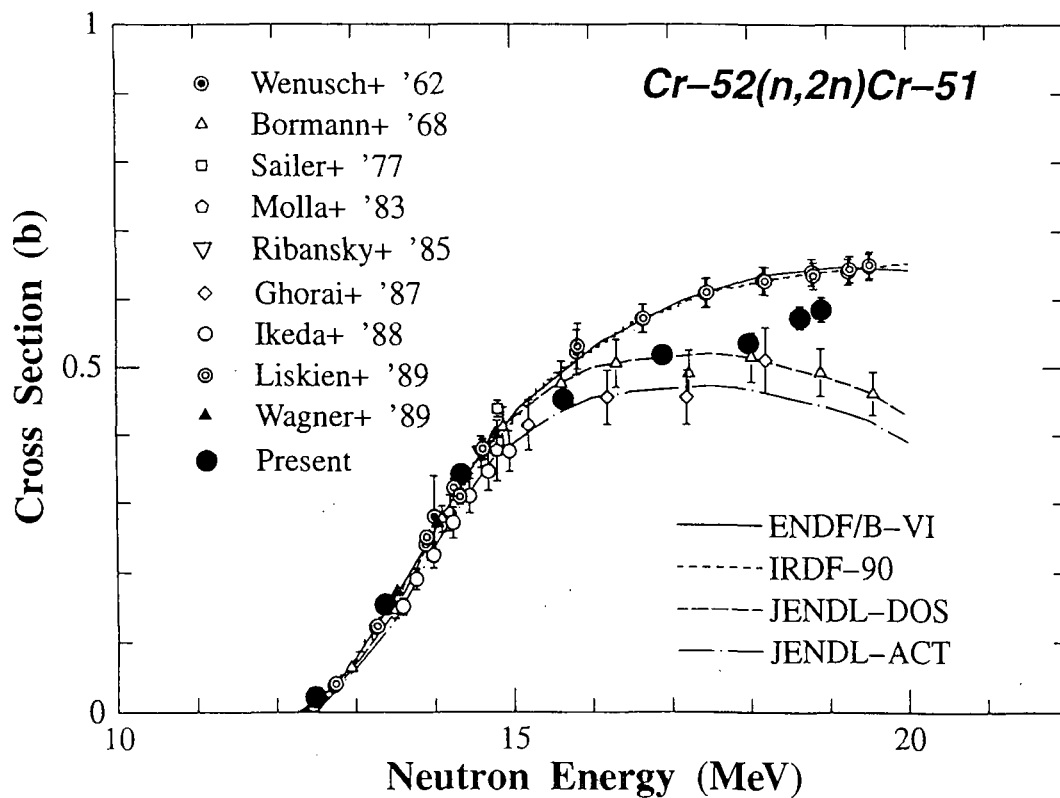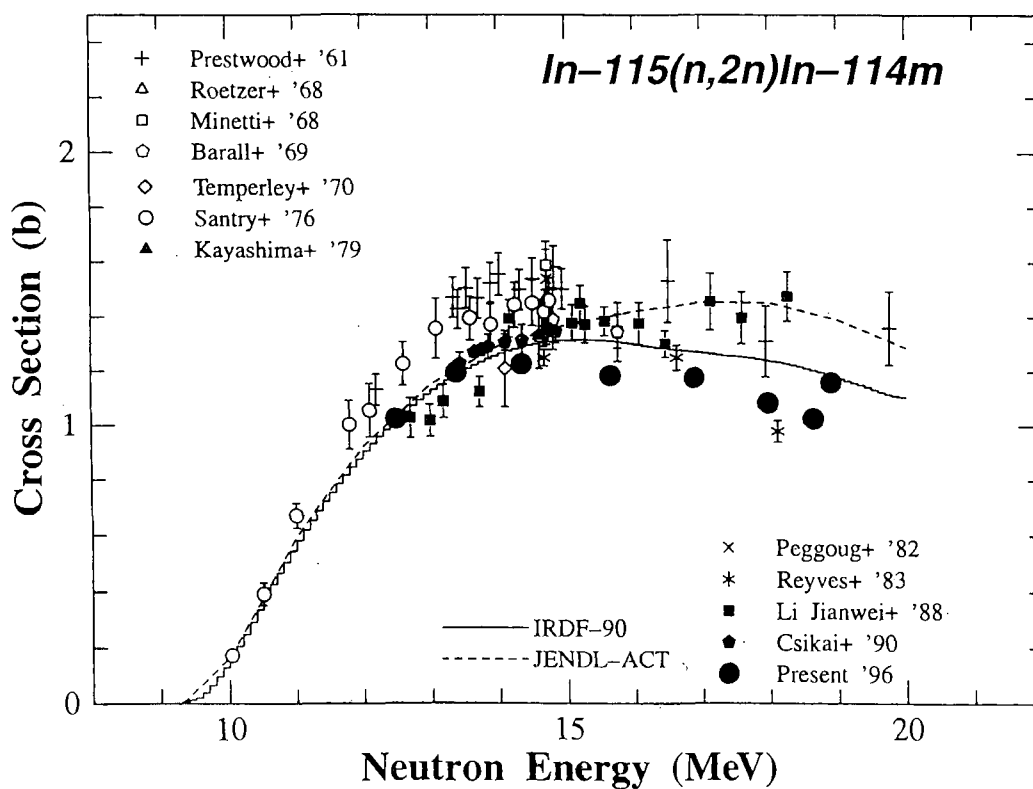

Fig. 4 Comparison of the present data with the previous experimental data as well as the curve of the files of JENDL ACT and IRDF-90 for ^{115}In(n,2n)^{114m}In reaction.

4. SUMMARY

Excitation functions of four (n,2n) reactions on [45]Sc, [52]Cr, [55]Mn, and [115]In were measured in the energy range from 12 to 19 MeV at Dynamitron Facility of Tohoku University, and briefly reported. As far as the measured reactions concerned, JENDL ACTIVATION File (JENDL DOSIMETRY File for some cases) and showed almost consistent with the present data, except for the indium in the higher energy region above 16 MeV, and are acceptable for the aimed applications of the files, e.g., the fusion activation evaluation.

ACKNOWLEDGEMENTS

REFERENCES

1. S. Iwasaki and N.Odano, Proceedings of the International Conference on Nuclear Data for Science and Technology, Gatlinburg, Tenn., USA, May 9-13, 1994.

2. M. Sakuma , S. Iwasaki, H. Shimada, N. Odano, K. Suda, J.R. Dumais and K.Sugiyama: JAERI-M 92-027, p.278 (1992).

3. S. Iwasaki, M. Sakuma, K. Sugiyama and N. Odano: JAERI-M 93-046, p.257, JAERI (1993).

4. S. Iwasaki, S. Matsuyama, T. Ohkubo, H. Fukuda, M. Sakuma, M. Kitamura and N. Odano: JAERI-Conf 95-008, p.165, JAERI (1995).

5. S. Iwasaki, S. Matsuyama, D. Soda, Y. Nauchi, H. Fukuda, M. Kitamura and N. Odano: JAERI-Conf 96-008, pp.157-164, JAERI (1996).

6. H.Vonach: 'Nuclear Standards for Nuclear Measurements', NEANDC-311"U", INDC (SEC) 101, NEA/OECD, p. 80, (1992).

7. J.H. Baard, W.L. Ziip, and H. J. Nolthenius, "Nuclear Data Guide for Reactor Neutron Metrology," Kluwer Academic Publishers (199).

8. Y. Nakajima, et al.: JAERI-Conf 96-008, pp.50-55, JAERI (1996).

9. M. Nakazawa, et al.: "JENDL Dosimetry File", JAERI 1325 (1991).

3.7 (n,α) Cross Section Measurement of Gaseous Sample
Using Gridded Ionization Chamber
- Cross Section Determination -

Toshiya SANAMI, Mamoru BABA, Keiichiro SAITO, Yasutaka IBARA and Naohiro HIRAKAWA

Department of Quantum Science and Energy Engineering, Tohoku University

Aramaki-aza-Aoba, Aoba-ku, Sendai-shi 980-77

e-mail : toshi@rpl.nucle.tohoku.ac.jp

We are developing a method of (n,α) cross section measurement using gaseous samples in a gridded ionization chamber (GIC). This method enables cross section measurements in large solid angle without the distortion by the energy loss in a sample, but requires a method to estimate the detection efficiency. We solve this problem by using GIC signals and a tight neutron collimation. The validity of this method was confirmed through the ^{12}C(n,α_0)^{9}Be measurement. We applied this method to the ^{16}O(n,α)^{13}C cross section around 14.1 MeV.

1 Introduction

The (n,α) cross section data are important in various fields. We have conducted double-differential (n,α) cross section measurement of Fe, Ni, ^{50}Cr and Cu using a gridded ionization chamber (GIC) and foil samples for 4 − 14 MeV neutrons [1,2]. For light nuclei such as C, N and O, measurments using gaseous samples of these nuclei are preferable. This method has advantages that it enables cross section measurements with very high geometrical efficiency without the effect of the energy loss in a sample. As descibed in the next section, however, utilizating gaseous samples gives rise to difficulties in determination of cross section values because of the uncertainties in the effective number of sample atoms, the detection probability of particles and the background determination.

To overcome these difficulties, we have developed a method to employ gaseous samples in GIC. This method employs tight neutron collimation and utilizes the information on event position obtained from GIC signals. We applied this method to the ^{12}C(n,α_0) reaction at 14.1 MeV to examine the detector behavior and the validity of the method. Furthermore, we measured the ^{16}O(n,α) reaction cross

section for 13.7 to 15.0 MeV neutrons. Preliminary results of the spectrum and cross sections for $^{16}O(n,\alpha)$ are presented.

2 Detection Method

To measure (n,α) cross sections of gaseous samples, we filled GIC with a counting gas in which contains the nucleide of interest. Figure 1 shows a schematic diagram of GIC with a gaseous sample. In the case of foil samples, the detector efficiency of α particles could be $\sim 100\%$ by setting the gas pressure so as to make α - particle range shorter than the cathode - grid distance. For the gaseous samples, as shown fig.1, the detector efficiency and the

Figure 1: Schematic view of GIC

number of sample atoms are not unique, but depend on the range [3], the production position of the particles and the neutron beam profile. In the case of GIC, the production position along the beam axis can be known from the anode and the cathode signals:

$$Pa = E + \sigma \cdot Pc \qquad \text{and} \qquad Pc = E \cdot (1 - x/d)$$

where E is the particle energy, σ is the grid inefficiency (5.9%), x is the distance from the cathode plate to the center-of-gravity of electrons produced by ionization (detection position) and d is the distance between the cathode and the grid. Therefore, the energy (E) and the detection position (x) for each event are known from Pa and Pc, and the events of full energy deposition can be selected by using its energy and position information. We determine the effective number of sample atoms and the detection probability of particles by employing an appropriate counting gas pressure, tight neutron collimation and the selection of events in the effective volume of GIC using output signals. Backgrounds can be estimated by comparing the yields for different sample gas content.

3 Experimental Procedure and Result

The experimental arrangement is same as previous 14.1 MeV experiment [1,2]. Neutrons were produced at a Ti-T target via the T(d,n) reaction using the Tohoku University 4.5 MV Dynamitron accelerator. The sample gas was a spectroscopic grade Kr+CH$_4$ for the $^{12}C(n,\alpha_0)$ and Kr+CO$_2$ mixture for the $^{16}O(n,\alpha)$ reaction. Neutrons from the target were collimated by a 20 cm Cu collimator

and its profile was measured using an imaging plate (IP) with a 0.5 mm thick polyethylene converter. For absolute normalization, the neutron flux was measured by a proton recoil telescope [4].

3.1 $^{12}C(n,\alpha_0)$ measurement

Figure 2 illustrates a two dimensional spectrum (Pa vs Pc) for the 4.0 kgf/cm^2 Kr+10%CH$_4$ gas. The anode channel corresponds to the particle energy and the cathode one to the detection point defined in sec.2. Straight diagonal lines represented by equations in sec.2, correspond to the detection position with 0.25 cm step. In this pressure, the maximum range of α particles from $^{12}C(n,\alpha_0)$ is about 1.33 cm and is shorter than cathode - grid distance 2.5 cm. Therefore, all α particles produced around the center of GIC were detected. In this figure, the events from the $^{12}C(n,\alpha_0)$ reaction form the vertical strip because the anode signal shows sum energy of α_0 and ^{9}Be particle.

Figure 3 shows the energy spectrum by the events in 1.3 - 1.7 cm region from the cathode for 3.0 kgf/cm^2 Kr+10%CH$_4$ counting gas. In this region, all events from $^{12}C(n,x\alpha)$ were detected as described in the next paragraph. The $^{12}C(n,\alpha_0)$ events form the peak around 8 MeV with $\sim$ 300 keV width in (3.8%) FWHM. The events below 6 MeV are α particles from the $^{12}C(n,n'3\alpha)$ reaction. This spectrum shows a continuous distribution because the neutron energies were not measured by GIC. Measurements with different sample gas content indicated that backgrounds by the Kr(n,α) events were negligibly small for the $^{12}C(n,\alpha_0)$ yield.

Figure 2: Tow dimentional spectrum of Kr+10%CH$_4$

Figure 3: The energy spectrum of Kr+10%CH$_4$ gas

Figure 4 shows the yield distributions of $^{12}C(n,\alpha_0)$ vs detection positions for 1.0 to 4.0 kgf/cm^2 counting gas pressure. It is found that the yields are low around at the positions of the cathode and

the grid (i.e. 0 and 2.5 cm, respectively) and shows peaks around 1.5 cm from the cathode. In the case for 3.0 and 4.0 kgf/cm^2, the yields at 1.5 cm are saturating and indicate almost 100% detection of α - particles. Therefore, the ^{12}C(n,α_0) cross section was deduced using these yields.

Table 1 shows the results in comparison with the data by the inverse reaction [5] and an evaluation. Although, our data contains uncertainties of absolute normalization and statistics, but do not contain these of region and the number of sample atoms. The present results are consistent with the inverse reaction data.

Table 1: ^{12}C(n,α_0) cross sections

	Cross section [mb]
Present	88.7 ± 4.5
Haight[5]	72.9 ± 9
ENDF/B-VI	81

Figure 4: The yield distributions of the ^{12}C(n,α_0) reaction

3.2 ^{16}O(n,α) cross section

We applied the method to the ^{16}O(n,α) reaction by using Kr+5%CO$_2$ counting gas. Neutrons of 13.7, 14.1 and 15.0 MeV were produced at 135°, 90° and 0° via the T(d,n) reaction, respectively. Figure 5 shows the energy spectra for 14.1 MeV neutrons in the region of 1.3 - 1.7 cm distance from cathode. The gas pressure of Kr+5%CO$_2$ and Kr+10%CH$_4$ were 3.0 kgf/cm^2. In Kr+5%CO$_2$ spectrum, two peaks around 11 and 7.5 MeV correspond to the ^{16}O(n,α_0)^{13}C$_{gs}$ and the ^{16}O(n,$\alpha_{1,2,3}$)^{13}C* events, respectively, and below 5 MeV, a continuum component corresponds to the ^{16}O(n,$\alpha_{4..}$) events are observed as well. The ^{12}C(n,α_0) and ^{12}C(n,n'3α) events are also observed in Kr+10%CH$_4$ spectrum. So we can obtain the spectrum of the ^{16}O(n,α) reaction by subtracting the Kr+10%CH$_4$ data from the

Figure 5: The energy spectra of Kr+5%CO$_2$ and Kr+10%CH$_4$

$Kr+5\%CO^2$ one.

Figure 6 illustrates the subtracted result, i.e., a net energy spectrum of the $^{16}O(n,\alpha)$ in comparison with a 14.1 MeV result measured using a cloud chamber by Lille et al [6]. From figure 5, however, this procedure might lead to over subtraction below around 4 MeV, because the H(n,p) reaction greatly contributes to the $Kr+10\%CH_4$ spectrum. However, as shown in fig.6, the data by Lillie shows similar spectrum with ones and ever lower values for $^{16}O(n,\alpha_{4..})$ components. Therefore, we deduced the $^{16}O(n,\alpha)$ cross section by using yields of region above 4 MeV.

Figure 7 shows our preliminary results of the $^{16}O(n,\alpha)$ cross section in comparison with other measurements [6-8] and evaluations. Absolute values were determined relating to the $^{12}C(n,\alpha_0)$ yield for the same gas pressure using the JENDL-3.2 data for $^{12}C(n,\alpha_0)$. Although, our data contain errors of absolute normalization and statistics, but do not contain these of region and the number of sample atoms. Above 14 MeV, the experimental data are about only one third compared with evaluation and should be examined.

4 Summary

We are developing a method of (n,α) cross section measurement using gaseous samples in a gridded ionization chamber and applied this method to the measurements of the $^{12}C(n,\alpha_0)^9Be$ and $^{16}O(n,\alpha)^{13}C$ cross sections around 14.1 MeV. From the consistency of the $^{12}C(n,\alpha_0)^9Be$ result with the data of inverse reaction, the validity of the method was confirmed. The $^{16}O(n,\alpha)$ result are consistent with other experimental data, but are about three times as large as JENDL-3.2 evaluations.

Reference

1. N.Ito et al., Nucl. Instr. Methods, **A337**, 474 (1994)
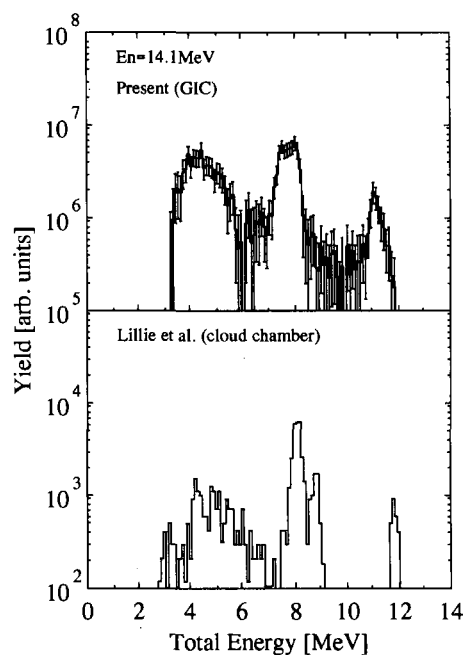
Figure 6: The energy spectra of $^{16}O(n,\alpha)$
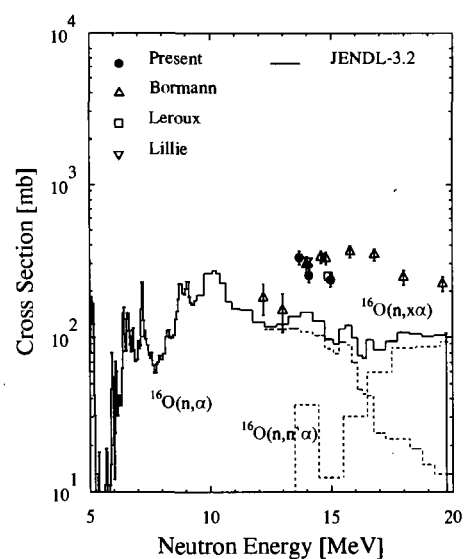
Figure 7: The $^{16}O(n,\alpha)$ cross section

2. M.Baba et al., J. Nucl. Sci. Technol., **31** [7], 745 (1994)

3. F.Gabbard et al., Nucl.Phys., **14**, 277 (1995)

4. M.Baba et al., Nucl. Instr. Methods, **A376**, 115 (1996)

5. R.C.Haight et al., Nucl. Sci. and Eng., **87**, 41 (1984)

6. A.Lillie, Phys.Rev., **87**, 716 (1952)

7. M.Bormann et al., Z.Phys., **174**, 1 (1963)

8. B.Leroux et al., Nucl.Phys., **A116**, 196 (1968)

3.8 Development of Whole Energy Absorption Spectrometer for Decay Heat Measurement on Fusion Reactor Materials

Fujio MAEKAWA and Yujiro IKEDA

Fusion Neutronics Laboratory, Japan Atomic Energy Research Institute

Tokai-mura, Naka-gun, Ibaraki-ken 319-11

e-mail: fujio@fnshp.tokai.jaeri.go.jp

To measure decay heat on fusion reactor materials irradiated by D-T neutrons, a Whole Energy Absorption Spectrometer (WEAS) consisting of a pair of large BGO scintillators was developed. Feasibility of decay heat measurement with WEAS for various materials and for a wide range of half-lives (seconds ~ years) was demonstrated by experiments at FNS. Features of WEAS, such as high sensitivity, radioactivity identification, and reasonably low experimental uncertainty of ~ 10 %, were found.

1. Introduction

Adequate estimation of decay heat on plasma facing components of a D-T fueled fusion reactor is important for safety designs of the reactor against loss of coolant/flow accidents and for planning of shutdown scenario. Induced radioactivity calculation codes and their data bases used for the designs should be validated by benchmark experiments. Many experimental studies have been devoted to induced radioactivies on fusion reactor materials irradiated with D-T neutrons. In these studies, gamma-rays emitted from the radioactivies are measured with HP-Ge detectors. These experiments, however, do not provide necessary informations for decay heat because beta-rays, which are the other sources of decay heat along with gamma-rays, are not measured. Thus, a Whole Energy Absorption Spectrometer (WEAS) was developed to measure decay heat on fusion reactor materials irradiated with D-T neutrons, as an R&D task (T-339) for the Engineering Design Activities of International Thermonuclear Experimental Reactor.

2. Whole Energy Absorption Spectrometer

Decay heat arises from deposited energies to the material by beta- and gamma-rays emitted from induced radioactivies. As shown in Fig. 1, the essential part of WEAS is consists of a pair of large bismuth-germanate (BGO) scintillators of 120 mm in diameter and 100 mm in thickness to measure whole energies of both beta- and gamma-rays emitted from an irradiated sample. The BGO scintillators are selected because of the following two substantial reasons: (i) the high detection efficiency due to the high Z-number of bismuth (83) and the high weight density (7.13 g/cm^3), (ii) no

hygroscopic character to eliminate window materials between the scintillators and a sample for beta-ray measurement, (iii) high transparency of the crystal for the scintillation light, and (iv) moderate decay constant of the scintillation light (0.3 μs) suitable for high counting rate measurements.

Irradiation samples are thin (~ 10 μm) foils to eliminate self-absorption of beta-ray energies in the samples, and sandwiched by the BGO scintillators. Energies of both beta- and gamma-rays emitted from the sample are deposited almost completely in the scintillators. The energy absorption efficiency, defined as a ratio of absorbed energies by BGO scintillators to total beta- and gamma-ray energies emitted from the sample, is calculated with the EGS4 code [1], as shown in Fig. 2. The efficiencies for electron are very close to 100 %, while those for photon are somewhat smaller than 100 %; which are ~ 90 % and ~80 % for 1 MeV and 2 MeV photons, respectively. The efficiencies for positron are almost equal to that of electron multiplied by that of 0.511 MeV photon. The efficiency curves are to be used for correction.

A diagram of the electronic circuit is shown in Fig. 1. The deposited energies are measured as a pulse height spectrum taken through photomultiplier tubes, amplifiers and a multi-channel analyzer. Each count of the pulse height spectrum is multiplied by the corresponding energy in electron-volt to obtain total deposited energies of the BGO scintillators. The total energies are divided by the counting time in second and multiplied by the conversion factor 1.602×10^{19} [J/eV], and after necessary corrections, a decay heat value averaged during the measurement period is derived in the unit of Watt/g.

3. Demonstration Experiment

Decay heat measurement on various materials were carried out at the Fusion Neutronics Source (FNS) facility in JAERI to demonstrate the feasibility of WEAS. Sample materials used in the measurements are listed in Table 1. About a half of them are thin foils with area of 25 x 25 mm^2, while the rest are in powder form sandwiched by two thin plastic tapes of 24 x 24 mm^2. The powder samples are used because of their availability due to chemical and physical stability. Carbon and oxygen atoms contained in parts of the powder samples do not cause significant decay heat except for ^{16}N nuclei with very short half-lives of 7.13 s produced by the ^{16}O(n,p) reactions. An aluminum foil of 50 μm in thickness with the same area as the sample is attached to the sample for determination of D-T neutron fluence with utilizing the ^{27}Al(n,α)^{24}Na reaction rate.

The samples were irradiated with D-T neutrons generated by FNS, and pulse height spectra were measured with WEAS as a function of cooling time. To obtain decay heat values for radioactivities having various half-lives, three types of combinations of irradiation and cooling time are adopted for the irradiation, as indicated in Table 2. Measurements for the cooling time up to 100 days have been finished, and the identified radioactivities of the longest half-life is ^{60}Co (5.27 years).

A typical example of the measured pulse height spectra for a titanium sample is shown in Fig. 3. The two spectra denoted as Det_A and Det_B are measured by individual scintillators (singles spectra), and the sum spectrum corresponds to total deposited energies for both the BGO scintillators (see Fig. 1). It is found in Fig. 3 that the two spectra denoted as Det_A and Det_B are almost identical because of the symmetric geometry of the scintillators. Scandium-48 nucleus

disintegrates with a beta-ray of maximum energy at 661 keV followed by three cascade gamma-rays of 984, 1037 and 1312 keV, with almost the 100 % probability. When the beta-ray energy is 0, the total deposited energy is the sum of three gamma-ray energies, i.e., 3333 keV, and when the beta-ray has the maximum energy, the total deposited energy corresponds to the Q_β (3994 keV) of ^{48}Sc. Thus, in Fig. 3, the pulse height spectrum of ^{48}Sc rises from 3333 keV and ends at 3994 keV (note that the measured pulse height spectrum is broadened by the energy resolution of the spectrometer).

Decay heat values were derived for all the measured pulse height spectra. Two examples of decay profiles for the measured decay heat are shown in Figs. 4 and 5 for 5 minutes and 7 hours irradiations, respectively (note that corrections for the energy absorption efficiency, energy cutoff (~ 50 keV) of pulse height spectra, and fluctuation of D-T neutron flux during the irradiations have not been performed). These are the first experimental data of decay heat on fusion reactor materials irradiated by D-T neutrons.

In the case of the copper sample, most of decay heat for the 5 minutes irradiation is dominated by ^{62}Cu ($T_{1/2}$ = 9.74 min) produced by the ^{63}Cu(n,2n) reactions. For the 7 hours irradiation, decay heat of copper for cooling time shorter than 3 days is due to ^{64}Cu ($T_{1/2}$ = 12.7 hr) produced mainly by the ^{65}Cu(n,2n) reactions, while the flat curve for cooling time longer than 10 days is due to ^{60}Co ($T_{1/2}$ = 5.27 y) produced by the ^{63}Cu(n,α) reactions.

As a consequence, these experiments demonstrated the feasibility of decay heat measurement with WEAS for various materials and for a wide range of half-lives (seconds ~ years).

4. Features of WEAS

The following features of WEAS are found:

(i)   high sensitivity, < 1 pW (almost corresponds to 2 Bq of ^{60}Co), needed for measurement of low-level radioactivities with long half-lives,

(ii) pulse height spectrum data for energy calibration with mono energy gamma-ray sources and for radioactivity identification by both the singles and the sum spectra,

(iii) small size sample (10~100 mg) for simultaneous irradiation of many samples, low cost, and low human dose for experimentalists, and

(iv) reasonably low experimental uncertainty around 10 %.

As expected from Fig. 3, the WEAS can be used for other types of experiment such as beta-ray spectrum measurements, Q_β determination and cross section measurements for pure beta-emitters.

Reference

[1]   Nelson W. R., Hirayama H. and Rogers D. W. O.: "The EGS4 code system", SLAC-265, Stanford Linear Accelerator Center (1985).

Table 1. Sample materials for the decay heat measurement.

Metallic Foil Sample		Powder Sample	
Al	Mo	B_4C	Y_2O_3
Ti	Ta	Na_2CO_3	SnO
V	W	SiO_2	$BaCO_3$
Fe	Pb	S	Re
Co	SS304	K_2CO_3	Bi
Ni	SS316	CaO	
Cu	Inconel-600	Cr	
Zr	NiChrom	Mn	
Nb	CF_2	$SrCO_3$	

Table 2. Combinations of irradiation and cooling time.

Irradiation Time	Cooling Time	Sample Materials
5 min	1 min ~ 60 min	All the samples in Table 1
1 hr	1 min ~ 12 hr	Ti, V, Cr, Fe, Co, Ni, Cu, Mo, Zr, SS316
7 hr	12 hr ~ years	All the samples in Table 1
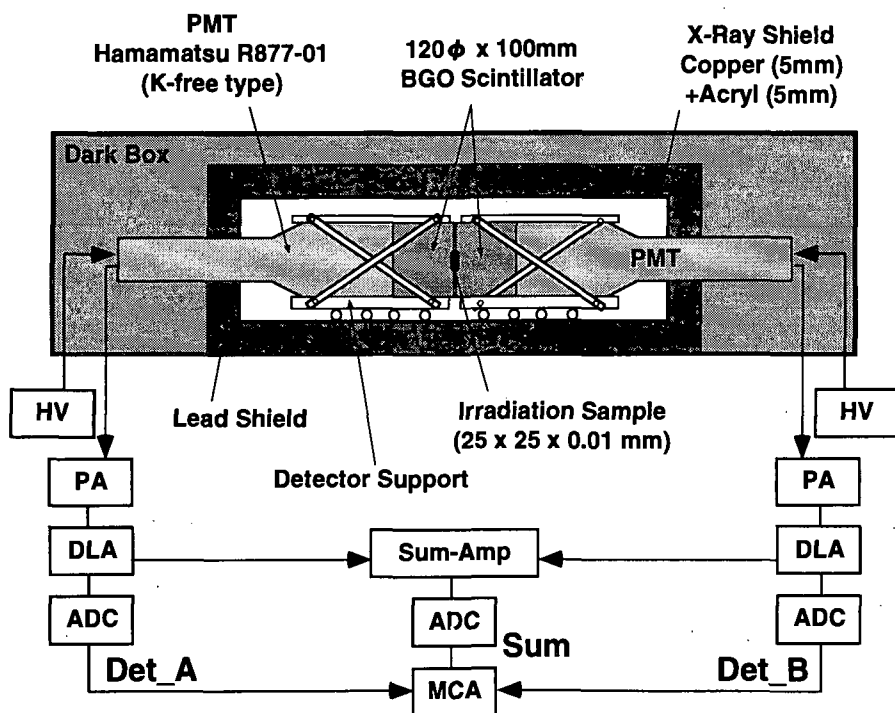
Fig. 1   A schematic diagram of the Whole Energy Absorption Spectrometer (WEAS) and the associated electronic circuit.
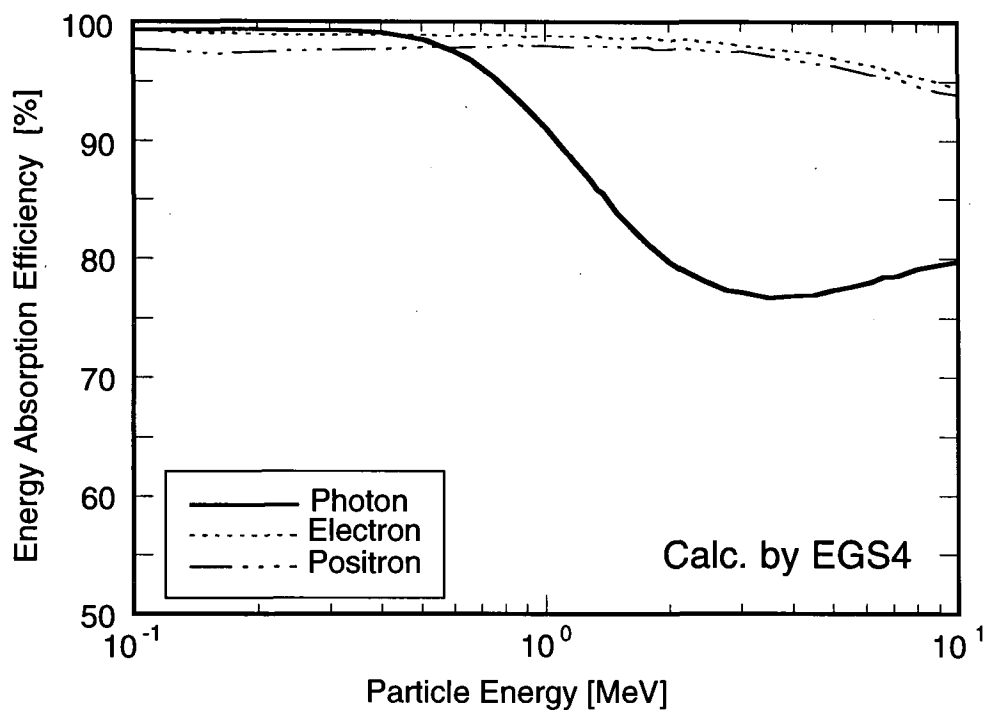
Fig. 2   Energy absorption efficiency of the WEAS for photon, electron and positron calculated
with the EGS4 code [1].
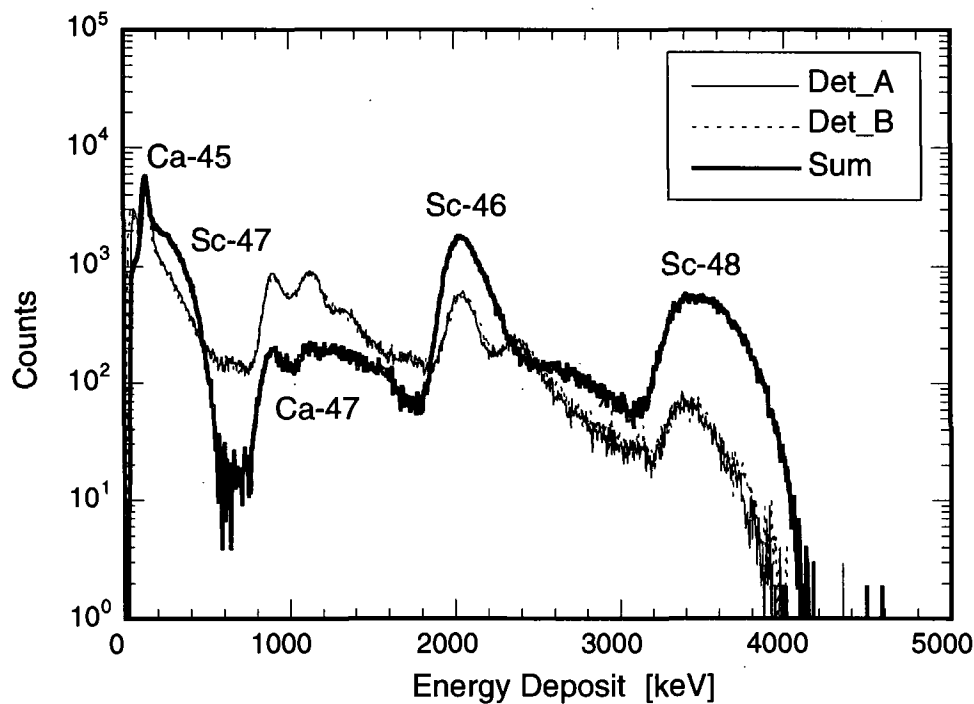
Fig. 3   A typical example of the measured pulse height spectra for a titanium sample irradiated
for 7 hours with cooling of 13 days. Spectra for Det_A and Det_B are almost
identical.
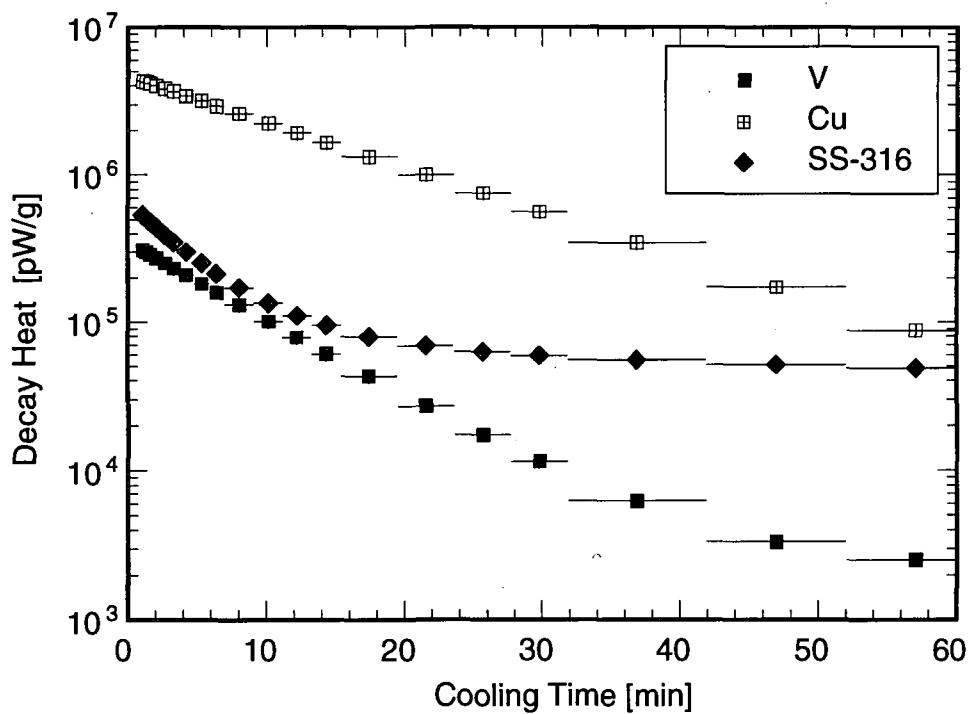
Fig. 4   Measured decay heat for vanadium, copper and SS316 irradiated with D-T neutron flux of 10^{10} [n/cm^2/s] for 5 minutes.
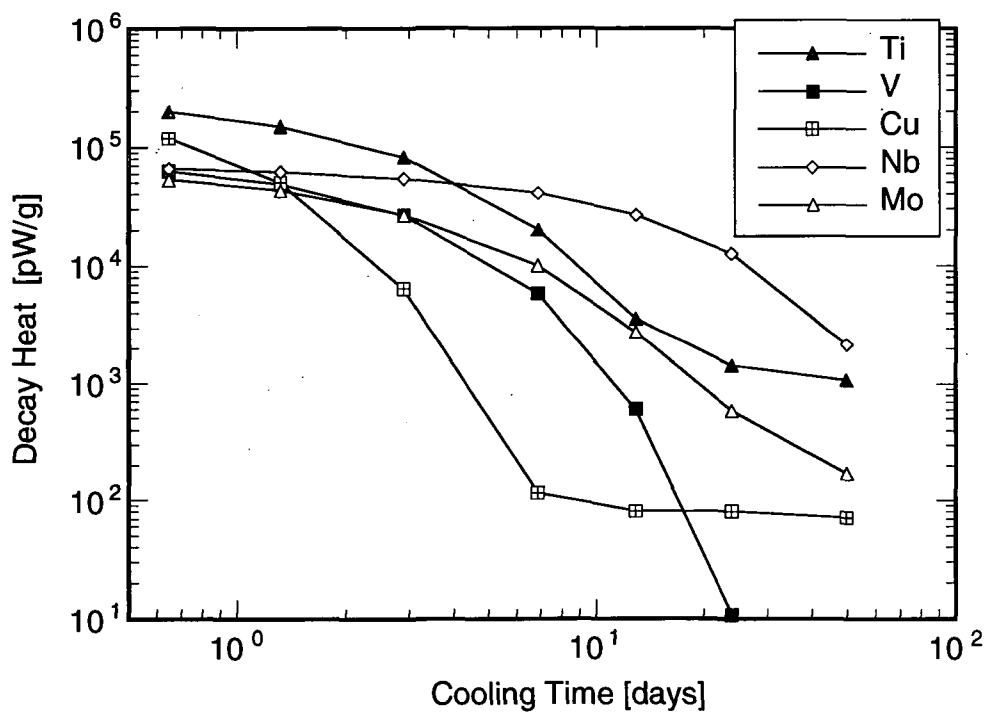
Fig. 5   Measured decay heat for titanium, vanadium, copper and niobium and molybdenum irradiated with D-T neutron flux of 10^{10} [n/cm^2/s] for 7 hours.

3.9 Evaluation of Induced Activity, Decay heat and Dose Rate Distribution after Shutdown in ITER

Koichi Maki, Satoshi Satoh[*1], Katsumi Hayashi[*2], Koubun Yamada[*3], Hideyuki Takatsu[*1], Hiromasa Iida[*4]

Hitachi Research Laboratory, Hitachi Ltd.
7-2-1 Omika-cho, Hitachi-shi, Ibaraki-ken,319-12 Japan

[*1]Naka Fusion Research Establishment, Japan Atomic Energy Research Institute
Naka-machi, Naka-gun, Ibaraki-ken 311-01 Japan

[*2]Hitachi Engineering Co., Ltd.
Saiwai-cho, Hitachi-shi Ibarali-ken 317 Japan

[*3]Mito Branch Office, Business Automation Ltd.,
Joonan, Mito-shi Ibaraki-ken 310 Japan

[*4] Garching Joint Work Site of ITER Max-Planck Institute für Plasmaphysik
Boltzmannstrasse 2 D85748 Garching bei Munchen Germany

Induced activity, decay heat and dose rate distributions after shutdown were estimated for 1MWa/m^2 operation in ITER. The activity in the inboard blanket one day after shutdown is 1.5x10^{11}Bq/cm^3, and the average decay heating rate 0.01w/cm^3. The dose rate outside the 120cm thick concrete biological shield is two order higher than the design criterion of 5μSv/h. This indicates that the biological shield thickness should be enhanced by 50cm in concrete, that is, total thickness 170cm for workers to enter the reactor room and to perform maintenance.

1. Introduction

The EDA (Engineering Design Activity) of ITER (International Thermonuclear Experimental Reactor)[1] was started at July in 1992, and its design concept has been being confirmed. Then it becomes necessary to evaluate induced activity, decay heat and dose rate distribution after shutdown, which have not been estimated yet with all significant quantities for reactor design, in order to perform remote maintenance design and safety design for radiation workers.

The objects of the present paper are as follows:
The first thing is to estimate induced activity, decay heat and dose rate distributions after shutdown for ITER, whose conceptual view and principal values are shown in Fig.1 and Table 1, respectively. The second thing is to recommend the required thickness of biological shield for workers to enter the reactor room and to perform directly maintenance. Further the third thing is to clarify what kinds of activation cross sections are necessary to be evaluate highly accurate in fusion reactor design.

2. Calculational method

Calculational procedure is shown in Fig.2 for computing nuclear properties during operation and after shutdown for fusion reactors. The neutron and gamma-ray fluxes during operation are calculated by two dimensional RZ
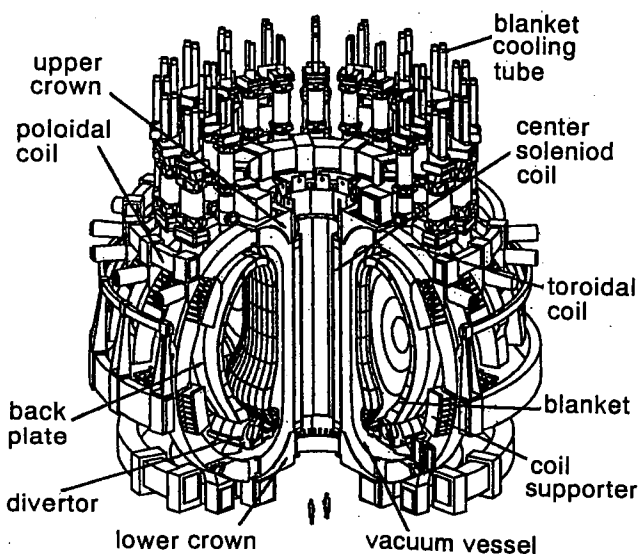
Fig. Conceptual view of ITER

Table 1. The principal values of ITER

Items	values
Fusion power	1500 MW
Average neutron wall loading	1 MW/m^2
Plasma major radius	8.1 m
minor radius	2.8 m
Plasma current	21 MA
Toroidal magnetic field on axis	5.7 T
maximum field	12.5 T
Plasma burning time	1000 s
Plasma heating power	100 MW

model with DOT3.5 code[2], and neutron and gamma-ray coupled transport group constant set of FUSION-40[3], which consists of neutron 42groups and gamma-ray 21 groups based on JENDL3[4]. Using the neutron flux, the induced activities, decay heat and gamma-ray source intensity one day after shutdown for the first wall neutron fluence operation or operating pulse pattern are computed by CINAC[5] code. On the basis of the gamma-ray source intensity, gamma-ray flux distribution is calculated by DOT3.5 code and gamma-ray transport group constant

Fig.2 Calculational procedure

set of GROUPIN[6] constructed with 54 groups, and dose rate distribution was converted from the gamma-ray flux distribution at a time point after shutdown.
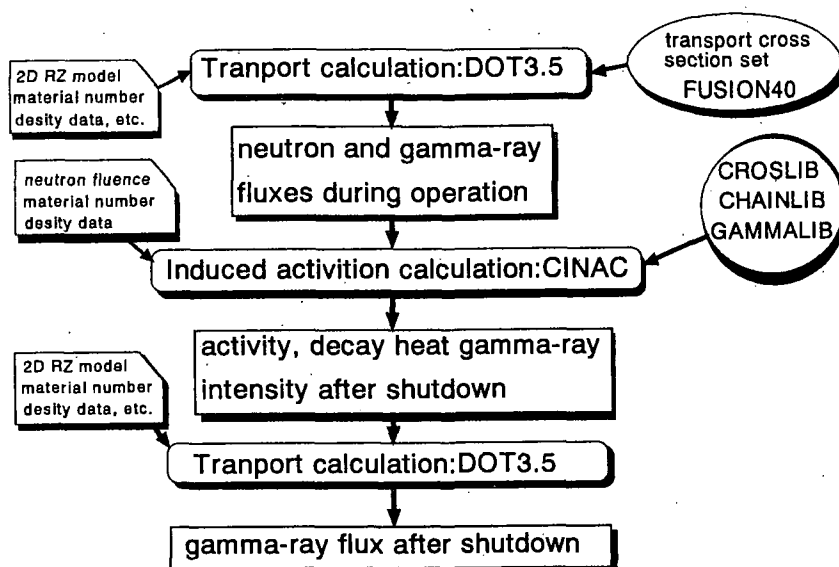
According to the conceptual design of ITER as shown in Fig.1, the two dimensional RZ torus model used in transport calculation is performed as illustrated in Fig.3. The neutron source intensity created in the plasma region by DT fusion reaction is 5.3194×10^{20} n/s for the fusion power of 1500MW during operation. The Legendre expansion order of P5 and the number of 160 angles in quadreture set are used in this calculation.

The time points estimating induced activities, decay heat and gamma-ray source intensity are 1 second, 1 minute, 1 hour, 1 day, 1 week, 1 month, 1 year, 10 years, 30 years and 100 years after shutdown of 1MWa/m^2 first wall neutron fluence operation.

3. Estimated results and discussion

Neutron and gamma-ray fluxes during operation were calculated as shown in Fig.4 and Fig.5. From these figures, maximum total neutron and gamma-ray fluxes can be seen respectively 4×10^{14} n/cm^{2}s and 2×10^{14} γ/cm^{2}s, which are shown at the plasma center and the upper point near the mid-plane of the outboard fisrt wall, respectively. Both the fluxes in the exhaust duct become approximately 10^{11} n/cm^{2}s by neutron and gamma-ray streaming through the ducts. Although, the fluxes in the ducts should be corrected from the view point of three dimensional configuration, since the ducts of this model is fully opened in the torus direction because of symmetry model in the torus direction.

Induced activities in the various components of ITER were calculated by using this neutron flux. At the same time, decay
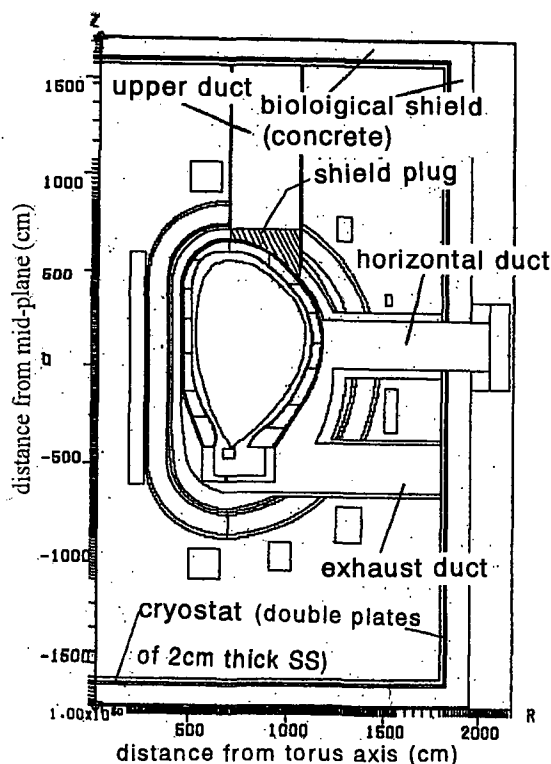
Fig.3 Two dimensional RZ torus model
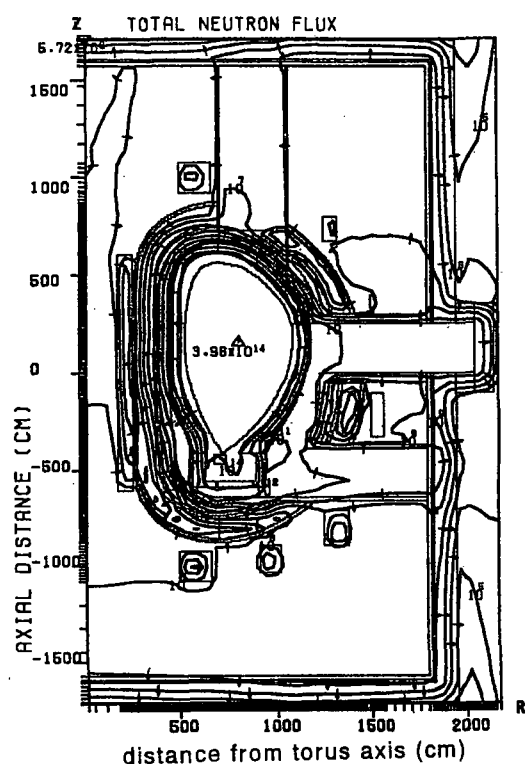
Fig.4 Total neutron flux contour in ITER for
the neutron first wall loading of 1MW/m²
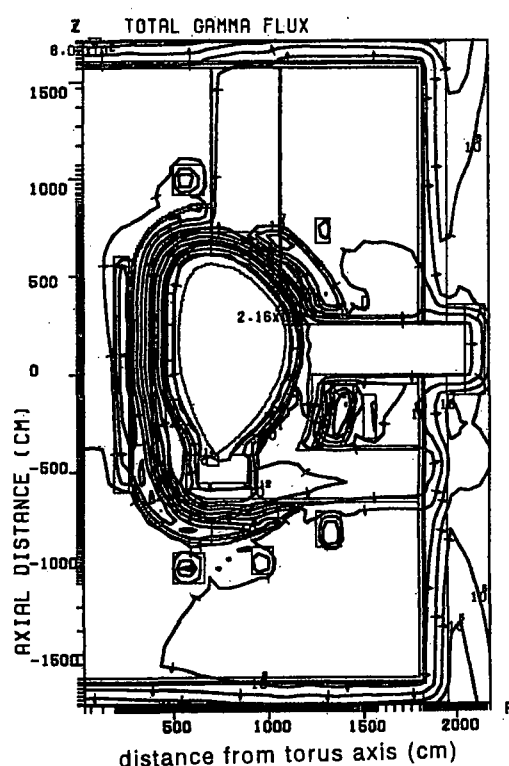
Fig.5 Gamma-ray flux contour in ITER for
the neutron first wall loading of 1MW/m²

heats in the various components were estimated for the first wall neutron fluence of 1MWa/m². Pairs of induced activity and decay heat in the inboard blanket, the inboard blanket back plate, the vacuum vessel and inboard toroidal coil leg of the ITER are represented Figs.6 and 7, Figs.8 and 9, Figs.10 and 11, Figs.12 and 13, respectively. The activity in the inboard blanket one day after shutdown is 1.5×10^{11}Bq/cm³, and the average decay heating rates in the component one second, one hour, one day and one week are 0.06w/cm³, 0.05w/cm³, 0.01w/cm³ and 0.007w/cm³, respectively. The activity in the back plate at the same time point is 2×10^{9}Bq/cm³, 2 order less than that in the blanket from Fig.6. The decay heating rates are also 2 order less than that in the blanket from Fig.7. Beyond expectations, the activity and decay heating rate in the vacuum vessel are 5 times higher than those in the back plate from Figs.8 and 9. This is the reason why vacuum vessel is irradiated from outside by the neutron leaking through the exhaust and horizontal ducts as shown in total neutron flux contour of Fig.4.

The principal nuclides contributing to the activity and decay heat after one day from shutdown are ^{51}Cr, [55]Fe(non gamma-ray), [57]Co, [58]Co and [54]Mn, etc.

The gamma-ray flux was computed on the basis of the gamma-ray source intensity radiated from decay nuclides. The gamma-ray flux distribution is illustrated Fig.14. According to the gamma-ray flux, the dose rate distribution was estimated by using the conversion factors from gamma-ray into dose rate. The dose rate distribution is also presented in Fig.15 for the first wall neutron fluence of 1MWa/m². According to this result, the dose rate in the plasma chamber is 2×10^{4}Sv/h in the maximum value one day after shutdown. The dose rate in the most space in the cryostat is less than 10mSv/h and that in the partial space near the exhaust and horizontal ducts is 10-100mSv/h. As described previously, corrected value with the factor= (real area)/(area in this model) concerning duct opening area is approximately 2 order less than the computed value by this model. If the factor has high reliability, there is a barely chance for workers to enter the cryostat with restricted period. In order to obtain exact dose rate, a three dimensional calculation must be necessary.
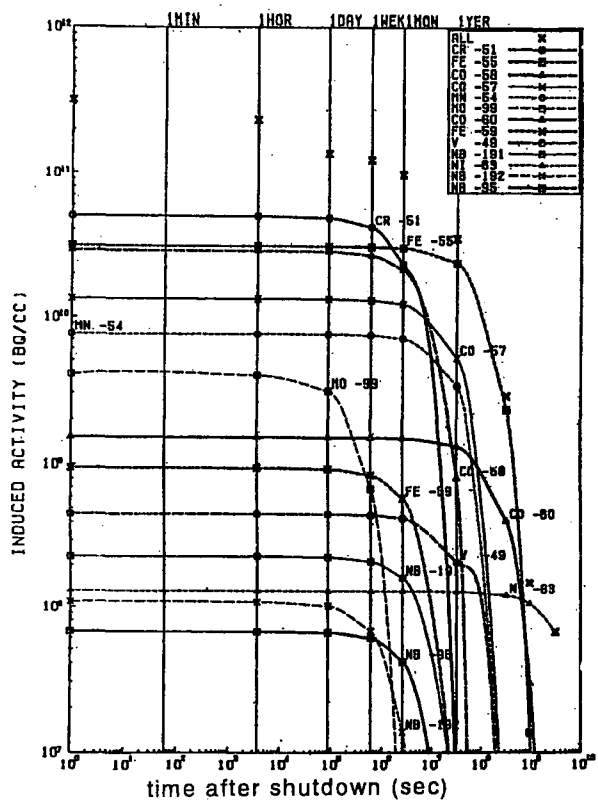
Fig.6 Induced activity in inboard blanket in ITER
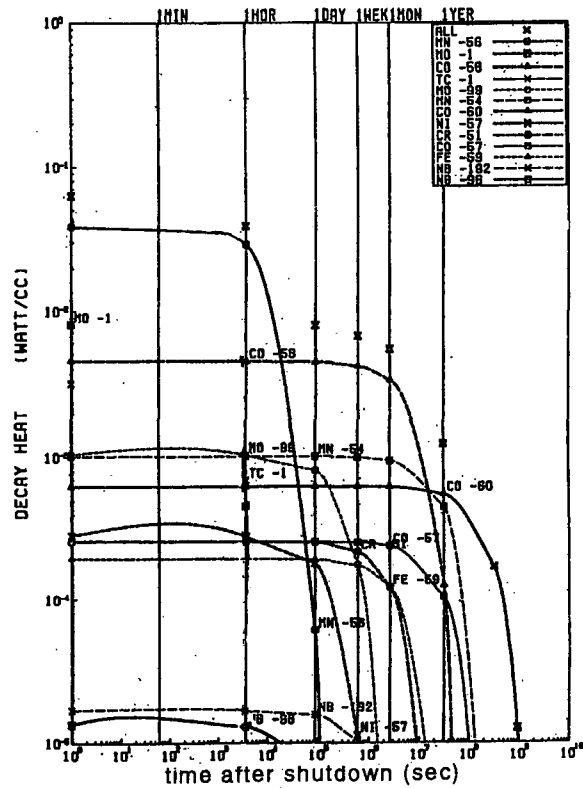
Fig.7 Decay heat in inboard blanket in ITER
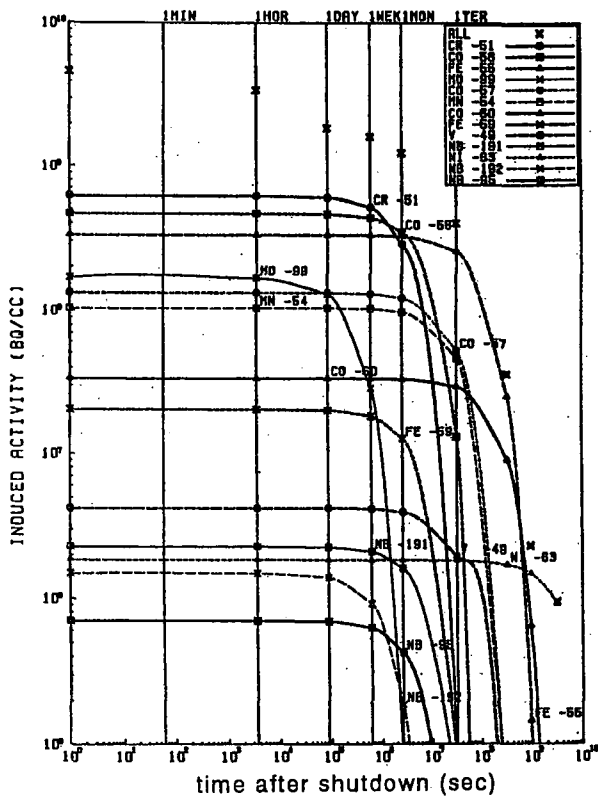
Fig.8 Induced activity in inboard blanket back plate in ITER

Fig.9 Decay heat in inboard blanket back plate in ITER

Fig.10 Induced activity in vacuum vessel
in ITER

Fig.11 Decay heat in vacuum vessel
in ITER

Fig.12 Induced activity in inboard leg
of toroidal coil in ITER
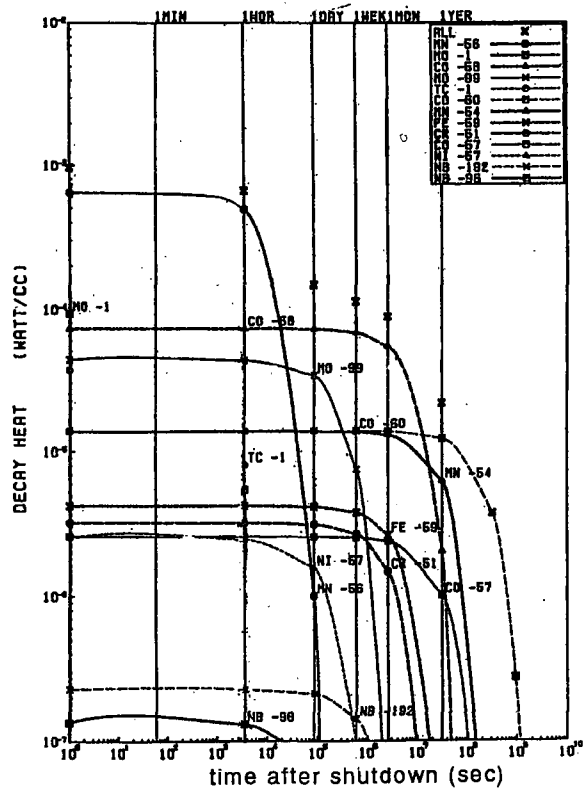
Fig.13 Decay heat in inboard leg
of toroidal coil in ITER
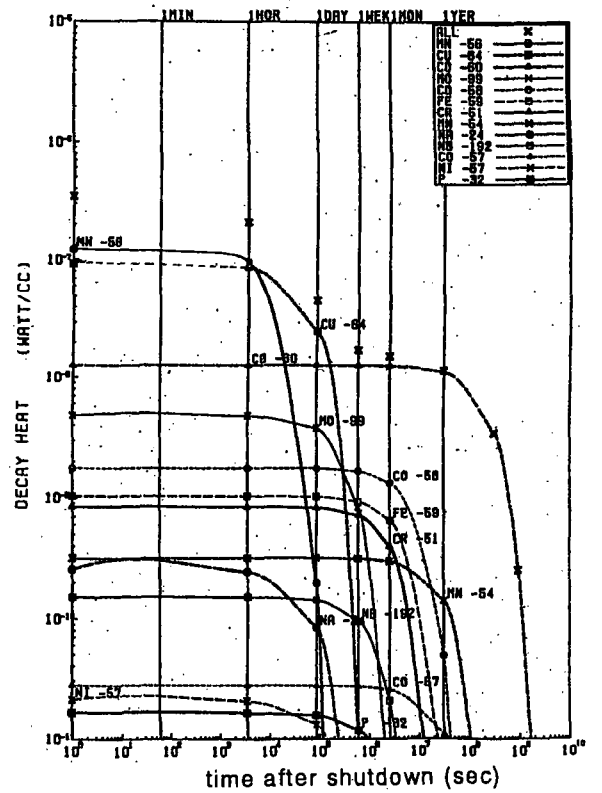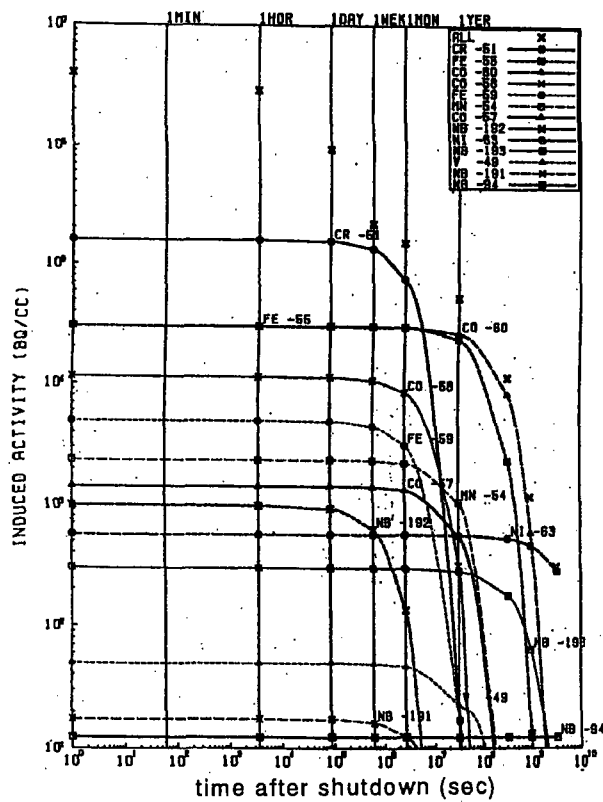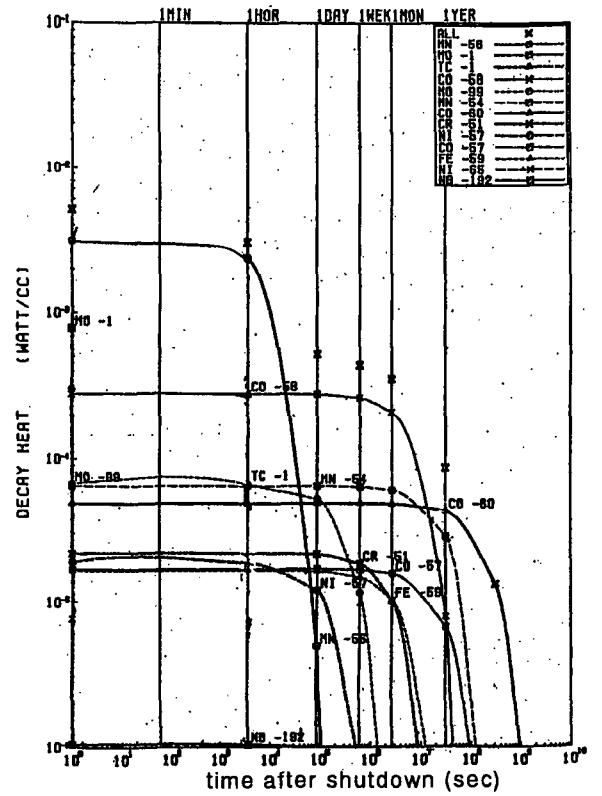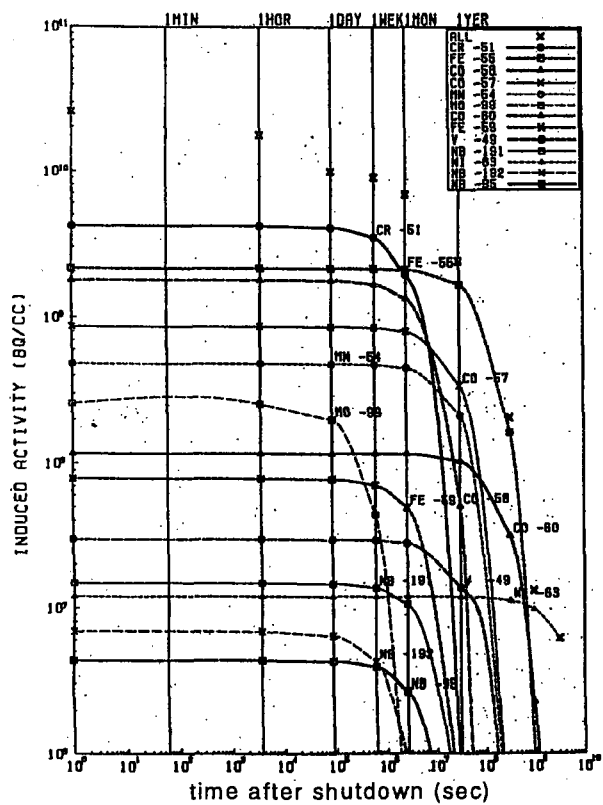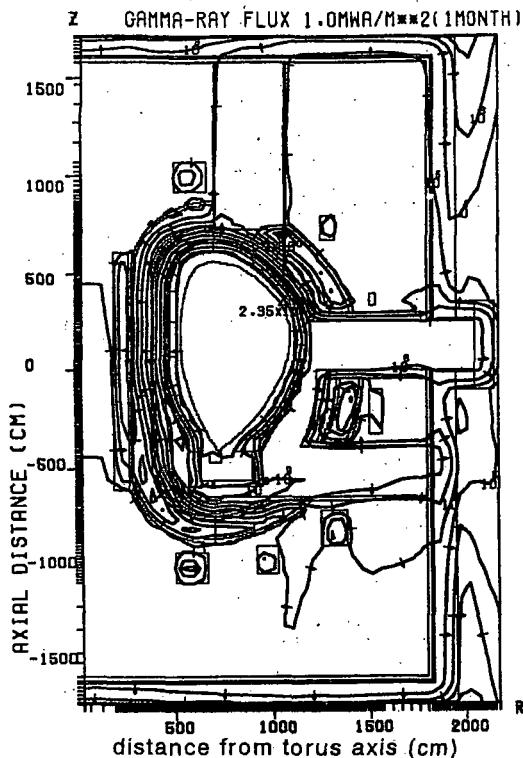
Fig.14 Gamma-ray flux conttour one day after shutdown of 1MWa/m² operation in ITER (γ/cm²s)
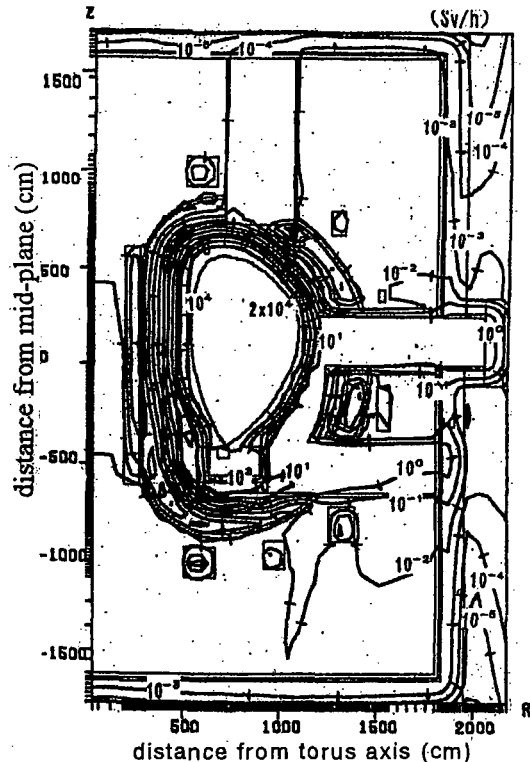
Fig.15 Gamma-ray dose rate conttour one day after shutdown of 1MWa/m² operation in ITER (Sv/h)

The dose rate outside the 120cm thick concrete biological shield is two order higher than the design criterion of 5µSv/h. This indicates that the biological shield thickness should be enhanced by 50cm in concrete, that is, total thickness 170cm for workers to be possible to enter the reactor room and to perform directly maintenance such as setting the maintenance machines and cutting the cooling tubes, etc.

4. Conclusion

Induced activity, decay heat and dose rate distributions after shutdown were estimated for 1MWa/m² operation in ITER, which in every component have not been estimated yet with all significant quantities for reactor design, in order to perform remote maintenance design and safety design for radiation workers.. From these calculations, we obtained the results as follows.

(1) The activity in the inboard blanket one day after shutdown is 1.5×10^{11}Bq/cm³.

(2) The average decay heating rates one second, one hour, one day and one week are 0.06w/cm³, 0.05w/cm³, 0.01w/cm³ and 0.007w/cm³, respectively.

(3) The dose rate outside the 120cm thick concrete biological shield is two order higher than the design criterion of 5µSv/h for workers in radiation field.

(4) The biological shield thickness is necessary to be enhanced by 50cm in concrete, that is, total thickness 170cm for workers to enter the reactor room and to perform maintenance.

References

[1] ITER Nuclear Design Group, ITER Documentation Series, No.29, IAEA, International Atomic Energy Agency (1991).

[2] W. A. Rhoades, F. R. Mynatt, The DOT-III Two Dimensional Discrete Ordinates Transport Code, ORNL-TN-4280, Oak Ridge National Laboratory (1973).

[3] K. Maki, et al., JAERI-M 91-072, Japan Atomic Energy Institute (1991).

[4] K. Shibata, et al., JAERI-1319, Japan Atomic Energy Institute (1990).

[5] H. Fukumoto, J. Nucl. Sci. Technol., 23, 97 (1986).

[6] Y. Seki, et al., JAERI 1301, Japan Atomic Energy Institute, (1986).

3.10 Measurements of Neutron Spallation Cross Section(2)

E. Kim, T.Nakamura (CYRIC,Tohoku Univ)

M.Imamura,N.Nakao,S.Shibata (INS,Univ.of Tokyo)

Y.Uwamino, N.Nakanishi (RIKEN)

Su.Tanaka (JAERI)

Neutron spallation cross section of ^{59}Co (n,xn) $^{60-x}$Co , ^{nat}Cu (n,sp) ^{56}Mn, ^{nat}Cu (n,sp) ^{58}Co, ^{nat}Cu (n,xn) ^{60}Cu , ^{nat}Cu (n,xn) ^{61}Cu and ^{nat}Cu (n,sp) ^{65}Ni was measured in the quasi-monoe nergetic p-Li neutron fields in the energy range above 40MeV which have been established at three AVF cyclotron facilities of 1)INS of Univ.of Tokyo,2)TIARA of JAERI and 3)RIKEN. Our experimental data were compared with the ENDF/B-VI high energy file data by Fukahori and the calculated cross section data by Odano.

1. INTRODUCTION

The high energy and high intensity of accelerator has developed with the increasing of its application using experiment in nuclear physics, nuclear medicine radiotherapy and so on. It was noticed that the induced radioactivity of the accelerators materials, shielding materials and the air of accelerator facility due to the primary accelerating charged particles as well as with the secondary neutrons are still problem. Nevertheless, neutron cross section data in the energy range above 20 MeV are very poor and no evaluated data file exists. In this study,we measured the neutron spallation cross section using quasi-monoenergetic p-Li neutrons in the energy range above 20MeV.

2.EXPERIMENTS

The experiments were performed at three cyclotron facilities of 1) Institute for Nuclear Study (INS), University of Tokyo, 2) Takasaki Research Establishments, Japan Atomic Energy Research Institute (TIARA) and 3) Institute of Physical and Chemical Research (RIKEN).

Irradiation experiments utilized quasi-monoenergetic neutrons which were produced by ^{7}Li(p,n)^{7}Be reaction of proton beams from AVF cyclotron. The Li-targets of 2 to 10 mm thicknesses were bombarded by proton beams of 20 to 120 MeV energies. The neutron produced in the forward direction from the target were transported through the collimator for sample irradiation and the proton beams passed through the target were swept out by the magnet to the beam dump. In the TIARA and RIKEN experiments, the neutron spectra were measured with the TOF method using a organic liquid scintillator. The absolute neutron fluence was determined with the PRT(Proton Recoil counter Telescope) at TIARA, and with the Li activation method to detect the ^{7}Be activity from the ^{7}Li(p,n)^{7}Be reaction at RIKEN. Fig. 1 and 2

showed the neutron spectra for 43, 58,68 and 88MeV proton incidence at TIARA and for 90,100,110 and 120MeV proton incidence at RIKEN, respectively.

The irradiation samples are ^{nat}Cu and ^{59}Co. Table 1 shows the physical data of irradiation samples. The samples were irradiated 400cm and 837cm behind the the Li-target at TIARA and RIKEN.

Irradiation consisted of short irradiation time (1 to 2 hours under 120MeV)and long irradiation time (about 20hours) by considering the half life of produced nuclei. During sample irradiation, proton beam currents were monitored with the digital current integrator and scalar. The gamma rays emitted from irradiated samples were measured with a high purity Ge detector.

The peak efficiency of Ge detector was obtained from the mixed standard source, QCD.1 and the EGS4 code[1] in TIARA and RIKEN.

The self absorption of samples was calculated with the PEAK code[2].

3.ANALYSIS

The reaction rates of identified radioisotopes were obtained by analyzing gamma-ray spectra after corrected for the peak efficiency, and self-absorption effects, also for the beam current fluctuation during sample irradiation.

3.1.Reaction Rate

The reaction rates of the irradiated samples were obtained by identified gamma ray peak area. The reaction rate corrected for the beam current fluctuation becomes

$$R = \frac{\lambda \cdot C}{N \cdot e \cdot g \cdot e^{-\lambda T_c} \cdot (1 - e^{-\lambda T_m}) \cdot \sum_i \{Q_i \cdot e^{-\lambda(n-i)\Delta t}\}} \qquad (1)$$

where N : Atomic number of the sample nuclide, C : Counts of gamma-ray peak area, T_i : Irradiation time of samples, T_m: Measurement time , T_c: Cooling time, ϵ : Peak efficiency, λ : Decay constant, γ : Emission rate of gamma rays. Q_i is beam current for Δt.

3.2.Cross Section

The cross section were obtained the reaction rate of equation(1), the reaction rate ratio and the peak neutron fluence which is given by PRT or Li activation method.

Finally, the cross section at E_{peak} can be estimated by

$$\sigma(E_{peak}) = \frac{R \times \frac{\int_{E_{min}}^{E_{max}} \sigma(E) \cdot \phi(E) \, dE}{\int_{E_{th}}^{E_{max}} \sigma(E) \cdot \phi(E) \, dE}}{\Phi(E_{peak})} \qquad (2)$$

R:The reaction rate by the eq.(1), ϕ (E): the measured by the TOF method , σ (E): estimated from our experimental data , the evaluated data file, ENDF/B-VI[3] by Fukahori , the calculated cross section data Odano[4].

3.3.Estimation of errors

The errors of cross section data were obtained from the error propagation law by combining the error of reaction rate (About 1 - 30%) ,peak neutron fluence (About 4 - 15%), FWHM of peak neutron spectrum(2.8～5.0MeV), contribution from the reference cross section used to estimate the low energy neutron component (About 5 - 40%).

4.RESULT AND CONCLUSION

We obtained the cross section values of ^{59}Co(n,xn) $^{60-x}$Co , ^{nat}Cu(n,sp) ^{56}Mn, ^{nat}Cu(n,sp) ^{58}Co, ^{nat}Cu(n,xn) ^{60}Cu, ^{nat}Cu(n,xn) ^{61}Cu and ^{nat}Cu(n,sp) ^{65}Ni reaction. Figs.3 to 10 give the obtained cross section data. The experimental cross section data of ^{59}Co(n,xn) $^{60-x}$Co and ^{nat}Cu(n,sp) ^{56}Mn to and ^{nat}Cu(n,sp) ^{65}Ni were compared with the calculation data by Odano and the ENDF/B-VI high energy file data calculated with the ALICE code[5].Our experimental results are the first experimental data and are generally good agreement.

Reference

[1]W.R.Nelson, H.Hirayama, and D.W.O.Rogers, SLAC-265
(Standard University, Standard 1985)

[2]T.Nakamura and T.Suzuki, Monte Carlo Calculation of Peak Efficiencies of Ge(Li) and pure Ge Detector to Voliminal Sources and Comparison with environmental Radioactivity Measurement . Nucl. Inst. and Meth. 205,211 (1983)

[3]National Nuclear data Center,Brookhaven National Laboratory, "Evaluated Nuclear data file" ENDF/B-VI(1990)

[4]N.Odano and S.Iwasaki, JAERI-M 94-019, p310-319, Proceedings of 1993 symposium on Nuclear Data,(1994)

[5]M.Blamm, CODE ALICE/89, private communication (1989)

Table.1:Physical data of irradiation samples

	Samples	Diameter	Thickness	Weight	Purity
TIARA EXP	^{59}Co	33mm	2.0mm	20g	99.99%
	^{nat}Cu	33mm	2.0mm	20g	99.99%
RIKEN EXP	^{nat}Cu	80mm	10mm	490g	99.99%
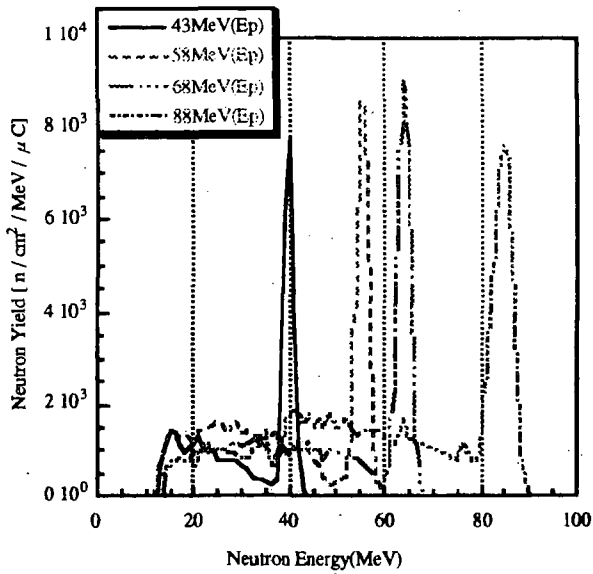
Fig 1. The neutron spectra of 43,58,68 and
88MeV p-Li reaction at TIARA
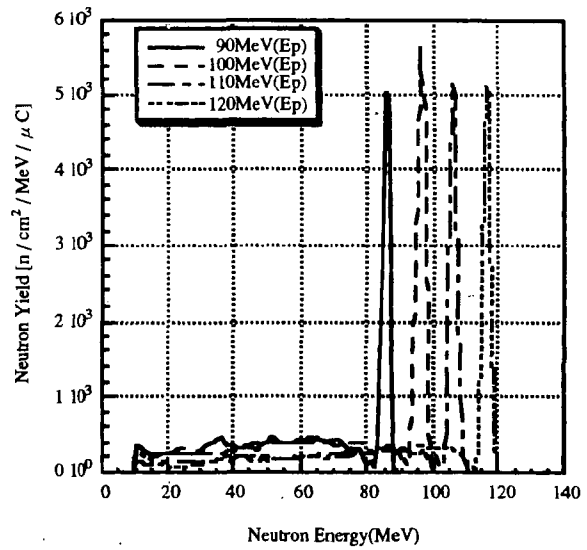
Fig 2. Neutron spectra of 90,100,110,
and 120MeV p-Li reactions at RIKEN
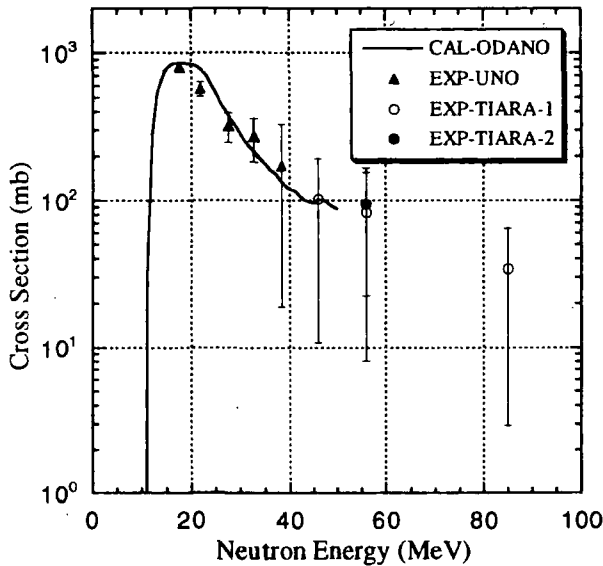
Fig.3 ^{59}Co(n,2n) ^{58}Co Cross Section
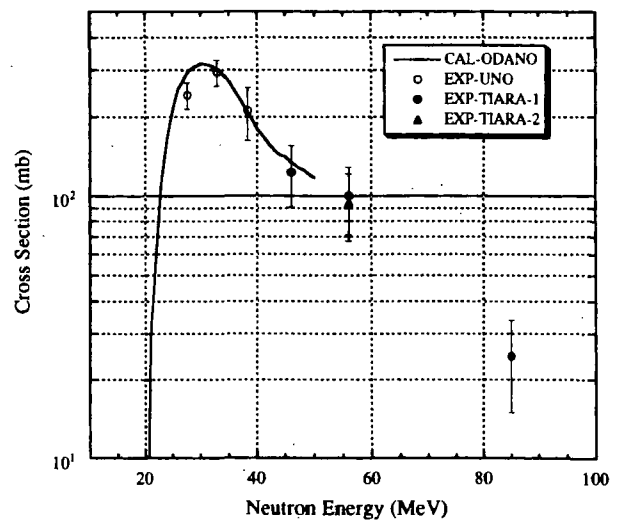
Fig.4 ^{59}Co(n,3n) ^{57}Co Cross Section
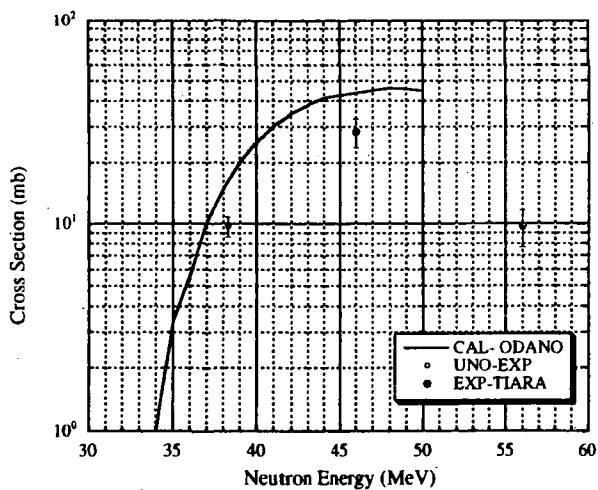
Fig.5 ^{59}Co(n,4n) ^{56}Co Cross Section
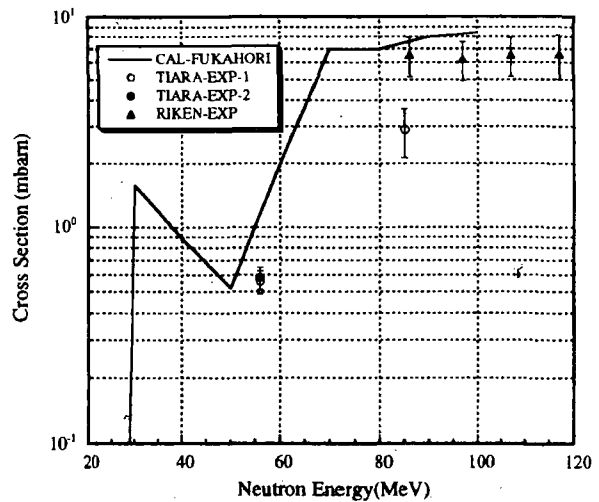
Fig.6 ^{nat}Cu(n,sp) ^{56}Mn Cross Section
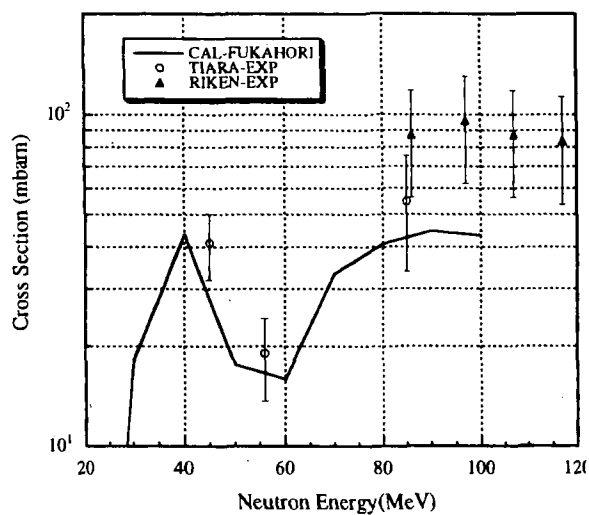
Fig.7 ^{nat}Cu(n,sp) ^{58}Co Cross Section
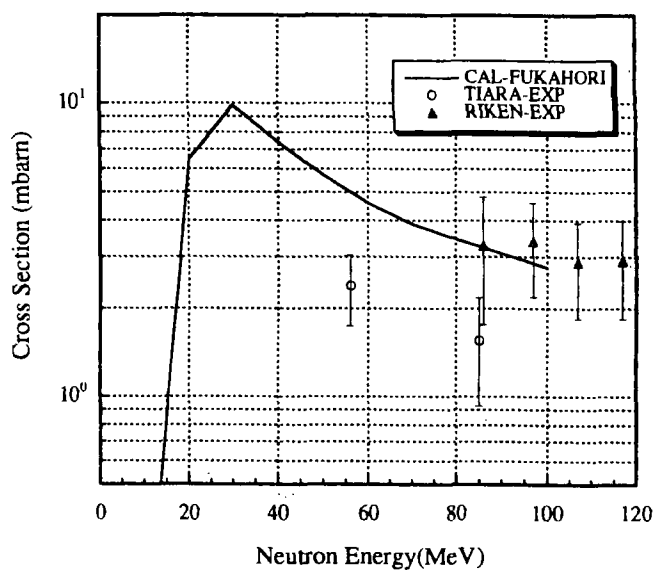
Fig.8 ^{nat}Cu(n,xn) ^{60}Cu Cross Section
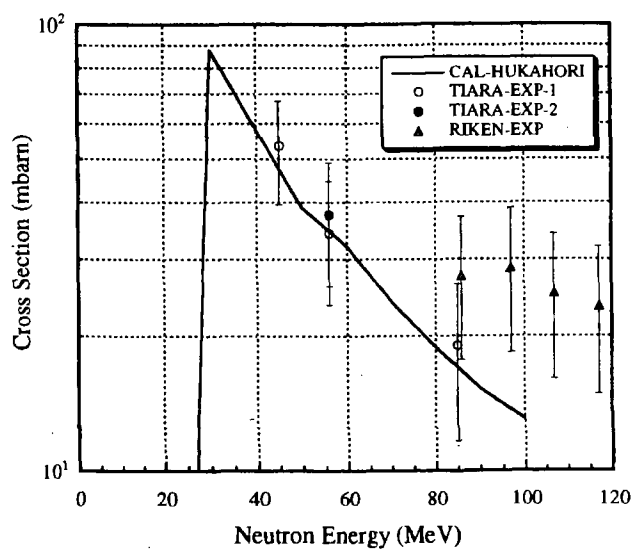
Fig.9 ^{nat}Cu(n,xn) ^{61}Cu Cross Section
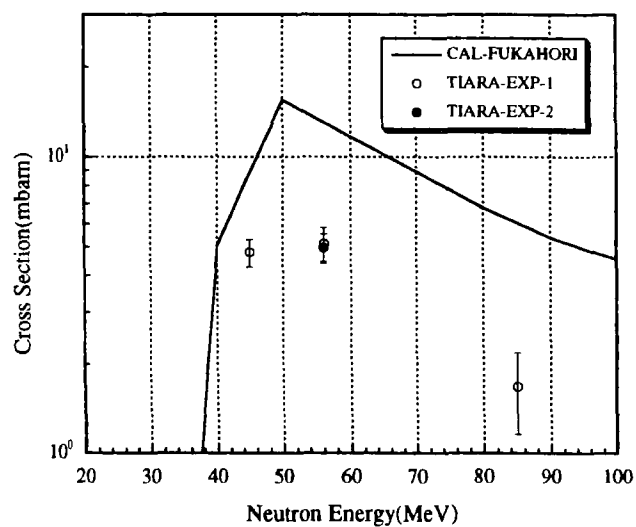
Fig.10 ^{nat}Cu(n,sp) ^{65}Ni Cross Section

3.11. Measurements of secondary neutrons producted from thick targets bombarded by heavy ions

T.Kurosawa[1], T.Nakamura[1], N.Nakao[2], T.Shibata[2]

Y.Uwamino[3], N.Nakanishi[3], A.Fukumura[4], Y.Kumamoto[4]

[1]*Cyclotron and Radioisotope center , Tohoku University*

Aoba, Aramaki, Sendai-shi, 980-77, Japan

[2]*Institute for Nuclear Study, University of Tokyo*

3-2-1, Midori-cho, Tanashi-shi, Tokyo, 188, Japan

[3]*The Insutitute of Physical and Chemical Research*

2-1, Hirosawa, Wako, Saitama, 351-01, Japan

[4]*National Institute of Radiological Sciences*

4-9-1, Anagawa, Inage-ku, Chiba-shi, Chiba, 263, Japan

Abstract

We measured neutron angular and energy distributions from high energy heavy ions stopping in targets of carbon, aluminum, copper and lead at HIMAC. These spectra are much harder for the lighter target nucleus like carbon. This means that the momentum transfer in the forward direction from heavy ion beam to lighter nuclei is much higher than that to heavier nuclei.

1. Introduction

At the National Institute of Radiological Sciences, the HIMAC accelerator (Heavy Ion Medical Accelerator in Chiba) is routinely used for the heavy ion cancer therapy. During operation of this machine, we started to measure the angular and energy distributions of secondary particles produced from thick targets bombarded by carbon and helium ion, especially secondary neutrons, whose experimental data are very scarce. These data are needful to design shielding for the heavy-ion accelerator facility, and also are of interest for estimating neutron doses producted by nuclear interactions during irradiation of cancerous tumors with heavy ions.

2. Experimental Procedure

The target materials with the thicknesses and the incident energies of carbon and helium ions are shown in Table 1. The target shape was 10cm by 10cm square. The target thickness was determined to stop the incident particles completely. The experimental set up is shown Fig. 1. We used three sets of NE213 organic liquid scintillator (12.7cm diam. by 12.7cm-long) for E counter and NE102A plastic scintillator (12.7cm by 12.7cm and 0.5cm thickness) for ΔE counter. A thin NE102A plastic scintillator(3cm diam. by 0.05cm thickness) was set near by the end of the beam line, and the output pulses of this scintillator were used as start signals of the TOF measurement and to count the absolute number of beam particles incident on the target.

For discriminating between neutrons and charged particles, we used the output pulses of the ΔE counter that was placed immediately in front of each E counter, and charged particles were identified from two-dimensional ΔE-E graphical plots.

The contribution of the background neutrons caused by the room-scattering was measured at 90 degree placing a rectangular iron block with the size of 15cm by 15cm by 60cm long between the target and detector.

A simplified schematic diagram of the electronics is shown in Fig.2. The beam-telescope timing signal started a 2048 channel CAMAC time-to-digital converter(TDC). Anode signals of the photomultipliers, which were connected NE213 scintillators, were branched out to three pulses. One pulse was put into CFD to produce the start signal of TDC.Two pulses were put into ADCs that collected the charge of pulse during the gate signal duration. In order to reject the events induced by gamma rays, the two-gate integration method[1] was adopted. For the measurement of the total and slow part of scintillation, timing of input signals was different. The total gate also employed to measure the pulse height of the scintillation.

3. Data Analysis

For discrimination between the neutrons and charged particles, we used the output pulses of the ΔE couter, and charged particles were identified from two-dimensional ΔE-E graphical plots (Fig.3). Next tne neutron and gamma ray events were distinguished from the charged particles, these were separated the neutron events and the gamma ray ones using two dimensional total-slow pulse height graphical plots (Fig.4). After the TOF spectrum of neutrons was obtained, was converted into the energy spectrum of the neutron by the following expression.

$$\Phi(E) = \frac{C(E, L_{th})}{\varepsilon(E, L_{th}) \cdot \Delta E \cdot Q \cdot \Delta\Omega} \cdot f_d$$

where $C(E, L_{th})$ is the energy distribution of neutron counts, ΔE the energy bin, $\Delta\Omega$ the solid angle sustained by the detector to the center of the target, Q the incident heavy ion counts, f_d the correction of dead time, $\varepsilon(E, L_{th})$ the detection efficiency for the neutron, L_{th} the discrimination level for the neutron pulse height, $\Phi(E)$ the energy neutron spectrum. The detection efficiencies were calculated with Cecil code.

4.Results
4.1. Neutron spectra

Neutron spectra are plotted in Fig.5-12. As an example, secondary neutron spectra from carbon, alminum, copper and lead target for 180MeV/nucleon carbon incidence are shown in Fig.5-8. Neutron spectra are spread up to about 370MeV and are much harder for a target of lighter nucleus like carbon. This means that the momentum transfer in the forward direction from carbon beam to lighter nucleid is much ligher than heavier nucleus.

4.2. Total Yields

The integrated neutron yields above 20MeV are shown in Fig. 13-16. The neutron yield at 0 degree is also larger for lighter target nucleus due to the stronger forwardness of secondary neutron production.

5.Conclusins

We measured neutron angular and energy distributions produced by helium and carbon ions stopping in targets of carbon, aluminum, copper, and lead. We are planning to do the repeated experiment for lower threshold. We are also proceeding the experiments for other heavy ions with several energies.

References
1) Z.W.Bell, Nucl. Instrum. Meth., 188, 105(1981).
2) R.A.Cecil, et al., Nucl. Instrum. Meth., 161, 439(1979).

Table 1 Projectile and target combinations and detector position for measuring the secondary particles.

Incident particle and energy [MeV/u]	Target thickness [cm]	Detector position[degree]
Helium 100	C[5] Al[4] Cu[1.5] Pb[1.5]	0, 7.5, 15
Helium 180	C[16] Al[12] Cu[4.5] Pb[5]	0, 7.5, 15, 30, 60, 90
Carbon 100	C[2] Al[2] Cu[1] Pb[1]	0, 7.5, 15, 30, 60, 90
Carbon 180	C[6] Al[4] Cu[1.5] Pb[1.5]	0, 7.5, 15, 30, 60, 90
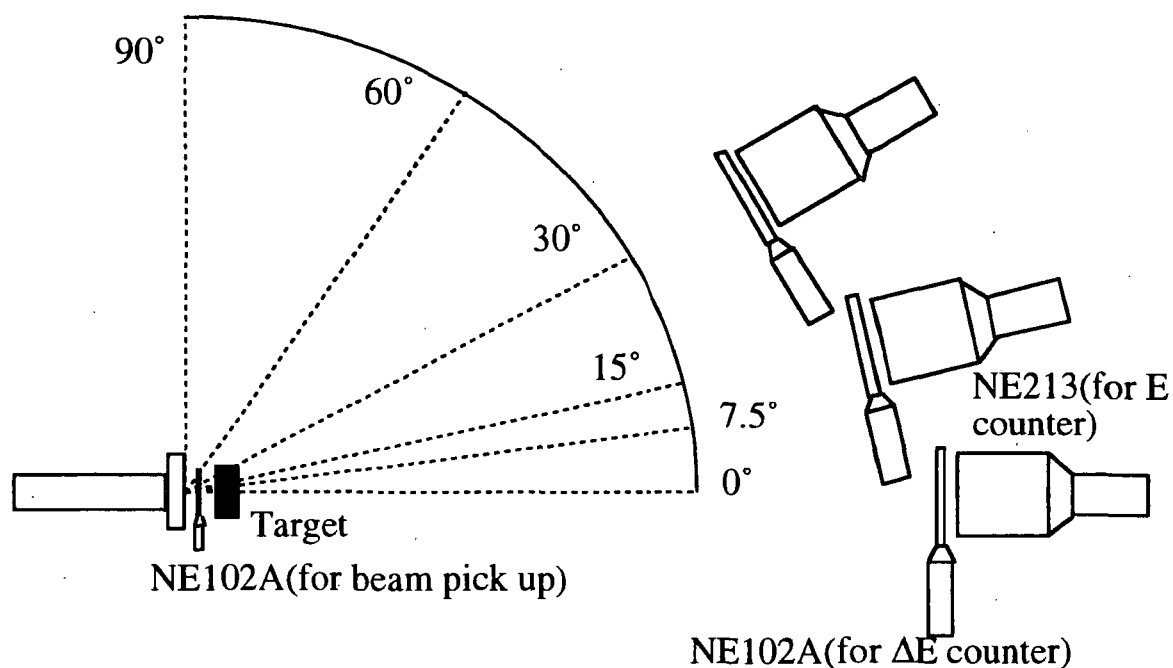
Fig. 1 : Experimental arrangement at HIMAC.
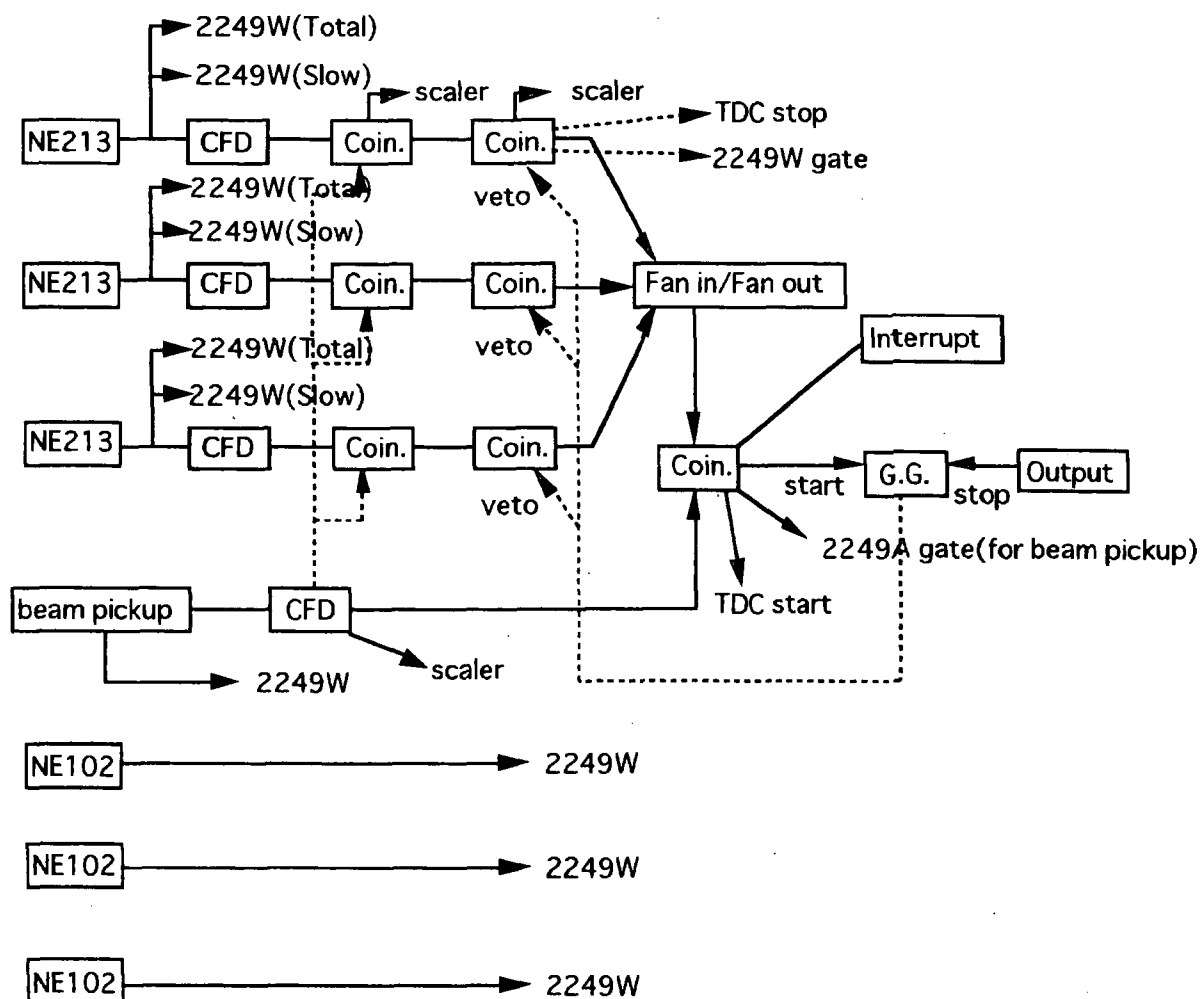
Fig. 2 : Simplified electronics diagram.

ΔE counter pulse height
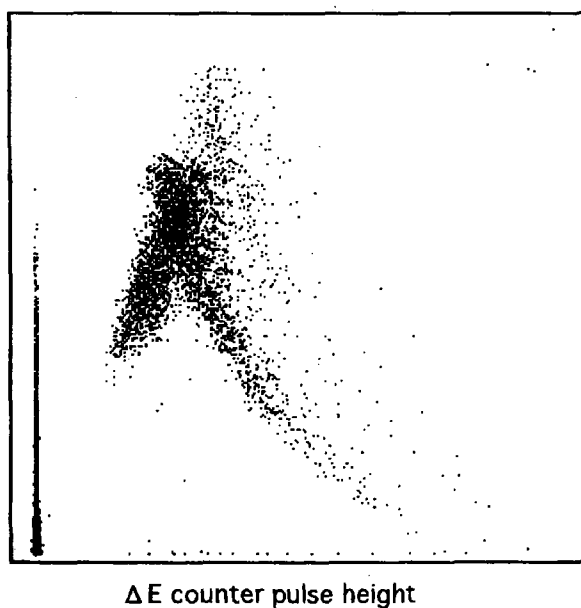
Fig. 3 : Two dimensional E-dE graphical plot.
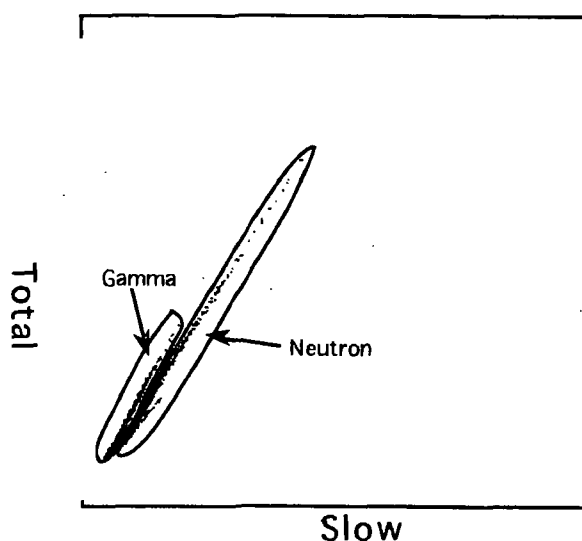
Fig. 4 : Two dimensional Total-Slow pulse height graphical plot.
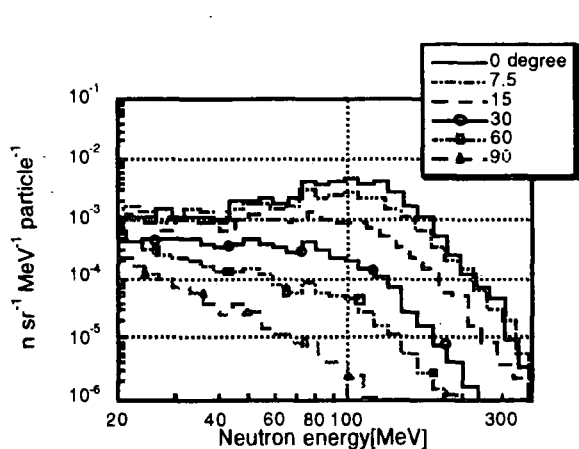
Fig. 5 : Neutron spectra from 180MeV/u carbon ions in a carbon target.
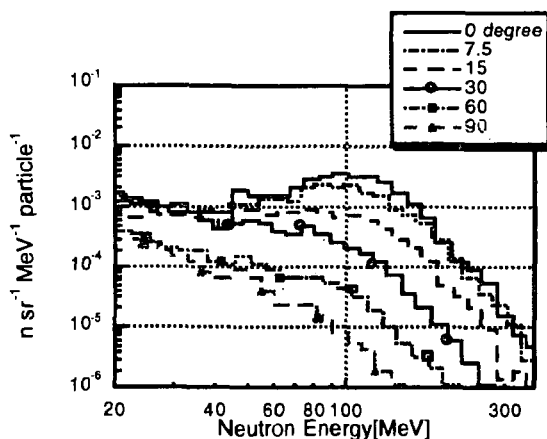
Fig. 6 : Neutron spectra from 180MeV/u carbon ions in a aluminum target.
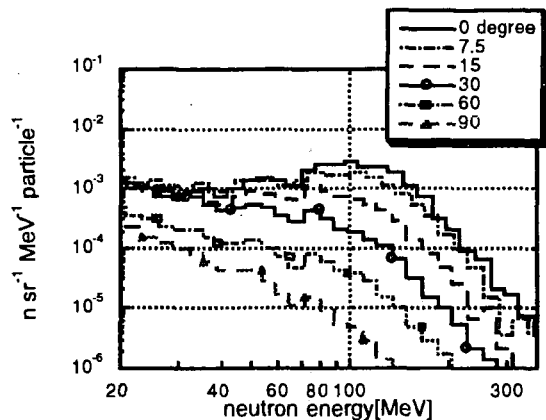
Fig. 7 : Neutron spectra from 180MeV/u carbon ions in a copper target.
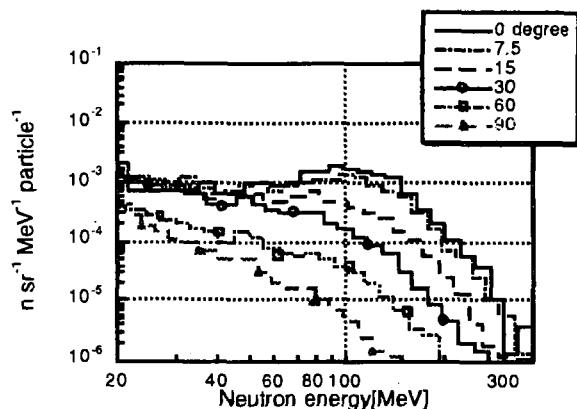
Fig. 8 : Neutron spectra from 180MeV/u carbon ions in a lead target.
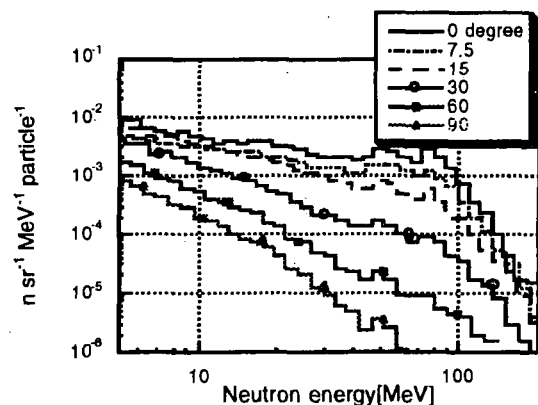
Fig. 9 : Neutron spectra from 100MeV/u carbon in a carbon target.
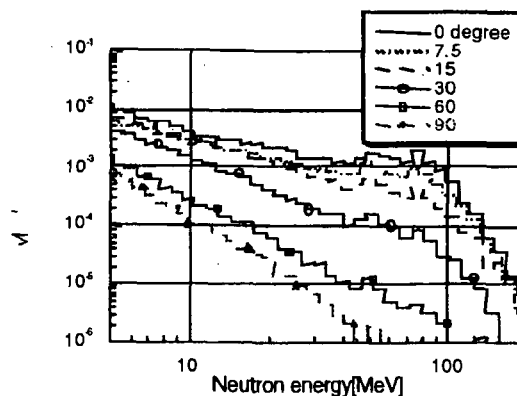
Fig. 10 : Neutron spectra from 100MeV/u carbon ions in a aluminum target.
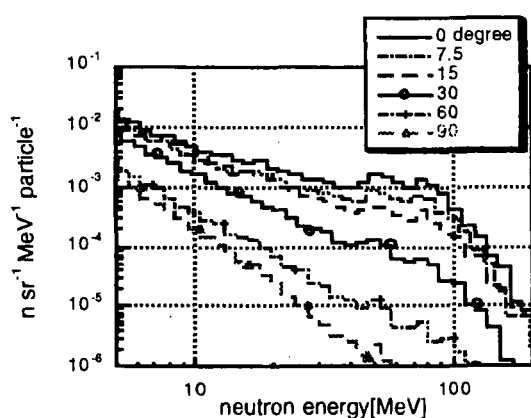
Fig.11 : Neutron spectra from 100MeV/u carbon ions in a copper target.
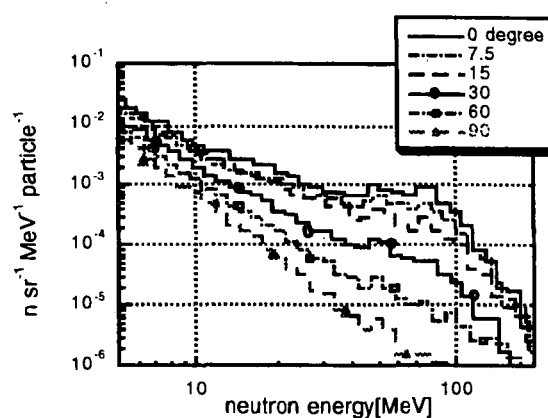
Fig. 12: Neutron spectra from 100MeV/u carbon ions in a lead target.
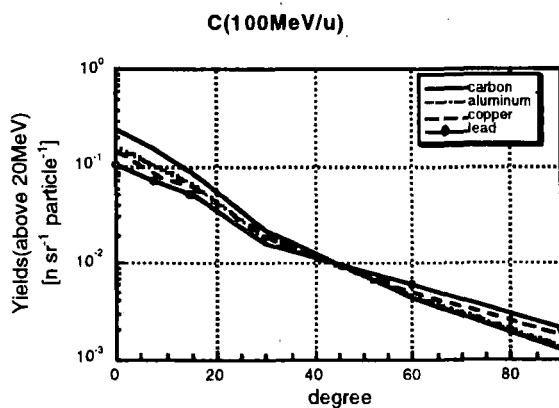
Fig. 13: The integrated neutron yields above 20MeV from 100MeV/u carbon ions.
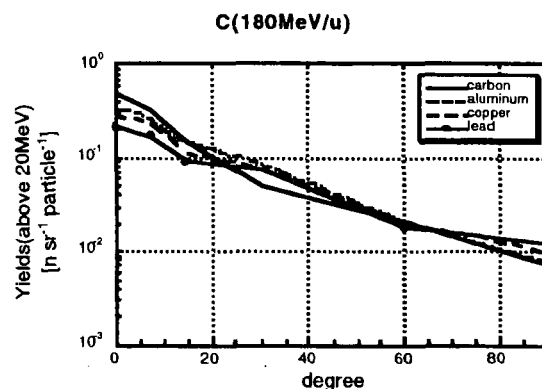
Fig. 14: The integrated neutron yields above 20MeV from 180MeV/u carbon ions.
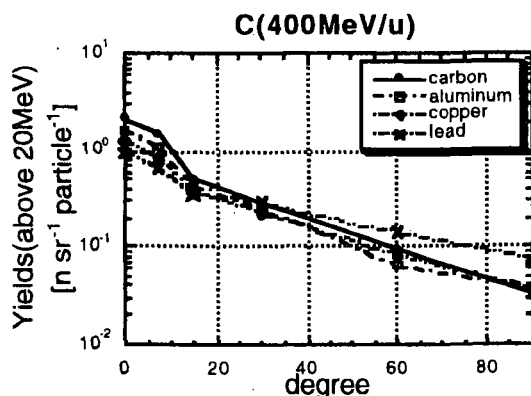
Fig. 15: The integrated neutron yields above 20MeV from 400MeV/u carbon ions.
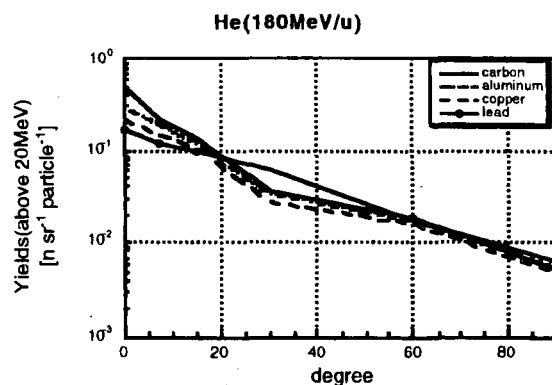
Fig. 16: The integrated neutron yields above 20MeV from 180MeV/u helium ions.

3.12 Measurements of Neutron Spectrum from Stopping-length Target Irradiated by Several Tens-MeV/u Particles

Shin-ichiro MEIGO[1], Hiroshi TAKADA, Hiroshi NAKASHIMA,Toshinobu SASA,
Susumu TANAKA*, Kazuo SHIN** and Shinji ONO**
Tokai Establishment, Japan Atomic Energy Research Institute, Tokai-mura 319-11
*Takasaki Establishment, Japan Atomic Energy Research Institute, Takasaki 370-12
**Department of Nuclear Engineering, Kyoto University, Sakyo-ku, Kyoto 606-01
[1]Email: meigo@linac.tokai.jaeri.go.jp

Using a Time-of-Flight technique, we have measured neutron spectra from stopping-length targets bombarded with 68-MeV protons and 100-MeV α-particles. The measured spectra were used to validate the results calculated by the Quantum Molecular Dynamics (QMD) plus Statistical Decay Model (SDM). The results of QMD plus SDM code agreed fairly well with the experimental data for the light target. On the other hand, the QMD plus SDM gives a larger value than the experimental for the heavy target.

1. Introduction

Applications of high energy light ion accelerators are rapidly growing in many fields such as the accelerator-based actinide transmutation system, the intensive neutron source based on the spallation reaction and a the cancer therapy. In the shielding and neutronics design of these facilities, detailed knowledge is crucially important on the neutron spectra produced by primary beam and their subsequent transport in bulk media. Historically, the cascade model such as NMTC/JAERI[1] has been employed as a tool to calculate the neutron spectra in such design studies. On the other hand, a code system based on the Quantum Molecular Dynamics (QMD) plus Statistical Decay Model (SDM) has been developed in JAERI[2] recently and was applied successfully to analyze the (p,xn) and (p,xp') reactions at intermediate energies [3,4]. These computational methods have been generally used to calculate the nuclear reactions in the energy region above approximately 100 MeV. However, validity of these models for lower energy region is not verified well. Furthermore, the QMD plus SDM approach has never been tested in a calculation for bulk media.

The purpose of this work is to measure the neutron spectra produced from stopping-length targets bombarded with 68-MeV protons and 100-MeV α-particles and validate the predictions by QMD model for such low-energy region. This paper describes the experimental procedure, data reduction method, computation methods and results of the comparison of measured and calculated values in the following sections.

2. Experimental Procedure

The experimental arrangement is shown in Fig. 1. The measurements were carried out at the HB beam course at the AVF-cyclotron in the TIARA facility of JAERI. By a chopper and buncher of the accelerator, incident ions were pulsed to a width of 1.4 and 2.5 ns in FWHM for proton and alpha particles, respectively. Targets were irradiated by 68-MeV protons and by 100-MeV alpha particles. The sizes of the targets are listed in table 1. Each target was thicker than the range of incident particles, but self-absorption of produced neutrons was negligibly small. The number of injected particles was counted with a digital current integrator (ORTEC 439) connected to the target that was surrounded by a -500V suppressor grid to repel secondary electrons. Neutrons were measured by the TOF method with an organic scintillator (BC501A) of 12.7 cm in diameter and 12.7 cm in length at emission angles of 0°, 15°, 30°, 45°, 60°, 90° and 120°. The flight path was 5.0 m for the measurements between 0° and 45°, and 2.5 m for those between 60° and 120°.

The BC501A scintillator was optically coupled to a photo-multiplier tube (HAMAMATU R4144). Three signals, pulse height, pulse shape and TOF were accumulated by a three-parameter data acquisition system

(CANBERRA GENIE system). The pulse height was calibrated by the standard sources of ^{137}Cs ($E\gamma$ = 0.66 MeV), ^{60}Co ($E\gamma$ = 1.17 ,1.33 MeV) and Am-Be ($E\gamma$ = 4.43 MeV). In order to discriminate between neutron and gamma-rays pulses, a pulse shape discriminator (CANBERRA 2160) having a dynamic-range over 500:1 was employed.

The contribution of the background neutrons caused by the room-scattering was measured at every angle placing a rectangular iron block with the size of 20 × 20 × 80 cm^3 and 20 × 20 × 40 cm^3 between the target and detector. By subtracting the contribution of background neutrons from the foreground spectra measured without the iron block, we obtained the net neutron spectrum produced from the target.

3. Data Reduction

The neutron TOF spectra were obtained by an off-line discrimination between the neutron and gamma pulses. By the following equation, the neutron energy spectrum was transformed from TOF spectrum,

$$\frac{d^2n}{dEd\Omega} = \frac{dn}{dt} \bullet \frac{dt}{dE} \bullet (Np\ \varepsilon \Delta\Omega)^{-1} \tag{1},$$

where, dn/dt is the neutron TOF spectrum, Np the number of incident particles, ε detection efficiency and $\Delta\Omega$ the solid angle sustained by the detector to the center of the target.

The detector bias was set at half height of ^{137}Cs Compton edge (0.497 MeVee). This bias enabled us to obtain the neutron spectra above 2.6 MeV. The detection efficiency for this bias was calculated with SCINFUL[5] which included modified deuteron light output[6] and the angular distribution of H(n,n) reaction cross-section[7]. In the neutron energies region below 50 MeV, the energy resolution and the uncertainty of neutron yield for the experimental data were smaller than 8% and 10 %, respectively. These values were much smaller than the ones obtained by the unfolding technique.

4. Calculation

In this study, the neutron spectrum was calculated by the QMD plus SDM code system. The neutron spectra were calculated based on the neutron production double differential cross sections (DDXs) that were obtained by the Quantum Mechanics Dynamics (QMD) theory[2] plus the statistical decay model (SDM)[2]. The neutron spectrum from the dynamical process was calculated by the QMD and the contribution from the statistical process was obtained by the SDM. The switching time from QMD to SDM was decided 5×10^{-22} s (100 fm/c). The maximum impact parameter was decided to $1.4 \times (A_i^{1/3} + A_t^{1/3})$ (fm), where A_i and A_t is mass number of the incident and target nucleus, respectively. The calculated energies for the incident protons are 10, 20, 30, 40, 50, 60 and 68 MeV and for the α particles are 10, 20, 40, 60, 80, 100 MeV.

The final neutron spectrum that has to be compared with the experimental data was calculated from the following equation using the DDXs as calculated by the QMD plus SDM,

$$\frac{d^2N}{d\Omega dE_n} = \int_0^{E_\alpha} n \frac{d\sigma}{d\Omega dE_n} \left|\frac{dE}{dx}\right|^{-1} \exp(-\int_B^{E_\alpha} \Sigma_{non}(E') \left|\frac{dE'}{dx}\right|^{-1} dE')dE \tag{2},$$

where $d^2N/d\Omega/dE_n$ is double differential neutron yields, n an atomic density of the target material (/cm^3), $d\sigma/d\Omega/dE_n$ (mb/sr/MeV) the neutron production DDX, E_α the incident energy of particle, dE/dx (MeV/cm) stopping power[8] and $\Sigma_{non}(E')$ the non-elastic cross section for incident particle with energy E'. The exponential term of the equation (2) shows the attenuation of the incident particles by the nuclear reaction in the target. The non-elastic cross section of the incident particles was calculated by the optical model using the code ECIS-79[9]. In the present calculation, the elastic scattering of the incident particles was ignored. Because the target is enough thinner than the mean free path of the measured neutron, the effect of the neutron reaction with the target nucleus was ignored.

5. Results

The measured neutron spectra from C, Al and Au targets irradiated by 68-MeV protons are compared in Fig. 2 with the predictions of QMD plus SDM models. For the calculation it is shown that the calculations reproduce the measured data fairly well for C and Al. For the data of Au target bombarded with protons, the QMD plus SDM calculation gives larger value than the experiment. The reason of having such overestimation in the neutron yield with the QMD plus SDM calculation is not yet clear. In Ref. [4] the double-differential (p,xp') and (p,xn) reactions of ^{27}Al were investigated with the QMD approach at 90 MeV: the calculated results agreed with the measured values very well. Nevertheless, applicability of the QMD approach may have to be investigated further in the energy region below 100 MeV.

Figure 3 exhibit the neutron spectra from C, Zr and Au targets irradiated by 100 MeV α particles. The measured data and results calculated by the QMD plus SDM approach were shown. The neutron spectra calculated by QMD plus SDM reasonably agreed with the experimental data. However, the shape of calculated spectra from C and Au targets were harder and softer, respectively, than the experimental results. In Fig. 4, the calculated spectra from thick C and Pb target irradiated by 710 MeV alpha particles are compared with the experimental neutron spectra[11]. For the incident energy higher than 100 MeV/u, the QMD plus SDM reproduces the experiment quite well. In the case of the incident energy below 100 MeV/u, the QMD approach may have some problems to predict the produced neutron spectrum.

For the examination of the dependence on the neutron spectrum for the switching time from QMD to SDM calculation, the calculations are performed using the three switching time i.e. 100, 150 and 200 fm/c. Figure 5 shows the comparison of the DDX of the (p,xn) and (α,xn) reaction between QMD plus SDM calculation and the experiment[12]. For light nucleus (Al), the calculated DDX have slightly dependence for the switching time and reproduce well the experiment. On the other hand, the calculated results for heavy nucleus (Bi) have a strong dependence on the switching time. In both figures, it is recognized that the calculated results reproduce well the shape of the experimental spectra, using the switching time of 100 fm/c adopted in the present analysis.

6. Summary

We have measured neutron spectra from stopping-length targets bombarded with 68-MeV protons and 100-MeV alpha particles. By using the time-of-flight technique, we obtained more precise spectra than ones obtained by the unfolding technique. The minimum energy of the measured neutron was 2.6 MeV.

It has been found through the comparison between the experimental and the calculated results of the target irradiated by protons that the calculated results of the QMD plus SDM system agreed well for light targets. For the heavy target, however, the calculated results are larger than the experimental ones. For the incident energy region less than 100 MeV/u, it would suggest that a further improvement of the QMD theory is necessary.

References

[1] Y. Nakahara and T. Tsutui, JAERI-M 82-198 (1982), (in Japanese).

[2] K. Niita, et al., Phys. Rev., C 52, 2620 (1995).

[3] M. B. Chadwick, et al., ibid., C 52, 2000 (1995).

[4] S. Chiba, et al., Phys. ibid., C 54, 285 (1996).

[5] J. K. Dickens, ORNL-6462, Oak Ridge National Laboratory (1988).

[6] S. Meigo, private communication.

[7] R. A. Arndt, et al., Phys. Rev., D 35, 128 (1987).

[8] S. Chiba, et al., J. Nucl. Sci. Technol, 33, 654 (1996).

[9] J. F. Janny, Atom. Data Nucl. Data Tabl., 27, 147 (1982).

[10] J. Ravnal, Notes on ECIS79, unpublished.

[11] R. A. Cecil, et. al., Phys. Rev, C 21, 2471 (1980).

[12] A. M. Kalend, et. al., ibid., C 28, 105 (1983).

Table 1. Size of the target and incident particle employed in the present experiment.

Target	Incident Particle	Target Size (mm)
C	p	ϕ30 x 31
	α	ϕ30 x 3.2
Nb	p	ϕ30 x 10
Zr	α	ϕ30 x 1.8
Au	p	ϕ30 x 6
	α	ϕ30 x 2
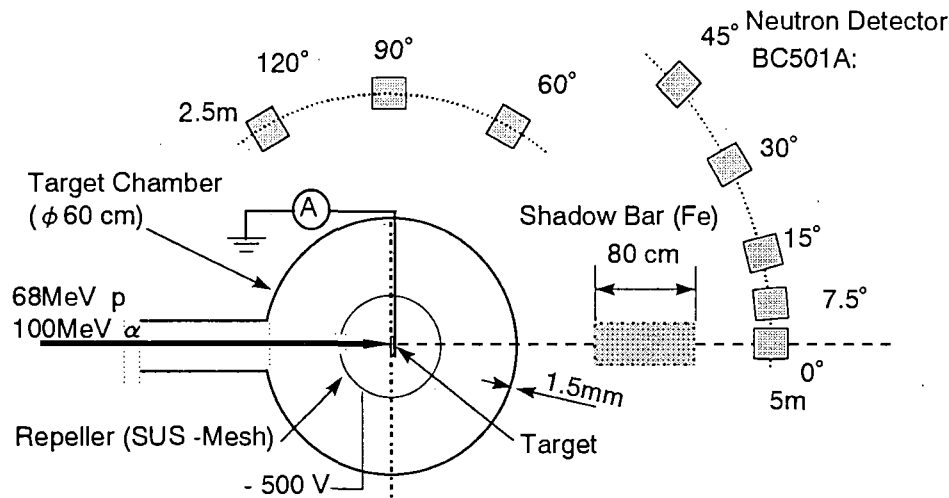
Fig. 1   Schematic view of the experimental setup
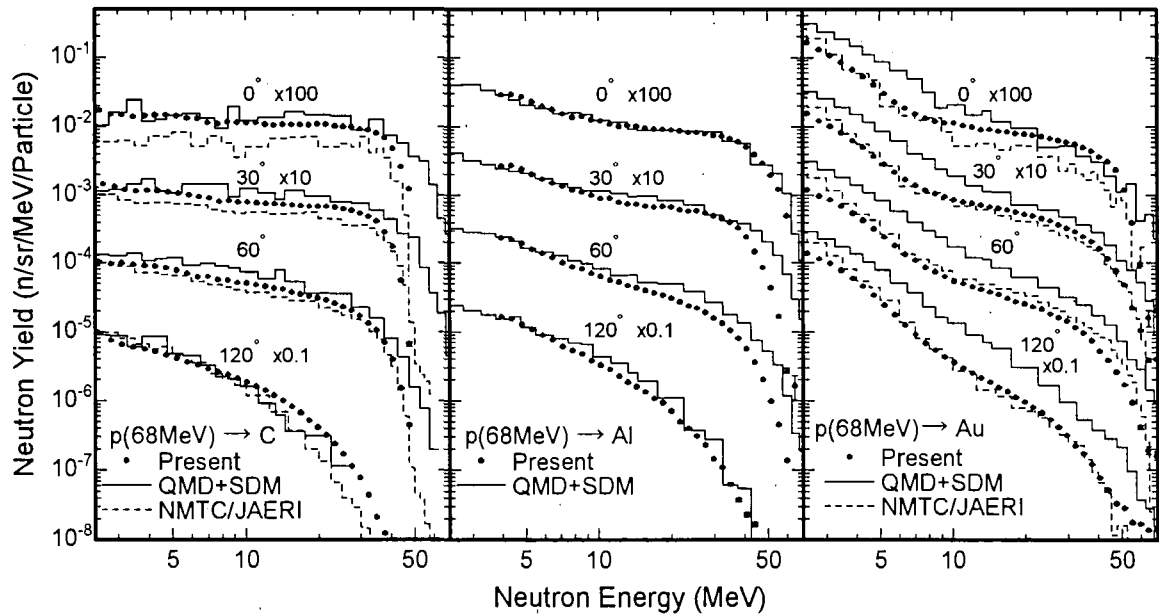
Fig. 2   Neutron energy spectra for 68 MeV proton incidence on stopping-length C, Al and Au target. The solid and the dashed lines stand for the results of calculation with QMD+SDM and NMTC/JAERI+MCNP-4A, respectively.
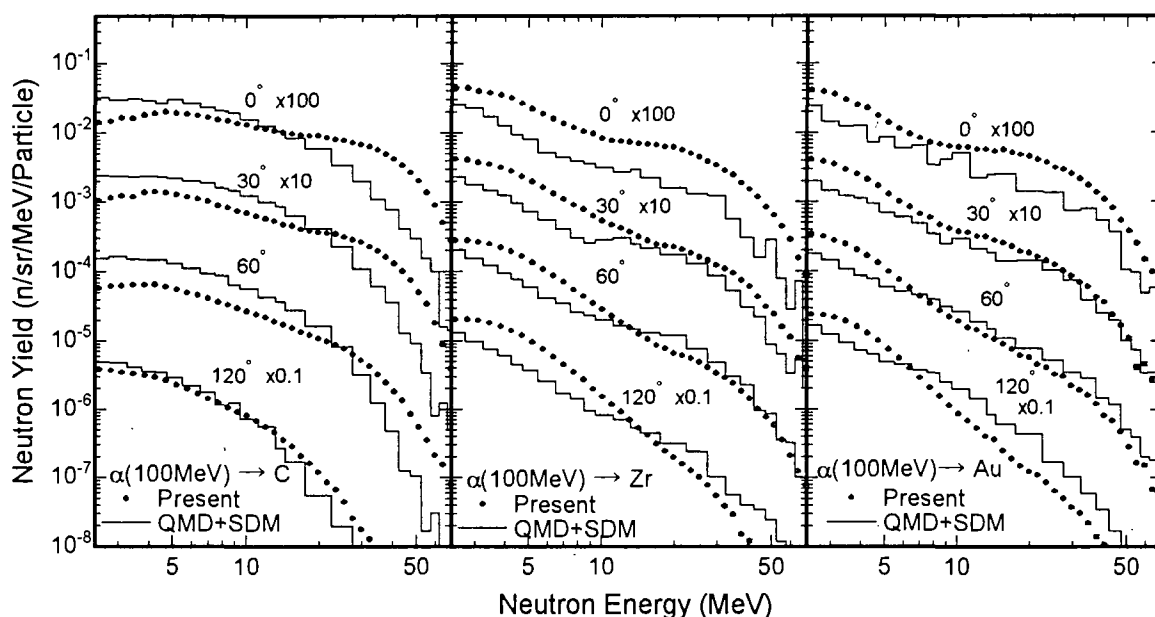
Fig. 3 Neutron energy spectra for 100 MeV alpha particle incidence on stopping-length C, Zr and Au target. The solid and the dashed lines stand for the results of calculation with QMD+SDM.
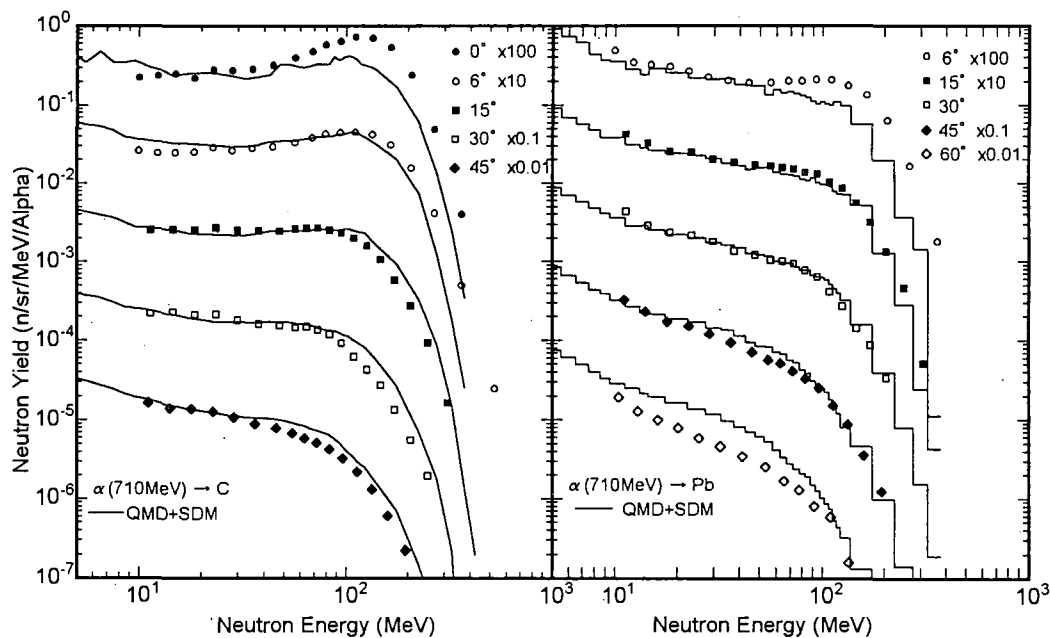
Fig. 4 Neutron energy spectra for 710 MeV alpha particle incidence on stopping-length C and Pb targets. The solid lines and marks stand for the results of calculation with QMD+SDM and the experimental data[11], respectively.
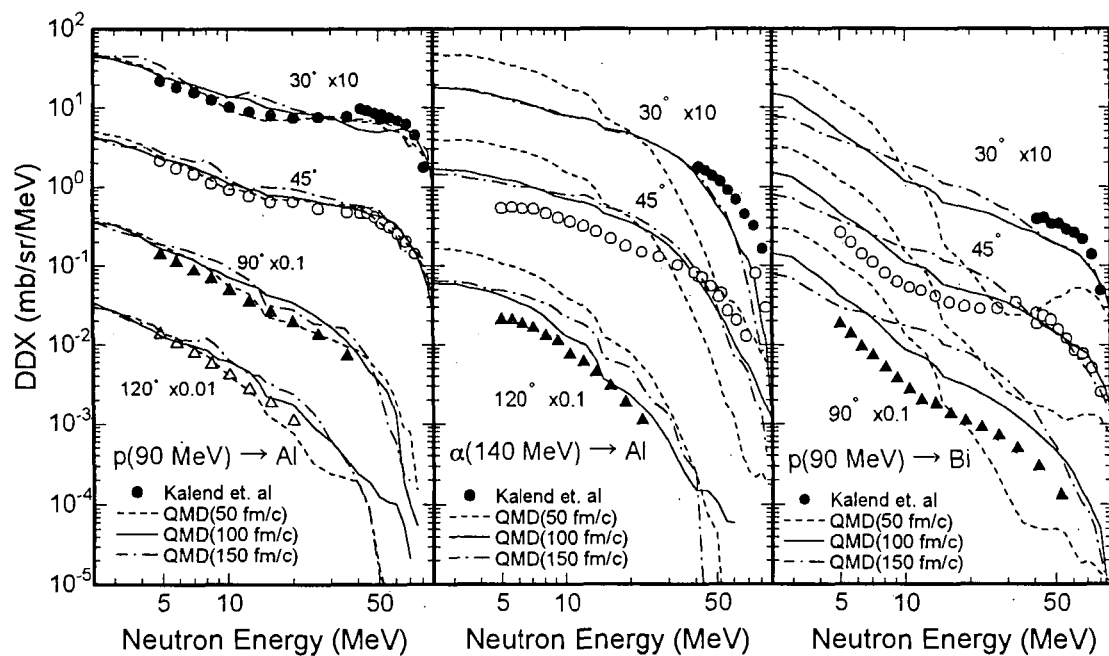
Fig. 5 Comparison of the neutron production double differential cross section(DDX) between the QMD+SDM calculation and the experiment[12]. Lines stand for the results of calculation with QMD+SDM using three switching time(50, 100 and 150 fm/c). Marks show the experimental data by Kalend et. al.[12].

3.13 Calculation of the Intermediate Energy Activation Cross Section

Shiori FURIHATA and Nobuaki YOSHIZAWA
Research Center for Safety Science, Mistubishi Research Institute, Inc.
2-3-6 Otemachi, Chiyoda-ku, Tokyo 100
e-mail:furihata@mri.co.jp

We discussed the activation cross section in order to predict accurately the activation of soil around an accelerator with high energy and strong intensity beam. For the assessment of the accuracy of activation cross sections estimated by a numerical model, we compared the calculated cross section with various experimental data, for $Si(p,x)^{22}Na$, $Al(p,x)^{22}Na$, $Fe(p,x)^{22}Na$, $Si(p,x)^7Be$, $O(p,x)^3H$, $Al(p,x)^3H$ and $Si(p,x)^3H$ reactions. We used three computational codes, i.e., quantum molecular dynamics (QMD) plus statistical decay model (SDM), HETC-3STEP and the semiempirical method developed by Silberberg *et.al*[3]. It is observed that the codes are accurate above 1GeV, except for ^7Be production. We also discussed the difference between the activation cross sections of proton- and neutron-induced reaction. For the incident energy at 40MeV, it is found that ^3H production cross sections of neutron-induced reaction are ten times as large as those of proton-induced reaction. It is also observed that the choice of the activation cross sections seriously affects to the estimate of saturated radioactivity, if the maximum energy of neutron flux is below 100MeV.

1. Introduction

Since new accelerators with higher energy and stronger intensity beam than we have ever had in Japan are planned recently, it becomes more important for radiation protection to estimate activation of soil. Especially the amount of water soluble radioactive elements such like ^3H and ^{22}Na are significant, because they spread rapidly into environment. In order to predict saturated radioactivity, neutron activation cross section and neutron flux are necessary. In this study, we focused on activation cross sections in the intermediate energy region.

It is very poor that the experimental data of neutron activation cross sections with their incident energies above 20MeV. To calculate saturated radioactivity, we have to use the activation cross sections computed by a numerical model, or substitute experimental values for proton-induced reaction instead of neutron.

In this work, we discussed three problems as the followings.
1. How accurately can a computational model predict an activation cross section?
   In order to assess the accuracy of activation cross sections estimated by a numerical model, we compared the calculated cross sections of proton-induced reactions with various experimental data in the energy region from 20MeV to 5GeV.
2. Does the activation cross section of proton-induced reaction approximate to the neutron-induced cross section?
   We compared the calculated cross sections of proton-induced reaction with those of neutron-induced reaction.
3. How sensitive are the saturated radioactivity to the activation cross sections?
   We calculated the saturated radioactivity due to $Si(n,x)^{22}Na$ reaction, and compared with the values estimated by the method of Shibata[4].

For the calculation of activation cross section, We used three numerical models, i.e, QMD+SDM[1], HETC-3STEP[2] and the semiempirical method[3]. We focused on

Si(p,x)^{22}Na, Al(p,x)^{22}Na, Fe(p,x)^{22}Na, Si(p,x)^{7}Be, O(p,x)^{3}H, Al(p,x)^{3}H and Si(p,x)^{3}H reaction. Si, O, Al, and Fe are main constituents of soil. Besides water soluble radioactive elements, we paid attention to ^{7}Be production, because ^{7}Be is known to have a large saturated radioactivity.

2. The accuracy of the numerical models

The analyses of the fragment cross sections of Al(p,x)^{22}Na, Al(p,x)^{3}H and Fe(p,x)^{22}Na by QMD+SDM were reported in 1996[1]. Added to these cross sections, O(p,x)^{3}H cross sections were computed by HETC-3STEP for the benchmark problems[5,6].

We used these codes for the assessment of the accuracy of the calculated activation cross sections. We also use the semiempirical method developed by Silberberg *et.al*[3] which can produce the Z>2 nucleus production cross section of proton-induced reaction.

In Fig.1, we show the activation cross sections of Si(p,x)^{22}Na reaction for the incident proton energy region from 20MeV to 5GeV. All experimental data in Fig.1 are tabled in the reference[7]. Above 100MeV, all the values by three numerical models are within experimental data, while below 50MeV, QMD+SDM and HETC-3STEP overestimate by 2 ~ 10 times of the measurements. It is shown in Fig.2 that all calculated values are in good agreement with experimental data for Al(p,x)^{22}Na reaction. Fig.3 shows that the QMD+SMD and HETC-3STEP underestimate the cross section of Fe(p,x)^{22}Na reaction below 500MeV, while the semiempirical method succeeded to reproduce them. It is observed in Fig. 4 that ^{7}Be production cross sections by the semiempirical method agreed with measurements and the values by two simulation methods are less than a half of experimental values. In Fig. 4, ^{7}Be production cross sections by QMD+SDM are not shown because the values are lower than 0.1mb. We show ^{3}H production cross sections from proton-induced reactions on Si, O, Al in Fig. 5 to Fig.7. The cross sections computed by two codes well agreed with experimental data in the energy region above 1GeV, however they disagree with the measurements below 1GeV.

QMD+SDM and HETC-3STEP can reproduce cross sections of activation whose mass is reduced from parent nucleus by seven or less. However they tend to underestimate for the activation whose mass is decreased to about a half of the mass of target nucleus. The semiempirical method agreed with the measurements for Z>2 residual nucleus production above 100MeV. For the precise evaluation of the codes' accuracy for ^{3}H production, we need more experimental data.

3. The Difference between proton- and neutron-induced reactions

The activation cross sections calculated by the QMD+SDM for proton- or neutron-induced on Si at 1GeV are shown in Fig.8. The calculated values for the incident energy at 40MeV are shown in Fig.9.

For 1GeV incident energy, no difference is observed between proton- and neutron-induced cross sections. On the other hand, for the incident energy at 40MeV, ^{24}Na and ^{3}H production cross sections of neutron-induced reaction are ten times as large as those of proton-induced reaction. The reason is that the number of the reaction channels which produce a specific activation differs between proton- and neutron-induced reaction, especially in low energy region. As the incident energy becomes higher, the channels which contribute to a specific activation production increase. Then the difference between proton- and neutron- induced cross section is reduced.

4. Saturated radioactivity

Saturated radioactivity can be obtained by the following equation,

$$\int_{E_{\min}}^{E_{\max}} \sigma(E) \cdot \phi(E) \cdot dE \tag{1}$$

where $\sigma(E)$ is activation cross section, $\phi(E)$ is neutron flux and E is energy of neutron flux. We calculated the saturated radioactivity due to Si(n,x)^{22}Na according to the method of Shibata[4]. In Shibata's work, neutron flux is assumed to be proportional to $1/E$. It is also presumed that the activation cross section is equal to 30mb despite energy. In this work, we assumed that the neutron flux is proportional to $1/E$, and that the activation cross section of proton-induced reaction is equal to neutron-induced one. As shown in Fig.9, ^{22}Na production cross sections of proton-induced reaction are almost equal to the cross sections of neutron-induced reaction. To avoid the ambiguity of the absolute value of neutron flux, we defined the normalized saturated radioactivity as the following equation.

$$\text{The normalized saturated radioactivity} \equiv \left(\int_{E_{\min}}^{E_{\max}} \sigma(E) \cdot E^{-1} \cdot dE \right) \bigg/ \left(30 \int_{E_{\min}}^{E_{\max}} E^{-1} \cdot dE \right) \tag{2}$$

For the estimate of the normalized saturated radioactivity, the activation cross sections shown in Fig.1 were used. The experimental data were averaged over in each energy bin of 20, 30, 40, 50, 60, 80, 100, 500, 1000, 2000MeV.

In Fig.10, the values of normalized saturated radioactivity are presented as a function of maximum energy of neutron flux. Below 100MeV, the choice of the activation cross sections seriously affects to the estimate of saturated radioactivity. At 100MeV, the normalized saturated radioactivity by HEST-3STEP is 20%, while the estimate by QMD+SDM is 60%. In the maximum energy region of neutron flux above 100MeV, the difference due to the choice of the activation cross sections is reduced. If the maximum energy of neutron flux is higher than 1GeV, the values of saturated radioactivity are 30% to 55% of those of calculated by constant activation cross section.

5. Summary

We examined three problems for the estimate of activation of soil around an accelerator with high energy and strong intensity beam. One is the accuracy of the activation cross section computed by numerical codes, second is the difference between proton- and neutron-induced reaction, and the last is the sensitivity of saturated radioactivity to the activation cross section. It is observed that the codes are accurate above 1GeV, except for ^{7}Be production. For ^{22}Na production from Si target, 40MeV proton-induced cross section is almost equal to neutron-induced one, however, ^{3}H production cross section from n+Si reaction is ten times as large as the result of p+Si reaction. It is also found that the choice of the numerical models seriously affects to the estimate of saturated radioactivity, if the maximum energy of neutron flux is below 100MeV.

Acknowledgments

References

[1] S. Chiba, O. Iwamoto, T. Fukahori and K. Niita, Phys. Rev. C54 (1996)285

[2] N. Yohizawa, K. Ishibashi and H. Takada, J. Nucl. Sci. Technol 32(1995)601

[3] R. Silberberg, C. H. Tsao and J. W. Letaw, Astro. J. Suppl 58(1985)873

[4] T. Shibata, Proceedings of a RIKEN symposium on Radiation Protection at RIKEN RI beam factory(1995)26

[5] H. Takada, N. Yoshizawa and K. Ishibashi, JAERI-Research 96-040(1996)

[6] R. Michel and P. Nagel, NEA/NSC/DOC(9)8, (1995)

[7] H. Shopper(Ed.), "LANDORT-BORNSTEIN, Numerical Data and Functional Relationships in Science and Technology, New Series, Group I: Nuclear and Particle Physics Vol. 13, Production of Radionuclides at Intermediate Energies, Subvol. a, Interactions of Protons with Targets from He to Br", Springer-Verlag, Berlin Heidelberg(1991)

[8] D. L. Olson, B. L. Berman, D. E. Greiner, H. H. Heckman, P. J. Lindstrom and H. J. Crawford, Phys. Rev. C28(1983)1602

[9] E. Brunix, CERN report 61-1, CERN, Geneva (1961)

[10] E. Brunix, CERN report 62-9, CERN, Geneva (1962)

[11] E. Brunix, CERN report 64-17, CERN, Geneva (1964)

[12] M. Noguchi, T. Miura, K. Kondo, T.Suzuki, Y. Oki, M. Takahashi, K. H. Tanaka and M. Ieiri, Appl. Radiat. Isot. 42(1991)577

[13] L. A. Currie and W. F. Libby and R. L. Wolfgang, Phys. Rev. 101(1956)1557
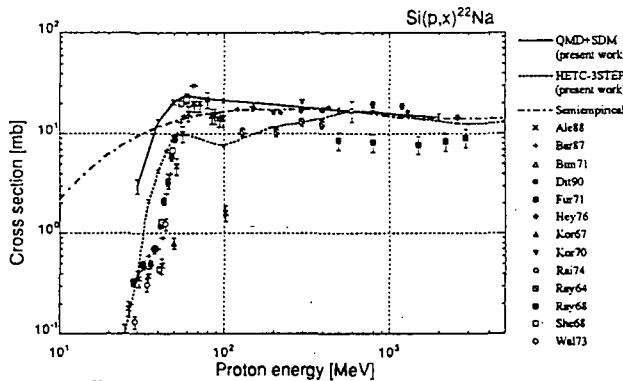
Fig.1 ^{22}Na production cross sections for proton-induced reaction on
^{nat}Si(^{28}Si for QMD+SDM). The marks indicate experimental data [7]. The notation of the marks is the same as reference [7].
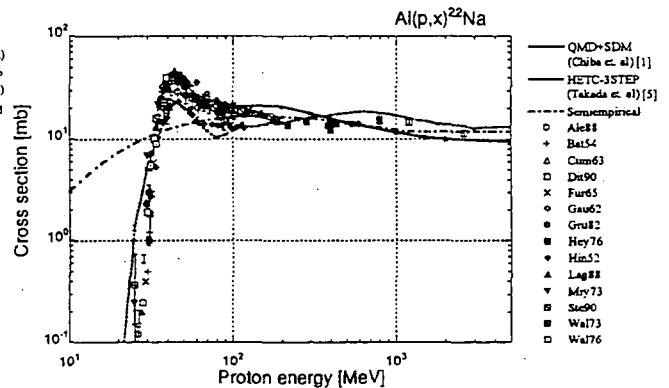
Fig.2 ^{22}Na production cross sections for proton-induced reaction on
^{nat}Al(^{27}Al for QMD+SDM).The marks indicate experimental data [7]. The notation of the marks is the same as reference [7].
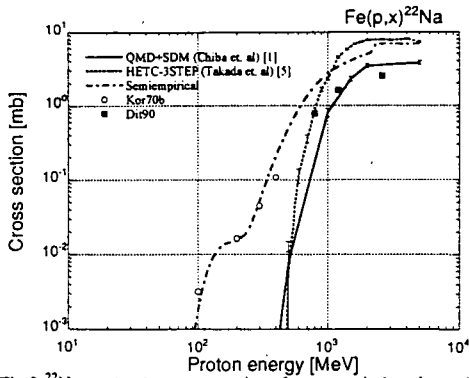
Fig.3 ^{22}Na production cross sections for proton-induced reaction on ^{nat}Fe(^{56}Fe for QMD+SDM). The marks indicate experimental data [7]. The notation of the marks is the same as reference [7].
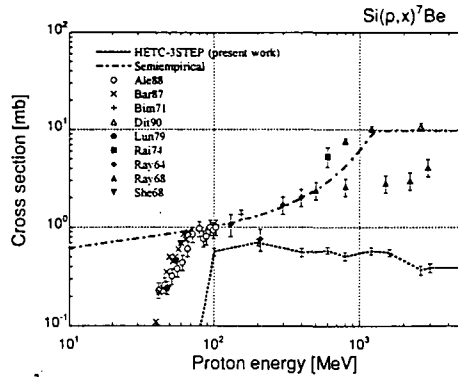
Fig.4 ^{7}Be production cross sections for proton-induced reaction on ^{nat}Si. All values by QMD+SDM are less than 0.1mb. The marks indicate experimental data [7]. The notation of the marks is the same as reference [7].
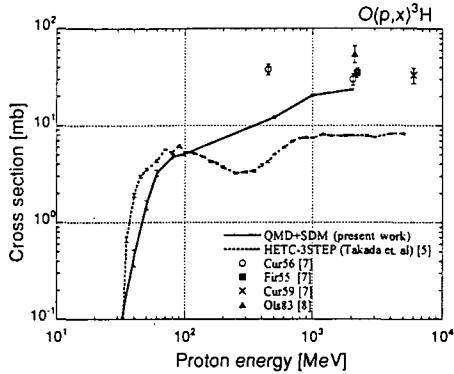
Fig.5 ^{3}H production cross sections for proton-induced reaction on ^{nat}O(^{16}O for QMD+SDM). The marks indicate experimental data [7, 8].
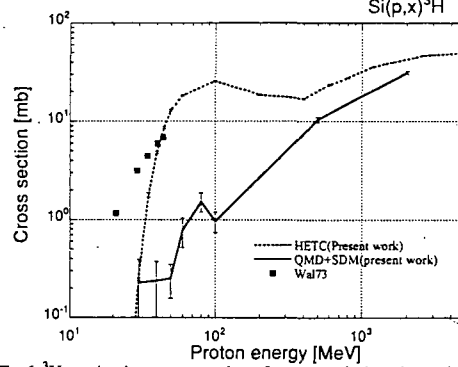
Fig.6 ^{3}H production cross sections for proton-induced reaction on ^{nat}Si(^{28}Si for QMD+SDM). The marks indicate experimental data [7]. The notation of the marks is the same as reference [7].
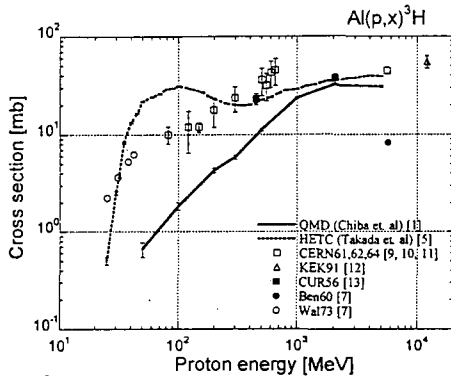
Fig.7 ^{3}H production cross sections for proton-induced reaction on ^{nat}Al(^{27}Al for QMD+SDM). The marks indicate experimental data [7, 9, 10, 11, 12, 13].
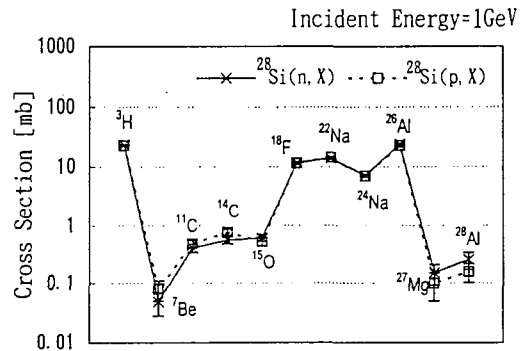
Fig.8 Production cross sections of various fragments for 1.0 GeV p or n+^{28}Si reactions. Both are calculated with QMD+SDM.
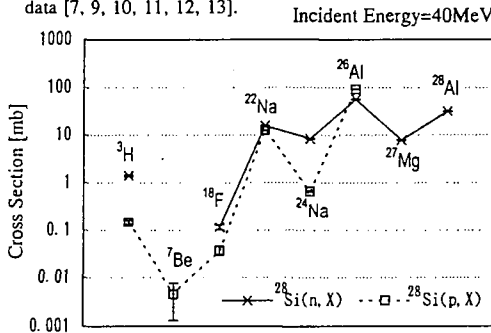
Fig.9 Production cross sections of various fragments for 40 MeV p or n+^{28}Si reactions. Both are calculated with QMD+SDM.
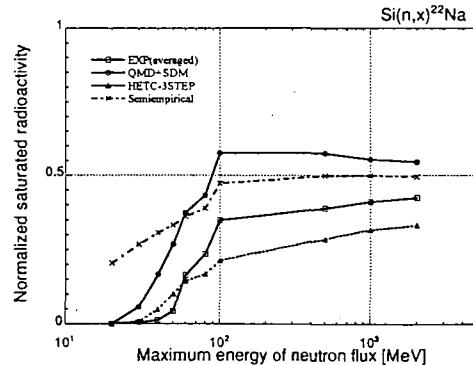
Fig.10 Normalized saturated radioactivity due to Si(n,x)^{22}Na reaction. The definition of normalized saturated radioactivity is shown by the equation (2). X-axis shows the maximum energy of neutron flux. Neutron flux is assumed to be proportional to 1/E. The activation cross sections for proton-induced reaction in Fig. 1 are used instead of neutron data.

3.14 Measurement of Reaction Cross Sections of ^{129}I Induced by DT Neutrons

Daisuke NAKANO, Isao MURATA and Akito TAKAHASHI

Department of Nuclear Engineering, Osaka University
Yamada-oka, 2-1, Suita 565, Japan
e-mail: daisuke@newjapan.nucl.eng.osaka-u.ac.jp

Abstract: The cross sections were measured for the ^{129}I(n,2n)^{128}I and ^{129}I(n,γ)^{130}I reactions by DT neutrons, at OKTAVIAN facility of Osaka University, Japan. The foil activation method was used in the measurement. The sample was a sealed source of ^{129}I, which was covered with a Cd foil. The irradiations were performed for 75 minutes to obtain the cross section of reaction producing ^{128}I ($T_{1/2}$=24.99m) and 22 hours for the ^{130}I ($T_{1/2}$=12.36h), respectively. The gamma-rays emitted from the irradiated sample were measured with a high purity Ge detector. The measured cross sections of ^{129}I(n,2n)^{128}I and ^{129}I(n,γ)^{130}I reactions were 0.92±0.11 barn and 0.013±0.002 barn, respectively. For the ^{129}I(n,2n)^{128}I reaction, the evaluation of JENDL-3.2 overestimates cross section about 60 % to the experimental result. However, especially for the ^{129}I(n,γ) reaction, the measured cross section may include the contribution from the neutrons in MeV region as well as epithermal ones. Also, the obtained cross section of the ^{129}I(n,γ)^{130}I reaction was evaluated as an effective production cross section of ^{130}I including ^{129}I(n,γ)^{130m}I reaction. In order to remove the contribution from the epithermal and MeV region neutrons. A new method was proposed for the measurement of (n,γ) reaction cross section.

1. Introduction

The transmutation methods of nuclear wastes, namely, minor actinides (MAs) and fission products (FPs), have been widely investigated. It is generally considered that the transmutation is performed by using fission reactor, fusion reactor, proton accelerator and so on. Recently, for the transmutation of FPs using fission reactor, the neutron capture cross sections of some FPs induced by thermal neutrons have been measured.[1][2] However, there exist few measured nuclear data to estimate the feasibility to transmute FPs with fusion reactor. In this study, ^{129}I, which is one of the most typical FPs from the standpoint of wastes transmutation due to its extremely long half life, was selected as a target sample. As shown later, ^{129}I has various advantages for the use of foil activation method. The DT

neutron induced cross sections of ^{129}I were measured using OKTAVIAN facility of Osaka University, Japan. The experimental results were compared with the evaluated nuclear data of JENDL-3.2.

2. Experiment

2.1 Sample for irradiation

In the measurement of reaction cross section of FP, because the irradiation sample is originally radioactive, a massive sample cannot be treated. Moreover the background due to the sample activity itself is very large. So, emitted secondary particles (neutron, gamma-ray and so on) cannot be utilized for the measurement. In this measurement, for these reasons, the foil activation method is used.

In this study, ^{129}I was selected as an irradiation sample. This nuclide has the following advantages of the measurement: (1) the number density of ^{129}I per unit activity is very large because it has the longest half life in the main target nuclides as shown in Table 1, (2) the energy of gamma-ray emitted following the beta decay of ^{129}I is so low that the gamma-ray cannot transmit the detector window, and the background from the sample itself can be suppressed, and (3) the radioactive nuclides produced by irradiation have the appropriate half lives (24.99 minutes and 12.36 hours) for measurement.

2.2 Experimental procedure

In the measurement, to realize quick loading and unloading of samples, pneumatic transport system was used. Neutron source is the DC line of OKTAVIAN. The mean neutron flux is $\sim 10^9$ n/cm^2/s at the sample position. The irradiation samples, whose dimensions are 1.3 cm ϕ × 1.5 cm, is 3.7 kBq of ^{129}I with and without a Cd filter. A Cd filter is used so as to remove the contribution of thermal neutrons from the measured cross section. As neutron flux monitors, a Nb foil of 1 cm^2 × 0.01 cm-t and a BF$_3$ proportional counter are used in the absolute and relative measurements, respectively. A MCS system was used to consider the time dependence of neutron flux. In the neutron energy measurement, the "Zr/Nb-ratio" method was adopted. The mean neutron energy was estimated to be 14.6 MeV. The gamma-rays emitted from the irradiated sample was measured by using a 180 cc high purity Ge detector. The schematic arrangement of the experiment is shown in Fig. 1. The sample was set up at 1.3 cm from the rotating tritium target, and irradiated for 75 minutes in the measurement of ^{129}I(n,2n)^{128}I reaction cross section and for 22 hours in ^{129}I(n,γ)^{130}I, respectively.

3. Results

The measured cross sections of ^{129}I(n,2n)^{128}I and ^{129}I(n,γ)^{130}I reactions at 14.6 MeV are 0.92±0.11 b and 0.013±0.002 b, respectively (see Table 2). The gamma-ray pulse height spectra associated with these measured cross sections are shown in Figs. 2 and 3. In the ^{129}I(n,2n)^{128}I reaction, the evaluation of JENDL-3.2 overestimates about 60 % to the experimental result. However, ^{129}I(n,γ)

reaction cross section is estimated as an effective production cross section of ^{130}I including ^{129}I(n,γ)^{130m}I reaction (see Figure 4). And, this value may include the contributions from epithermal and MeV region neutrons. The error estimations of the results is summarized in Table 3.

4. Proposal of a new method

As described in chapter 3, the measured cross section of ^{129}I(n,γ)^{130}I reaction may include the contribution from the neutrons in MeV region as well as epithermal ones. To find out each contribution, MCNP calculation was performed with a precise model including neutron source and irradiation room as wall as sample. The result showed that contributions for thermal, epithermal, MeV region and DT neutrons were about 30 %, negligible, 50 % and 20 %, respectively. And it was also confirmed that the thermal neutron contribution could be removed with a Cd filter. Consequently, MeV region neutron contribution is required to be removed by another measurement method. The MeV region neutrons are produced in mainly structure materials of the rotating target by one or more scatterings, while DT neutrons enter the sample directly without scattering. Therefore a new method is proposed that putting a small absorber between neutron source and a sample can reduce only DT neutrons without reducing MeV region neutrons. To confirm above discussion MCNP calculation was conducted using the calculation model as shown in Fig. 5. The result is shown in Fig. 6. By comparing the results with and without the absorber, the contribution from MeV region can be clarified. So it means that we can estimate the contribution only from DT neutrons.

5. Conclusion

The cross sections were measured for the ^{129}I(n,2n)^{128}I and ^{129}I(n,γ)^{130}I reactions by DT neutrons. The new measurement method to remove the MeV region contribution was proposed. It was confirmed from the MCNP calculation that it was possible to measure ^{129}I(n,γ) reaction cross section by DT neutron with this method.

References

(1) T.SEKINE, Y.HATSUKAWA, K.KOBAYASHI, H.HARADA, H.WATANABE and T.KATOH: J.Nucl.Sci.Technol., 30[11], 1099 (1993).
(2) H.HARADA, T.SEKINE, Y.HATSUKAWA, N.SHIGETA, K.KOBAYASHI, T.OHTSUKI and T.KATOH: J.Nucl.Sci.Technol., 31[3], 173 (1994).

Table 1 Main transmutation target FPs

	E_γ(keV)	$T_{1/2}$(year)	Atom/μCi	Problem
^{137}Cs	662	30.07	$\sim 10^{14}$	Heat source
^{90}Sr	-	28.78		
^{99}Tc	-	2.111×10^5	$\sim 10^{18}$ ($\sim 1\mu$g)	Inherent risk
^{135}Cs	-	2.3×10^6		
^{129}I	39.6	1.57×10^7		

Table 2 Measured cross sections compared with evaluation

	Cross section at 14.6MeV (barn)	
	Experiment *	JENDL-3.2
^{129}I(n,2n)^{128}I	0.92±0.11	1.50
^{129}I(n,γ)^{130}I	0.013±0.002 **	1.00×10^{-3}

* Erros in measurements are summarized in Table 3

** Effective production cross section,

which may contain epithermal and MeV region

Table 3 Error estimation

Items		Error (%)
Sample	Activity	6
	Half life	2.6
Foil	Weight	1.2
	Measurement	1.0
Position of the sample and foil		5
Production nuclide	Measurement	5
Reference source	Activity	5
	Half life	<1.4
Total error		<11
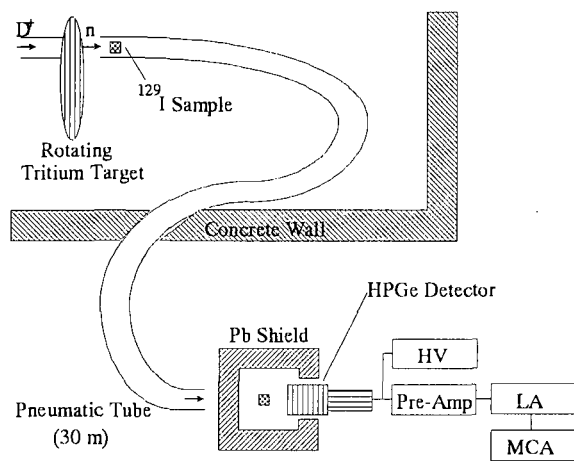
Figure 1   Schematic arrangement of the experiment
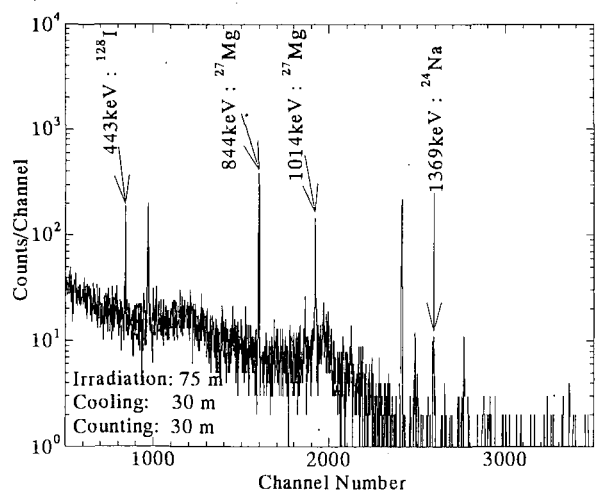
Figure 2   Gamma-ray pulse height spectrum associated with the measurement
of the (n,2n) reaction cross section
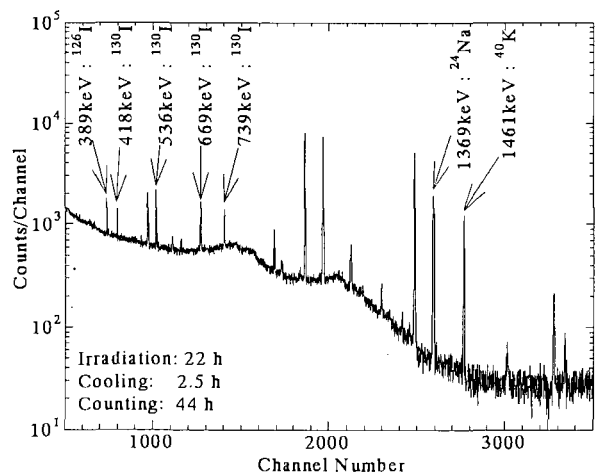
Figure 3   Gamma-ray pulse height spectrum associated with the measurement
of the (n,γ) reaction cross section
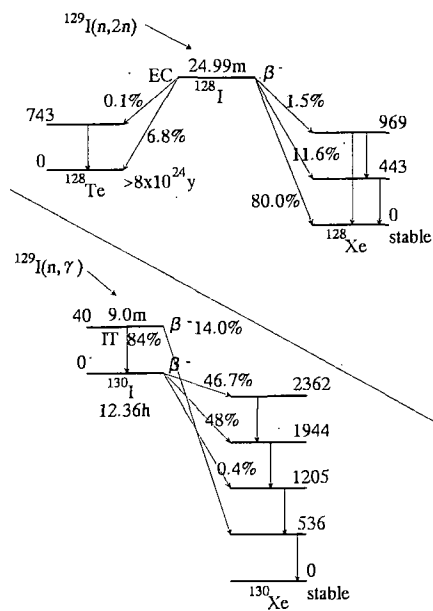
Figure 4   Decay schemes of ^{128}I and ^{130}I
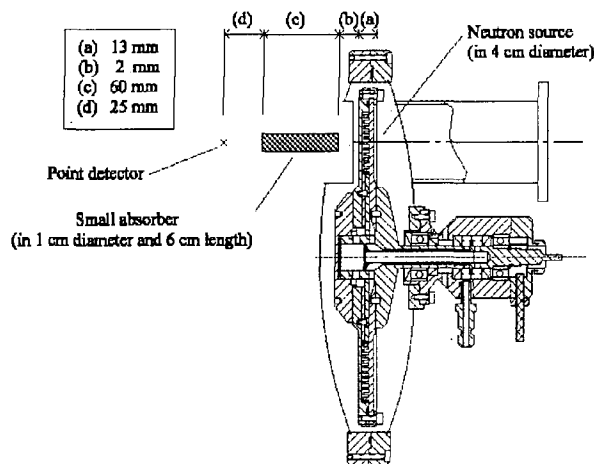
Figure 5   Geometrical model of MCNP calculation for a new method
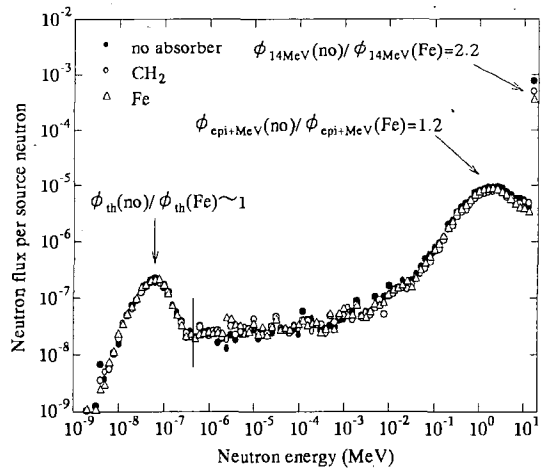
Figure 6   Results of MCNP calculation

3.15 Measurement of Thermal Neutron Cross Section and Resonance Integral of the Reaction ^{135}Cs(n, γ)^{136}Cs

Toshio KATOH[1]†, Shoji NAKAMURA[1], Hideo HARADA[1],
Yuichi HATSUKAWA[2], Nobuo SHINOHARA[2], Kentaro HATA[2],
Katsutoshi KOBAYASHI[2], Shoji MOTOISHI[2] and Masakazu TANASE[2]
1) *Power Reactor and Nuclear Fuel Development Corp**.
2) *Japan Atomic Energy Research Institute**
* Tokai-mura, Ibaraki-ken, 319-11

Abstract: The thermal neutron(2,200 m/s neutron) capture cross section(σ_0) and the resonance integral(I_0) of the reaction ^{135}Cs(n, γ)^{136}Cs were measured by an activation method. Targets of radioactive cesium, which include ^{135}Cs, ^{137}Cs and stable ^{133}Cs, were irradiated with reactor neutrons within or without a Cd shield case. The ratio of the number of nuclei of ^{135}Cs to that of ^{137}Cs was measured with a quadrupole mass spectrometer. This ratio and the ratio of activity of ^{136}Cs to that of ^{137}Cs were used for deduction of the σ_0 and the I_0 of ^{135}Cs. The σ_0 and the I_0 of the reaction ^{135}Cs(n, γ)^{136}Cs were 8.3 $\pm$ 0.3 barn and 38.1 $\pm$ 2.6 barn, respectively.

1. Introduction

Accurate nuclear reaction cross sections of radioactive fission products and transuranic elements are required for research on nuclear transmutation methods in nuclear waste management. Important fission products in the nuclear waste management are ^{137}Cs, ^{135}Cs, ^{90}Sr, ^{99}Tc and ^{129}I because of their large fission yields[1] and long half-lives[2]. The present authors have measured neutron capture cross sections(σ_0) and resonance integrals(I_0) of fission products, ^{137}Cs[3],[4], ^{90}Sr[5], ^{99}Tc[6] and ^{129}I[7].

The thermal neutron capture cross section(σ_0) of ^{135}Cs has been reported in two papers. Sugarman reported the cross section obtained by a radiochemical method as 14.5 ($\pm$ 30%) barn[8]. Baerg et al. reported the cross section measured by a 4π-ß

---

† Partly at Gifu College of Medical Technology

counting method[9].   The latter authors obtained the values of the neutron capture cross section and the resonance integral as 8.7 ± 0.5 barn and 61.7 ± 2.3 barn, respectively.

The present experiment was designed to obtain more reliable values of the cross section and the resonance integral of the reaction $^{135}Cs(n, \gamma)^{136}Cs$.

2. Experiment

a) Target Preparation

Since it was hard to obtain pure substance of ^{135}Cs, ^{135}Cs included in the "Standardized Solution" of ^{137}Cs solution was used for the present experiment.   Two targets of ^{135}Cs-^{137}Cs were prepared.   Each target contained about 0.37 MBq of ^{137}Cs solution.   The ratio of the number of nuclei of ^{135}Cs to that of ^{137}Cs was determined with a quadrupole mass spectrometer.   A measurement of accurate number of target nuclei was not necessary as in the case of the cross section measurement of ^{137}Cs[3],[4]. The solution of CsCl containing ^{135}Cs-^{137}Cs nuclide was poured into a quartz tube. The tube was sealed and wrapped with an aluminum foil together with neutron flux monitors, Co/Al and Au/Al alloy wires.   One set of a cesium solution tube(target A) and monitor wires was housed in an aluminum capsule for neutron irradiation without a Cd shield case.   Another set of a cesium tube(target B) and monitor wires was put in a Cd shield case to monitor the epithermal fraction of the neutron flux at the cesium target and monitor wires.   This was also housed in another irradiation capsule.   The Cd shield case was used to reduce the thermal neutron flux at the cesium target and the monitor wires.

b) Mass Analysis of the Target

The mass analysis of target solution was performed to obtain the ratio of the number of nuclei of ^{135}Cs to that of ^{137}Cs in the samples by using a quadrupole mass spectrometer.   Detail of the performance characteristics of the spectrometer will be reported elsewhere[10].   Since the ß-decay product of ^{137}Cs is ^{137}Ba, contamination of ^{137}Ba was checked.   The test was made by using mixture of natural cesium chloride and barium chloride.   A mass peak at the mass 138, which corresponded to the mass of natural barium, did not appear up to 800°C.   It is therefore concluded that mass peaks in the spectra taken at the temperature below 800°C were those of the cesium isotopes without the barium isotope.   Clear peaks were seen at the masses of 135 and 137 in the mass spectrum obtained at around 340°C.   The isotopic ratio(P_1), the ratio of the number of nuclei of ^{135}Cs to that of ^{137}Cs, was obtained from the spectra observed and was 0.89 ± 0.03.

c) Neutron Irradiation and Activity Measurement

The neutron irradiation of targets was performed at the hydraulic tube facility of the JRR-3 Reactor of Japan Atomic Energy Research Institute(JAERI). The irradiation of target A and monitor wires without the Cd shield case was made for 1 hour. The irradiation of target B and monitor wires within the Cd shield case was made for 24 hours.

A Ge detector with a 90% relative efficiency was employed for measurements of γ-ray spectra. The energy resolution of the detector was 2.1 keV FWHM at 1.33 MeV. The full energy peak efficiencies of the detector were calibrated with a standard ^{152}Eu γ-ray source. Pulse pile-up loss of the full energy peak intensities was corrected. The amount of this correction was small and the error associated with this correction was negligible.

After three days from the end of the neutron irradiation, γ-rays from the Au/Al monitor wire irradiated without the Cd shield was measured for 10 min. The distance between the monitor wires(or samples) and the detector was 15 cm for the present experiment. Gamma-rays from the irradiated cesium(^{135}Cs-^{137}Cs) target A was measured for 12 hours. The 12 hour measurements of γ-rays from the cesium target A were repeated 6 times sequentially, and the decay of the γ-ray intensities were followed by recording the spectrum of each measurement. After one week from the end of the irradiation, a measurement of γ-ray spectrum of the Au/Al monitor wire irradiated within the Cd shield was made for 10 min, and then, 12 hour measurements of γ-rays from the irradiated cesium target B were carried out and repeated 8 times. The decay of γ-ray intensities were also followed. After this measurement, γ-rays from Co/Al monitor wires irradiated without or within the Cd shield and Au/Al monitor wires irradiated without or within the Cd shield were measured, successively. This sequence of measurements were repeated for 4 times. Gamma-rays from ^{136}Cs are observed at the energies of 0.819, 1.048 and 1.235 MeV together with γ-rays from ^{134}Cs and ^{137}Cs. Decays of intensities of these γ-rays were followed by the spectra taken sequentially. The half-life of ^{136}Cs was determined from the decay curves of γ-ray intensities. A weighted average of values obtained from the decay of γ-rays observed is 12.63 $\pm$ 0.04 days and close to the half-life of ^{136}Cs(13.16 d) reported previously[2]. Therefore, these γ-rays were considered to be γ-rays from the product nuclide, ^{136}Cs, of the reaction ^{135}Cs(n, γ)^{136}Cs.

3. Analysis and Results

The radioactivities of [136]Cs and ^{137}Cs in the cesium samples and those of ^{60}Co and [198]Au in the flux monitor wires at the end of irradiation were obtained from the observed γ-ray intensities.　Self-absorption of γ-rays were estimated for the flux monitor wires in the same manner as described in Ref.(6).　The reaction rate R was deduced from the activity observed.

Practically, the reaction rate R can be calculated by the following equation[3],[4],

$$R = \frac{n_2 b_1 \varepsilon_1}{n_1 b_2 \varepsilon_2} \cdot \frac{\lambda_1 \lambda_2 (t_2 - t_1)}{[\exp(-\lambda_2 t_1) - \exp(-\lambda_2 t_2)]} \frac{1}{[1 - \exp(-\lambda_2 t_{ir})]} \cdot \quad (1)$$

Here, the meaning of the symbols are as follows:

n_1, n_2 :　total counts of γ-ray peaks from the target nuclei and the product nuclei, respectively, observed in the same γ-ray spectrum,

b_1, b_2 :　gamma-ray emission probabilities per decay from the target nuclei and the product nuclei, respectively,

ε_1, ε_2 :　full energy peak efficiencies of the Ge detector for the γ-rays from the target nuclei and the product nuclei, respectively,

λ_1, λ_2 :　decay constants of the target nuclide and the product nuclide, respectively,

t_1, t_2 :　start time and stop time of γ-ray measurement from the end of neutron irradiation, respectively,

t_{ir} :　total period of neutron irradiation.

Since the target nuclide, [135]Cs, of the present experiment does not emit any γ-rays, the nuclide ^{137}Cs included in the target samples, was used as a tracer of the nuclide [135]Cs, and the 0.662 MeV γ-ray peak was used for this purpose.　The isotopic ratio($P_1 = N([135]Cs) / N([137]Cs)$; N means the number of the nuclei in the parenthesis) was measured in advance as mentioned above.　　The Eq.(1) was modified by using P_1 as follows:

$$R = \frac{n_2 b_0 \varepsilon_0}{n_0 b_2 \varepsilon_2 P_1} \cdot \frac{\lambda_0 \lambda_2 (t_2 - t_1)}{[\exp(-\lambda_2 t_1) - \exp(-\lambda_2 t_2)]} \cdot \frac{1}{[1 - \exp(-\lambda_2 t_{ir})]} , \quad (2)$$

where n_0 means a total counts of the 0.662 MeV γ-ray peak from ^{137}Cs, b_0 the emission probability per decay of the 0.662 MeV γ-ray, ε_0 the full energy peak efficiency for the 0.662 MeV γ-ray, and λ_0 the decay constant of [137]Cs.　The meaning of other parameters are the same as those in Eq.(1).　Thus, the reaction rate R can be obtained from a ratio of γ-ray intensity of the product nuclei, [136]Cs, to that of the tracer nuclei,

[137]Cs, and was used to derive the thermal neutron cross section and the resonance integral as was done before[3] ~ [5].

According to the Westcott convention[11], relations between reaction rate(R) and thermal neutron cross section(σ_0) can be written in a simplified form[4]~[7], as

$$R/\sigma_0 = \phi_1 + \phi_2 s_0 , \qquad (3)$$

for irradiation without a Cd shield case, and

$$R'/\sigma_0 = \phi'_1 + \phi'_2 s_0 , \qquad (4)$$

for irradiation within a Cd shield case.

The s_0 is defined by

$$s_0 = \frac{2}{\pi^{1/2}} \frac{I'_0}{\sigma_0} \qquad (5)$$

with I'_0, the resonance integral after subtracting the $1/v$ component.

The values of simplified flux factors, $\phi_{1,2}$ and $\phi'_{1,2}$ were determined using the R and R' values of the flux monitor wires, Co/Al and Au/Al, of which σ_0's were known.

Because Eqs.(3) and (4) give a relation,

$$s_0 = - \frac{\phi_1 - \phi'_1 (R/R')}{\phi_2 - \phi'_2 (R/R')} , \qquad (6)$$

the s_0 value of the [135]Cs(n, γ)[136]Cs reaction is deduced from the R/R' value of irradiated [135]Cs samples. The value of σ_0 can be obtained by substituting the s_0 into Eq.(3). The value of I'_0 is then obtained using Eq.(5).

The resonance integral I_0 can be calculated by assuming the Cd cut-off energy to be 0.5 eV. Then, the resonance integral I_0 is given by

$$I_0 = I'_0 + 0.45\sigma_0 , \qquad (7)$$

where $0.45\sigma_0$ is the $1/v$ contribution.

In addition to the statistical errors, the following systematic errors were included in the errors of σ_0 and I_0.

1) Error in the γ-ray full energy peak efficiency resulting from the uncertainty of the source intensity used for the calibration ・・・ 1.5%

2) Error in the measurement of the neutron flux ・・・・・・ 1.5%

3) Error in the emission probability per decay of each γ-ray ・・・・ 1.0%

4) Error in the measurement of the isotopic ratio of [135]Cs and ^{137}Cs by the quadrupole mass spectrometer ・・・・・・・ 3 %

The thermal neutron capture cross section(σ_0) and the values of s_0, I_0' and I_0 were obtained from the above analysis of each γ-ray. Weighted average of these values are shown in Table 1 together with data reported in references[8],[9]. The value of the thermal neutron capture cross section(σ_0) obtained is in agreement with that reported by Baerg et al.[9], while the value of the resonance integral(I_0) is about 2/3 of that obtained by Baerg et al[9].

Table. 1   Results of the present experiment and the previous reports[8],[9]

	Present Result	Baerg et al.[9]	Sugarman[8]
σ_0(b)	8.3 ± 0.3	8.7 ± 0.5	14.5 ± 30%
s_0	4.66 ± 0.29	------	------
I_0'(b)	34.4 ± 2.5	------	------
I_0(b)	38.1 ± 2.6	61.7 ± 2.3	------

References
(1) Tasaka, K., Katakura, J., Ihara, H., Yoshida, T., Iijima, S., Nakasima, R., Nakagawa, T., Takano, H.: JAERI 1320, (1990).
(2) Firestone, R. B., Shirley, V. S., Baglin, C. M., Chu, S. Y. F., Zipkin, J. : "Table of Isotopes(8th ed,)", John Wiley & Sons Inc., New York, (1996).
(3) Harada, H., Watanabe, H., Sekine, T., Hatsukawa, Y., Kobayashi, K., Katoh, T.: J. Nucl. Sci. Technol., 27, 577 (1990).
(4) Sekine, T., Hatsukawa, Y., Kobayashi, K., Harada, H., Watanabe, H., Katoh, T.: Ibid., 30, 1099 (1993).
(5) Harada, H., Sekine, T., Hatsukawa, Y., Shigeta, N., Kobayashi, K., Ohtsuki, T., Katoh, T: ibid., 31, 173 (1994).
(6) Harada, H., Nakamura, S., Ogata, Y., Katoh, T.: Ibid., 32, 395 (1995).
(7) Nakamura, S., Harada, H., Katoh, T., Ogata, Y.: Ibid., 33, 283 (1996).
(8) Sugarman, N.: Phys. Rev., 75, 1473 (1949).
(9) Baerg, A. P., Brown, P., Lounsbury, M. : Can. J. Phys., 36, 863 (1958).
(10) Harada, H., Nakamura, S., Katoh, T.: J. Nucl. Sci. Technol., to be published.
(11) Westcott, C, H., Walker, W. H., Alexander, T. K. : "Proc. 2nd Int. Conf. Peaceful Use of Atomic Eneergy, Geneva", United Nations, New York, Vol. 16, 70 (1958).

3.16 Calculation of Prompt Neutron Spectra for Curium Isotopes

Takaaki OHSAWA

Atomic Energy Research Institute, Kinki University,

3-4-1 Kowakae, Higashi-osaka , Osaka 577 Japan

With the aim of checking the existing evaluations contained in JENDL-3.2 and providing new evaluations based on a methodology proposed by the author, a series of calculations of prompt neutron spectra have been undertaken for curium isotopes. Some of the evaluations in JENDL-3.2 was found to be unphysically hard and should be revised.

1. Introduction

Recent interest in transmutation of long-lived actinide nuclides and shielding design of reprocessing facilities for highly-burnt nuclear fuels necessitates improved data for the prompt neutron spectra from neutron-induced and spontaneous fission of minor actinides. For many of the minor actinides, experimental data are very poor or completely lacking. It has been customary to use the systematics of Smith[1] to infer the effective nuclear temperatures of the Maxwellian distribution for nuclei for which experimental data are absent. For curium isotopes this convention was used to produce the evaluated data for JENDL-3.2. On the other hand, we have developed a prescription which enables calculation of prompt neutron spectra for any actinides[2]. Thus it is interesting to compare the results of this calculation with the evaluations in JENDL-3.2.

2. Methodology

Studies in the last decade[3] have made it clear that the well-known representation of the fission neutron spectra with the Maxwellian distribution is only an approximation and tends to overestimate the high energy component of the spectrum. Among several models newly proposed, that of Madland-Nix (MN)[4] was found to give adequate description of the spectrum to the degree of accuracy required from nuclear design and dosimetry calculations, without requiring too much input data and computing time. Our prescription of evaluation is based on the MN model with some improved characterization of input parameters. The flow chart of the evaluation is shown in **Fig.1**.

The improved features in the present calculations are the followings:
(1) Level density parameters for fission fragments: In the MN model[4], the
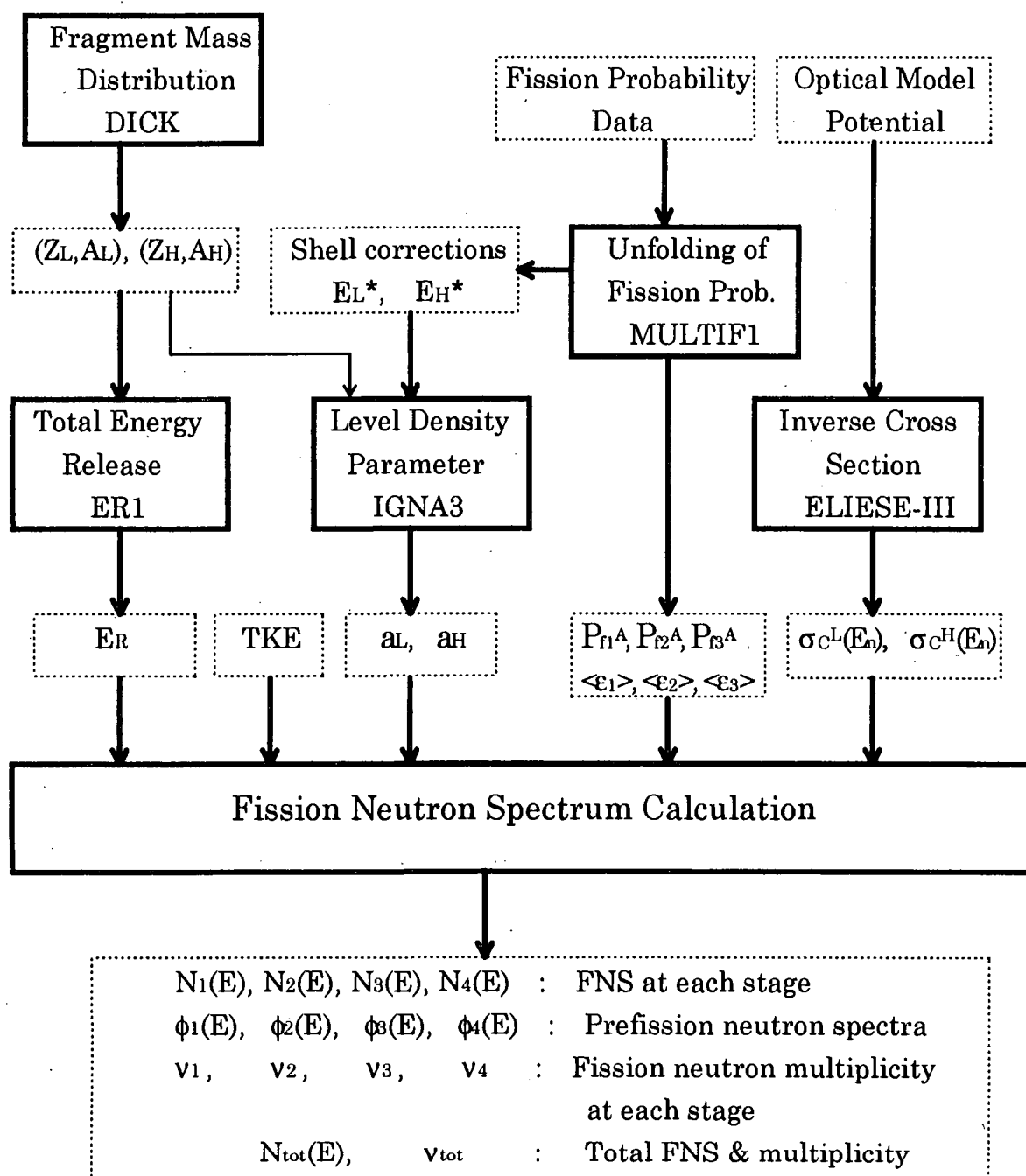
Fig.1. The flow chart of evaluation of the fission neutron spectrum. The solid boxes indicate programs and the dotted boxes sets of data.

linear approximation $a = A/C$ was used for the level density parameter (LDP) a, where A is the mass number and C is an adjustable parameter ranging from 8 to 11, for both the light fragment (LF) and heavy fragment (HF). However, this approximation does not consider the shell effects on the fragments. Especially the LDPs of heavy fragments are strongly deviated from the linear approximation **(Fig.2)**. So, we used the Ignatyuk model (the 1979 version)[5] to take into consideration the fragment shell effects.
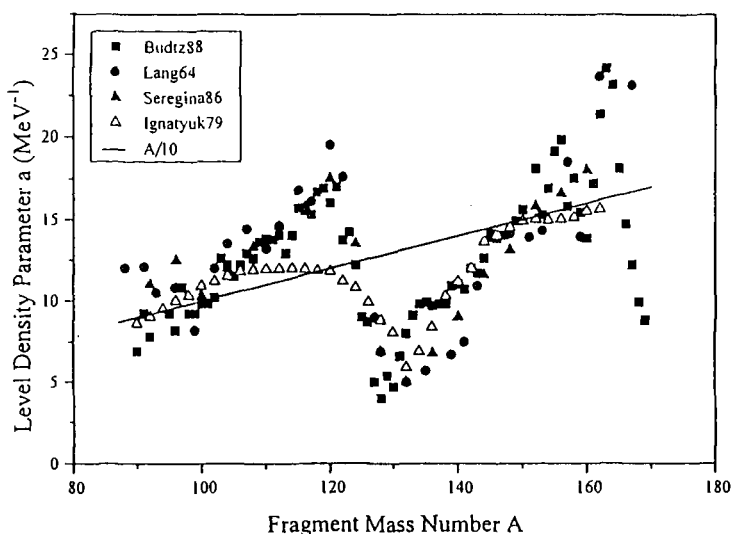
Fig.2. The level density parameters of the fission fragments. Closed symbols with error bars
stand for experimental data, open triangles the calculation by the Ignatyuk model.

(2) Energy-dependence of the inverse cross section : In the evaluation for
JENDL-3.1, the constant-inverse-cross section assumption was used. This
assumption simplified the formula, but led to inaccurate spectral shape. In
the present evaluation, the energy-dependent reaction cross sections for the
typical LF and HF generated by using the optical model potentials of Bec-
chetti-Greenlees[6] and Walter-Guss[7] were adopted.

(3) Systematics of fragment mass distribution : Dickens[8] proposed a five
Gaussian representation of the fragment mass distributions on the basis of
available measurements including his own data for curium isotopes. **Figure
3** compares the mass distributions for Cm-242, -243, -244, - 246 and -248 calcu-
lated with his formula. This representation was used to calculate the aver-
age LF and HF. The most probable charges were obtained from Wolfsberg[9]
and Netherway[10].

(4) Total energy release of fission : The total energy release of fission was
calculated using the seven-point approximation[4], in which seven fragment
pairs around the typical fragment are chosen and the total energy releases for
each pair were averaged by weighting them with respective fission yields.
The mass formula of Tachibana *et al.*[11] (abbreviated as TUYY formula) was
used to calculate the total energy release, because this formula is known to
yield adequate values for nuclei far from beta-stability line.

3. Results and Discussion

Calculations were made for five curium isotopes Cm-242, -243, -244, -246
and -248. Main fission properties (the average light and heavy fragments, the
total energy release E_R, the total kinetic energies TKE, the effective Max-wel-
lian temperatures T_M) for curium isotopes are summarized in Table 1.
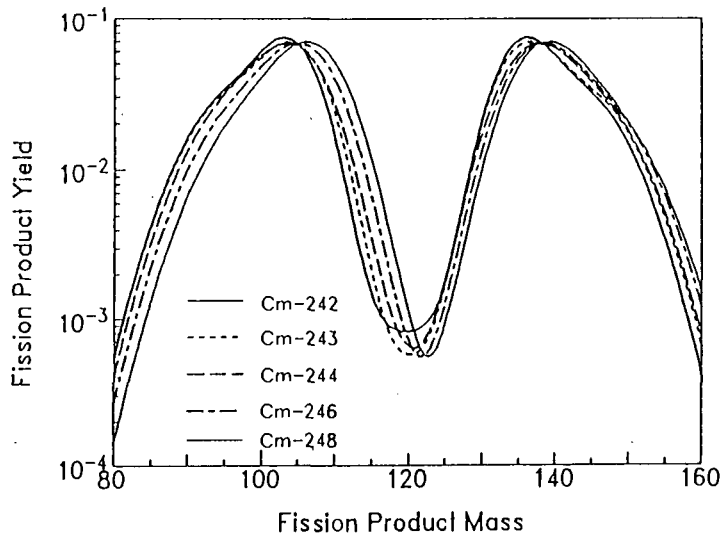
Fig.3 The fragment mass distributions for curium isotopes as calculated with the Dickens' formula.

Table 1. Main fission properties of curium isotopes.

Nuclide/Type	LF	HF	E_R (MeV)	TKE (MeV)	T_M (MeV)
Cm-241(n,f)	------	-------	------	------	1.440(?)
Cm-242(n,f)	Nb-102	Cs-141	209.05	188.05	1.414
Cm-243(n,f)	Nb-103	Cs-141	207.91	186.89	1.408
Cm-244(sf)	Nb-103	Cs-141	207.87	187.00	------
Cm-242(n,f)	Nb-103	Cs-142	207.49	185.73	1.402
Cm-246(n,f)	Nb-105	Cs-142	207.93	183.42	1.480(?)
Cm-247(n,f)	------	------	------	-----	1.470(?)
Cm-248(n,f)	Nb-106	Cs-142	207.52	182.40	1.380

The calculated prompt neutron spectra for ^{242}Cm(n_{th},f) are shown in **Fig.4** for two cases in which optical potentials of Becchetti-Greenlees and Walter-Guss were used to generate the inverse cross sections. Note that in these figures the ratio to the Maxwellian distribution with the effective temperature as given in JENDL-3.2 are plotted. It can be seen that (i) the calculated spectra are considerably deviated from the Maxwellian distribution, and (ii) no great difference is observed between the results for the two potentials. Similar results are obtained for other isotopes of curium.

Figure 5 compares the calculated prompt neutron spectra and the JENDL-3.2 evaluation for ^{246}Cm, the latter being the Maxwellian shape with T_M=1.48 MeV. The apparent difference is due to the too high value of T_M, exceeding even that (T_M=1.42 MeV) for ^{252}Cf(sf), which is unphysical. Similar anomaly is observed for ^{241,247}Cm; these are marked with (?) in Table 1. This is probably due to miscalculation of the effective temperature.
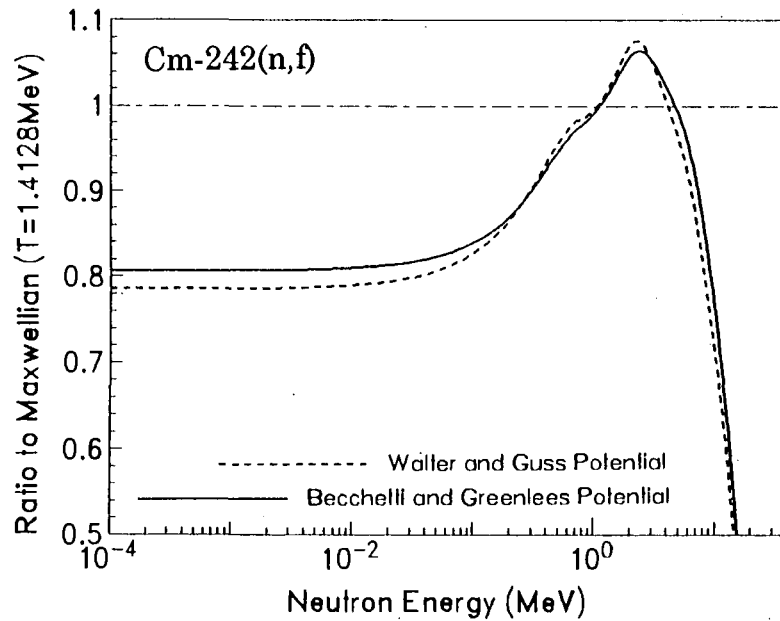
Fig.4 The calculated prompt neutron spectra for ^{242}Cm(nth,f). Two results using the Becchetti-Greenlees (solid curve) and the Walter-Guss (dashed curve) potentials are compared.
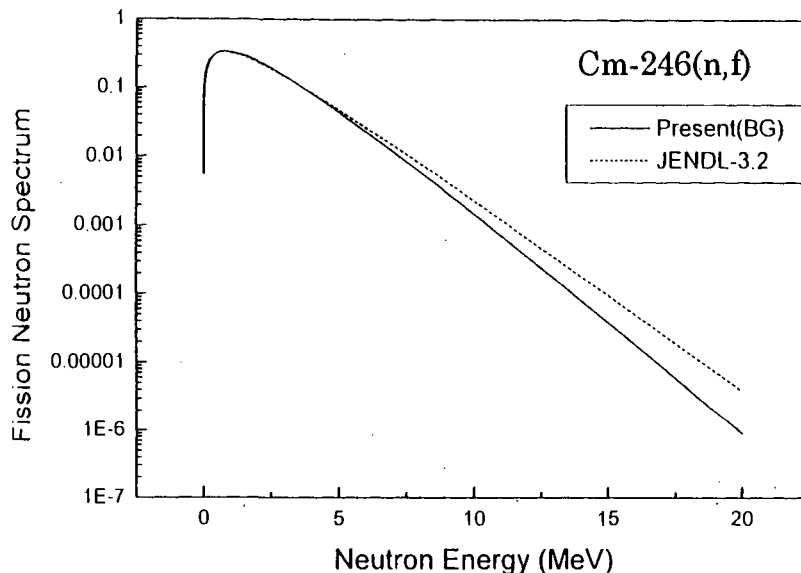
Fig.5. Comparison of the calculated prompt neutron spectra and the JENDL-3.2 evaluation (Maxwellian with T_M=1.48MeV) for ^{246}Cm.

It would be interesting to compare the spectra for ^{243}Cm(nth,f) and ^{244}Cm(sf), for which the fissioning nucleus is identical. **Figure 6** compares the spectra for the two cases, together with that for ^{235}U(nth,f). It can be seen that the spectrum for ^{243}Cm(nth,f) is harder than that for ^{244}Cm(sf), that for ^{235}U(nth,f) coming in between. This is due to the fact that the average total excitation energy of the fragments is 33.3MeV for ^{243}Cm(nth,f), while it is 25.2MeV for ^{244}Cm(sf), the difference being the neutron binding energy plus the difference in the total kinetic energy.
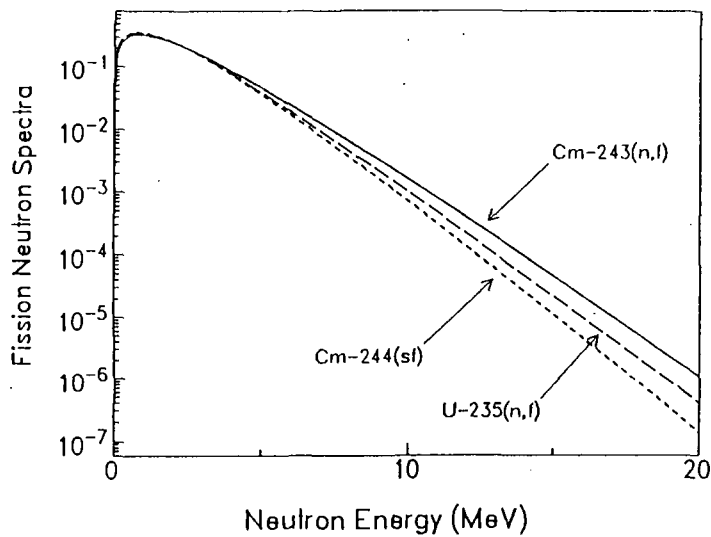
Fig.6. Comparison of the fission neutron spectra for ^{243}Cm(nth,f), ^{244}Cm(sf) and ^{235}U(nth,f).

4. Conclusions

Calculations of the prompt neutron spectra were made for five curium isotopes $^{242, 243, 244, 246}$Cm and ^{248}Cm. The Maxwellian temperatures for $^{241, 246, 247}$Cm in JENDL-3.2 were found to be unphysically high.

Acknowledgments

The author is very grateful to Mr. Y.Ito of Osaka University for performing numerical calculations.

References

1. A.B.Smith et al., ANL/NDM-50 (1970)
2. T.Ohsawa and T.Shibata, Proc. Int. Conf. on Nuclear Data for Science and Technology, Gatlinburg, 1994, Vol.2 (1994) p.639.
3. See for example: S.Ganesan (ed.), Nuclear Data for Neutron Emission in the Fission Process, INDC(NDS)-251, IAEA (1991)
4. D.G.Madland and J.R.Nix, Nucl. Sci. Eng. 81 (1982) 213.
5. A.V.Ignatyuk, Sov. J. Nucl. Phys. 29 (1979) 450.
6. F.D.Becchetti, Jr., and G.W.Greenlees, Phys. Rev. 182 (1969) 1190.
7. R.I.Walter and P.P.Guss, Proc. Int. Conf. on Nuclear Data for Basic and Applied Science, Santa Fe, 1985, Vol.2 (1986), p.1079
8. J.K.Dickens, Nucl. Sci. Eng. 96 (1974) 8.
9. K.Wolfsberg, Phys. Rev. B137 (1965) 929.
10. D.R.Netherway, UCRL-51640 (1974)
11. T.Tachibana, M.Uno, M.Yamada, S.Yamada, Atomic Data and Nuclear Data Tables, 39 (1988) 251

3.17 One-Group Constant Libraries for Nuclear Equilibrium State

Akihiko MIZUTANI and Hiroshi SEKIMOTO
Research Laboratory for Nuclear Reactors, Tokyo Institute of Technology
O-okayama, Meguro-ku, Tokyo
e-mail: amizutan@nr.titech.ac.jp

One-group constant libraries for the nuclear equilibrium state were generated for both liquid sodium cooled MOX fuel type fast reactor and PWR type thermal reactor with Equilibrium Cell Iterative Calculation System (ECICS) using JENDL-3.2, -3, -2 and ENDF/B-VI nuclear data libraries. ECICS produced one-group constant sets for 129 heavy metal nuclides and 1238 fission products.

1. Introduction

One-group constants are generated for many reactor types and for neutron spectra, but most of them are for fresh fuel reactors. We do not have any good libraries for the nuclear equilibrium state. An equilibrium cell iterative calculation system (ECICS) has been developed to obtain the consistent neutron spectrum, one-group nuclear constant set and nuclide number density which characterize the nuclear equilibrium state.

In this paper, we make one-group nuclear constant libraries at the equilibrium state for a liquid sodium cooled MOX fuel type fast reactor and a PWR type thermal reactor by ECICS calculations.

2. Calculation Method by ECICS

The flow chart of the equilibrium cell iterative calculation system (ECICS) is shown in Fig. 1. This system employs an iterative procedure of a cell neutron transport calculation and an equilibrium nuclide density calculation. At first, we perform the equilibrium calculation in which the material balance equations within the fuel pellet region for heavy metals and fission products are solved[1,2]. The equation with respect to the fuel supply rate is solved simultaneously with the material balance equations. These equations are solved on condition that the total number density of nuclides associated with the fuel is fixed. In this condition for the fixed total number density, the number density of fission products is divided by 2 since one fission makes two fission products. This equilibrium calculation treats 129 heavy nuclides and 1238 fission products (FPs). Next, the one-group scalar neutron flux level is normalized by the given power density. This iterative calculations (flux level iteration) are continued until both flux level and each nuclide number density are converged.

After this flux level iteration is converged, we perform the cell calculation to obtain the neutron spectrum and fine-group microscopic cross sections of each nuclide. The cell calculation is performed by the SLAROM code for the fast reactor with JFS-3-J3 nuclear data set, and we make the JFS format FP libraries by using the NJOY code from ENDF/B-VI nuclear data library[3]. For the thermal reactor we use the SRAC code with JENDL-3.2, JENDL-2 and ENDF/B-VI nuclear data libraries[4]. The multi-group cross sections that are obtained by these cell calculation codes are collapsed into the one-group cross sections. Although the equilibrium calculation employs 129 heavy metals and 1238 FPs, the cell calculation employs 27 important heavy metals and 20 FPs for the fast reactor, and 26 heavy metals and 16 FPs for the thermal reactor, respectively.

Then the equilibrium calculation is performed again with these one-group cross sections. The whole set of equilibrium calculation with the flux level iteration and the cell calculation is repeated until each of the one-group scalar neutron flux level, nuclide densities and one-group microscopic cross sections satisfies its corresponding convergence criterion.

After this ECICS calculations are converged, the one-group nuclear constants for nuclides which are not treated in the cell calculations are made by using the CRECTJ5 code by means of the converged neutron spectrum which is obtained in ECICS calculations.

3. Calculation Condition

As the equilibrium nuclear fuel cycle model, we assume the actinides confining fuel cycle. In this model all of the generated actinides (including Ra) are confined in the reactor. The stable lead and bismuth and stable fission products are taken out continuously from the fuel cycle. The discharged radioactive nuclides are stored in the repository, and are also removed from the fuel cycle after decaying. In the present study, the half amounts of FPs are discharged continuously from the fuel cycle in one year, and the long-life fission products are also to be taken out from the fuel cycle.

We perform ECICS for two types of cell elements. One cell consists of oxide fuel, SUS-316 cladding and liquid sodium coolant for a fast reactor, and the other consists of oxide fuel, Zircaloy-4 cladding and light water coolant for a PWR type reactor. The condition of cell calculation is shown in Table 1. The power densities in the fuel pellet are assumed to be 810 W/cc for the fast reactor and 140W/cc for the thermal reactor, respectively

4. Calculated Results

We calculate neutron spectrum, one-group nuclear constant, nuclide number density and criticality in the nuclear equilibrium state for the above mentioned fast and thermal reactors by using ECICS calculation. In the present calculation, natural uranium is supplied continuously to the reactor as a fuel for the fast reactor, and 3% enriched uranium is supplied for the thermal reactor. The converged neutron flux level is 4.72×10^{15} and 2.14×10^{14} (#/cm$^2 \cdot$ s) for the fast and thermal reactors, respectively.

The neutron spectrum for the fast reactor is shown in Fig. 2 and for the thermal reactor is shown in Fig. 3, respectively. We show the one-group nuclear constants of important nuclides

in Table 2 and Table 3. Figure 4 and Fig. 5 show the nuclide number densities for the fast and thermal reactors, respectively. To investigate the criticality performance, the nuclear equilibrium study usually evaluate the h-value and the infinite neutron multiplication factor, which are defined as

$$h = \frac{\nu\Sigma_f^{HM}}{\Sigma_a^{HM,FP}}, \qquad k_\infty = \frac{\nu\Sigma_f^{HM}}{\Sigma_a^{HM,FP,CLAD,COOL} - \Sigma_{n2n}^{HM,FP,CLAD,COOL}}$$

where $\nu\Sigma_f$, Σ_a and, Σ_{n2n} are ν-value times fission cross section, absorption cross section and n2n reaction cross section, respectively. The superscript HM, FP, CLAD and COOL are heavy metals, fission products, cladding materials and coolant materials, respectively. The calculated h-values and infinite neutron multiplication factors for fast and thermal reactors are shown in Table 4. In our calculation condition it is difficult to attain the nuclear equilibrium state by thermal reactor because of its criticality, even if 3% enriched uranium is supplied to the reactor as a fuel.

5. Conclusion

The one-group nuclear data set which are consistent with the equilibrium nuclide densities is important for evaluating reactor characteristics in the nuclear equilibrium state. By employing the iterative calculation scheme combining the cell calculation and the equilibrium one, the computing system of ECICS was made to obtain consistent neutron spectrum, one-group nuclear constants and nuclide number densities which characterized the nuclear equilibrium state. We performed the ECICS for the oxide fuel liquid sodium cooled fast reactor and PWR type thermal reactor, and made the one-group nuclear constant libraries for the nuclear equilibrium state. We would be able to investigate the characteristics of the nuclear equilibrium state with these one-group cross section sets. Although we showed only two calculation results in this paper, we were able to obtain the consistent one-group nuclear constant set for various reactor types and cell structures, and perform the accurate evaluation of the core characteristics at the equilibrium state by using the ECICS calculation[5].

	Fast Reactor	Thermal Reactor
h	1.222	0.9526
k_∞	1.146	0.8907

Table 4 Calculated h-values and infinite multiplication factors

ECICS calculation

Equilibrium Calculation

$$\frac{dn^{HM}}{dt} = \cdots = 0 \quad \text{HM: 129nuclides}$$

$$\frac{dn^{FP}}{dt} = \cdots = 0 \quad \text{FP: 1238nuclides}$$

$$s^{HM} = \kappa^{HM} \cdot S$$

$$\sum \left(n^{HM} + n^{FP}/2\right) = N_{total}$$

$n^{HM,FP}$

Cell Calculation

SLAROM code
for FAST reactor with JFS-3-J3

SRAC code
for THERMAL reactor
with JENDL-3.2, -2, ENDF/B-VI

$\sigma_{x,1group}^{HM,FP}$

$\phi_g \quad \sigma_{x,g}^{HM,FP}$

ϕ n^{HM}

Normalization by Power Density

$$\Gamma \sum n^{HM} \sigma_{fission}^{HM} \phi = P$$

Collapse of Multi-Group Cross Section

$$\sigma_{x,i}^{1group} = \frac{\sum_g \sigma_{x,i}^g \phi^g}{\sum_g \phi^g}$$

Iterations of ECICS are converged

Important Nuclides   Except Important Nuclides

Converged Neutron Spectrum → CRESTJ5 code ← JENDL-3 and ENDF/B-VI data libraries

We obtain
consistent neutron spectrum, one-group microscopic cross section
and nuclide number density at the nuclear equilibrium state

Fig. 1 Flow chart of equilibrium cell iterative calculation system

Table 1 Condition of cell calculation

		Fast Reactor		Thermal Reactor	
Cell Composition	Fuel Pellet	MOX	(37%)	MOX	(36%)
	Cladding	SUS-316	(23%)	Zircaloy-4	(16%)
	Coolant	Na	(40%)	H2O	(48%)
Fuel Pellet Diameter		6.00mm		8.00mm	
Pin Diameter		7.64mm		9.60mm	
Pin Pitch		9.40mm		12.7mm	
Cell Geometry		One dimensional cylindrical geometry			

( ) shows the volume fraction
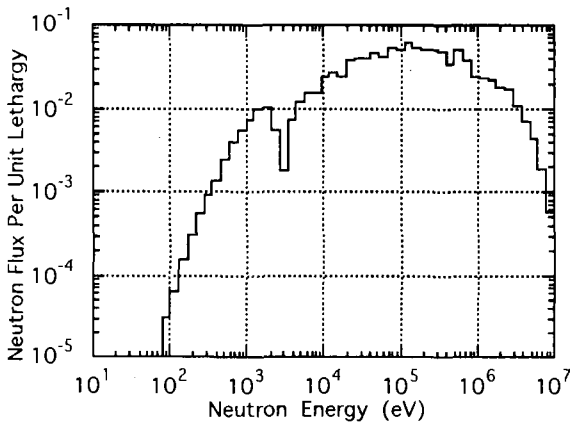
Fig. 2 Neutron spectrum for fast reactor
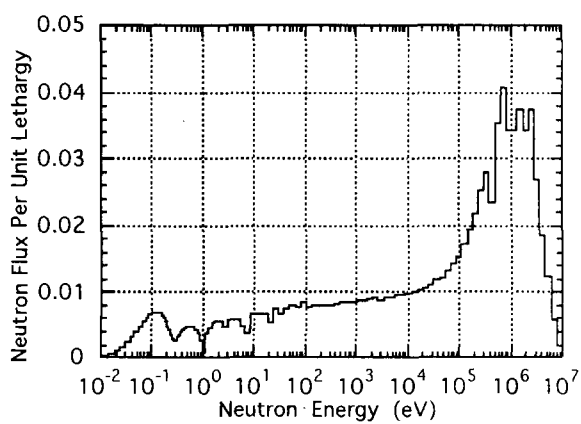
Fig. 3 Neutron spectrum for thermal reactor

(atoms/barn/cm)
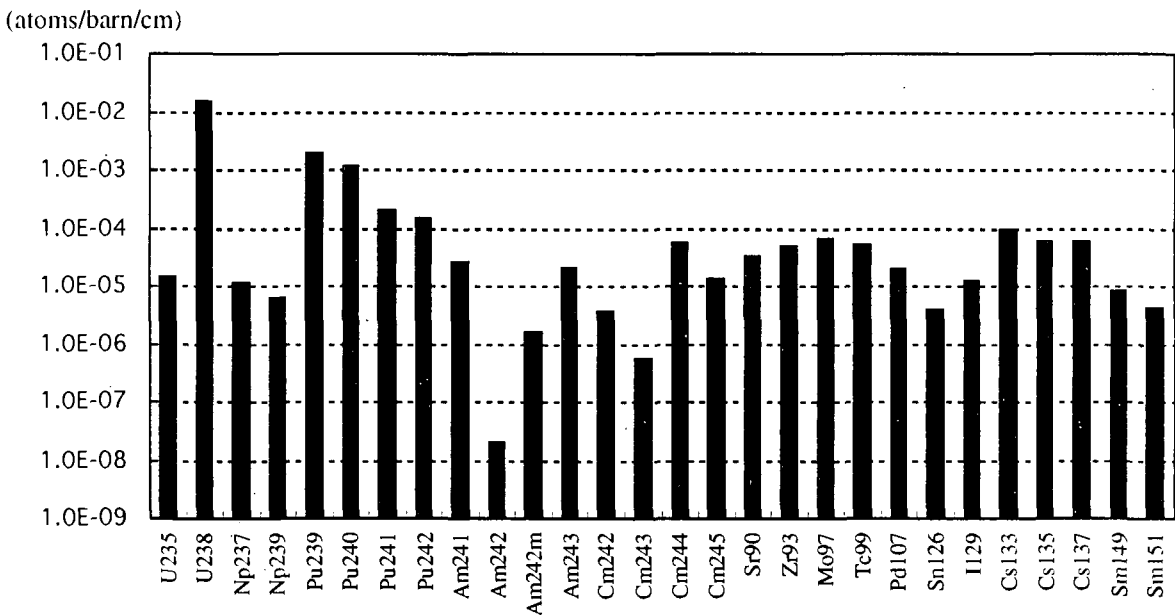
Fig. 4 Nuclide number density of fast reactor

(atoms/barn/cm)
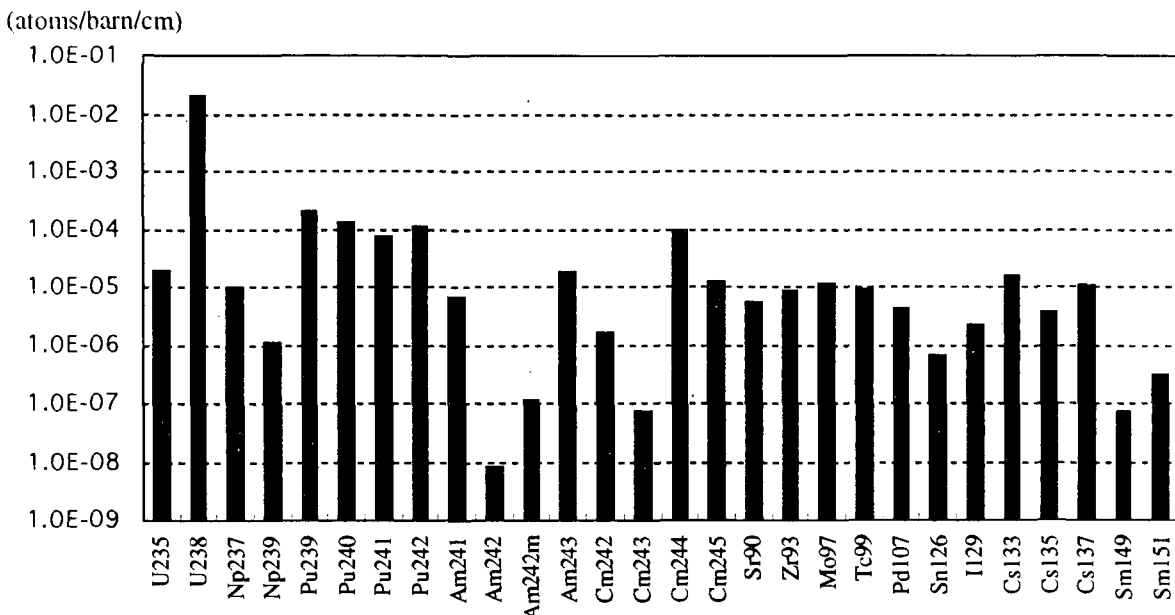
Fig. 5 Nuclide number density of thermal reactor

Nuclide	Capture	Fission	ν	Nuclide	Capture	Fission	ν
U-235	6.481E-01	2.014E+00	2.453E+00	Cm-244	7.726E-01	4.030E-01	3.510E+00
U-238	3.033E-01	4.286E-02	2.748E+00	Cm-245	3.752E-01	2.803E+00	3.627E+00
Np-237	1.847E+00	3.060E-01	2.773E+00	Sr-90	1.384E-02		
Np-239	2.178E+00	4.229E-01	2.909E+00	Zr-93	9.662E-02		
Pu-239	5.859E-01	1.856E+00	2.949E+00	Mo-97	3.305E-01		
Pu-240	6.476E-01	3.588E-01	2.992E+00	Tc-99	6.882E-01		
Pu-241	5.293E-01	2.685E+00	2.970E+00	Pd-107	1.035E+00		
Pu-242	5.385E-01	2.462E-01	3.046E+00	Sn-126	7.130E-03		
Am-241	1.958E+00	2.615E-01	3.513E+00	I-129	3.854E-01		
Am-242	6.461E-01	3.380E+00	3.314E+00	Cs-133	5.293E-01		
Am-242m	5.903E-01	3.271E+00	3.317E+00	Cs-135	7.828E-02		
Am-243	1.748E+00	1.912E-01	3.542E+00	Cs-137	1.553E-02		
Cm-242	5.749E-01	7.007E-01	3.423E+00	Sm-149	2.663E+00		
Cm-243	4.153E-01	3.188E+00	3.479E+00	Sm-151	2.948E+00		

(Capture,Fission: barn)

Table 2 One-group nuclear constant of fast reactor

Nuclide	Capture	Fission	ν	Nuclide	Capture	Fission	ν
U-235	6.850E+00	2.640E+01	2.436E+00	Cm-244	1.039E+01	8.756E-01	3.499E+00
U-238	8.821E-01	1.013E-01	2.784E+00	Cm-245	1.101E+01	7.000E+01	3.534E+00
Np-237	2.673E+01	5.451E-01	2.830E+00	Sr-90	6.615E-02		
Np-239	1.191E+01	6.764E-01	2.979E+00	Zr-93	1.030E+00		
Pu-239	3.190E+01	5.715E+01	2.876E+00	Mo-97	7.184E-01		
Pu-240	5.342E+01	5.696E-01	3.077E+00	Tc-99	7.923E+00		
Pu-241	2.170E+01	6.347E+01	2.934E+00	Pd-107	3.593E+00		
Pu-242	1.489E+01	4.509E-01	3.101E+00	Sn-126	7.649E-03		
Am-241	6.517E+01	9.197E-01	3.435E+00	I-129	1.871E+00		
Am-242	1.816E+02	1.031E+02	3.277E+00	Cs-133	1.052E+01		
Am-242m	6.777E+01	3.414E+02	3.275E+00	Cs-135	2.345E+00		
Am-243	4.134E+01	5.698E-01	3.519E+00	Cs-137	2.367E-02		
Cm-242	4.310E+00	9.510E-01	3.755E+00	Sm-149	3.268E+03		
Cm-243	1.378E+01	7.958E+01	3.434E+00	Sm-151	3.870E+02		

(Capture,Fission: barn)

Table 3 One-group nuclear constant of thermal reactor

References

[1] H. SEKIMOTO and N. TAKAGI, J. Nucl. Sci. Technol., 28[10], 941 (1991).

[2] N. TAKAGI and H. SEKIMOTO, J. Nucl. Sci. Technol., 29[3], 276 (1992).

[3] M. NAKAGAWA and K. TSUCHIHASHI, "SLAROM", JAERI-1294 (1984).

[4] K. TSUCHIHASHI, et al., "Revised SRAC Code System", JAERI-1302 (1986).

[5] A. MIZUTANI and H. SEKIMOTO, Proc. of Int. Conf. on the Physics of Reactors, PHYSOR 96, Mito, Japan, 1996.

3.18 Development of a System of Measuring Double-differential Cross Sections for Proton-induced Reactions

M. Harada, Y. Watanabe, K. Sato and S. Meigo*

Department of Energy Conversion Engineering, Kyushu University, Kasuga, Fukuoka 816
*Japan Atomic Energy Research Institute, Tokai-mura, Naka-gun, Ibaraki 319-11
e-mail : harada@ence.kyushu-u.ac.jp

We report the present status of a counter telescope and a data acquisition system which are being developed for the measurement of double-differential cross sections of all light-charged particles emitted from proton-induced reactions on ^{12}C at incident energies less than 90 MeV. The counter telescope consists of an active collimator made of a plastic scintillator, two thin silicon ΔE-detectors and a CsI(Tl) E-detectors with photo-diode readout. Signals from each detector are processed using the data acquisition system consisting of the front-end electronics (CAMAC) and two computers connected with the ethernet LAN: a personal computer as the data collector and server, and a UNIX workstation as the monitor and analyzer.

1. Introduction

Intermediate energy neutron and proton nuclear data for major elements contained in a human body, such as C, N, and O, are required with high priority in the advanced cancer therapy using a neutron beam or a proton beam. Recently, we have evaluated neutron nuclear data and kerma factors of ^{12}C for incident energies up to 80 MeV to meet the requirement[1]. As the next research program, we have recently started the evaluation of proton nuclear data of ^{12}C in the energy range up to 200 MeV.

Double-differential cross sections (DDXs) are indispensable to transport calculations of particles in matter. A few experimental data of DDXs are available for proton-induced reactions on ^{12}C as listed in Table I. Available evaluated data files are also limited at present. Therefore, further effort on systematic measurements of DDXs are necessary for energies ranging from a few tens MeV to 200 MeV. Moreover, analyses of precise proton data are useful to make neutron nuclear data evaluation more reliable, because the proton data generally play a complementary role to the neutron data.

Under these circumstances, we have proposed a new experiment to measure the DDXs of all light-charged particles (p, d, t, ^{3}He, and α) emitted from the p+^{12}C reactions at 45, 70 and 90 MeV using the AVF cyclotron at TIARA facility of JAERI. Up to now, a counter telescope and a data acquisition system have been developed for the measurement. The status of the preparation is described in this paper.

2. Development of the counter telescope

2.1. Outline of the ΔE-E counter telescope

Fig. 1 illustrates a side view of the counter telescope which has been designed in this work. It is of a conventional type, consisting of four detectors: an NE102A plastic scintillator (is 1 to 4 mm, whose thickness depending on the incident energy) as an active collimator, two thin silicon ΔE-detectors (30 μm and 500 μm in thickness, respectively), and a CsI(Tl) E-detector (18 mm $\times$ 18 mm $\times$ 30 mm). The thickness and size of those detectors were optimized using a Monte Carlo simulation of the energy deposit in which the effect of energy straggling was considered by assuming the Vavilov distribution. From the result of the simulation, the counter telescope was found to be capable of detecting light-charged particles over a wide dynamic energy range from a few MeV to 90 MeV using three-stacked ΔE

and E detectors. Particle identification is possible by means of two-demensional contour plot of ΔE and E signals: $\Delta E_1(30 \, \mu m) \times (\Delta E_2(500 \, \mu m)+E)$ for low energy range and $(\Delta E_1 + \Delta E_2) \times E$ for high energy range.

The CsI(Tl)-E detector is connected with a silicon photo-diode (Hamamatsu 3204-08) which has the well-matched spectral response characteristics for scintillation light from CsI(Tl). The use of the photo-diode has an advantage on the fabrication of such a compact counter telescope as shown in Fig. 1, because the counter telescope will be placed in a small scattering chamber 60 cm in diameter.

The active collimator is also used because it has proved to be crucial for reduction of the background due to the edge-penetration or edge-scattering in the defining slit[2], particularly in the small-angle measurements.

2.2. Nuclear reaction component in the CsI(Tl) detector

Nuclear reactions in a thick E-detector bring a serious background for the measurement of the continuum energy spectra. In particular, the background becomes a problem in the small-angle measurements because of the large elastic proton yield, according to our experiences on the measurements of continuum (p,p') spectra at 14.1 and 26 MeV[3]. Hence we have estimated the response function of the CsI(Tl) to see the influence of nuclear reactions generated in the CsI(Tl) by the elastically-scattered protons. Proton transport calculations in the CsI(Tl) were made for the estimation. The incident proton was assumed to lose its kinetic energy continuously in the CsI(Tl) until it stops or gives rise to nuclear reactions, and to deposit its energy no more if the nuclear reaction takes place. The transport of secondary particles emitted by the nuclear reactions and elastically-scattered protons to large angles was not taken into consideration in this estimation. The most important input data for the calculation are total nuclear reaction cross sections as a function of proton energy. The latest empirical formula given by Wellish et al.[4] was used.

The "tail" spectra due to the nuclear reactions were estimated for three incident proton energies of 45, 70 and 90 MeV. The results are presented in Fig. 2. The relative yield per MeV of the tail component does not depend strongly on the incident and outgoing energy and is rather constant at low outgoing energies. In addition, we have calculated the tail-to-peak ratio. The result is shown in Fig. 3 together with Janni's evaluation[5]. Our result is in good agreement with his evaluation. This implies that our estimation is reliable. The reaction component in the low energy region is considerably small, but increases with increasing incident energy, and amounts to a 9% at 100 MeV. Calculations taking into account the effect of protons escape by elastic scattering will be necessary for more reliable estimation.

3. Development of the DAQ system

The hardware and software configurations of the DAQ system are shown in Fig. 4. The personal computer PC486SR interfaced to the CAMAC crate controller has a role as the data collector and server; the PC works with the operating system of FreeBSD. It is connected with the workstation (SUN SPARC 10) via the ethernet LAN. The acquired raw data are transferred from the PC to the WS using the Inter Process Communication function and are analyzed with a package of CERNLIB on the WS. Finally, the analyzed data are displayed graphically on the screen.

A simple stand-alone DAQ system consisting of only a PC has been developed as the first stage toward completion of the above-mentioned DAQ system. The software works under the operating system of MS-DOS on the PC. The DAQ system was used in a measurement of DDXs of (p, charged particles) on ^{90}Zr using a 26 MeV proton beam from JAERI Tandem accelerator to test the performance[3,6]. A typical two-dimensional scatter plot (the x-axis: the energy of outgoing particles; the y-axis: the particle identifier output) is shown in Fig. 5. From this test experiment, it has proved that the stand-alone DAQ system worked well for the multiparameter data acquisition.

The network function and the software required for the WS are being developed toward completion of the DAQ system shown in Fig. 4. Also, a method of reducing the dead time of CAMAC-DAQ is being studied using the FERA bus.

4. Summary

The present status of the ΔE-E counter telescope and DAQ system which are being developed for the measurement of DDXs for the p+^{12}C reactions was reported. The counter telescope is composed of two Si ΔE-detectors and a CsI(Tl) E-detector. The active collimator made of the NE102A is used to reduce the background due to the edge-penetration in the defining slit. The signals from each detector are processed and analyzed using the CAMAC-DAQ and analysis system which makes use of the advantages of the ethernet LAN.

The response function of the CsI(Tl) was estimated by the Monte Carlo simulation using the latest empirical formula of the reaction cross sections. It was found that the tail component appearing in the response function becomes large with an increase in the incident proton energy. Since it causes a large background in the continuum part of the (p,p'x) spectra observed at small angles, careful attention to the elimination should be needed. The estimation of the response function of the CsI(Tl) is indispensable to the data analysis concerning the elimination of the background.

Our experiment is scheduled from FY1997 to FY1999 in the University-JAERI collaborative Program at TIARA. Before the full measurements of DDXs, some test experiments are planned: investigations of the energy dependence of light output and the tail-to-peak ratio for the CsI(Tl) detector, performance tests of the distributed type of DAQ system, etc.

References
[1] M. Harada et al., to be published in J. Nucl. Sci. Technol. (1997).
[2] M. Hayashi et al., Proc. of the 1994 Symp. on Nuclear Data, JAERI-Conf. 95-008, p.225 (1995).
[3] S. Yoshioka et al., presented at this symposium.
[4] H. P. Wellisch & D. Axen, Phys. Rev. C, 24, p.1329 (1996).
[5] J. F. Janni, Atom. Data & Nucl. Data Tab., 27, p.147 (1982).
[6] K. Sato et al., presented at the Kyushu branch of Meeting of the Atomic Energy Society of Japan, Dec. 20, 1996, Kyushu University, Fukuoka.
[7] S. Pearlstein et al., Brookhaven National Laboratory, BNL-48035 (1993).
[8] P. G. Young, et al., Los Alamos National Laboratory, report LA-11753-MS (1989).
[9] F. E. Bertrand and R. W. Peelle, Phys. Rev. C, 8, p.1045 (1973).
[10] S. V. Förtsch et al., Nucl. Phys., A485, p.258 (1988).
[11] H. Kashimoto et al., Master thesis, Kyushu University (unpublished) (1993).
[12] G. J. Arendse et al., NAC Annual Report, NAC/AR/95-01, p.9 (1995).

Table I : DDXs data for energies from a few tens MeV to 200 MeV

[a] : Reference[7] [b] : Reference[8] [c] : Reference[9]
[d] : Reference[10] [e] : Reference[11] [f] : Reference[12]

Evaluated nuclear data	ENDF/B-VI/He[a]	1 MeV ~ 10 GeV
	Los Alamos evaluation[b]	10^{-11} ~ 100 MeV
Experimental data	Bertrand et al. (1973)[c] ^{12}C(p, x), x = p, d, t, ^{3}He, α	29, 39, 62 MeV
	Förtsch et al. (1988)[d] ^{12}C(p, p')	90, 200 MeV
	Kashimoto et al. (1993)[e] ^{12}C(p, p'), (p, α)	26 MeV
	Arendse et al. (1995)[f] ^{12}C(p, x), x = p, d, t, ^{3}He, α	150 MeV
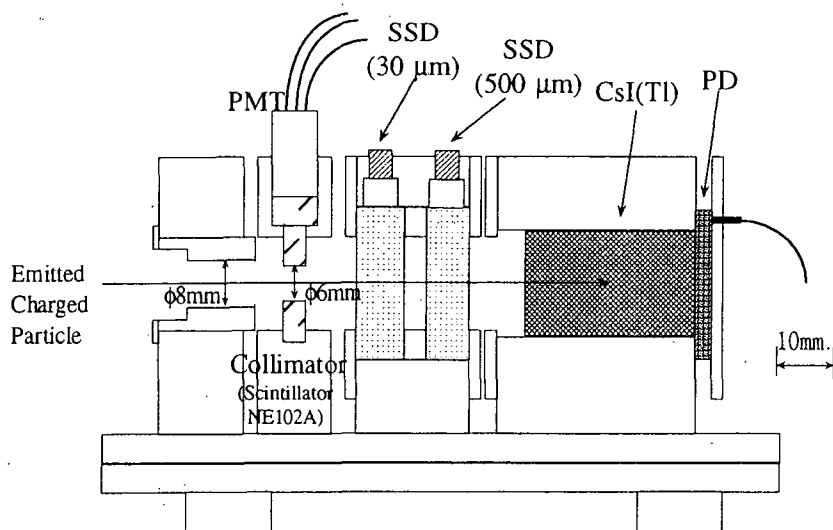
Fig. 1 : Side view of the counter telescope
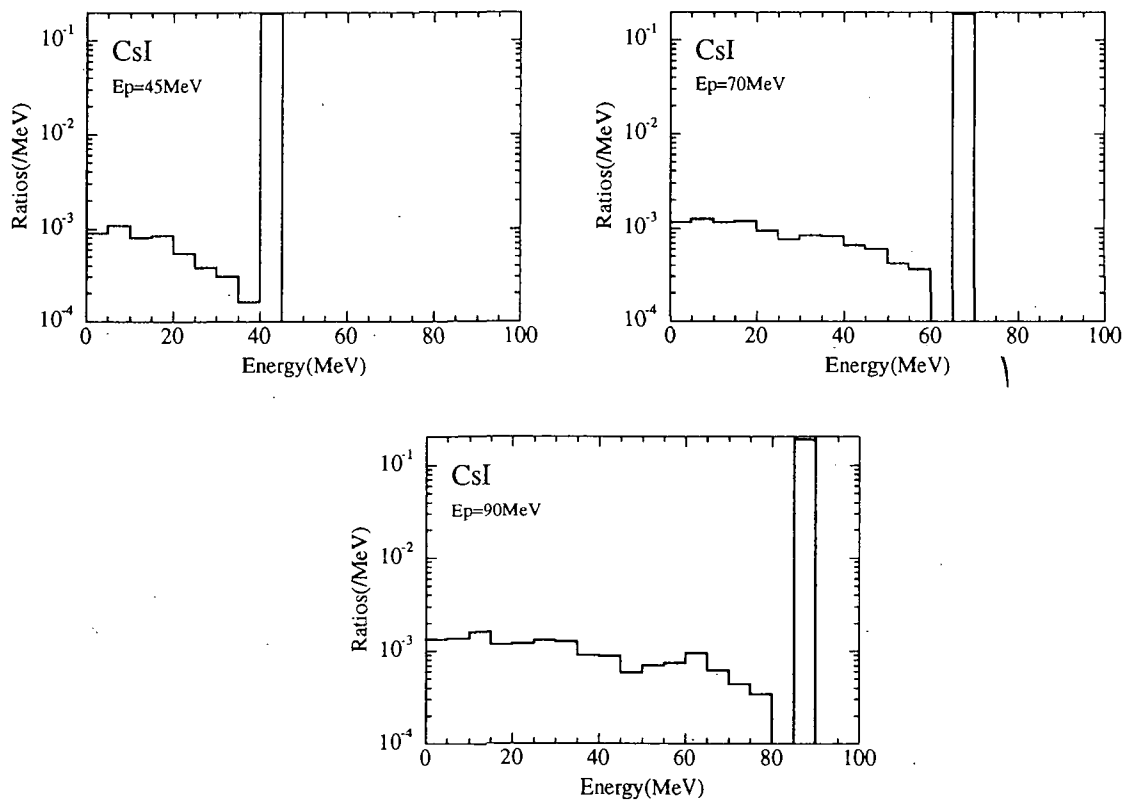
Fig 2 : Reaction component by 40,70 and 90MeV protons
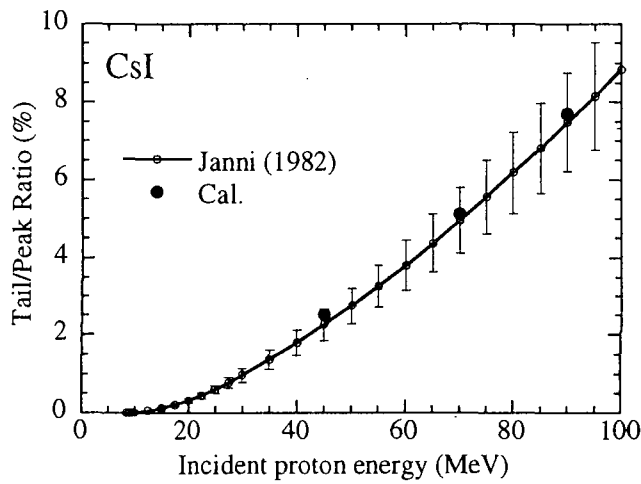
Fig. 3 : Tail/Peak ratio as a function of incident energy
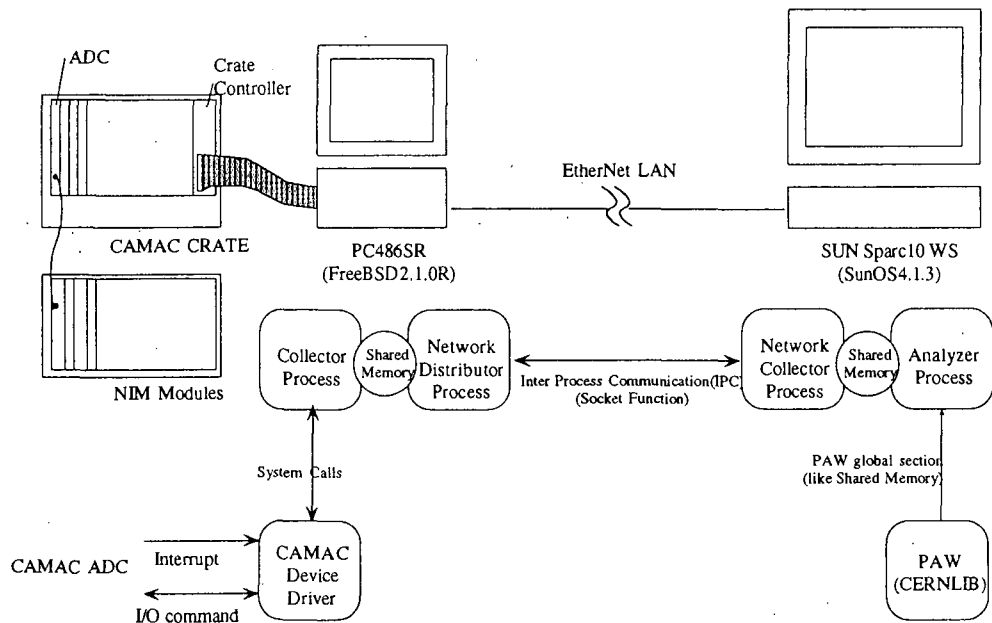
Fig. 4 : The hardware and software configuration of the DAQ system
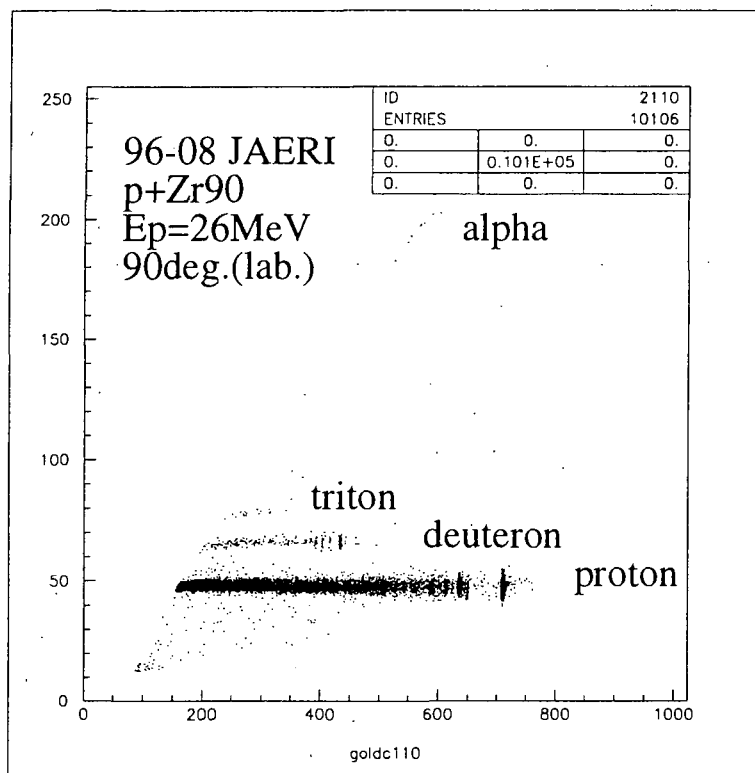
Fig. 5 : PI-E scatter plot of the data measured using the stand alone DAQ system

3.19 Measurement of Fission Cross Section with Pure Am-243 Sample using Lead Slowing-Down Spectrometer

Katsuhei Kobayashi[1], Shuji Yamamoto[1], T. Kai[1], Yoshiaki Fujita[1],
Hideki Yamamoto[2], Itsuro Kimura[2] and Nobuo Shinohara[3]

1 Research Reactor Institute, Kyoto University
Kumatori-cho, Sennan-gun, Osaka 590-04, Japan
2 Department of Nuclear Engineering, Kyoto University
Yoshidahonmachi, Sakyo-ku, Kyoto 606-01, Japan
3 Isotope Products Laboratory, Japan Atomic Energy Research Institute
Tokai-mura, Naka-gun, Ibaraki 319-11, Japan

By making use of back-to-back type double fission chambers and a lead slowing-down spectrometer coupled to an electron linear accelerator, the fission cross section for the ^{243}Am(n,f) reaction has been measured relative to that for the ^{235}U(n,f) reaction in the energy range from 0.1 eV to 10 keV. The measured result was compared with the evaluated nuclear data appeared in ENDF/B–VI and JENDL–3.2, whose evaluated data were broadened by the energy resolution function of the spectrometer. General agreement was seen between the evaluated data and the measurement except that the ENDF/B–VI data were lower in the range from 15 to 60 eV and that the JENDL–3.2 data seemed to be lower above 100 eV.

1. Introduction

Americium isotopes are minor actinides which are produced subsequently to ^{237}Np nuclide in light water reactors. The nuclear data for the minor actinides are of great interest in the design of reactors with MOX or Pu fuels and for the design of systems for spent fuel reprocessing or waste disposal. The fission cross sections are important for transmutation of the burdensome actinides[1,2].

Numerous measurements of the nuclear data for ^{237}Np and ^{241}Am have been made previously [3]. Recently, the authors have also measured the fission cross sections of ^{237}Np and ^{241}Am in the neutron energy range from 0.1 eV to 10 keV[4,5]. However, the fission cross section for ^{243}Am is not always enough both in quality and in quantity, especially, the measured data have not been reported below 5 keV except for thermal neutron energy[3,6]. In the lower energy region, ^{243}Am has a small subthreshold fission cross section. However, the cross section is still important not only for systematic studies of fission mechanism but also for transmutation in light water reactors because they have higher neutron fluxes at the relevant energies.

In the present study, at first, we have prepared the pure ^{243}Am sample by anion-exchange method to remove the ^{239}Pu impurity produced through the alpha-decay of ^{243}Am. After the chemical purification, the fission cross section for the ^{243}Am(n,f) reaction has been measured

relative to that for the ^{235}U(n,f) reaction by making use of back—to—back type double fission chambers and a lead slowing—down spectrometer coupled to 46 MeV electron linear accelerator (linac) of Research Reactor Institute, Kyoto University (KURRI). The experimental technique is the same as before[4,5]. The measured result is compared with the evaluated data in JENDL-3.2[7] and ENDF/B-VI[8].

2. Experimental Methods

2.1. Lead Slowing—down Spectrometer

The lead slowing—down spectrometer was recently installed coupling to the 46 MeV electron linear accelerator (linac) at Research Reactor Institute, Kyoto University (KURRI). The Kyoto University Lead Slowing-down Spectrometer (KULS) is composed of 1600 pieces of lead blocks (each size : 10x20x20 cm^3, and purity : 99.9 %) and these are piled up to make a cube of 1.5x1.5x1.5 m^3 (about 40 tons) without any structural materials[9], as seen in Fig. 1. At the center of the KULS, we have set an air—cooled photoneutron target of Ta to generate pulsed fast neutrons. Thermocouples were attached on the surface of the target case to monitor the temperature. The linac was operated to keep the temperature less than 300 °C. The KULS has eight experimental/irradiation holes (10x10 cm^2, 55 or 45 cm in depth), and one of the holes is covered by bismuth layers of 10 to 15 cm in thickness to shield high energy gamma—rays (6 to 7 MeV) produced by the Pb(n,γ) reaction in the spectrometer.

Characteristic behavior of neutrons in the KULS was studied by calculations with the continuous energy Monte Carlo code MCNP[10] and by experiments with resonance filter method [4,9]. It was found that the slowing—down constant K in the relation of energy and slowing—down time E=K/t^2 was determined to be 190 ± 2 and 156 ± 2 (keV μs^2) for the bismuth and the lead experimental holes. The energy resolution was around 40 % for both experimental holes at energies from a few eV to about 500 eV and was larger in the lower and the higher energy regions. More detailed characteristics of the KULS are given elsewhere [4,9].

2.2. ^{243}Am and ^{235}U Samples

The americium sample was purified at Isotope Products Laboratory,
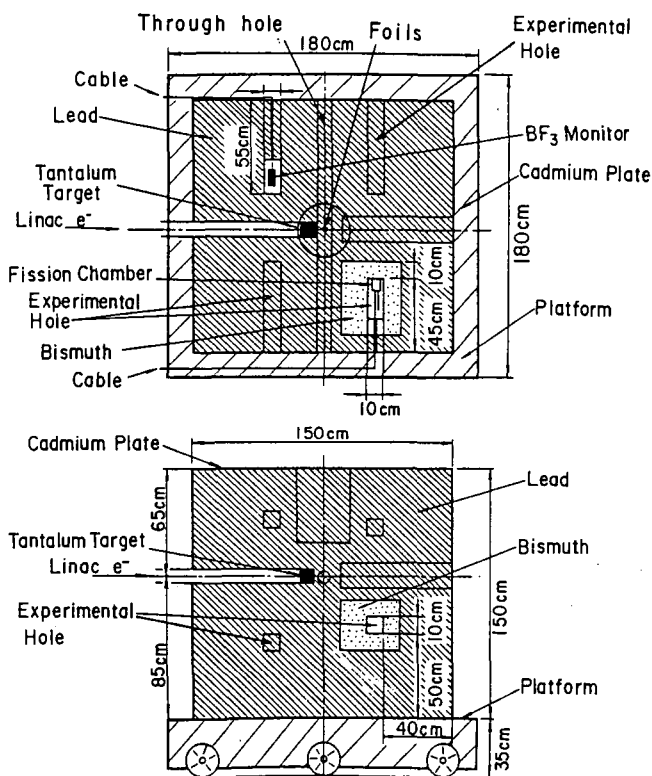
Fig. 1 Cross—sectional view of Kyoto University Lead Spectrometer, KULS.

Japan Atomic Energy Research Institute by anion–exchange method using nitric acid methyl alcohol–mixed media [11], in order to remove uranium, neptunium, plutonium and curium from the americium sample. The purified americium solution and isopropyl alcohol were mixed thoroughly and electrolyzed on a stainless steel disk (28 mm in diameter and 0.2 mm in thickness) for preparing an americium deposit (radioactive area of 20 mm in diameter)[12]. After electrodeposition, the sample was sintered with a gas burner to fix the americium layer on the disk by making americium oxide.

Alpha–ray from the deposit was measured with a silicon surface barrier detector. The pulse height distribution of the ^{243}Am sample is shown in Fig. 2. Although small amount of impurities of ^{241}Am and ^{243}Cm are observed in the figure, their counting rate ratios for ^{241}Am/^{243}Am and Cm/^{243}Am are 0.007 and 0.00004, respectively. We have found that these impurities have no influence on the result of the ^{243}Am (n,f) cross section measurement, considering their cross sections and half–lives or numbers of their atoms.

Fig. 2 Alpha–ray spectrum of ^{243}Am.

In addition, 74.7 keV gamma–ray from ^{243}Am was measured with a HPGe detector and the number of ^{243}Am was also determined by analyzing the gamma–ray spectrum obtained. The results measured by both detectors are in good agreement within the uncertainty of 2 %. The number of ^{243}Am atoms is determined to be $(3.33 \pm 0.11) \times 10^{17}$, where the error was estimated by taking into account (i) statistics of the activity measurements, (ii) geometrical detection efficiencies, and (iii) uncertainties of the decay data used.

Highly enriched uranium oxide (99.91 % of ^{235}U) got from ORNL was chemically treated as almost same technique as the americium sample. The uranium deposit on the stainless steel disk was prepared at KURRI by the electrodeposition method. This ^{235}U sample was used to monitor the neutron flux in this study as the well–known reference cross section of the ^{235}U(n,f) reaction. Alpha–ray and gamma–ray spectrometries were carried out to determine the number of the uranium atom as well as the americium sample. From the analyses of the alpha–rays with 4.152 to 4.597 MeV from ^{235}U, the number of ^{235}U atoms was determined to be $(2.81 \pm 0.03) \times 10^{16}$. The gamma–ray measurement by 185.7 keV of ^{235}U showed good agreement within 1.5 % with the alpha–ray measurement.

2.3. Fission Chambers

The fission chambers employed for the present measurement are composed of two parallel plate type ionization chambers[4,5] as shown in Fig. 3. The back sides of a sample deposit (^{243}Am) and a reference one (^{235}U) are faced each other, and it is called back–to–back type. The chambers were made of Al and filled with a mixed gas (97% Ar and 3% N 2) at 1 atm.

2.4. Data Taking and Fission Rate Measurement

The back-to-back type fission chambers were put in the Bi-covered hole of the KULS. Since we used quite thin [243]Am(43 μg/cm^2) and [235]U(3.5 μg/cm^2) deposits, fission pulses were clearly discriminated from background pulses caused by alpha-rays, and led to the respective time analyzer, as before[4,5]. The start signal for timing was taken from the linac electron burst. The channel number and the time width of each time analyzer were 4096 and 62.5 or 500 ns, respectively. The linac was operated with pulse width of 22-33 ns, repetition rate of 200 Hz, electron peak current of about 1.9 A, and accelerating energy of about 30 MeV. After about 50 hours' experiment, the [243]Am and the [235]U deposited plates were exchanged each other and had another 30 hours, to eliminate the systematic and statistic uncertainties in the cross section measurement.

Fig. 3 Cross-sectional view of back-to-back type fission chambers.

The fission cross section of [243]Am is obtained by

$$\sigma_{Am}(E) = \frac{C_{Am}}{C_U} \frac{N_U}{N_{Am}} \sigma_U(E)$$

where

C_{Am} : fission counts of [243]Am,

C_U : fission counts of [235]U,

N_{Am} : number of [243]Am atoms in the sample deposit,

N_U : number of [235]U atoms in the reference deposit,

$\sigma_U(E)$: energy dependent fission cross section of [235]U.

We cited the numerical values of $\sigma_U(E)$ from ENDF/B-VI[8].

Figure 4 shows the cross sections measured at the time when 4 weeks, 5 months and 13 months have passed after the chemical purification. In the neutron energy region around 0.3 eV, one can see that the cross sections are getting higher as the time passes, due to the accumulated impurity of [239]Pu by the alpha-decay of [243]Am. With the repeated experiments as seen in Fig. 4, we could experimentally investigate the influence of the [239]Pu impurity and correct the measured results to give the data at the point of time when the chemical process was done. The details are described elsewhere[13].

3. Results and Discussion

The present result, which has been corrected with the growth influence of the [239]Pu impurity, is shown in Fig. 5 and is compared with the evaluated cross sections in JENDL-3.2[7] and

Fig. 4 Comparison of the measured data depending on the time
after the chemical purification.

ENDF/B-VI[8], which are broadened by the energy resolution function of the KULS. The experimental uncertainties are considered to be mainly due to (1) the statistical error in fission counts, (2) assignment of fission counts, (3) number of atoms for the ^{243}Am and the ^{235}U deposits, and (4) the reference fission cross section for the ^{235}U(n,f) reaction. Total amount of the experimental uncertainties is 4 to 6 %.

It is seen in Fig. 5 that both of the evaluation data are discrepant each other in the energy regions below 0.3 eV and above 15 eV. Although the ENDF/B-VI data are in general agreement with the present measurement, they are lower at energies between 15 and 60 eV. The JENDL-3.2 data seem to be lower than the measurement in general above 100 eV. At the narrow dip of around 3 eV, one can see discrepancy between the evaluated and the measured data. The reason would be due to the inappropriate resolution function of the lead slowing-down spectrometer.

References

1. D. Lancaster, "Actinide Burning in a Standard Pressurized Water Reactor", Proc. of the Int'l Conf. and Technol. Exposition on Future Nucl. Systems: Global '93", Sept. 12–17, 1993, p.609, ANS, La Grange Park, Illinois, 1993.

2. J. Tommasi, et al., "Long-Lived Waste Transmutation in Reactor", ibid., p.1252, ANS, La Grange Park, Illinois, 1993.

3. V. McLane, et al., "Neutron Cross Sections", Vol.2, Neutron Cross Section Curves, Academic Press, Inc., London, 1988.

4. A. Yamanaka, et al., J. Nucl. Sci. Technol., 36, 863 (1993).

5. K. Kobayashi, S. Yamamoto, et al., "Measurement of Fission Cross Section with Pure Am-241 Sample using Lead Slowing-down Spectrometer", JAERI-Conf 96-008, p.117 (1996).

6. K. Wisshak and F. Kappeler, Nucl. Sci. Eng., 85, 251 (1983).

7. T. Nakagawa, "Evaluation of Nuclear Data for Americium Isotopes", JAERI–M, 89–008 (1989), and J. Nucl. Sci. Technol., Vol.32, 1259 (1995).

8. R. F. Rose (Ed.), "ENDF/B Summary Documentation", BNL–NCS–17541, 4th Ed. (ENDF/B–VI) 1991.

9. K. Kobayashi, et al., "Characteristic Behavior of Neutrons in the Lead Slowing–down Spectrometer Coupled to Electron Linac", JAERI–M 93–046, p.360, JAERI, 1993, and Nucl. Instr. Methods, Phys. Res. A, in print.

10. "MCNP – A General Monte Carlo Code for Neutron and Photon Transport, Version 3A", LA–7396–M, Rev.2, Los Alamos National Laboratory (1986).

11. S. Usuda and N. Kohno, Separation Science and Technology, 23, 1119 (1988).

12. N. Shinohara and N. Kohno, Appl. Radiat. Isot., 40, 41 (1989).

13. T. Kai, K. Kobayashi, et al., "The Influence of Impurities for Cross Section Measurement of ^{241,243}Am(n,f) Reactions", presented in this Symposium.
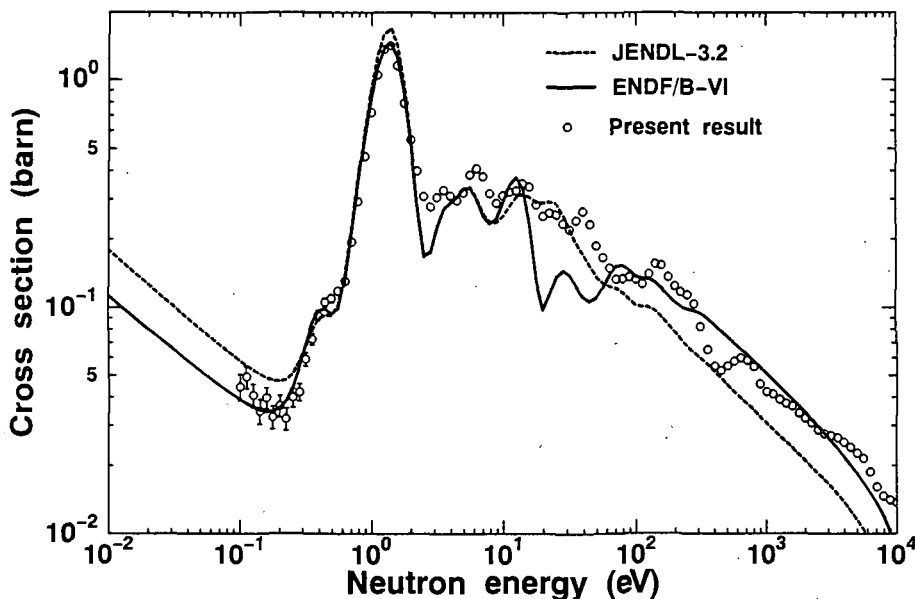
Fig. 5 Comparison of the evaluated fission cross sections of ^{243}Am with the present measurement.

3.20 Quasi-Elastic Cross Sections for 1GeV Proton Incident on ^{4}He and ^{12}C

M.Nishimura[1], T.Nakamoto[1], N.Shigyo[1], K.Iga[1], S.Maruyama[1], K.Maehata[1], K.Ishibashi[1]

S.Meigo[2], H.Takada[2], H.Hirayama[3], S.Ban[3], M.Numajiri[3] and T.Shibata[4]

1. *Department of Nuclear Engineering, Kyushu University*

Hakozaki, Higashi-ku, Fukuoka 812-81, Japan

e-mail: nisimura@kune2a.nucl.kyushu-u.ac.jp

2. *Japan Atomic Energy Research Institute*

Tokai-mura, Naka-gun, Ibaraki 319-11, Japan

3. *National Laboratory for High Energy Physics, KEK*

Oho, Tukuba, Ibaraki 305, Japan

4. *Institute for Nuclear Study, Univ. of Tokyo*

Midorimachi, Tanashi, Tokyo 188, Japan

The experiment of p-n quasi-elastic scattering cross sections was carried out for 1 GeV protons on ^{4}He and ^{12}C. The coincident measurement was made at c.m. angles of $\pm$ 90°. The experiment was simulated by the use of HETC (High Energy Transport Code). It was examined to apply the p-n quasi-elastic scattering cross sections to neutron flux measurement.

1.Introduction

Neutron-incident experimental data are very important for the design of facilities of transmutation for radioactive nuclear wastes and accelerator etc. For this reason, neutron-incident experiments will be performed at wide variety of energies in future. When such experiments were actually carried out, the intensity of incident neutron flux should be obtained exactly. The recoiled-proton spectrometers have usually been used for the measurement of neutron flux. The method requires the n-p elastic scattering cross sections; accumulation of these data is not enough at high energies (~GeV) to give a precise intensity of the neutron flux because of the difficulty of high energy neutron beam experiments. Therefore we examine a method of using the results of nuclear targets bombarded by protons, since the p-n quasi-elastic scattering cross sections are essentially equivalent to those of the n-p elastic scattering at high energies.

2.Experimental methods

If protons with energies of GeV region are incident to symmetric (Z=N) nuclei, the p-n quasi-elastic

scattering cross section is basically the same as the n-p quasi-elastic scattering cross section induced by neutrons. When the proton-incident p-n quasi-elastic scattering cross section is known for the nuclei, it is possible to obtain the neutron flux from the p-n coincident measurement by using the p-n quasi-elastic cross section instead of n-p one, as shown in Fig.1.

The experiments for the p-n cross section were performed at the $\pi 2$ beam line of the 12 GeV proton synchrotron in National Laboratory for High Energy Physics (KEK). The experimental arrangement is illustrated in Fig.2. At the $\pi 2$ beam line, the beam intensity was very weak in a level of 10^5 protons/2.5 sec. The protons came as low intensity pulsed beam and were able to be individually counted one by one. The weakness of the incident beam forced us to make short the length of the flight path between the target and detector. We used ^{12}C and ^{4}He as the symmetric nuclei targets. The reason of selecting these targets is that quasi-elastic scattering events appear more obviously with decreasing number of nucleons. The incident proton beam energy was 1GeV. The energy of emitted particles from the target was determined by time-of-flight (TOF) technic with NE213 liquid scintillators. The size of these scintillators is 12.7 cm thick and 12.7 cm in diameter. The flight path length was 1.25 m (carbon) and 1.0 m (helium). The emitted protons and neutrons from the target were detected in coincidence by NE213 detectors placed in pairs in the direction of 90° in the center of mass system. In front of individual NE213 detectors, NE102A plastic scintillators of 1 cm thick were mounted as veto to distinguish between charged particle events and non-charged particle by the anticoincidence method.

The block diagram of the measurement circuit is shown in Fig.3. Time-to-digital converters (TDCs) were used for measuring the TOF that was given by differences of times between tha start pulse from the coincidence module and the stop pulse from the incident proton beam monitor. The charges of the anode pulses from photomultipliers of the NE213 neutron detectors were branched into two by the signal dividers and were recorded by charge-sensitive analogue-to-digital converters (ADCs).

3.Data analysis

It is very important to perform the pulse-shape discrimination between neutrons and gamma-rays particularly in the short flight path experiment. Since two-gate integration method[1),2),3)] is able to eliminate gamma-ray events to high energy ($\sim$GeV)[4)], this method was useful as shown in Fig.4. The discrimination between high energy protons and pions was made by both the ΔE-E and the two-gate integration method. Fig.5 shows that there is a subtle distinction between protons and pions. The delayed component of scintillation depends on a stopping power of particle. Since a stopping power depends on a velocity in the Bethe equation, the stopping power of proton is equal to that of pion in a rough estimation. However if we take reduced mass and recoil angle into consideration, the energy loss density by proton is slightly different from that by pion. Due to this subtle difference of energy loss densities between protons and pions, these particles are able to be discriminated by the two-gate integration method.

4.Results

A TOF spectrum of quasi-elastic scattering in ^{12}C and ^{4}He is shown in Figs.6 and 7. The quasi-elastic

scattering peak of carbon is less sharp than that of helium. This is ascribed to the fact that the number of nucleon of helium is fewer than that of carbon. We simulated the quasi-elastic scattering spectra by High Energy Transport Code[5] (HETC) and calculated the quasi-elastic scattering cross sections. Table 1 summarizes p-n quasi-elastic scattering cross sections of experiment and HETC calculation. For carbon target, the experimental cross section is good agreement with that of HETC, while it exceeds the calculation results by 30 % for helium. In case of the calculation for ^{4}He, there is a following problem; it does not follow that the density of nucleons is homogeneity in nuclei. The detection system of this experiment enables the error of detection to cancel out in neutron-incident experiments.

5.Conclusion

We confirmed that the quasi-elastic scattering was measured by the experiment of a short flight path length. For helium target, the experimental cross section is disagreement with that of HETC due to the density of nucleons in HETC. In neutron flux measurement, carbon is easier to use as target.

The discrimination between protons and pions with NE213 at high energy region was made successfully by the two-gate integration method.

Acknowledgements

The authors express their gratitude to the beam channel staff of KEK for their cointinuous encouragement and general support of this experiment.

References

1) CHANDLER, K. C. and ARMSTRONG, T. W., *CCC-178*, Radiation Shielding Information Center, Oak Ridge National Laboratory (1977)

2) BELL, Z. W., *Nucl. Instrum. Methods* **188**, 105 (1981)

3) ZUCKER, M. S. and TSOUPAS, N., *Nucl. Instrum. Methods* A **299**, 281 (1990)

4) NAKAMOTO, T., et al., *ISSN 0023-6160* (1995)

5) MOSZYNSKI, M., et al., *Nucl. Instrum. Methods* A **343**, 563 (1994)

Table 1. p-n quasi-elastic scattering cross sections

	experiment (mb/sr)	calculation* (mb/sr)
helium	0.67±0.07** ±0.12***	0.50
carbon	0.69±0.08** ±0.14***	0.67

* calculated by HETC (High Energy Transport Code)
** statistical error
*** efficiency of neutron detection and statistical error
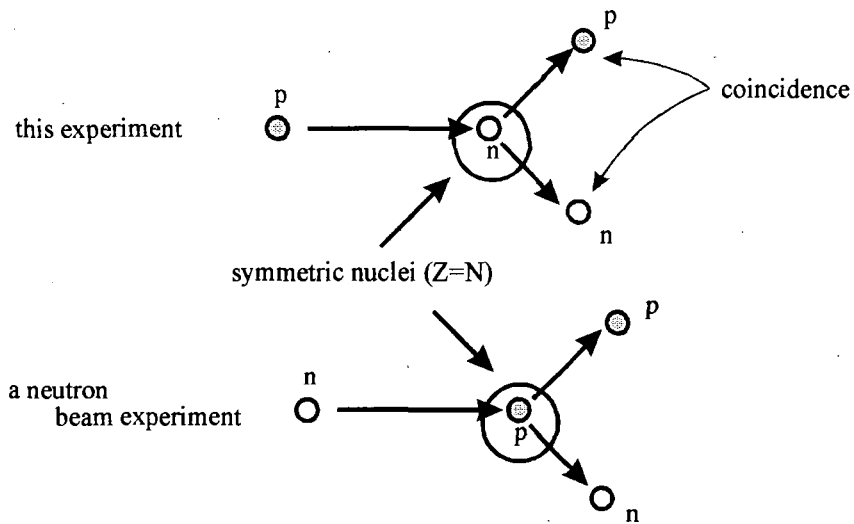
Fig.1   The principle of this experiment. With energies of GeV region, the p-n
        quasi-elastic scattering cross section is basically the same as the n-p
        quasi-elastic scattering cross section induced by neutrons.
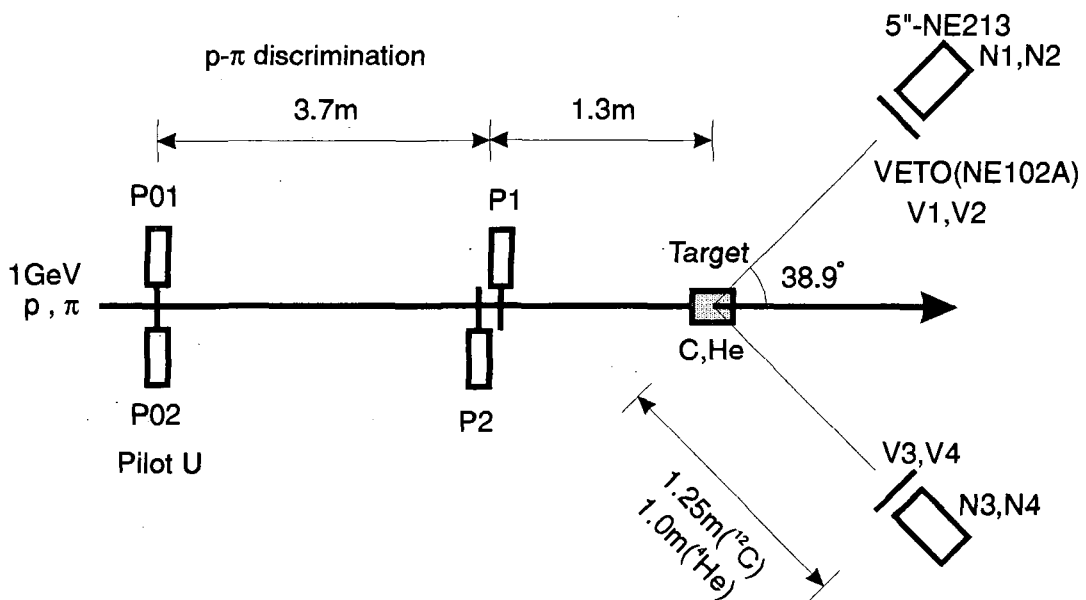
Fig.2 Illustration of the experimental arrangement
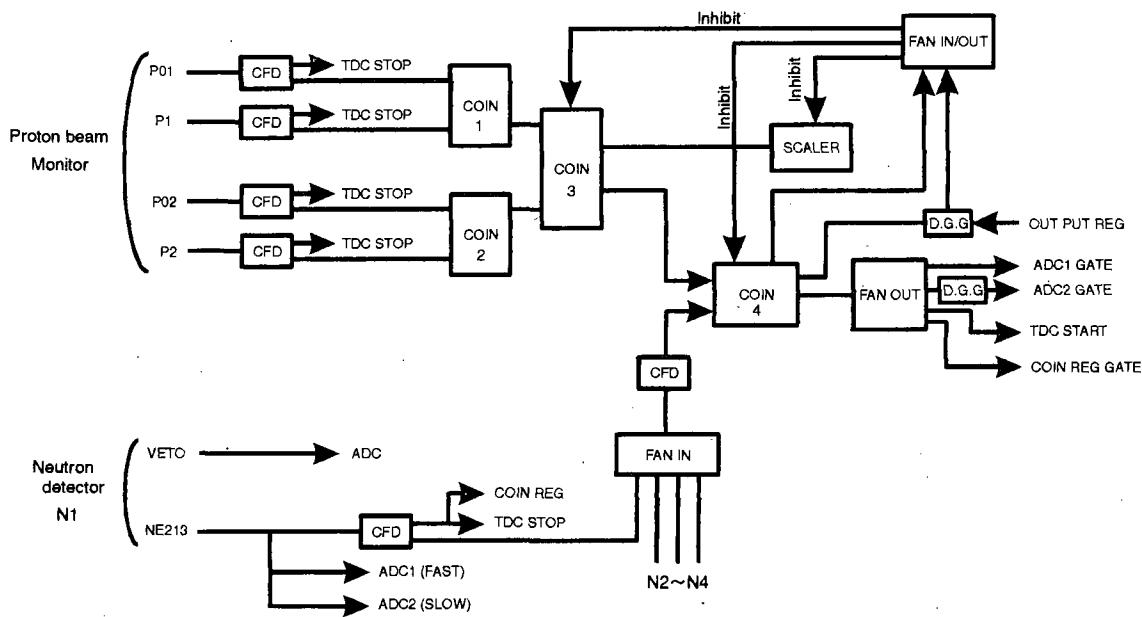
Fig.3 Block diagram of the measurement cicuit
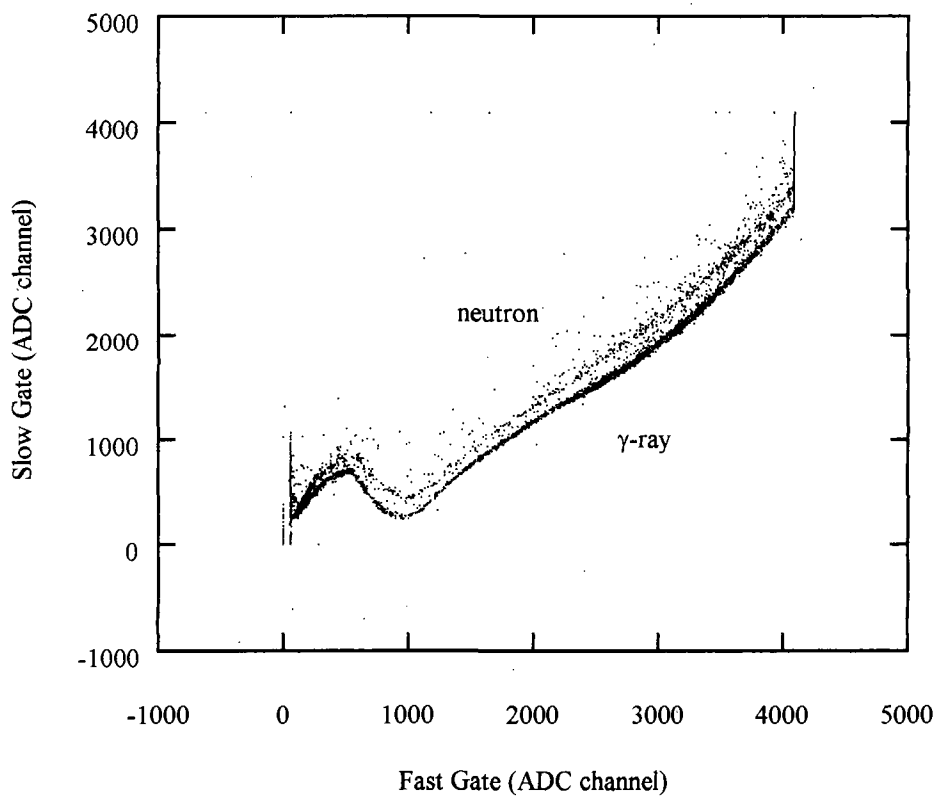
Fig.4 Neutron and gamma-ray pulse-shape discrimination by two-gate integration method
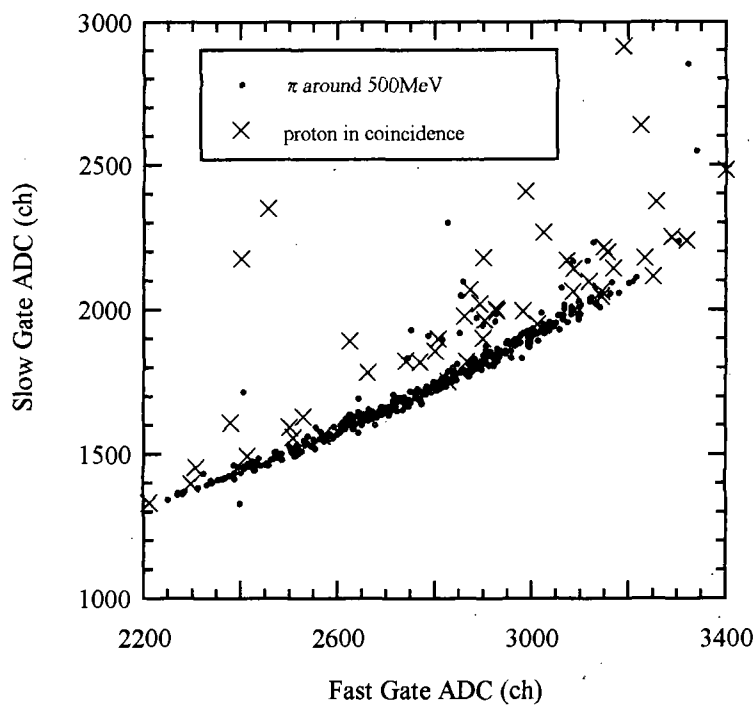
Fig.5 Proton and pion pulse-shape discrimination
by two-gate integration method
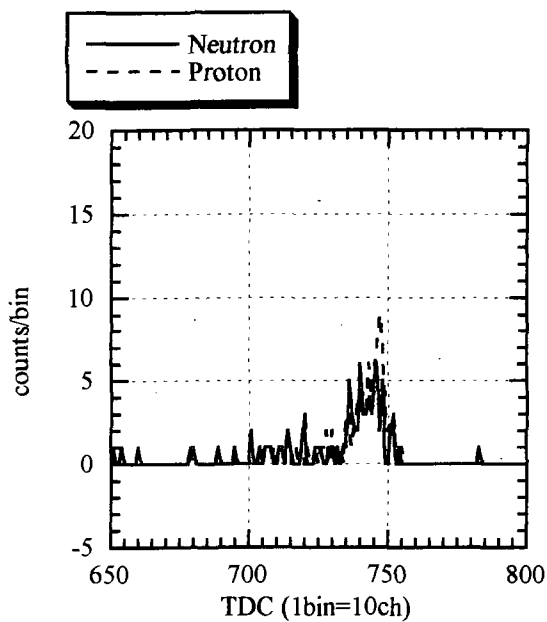
Fig.6 Quasi-elastic scattering spectrum of ^{12}C
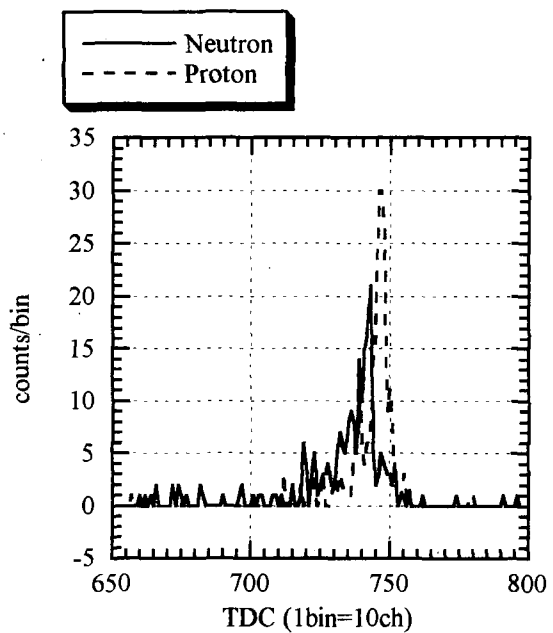
Fig.7 Quasi-elastic scattering spectrum of ^{4}He

3.21   Cross Section Measurement for (n,nα) Reactions by 14 MeV Neutrons

Y. Kasugai, Y.Ikeda, Y. Uno,
*H.Yamamoto, *K. Kawade

Fusion Neutronics Laboratory, Japan Atomic Energy Research Institute
*Department of Energy Engineering and Science, Nagoya University

Nine (n,nα) cross sections for (n,nα) reactions induced by 13.5-14.9 MeV neutrons were measured for ^{51}V, ^{65}Cu, ^{71}Ga, ^{76}Ge, ^{87}Rb, ^{91}Zr, ^{93}Nb, ^{96}Zr and ^{109}Ag isotopes by using Fusion Neutronics Source (FNS) at JAERI. The reactions for 91Zr and 96Zr were measured for the first time. The evaluated data of JENDL-3 and ENDF/B-VI were compared with the present data. Some of the evaluated values are much different from our data by a factor more than ten.

1. Introduction

Activation cross sections of (n,nα) reactions by 14 MeV neutrons have been reported on several target nuclide. In most cases, however, only upper limits of cross sections were given because activities produced via (n,nα) reactions were weak[1]. Recently we can use the HPGe detectors with large efficiency and excellent energy resolution. By using them, it is possible to detect weaker activities than before.

Nine cross sections for (n,nα) reactions induced by 13.5-14.9 MeV neutrons were measured using Fusion Neutronics Source (FNS) at JAERI.   The measured reactions were listed in Table 1 with decay parameters of the products.

2. Experiment

The cross sections were measured by means of the activation method. The sample was sandwiched by Al or Nb foils to measure the neutron flux at a sample position with use of ^{27}Al(n,p)^{27}Mg or ^{93}Nb(n,2n)^{92m}Nb reactions as the standard. The typical neutron flux at the irradiation position was 2.0×10^8 n/cm²·s. If the product was short-lived nuclei, the pneumatic transport system was used for irradiation. The sample and the arrangement of pneumatic tubes is shown in Fig.1. After irradiation, gamma-rays emitted from the irradiated samples were measured with HPGe detectors. The main error sources were due to gamma-ray detection efficiency (2%), the standard reaction cross section of ^{27}Al(n,p)^{27}Mg or ^{93}Nb(n, 2n)^{92m}Nb (3%), and statistics(3-45%).

3. Results

In Fig.2.1-2.9 cross sections measured in this work are shown with the data reported previously and the evaluation data of JENDL-3 and ENDF/B-VI. The cross sections of ^{91}Zr(n,nα)^{87m}Sr, ^{96}Zr(n,nα)^{92}Sr and ^{109}Ag(n,nα)^{105}Rh were measured

for the first time. For the (n,nα) reactions on 71Ga and 93Nb, the partial excitation functions between 13.5 and 14.9 MeV were obtained for the first time by the measurement at multiple neutron energy points. Some of the evaluated values are much different from our data by a factor more than ten.

The cross section data at 14.9 MeV are plotted as functions of the asymmetry parameter (N-Z)/A of the target nucleus and the threshold energy in Fig. 3. No distinct trend can be observed in Fig.3.

4. Conclusion

Nine cross sections for (n,nα) reactions induced by 13.5-14.9 MeV neutrons were measured using Fusion Neutronics Source (FNS) at JAERI. In this work, two cross sections and two partial excitation functions were measured for the first time. There were some extreme differences between the evaluation and our data. We tried to find the systematics of (n,nα) reactions on the basis of our data , but no distinct trend can be observed. More data are needed for a detailed analysis.

References
(1)   S. M. Qaim, Nucl. Phys. A458 (1986) 237.

Table 1   Measured reactions and decay parameters

Reaction	$T_{1/2}$	Eγ(keV)	Iγ(%)	Q(MeV)
51V(n,nα)47Sc	3.34 d	159.4	68±2	-10.68
65Cu(n,nα)61Co	1.65 h	67.6	84.7±0.4	-6.25
71Ga(n,nα)67Cu	2.58 d	184.6	48.6±0.8	-5.47
76Ge(n,nα)72Zn	1.98 d	144.7	83±2.0	-7.83
87Rb(n,nα)83Br	2.38 h	529.7	1.30±0.03	-7.81
91Zr(n,nα)87mSr	2.80 h	388.4	82.3±0.8	-8.09
96Zr(n,nα)92Sr	2.71 h	1384.1	90±10	-4.91
93Nb(n,nα)89mY	16.06 s	909.2	99.14	-5.55
109Ag(n,nα)105Rh	1.47 d	319.2	19.0±0.4	-3.51
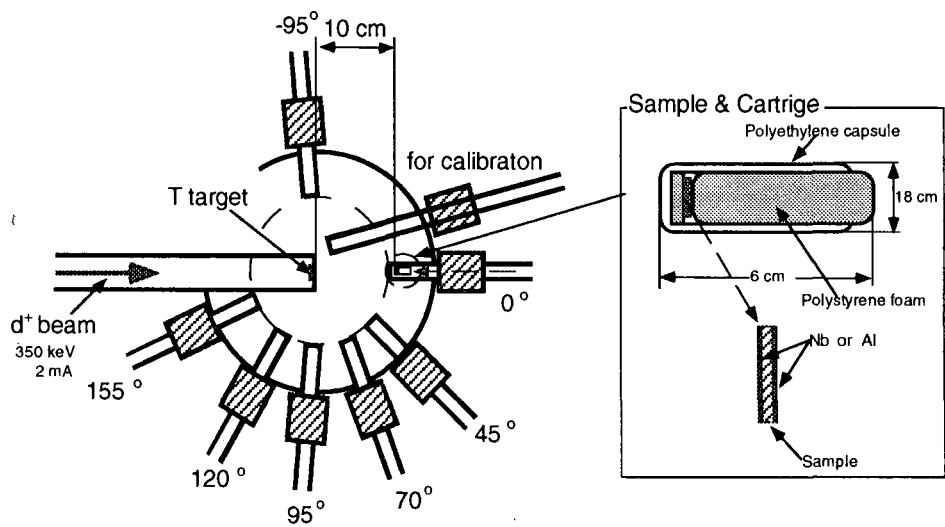
Fig. 1   Arrangement of pneumatic tubes around T-target. Samples are sandwiched between Nb or Al foils, and they are transported to the irradiation position by using the cartrides.
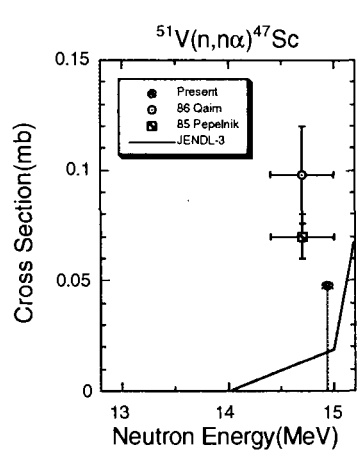
Fig 2.1   Cross section of $^{51}V(n,n\alpha)^{47}Sc$.
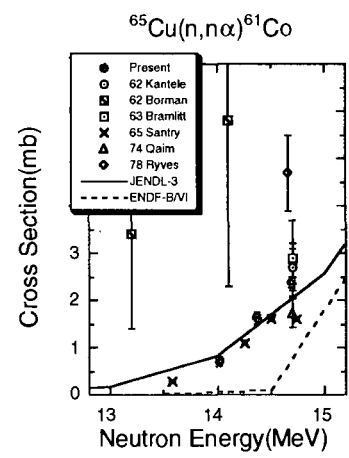
Fig.2.2   Cross section of $^{65}Cu(n,n\alpha)^{61}Co$.
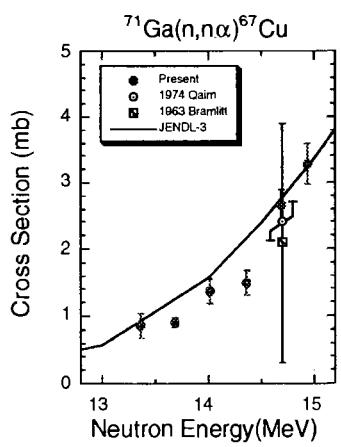
Fig.2.3   Cross section of $^{71}Ga(n,n\alpha)^{67}Cu$.
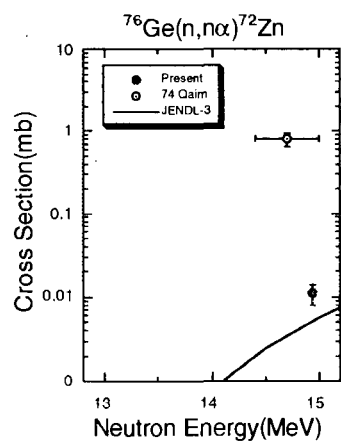
Fig.2.4   Cross section of $^{76}Ge(n,n\alpha)^{72}Zn$
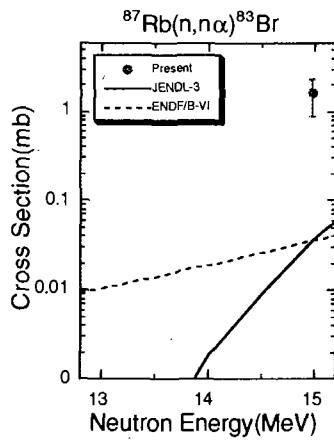
Fig.2.5 Cross section of ^{87}Rb(n,nα)^{83}Br.
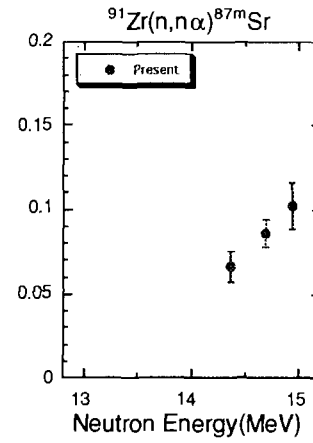
Fig.2.6 Cross section of ^{91}Zr(n,nα)^{87m}Sr.
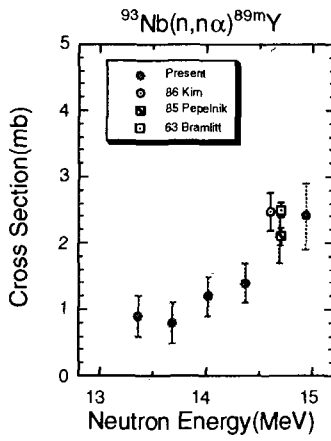
Fig.2.7 Cross section of ^{93}Nb(n,nα)^{89m}Y
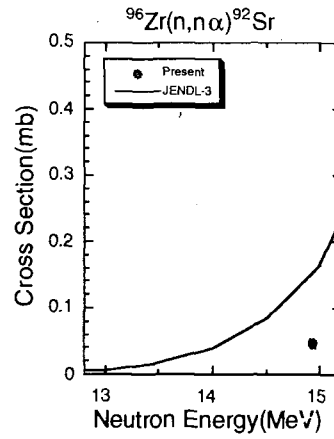
Fig.2.8 Cross section of ^{96}Zr(n,nα)^{92}Sr
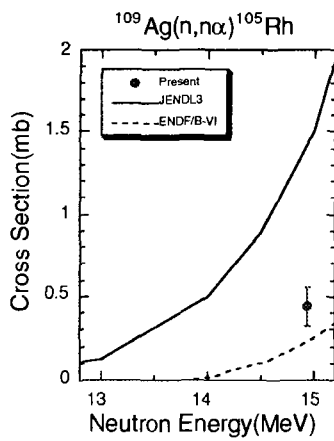
Fig.2.9 Cross section of ^{109}Ag(n,nα)^{105}Rh
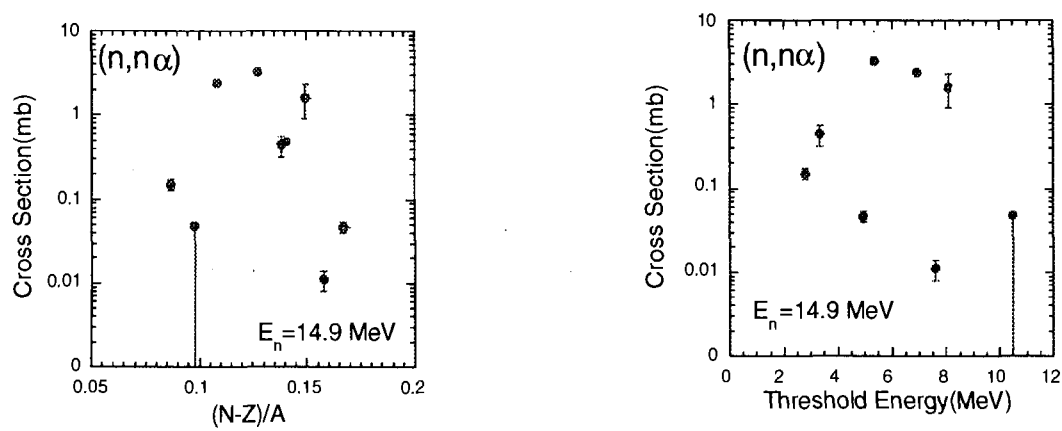
Fig. 3 Syatematics of activation cross sections induced by 14.9 MeV neutrons. The cross sections are plotted as functions of the asynmetry parameter (N-Z)/A of the target nucleus and thereshold energy of the reactions.

3.22 Measurement of Cross Sections Producing Short-lived Nuclei by 14 MeV Neutron -Br, Te, Dy, Ho, Yb-

H.Sakane, T.Matsumoto, T.Iida*, A.Takahashi*, H.Yamamoto and K.Kawade
Department of Energy Engineering and Science, Nagoya University
*Department of Nuclear Engineering, Osaka University
e-mail:h956316m@eds.ecip.nagoya-u.ac.jp

Nine neutron activation cross sections producing the nuclei with half-lives between 2 min and 57 min have been measured at energy range between 13.4 and 14.9 MeV for Br, Te, Dy, Ho, Yb. The cross sections of ^{81}Br(n,p)^{81m}Se, ^{128}Te(n,p)^{128m}Sb, ^{128}Te(n,α)^{125m}Sn, ^{164}Dy(n,p)^{164}Tb, ^{165}Ho(n,α)^{162}Tb, ^{176}Yb(n,p)^{176}Tm were newly obtained at the six energy points between 13.4-14.9 MeV, although the previous results have been obtained at one energy point. ^{79}Br(n,2n)^{78}Br, ^{164}Dy(n,p)^{164}Tb are compared with evaluated data of JENDL-3.2. The evaluations for these reactions agree reasonably well with experimental results. The cross sections of (n,p) reaction are compared with systematics by Kasugai et.al. The systematics agrees with experimental results.

1 Introduction

Neutron activation cross section data around 14 MeV have become important from the view point of fusion reactor technology,especially for calculations on radiation damage,nucleartransmutation,induced activity and so on. However the cross section data have not often been measured in reasonable accuracy,or there are no available data on some reactions because of difficulty in measuring short-lived activities.As a result,the evaluated data will not be unreliable. We have been measuring activation cross sections of short-lived nuclei by 14 MeV neutron at the Intense 14 MeV Neutron Source Facility (OKTAVIAN) of OsakaUniversity. In this work nine cross sections for the (n,2n),(n,p) and (n,α) reaction leading to short-lived nuclei with half-lives between 2 min and 57 min were measured at neutron energy from 13.4-14.9 MeV in a qualified experimental condition.

2 Experimental

Experiment were carried out at OKTAVIAN. A pneumatic transport system was used for the irradiation of sample. The angles of the irradiation potision to the d$^+$ beam were 0°,50°,75°, 105°,125° and 155°, which covered the neutron energies ranging from 14.9 to 13.4 MeV. The distance between the T-target and the irradiation position was 15 cm . When high neutron flux was required , an additional tube set at 0° and at 1.5 cm was set. The induced activity were measured by 12 % and 16 % HPGe detectors. The neutron flux at the irradiation position was measured by using substandard ^{27}Al(n,p)^{27}Mg (T$_{1/2}$=9.462 min) reaction, whose cross sections were determined by refering ^{27}Al(n,α)^{24}Na reaction (ENDF/B-VI). The samples were sandwiched between two

aluminium foils of 10 mm × 10 mm × 0.2 mm thick. The effective energy of incident neutron at the irradiation position was determined by the ratio of the ^{90}Zr(n,2n)^{89}Zr and ^{93}Nb(n,2n)^{92m}Nb cross sections (Nb/Zr method 5)). The error in the neutron energy were estimated to be about 90 keV. Mass separated isotopes and samples of natural abundance were used as samples. Powder samples were wrapped in powder papers (size:10 mm × 10 mm and about 1 mm thick). Measured reactions and decay parameters are listed on Table 1. Correctons were made for time fructuation of neutron flux, thickness of samples, selfabsorption of gamma-ray, sum-peak effect of gamma-ray and contribution of low energy neutrons below 10 MeV. The details of the correction are described eleswhere.[1)2)3)4)] The total errors (δ_t) were described by combining the experimental errors (δ_e) and the errors of nuclear deta (δ_r) in quadratic: $\delta_t^2 = \delta_e^2 + \delta_r^2$.

3 Results

Numerical data table of cross section are given in Table 2 and the example of graphs is given in Fig.1. The cross sections of ^{81}Br(n,p)^{81m}Se, ^{128}Te(n,p)^{128m}Sb, ^{128}Te(n,α)^{125m}Sn, ^{164}Dy(n,p)^{164}Tb, ^{165}Ho(n,α)^{162}Tb, ^{176}Yb(n,p)^{176}Tm were newly obtained at the six energy points between 13.4-14.9 MeV, although the previous results have been obtained at one energy point. ^{79}Br(n,2n)^{78}Br, ^{164}Dy(n,p)^{164}Tb are compared with evaluated data of JENDL-3.2. The evaluations for these reactions agree reasonably well with experimental results. The cross sections of (n,p) reaction are compared with systematics by Kasugai et al[6]. The systematics agrees with experimental results.

4 Conclusion

Nine activation cross sections were obtained. The evaluated data of JENDL-3.2 agree well with experimental results. The systematics by Kasugai et al agrees with experimental results. The systematics predicts the excitation functions around 14 MeV.

References

[1] T.Katoh et al.:JAERI-M 89-083 (1989) (in Japanese)

[2] K.Kawade et al.:JAERI-M 90-171 (1990)

[3] K.Kawade et al.:JAERI-M 92-020 (1992)

[4] K.Kawade et al.:JAERI-M 93-124 (1993)

[5] E.Browne et al.:"Table of Radioactive Isotopes 8th Edition",John Wiley & Sons,New York(1996)

[6] Y.Kasugai et al.: to be published.

Table 1: Reactions and decay parameter[a]

Reaction[b]	$T_{1/2}$	E_γ(keV)	I_γ (%)	Q(MeV) [c]
^{79}Br(n,2n)^{78}Br	6.46(4)m	613.85	13.6(4)	-9.12
^{81}Br(n,p)^{81m}Se	57.28(5)m	102.98	12.7(3)	-0.91
^{128}Te(n,p)^{128m}Sb	10.4(2)m	314.15	89(5)	$\leq$ -3.48
^{128}Te(n,α)^{125m}Sn	9.52(5)m	332.04	97.0(19)	2.42
^{164}Dy(n,p)^{164}Tb	3.0(1)m	168.829	24.0(12)	-3.07
^{165}Ho(n,2n)^{164m}Ho	37.5(10)m	93.99	0.141(15)	-6.01
^{165}Ho(n,2n)^{164g}Ho	29.0(5)m	73.356	1.97(13)	-6.47
^{165}Ho(n,α)^{162}Tb	7.7(2)m	260.080	79(5)	6.51
^{176}Yb(n,p)^{176}Tm	1.9(1)m	189.80	44(4)	-3.12
^{27}Al(n,α)^{24}Na[e]	14.959h	1368.6	99.994(3)	-3.13
^{27}Al(n,p)^{27}Mg[f]	9.46m	843.8	72.0(4)	-1.83

a)taken from ref.5

b)(n,np) means [(n,d)+(n,n'p)+(n,pn)]

c)Q(n,n'p) is given here. Q(n,d)=Q(n,n'p)+2.225 MeV

d)measured by Well type Ge detector

e)Standard reaction(ENDF/B-VI) used in this work

f)Secondary conventional reaction used for short-lived nuclei
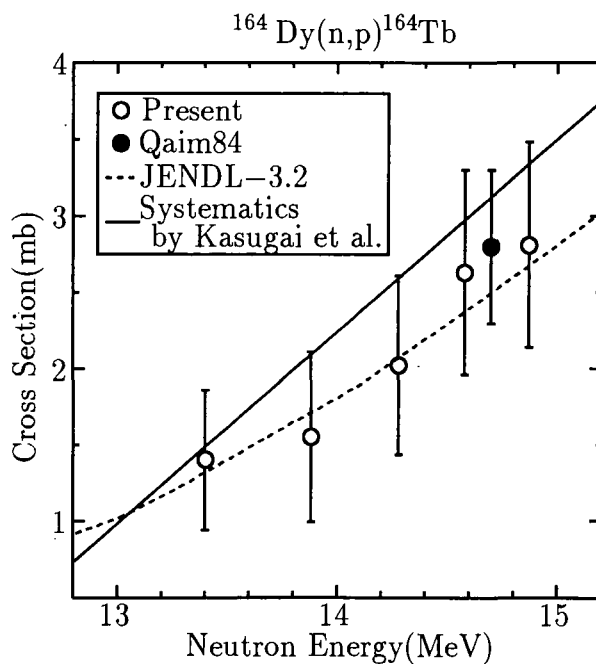
Fig.1 Cross section ^{164}Dy(n,p)^{164}Tb(3.0 min)

Table 2: Activation cross sections of short-lived nuclei

^{79}Br(n,2n)^{79}Br (6.46m)

En(MeV)	σ (mb)	δ e(%)	δr (%)	δt (%)
14.87	987.20	3.70	4.20	5.60
14.58	871.37	3.65	4.20	5.57
14.28	853.71	3.66	4.20	5.57
13.88	877.50	3.62	4.20	5.55
13.65	797.92	3.66	4.20	5.57
13.40	723.48	3.69	4.20	5.59

^{81}Br(n,p)^{81m}Se(57.28m)

En(MeV)	σ (mb)	δe (%)	δr (%)	δt (%)
14.87	10.6	18.2	3.82	18.6
14.58	7.19	12.7	3.82	13.3
14.28				
13.88				
13.65	5.60	30.3	3.82	30.5
13.40	1.83	55.1	3.82	55.3

^{128}Te(n,p)^{128m}Sb(10.4m)

En(MeV)	σ (mb)	δ e(%)	δ r(%)	δ t(%)
14.87	1.14	5.9	4.9	7.7
14.58	1.06	6.0	4.9	7.7
14.28	1.05	6.7	4.9	8.3
13.88	0.58	8.9	6.8	11
13.65	0.44	22	5.9	23
13.40	0.55	15	5.9	16

^{128}Te(n,α)^{125m}Sn(9.52m)

En(MeV)	σ (mb)	δ e(%)	δ r(%)	δ t(%)
14.87	0.56	14	3.6	14
14.58	0.42	24	3.6	24
14.28	0.56	20	3.6	20
13.88	0.49	9.8	3.6	10
13.65	0.40	17	3.6	18
13.40	0.36	17	3.6	17

^{164}Dy(n,p)^{164}Tb(3.0m)

En(MeV)	σ (mb)	δ e(%)	δ r(%)	δ t(%)
14.87	2.81	24	6.0	25
14.58	2.63	30	6.0	31
14.28	2.02	28	7.1	29
13.88	1.55	35	7.1	36
13.65				
13.40	1.40	32	7.1	33

^{165}Ho(n,2n)^{165m}Ho(37.5m)

En(MeV)	σ (mb)	δ e(%)	δ r(%)	δ t(%)
14.87	1129.69	7.58	11.8	14.0
14.58	1051.04	7.44	11.8	13.9
14.28	981.43	8.45	11.8	14.5
13.88	949.89	7.34	11.8	13.9
13.65	947.14	7.56	11.8	14.0
13.40	941.29	8.70	11.8	14.6

^{165}Ho(n,2n)^{165g}Ho(29.0m)

En(MeV)	σ (mb)	δ e(%)	δ r(%)	δ t(%)
14.87	689.50	5.97	7.91	9.91
14.58	619.48	5.87	7.91	9.84
14.28	733.47	6.00	7.91	9.92
13.88	702.01	5.95	7.91	9.90
13.65	724.50	6.25	7.91	10.1
13.40	720.06	5.85	7.91	9.84

^{165}Ho(n,α)^{162}Tb(7.7m)

En(MeV)	σ (mb)	δ e(%)	δ r(%)	δ t(%)
14.87	0.90	15.0	5.19	15.8
14.58	0.86	14.6	5.19	15.5
14.28	0.82	17.1	5.19	17.9
13.88	0.78	14.5	5.19	15.4
13.65	0.81	14.9	5.19	15.8
13.40	0.60	17.4	5.19	18.2

^{176}Yb(n,p)^{176}Tm(1.9m)

En(MeV)	σ (mb)	δ e(%)	δ r(%)	δ t(%)
14.87	1.82	29.1	10.5	31.1
14.58	1.74	36.0	10.9	37.7
14.28				
13.88	1.48	26.2	10.9	28.4
13.65				
13.40	1.35	37.5	10.9	39.1

3.23 Systematic Measurement of Beta-decay Half-lives of Short-lived Isotopes

T. Hirose, H. Yamamoto, T. Iida*, A. Takahashi*, Y. Kasugai**, Y. Ikeda**
and K. Kawade
Department of Energy Engineering and Science, Nagoya University
Furo-cho, Chikusa-ku, Nagoya, 464-01, Japan
*Department of Nuclear Engineering, Osaka University
Yamadaoka, Suita-shi, Osaka, 565, Japan
**Japan Atomic Energy Research Institute
Tokai-mura, Naka-gun, Ibaraki-ken, 319-11, Japan

e-mail:h966425m@eds.ecip.nagoya-u.ac.jp

Abstract

We have measured the half-lives of short-lived isotopes for past decade and deduced the half-lives of 6 isotopes further. These results demonstrated that most of the literature values shorter than 10 min systematically deviated from our measurement ones. The cause seems to be that a large number of the previous half-life studies were performed with scintillation counters before 1970 and they had a difficulty in distinguishing the interest γ-ray from the contamination and correcting for pile-up and dead-time losses. Moreover, the deviated data found to be quoted for evaluation.

1 Introduction

The half-life of β-decay is one of the most fundamental constants on radioisotopes. In the activation cross section measurement, the uncertainty brings a strong effect to the result and it is required that the values are determined precisely and reliably. The literature values, however, have large uncertainties and sometimes show the substantial discrepancies exceeding the individual uncertainties. This leads to two assumptions as follows. The one is due to contamination. In the investigations with GM counters, proportional counters, ionization chambers and scintillation counters, it is difficult to distinguish the interest activity from the interference derived from impurities or competing reactions. The second is the influence of pile-up and dead-time losses. In the case of short half-life investigations, it is likely to detect the intense activities so as to attain good statistics during the short period. The counting losses increase as the counting rates become higher. If the correction for such losses is not enough, the decay curve will show

a longer half-life compared with the true value since more counts are lost initially than later.

We have measured the half-lives of short-lived nuclides with HPGe detectors for past decade by applying the plausible correction method for counting losses, which combined the source and constant-pulser methods. We have already recognized that most of the previous values shorter than 10 min were systematically longer than our experimental ones. We deduced the half-lives of 6 isotopes further (^{23}Ne, ^{50}Sc, ^{54}V, ^{75m}Ge, ^{77m}Se and ^{84m}Rb), and examined the details about those discrepancies.

2 Experiment and results

Sources of ^{23}Ne, ^{50}Sc, ^{54}V and ^{84m}Rb were produced by 14 MeV neutron bombardments at the intense 14 MeV neutron generator of Osaka University (OKTAVIAN) and the facility of Fusion Neutronics Source of JAERI (FNS). The samples of ^{75m}Ge and ^{77m}Se were activated in the TRIGA-II reactor of Rikkyo University. The γ-rays were detected with ORTEC 22 % HPGe detector in the spectrum multi-scaling mode. We utilized a High-rate spectroscopy amplifier for high counting rates. Decay was followed for about 10 times the half-life at equal intervals of 1/3 of half-life. A long-lived γ source and a constant-pulser were simultaneously measured together with the short-lived activity to correct for the pile-up and the dead-time losses (source method, pulser method).

A γ-ray spectrum and a decay curve of ^{75m}Ge are shown in Figs. 1 and 2, respectively. The results of all isotopes are summarized in Table 1 together with production reactions, energy of γ-rays, measured and evaluated values [1, 2] and the results of ^{75m}Ge and ^{84m}Rb are compared with the previous works in Figs. 3 and 4. The half-life values were deduced with accuracy of 0.15–0.75 % and indicated the same tendency as we expected (Fig. 5).

3 Discussion

We examined the details of these discrepancies. The literature and evaluated data are taken from ref. [1–3].

3.1 Year and detector

Figs. 6 and 7 show the dependence of these deviations on the reported year and the employed detector. It is apparent that the works before 1970 showed larger discrepancies. In this period, half-life measurements were dominantly performed with the scintillation counters, with which it is hard to identify only the interest γ-ray because of the poor resolution and to compensate for pile-up and dead-time losses. In fact, the works in

conjunction with this apparatus were in disagreement with our results as depicted in Fig. 7. On the other hand, the studies after 1970 agreed with our experimental ones reasonably and this is consistent with the fact that the works with Ge(Li) detectors, which have been widely used in the latter half of 1960's, were in better agreement with ours (Fig. 6). Some values shorter than 2 min, however, deviated and this might be due to insufficient corrections for counting losses.

3.2 Evaluated values

The remarkable deviations for evaluated values shorter than 2 min and the deviations of about 2 % in the vicinity of 4 min were seen in Fig. 8. The cause results from that the deviated values were adopted into evaluated ones directly, which were obtained with the scintillation counters before 1970 and/or reported by the specific authors given in Table 2, by whom the half-life values differed noticeably, or the mean values between the deviated and agreeable data were used as evaluated values. It is concluded that the reference data contain a serious source in both cases, while the latter have the problem in the way of evaluation.

4 Summary

Not only the literature values but also evaluated ones have been found to deviate. We emphasize that it is necessary to re-determine and re-evaluate the half-lives of short-lived isotopes with proper method.

References

[1] R. B. Firestone and V. S. Shirley, *Table of Isotopes 8th Ed.*, (1996) John Wiley & Sons, New York

[2] Nuclear Data Sheets

[3] C. M. Lederer and V. S. Shirley, *Table of Isotopes 7th Ed.*, (1978) John Wiley & Sons, New York

[4] J. O. Elliot and F. C. Young, Nucl. Sci. and Eng. 5 (1959) 55

[5] R. G. Wille and R. W. Fink, Phys. Rev. 118 (1960) 242

[6] S. Malmskog and J. Konijin, Nucl. Phys. 38 (1962) 196

[7] H. P. Yule, Nucl. Phys. A94 (1967) 442

[8] T. E. Ward, P. H. Pile and P. K. Kuroda, Nucl. Phys. A134 (1969) 60

[9] B. Ehrenberg and S. Amiel, Phys. Rev. C6 (1972) 618

Table 1: Results of half-life measurement.

Nuclide	Production reaction	Energy [keV]	Number of measurement	Half-life Present	Half-life Evaluated[a]
^{23}Ne	^{23}Na(n,p)	440	7	37.25(16) s	37.24(12) s
^{50}Sc	^{50}Ti(n,p)	1121	3	100.4(4) s	102.5(5) s
^{54}V	^{54}Cr(n,p)	835	5	48.4(3) s	49.8(5) s
^{75m}Ge	^{74}Ge(n,γ)	140	4	47.29(12) s	47.7(5) s
^{77m}Se	^{76}Se(n,γ)	162	5	17.29(13) s	17.36(5) s
^{84m}Rb	^{85}Rb(n,2n)	248	3	20.28(3) m	20.26(4) m

a) Taken from ref. [1, 2].

Table 2: The authors whose works remarkably deviated from our experimental results. The nuclides whose half-life values were used as reference for evaluation in Nuclear Data Sheets are emphasized.

Author[a]	Detector	Nuclides shown deviations
J. O. Elliot et al.	NaI(Tl)	^{16}N, ^{28}Al, ^{37}S, ^{104m}Rh
R. G. Wille et al.	Proportional Counter	^{138g}Cs, ^{139m}Ce, ^{161}Gd, ^{174}Tm
S. Malmskog et al.	NaI(Tl)	^{16}N, ^{19}O, ^{20}F, ^{28}Al, ^{77m}Se
H. P. Yule	NaI(Tl)	^{19}O, ^{20}F, ^{23}Ne, ^{77m}Se, ^{86m}Rb, ^{89m}Y
T. E. Ward et al.	Ge(Li)	^{53}V, ^{63}Co
B. Ehrenberg et al.	Proportional Counter	^{138g}Cs, ^{139}Ba

a) Taken from ref. [4–9].
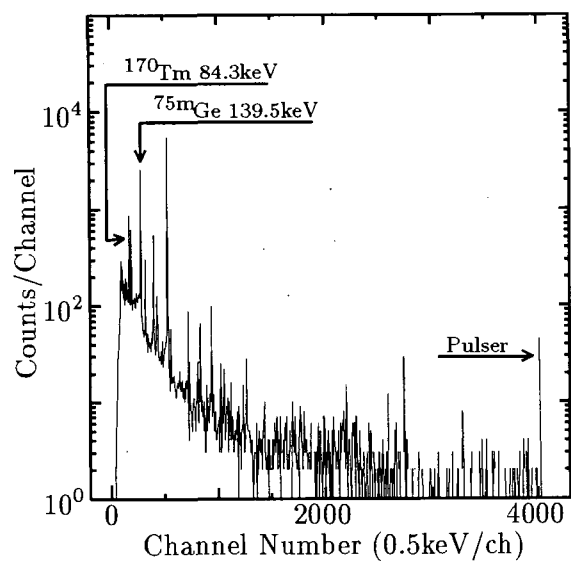
Fig. 1: Gamma-ray spectrum in the decay of ^{75m}Ge.
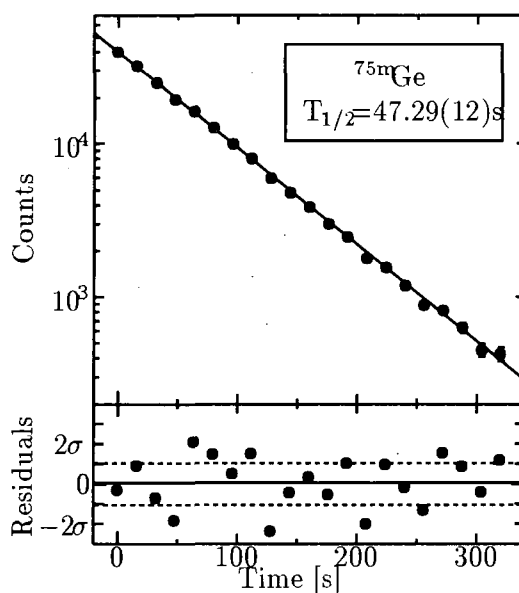
Fig. 2: Decay curve of ^{75m}Ge and residuals from a least squares fitting curve.
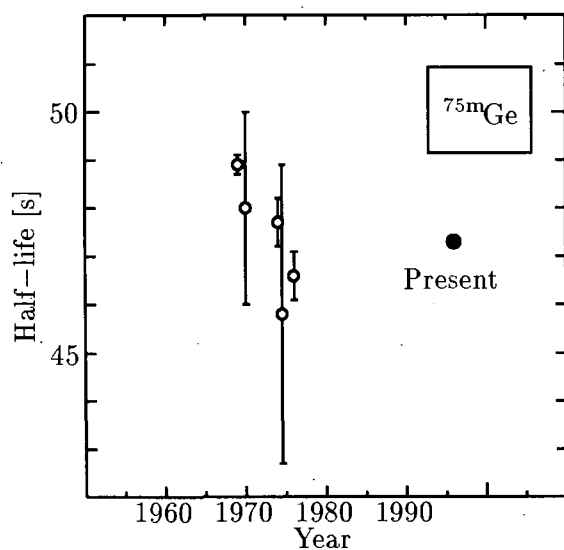
Fig. 3: Result of ^{75m}Ge and comparison with the previous works.
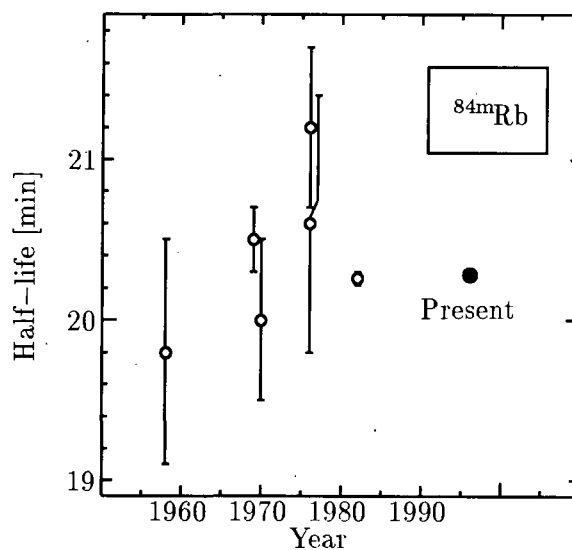
Fig. 4: Result of ^{84m}Rb and comparison with the previous works.
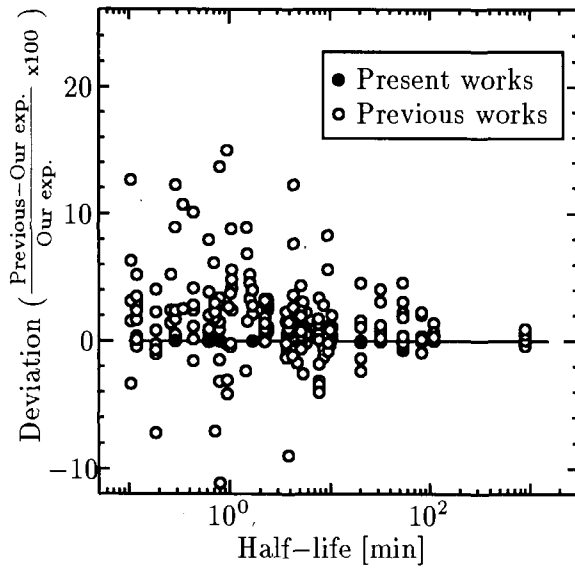
Fig. 5: Relative deviations of previous works from our experimental ones. Most of the previous values shorter than 10 min were systematically longer.
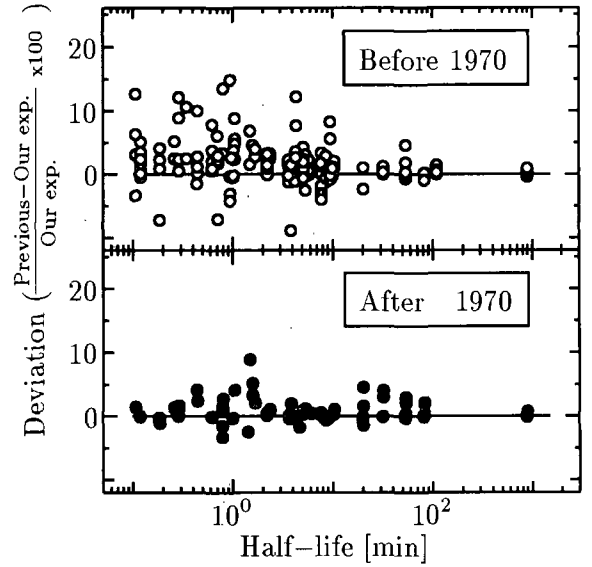
Fig. 6: Dependence of the deviations on reported year. The upper and lower parts show the deviations of works before 1970 and after 1970, respectively.
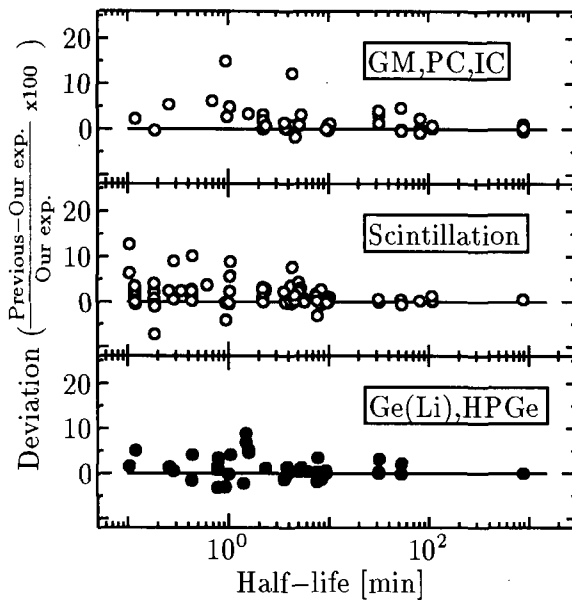
Fig. 7: Dependence of the deviations on employed detector. Upper: GM counters, Proportional counters(PC) and Ionization chambers(IC). Middle: Scintillation counters. Lower: Ge(Li) and HPGe detectors.
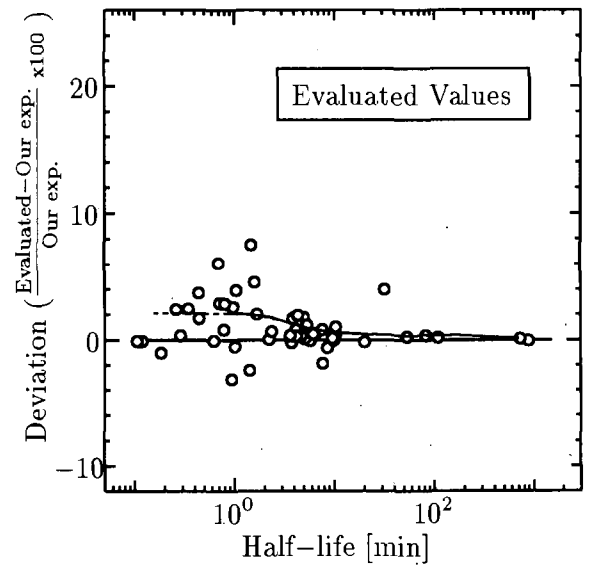
Fig. 8: Relative deviations of evaluated values from our measurement ones. The tendency of evaluated values corresponds with that of the previous ones.

3.24 Double Differential Charged Particle Emission Cross Sections of Vanadium for 14.1 MeV Incident Neutrons

Kokooo, Isao Murata and Akito Takahashi
Department of Nuclear Engineering, Osaka University
Yamadaoka 2-1, Suita, Osaka 565, Japan

The double differential cross sections of V(n,xp) and V(n,x α) reactions have been measured by using the E-TOF spectrometer. The measured data were compared with other experimental data and evaluated nuclear data of JENDL Fusion-File.

1. Introduction

The double differential cross sections of charged particle emission reactions induced by 14.1 MeV incident neutrons are important for evaluating nuclear heating and material damages in D-T fusion devices. Until now only a few data have been measured worldwide because of experimental difficulties in high backgrounds and low counting rates. Vanadium has high potential as an element of structural materials for fusion power reactors because of its very low activation property by fast neutrons and favorable balance between neutron absorption and multiplication reactions. In the present experiment, the DDX data for vanadium were measured at emission angles of 30° , 70° and 120° for the ^{51}V(n,xp) reaction and at 70° for the ^{51}V(n,x α) reaction.

2. Experimental

2.1. Experimental procedure

The DDXs of vanadium have been measured at 14.1 MeV incident neutrons by using the charged particle spectrometer[1] with 3 ns pulsed D-T neutron source of OKTAVIAN, the Intense 14 MeV Neutron Source Facility of Osaka University. This spectrometer is based on the two dimensional analysis of energy and time-of-flight spectra, combined with the pulse shape discrimination technique. The CsI(Tl) scintillater, 2mm in thickness and 5 cm in diameter, is used as charged particle detector because of its good performance in pulse shape discrimination. The two-dimensional E-TOF analysis for charged particles is based on the following equation,

$$T = d \sqrt{\frac{m}{2E}}$$

where, T = the time-of-flight,

      d = the flight path,

      E = the energy of the emitted particle and

      m = the mass of the particle.

According to the above equation, the graph of energy and time-of-flight can be drawn as shown in Fig.1.

2.2. Charged Particle Spectrometer

      The schematic diagram of the charged particle spectrometer is shown in Fig.2. The spectrometer is arranged in the vacuum chamber of 1 m Φ $\times$ 1 m . The chamber is kept at the pressure of about 1.3 Pa. The target is positioned in a stainless steal through-tube and out of the vacuum chamber. The backgrounds were reduced by the pulse shape discrimination technique and the iron + lead + polyethylene shielding set. The detector is placed inside the hole of lead shield. An example of two dimensional energy-rise-time distributions of α, p and γ, by using CsI(Tl) detector is shown in Fig.3. The proton reference source is obtained by bombarding the polyethylene sample by D-T neutrons and independently ^{241}Am is used as the α reference source. It can be seen that the contours of α, p and γ were well separated each other. Therefore, we can eliminate obstructive backgrounds and choose a contour of either alpha particle or proton.

      The spectrometer can be used to measure the DDX data for the emission angle between 30° and 135° . The flight path varied from 32.0 cm to 56.7 cm according to the change of emission angle. The sample position for various scattering angle can be seen in Fig.4. The vanadium samples of 10 μ m and 25 μ m thickness have been used in proton and α measurement, respectively. The diameter of the sample is 6 cm.

2.3. Data Acquisition System

      The block diagram of the measuring system is shown in Fig.5. The two dimensional data acquisition has been done by using the pulse height of dynode signal corresponding to energy and the time-of-flight signal. The time-of-flight signal is created by the time to pulse height converter using the fast signals of anode as start signal and the stop signal(with delay) from the beam pick up ring. The logic signal created by pulse shape discrimination circuit has been used as the gate signal for two-dimensional acquisition. The NE213 detector was used as relative source neutron flux monitor. The TOF-gated method in coincidence with the signal of pulse shape discriminator has been used to count only 14 MeV neutrons by pulsed deuteron beams..

3. Results

3.1. Data Analysis

      The net raw data have been deduced by subtracting the background data from the

foreground data. The background run has been done by removing the sample. In Fig.6, the net raw data spectrum of protons for a CH₂ sample at the emission angle of 45° is shown as an example. The integral counts of respective charged particle for each energy channel, namely the net pulse height spectrum, have been measured by properly choosing the region of interest within the corresponding contour of the net raw data spectrum. From Fig.6, it can be seen that the obstructive backgrounds can be eliminated by selecting the appropriate region of interest.

The DDX, $\sigma(E, \theta)$ barn/sr/MeV can be obtained from the net pulse height spectrum by using the following equation,

$$\sigma(E,\theta) = \frac{R(E)f_p}{\phi \cdot N \cdot S_d}$$

where,　$R(E)$　= the net count rate per unit energy,

f_p　= the flight path,

ϕ　= the neutron flux at the sample,

N　= the atomic number density of the sample and

S_d　= the area of the detector.

In the present experiment, the ADX data of H(n,p) reaction for CH₂ sample, 2.5 cm diameter and 18 μ m thickness, were used as the reference for the cross section normalization. Therefore, the new expression can be deduced from the above and it becomes,

$$\sigma(E,\theta) = \sigma_r(\theta) \cdot \frac{R(E)}{\int R_r(E)dE}$$

where,　$\sigma_r(\theta)$ = the reference cross section of the H(n,p) reaction for the same incident energy and

$R_r(E)$ = the net count rate per unit energy for the reference cross section measurement.

In the proton measurement, the energy calibration constants were estimated by doing three measurements for CH₂ sample at the emission angles of 30° , 45°　and 60°　respectively. The proton energy of the respective angle has been measured by the equation,

$$E_p = E_n \cos^2 \theta$$

where,　E_p =　the emitted proton energy,

E_n =　the incident neutron energy and

θ =　the emission angle.

In the case of α measurement, the [241]Am standard source and two Al foils of 5 μ m and 10 μ m thickness have been used to measure the calibration constants. A research pulser has been used to determine the zero-energy channel in the pulse height analyzer

3.2. Data Correction

The raw data must be corrected because the broadening functions of angular resolution and the energy loss of the charged particle in the sample were not negligible. The Monte Carlo

simulation with the JENDL Fusion-File cross section data were used to obtain the correction factors for every angle point. The block diagram of data correction method is shown in Fig.7. The correction factor for the emission angle of 70° is shown in Fig.8. The comparison among the Monte Carlo simulation, the evaluated data and the experimental data can be seen in Fig.9. In Fig.10, the comparison of corrected data and uncorrected data are shown.

3.3. Results and Discussions

The experimental results of DDX of the ^{51}V(n,xp) reaction at the emission angle of 70° compared with the JENDL Fusion-File and Grimes' experimental data[2] are shown in Fig.11. It can be seen that the three data are in good agreement in each other. The experimental result of DDX$_p$ compared with the JENDL Fusion-File data for the emission angle of 30° is shown in Fig.12. For the proton DDXs, JENDL-FF can well reproduce each experimental result.

In Fig.13, the DDX $_\alpha$ data of the experiment and JENDL fusion-file for the emission angle of 70° are shown. In the present experiment, the DDXs of the ^{51}V(n,x α) reaction were very difficult to measure because of very small reaction cross section values. In the measured spectrum, there exists therefore large statistical errors. However, a fairly good agreement between the present result and JENDL-FF was obtained.

4. Summary

The double differential cross sections of ^{51}V(n,xp) and ^{51}V(n,x α) have been measured at the emission angles of 30° , 70° and 120° in the case of proton and at 70° in the case of α, respectively. The experimental data have been compared with other experimental data and evaluated data of JENDL fusion-file. The data were in good agreements in each other.

References:

(1)S.Ogino, et. al., "Development of Neutron Induced Secondary Charged Particle Spectrometer Based on Two-dimensional E-TOF Analysis", OKTAVIAN Rep., A-91-01(1991).

(2)S.M. Grimes, et al., Phys. Rev., C17,508(1978)
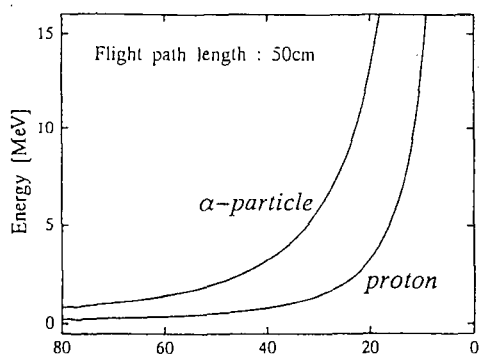
Fig.1 The ideal energy and time-of-flight spectrum
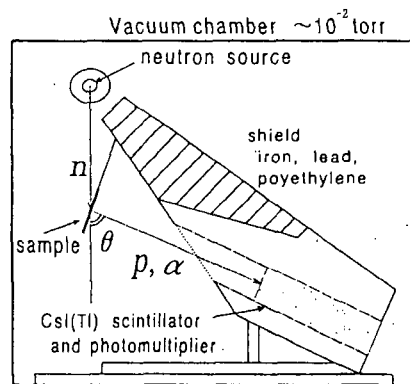
Fig.2 Schematic diagram of charged particle spectrometer
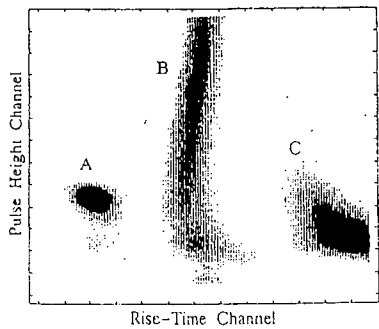
Fig.3 The two dimensional energy-
rise time distribution

A=α spectrum, B=p spectrm

C=γ spectrum
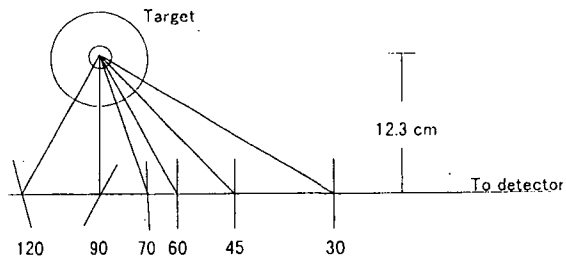
Fig.4 The sample position for the various
scattering angle.
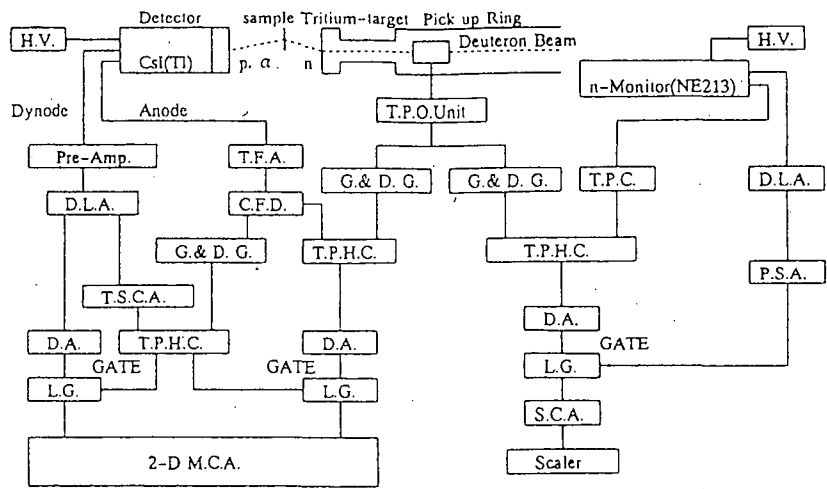
Fig.5 The block diagram of data acquisition system
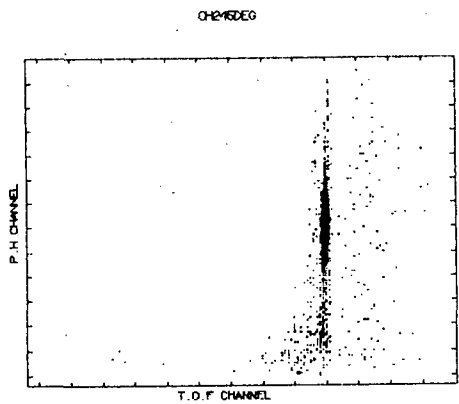
Fig.6 The net raw data of CH₂ sample
at 45 degree
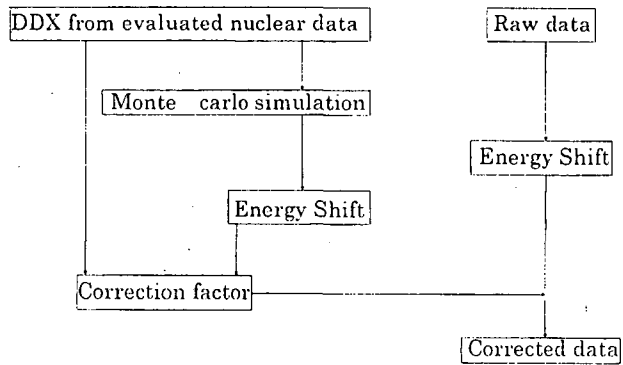
Fig.7 The block diagram of data correction method
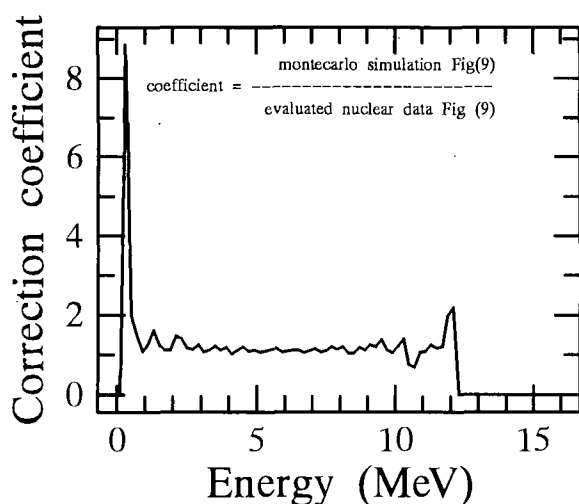
Fig.8 The correction coefficient for V(n,p) reaction
at 70 degree
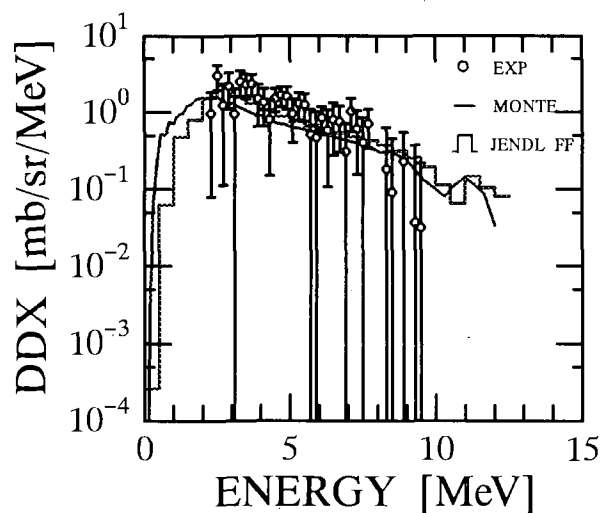
Fig.9 The comparison among the experiment
monte—carlo simulation and JENDL FF
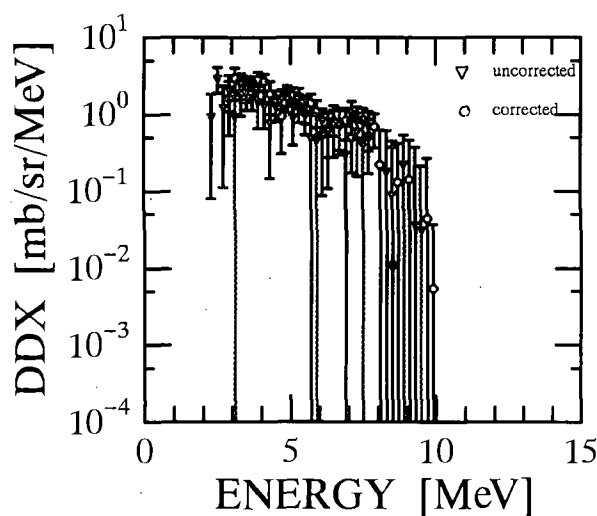
Fig.10 The comparison between corrected data

and uncorrected data
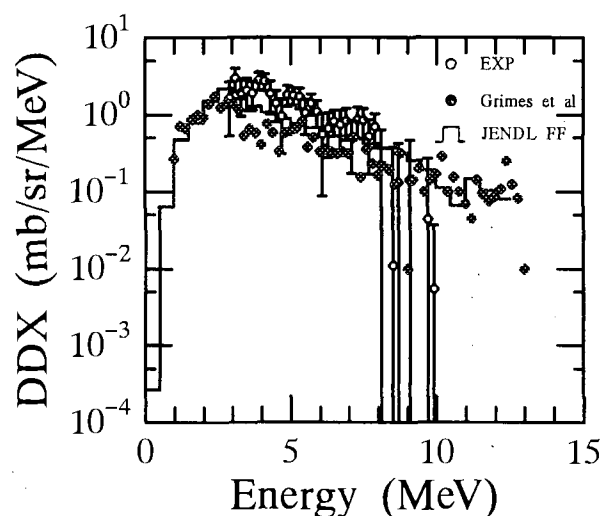
Fig.11 The DDX for V(n,xp) reaction at 70 degree
compared with JENDL FF Grimes et al.
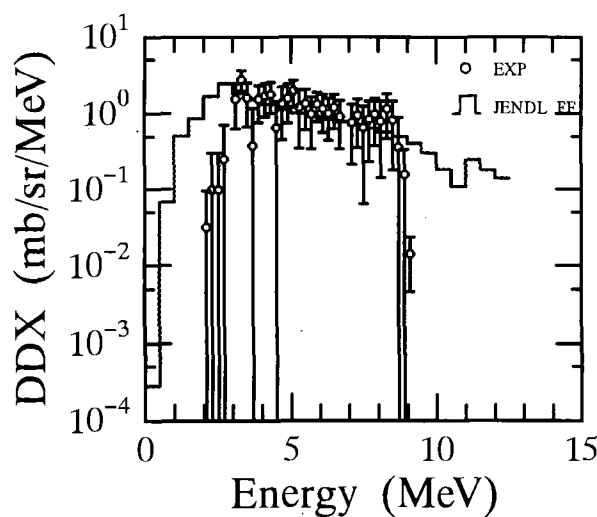
Fig.12 The DDX of proton emission reaction
at 30 deg
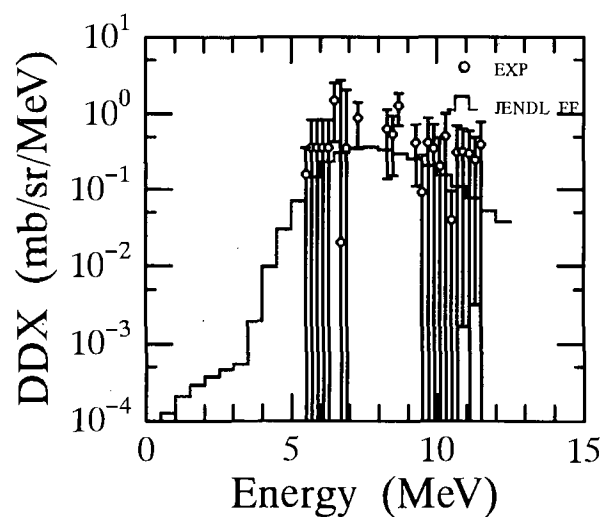
Fig.13 The DDX of alpha emission reaction
at 70 degree

3.25 Direct Neutron Capture in a Dispersion Potential of Light Nuclei

Hideo KITAZAWA

Department of Energy Sciences, Interdisciplinary Graduate School of Science and Engineering, Tokyo Institute of Technology, 4259 Nagatsuta-cho, Midori-ku, Yokohama 226, Japan (e-mail:kitazawa@es.titech.ac.jp)

Masayuki IGASHIRA

Research Laboratory for Nuclear Reactors, Tokyo Institute of Technology, 2-12-1 O-okayama, Meguro-ku, Tokyo 152, Japan

Yoshiko HARIMA

CRC Research Institute, Inc., 2-7-5 Minamisuna, Koto-ku, Tokyo 136, Japan

A paper on this subject was presented at 9th International Symposium on Capture Gamma-Ray Spectroscopy and Related Topics, Budapest, Hungary, 8-12 October 1996 with the following abstract:

Low-energy neutron capture reactions on light nuclei are supposed to play an important role in the nucleosynthesis of intermediate-mass nuclei in an inhomogeneous big-bang model and in that of heavy elements during steller evolution. Also, drip-line light nuclei are found to have a radius much larger than other neighboring nuclei. It suggests the existence of a neutron-halo structure in those nuclei.

Stimulated by the above findings, a lot of experimental work has recently been performed to obtain neutron-capture cross sections of light nuclei in the steller energy region. Simultaneously, those cross sections have been calculated in the framework of a direct-capture model, because the reactions may be decoupled from resonance states. Consequently a reasonable agreement was found between theory and experiment. However, the results do not guarantee that the optical-potential parameters used in the calculations reproduce the observed total cross sections in this energy region.

The direct-capture cross section is generally sensitive to the incident wave function in the channel region, i.e. to optical-potential parameters. In the present study, we describe low-energy neutron direct-capture reactions on ^{12}C-nuclei, using the optical potential derived form the dispersion theory. This potential is quite successfully applied to direct-capture model calculations in explaining off-resonance neutron-capture cross sections of ^{12}C observed at 20-600keV. We also emphasize that the spatial nonlocality of a neutron-nucleus interaction potential for negative energies should be taken into account to describe the direct capture of low-energy neutrons by light nuclei.

3.26 The Influence of Impurities for
Cross Section Measurement of ^{241,243}Am(n,f) Reactions

Tetsuya Kai[1], Katsuhei Kobayashi[1], Shuji Yamamoto[1], Yoshiaki Fujita[1],
Itsuro Kimura[2], Mitsuharu Miyoshi[2], Hideki Yamamoto[2] and Nobuo Shinohara[3]

1 Research Reactor Institute, Kyoto University
2 Department of Nuclear Engineering, Kyoto University
3 Japan Atomic Energy Research Institute

e-mail:tkai@rri.kyoto-u.ac.jp

The influence of the impurities on the fission cross section measurements for ^{241}Am and ^{243}Am has been investigated with the practical results. Following cases have been considered as the influence of impurities; (a)experiments with the ^{241}Am sample that contains impurities originally, and (b) experiments with the ^{243}Am sample that contains impurities produced by α, β decays after the chemical purification. The present study has demonstrated the usefulness of pure samples by the comparison of the experiments using the sample on the market with those using the pure sample processed by the authors. Particularly on the case(b), the correction of the impurity through the periodical measurements was experimentally performed (about 18% around 0.3 eV in 4 weeks after the chemical purification).

1.Introduction

For the nuclear data measurements, in general, cross section value of the sample containing impurities may be bigger than that with the pure sample depending on the amount of impurities and on the nuclear characteristics[1][2]. Particularly, it have to be careful to measure the fission cross sections of minor actinides because many kinds of them are produced and accumulated in the sample through the complicated decay processes. Therefore, the extensive experimental studies have recently been concentrated on the importance of the chemical and isotopic composition of the sample materials and of its physical properties[1][2][3].

In an earlier measurement, we had the experience of obtaining a much larger fission cross section for ^{241}Am, being the measurement made with a sample on the market[4]. Through the careful and systematic investigation of the ^{241}Am sample by α-ray spectrometry, we found that the sample contained the ^{239}Pu impurity of about 0.3%[5]. On the other hand, the measurement of ^{243}Am fission cross section have to be also performed with careful consideration of ^{239}Pu ingrowth, because it is produced through the following decay chaain;

$$^{243}\text{Am} \xrightarrow[7370y]{\alpha} {}^{239}\text{Np} \xrightarrow[2.355d]{\beta^-} {}^{239}\text{Pu} \xrightarrow[24110y]{\alpha} {}^{235}\text{U}$$
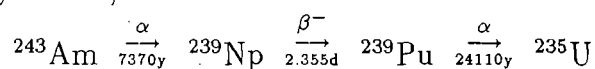
This ^{239}Pu ingrowth makes an important contribution to the measured fission cross section even if we have purified the ^{243}Am sample by the chemical processing.

In the present study, following cases have been considered as the influence of impurities for fission cross section measurements with:

(a) the sample which contains impurities originally.

(b) the sample whose decay products are accumulated as impurities after chemical purification.

In practice, the impurity problems have been investigated as typical examples for the measurements of the ^{241}Am(n,f) and ^{243}Am(n,f) cross sections, respectively[4][5][6]. The experiments have been performed by making use of back-to-back type double fission chambers using the Am and the ^{235}U deposits and of a lead slowing-down spectrometer coupled to an electron linear accelerator[7][8].

2.Experimental Methods

2.1. Lead Slowing-down Spectrometer

The fission cross section measurements for ^{241}Am and ^{243}Am have been made in the energy range from 0.1 eV to 10 keV with Kyoto University Lead Slowing-down Spectrometer (KULS)[7]. The KULS is composed of 1600 lead blocks (each size:10 × 10 × 20cm^3, purity:99.9%) and the blocks are piled up to make a cube of 1.5 × 1.5 × 1.5m^3(40 tons) without any structural materials. We covered the KULS with Cd sheets of 0.5 mm in thickens. At the center of the KULS, an air-cooled photoneutron source of Ta is set to generate pulsed fast neutrons. One of the experimental holes in the KULS was covered by Bi layers of 10 to 15 cm in thickness to shield high energy gamma-rays (6 to 7 MeV) produced by the Pb(n,γ) reaction in the spectrometer.

The characteristics of the spectrometer (the relation between neutron slowing-down time and energy, and the resolution) have been obtained by the measurements and the calculations. The detailed description is given elsewhere[7].

2.2. ^{241}Am and ^{243}Am Samples

Two kinds of Am samples were used; one was commercially available[4] and the other was prepared by ourselves with the chemical processing using anion-exchange methods. Both types of the Am samples were deposited on stainless steel plates of 28 mm in diameter and 0.2 mm thick (radioactive area:20 mm in diameter). In the α-ray spectrum of the purified ^{241}Am sample, no other α-ray peak was observed. For the ^{243}Am spectrum measurement, although small amount of impurities of ^{241}Am and ^{243}Cm were observed, the counting rate ratios for ^{241}Am/^{243}Am and ^{243}Cm/^{243}Am were 0.007 and 0.00004, respectively. These results were found to be negligible in the ^{243}Am(n,f) cross section measurement at the relevant energies.

2.3. Fission Chambers

The fission chambers employed for the present measurements are composed of two parallel plate type ionization chambers[8]. The back sides of a sample deposit (Am) and a reference one (^{235}U) are faced each other, therefore it is called back-to-back type. The chambers were made of aluminum and filled with a mixed gas (97% Ar and 3% N$_2$) at 1 atm. Enrichment of the reference ^{235}U sample was 99.91%.

3. Fission Cross Section Measurement

Each of the fission cross section for ^{241}Am and ^{243}Am is obtained by the following

equation;

$$\sigma_{Am}(E) = \frac{C_{Am}}{C_U} \frac{N_U}{N_{Am}} \sigma_U(E)$$

where C_{Am} : fission counts of Am,
  C_U : fission counts of ^{235}U,
  N_{Am} : number of Am atoms in the sample deposit,
  N_U : number of ^{235}U atoms in the reference deposit,
  $\sigma_U(E)$: energy dependent fission cross section of ^{235}U.

The reference cross section values were cited from ENDF/B-VI[10]. More detailed experimental descriptions are given elsewhere[6][9].

4.Results and discussion

The result with the ^{241}Am sample on the market is shown in Fig. 1, and is compared with the evaluated data in JENDL-3.2[11] and ENDF/B-VI[10], where the evaluated data were broadened by the energy resolution of the KULS. The fission cross section for the pure ^{241}Am sample has also been shown in Fig. 2, where the measurement is in good agreement with the evaluated data. It is clear that the larger cross section for the purchased sample is due to the impurities. We have experimentally investigated the problem and found that the purchased sample contained ^{239}Pu impurity of about 0.3 % at least by the careful α-ray spectrometry. The sample contains some other impurities in addition to ^{239}Pu because the larger cross section has not been corrected properly with the amount of ^{239}Pu impurity except for the energy region around the 0.3 eV resonance. It is shown in Fig. 3 that we have simulated the impurity corrections not only with ^{239}Pu but also with ^{242m}Am. The amount of ^{242m}Am impurity was assumed to be 0.25% to fit the analytical result to the measurement around higher neutron energy region. The result of this correction means that the ^{242m}Am impurity was overestimated and there were any other impurities in the sample because of the inadequate correction around lower neutron energy region.
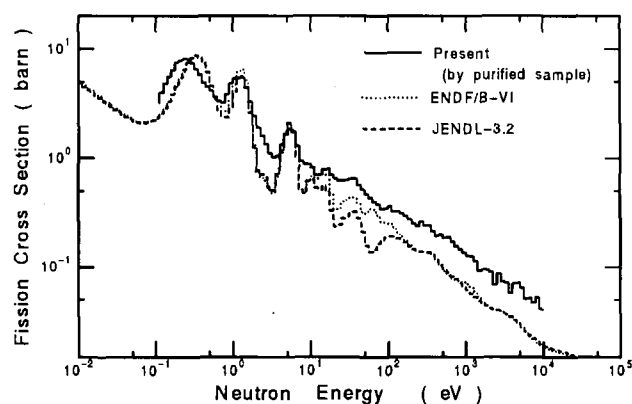
Fig. 1   Comparison of the measured cross section for the purchased sample and the evaluated.
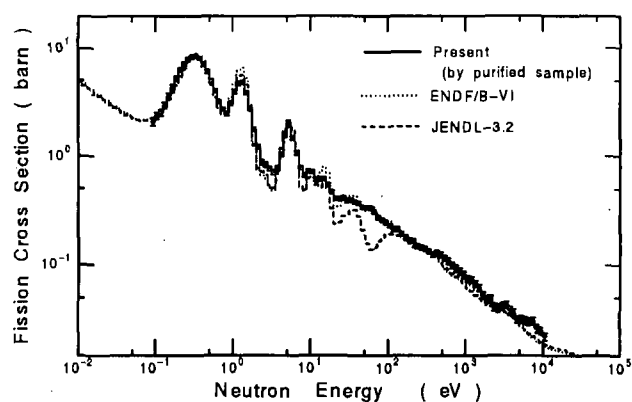
Fig. 2   Comparison of the measured cross section for the purified sample and the evaluated.
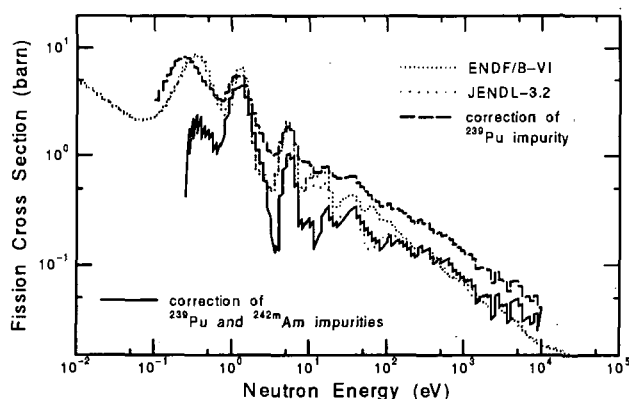
Fig. 3 Corrected cross section for the purchased ^{241}Am sample.

Figure 4 also shows the ^{243}Am(n,f) cross section measured with the sample on the market. There is a remarkable difference between this result and the evaluated data around 0.3 eV, which is clearly cause by ^{239}Pu impurity produced by the α-decay of ^{243}Am. We have followed the growth of ^{239}Pu impurity in the ^{243}Am sample after the chemical purification by the calculation and periodical measurements. In Fig. 5, the results of the measurements performed at 4 weeks, 21 weeks and 55 weeks after the purification is shown. It is obviously observed that the measured values around 0.3 eV increased depending on the time after the purification.

Fig. 4 Comparison of the measured cross section for the purchased sample and the evaluated.

The influence of ^{239}Pu ingrowth around its 0.3 eV resonance is illustrated in Fig. 6, where the solid line means the measured cross sections and the broken line indicates the estimated contribution of ^{239}Pu ingrowth using the cross sections cited from ENDF/B-VI[10]. Good agreement is seen between them. Figure 7 shows the energy dependent influence of the ^{239}Pu ingrowth. As a result, the present cross section for the ^{243}Am(n,f) reaction has been derived and displayed in Fig. 8 with the correction of ^{239}Pu accumulation (about 18 % around 0.3 eV in 4 weeks after the chemical process). Through the present experimental investigation, it is found that the measurement has to be done as soon as possible after the chemical purification not to make the correction large and that the pure sample is indispensable for these kinds of measurements.
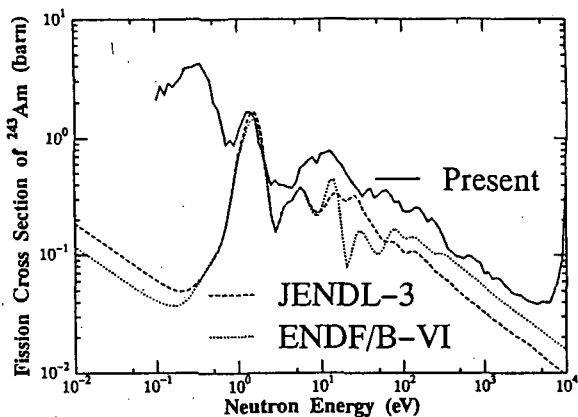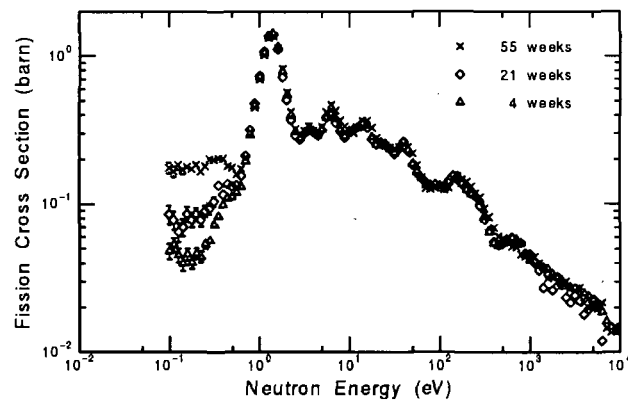
Fig. 5 Ingrowth of ^{239}Pu in ^{243}Am(n,f) cross section after chemical separation.
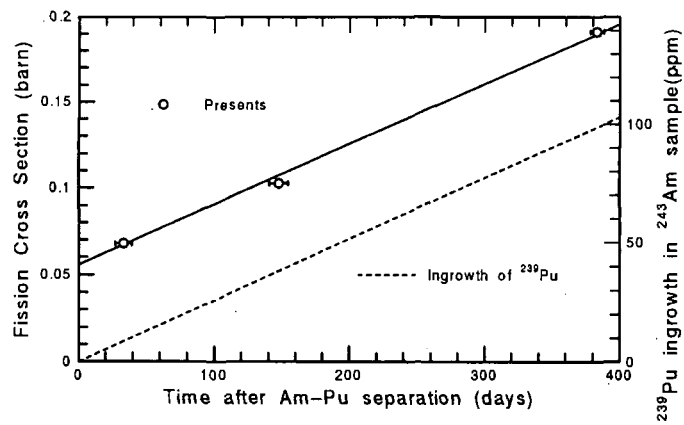
Fig. 6 Contribution of ^{239}Pu around 0.3 eV.
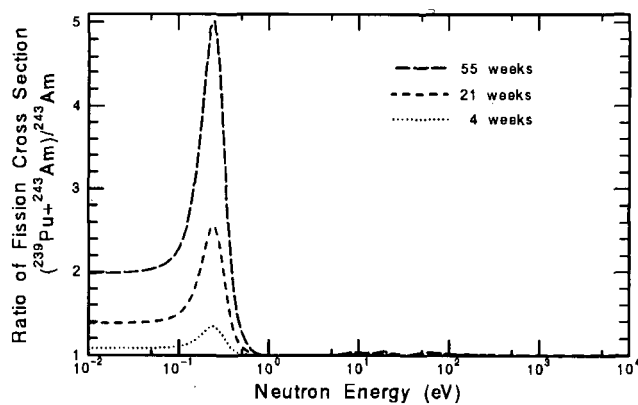
Fig. 7 Energy dependent influence of ^{239}Pu ingrowth.
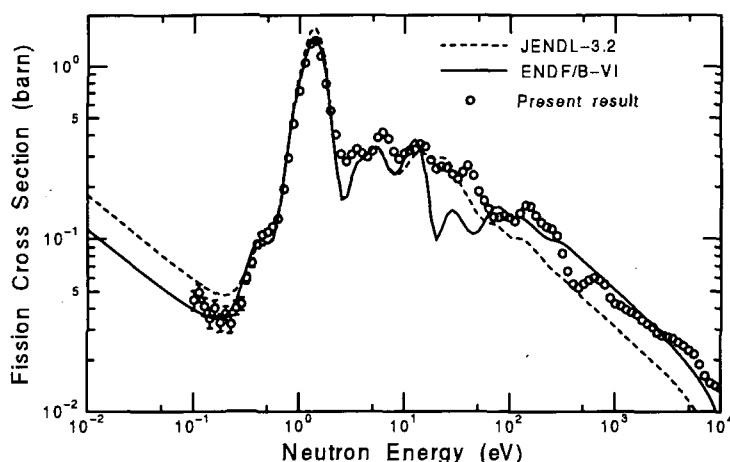
Fig. 8 Present ^{243}Am(n,f) cross section with the correction of ^{239}Pu ingrowth.

Reference

[1] C. Wagemans: *Nucl. Instr. Meth.*, **A236**, 429(1985).

[2] C. Wagemans, et al.: *Nucl. Phys.*, **A597**, 188(1996).

[3] N. Shinohara: to be published in *J. Nucl. Sci. Technol.*.

[4] K. Kobayashi, et al.: *Proc. Int'l Conf. on Nucl. Dara for Sci. and Technol., Gatlinburg,* **Vol.1**, p242(1994).

[5] M. Miyoshi: "Measurement of Nutron Energy Dependent Fission Cross Section of ^{241}Am", Master Thesis in Japanese, Department of Nuclear engineering, Kyoto University, 1995.

[6] K. Kobayashi, et al.: "Measurement of Fission Cross Section with the Pure Am-243 Sample using Lead Slowing-Down Spectrometer", presented in this Symposium.

[7] K. Kobayashi, S. Yamamoto, A.Yamanaka, et al.: "Characteristics of Kyoto University Lead Slowing-down Spectrometer Coupled to an Electron Linac" JAERI-M 93-046,p360(1993) and to be published in *Nucl. Instr. Methods in Phys. Res.*.

[8] M. Obu: "Preparation and Characteristics of Fission Chambers with Actinide Nuclides" JAERI-M 9757(1981) and to be published in *Nucl. Sci. Eng.*.

[9] K. Kobayashi, S. Yamamoto, et al.: "Measuement of Fission Cross Section with Pure Am-241 Sample using Lead Slowing-down Spectrometer", JAERI-Conf 96-008, p.117(1996).

[10] R. F. Rose(Compiled and Edited): "ENDF-201, ENDF/B-VI Summary Documentation", BNL-NCS-17541, 4th Ed. (ENDF/B-VI)(1991.13).

[11] T. Nakagawa, et al.: *J. Nucl. Sci. Technol.,* **Vol.32**, No.12, 1259(1995) and "Evaluation of Nuclear Data for Americium Isotopes", JAERI-M, 89-008(1989).

3.27 Modification of EXIFON Code
and Analysis of O16+n Reactions in En=20-50 MeV *

Toru Murata
Nippon Nuclear Fuel Development Co.
Oarai-Machi,Ibaraki-Ken.311-13,Japan

Abstract

To evaluate the nuclear data concerning neutron induced reactions of O-16 and N-14 in the incident energy range of 20-50 MeV, the statistical multistep reaction code EXIFON was modified to include the outgoing channels of deuteron,triton and He-3. The calculated double differential cross sections (DDXs) with the modified code are compared with experimental DDXs.

1.Introduction

The statistical multistep direct and compound reaction code EXIFON has been formulated and developed by Kalka[1], and can predicts emission spectra for neutrons,protons,alphas and photons by the reaction of neutron,proton and alpha incident on the target nucleus which mass number greater than 20,in the incident energy region below 100 MeV.

Nuclear data evaluation concerning the neutron induced reactions on O-16 and N-14 are planned to be made using the EXIFON code in the incident energy region 20 to 50 MeV. For light nuclei, cross sections of deuteron,triton and He-3 emission reactions are not negligible, so these particle emission channels are added to the EXIFON code and some other modification of the code were made.

Calculated DDXs with the modified code are compared with the experimental data measured by Subramanian et al.[2]. Ways to obtain better agreement are discussed.

2. Modification
1) Addition of reaction channels

Though reaction channels of deuteron, triton and He-3 emission were added to the original EXIFON channels, it is assumed,for multiple particle emission that the first chance emission particle is restricted to neutron,proton or alpha. Table 1 shows all of the present reaction channels.

The cluster formation factors of deuteron,triton and He-3 were calculated with the EXCIT code[3]. The predominant factor for the emission in the present energy region were reproduced with the following quadratic formula of emitted particle energy E.

Deuteron :

$$F11=1.025-0.0291*E+1.965*10^{-4}*E^2 \quad (E<=40 \text{ MeV })$$
$$F11=0.175 \quad (E> 40 \text{ MeV })$$

Triton   :

$$F12=0.5144-0.0142*E+9.423*10^{-5}*E^{2} \qquad (\; E<=40 \; MeV \;)$$
$$F12=0.097 \qquad (\; E> \; 40 \; MeV \;)$$

He-3   :

$$F12=0.5008-0.0146*E+1.008*10^{-4}*E^{2} \qquad (\; E<=40 \; MeV \;)$$
$$F12=0.077 \qquad (\; E> \; 40 \; MeV \;)$$

Another factor which should be multiplied to the cluster formation factor is originated from particle state density. Though the factor propotional to (particle reduced mass)$^{3/2}$, deuteron,triton and He-3 would not behave as a particle in a nucleus and the factor equal to 1.5 for deuteron, and 1.0 for triton and He-3 gave adequate agreement with the exerimental DDXs.These values were adopted for the present calculation.

The reaction Q-values and other parameters were also added to the original input files.

2) Calculation of the optical model reaction cross sections

The optical model reaction cross sections were calculated for incident particles of n,p,d,t,He-3 and alpha particle on target nucleus of He-3 to O-18, in the incident energy range below 100 Mev. For neutron , the optical model potential by Wilmore and Hodgeson[4], for proton,by Perey[5],for deuteron,by Perey and Perey[6],for triton and He-3,by Becchetti and Greenlees[7] and for alphas,by Igo[8] were adopted.

The calculated cross sections were devided into two region and reproduced with the formula : C1*Ei+C0+C2/Ei ,where Ei is the incident particle energy, and coefficients C0,C1,C2 were fitted with quadratic formula of mass number by element to element. In the incident energy region higher than about 20 MeV, the original EXIFON gives rather small reaction cross section for light nucleus.

3) Miscellaneous revision

The charged particle barrier penetration factor calculated using the ratio of optical model reaction cross section to that of the same energy neutrons is corrected by reduced mass ratio.

The penetration factor which unified with the cluster formation factor in the code is classified into incident channel and outgoing channel.

Recoil energy of the residual nucleus is subtructed from outgoing channel energy to obtain outgoing particle energy.

Direct reaction cross sections are given as input data, and subtructed from the optical model reaction cross section,to obtain compound process cross sections.

3. Results and discussion

The calculated DDXs in the center of mass system with the modified EXIFON code were converted to the laboratory system using the two-body kinematics and angular distribution systemsatics given by Kalbach[9], then compared with the experimental data of Subramanian et al.[2] at the angles of forwardmost,medium and backward.

1) Proton emission DDX

Figure 1 shows the proton emission DDXs. The modified EXIFON underestimates the DDX considerably (solid line). The posibility that the direct (n,p) process would explain the difference was

suggested by Watanabe[10]. The direct reaction DDX was estimated using the quasi-free (n,p) scattering model[11],tentatively. Sum of the modified EXIFON DDX and the quasi-free (n,p) DDX is shown by dashed line in Fig.1. There still remain some differences at En=60.7 MeV,in forward angle..

2) Deuteron emission DDX

Figure 2 shows the deuteron emission DDXs. Experimental DDXs show clearly two peaks caused by the direct (n,d) reactions. The proton pickup direct reaction differential cross sections were calculated with the DWBA code DWUCK4 [12] and normalized to experimental data as a whole. Solid lines in Fig.2 show the sum of the direct and the multistep DDXs.

3) Triton emission DDX

Figure 3 shows the trition emission DDXs. In the low incident energy region, the modified EXIFON code underestimates the DDX. There are possibility that the deuteron pickup direct reaction is the predominant process in this energy region.

4) He-3 emission DDX

Figure 4 shows the He-3 emission DDXs. No experimental data were given in the lowest incident energy. Agreement between the experiment and the present calculation is good.

5) Alpha particle emission DDX

Figure 5 shows the alpha particle emission DDXs. Agreement between the experiment and the present calculation is fairly good generally.

4. Conclusion

A modified EXIFON code has been developed to evaluate the nuclear data of neutron induced reactions for light nuclei,in the incident energy range from 20 to 50 MeV. Though the modified code gave good results for some reaction channels, for other channels, the direct reactions should be taken into account.

Thanks are due to Dr.Y.Watanabe (Kyushu.Univ.) for helpful discussion and instruction, and also due to Drs.S.Chiba,T.Fukahori and K.Shibata (JAERI) for kindly suggestion and preparing analysis codes.

References

[1] Kalka,H.: Z.Phys.A341,289(1992)
[2] Subramanian,T.S.et al.: Phys.Rev.C34,1580(1986)
[3] Sato,K.,Iwamoto,A.,Harada,K.:Phys.Rev.C28,1527(1983)
[4] Wilmore,D.,Hodgson,P.E.:Nucl.Phys.32,353(1962)
[5] Perey,F.G.:Phys.Rev.131,745(1963)
[6] Perey,C.M.,Perey,F.G.:Phys.Rev.132,755(1963)
[7] Becchetti,F.D.,Greenlees,G.W.:"Polarization Phenomena in Nucl. Reaction",p.628 (The Univ.of Wisconsin Press,1971)
[8] Igo,G.:Phys.Rev.115,1665(1960)
[9] Kalbach,C.:Phys.Rev.C37,2350(1988)
[10] Watanabe,Y.: Private Communication
[11] Kikuchi,K.,Kawai,M.: "Nuclear Matter and Nuclear Reactions" (North Holland,1968),chapter 2
[12] Kunz,P.D.: Private Communication

Table 1. Reaction Channels of the Modified EXIFON Code

IS \ I	1	2	3	4	5	6	7
1 (SMD)	i,n	i,p	i,d	i,t	i,h	i,a	i,g
2 (SMC)	i,n	i,p	i,d	i,t	i,h	i,a	i,g
3 (SMC)	i,nn	i,np	i,nd	i,nt	i,nh	i,na	i,ng
4 (SMC)	i,pn	i,pp	i,pd	i,pt	i,ph	i,pa	i,pg
5 (SMC)	i,an	i,ap	i,ad	i,at	i,ah	i,aa	i,ag
6 (SMC)	i,2nn	i,2np	i,2nd	i,2nd	i,2nh	i,2na	i,2ng

i : incident particle, h : He-3, a : alpha, g : gamma-ray
SMD : Statistical Multistep Direct Reaction
SMC : Statistical Multistep Compound Reaction
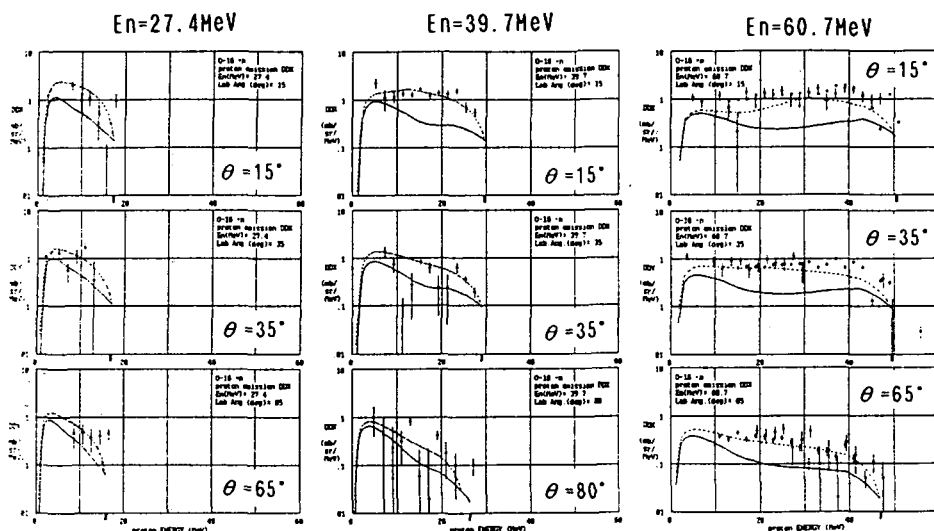
Fig.1 Proton DDXs of the O-16(n,xp) reaction : Comparison of the present calculation and the experimental data measured by Subramanian et al./2/. Solid line:modified EXIFON, Dashed line: modified EXIFOM + Quasi-free (n,p)
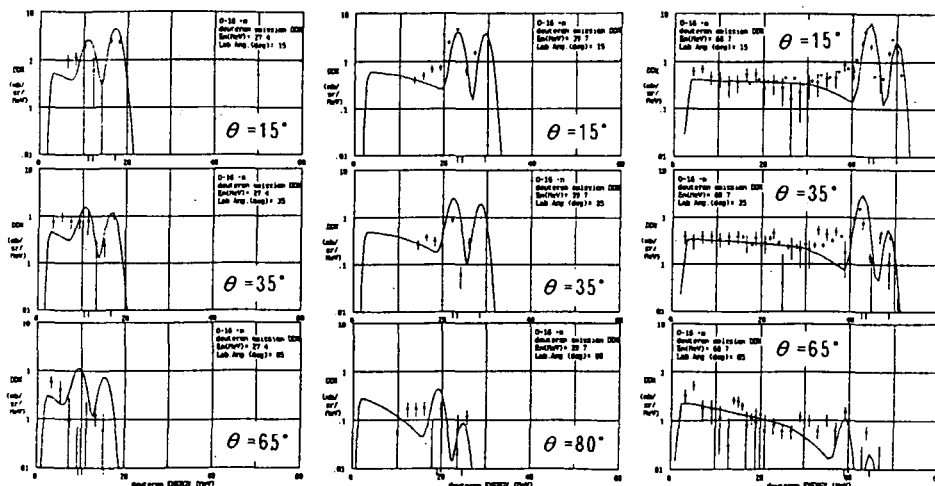
Fig.2 Deuteron DDXs of the O-16(n,xd) reaction : Comparison of the present calculation and the experimental data measured by Subramanian et al./2/. Solid line:modified EXIFON + DWBA

En=27.4MeV   En=39.7MeV   En=60.7MeV
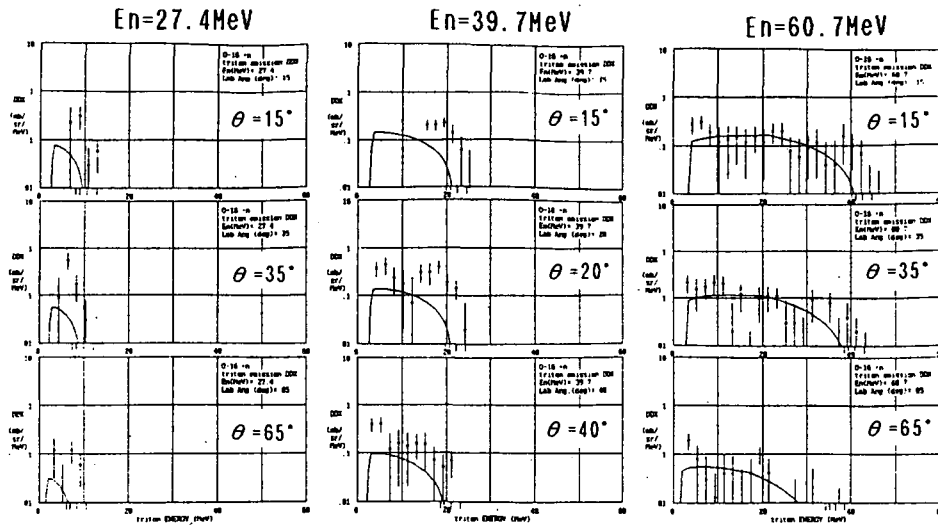
Fig.3 Triton DDXs of the O-16(n,xt) reaction : Comparison of the present calculation and the experimental data measured by Subramanian et al./2/. Solid line:modified EXIFON
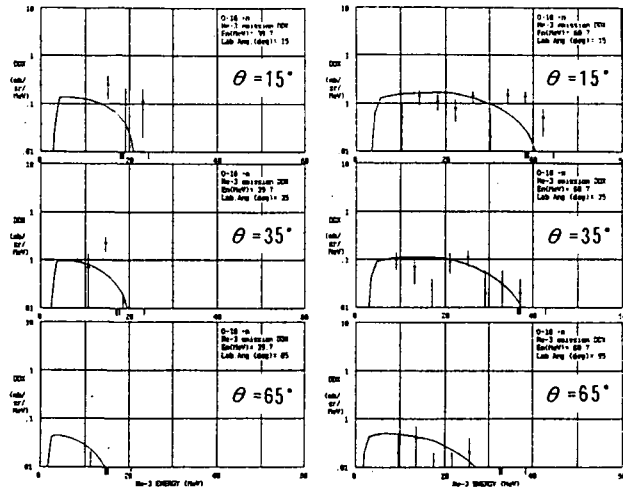
Fig.4 He-3 DDXs of the O-16(n,xHe3) reaction : Comparison of the present calculation and the experimental data measured by Subramanian et al./2/. Solid line:modified EXIFON
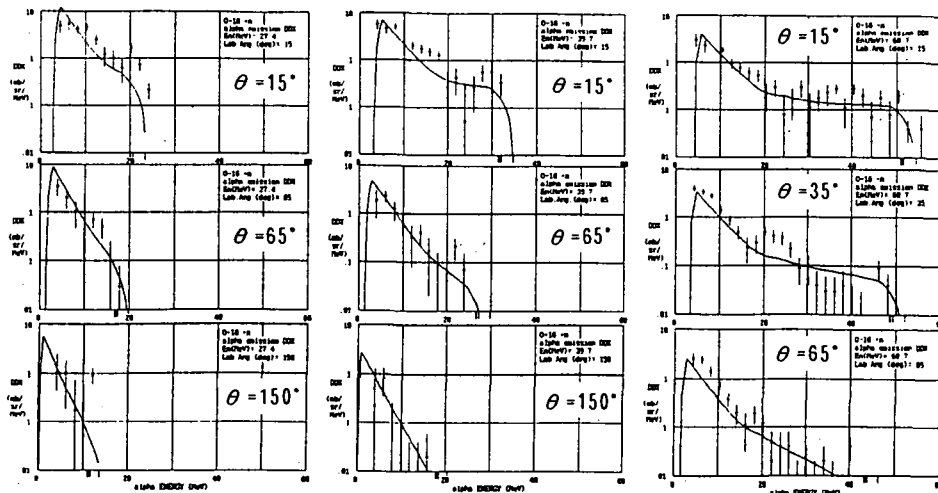
Fig.5 Alpha particle DDXs of the O-16(n,xa) reaction : Comparison of the present calculation and the experimental data measured by Subramanian et al./2/. Solid line:modified EXIFON

3.28 HETC-3STEP Included Fragmentation Process

Nobuhiro SHIGYO, Kiminori IGA and Kenji ISHIBASHI
Department of Nuclear Engineering, Kyushu University
Hakozaki, Higashi-ku, Fukuoka-shi 812-81
e-mail: shigyo@nucl.kyushu-u.ac.jp

High Energy Transport Code (HETC) based on the cascade-evaporation model is modified to calculate the fragmentation cross section. For the cascade process, nucleon-nucleon cross sections are used for collision computation; effective in-medium-corrected cross sections are adopted instead of the original free-nucleon collision. The exciton model is adopted for improvement of backward nucleon-emission cross section for low-energy nucleon-incident events. The fragmentation reaction is incorporated into the original HETC as a subroutine set by the use of the systematics of the reaction. The modified HETC (HETC-3STEP/FRG) reproduces experimental fragment yields to a reasonable degree.

1. Introduction

Reliable high-energy nuclear data have been required for application of the spallation reaction to facilities such as the high intensity neutron source[1] and the accelerator based transmutation[2]. Cross sections of the fragmentation reaction which is induced by incident nucleons of energies above several hundred MeV are necessary for engineering design. Since it is difficult to obtain the whole fragmentation data by experiments, calculation models need to be developed.

High Energy Transport Code (HETC)[3] is currently often used for engineering purposes at intermediate energies. The code mainly considers the intranuclear-cascade and evaporation processes in the nuclear-reaction part. The production yields of the fragments such as ^{7}Be and ^{22}Na are not represented by HETC, since the fragmentation process does not taken into consideration. We, therefore, have modified this code as HETC-FRG to calculate the intermediate-energy proton-incidence fragmentation cross sections.

For further improvement of the code, the nuclear in-medium correction is taken into account in the intranuclear-cascade process, and the exciton model is adopted for better reproduction of the nucleon emission cross sections for nucleon-incidence at low energies. This code is designated HETC-3STEP/FRG.

2. Nuclear in-medium correction

The free-space nucleon-nucleon (NN) cross sections are used in the intranuclear-cascade process of HETC. Since the NN collisions occur in the nuclear medium, however, it is important to consider the in-medium NN cross section correction[4]. The NN cross sections in the intranuclear-cascade process of HETC are modified for this reason. The cross sections in medium are obtained by simple and practical parameterization[5]. These parametrization are applicable to energies up to 300 MeV. Above 300 MeV, the NN cross section in medium is postulated to increase linearly, and is equal to the free-space NN cross section at the energy of 500 MeV.

3. Incorporation of fragmentation into HETC

Before incorporation of the proton incident fragmentation process into HETC, systematics on the mass yields and the kinetic energy spectra of the process have been constructed[6]. The former was obtained on the basis of a liquid-gas phase transition model[7], and was parametrized by the incident proton energy, the target and the fragment mass numbers and the fragmentation nuclear temperature. For the latter, a formula was devised to have a simple expression considering the Coulomb barrier. The kinetic energy spectra were represented by the parameters of the fragmentation nuclear temperature, the fragment and the target mass numbers and the incident proton energy. The nuclear temperature of the fragmentation was determined in average by the incident proton energy.

For the calculation in HETC, it is assumed that the fragmentation process occurs between the cascade and the evaporation processes. The systematics are incorporated with some modification as a subroutine set into HETC[8]. The probability of the fragmentation occurrence is evaluated by the excitation energy after the cascade process, instead of the use of incident proton energy. The nuclear temperature is at first obtained as liquid-phase one after the cascade process without considering a degree of freedom of the fragmentation: This temperature is given by the excitation energy and the mass number of the nucleus after the cascade process. Then, the temperature considering the fragmentation is presented as a function of the liquid-phase temperature. This method takes into account information on the nucleus after the cascade process such as excitation energy and mass number to some extent.

4. Exciton model

The original HETC based on cascade and evaporation processes is known to underestimate the nucleon emission cross section in the backward direction when incident nucleon energy is around or below 100 MeV. To solve this problem simply, the exciton model[9] is adopted as the intermediate process between the intranuclear-cascade and the evaporation processes. The model considers the mass and the atomic numbers, the excitation energy and the number of the excitons after the intranuclear-cascade process.

The exciton model is only effective in the case that the number of excitons is small, i.e., relatively low excitation energy after the intranuclear-cascade process. On the contrary, the fragmentation tends to occur in a high excitation state, where the number of excitons is large. At a number of excitons of 15, the calculation is determined to be switched from the process of fragmentation to exciton model. If the number of exciton is below 15, the exciton model calculation follows to the cascade process, whereas the fragmentation process is run if it exceeds 15.

5. Calculation results

The cross sections of the fragmentation are first calculated by the fragmentation-incorporated HETC (HETC-FRG). This calculation includes the fragmentation as the intermediate process. Fig. 1 is the mass yields of the fragments from Ag and Xe targets[10, 11, 12]. This figure indicates that the cross sections by HETC-FRG are in good agreement with the experimental data.

Figures 2 - 8 are the nuclide production yields from Al, Fe, Zr and Au targets. In these figures, marks indicate the experimental data[13, 14], short dashed lines show the cross sections calculated by HETC-FRG, and solid lines present those by HETC-3STEP/FRG that considers both the fragmentation and the exciton processes. For comparison, long dashed lines are given by HETC-3STEP[15] that includes the exciton model alone. In Fig. 2, HETC-3STEP/FRG is more appropriate than HETC-FRG below 1 GeV. This is because the exciton phenomenon is dominant in this energy region. Fig. 3 indicates that both HETC-FRG and HETC-3STEP/FRG reproduce the production yield of ^{7}Be within a factor of five at incident proton energies above 300 MeV. Since ^{7}Be is mainly produced by the fragmentation process, the results of HETC-3STEP are apart from the experimental data. In the case of Zr target, this tendency is more evident as shown in Fig. 10. Figure 12 also shows same results in the case of Au target. The results of the production cross sections near the target nucleus by HETC-3STEP, HETC-FRG, and HETC-3STEP/FRG reproduce the experimental cross sections for Fe, Zr and Au targets to some degree in Figs. 4, 6, and 8.

6. Summary

In order to calculate the cross section of the proton-incidence fragmentation reaction, HETC was modified. The nucleon-nucleon cross sections in the intranuclear-cascade process were changed from free-space values to in-medium ones. The fragmentation reaction is incorporated into the code as a subroutine set on the basis of the systematics of the proton-induced reaction. The exciton model is adopted to improve the nucleon emission cross section in the backward direction. The resultant HETC-3STEP/FRG is appropriate to obtain the fragmentation cross sections in the wide target mass range at incident proton energies above several hundred MeV. Although the original HETC is incapable of reproducing the experimental production yields of the light mass fragments like ^{7}Be, HETC-3STEP/FRG represents them to a considerable degree.

References

[1] Carpenter, J.M., et al.: Proceedings of the twelfth Meeting of International Collaboration on Advanced Neutron Sources 24 - 28 May 1993, Rutherford Appleton Laboratory Report, 94-025, T-95 (1994).

[2] Bowman, C.D., et al.: Nucl. Instr. and Meth., A320, 336 (1992).

[3] Chandler, K.C., and Armstrong, T.W.: ORNL 4744 (1972).

[4] Suetomi, E. et al.: Phys. Lett., B333, 22 (1994).

[5] Li, G.Q., and Machleidt, R.: Phys. Rev., C48, 1702 (1993); Li, G.Q., and Machleidt, R.: ibid, C49, 566 (1994).

[6] Shigyo, N., et al.: J. Nucl. Sci. Technol., 32, 1 (1995).

[7] Panagiotou, A.D., et al.: Phys. Rev., C31, 55 (1985).

[8] Shigyo, N., et al.: JAERI-Conf., 95-008, 217 (1995); Shigyo, N., et al.: ibid, 96-008, 272 (1995).

[9] Gudima, K.K., et al.: Nucl. Phys., A401, 329 (1983).

[10] Green, R.E.L., et al.: Phys. Rev., C29, 1806 (1984).

[11] Andronenko, L.N., et al.: Phys. Lett., B174, 18 (1986).

[12] Porile, N.T., et al.: Phys. Rev., C39, 1914 (1989).

[13] Michel, R., et al.: Nucl. Instr. and Meth., B103, 183 (1995).

[14] Iljinov, A.S., et al.: "Production of Radionucleids at Intermediate Energies ", Springer Verlag, Landolt-Bornstein, New Series, subvolumes I/13a (1991), I/13b (1992), I/13c (1993), I/14d (1994).

[15] Takada, H., et al.: JAERI-Research, 96-040 (1996).
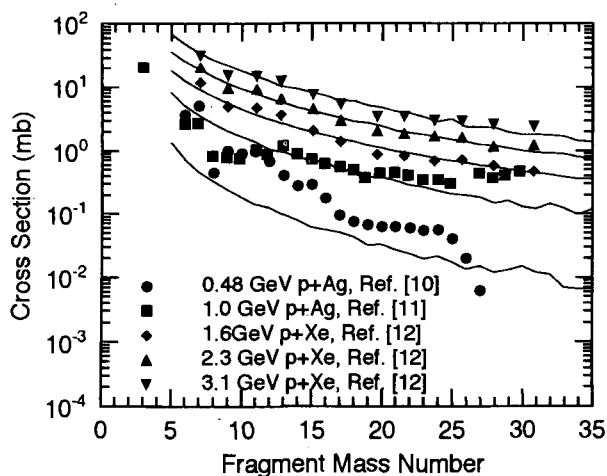
Fig. 1 Fragment mass yields. Marks show experimental values, and lines are results of HETC-FRG.
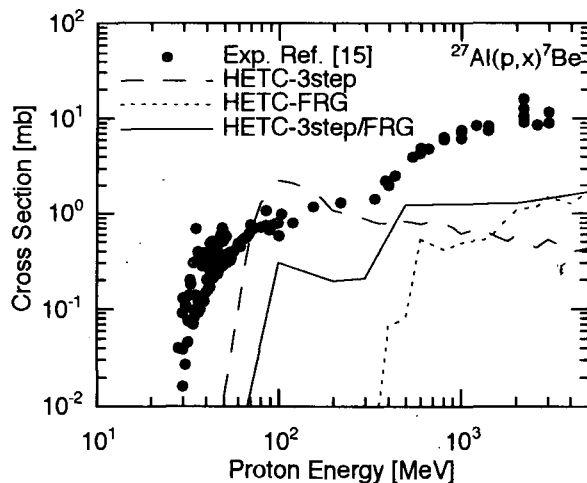
Fig. 2 Production cross section of ^{7}Be from ^{27}Al.
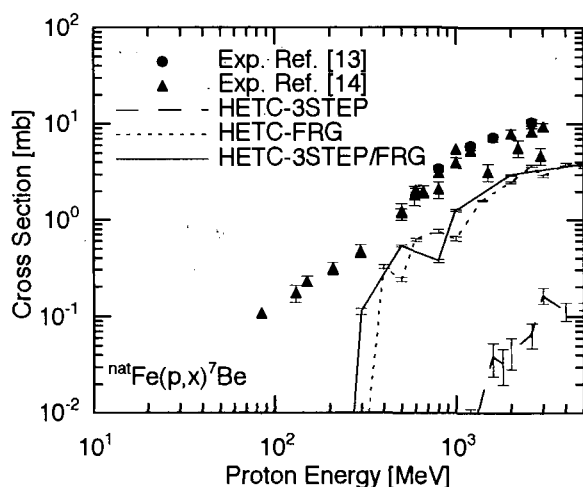
Fig. 3 Production cross section of ^{7}Be from ^{nat}Fe.
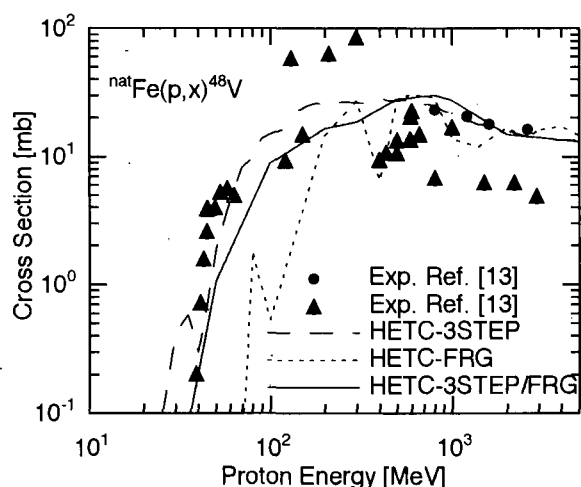
Fig. 4 Production cross section of ^{48}V from ^{nat}Fe.
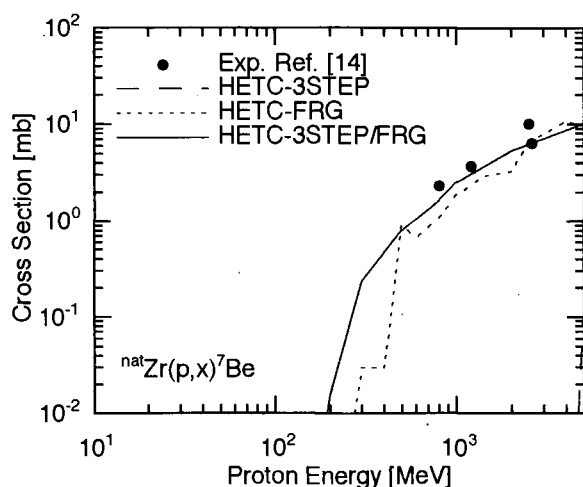
Fig. 5 Production cross section of ^{7}Be from ^{nat}Zr.
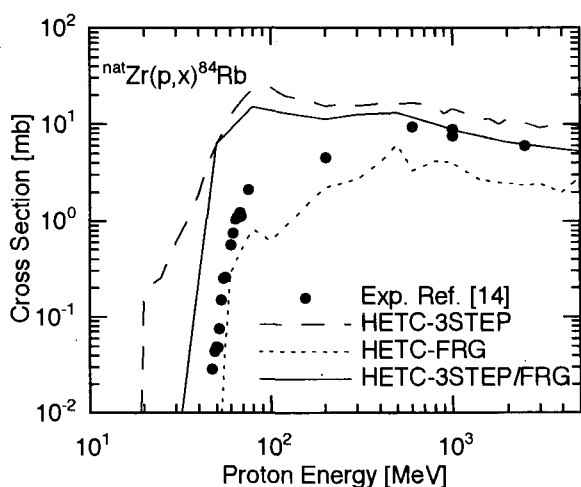
Fig. 6 Production cross section of ^{84}Rb from ^{nat}Zr.
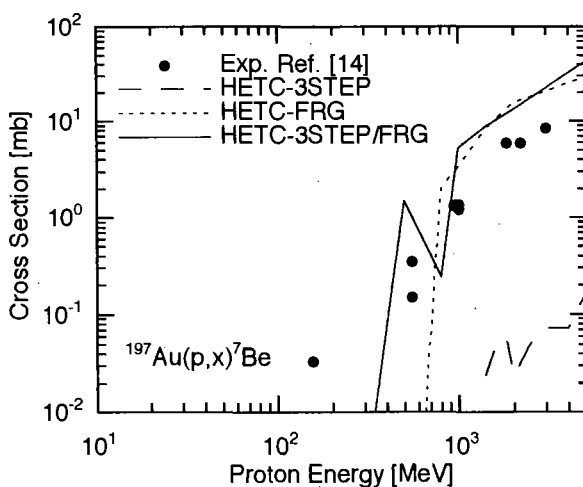
Fig. 7 Production cross section of ^{7}Be from ^{197}Au.
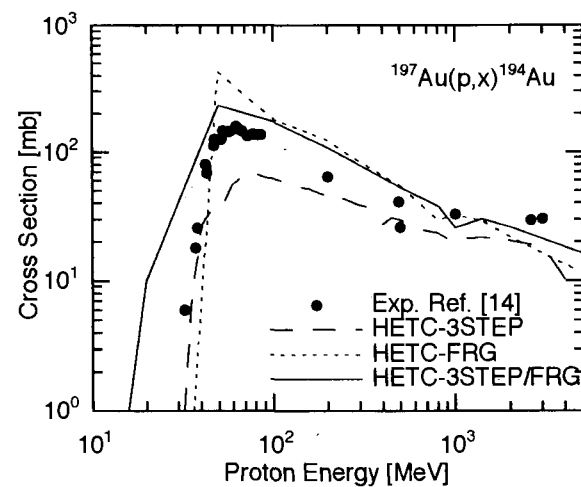
Fig. 8 Production cross section of ^{194}Au from ^{197}Au.

3.29 Phenomenological Dirac optical potential for neutron cross sections

Shin-ichi Maruyama, Hirohiko Kitsuki, Nobuhiro Shigyo and Kenji Ishibashi

Department of Nuclear Engineering, Kyushu University

Hakozaki, Higashi-ku, Fukuoka, 812-81 Japan

e-mail: maru@meteor.nucl.kyushu-u.ac.jp

Because of limitation on neutron-incident data, it is difficult to obtain global optical model potential for neutrons. In contrast, there are some global optical model potentials for proton in detail. It is interesting to convert the proton-incident global optical potentials into neutron-incident ones. In this study we introduce $(N-Z)/A$ dependent symmetry potential terms into the global proton-incident optical potentials, and then obtain neutron-incident ones. The neutron potentials reproduce total cross sections in an acceptable degree. However, a comparison with potentials proposed by other authors brings about a confused situation in the sign of the symmetry terms.

1. Introduction

Some proton-incident data have been published on elastic-scattering and total-reaction cross sections in the intermediate energy region. Such results as well as experimental data obtained by polarized proton beams are useful for parametrizing global optical model potentials in detail. Phenomenological Dirac optical model potential parameters were obtained in a global form by Cooper et al.[1]. In contrast, neutron-incident experiments on elastic scattering are more difficult than proton ones, so that there is a limitation on neutron-incident data. Shen et al.[2] determined the parameters neutron-incident phenomenological Dirac optical model potentials; their validity is in question due to the situation that only limited quantities of the neutron data are available.

There is an approach to determine the symmetry term that includes $(N-Z)/A$ dependence, according to Lane model[3]. Kozack and Madland[4] made potential parametrization taking the symmetry term into account, for a target nucleus ^{208}Pb for both proton and neutron incidence in the energy range of 95 to 300MeV. In this study an attempt is carried out to find how the symmetry term approach is useful for deriving global neutron-incident potentials from those of proton incidence. Potentials of interest in this study are in the range of neutron energies of 100 to 1000MeV and targets of C to U.

2. Potentials based on the Dirac-Schrödinger equation

Because of treatment in the intermediate range, the Dirac equation is suitable for potential parametrization. The time-like four-vector potential U_V and the Lorentz scalar potential U_S are chosen in the following form:

$$U_V(r,E) = V_V(E)f_V(r,E) + i\left[W_V(E)g_V(r,E) + W_{VSP}(E)h_V(r,E)\right],$$

$$U_S(r,E) = V_S(E)f_S(r,E) + i\left[W_S(E)g_S(r,E) + W_{SSP}(E)h_S(r,E)\right],$$

In these potentials, $V_V(E), V_S(E), W_V(E)$ and $W_S(E)$ show the volume term, and are approximately proportional to the nucleon density. Symbols of $W_{VSP}(E)$ and $W_{SSP}(E)$ indicate the surface term; they increase at the nuclear surface and are influential for low energy incidence. Values of $f(r,E)$ and $g(r,E)$ stand for the nuclear density distribution; either Wood-Saxon[1] or symmetrized forms[2,4] are utilized. Quantity of $h(r,E)$ is the differentiated function of $f(r,E)$, and accordingly takes a large value at the nuclear surface.

To simplify the calculation, the Dirac equation is often rearranged into a Schrödinger-type equation (Dirac-Schrödinger equation). Correspondingly, U_V and U_S are converted into the central potential U_{cent} and the spin-orbit potential U_{so} as

$$\left[p^2 + 2E\left(U_{cent} + U_{SO}\vec{\sigma}\cdot\vec{L}\right)\right]\phi(r) = \left[(E-V_c)^2 - m\right]\phi(r),$$

$$U_{cent} = \frac{1}{2E}\left(2EU_V + 2mU_S - U_V^2 + U_S^2 - 2V_cU_V + 2EU_{Darwin}\right),$$

$$U_{so} = -\frac{1}{2EAr}\frac{\partial A}{\partial r}, \quad U_{Darwin} = -\frac{1}{2}\frac{1}{Ar^2}\left(\frac{\partial}{\partial r}r^2\frac{\partial}{\partial r}A\right) + \frac{3}{4}\frac{1}{A}\left(\frac{\partial}{\partial r}A\right),$$

$$A = \frac{E + m + U_S - U_V - V_c}{E + m}.$$

Partial wave analysis is made by the Dirac-Schrödinger equation, and cross sections such as elastic scattering and reaction are obtained.

3. Determination of potential parameters

In the intermediate energy region, the potential is based on the sum of interactions between incident nucleon and individual nucleons in the nucleus. From this point of view, the optical model potential consists of potentials of proton-proton, proton-neutron and neutron-neutron. The symmetry of nuclear force on iso-spin gives the equivalence of interactions of proton-proton and neutron-neutron.

When a proton is incident on the target, a local value of potential V has the following dependence in a rough approximation.

$$V \propto \frac{Z}{A}V_{pp} + \frac{N}{A}V_{pn} = \frac{V_{pp} + V_{pn}}{2} + \frac{V_{pp} - V_{pn}}{2}\frac{N-Z}{A}$$

The first term in the right side is the average term, and the second the symmetry term. When a neutron is incident on the same target, the potential has the following dependence.

$$V \propto \frac{Z}{A}V_{pp} + \frac{N}{A}V_{pn} = \frac{V_{pp} + V_{pn}}{2} + \frac{V_{pp} - V_{pn}}{2}\frac{N-Z}{A}$$

This is coincides with the proton potential having the changed sign of the symmetry term.

The global parametrization by Cooper et al is utilized as proton-incident potentials in this study. As a first approach, the symmetry term was simply derived from the potentials, on the basis of their dependence on (N-Z)/A. After changing the sign of the symmetry term, the total cross sections for neutron incidence were calculated. The result are plotted by dashed line in Fig.1. One can see that the dashed lines are in good agreement with the

experimental data for ^{56}Fe to ^{208}Pb at energies of 200 to 300 MeV. It is quite interesting that the simple estimation of symmetry term based on the difference of potentials between ^{90}Zr and ^{208}Pb holds good in this energy region. The dashed lines underestimate the experimental data in the energy region of 80 to 200 MeV, and also in the range above 300 MeV.

Table 1 Values of the symmetry term

T(MeV)	b_{VV}	b_{WV}	b_{VS}	b_{WS}	b_{WVSP}	b_{WSSP}
50	188	84.7	-280	-118	4.69	-4.41
100	188	84.5	-280.7	-118	4.10	-4.03
200	185	89.7	-279	-123	-0.587	-0.346
300	179	93.5	-272	-127	-3.35	1.89
400	173	94.7	-265	-131	-3.36	2.68
500	169	94.9	-260	-135	-1.86	3.53
700	175	97.52	-267	-153	1.12	9.64
1000	213	114.7	-318	-205	-2.10	34.1

To find the influence of the symmetry term, a quantity of

$$f = (\sigma_1 - \sigma_0)/(\sigma_e - \sigma_0)$$

is evaluated, where

σ_0 : the calculated cross section for incident protons without the Coulomb potential

σ_e : the experimental cross sections

σ_1 : the calculated cross section after sign change of the symmetry term (neutron incidence).

Then the value of f are fitted by a smooth function as

$$f = \frac{1}{1 + e^{-(T-T_1)/a_1}} \frac{1}{1 + e^{(T-T_2)/a_2}}$$

The parameters are listed in Table.2, and the results are plotted in Fig1 by solid line. For heavy nuclei like ^{181}Ta and lighter ^{56}Fe, the solid lines reproduce the experimental data completely in the whole energy region, and give better results than chain lines obtained from the potentials by Shen et al. For ^{107}Ag and ^{63}Cu, the solid lines represent better the experimental data than the chain ones in the energy range below 400 MeV, but underestimate the data above this energy. The behavior of cross sections of ^{107}Ag and ^{63}Cu above 400 MeV seems to be different in quality from those of ^{181}Ta and ^{56}Fe.

Table 2 Parameters for the adjustment factor f. The parameters
are expressed in a form of $c_1 + c_2(N-Z)/A$.

	T_1	a_1	T_2	a_2
c_1	152	-4.42	379	-17.2
c_2	20.5	127	72.6	322

4. Neutron-incident differential cross sections

Neutron incident differential cross sections for the elastic scattering are calculated by the use of potentials obtained above. The results are plotted by solid lines in Fig. 2. The solid line for ^{63}Cu is almost the same as the chain line by the potentials of Shen et al. For ^{208}Pb, the solid line gives similar results to the dotted one of Kozack.

at angles below 9°, whereas the solid line deviates from the lines of Kozack. exponential type parametrization and Shen et al. The deviation may come mainly from invalidity of the original global parametrization of Cooper et al. for proton incidence on ^{208}Pb.
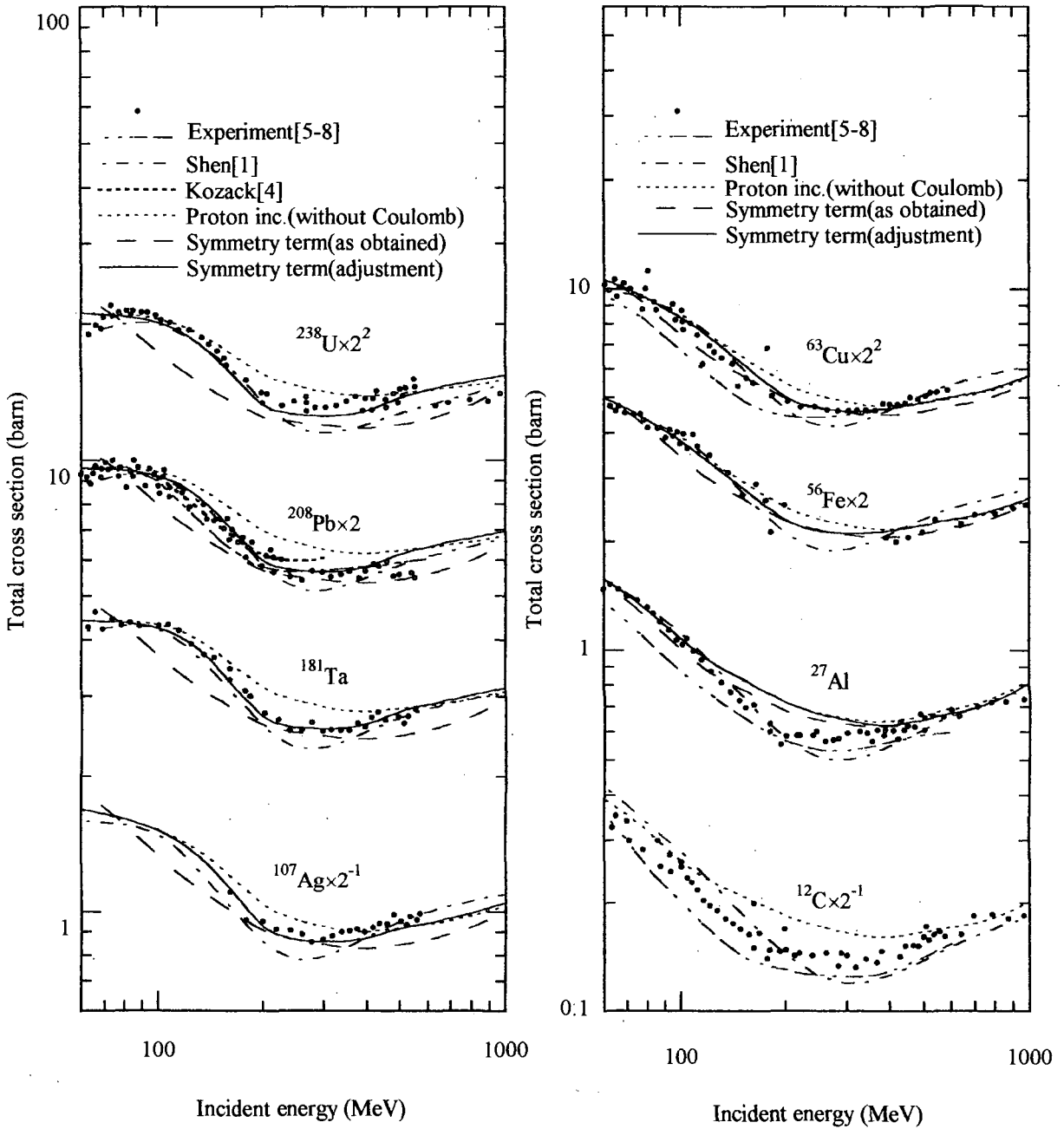
Fig.1 Neutron total cross section
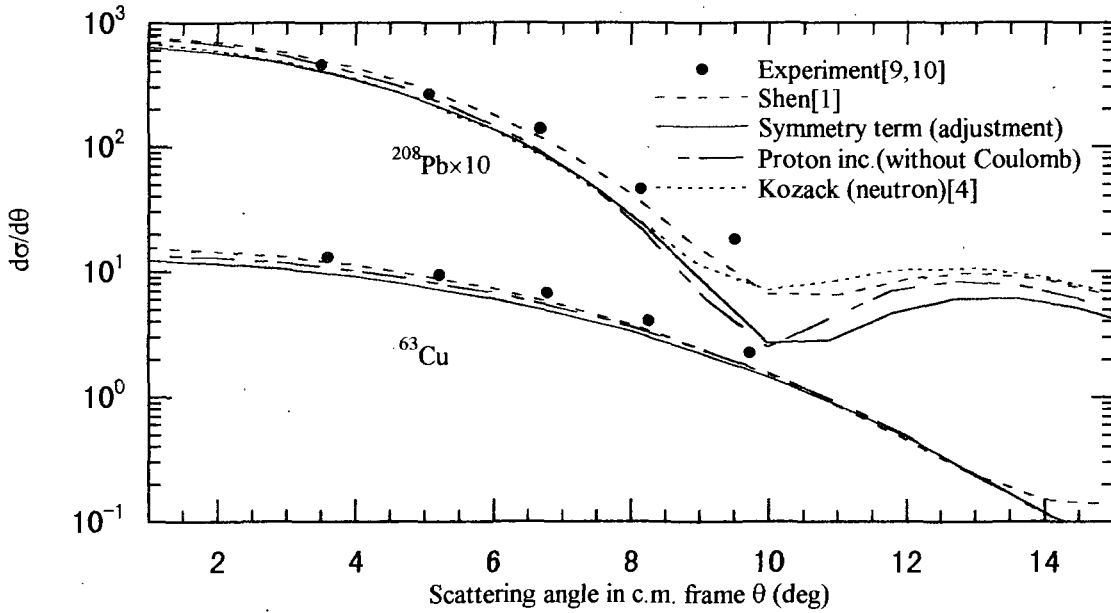
Fig.2 Neutron-incident differential cross section at T=155MeV

5. Comparison between potentials

Present potentials for ^{208}Pb are plotted in Fig. 3 together with those of Kozack and Madland and Shen et al. The potentials are displayed in a form of volume integral for proton and neutron incidence, to make clear the size of the symmetry terms. Although Shen et al. parametrized the potential parameters for neutrons with symmetry terms, the potentials for protons are simply deduced by changing the sign of symmetry terms. For U_{VR} at an energy of 200 MeV, the solid line for proton incidence in the present parametrization decreases to the chain line for neutron, i.e. a positive value of b in the symmetry term. In contrast, potentials by Shen et al. has no change in U_{VR} for proton and neutron incidence, and the dashed line for proton incidence in Kozack. increases to the dotted line for neutron, corresponding to a negative value of b. For U_{VI}, both present parametrization and Shen et al. have positive values of b, whereas that of Kozack owns a negative quantity. A similar contradiction appears in U_{SR} and U_{SI}. Although the sign of symmetry term is based on dependence of proton incidence parameters on target nuclei, it brings about a confusion in the sign of symmetry term. More studies are required to clear up the confused situation.

6. Concluding remarks

Neutron-incident optical model potentials were obtained by introduction of the symmetry term into proton-incident global potentials. The symmetry term shows a special tendency as a function of the incident energy, and its behavior in the energy region of 200 to 300 MeV is different from that out of the region. The potentials obtained for neutron incidence reproduce the total cross sections for Fe or heavier nuclei at neutron energies of 100 to 300 MeV. The calculated neutron-incident differential cross sections for elastic scattering are in fair agreement with the experimental data for target nuclei. For potentials proposed by present and other authors, the

confused situation remains in the sign of the symmetry terms.
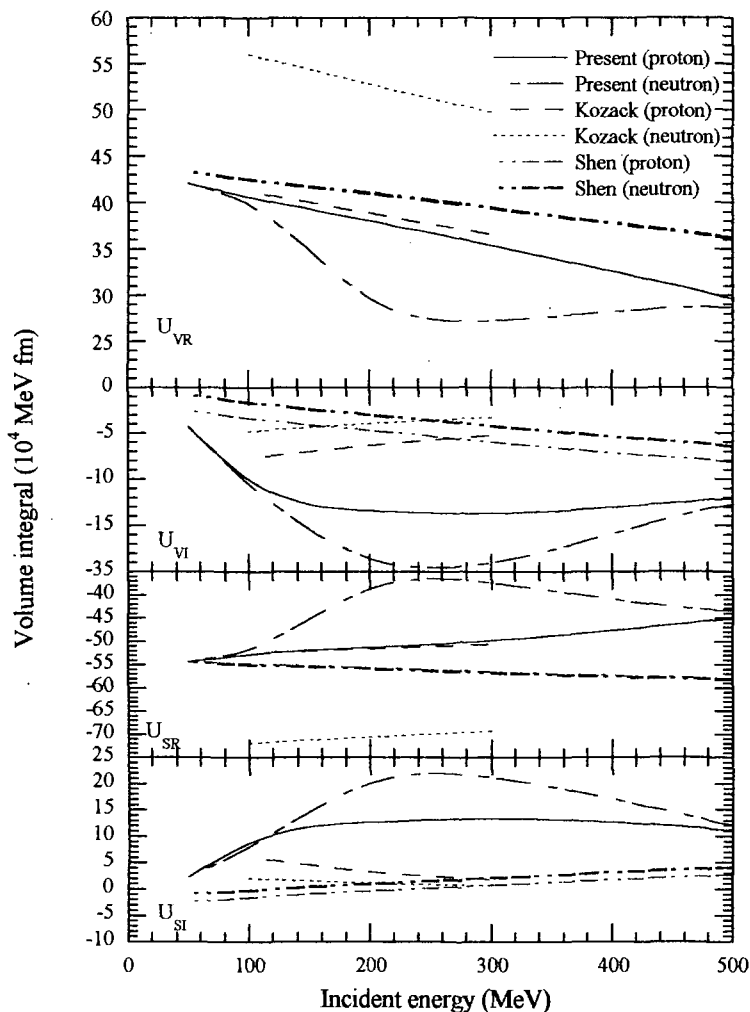
Fig.3 Volume Integral for ^{208}Pb

Acknowledgments

Referencese

[1] Shen, Q.B., Feng, D.C., and Zhuo, Y.Z.: *Phys. Rev.*, **C43**, 2773 (1991).

[2] Cooper, S., et al.: *Phys. Rev.*, **C47**, 297 (1993).

[3] Lane, A.M.: *Nucl. Phys.*, **35**, 676 (1962)

[4] Kozack, R., Madland, D.G.: *Phys. Rev.*, **C41**, 2737 (1990).

[5] Franz, J., et al.: *Nucl. Phys.*, **A 490**, 667 (1988), Pearlsteinin, S.: *Nuclear Data for Basic and Applied Science Proceedings of the International Conference Santa Fe*, New Mexico.

[6] Mclane, V., Dunford, C.L., and Rose, P.F.: *ÔNeutron Cross SectionsÔ*, Vol. 2.

[7] Schutt, R.L. et al.: *Phys. Lett.*, **B203**, 22 (1988).

[8] Finlay,R.W. et al.: *Phys. Rev.*, **C47**, 237 (1993).

[9] Salmon, G.L.: *Nucl. Phys.*, **21**, 15 (1960).

[10] Harding, R.S.: *Phys. Rev.*, **111**, 1164 (1958).

3.30 A Consistent Analysis of (p,p') and (n,n') Reactions Using the Feshbach-Kerman-Koonin Model

S. Yoshioka, Y. Watanabe, M. Harada, K. Sato, Y. Nakao, H. Ijiri
Department of Energy Conversion Engineering, Kyushu University, Kasuga, Fukuoka 816
e-mail: watanabe@ence.kyushu-u.ac.jp

S. Chiba, T. Fukahori, S. Meigo, M. Iwamoto
Japan Atomic Energy Research Institute, Tokai, Ibaraki 319-11

N. Koori
Faculty of Integrated Arts and Sciences, The University of Tokushima, Tokushima 770,

Double-differential proton emission cross sections were measured for proton-induced reactions on several medium-heavy nuclei (^{54,56}Fe, ^{60}Ni, ^{90}Zr, and ^{93}Nb) at two incident energies of 14.1 and 26 MeV. The (p,p') data for ^{56}Fe and ^{93}Nb were compared with available data of (n,n') scattering for the same target nuclei and incident energies, and both data were analyzed using the Feshbach-Kerman-Koonin model to extract the strength V_0 of the effective N-N interaction which is the only free parameter used in multistep direct calculations.

1. Introduction

The statistical multistep reaction theory of Feshbach-Kerman-Koonin (FKK) has been applied to analyze experimental data for nucleon-induced preequilibrium reactions with interests in basic and applied nuclear physics[1,2,3,4]. The FKK model reproduces various experimental data well by adjusting some model parameters, for instance, the strength V_0 of the effective N-N interaction used in the calculation of multistep direct (MSD) processes. The systematics of V_0 values (i.e., the dependence of incident energy and mass number) has been investigated through FKK analyses of (N,N'x) data. Recent analyses[5,6] for low incident energies less than 26 MeV have found that different V_0 values between (n,n') and (p,p') reactions are required to fit the experimental data. However, there was no available data set of (n,n') and (p,p') for the same targets and incident energies in those analyses. In the present work, therefore, we have undertaken to measure preequilibrium (p,p') spectra for the same targets and incident energies as in the previous (n,n') measurements[7,8] in order to see whether or not both (p,p') and (n,n') data can be described consistently well by the FKK model.

2. Experimental procedure and results

The experiments were performed using a 14.1 MeV proton beam from the Kyushu University Tandem accelerator and a 26 MeV proton beam from the JAERI Tandem accelerator. The experimental procedures were basically same as those reported in Refs. [5,9]. The targets used and their thicknesses are summarized in Table I. In the present measurements, we have used a new stacked ΔE-E silicon detector counter telescope with an active collimator made of an NE102A plastic scintillator. The thicknesses of ΔE and E silicon detectors are 75 μm and 2000 μm for the 14.1 MeV experiment, and 30 μm, 200 μm, 5000 μm for the 26 MeV experiment, respectively. Details of the counter telescope have been reported in Refs.[10,11]. The active collimator (AC) had a role as a veto detector to reduce the continuum background component due to the edge-penetration which makes it difficult to measure continuum (p,p') spectra at small angles. Signals from each detector were processed using commercially available NIM modules and a PC-based multiparameter data taking system. In the case of 14.1 MeV, energy spectra of emitted protons were measured at angles in steps of 10° from 20° to 160°; additional data were taken at 15° for ^{56}Fe and ^{60}Ni. On the

other hand, the measurement of (p,xp) spectra for 26 MeV were carried out in steps of 10° in the angular range between 30° and 150°.

As for the experiment of 26 MeV at JAERI, we have performed the measurements twice. In the first measurement, the ΔE(30 μm) silicon detector and the AC was not employed owing to some trouble. The silicon detector 200 mm in thickness was used as a ΔE detector, As a result, he threshold energy of protons to be detected was about 6 MeV. In the second measurement, the three-stacked ΔE-E silicon detector counter telescope was operated successfully. The data processing for the second measurement is now in progress and the final result has not yet been obtained. Hence we present the experimental result and analysis of the first measurement for 26 MeV in this paper.

Experimental double-differential cross sections of ^{93}Nb(p,p') at incident energies of 14.1 and 26 MeV are shown for four angles in Figs. 1 and 2. In the case where the backgrounds due to impurities (H, ^{12}C, ^{16}O) on the target and the nuclear reaction in E-detector (Si) were not completely eliminated, the positions are indicated in these figures. The continuum parts in the intermediate ejectile energy region exhibit obviously smooth and forward-peaked angular distributions which characterize preequilibrium particle emission. In Fig.2, the data of Moroz et al.[12] (open circles) are compared with our data (closed circles). Their experimental data at 30° are larger than our data over the whole continuum region, although the data at other angles are almost same except for the difference in the experimental threshold energy. From the fact that no active collimator was used in both the experiments, it seems that the data of Moroz et al. contain additional backgrounds other than the edge-penetration in the collimator slit, *e.g.*, the backgrounds due to the halo component in the incident proton beam and the nuclear reactions in E-detector by elastically-scattered protons.

3. FKK model analysis and discussions

The ^{93}Nb(p,p') data were analyzed together with (n,n') for the same incident energies using the modified FKK-GNASH code[5,13] in which the FKK model for the preequilibrium process and the Hauser-Feshbach (HF) model for the compound process are used. First of all, the strength V_0 of the effective N-N interaction was extracted using the same subtraction method as described in Ref.[5]. The other parameters used were same as those in REf.[5]. Typical results of the subtraction method are presented for the ^{93}Nb(p,p') reaction at 14.1 MeV in Fig. 3. The calculated one-step MSD cross section was normalized to the data by adjusting the strength V_0. The best fit V_0 values were 55.9 ± 2.3 MeV for 14.1 MeV and 42.8 ± 1.7 MeV for 26 MeV, respectively.

In Fig.4, the V_0 values are plotted for both (p,p') and (n,n') as a function of the incident energy together with our previous results[5]. As a result, there was found to be an obvious difference in V_0 between (p,p') and (n,n') even for the same target (^{93}Nb) and incident energy (14.1 MeV). However, both V_0 values for 26 MeV are not so different. Figure 4 shows that the incident energy dependence of V_0 values between (p,p') and (n,n') is different. The reason seems not clear at present, although the inclusion of the density-dependence of effective interaction[14] might explain the difference. Similar analyses for the other target nuclei are now in progress to investigate whether the above-mentioned trend of V_0 values depends upon the mass number of target nuclei.

Using each best fit V_0 value, we have calculated the angle-integrated (p,p') and (n,n') spectra for ^{93}Nb at 14.1 MeV using the modified FKK-GNASH code and compared them with the experimental data. The result is shown in Fig. 5. The same input parameters were used for both (p,p') and (n,n') except V_0 values. In the HF calculation of (p,p'), the isospin was taken into account as an additional quantum number in a manner corresponding to the case (B) in Ref.[13]. The isospin mixing parameter μ used was 51 %, which was almost same as that used for ^{98}Mo[14]. The calculations provide good agreement with both the experimental data of (p,p') and (n,n') in the continuum region lower than 10 MeV as can be seen in Fig.5.

4. Concluding remarks

The double differential cross sections of (p,xp) reactions were measured for ^{56}Fe, ^{60}Ni, and ^{93}Nb at 14.1 MeV and ^{54,56}Fe, ^{90}Zr, and ^{93}Nb at 26 MeV. In the measurements, the active collimator (the NE102A plastic scintillator) was installed in the ΔE-E silicon detector counter telescope and played a crucial role to reduce the continuum background due to the edge-penetration of elastically-scattered protons in the metallic collimator at angles less than 40°.

The FKK model was applied to the preequilibrium analysis of both the (p,p') and (n,n') for ^{93}Nb. The subtraction method was used to extracted the strength V_0 of the effective N-N interaction necessary in the FKK-MSD calculation. The extracted V_0 values showed the differences between (p,p') and (n,n'), which depend upon the incident energy. Further detailed analysis would be necessary to understand the reason why the difference appears. The FKK-GNASH calculations with common input parameters except V_0 values reproduced well the experimental angle-integrated spectra of (p,xp) and (n,xn) on ^{93}Nb.

Acknowledgments

References

[1] H. Feshbach, A. Kerman, and S. Koonin, Ann. Phys. (N.Y.) **125** (1980) 429.
[2] E. Gadioli and P.E. Hodgson, *Preequilibrium Nuclear Reactions,* (Oxford University Press 1992).
[3] R. Bonetti, M.B. Chadwick, P.E. Hodgson, B.V. Carlson, and M.S. Hussein, Phys. Rep. **202** (1991) 171; R. Bonetti, A.J. Koning, J.M. Akkermans, and P.E. Hodgson, Phys. Rep. **247** (1994) 1.
[4] See for instance, P.E. Hodgson and M.B. Chadwick, *Proc. of Int. Conf. on Nuclear Data for Science and Technology*, Gatlinburg, Tennessee, U.S.A, May 9-13, 1994, Ed. by J.K. Dickens, (American Nuclear Society, Inc., 1994), p. 519.
[5] Y. Watanabe et al., Phys. Rev. C **51** (1995) 1891.
[6] P. Demetriou et al., J. Phys. G **22** (1996) 629.
[7] A. Takahashi et al., Osaka University, OKTAVIAN Report No. A-92-01 (1992).
[8] M. Baba et al., J. Nucl. Sci. Technol. **31** (1994) 757.
[9] Y. Watanabe et al., Phys. Rev. C **36** (1987) 1325.
[10] M. Hayashi et al., *Proc. of the 1994 Symp. on Nuclear Data*, November 17-18, 1994, JAERI, Tokai, JAERI-Conf 95-008 (1995), p. 225.
[11] Y. Nakao et al., Kyushu University Tandem Laboratory, KUTL report-5 (1995), p. 115.
[12] Z. Moroz et al., Soltan Institute for Nuclear Studies, SINS Report (1996).
[13] Y. Watanabe, *Proc. of Int. Symp. on Pre-Equilibrium Reactions*, Smolenice, Slovakia, October, 1995, acta physica slovaca **45** (1995) 749.
[14] M. Avrigeanu et al., to be published in Phy. Rev. C (1996).

Table I Targets used in the experiments and their thickness

14.1 MeV		26 MeV	
^{56}Fe	570 μg/cm^2	^{54}Fe	480 μg/cm^2
^{60}Ni	760	^{56}Fe	445
^{93}Nb	545	^{90}Zr	475
		^{93}Nb	490
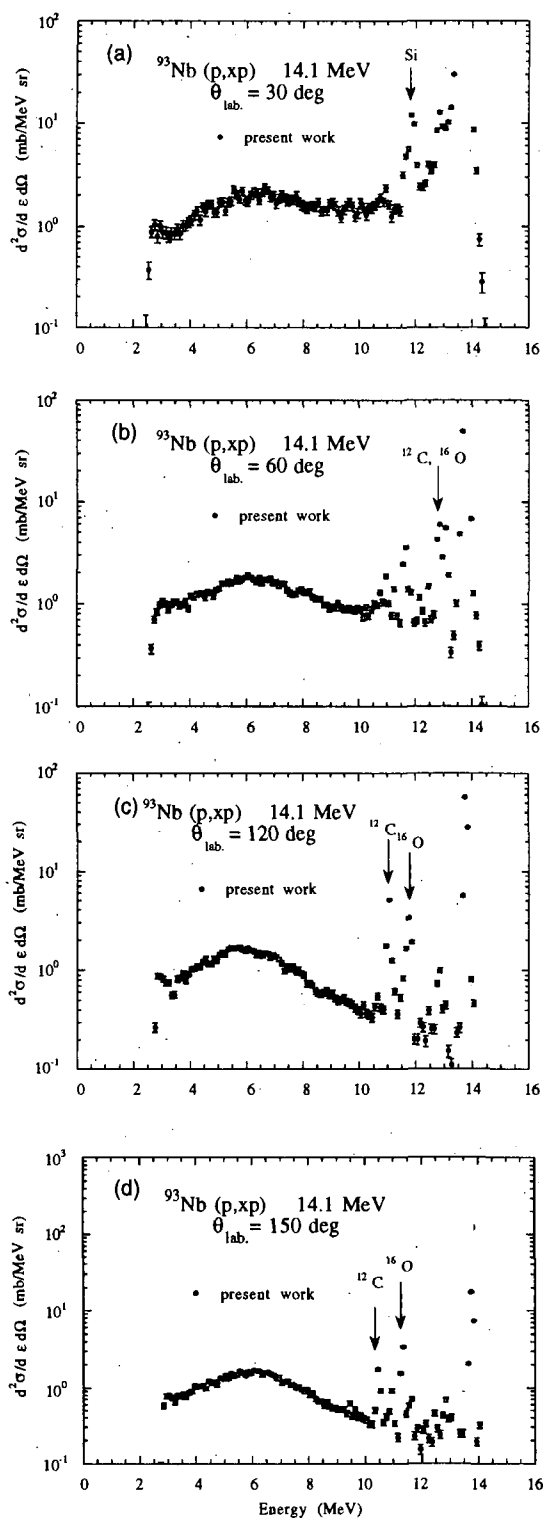
Fig.1 Experimental double-differential (p,p') cross sections for ^{93}Nb at E_p=14.1 MeV.
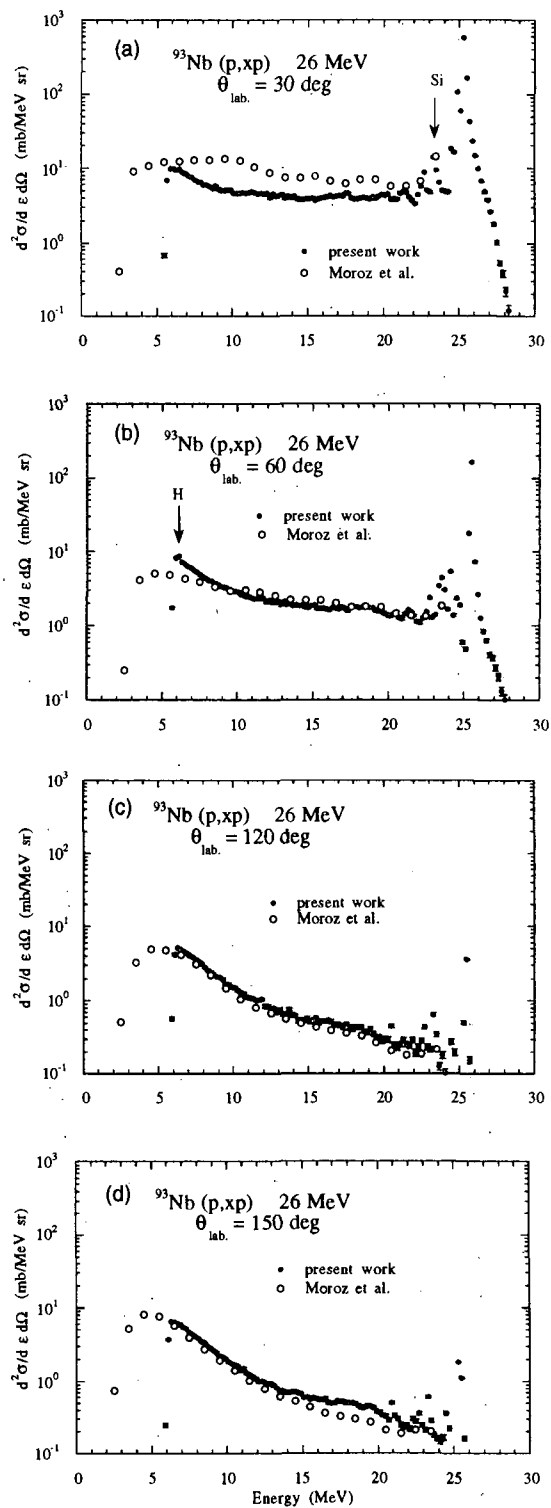
Fig.2 Same as in Fig.1 but for E_p=26 MeV.
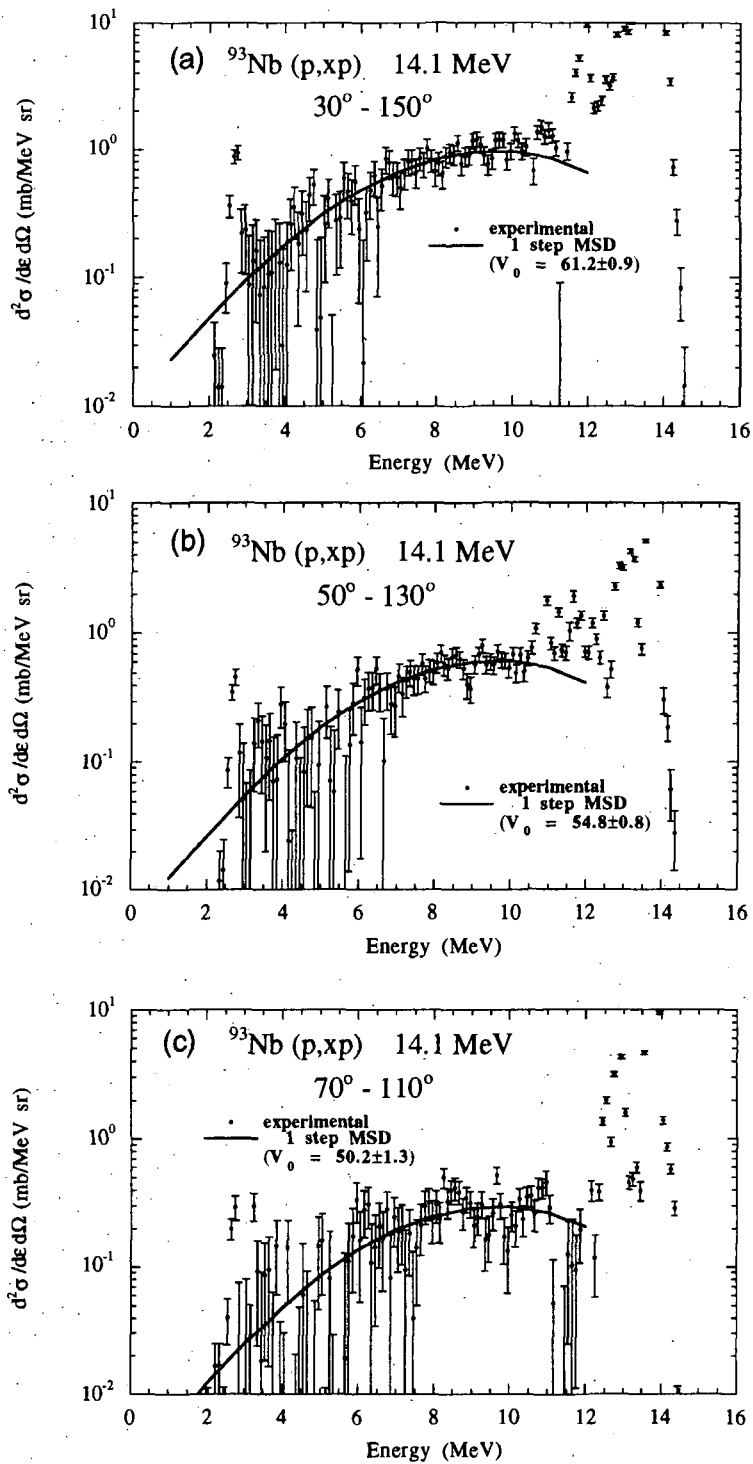
Fig.3   Subtracted double-differential cross sections for 14.1 MeV (p,p') on ^{93}Nb for three pairs of complementary angles. The solid curves are subtracted double-differential cross sections of the one-step MSD component. The curves are normalized to the data and the extracted best fit V_0 and the error are indicated in each figure.
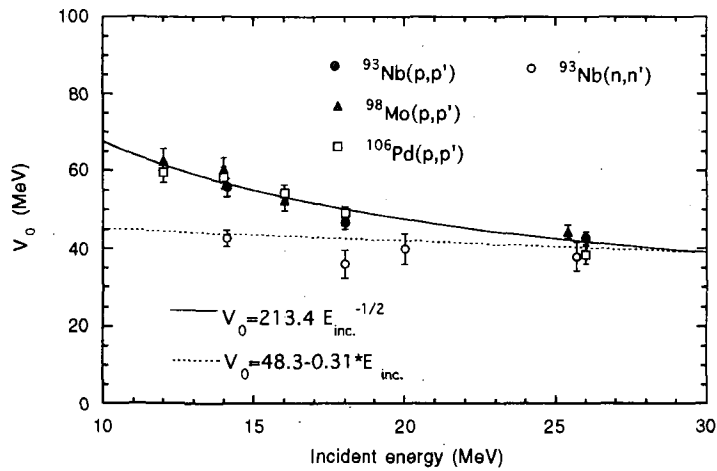
Fig.4   The extracted strength V_0 plotted as a function of the incident energy. The V_0 values are taken from Ref.[5] except for those of the ^{93}Nb(p,p') reactions at 14.1 and 26 MeV.
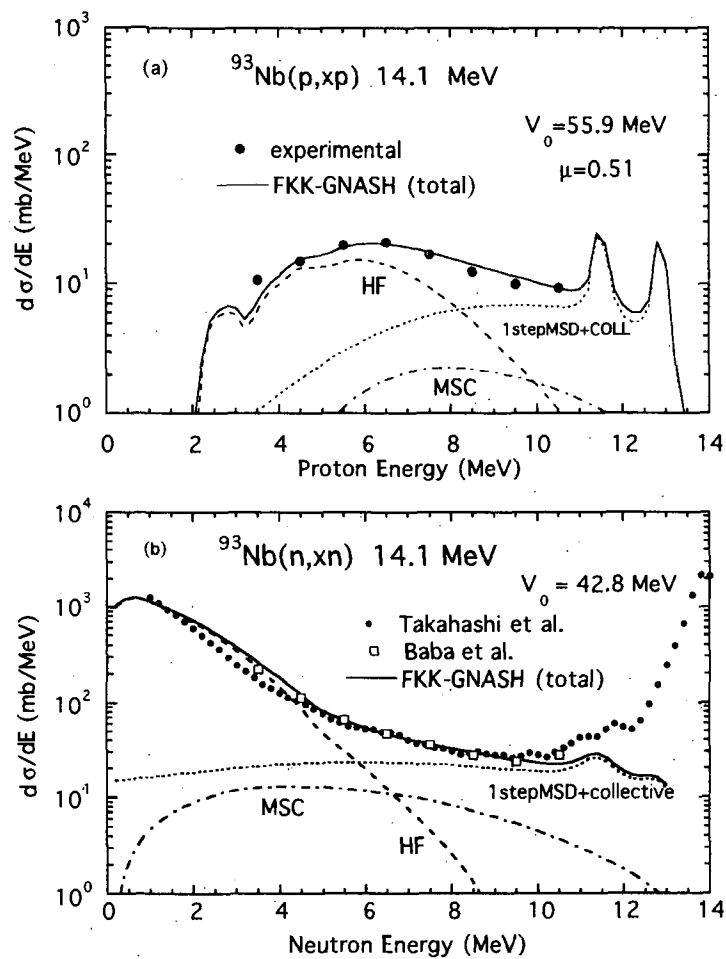
Fig.5   Comparison of the angle-integrated (N,N') spectra for ^{93}Nb at 14.1 MeV with the modified FKK-GNASH calculations: (a) (p,p') and (b) (n,n').

3.31 Construction of a Nuclear Data Server using TCP/IP

Toshihiko KAWANO[†] and Osamu SAKAI[‡]
Energy Conversion Engineering, Kyushu University
6-1 Kasuga-kouen, Kasuga 816, Japan
e-mail[†]: kawano@ence.kyushu-u.ac.jp
e-mail[‡]: sam@ence.kyushu-u.ac.jp

We construct a nuclear data server which provides data in the evaluated nuclear data library through the network by means of TCP/IP. The client is not necessarily a user but a computer program. Two examples with a prototype server program are demonstrated, the first is data transfer from the server to a user, and the second is to a computer program.

1. Introduction

Nuclear data have been provided with various media — namely magnetic tape, a disk, and so on, however the nuclear data recently became more accessible since network environment is expanding over the whole world. There are several ways to transmit data through the network. TCP/IP (Transmission Control Protocol/Internet Protocol) is one of the most popular protocol[1], and it has been used to transmit scientific data over the Internet. FTP (File Transfer Protocol) is one of the standard application protocol which is defined by the TCP/IP. A file transfer client which uses the FTP allows a user to transfer files to and from a network, and the nuclear data have been mainly provided using the FTP program.

Use of a standard application service such as the file transfer program makes it possible to communicate with the other networks easily. The protocol is, however, designed to transfer a file, not the numerical data themselves. We planed to construct a nuclear data server which provides data in the evaluated nuclear data library through the network. A conceptual design and examples with a prototype are shown in this study. The nuclear data server is designed using the TCP/IP in order to avoid machine dependent feature, but the protocol is locally-defined. The client is not necessarily a user. The server is designed so as to send nuclear data to users as an interactive system, but also it provides data to computer programs automatically.

2. Server

The nuclear data server has following components:

- Server daemon program

  - Primary server
  - Secondary server, and data cache system

- Evaluated nuclear data library search system

- Client program – network interface library

Physical configuration of the data server system is shown in Fig.1.

The primary server is installed somewhere in the Internet, where the organization has the authorized data-base. Data maintenance should be done to this server. The secondary server is in the local area network (LAN). The secondary server does not keep any data at first. When the secondary server accepts clients' requests it forwards the requests to the primary server and gets requisite data, then the secondary server feeds the data to the clients. At the same time, the secondary server copies the data (Cache) to local storage in order to reuse the data for a repeated request. The scheme of the data flow is illustrated in Fig.2.
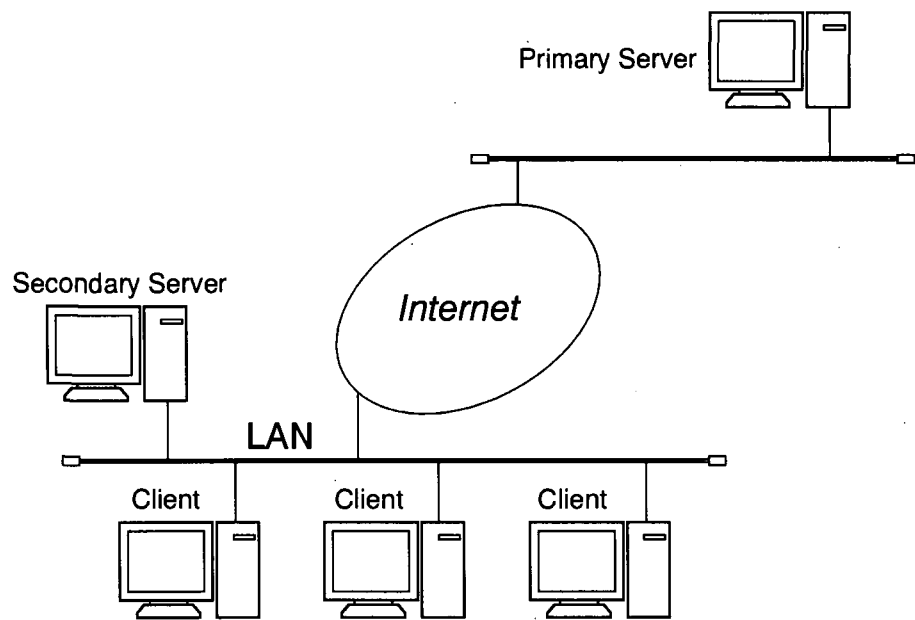
Fig.1 : Network configuration
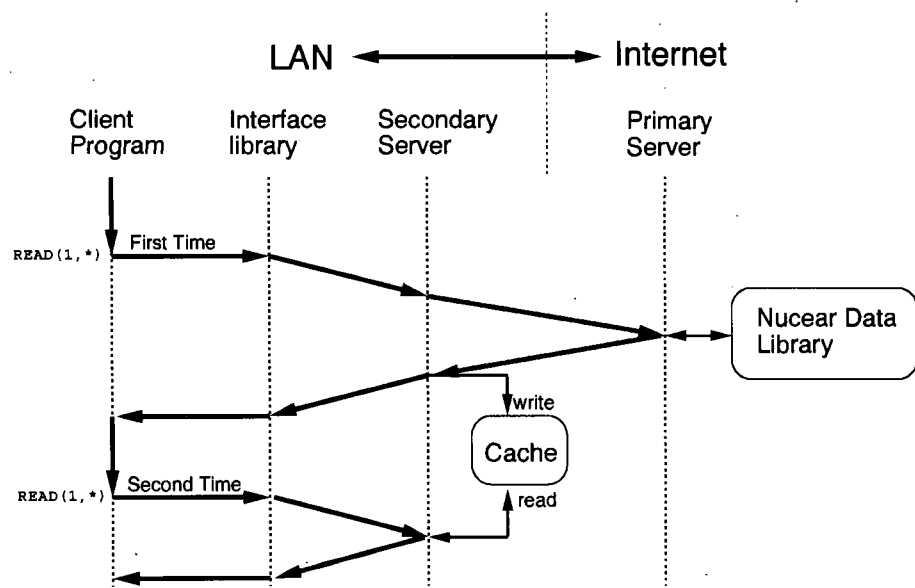
Fig.2 : Flow of the message between a client and servers

The server program uses socket interface which was implemented in the BSD (Berkeley Software Distribution) UNIX. The socket interface has been adopted by many vendors and it is *de facto* standard. The server program listens clients' requests on the network (`listen` system call). When a client computer program needs nuclear data, which is usually a cross section of a specific reaction type and an energy, it calls `connect` system call to establish a connection, and sends the request with `write` system call. The server receives the request (`read`) it looks up the value in the data-base and returns the value(`write`).

3. Client

Clients are programs which require the nuclear data library. An interactive use such as nuclear data search and the data retrieval is provided by a user-interface program. These client programs lies in an application layer and they can access to the TCP/IP layer with an interface library. The interface library lies between the application program and the TCP/IP layer and it simplifies a coding of programs which use the TCP/IP. We supply two libraries, FORTRAN and C.

The client programs drive the server in various modes. Some examples of feasible use are shown in Fig.3. The server transfers ASCII data to the clients when the clients are user-interface programs or applications. In Fig.3 a possible user-interface application is a WWW browser through CGI (Common Gateway Interface). In the BINARY mode the server transfer binary data. This mode is mainly used by nuclear data process programs.
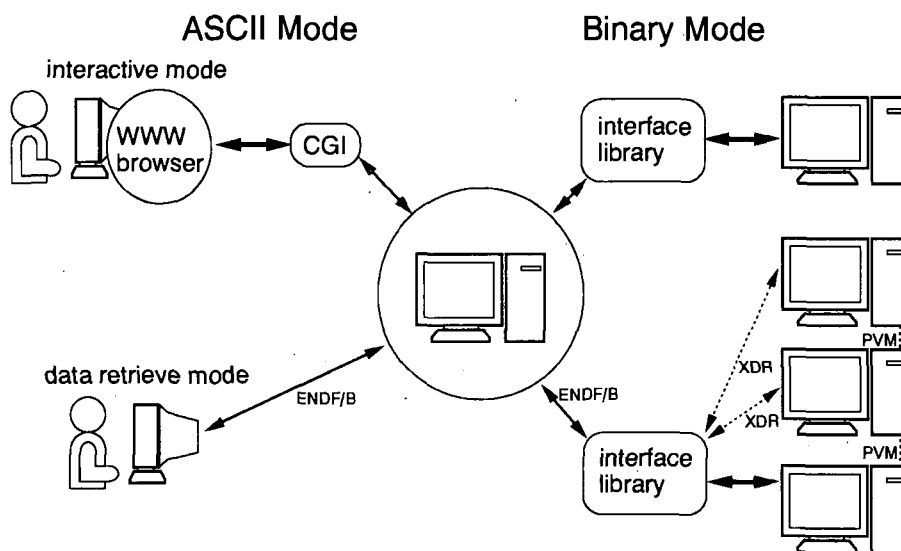
Fig.3 : Examples of the nuclear data server use

4. Examples and Discussion

Two examples using the nuclear data server are shown in Figs.4 and 5. In these examples clients access directly to the primary server which is installed in LAN.

The first example demonstrates communication between a user and the server through a user-interface program. The program allows user to retrieve nuclear data if one gives ZA, MF, and MT numbers. The program sends a request to the server by means of the socket library, receives asked data from the server, and displays the result. In this example the user input is ^{238}U total inelastic scattering data, and the output is ENDF-B formatted ASCII data.

```
% Data_Retrieval_Program
Enter ZA number (Z*1000+A): (92238)
Enter MF number: ③                        User Input
Enter MT number: ④
  9.2238e+04 2.3601e+02        0      99      0       03926 3  4
  0.0000e+00-4.4910e+04        0       0      1     1273926 3  4
        127          2         0       0      0       03926 3  4
  4.5100e+04 0.0000e+00 5.0000e+04 3.8658e-04 5.5000e+04 8.2189e-023926 3  4
  6.0000e+04 1.5349e-01 6.5000e+04 2.1875e-01 7.0000e+04 2.7754e-013926 3  4
  7.5000e+04 3.3073e-01 8.0000e+04 3.7928e-01 8.5000e+04 4.2421e-013926 3  4
  9.0000e+04 4.6609e-01 9.5000e+04 5.0496e-01 1.0000e+05 5.4152e-013926 3  4
..........
  1.1500e+07 8.3299e-01 1.2000e+07 7.9039e-01 1.3000e+07 7.1594e-013926 3  4
  1.4000e+07 6.9826e-01 1.5000e+07 6.6363e-01 1.6000e+07 6.4090e-013926 3  4
  1.7000e+07 6.1818e-01 1.8000e+07 5.9545e-01 1.9000e+07 5.7273e-013926 3  4
  2.0000e+07 5.5000e-01                                      3926 3  4
%
```

Fig.4 : An example of use : communicate with a user-interface program

Case 1   Case 2

exec time: ca. 10 sec   exec time: ca. 40 sec
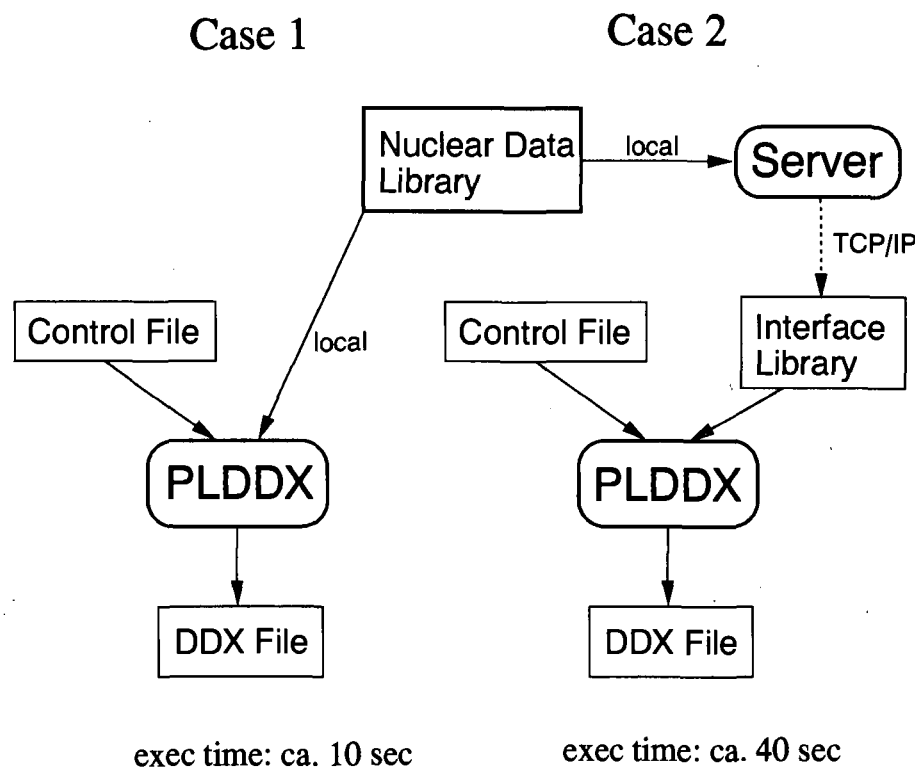
Fig.5 : An example of use : communicate with the nuclear data process program

The second example is data transfer from the server to a nuclear data processing computer program, PLDDX[2], which generates double differential cross sections from the cross sections (MF=3), the angular distributions (MF=4), and the energy spectra (MF=5) in the evaluated nuclear data library.

PLDDX calculation took about 10 seconds when the nuclear data library was prepared in the local hard drive (Case 1). When the data stored in the server and PLDDX read the data through the network it took about 40 seconds (Case 2). Obvious deterioration of the performance is demonstrated here. The slowest process during the communication is not a data tranfer part but a data search part. At the moment we have not optimized the data search system and the data search consumes much of the data transfer time.

We have examined performance of the client and the server inside the local area network. As seen in two examples the nuclear data server is practical, however, there seems to be some room to make an improvement. One of the problems is slow response of the server, and this may be improved if one uses suitable data-base format. When the data are transfered over the Internet a security problem becomes crucial, since the server is accessible without any authorization so far.

5. Conclusion

We proposed a nuclear data server which uses the TCP/IP, and some examples with a prototype server program were demonstrated. The first example showed that users are accessible interactively to the nuclear data library through a user-interface program. The second example showed that it is possible to transfer nuclear data from the server to a computer program, but the performance should be improved.

References

[1] Comer, D.E., Stevens, D.L., : "Internetworking With TCP/IP," Prentice-Hall, Inc. (1993).

[2] Fukahori, T., Chiba, S., and Asami, T.: JAERI-M 92-053, 201 (1992).

3.32 Decay Data File Based on the ENSDF File

J. Katakura

Nuclear Data Center

Japan Atomic Energy Research Institute

Abstract

A decay data file with the JENDL (Japanese Evaluated Nuclear Data Library) format based on the ENSDF (Evaluated Nuclear Structure Data File) file was produced as a tentative one of special purpose files of JENDL. The problem using the ENSDF file as primary source data of the JENDL decay data file is presented.

1 Introduction

As one of special purpose files of JENDL (Japanese Evaluated Nuclear Data Library), a decay data file is planned to be compiled. The decay data file is expected to include the decay data of all radioactive nuclides needed for application fields because the file is supposed to be applied to not only light water reactor field but also accelerator, actinide incineration fields and so on. As for the application to the light water reactor field, Japanese Nuclear Data Committee has released the second version of Nuclear Data Library of Fission Products [1] (JNDC-V2 library) which is the data library for decay heat evaluation in reactors and includes all the necessary decay data for it. The planed decay data file is expected to be consistent with the library and is therefore considered to be the extension of the library. The feature of the JNDC-V2 library is adoption of model calculated decay data to the nuclides without reliably measured data. The primary data source, however, is experimentally measured ones and the model calculated data are used to compensate the defect of the measured data.

As the primary data source of compiling the decay data file of JENDL, the ENSDF [2] (Evaluated Nuclear Structure Data File) file is suitable one because the file is internationally recognized comprehensive data base of nuclear structure and decay data and includes all experimentally measured decay data. The included data are considered to be the newest ones because of expected regularly updating. However, there is disadvantage using the ENSDF file because some nuclides have incompletely measured decay data.

The purpose of making a tentative decay data file with the JENDL format is to get the understanding of problems using the ENSDF file as source data file and to make the way to the future compilation of the JENDL decay data file.

2 Processing the ENSDF file

The ENSDF file is made up of a collection of "data sets" which present one of the following kinds of information [3]:

- The evaluated results of a single experiment, e.g., a radioactive decay or a nuclear reaction.

- The combined evaluated results of a number of experiments of the same kind, e.g., (Heavy ion,xnγ), Coulomb excitation, etc.

- The adopted properties of the nucleus.

- The references used in all the data sets for the given mass number. This data set is based upon reference code (key numbers) used in various data sets for a given mass number and is added to the file by NNDC (National Nuclear Data Center).

- The summary information for a mass chain giving information, e.g., evaluator's name and affiliations, cutoff date, Nuclear Data Sheets publication details, etc.

In the processing of the ENSDF file, at first, decay data sets like β^- decay, β^+ and/or ϵ decay and IT decay are retrieved from the ENSDF file, but the SF(Spontaneous Fission) decay data sets are excluded in the present purpose. The decay data are converted to the JENDL format (the same as the ENDF format [4]) with the utility code RADLST [5]. The decay data file produced by this way can not be directly served as a JENDL decay data file because there is a possibility that the file have some problems. One of those is that the the data of some nuclides in the ENSDF file are incomplete because of the difficulty of experiment to get the data. Especially the decay data of nuclides with short half-life are not always completely given by the experiment. Therefore the need of the modification of the decay data file is required. And also there may be no experimental data for the nuclides needed for some applications. For such nuclides the needed data should be added by some model calculations. The procedure of making the JENDL decay data file is shown in Fig 1. In the present report the modification of the decay data file, however, has not been performed yet.

The number of decay data sets thus processed is tabulated in Table 1. As seen in the table, total 3159 decay data sets were processed, but 743 sets had some errors and the JENDL format data for them were not produced. Therefore the JENDL format file including 2416 decay data sets were produced. As for the 734 data sets with error detailed examination of the cause of the error is needed and the effort of removing the error is going to be done.

Table 1: Number of decay data processed

Mass number	Processed	Error	No error
1-50	277	92	185
51-100	564	107	457
101-150	874	184	690
151-200	854	239	615
201-266	590	121	469
Total	3159	743	2416

The examples of the ENSDF decay data set and the produced decay data for ^{51}K β^- decay are shown in Fig 2 and 3.
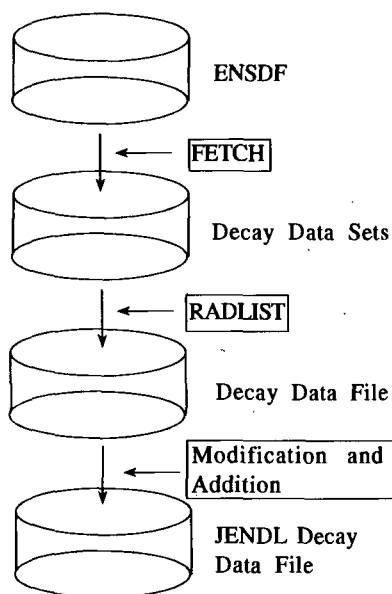
Figure 1: Flow of JENDL Decay Data File Production

3 Produced Decay Data File

The directly produced decay data file from the ENSDF file as mentioned above has following problems:

- The data of the nuclide with more than one decay mode are produced for each decay mode.

- The identification number of the produced data is different from that of the JENDL file.

- Incomplete decay data of some short lived nuclides.

In the ENSDF file, the nuclide with more than one decay mode, for example β^- decay and isomeric transition modes, has two data sets, β^- data set and IT data set. Processing them with the RADLST code two JENDL format data sets with the same ID number are produced. They have to be merged to one data set as the JENDL data. The problem concerning ID number will be settled by changing the ID number. The incomplete decay data mean that spectroscopic measurement which is the basis of the ENSDF data often misses higher energy levels of the daughter nucleus and the related β and γ transitions. That leads to the overestimated β energy and the underestimated γ energy per decay. As examples of incomplete decay data, beta ray spectra of the ENSDF file are shown in Fig 4 and 5 comparing with the directly measured beta ray spectra [6].

```
1.90510+04 5.05379+01        -1          0          1      11951 1451
0.00000+00 1.00000+00         0          0          0      61951 1451
0.00000+00 0.00000+00         0          0          4      61951 1451
0.00000+00 0.00000+00         0          0         23      21951 1451
19-K - 51 BNL        EVAL-FEB96 CONVERSION OF ENSDF        1951 1451
/ENSDF/              DIST-AUG91 REV1-                       1951 1451
---- ENDF/A-6        MATERIAL 1951                          1951 1451
----- DECAY DATA                                           1951 1451
------ ENDF-6                                              1951 1451
  51K B- DECAY (365 MS 5)          I(MIN)=0.0010%           1951 1451
       RADLST 5.5 [ 5-OCT-88].                              1951 1451
83RAZR: SOURCE PRODUCED BY U(P,X) E=600 MEV; MEASURED B-DELAYED  1951 1451
        NEUTRON, BN, BG, BGN. SHELL-MODEL CALCULATIONS.    1951 1451
81LA23: SOURCE PRODUCED BY IR(P,X) E=10 GEV; MEASURED B-DELAYED  1951 1451
        NEUTRON YIELD, EMISSION PROBABILITY, AND T1/2.     1951 1451
SEE ALSO 86LY02 AND 83LY06.                                1951 1451
BETAS:           ALL DATA ARE FROM 83RAZR, EXCEPT AS NOTED. 1951 1451
BETAS:    IB     FROM INTENSITY IMBALANCE AT EACH LEVEL.   1951 1451
BETAS:    IB(A)  DIB ESTIMATED TO BE 15%.                   1951 1451
GAMMAS:          ALL DATA ARE FROM 83RAZR; DE AND IG ARE NOT 1951 1451
        GIVEN.                                             1951 1451
GAMMAS:  RI$RELATIVE INTENSITY NORMALIZED TO IG(3462G)=100 15. 1951 1451
        VALUES FROM IB.                                    1951 1451
NORMALIZATION: NR     FROM IB(TO 3462)=10.7 16 AND IB(TO   1951 1451
        3530)=2.3 3 AND G'S TO GS                          1951 1451
NORMALIZATION: BR     %B-=100 (83RAZR AND 81LA23)          1951 1451
NORMALIZATION:  0.107                  1.0                 1951 1451
0.00000+00 0.00000+00         1        451         28      01951 1451
0.00000+00 0.00000+00         8        457          0      01951 1451
0.00000+00 0.00000+00         0          0          0      01951  1 0
0.00000+00 0.00000+00         0          0          0      01951  0 0
1.90510+04 5.05379+01         0          0          0      21951 8457
3.65000-01 5.00000-03         0          0          6      01951 8457
3.50000+06 3.00000+05 4.50000+05 6.00000+04 1.02000+03 8.00000+011951 8457
-7.77770+01 0.00000+00         0          0          6      11951 8457
1.00000+00 0.00000+00 1.26000+07 0.00000+00 1.00000+00 0.00000+001951 8457
0.00000+00 0.00000+00         0          0          6      21951 8457
1.07000-03 0.00000+00 4.50000+05 6.00000+04 0.00000+00 0.00000+001951 8457
3.46200+06 0.00000+00         0          0          4      01951 8457
1.00000+00 0.00000+00 1.00000+02 1.50000+01                 1951 8457
3.53000+06 0.00000+00         0          0          4      01951 8457
1.00000+00 0.00000+00 2.20000+01 3.00000+00                 1951 8457
0.00000+00 1.00000+00         0          0          6      101951 8457
1.00000-02 0.00000+00 3.50000+06 3.00000+05 0.00000+00 0.00000+001951 8457
4.68900+06 0.00000+00         0          0          4      01951 8457
1.00000+00 1.00000+00 7.00000+00 2.00000+00                 1951 8457
5.14900+06 0.00000+00         0          0          4      01951 8457
1.00000+00 1.00000+00 1.20000+01 4.00000+00                 1951 8457
5.77800+06 0.00000+00         0          0          4      01951 8457
1.00000+00 1.00000+00 1.10000+01 2.00000+00                 1951 8457
5.94800+06 0.00000+00         0          0          4      01951 8457
1.00000+00 1.00000+00 1.50000+01 3.00000+00                 1951 8457
6.55800+06 0.00000+00         0          0          4      01951 8457
1.00000+00 1.00000+00 5.00000+00 2.00000+00                 1951 8457
7.07800+06 0.00000+00         0          0          4      01951 8457
1.00000+00 1.00000+00 1.60000+01 4.00000+00                 1951 8457
7.40800+06 0.00000+00         0          0          4      01951 8457
1.00000+00 1.00000+00 1.00000+00 1.00000+00                 1951 8457
9.06740+06 2.00000+03         0          0          4      01951 8457
1.00000+00 1.00000+00 2.30000+00 3.00000-01                 1951 8457
9.13540+06 1.00000+03         0          0          4      01951 8457
1.00000+00 1.00000+00 1.07000+01 1.60000+00                 1951 8457
1.26000+07 0.00000+00         0          0          4      01951 8457
1.00000+00 1.00000+00 1.90000+01 3.00000+00                 1951 8457
0.00000+00 0.00000+00         0          0          0      01951  8 0
0.00000+00 0.00000+00         0          0          0      01951  0 0
0.00000+00 0.00000+00         0          0          0       0  0 0 0
```

```
51CA    51K B- DECAY            83RAZR,83LA23        91NDS    910807
51CA C  83RAZR: SOURCE PRODUCED BY U(P,X) E=600 MEV; MEASURED B-DELAYED
51CA2C  NEUTRON, BN, BG, BGN. SHELL-MODEL CALCULATIONS.
51CA C  81LA23: SOURCE PRODUCED BY IR(P,X) E=10 GEV; MEASURED B-DELAYED
51CA2C  NEUTRON YIELD, EMISSION PROBABILITY, AND T1/2.
51CA C  SEE ALSO 86LY02 AND 83LY06.
51CA CL         ALL DATA ARE FROM 83RAZR, EXCEPT AS NOTED.
51CA CL E       DE NOT GIVEN (83RAZR).
51CA CL J       FROM ADOPTED LEVELS.
51CA CB         ALL DATA ARE FROM 83RAZR, EXCEPT AS NOTED.
51CA CB IB      FROM INTENSITY IMBALANCE AT EACH LEVEL.
51CA CB IB(A)   DIB ESTIMATED TO BE 15%.
51CA CB LOGFT   CALCULATED BY USING LOGFT PROGRAM.
51CA CG         ALL DATA ARE FROM 83RAZR; DE AND IG ARE NOT GIVEN.
51CA CG RI$RELATIVE INTENSITY NORMALIZED TO IG(3462G)=100 15. VALUES FROM
51CA2CG IB.
51K   P 0.0         (1/2+,3/2+)      365 MS  5          12600    CA
51CA  N 0.107                         1         1
51CA  CN NR    FROM IB(TO 3462)=10.7 16 AND IB(TO 3530)=2.3 3 AND G'S TO GS
51CA  CN BR    %B-=100 (83RAZR AND 81LA23)
51CA  PN 0.107                 1.0
51CA  L 0.0         (3/2-)
51CA  B         19      3              6.05 7
51CAS B EAV=    5998
51CA4 B FLAG=A$
51CA  L 3462      1(1/2+,3/2+,5/2+)
51CA  B         10.7    16             5.64 7
51CAS B EAV=  4299.2 5
51CA4 B FLAG=A$
51CA  G 3462      100     15                              C
51CA  L 3530      2(1/2,3/2,5/2)
51CA  B         2.3     3              6.29 6
51CAS B EAV=  4265.8 10
51CA4 B FLAG=A$
51CA  G 3530      21.5    28
51CA  L 5190      (1/2,3/2,5/2)                            C
51CA2 L %B-N <2$
51CA  B         2       LT             5.9 GT
51CAS B EAV=    3450
51CA  L 5520      (1/2+,3/2+,5/2+)
51CA2 L %B-N=16.0 43$
51CA  B         16      4              4.9511
51CAS B EAV=    3288
51CA  L 6040      (1/2+,3/2+,5/2+)
51CA2 L %B-N=5 2$
51CA  B         5       2              5.3018
51CAS B EAV=    3033
51CA  L 6650      (1/2+,3/2+,5/2+)
51CA2 L %B-N=15 3$
51CA  B         15      3              4.63 9
51CAS B EAV=    2734
51CA  L 6820      (1/2+,3/2+,5/2+)
51CA2 L %B-N=11 3$
51CA  B         11      2              4.70 8
51CAS B EAV=    2651
51CA  L 7450      (1/2+,3/2+,5/2+)
51CA2 L %B-N=12 4$
51CA  B         12      4              4.4315
51CAS B EAV=    2342
51CA  L 7910      (1/2+,3/2+,5/2+)
51CA2 L %B-N=7.0 27$
51CA  B         7       2              4.4813
51CAS B EAV=    2118
```

Figure 2: ENSDF format data
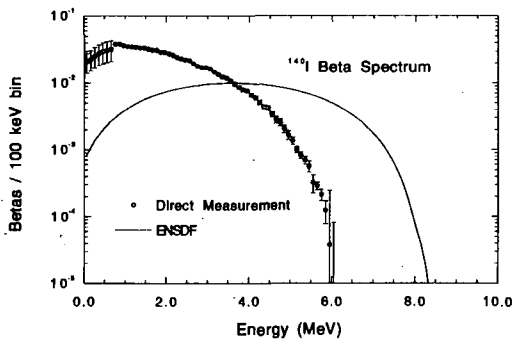
Figure 3: Produced ENDF format data
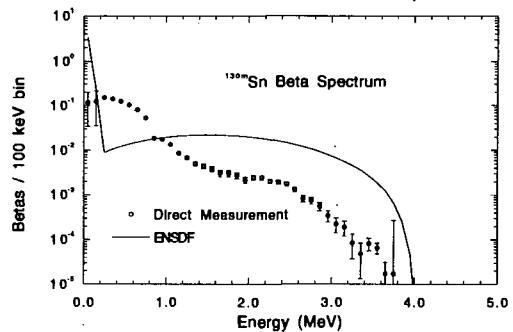

Figure 4: Beta ray spectrum of ^{140}I

Figure 5: Beta ray spectrum of ^{130m}Sn

In these figures directly measured spectra are indicated by circle and the spectra calculated from the ENSDF data by solid lines. The ENSDF data extend the beta ray to higher energy region than the directly measured data which means the spectroscopic data exaggerate the high energy β ray, that is, β transition to lower levels of daughter nucleus, and the resultant average β energy is overestimated. This problem has been recognized in the application to the decay heat analysis in a reactor. In order to remove the problem model calculated data have been applied to the incomplete decay data as in JNDC-V2 library and ENDF/B-VI decay data file [7]. In the expected JENDL decay data file the model calculated data will be incorporated into the file in order to remove the problem due to the incompleteness of the measured data in the ENSDF file.

4   Summary

Decay data file with the JENDL format was produced from the ENSDF file as a tentative JENDL decay data file. 3159 decay data in the ENSDF file were processed. Of these data 2416 decay data were produced with RADLST code. Other 743 data showed some error when processed. These data will be checked and corrected for JENDL decay data file. The produced data of some nuclides with more than one decay mode are needed to be merged. And also the ID number of the produced data will be changed to fit the JENDL ID number. The present decay data file is a tentative one and problems producing the decay data file from the ENSDF file are searched. These problems are going to be removed when the JENDL decay data file is compiled.

Acknowledgement

The author wishes to thanks to Mr. Ichimiya, The Japan Radioisotope Association, for running the RADLST code.

References

[1] Tasaka, K. et al.: "JNDC nuclear data library of fission products - second version," JAERI 1320, Japan Atomic Energy Research Institute (1990).

[2] "Evaluated Nuclear Structure Data File (ENSDF)," National Nuclear Data Center, Brookhaven laboratory.

[3] Tuli, J.K.: "Evaluated Nuclear Structure Data File - A Manual for Preparation of Data Sets," Report BNL-NCS-51655-Rev. 87, Brookheaven National Laboratory (1987)

[4] Rose, P.F. and Dunford, C.L.: "Data formats and procedures for the Evaluated Nuclear Data File ENDF-6," Report BNL-NCS-44945 (ENDF-102) Rev. 10/91, Brookhaven National Laboratory (1991)

[5] Burrows, T.W.: The Program RADLST, Report BNL-NCS-52142, Brookhaven National Laboratory (1988)

[6] Rudstam, G. et al.: At. Data Nucl. Data Tables, 45 239 (1990)

[7] Katakura, J.: "Augmentation of ENDF/B Fission Product Gamma-Ray Spectra by Calculated Spectra," LA-12125-MS (ENDF-352), Los Alamos National Laboratory (1991)

国際単位系 (SI) と換算表

表1 SI基本単位および補助単位

量	名 称	記 号
長 さ	メ ー ト ル	m
質 量	キ ロ グ ラ ム	kg
時 間	秒	s
電 流	ア ン ペ ア	A
熱力学温度	ケ ル ビ ン	K
物 質 量	モ ル	mol
光 度	カ ン デ ラ	cd
平 面 角	ラ ジ ア ン	rad
立 体 角	ステラジアン	sr

表3 固有の名称をもつSI組立単位

量	名 称	記号	他のSI単位による表現
周 波 数	ヘ ル ツ	Hz	s^{-1}
力	ニ ュ ー ト ン	N	$m \cdot kg/s^2$
圧 力 , 応 力	パ ス カ ル	Pa	N/m^2
エネルギー, 仕事, 熱量	ジ ュ ー ル	J	$N \cdot m$
工 率 , 放 射 束	ワ ッ ト	W	J/s
電 気 量 , 電 荷	ク ー ロ ン	C	$A \cdot s$
電位, 電圧, 起電力	ボ ル ト	V	W/A
静 電 容 量	フ ァ ラ ド	F	C/V
電 気 抵 抗	オ ー ム	Ω	V/A
コンダクタンス	ジ ー メ ン ス	S	A/V
磁 束	ウ ェ ー バ	Wb	$V \cdot s$
磁 束 密 度	テ ス ラ	T	Wb/m^2
インダクタンス	ヘ ン リ ー	H	Wb/A
セルシウス温度	セルシウス度	℃	
光 束	ル ー メ ン	lm	$cd \cdot sr$
照 度	ル ク ス	lx	lm/m^2
放 射 能	ベ ク レ ル	Bq	s^{-1}
吸 収 線 量	グ レ イ	Gy	J/kg
線 量 当 量	シ ー ベ ル ト	Sv	J/kg

表2 SIと併用される単位

名 称	記 号
分, 時, 日	min, h, d
度, 分, 秒	°, ′, ″
リ ッ ト ル	l, L
ト ン	t
電 子 ボ ル ト	eV
原子質量単位	u

$1 eV = 1.60218 \times 10^{-19} J$

$1 u = 1.66054 \times 10^{-27} kg$

表4 SIと共に暫定的に維持される単位

名 称	記 号
オングストローム	Å
バ ー ン	b
バ ー ル	bar
ガ ル	Gal
キ ュ リ ー	Ci
レ ン ト ゲ ン	R
ラ ド	rad
レ ム	rem

$1 Å = 0.1 nm = 10^{-10} m$

$1 b = 100 fm^2 = 10^{-28} m^2$

$1 bar = 0.1 MPa = 10^5 Pa$

$1 Gal = 1 cm/s^2 = 10^{-2} m/s^2$

$1 Ci = 3.7 \times 10^{10} Bq$

$1 R = 2.58 \times 10^{-4} C/kg$

$1 rad = 1 cGy = 10^{-2} Gy$

$1 rem = 1 cSv = 10^{-2} Sv$

表5 SI接頭語

倍数	接頭語	記 号
10^{18}	エ ク サ	E
10^{15}	ペ タ	P
10^{12}	テ ラ	T
10^{9}	ギ ガ	G
10^{6}	メ ガ	M
10^{3}	キ ロ	k
10^{2}	ヘ ク ト	h
10^{1}	デ カ	da
10^{-1}	デ シ	d
10^{-2}	セ ン チ	c
10^{-3}	ミ リ	m
10^{-6}	マ イ ク ロ	μ
10^{-9}	ナ ノ	n
10^{-12}	ピ コ	p
10^{-15}	フ ェ ム ト	f
10^{-18}	ア ト	a

(注)

1. 表1－5は「国際単位系」第5版, 国際度量衡局 1985年刊行による。ただし, 1 eV および1 uの値はCODATAの1986年推奨値によった。
2. 表4には海里, ノット, アール, ヘクタールも含まれているが日常の単位なのでここでは省略した。
3. bar は, JISでは流体の圧力を表わす場合に限り表2のカテゴリーに分類されている。
4. EC閣僚理事会指令では bar, barn および「血圧の単位」mmHg を表2のカテゴリーに入れている。

換 算 表

力	N(=10^5dyn)	kgf	lbf
	1	0.101972	0.224809
	9.80665	1	2.20462
	4.44822	0.453592	1

粘 度 $1 Pa \cdot s(N \cdot s/m^2) = 10 P(ポアズ)(g/(cm \cdot s))$

動粘度 $1 m^2/s = 10^4 St(ストークス)(cm^2/s)$

圧 力	MPa(=10 bar)	kgf/cm^2	atm	mmHg(Torr)	lbf/in^2(psi)
	1	10.1972	9.86923	7.50062×10^3	145.038
	0.0980665	1	0.967841	735.559	14.2233
	0.101325	1.03323	1	760	14.6959
	1.33322×10^{-4}	1.35951×10^{-3}	1.31579×10^{-3}	1	1.93368×10^{-2}
	6.89476×10^{-3}	7.03070×10^{-2}	6.80460×10^{-2}	51.7149	1

エネルギー・仕事・熱量	J(=10^7 erg)	kgf・m	kW・h	cal(計量法)	Btu	ft・lbf	eV
	1	0.101972	2.77778×10^{-7}	0.238889	9.47813×10^{-4}	0.737562	6.24150×10^{18}
	9.80665	1	2.72407×10^{-6}	2.34270	9.29487×10^{-3}	7.23301	6.12082×10^{19}
	3.6×10^6	3.67098×10^5	1	8.59999×10^5	3412.13	2.65522×10^6	2.24694×10^{25}
	4.18605	0.426858	1.16279×10^{-6}	1	3.96759×10^{-3}	3.08747	2.61272×10^{19}
	1055.06	107.586	2.93072×10^{-4}	252.042	1	778.172	6.58515×10^{21}
	1.35582	0.138255	3.76616×10^{-7}	0.323890	1.28506×10^{-3}	1	8.46233×10^{18}
	1.60218×10^{-19}	1.63377×10^{-20}	4.45050×10^{-26}	3.82743×10^{-20}	1.51857×10^{-22}	1.18171×10^{-19}	1

1 cal = 4.18605 J (計量法)

= 4.184 J (熱化学)

= 4.1855 J (15 ℃)

= 4.1868 J (国際蒸気表)

仕事率 1 PS (仏馬力)

= 75 kgf・m/s

= 735.499 W

放射能	Bq	Ci
	1	2.70270×10^{-11}
	3.7×10^{10}	1

吸収線量	Gy	rad
	1	100
	0.01	1

照射線量	C/kg	R
	1	3876
	2.58×10^{-4}	1

線量当量	Sv	rem
	1	100
	0.01	1

(86年12月26日現在)